

University of Nottingham
UK | CHINA | MALAYSIA

The Roles of *def6a* and *swap70b* in Zebrafish Embryogenesis and Haematopoiesis and DEF6 Interactome Analysis in Jurkat T Cells

By

Deniz Akdeniz, MSc

Thesis submitted to the University of Nottingham for the degree of Doctor of Philosophy

March 2018

Acknowledgements

I would like to express my very great appreciation to Prof. Fred Sablitzky, my research supervisor, for his valuable suggestions and guidance during the planning and development of the research project. His helpful critiques, positive encouragements and experienced recommendations motivated me to find the solutions when I had problems during the project. His willingness to give his time so generously is very much appreciated. I could not have imagined having a better advisor and mentor for my PhD study. My grateful thanks are also extended to Dr. Peter Jones for his help in cell culture and protein techniques.

My sincere thanks also goes to Dr. Martin Gering, my second supervisor, for his guidance and suggestions throughout my research and permission to use the microscopes and injection equipment in his laboratory.

I am thankful to Dr. Keith Joung and Dr. Kyle Roux for generating the TALEN and BioID plasmids, respectively and to Dr. Andrew Bottrill for his help in mass spectrometry. I would like to thank the project students, Nadia Ullrich, Jack Taylor, Andreas Papasozomenos, Matthew Jones and Matthew J. Riley for making wnt11, wnt5 and hoxb1a probes.

I am particularly grateful for the guidance and advice given by Tamilvendhan Dhanaseelan who taught me injections and zebrafish techniques. Thanks to the BMSU staff for looking after the fish. Special thanks should be given to Dr. Joanna Richens for her help and advice in the experiments. A big thank you goes to Huaitao Cheng, Kerry Remon, Chen Chen, Yasmin Hough and Peter Jessop for their friendship and advice in the laboratory. It was great sharing laboratory with all of you during the last four years. I must express my special gratitude to Maha Alsayegh, my best friend, for her continued support, help and encouragement. She has become a part of my life since the first day we met and I wish our friendship lasts forever.

Most importantly, I am extremely grateful to my parents, Fehmi and Cemaziye, my siblings Ozgur and Derya and my sister and brother-in laws Ozlem and Yunus for their love, prayers, caring and sacrifices throughout my entire life. I could not have finished my research without their moral and emotional support. Thank you all for providing the opportunity to follow my dreams and putting up with me through the toughest moments of my life. You are the biggest inspiration in my life.

Last but not least, I wish to thank my loving, patient and supportive boyfriend, Aytac Kadioglu whose love and guidance are with me in all my pursuits. His faithful support throughout this PhD is so much appreciated.

Abstract

Medio-lateral narrowing (convergence) and anterior-posterior elongation (extension) are two of the most important cell movements of the gastrulation period leading to the formation of embryonic body axis. In vertebrates, convergence and extension (CE) cell movements are regulated by the non-canonical Wnt/Planar cell polarity (PCP) signalling pathway which requires the activation of its downstream effectors, Rho GTPases. DEF6 and SWAP70 are guanine nucleotide exchange factors (GEFs) catalysing the activation of Rho GTPases to regulate the re-arrangement of actin cytoskeleton, cell polarity and cell movements. Although it has been shown that the zebrafish orthologous, Def6a and Swap70b, act downstream of Wnt5b or Wnt11 signalling pathway, respectively, regulating the CE cell movements during gastrulation, little is known about the underlying molecular mechanisms and direct downstream targets of Def6a and Swap70b. To further elucidate the function of *def6a* and *swap70b* within the non-canonical Wnt/PCP signalling pathway, Transcription Activator-Like Effector Nucleases (TALENs)-induced mutagenesis was employed to establish knock-out mutant lines lacking either *def6a (qmc811), swap70b (qmc809)* or both (*qmc813*). Phenotypic and whole-mount *in situ* hybridisation analyses have revealed that the anterior movement and the convergence of the lateral mesendodermal and ectodermal cells were severely impaired in *def6a* and/or *swap70b*-deficient zebrafish embryos, indicating that *def6a* and *swap70b* are required for normal CE cell movements during gastrulation. Ectopic expression of Cdc42 GTPase robustly rescued the CE cell movement defects in both *def6a*$^{qmc811/qmc811}$ and *swap70b*$^{qmc809/qmc809}$ homozygous mutant lines whereas ectopic expression of RacI robustly rescued CE cell movement defects only in *swap70b*$^{qmc809/qmc809}$ homozygous mutant line, suggesting that Def6a and Swap70b acts upstream of Cdc42 and Cdc42/RacI respectively. Elevated expression of *wnt5b* and *wnt11* detected in the mutant lines indicated that abrogation of *def6a* and *swap70b* functions interfered with Cdc42/RacI-mediated Jnk activation that negatively regulates expression of *wnt11* and perhaps *wnt5b*. In adult *def6a* and/or *swap70b*-deficient fish, a decreased number of myeloid population was observed, suggesting that both proteins are required for balanced cell differentiation during haematopoiesis. Generation of the double homozygous mutant line revealed that *def6a* and *swap70b* act in a partially redundant manner during zebrafish embryogenesis and in a non-redundant manner during haematopoiesis. DEF6 is highly expressed in T cells and plays an immunoregulatory role in cell polarity-induced immunological synapse (IS) formation, T cell receptor (TCR) signalling, T cell activation, differentiation and inflammatory responses. Recently, it has been shown that DEF6 may also be involved in the mRNA surveillance and translation. However, the molecular

mechanisms that it may be involved in and its interactors in T cells are still unknown. Hence, a novel method, BioID, which enables the promiscuous biotinylation of proximal and interacting proteins of a target protein in mammalian cells, was adapted to identify DEF6 interactome in Jurkat T cells. Notably, *in vivo* BioID-DEF6 fusions yielded 127 clusters of interacting and vicinal proteins, including 2 known binding partners, Rac2 and PKC and 1 known close proximity partner, PABP. GO-term classification of the identified proteins showed that the proteins are enriched not only in actin cytoskeleton organisation and mRNA translation, but also in transcription, mRNA splicing/processing, protein folding/modification and metabolic processes. Co-localisation of DEF6 with Coronin1A (CORO1A), an actin cytoskeleton regulator during IS formation, in resting and activated cells provided proof of principle for the interactome analysis suggesting that DEF6 is a multifunctional protein involved in the regulation of cytoskeletal organisation, transcription, mRNA splicing, protein folding/processing and metabolic processes.

Abbreviations

AGM	Aorta-Gonad-Mesonephros
AID	Activation-Induced cytidine Deaminase
ALM	Anterior Lateral Mesoderm
AP	Alkaline Phosphatase
APC	*Adenomatous Polyposis Coligene*
APC	Antigen Presenting Cell
APS	Ammonium Persulfate
BAL	Broncho Alveolar Lavage
BCCP	Biotin Carboxyl Carrier Protein
BCR	B-cell Receptor
BioAMP	Biotinoyl-5′-AMP
BioID	Biotin Identification
BMMC	Bone Marrow Mast Cells
Bmp	Bone Morphogenetic Protein
Boz	Bozozok
Bp	Base pair
BPL	Biotin Protein Ligase
BSA	Bovine Serum Albumin
CA	Constitutively Active
CaM	Calmodulin
CAMK II	Calmodulin-Dependent Kinase II
Cdc42	Cell Division Control Protein 42 homolog
Cdx	Caudal Homeobox Transcription Factor
CE	Convergent and Extension
Chd	Chordin
CHT	Caudal Hematopoietic Tissue
CK 1	Casein Kinase 1
CLPs	Common Lymphoid Progenitors
CMPs	Common Myeloid Progenitors
CNS	Central Nervous System
CORO1A	Coronin-1A

CRD	Cysteine Rich Domain
CRISPR)/Cas	Clustered regulatory interspaced short palindromic repeats CRISPR-associated (Cas)
cSMAC	Central Supramolecular Activation Cluster
C-ter	C terminal
DAAM 1	Dishevelled-Associated Activator of Morphogenesis 1
DAG	Diacylglycerol
DCP1	Decapping Enzyme 1
DEF6	Differentially Expressed in FDCP cells
DEL	Deep Cells
DEP	Dishevelled/EGL-10/Pleckstrin
Dgo	*Diego*
DH	Dbl Homology
DHL	Dbl Homology-Like
DHR	Dock-Homology Region
Dig	Digoxigenin
DIX	Dishevelled/Axin
DKK 1	Dickkopf 1
DKO	Double Knock Out
Dlx	Distal-Less Homeobox
DN	Dominant Negative
DNA	Deoxyribonucleic Acid
Dpf	Days Post Fertilisation
DSB	Double Strand Break
DSH	DEF6/SWAP70 Homology domain
Dsh/Dvl	Dishevelled
dSMAC	Distal Supramolecular Activation Cluster
4E-T	Eukaryotic Translation Initiation Factor 4E Transporter
EAE	Experimental Autoimmune Encephalomyelitis
EAU	Experimental Autoimmune Uveitis
ECL	Enhanced ChemiLuminescence
ECM	Extracellular Matrix
EDTA	Ethylenediaminetetraacetic Acid
EF	EF-Hand Region

Egr	Early Growth Response
eIF	Eukaryotic Initiation Factor
eIF4E	Eukaryotic Translation Initiation Factor 4E
EMS	Ethyl Methane Sulfonate
ER	Endoplasmic Reticulum
ERK	Extracellular signal-Regulated Kinase
Ery	Erythrocytes
EVL	Enveloping Layer
FACS	Fluorescence Activated Cell Sorting
F-actin	Filamentous actin
FBS	Foetal Bovine Serum
FGF	Fibroblast Growth Factor
Fmi	*Flamingo*
FSC	Forward Scatter
FYN	Fgr/Yes related novel protein
Fz	Frizzled
GAP	GTPase-Activating Protein
GDI	Guanine nucleotide Dissociation Inhibitor
GDP	Guanosine Diphosphate
GEF	Guanine nucleotide Exchange Factor
GFP	Green Fluorescent Protein
GMPs	Granulocyte-Monocyte Precursors
GO	Gene Ontology
GSK 3	Glycogen Synthase Kinase 3
GST	Glutathione S-transferase
GTI	Gene-Trap Integration
GTP	Guanosine Triphosphate
GTPase	Guanosine Triphosphate Hydrolase
HDR	Homology-Directed Repair
Hgg	Hatching Gland Gene
HNRNP	Heterogeneous Nuclear Ribonucleoprotein
Hox	Homeobox gene
Hpf	Hours Post Fertilisation
HRMA	High Resolution Melt Analysis

HSCs	Hematopoietic Stem Cells
HSPCs	Haematopoietic Stem and Precursor Cells
HSPG	Heparin-Sulfated forms of Proteoglycans
IBP	IRF-4 Binding Protein
ICAM 1	Intercellular Adhesion Molecule 1
ICM	Intermediate Cell Mass
IRBP	Interphotoreceptor Retinoid-Binding Protein
IRF4	Interferon-Regulatory Factor 4
IFN	Interferon
IL	Interleukin
In-del	Insertion and deletion mutations
$InsP_3$	Inositol-1,4,5-trisphosphate
IP_3R1	Inositol 1,4,5-trisphosphate receptor type 1
IS	Immunological Synapse
ITAM	Immunoreceptor Tyrosine-based Activation Motif
ITK	Interleukin-2 inducible T-cell Kinase
JUN	Jun proto-oncogene
JNK	JUN N-terminal Kinase
JNKK	JNK Kinase
Kny/gpc4	*knypek/glypican 4*
LAT	Linker for Activation of T cells
LB	Luria-Bertani
LCA 1	Leukocyte Function-Associated Antigen 1
LCK	Lymphocyte-Specific Protein Tyrosine Kinase
LN	Lymph Node
LRP	Lipoprotein Receptor-Related Protein
LSK	Lineage-negative, Sca1-positive, c-Kit positive
Lym	Lymphocytes
MAB	Maleic Acid Buffer
MABT	Maleic Acid Buffer with Tween-20
MAPK	Mitogen-Activated Protein Kinase
MBT	Midblastula Transition
MEPs	Megakaryocyte-Erythrocyte Progenitors
MO	Morpholino

MRF	Myogenic Regulatory Transcription Factor
mRNA	Messenger RNA
MS	Mass Spectrometry
MUSK	Muscle Skeletal Receptor Tyr Kinase
Mye	Myelomonocytes
MyoD	Myogenic Differentiation
MZ	Maternal Zygotic
NES	Nuclear Export Signal
NFAT	Nuclear Factor of Activated T cells
NHEJ	Non-Homologous End Joining
NK	Natural Killer
NLS	Nuclear Localisation Signal
NMD	Nonsense-Mediated Decay
NS	No Significant
N-ter	N terminal
Ntl	No tail
Otx	Orthodenticle homeobox
PABP	Poly (A) Binding Protein
PAM	Protospacer-Adjacent Motif
Pax	Paired box gene
P-body	Processing Body
PBS	Phosphate Buffered Saline
PBST	Phosphate Buffered Saline with Tween-20
PCP	Planar Cell Polarity
PCR	Polymerase Chain Reaction
PDGF	Platelet-Derived Growth Factor
PDZ	PSD-95/DLG/ZO1
PFA	Paraformaldehyde
Pg	Pico gram
PH	Pleckstrin Homology
Pk 1	*prickle 1*
PKC	Protein Kinase C
PLA	Proximity Ligation Assay
PLC	Phospholipase

PLM	Posterior Lateral Mesoderm
Ppt/wnt5	*pipetail/wnt5*
Pre	Precursors
pSMAC	Peripheral Supramolecular Activation Cluster
$PtdIns_{(4,5)}P_2$	Phosphatidylinositol-4,5-biphosphate
$PtdIns_{(3,4,5)}P3$	Phosphatidylinositol 3,4,5 triphosphate
PTK 7	Protein Tyr Kinase 7
PVDF	Hybond-P Polyvinylidene Fluoride
RacI	Ras-Related C3 Botulinum Toxin Substrate I
RhoA	Ras Homolog Gene Family Member A
RNA	Ribonucleic acid
RNAi	RNA interference
ROCK	Rho-Associated Kinase
ROR	Receptor Tyr kinase-like Orphan Receptor
RPMI	Roswell Park Memorial Institute 1640
Rspo 2	R-spordin 2
RT	Reverse Transcriptase
S. aureus A/B	*Staphylococcus aureus* enterotoxin A and B
SDS	Sodium Dodecyl Sulphate
SDS-PAGE	Sodium Dodecyl Sulphate Polyacrylamide Gel Electrophoresis
sgRNA	Guide RNA
SLAT	SWAP70-Like Adaptor of T-cells
Slb/wnt11	*silberblick/wnt11*
SMAC	Supramolecular Activation Cluster
SRSF	Serine/Arginine-Rich Splicing Factor
SSC	Side Scatter
SSC	Sodium Sulphate Saline
SSCT	Sodium Sulphate Saline with Tween-20
Sqt	*squint*
SWAP70	Switch Associated Protein-70kDa
Syx	Synectin-binding RhoA Exchange Factor
RVD	Repeat Variable Di-Residue
TALEs	Transcription Activator-Like Effectors
TALENs	Transcription Activator-Like Effector Nucleases

TBE	Tris-Borate-EDTA
TCF/LEF	T Cell Factor/Lymphoid Enhancer Factor
TCR	T-Cell Receptor
Th	T Helper
TILLING	Targeting Induced Local Lesions in Genomes
TLR	Toll-like Receptor
tracrRNA	trans-activating CRISPR crRNA
tri/vangl2	*trilobite/van gogh-like 2*
UTR	Untranslated Region
UV	Ultra Violet
v/v	volume/volume
WASP	Wiskott-Aldrich Syndrome Protein
WAVE	WASP-family Verprolin Homologous Protein
WGEF	Weak-similarity GEF
WISH	Whole Mount *In Situ* Hybridisation
WT	Wild Type
w/v	weight/volume
YSL	Yolk Syncytial Layer
ZAP70	Zeta-Chain-Associated Protein Kinase 70
ZFNs	Zinc-Finger Nucleases

List of Contents

Acknowledgements ……..i

Abstract ..……...ii

Abbreviations ..……....iv

List of Contents ..……..x

List of Figures ……xviii

List of Tables ……xxiii

Chapter 1 Introduction ..……...1

1.1. The Wnt signalling pathways ……..……..1

1.1.1. The multiple pathways of Wnt signalling ……4

1.1.1.1. The canonical Wnt/β-catenin signalling pathway ……..……6

1.1.1.2. The non-canonical Wnt/Planar Cell Polarity (PCP) signalling pathway .....……7

1.1.1.3. The non-canonical Wnt/Ca2+ signalling pathway ..……....8

1.2. The role of Wnt signalling in zebrafish embryonic development ……..……10

1.2.1. Early zebrafish development .....……....……10

1.2.1.1. Zebrafish as a model organism …...……10

1.2.1.2. Embryonic developmental stages of zebrafish ……..11

1.2.2. The canonical Wnt/β-catenin signalling pathway regulates cell fate specification and axis formation ..……...19

1.2.3. The non-canonical Wnt/PCP signalling pathway regulates cell movements during gastrulation ..……20

1.2.3.1. Wnt ligand mutants ……..……..……..…..21

1.2.3.2. Transmembrane and membrane-associated protein mutants 22

1.2.3.3. Frizzled receptor mutants 23

1.2.3.4. Wnt co-factor mutant 23

1.3. Rho GTPases and their role in the regulation of actin cytoskeleton 25

1.3.1. The regulators of Rho GTPases 29

1.3.1.1. GTPase activating proteins (GAPs) 30

1.3.1.2. Guanine nucleotide dissociation inhibitors (GDIs) 31

1.3.1.3. Guanine nucleotide exchange factors (GEFs) 31

1.4. DEF6 and SWAP70 are novel GEFs 35

1.4.1. The isolation and identification of DEF6 and SWAP70 35
1.4.1.1. The isolation and identification of DEF6 35
1.4.1.2. The isolation and identification of SWAP70 36
1.4.2. The structures of DEF6 and SWAP70 proteins 37
1.5. The proposed roles of DEF6 and SWAP70 43
1.5.1. DEF6 and SWAP70 act as GEFs 43
1.5.1.1. The role of DEF6 as a GEF 43
1.5.1.2. The role of SWAP70 as a GEF 44
1.5.2. The roles of Def6 and Swap70 in the immune system 46
1.5.2.1. The role of Def6 in the immune system 46
1.5.2.2. The role of Swap70 in the immune system 49
1.5.3. The roles of Def6 and Swap70 in embryogenesis 50
1.5.3.1. The identification of DEF6 and SWAP70 within the zebrafish genome 50
1.5.3.2. The role of *def6a* in the zebrafish embryonic development 55
1.5.3.2.1. Expression of *def6a* during zebrafish embryonic development 55
1.5.3.3. The role of *swap70b* in the zebrafish embryonic development 58
1.5.3.3.1. Expression of *swap70b* during zebrafish embryonic development 58
1.6. Targeted genome editing to study gene functions 62
1.6.1. Zinc-Finger Nuclease (ZFN) based genome editing 63
1.6.2. Transcription Activator-Like Effector Nuclease (TALEN) based genome editing 65
1.6.3. Clustered Regularly Interspaced Short Palindromic Repeats (CRISPR)/ CRISPR-associated (CRISPR-Cas) based genome editing 65
1.7. Identification of proximal and interacting proteins in mammalian cells by using BioID technique 68
1.8. Research aims and objectives 70-71
Chapter 2 Materials and Methods 72
2.1. Materials 72
2.1.1. Molecular biology and microbiological materials 72
2.1.1.1. Plasmids 72
2.1.1.2. Solutions, buffers and reagents 73

2.1.1.3. Reaction kits 75
2.1.1.4. Enzymes 76
2.1.1.5. Competent cells 76
2.1.2. Technical equipment 77
2.1.3. Zebrafish and microinjection equipment 78
2.1.4. Whole mount *in situ* hybridisation materials 79
2.1.5. Fluorescence activated cell sorting (FACS) materials 80
2.1.6. Cell culture, Western blotting, co-immunoprecipitation and immunostaining materials 81
2.1.7. Databases, software and online programmes 84
2.2. Methods 85
2.2.1. Molecular biology and microbiological techniques 85
2.2.1.1. Streaking the bacterial stab for purification of the plasmid DNA 85
2.2.1.2. Small and large scale preparation of plasmid DNA 85
2.2.1.3. Quantification of nucleic acid concentrations and purity 86
2.2.1.4. Restriction endonuclease digestion 86
2.2.1.5. Phenol-Chloroform extraction and ethanol precipitation of DNA 87
2.2.1.6. Agarose gel electrophoresis 88
2.2.1.7. DNA extraction from agarose gels and purification of PCR products .88
2.2.1.8. DNA ligation 88
2.2.1.9. Transformation 89
2.2.1.10. DNA sequencing 89
2.2.2. Polymerase Chain Reaction (PCR) 90
2.2.3. *In vitro* transcription of mRNAs for microinjection and whole mount *in situ* hybridisation 92
2.2.3.1. *In vitro* transcription and phenol-chloroform extraction of TALEN mRNAs and mRNAs for microinjections into embryos 92
2.2.3.2. *In vitro* transcription of mRNA probes for whole mount *in situ* hybridisation 93
2.2.4. Zebrafish techniques 93
2.2.4.1. Embryo culture, crosses and zebrafish stock maintenance 93
2.2.4.2. TALEN mRNAs microinjection into one-cell stage embryos 94
2.2.4.2.1. Preparation of microinjection needle 94
2.2.4.2.2. TALEN mRNAs microinjections 94

2.2.4.3. Genomic DNA extraction from embryos 95
2.2.4.4. Fin clipping genotyping 95
2.2.4.5. Fixation and storage of zebrafish embryos for whole mount *in situ* hybridisation 95
2.2.4.6. Whole mount *in situ* hybridisation of zebrafish embryos 95
2.2.4.7. Genotyping after whole mount *in situ* hybridisation 96
2.2.4.8. Actin staining of zebrafish embryos 97
2.2.4.9. Imaging of zebrafish embryos 97
2.2.4.10. Flow cytometry analysis of cells isolated from adult kidney marrow .97
2.2.4.11. Data quantification and statistical analysis 98
2.2.5. Cell culture techniques 98
2.2.5.1. Maintenance and passaging of suspension cells 98
2.2.5.2. Cell counting using a haemocytometer 98
2.2.5.3. Precipitation of DNA for the transfection of cells 98
2.2.5.4. Transient transfection of Jurkat T cell lines 99
2.2.6. Protein techniques 99
2.2.6.1. Cell lysis and SDS-PAGE 99
2.2.6.2. Western blotting and immunodetection 100
2.2.6.3. PVDF membrane antibody stripping and re-probing 100
2.2.6.4. Affinity capture of the biotinylated proteins 100
2.2.6.5. Mass spectrometry (MS) 101
2.2.6.6. Immunological synapse formation 101
2.2.6.7. Immunofluorescence 101
2.2.6.8. Confocal microscopy and analysis of images 102
Chapter 3 Results- Establishment of *def6a* and *swap70b* mutant zebrafish 103
3.1. TALEN-mediated mutagenesis of *def6a* and *swap70b* loci 103
3.2. Construction and design of TALENs targeting *def6a* and *swap70b* loci 105
3.3. TALEN-mediated targeted mutations at *def6a* and *swap70b* loci 107
3.3.1. *In vitro* transcription of *def6a* and *swap70b* TALEN mRNAs 107
3.3.2. Optimising the amount of TALEN mRNAs injected for efficient mutagenesis ..108
3.3.2.1. Genotyping and analysing the mutation efficiency in *def6a* locus 108
3.3.2.2. Genotyping and analysing the mutation efficiency in *swap70b* locus108
3.3.3. TALEN mRNAs-induced somatic mutations at *def6a* and *swap70b* loci 109

3.3.4. Germline transmission of TALEN-induced mutations 113

3.3.5. Establishment of *def6a*$^{qmc811/qmc811}$ and *swap70b*$^{qmc809/qmc809}$ mutant lines 117

3.3.6. Establishment of double knock-out mutant line, qmc813, lacking both *def6a* and *swap70b* 125

3.4. Summary 130

Chapter 4 Results- *def6a* and/or *swap70b*-deficiency results in CE cell movement defects during zebrafish gastrulation 131

4.1. Loss of *def6a* and/or *swap70b* resulted in shortened body axis and developmental delay during gastrulation 131

4.2. Normal cell fate specification in single and double homozygous *def6a* and *swap70b* mutants 137

4.3. Single *def6a*$^{qmc811/qmc811}$ and *swap70b*$^{qmc809/qmc809}$ and double *def6a*$^{qmc811/qmc811}$; *swap70b*$^{qmc809/qmc809}$ homozygous mutants displayed posterior shift, reduction and expansion in neuroectoderm markers 141

4.4. *def6a* and *swap70b* are required for convergence and extension (CE) cell movements during gastrulation 146

4.5. Single and double homozygous mutants displayed normal development of anterior and posterior body parts after gastrulation 155

4.5.1. Single and double homozygous mutants displayed normal neural patterning and brain morphogenesis during segmentation 155

4.5.2. Single and double homozygous mutants displayed normal development of somite and tail structures during segmentation 157

4.6. Summary 159

Chapter 5 Results- *def6a* and *swap70b* regulate actin cytoskeleton and *wnt5b/wnt11* expression through Cdc42 and Racl in the non-canonical Wnt/PCP/Ca^{2+} signalling pathways 160

5.1. CE cell movement defects in *def6a*$^{qmc811/qmc811}$ mutants were robustly rescued by overexpression of Cdc42, while overexpression of either Cdc42 or Racl rescued *swap70b*$^{qmc809/qmc809}$ mutants 160

5.1.1. Overexpression of Cdc42 robustly rescued CE cell movement defects in *def6a*$^{qmc811/qmc811}$ mutants 160

5.1.2. Overexpression of either Racl, RhoA or Gfp in *def6a*$^{qmc811/qmc811}$ mutants had no effect on CE cell movement defects 164

5.1.3. Overexpression of either Cdc42 or Racl rescued CE cell movement defects in *swap70b*$^{qmc809/qmc809}$ mutants 172

5.1.4. Overexpression of either RhoA or Gfp in *swap70b*$^{qmc809/qmc809}$ mutants did not restore CE cell movement defects 178

5.2. *def6a*$^{qmc811/qmc811}$ and *swap70b*$^{qmc809/qmc809}$ mutants displayed fewer cell protrusions and fewer polarised cell shape during gastrulation 185

5.3. Expression of *wnt5b* and *wnt11* are upregulated in single and double homozygous mutants 188

5.4. Summary 190

Chapter 6 Results- Myelopoiesis is impaired in adult zebrafish lacking either *def6a, swap70b* or both 191

6.1. Introduction 191

6.2. Development of myelomonocytes in adult zebrafish is significantly affected in the absence of *def6a, swap70b* or both 194

6.3 Summary 196

Chapter 7 Results- BioID-mediated identification of proximal and interacting proteins of DEF6 in Jurkat T cells 197

7.1. BioID-mediated identification of protein-protein interactions in mammalian cells 197

7.2. Construction of BirA-DEF6 and BirA-Truncated DEF6 fusion vectors 200

7.2.1 Establishment of BirA* DEF6 fusion vectors 202

7.2.2 *In vivo* biotinylation of DEF6 interactome in Jurkat T cells 204

7.2.3 Identification and classification of DEF6 interactome 207

7.3. DEF6 might be involved in several processes in Jurkat T cells 222

7.3.1 Actin Cytoskeleton Organisation 222

7.3.2 RNA Splicing and Processing 230

7.3.3 mRNA translation 235

7.3.4 Transcription 239

7.3.5 Metabolic Processes 242

7.3.6 Protein Processing 248

7.4. Summary 252

Chapter 8 Discussion 253

8.1. TALEN-mediated targeted mutations were generated at *def6a* and *swap70b* loci and *qmc809, qmc811* single and *qmc813* double mutant lines were established 253

8.2. The roles of *def6a* and *swap70b* in zebrafish gastrulation 255

8.2.1. *def6a* and *swap70b* are required for CE cell movements but not for cell fate specification during gastrulation 255

8.2.2. Def6a and Swap70b act upstream of Cdc42 and Cdc42/Racl GTPases, respectively in the non-canonical Wnt/PCP/Ca^{2+} signalling pathway to regulate CE cell movements 259

8.3. *def6a* and *swap70b* play a role in the development of myeloid cells during zebrafish haematopoiesis 263

8.4. *def6a* and *swap70b* act in a partially redundant manner during zebrafish embryogenesis and in a non-redundant manner during haematopoiesis 264

8.5. Comparison of knock-out mice and knock-out zebrafish phenotypes 265

8.6. BioID-mediated identification of DEF6 interactome in Jurkat T cells 265

8.7. Conclusion 268

References 269

Appendices 315

List of Figures

Figure 1.1 Schematic representation of Wnt proteins.....2

Figure 1.2 Schematic representation of Frizzled proteins 3

Figure 1.3 Schematic representation of the domain structure of Dishevelled (Dsh) 4

Figure 1.4 The canonical and non-canonical Wnt signalling pathways 5

Figure 1.5 Schematic representations exhibiting the early stages of zebrafish embryonic development 16

Figure 1.6 Gastrulation cell movements in zebrafish 17

Figure 1.7 Cell fate maps of zebrafish 18

Figure 1.8 *ppt/wnt5*, *slb/wnt11* and *slb;ppt* double mutants exhibited CE cell movement defects at tail-bud stage 24

Figure 1.9 Arrangement of actin cytoskeleton components and cell migration 26

Figure 1.10 Regulators of Rho GTPases 30

Figure 1.11 Domain structures of some Dbl-family GEFs exhibiting a conserved DH-PH cassette and multifunctional domains regulating distinct biological functions 34

Figure 1.12 Domain structures of DEF6 and SWAP70 proteins exhibiting the unusual PH-DH domain arrangement 38

Figure 1.13 Amino acid comparison of *def6a* and *swap70b* to human and mouse DEF6 and SWAP70 53

Figure 1.14 Developmental expression levels of *def6* paralogous at different time points 54

Figure 1.15 Expression pattern of *def6a* during zebrafish embryonic development 56

Figure 1.16 Expression pattern of swap70b during zebrafish embryonic development 59

Figure 1.17 Possible genome editing pathways using locus-specific engineered nucleases or CRISPR/Cas system 64

Figure 1.18 Schematic representations of engineered nucleases 67

Figure 1.19 Schematic representation demonstrating the application of BioID method 69

Figure 3.1 Overview of the TALEN-mediated establishment of the *def6a* and *swap70b* homozygous mutant lines 104

Figure 3.2 Left and right TALEN binding sequences targeting exon-1 of *def6a* and *swap70b* loci to generate knock-out zebrafish lines 106

Figure 3.3 Linearisation of *def6a* and *swap70b* TALEN plasmids and *in vitro* transcription of *def6a* and *swap70b* TALEN mRNAs 107

Figure 3.4 Induction of somatic mutations at the targeted locus by injecting *def6a* TALEN mRNAs 110

Figure 3.5 Induction of somatic mutations at the targeted locus by injecting *swap70b* TALEN mRNAs 111

Figure 3.6 Chart indicates the mutation efficiencies after two sets of *def6a* and *swap70b* TALEN mRNAs injection 112

Figure 3.7 Charts illustrate the germline transmission of TALEN-induced mutations and germline transmission efficiency for both *def6a* and *swap70b* TALEN mRNAs-injected F_0 embryos 114

Figure 3.8 In frame and out of frame mutations were inherited from 250pg def6a TALEN mRNAs-injected F_0 founders 115

Figure 3.9 In frame and out of frame mutations were inherited from 500pg *swap70b* TALEN mRNAs-injected F_0 founders 116

Figure 3.10 Fin-clip genotyping to find heterozygous F1 carriers 120

Figure 3.11 Mutated DNA and predicted protein sequences of $def6a^{qmc811/qmc811}$ and $swap70b^{qmc809/qmc809}$ mutant lines 121

Figure 3.12 Distribution of $qmc811^{def6a}$ and $qmc809^{swap70b}$ mutant alleles were found at the expected Mendelian rate 122

Figure 3.13 Fin-clip genotyping to find F2 homozygous carriers 123

Figure 3.14 Genotyping of $def6a^{qmc811/qmc811}$ and $swap70b^{qmc809/qmc809}$ lines to confirm their homozygosity 124

Figure 3.15 Fin clip genotyping confirmed the double heterozygosity for both *def6a* and *swap70b* genes 126

Figure 3.16 Fin-clip genotyping to identify double homozygous mutants 128

Figure 3.17 Sequencing analysis confirmed the double homozygosity of the qmc813 *def6a*; *swap70b* mutant line 129

Figure 4.1 Morphological analysis of WT, single and double homozygous mutants 133

Figure 4.2 Single and double homozygous mutants showed reduced extension of the body axis at tail bud stage (10hpf) compared to WT controls 135

Figure 4.3 Cell specification was not altered in single and double homozygous mutants 139

Figure 4.4 chd expression was not altered in single mutants during gastrulation 140

Figure 4.5 Posterior shift, reduction and expansion in the neuroectoderm markers, pax2a, fgf8, krox20 and hoxb1a were observed in single and double homozygous mutants during gastrulation 144

Figure 4.6 Single and double mutants displayed impaired convergence and extension (CE) cell movements during gastrulation 149

Figure 4.7 Impaired CE cell movements in single and double mutants were confirmed by statistical analyses 153

Figure 4.8 Single and double mutants displayed normal neural patterning and brain morphogenesis during segmentation 156

Figure 4.9 Single and double mutants displayed normal development of somite and tail structures during segmentation 158

Figure 5.1 Injection of *gfp-cdc42* mRNA robustly rescued the CE cell movement defects in *def6a*$^{qmc811/qmc811}$ mutants 162

Figure 5.2 Injection of *gfp-racI* mRNA did not rescue the CE cell movement defects in *def6a*$^{qmc811/qmc811}$ mutants 165

Figure 5.3 Injection of *gfp-rhoA* mRNA did not rescue the CE cell movement defects in *def6a*$^{qmc811/qmc811}$ mutants 167

Figure 5.4 Injection of *gfp* mRNA did not rescue the CE cell movement defects in *def6a*$^{qmc811/qmc811}$ mutants 169

Figure 5.5 Summary of the quantitative analysis indicating robust rescue of the CE cell movement defects by overexpression of *gfp-cdc42* in *def6a*$^{qmc811/qmc811}$ mutants 171

Figure 5.6 Injection of *gfp-cdc42* mRNA robustly rescued the CE cell movement defects in *swap70b*$^{qmc809/qmc809}$ mutants 173

Figure 5.7 Injection of *gfp-racI* mRNA robustly rescued the CE cell movement defects in *swap70b*$^{qmc809/qmc809}$ mutants 176

Figure 5.8 Injection of *gfp-rhoA* mRNA did not rescue the CE cell movement defects in *swap70b*$^{qmc809/qmc809}$ mutants 180

Figure 5.9 Injection of *gfp* mRNA did not rescue the CE cell movement defects in *swap70b*$^{qmc809/qmc809}$ mutants 182

Figure 5.10 Summary of the quantitative analysis demonstrating robust rescue of the CE cell movement defects by overexpression of either *gfp-cdc42* or *gfp-racI* in *swap70b*$^{qmc809/qmc809}$ mutants 184

Figure 5.11 *def6a*$^{qmc811/qmc811}$ and *swap70b*$^{qmc809/qmc809}$ mutants displayed fewer cell protrusions and fewer elongation of actin stained dorsal ectodermal cells than the WT controls 186

Figure 5.12 *wnt5b* and *wnt11* expression were upregulated in single *def6a*$^{qmc811/qmc811}$ and *swap70b*$^{qmc809/qmc809}$ and double *def6a*$^{qmc811/qmc811}$*; swap70b*$^{qmc809/qmc809}$ mutants 189

Figure 6.1 Overview of zebrafish haematopoiesis 193

Figure 6.2 Flow cytometric analysis of the blood cell lineages of WT, single and double mutants revealed that the development of myelomonocytes was significantly reduced in all mutants 195

Figure 7.1 Overview of the BioID method demonstrating DEF6 and its truncations as bait proteins 199

Figure 7.2 Illustration of BirA*-DEF6 and BirA*-N-terminal DEF6, BirA*-PH, BirA*-C-terminal DEF6 fusions 201

Figure 7.3 Cloning of human FL, truncated N-terminal, PH, and C-terminal DEF6 into the pcDNA3.1 mycBioID vector was confirmed by agarose gel electrophoresis 203

Figure 7.4 Western blot analysis demonstrating the biotinylation of interacting or proximal endogenous proteins in Jurkat cells expressing the fusions in the presence of 50μM biotin 205

Figure 7.5 Western blot analysis after affinity capture of biotinylated proteins 206

Figure 7.6 Venn diagrams demonstrating the detected protein numbers for each sample 209

Figure 7.7 Interaction network demonstrating the interaction of 127 proteins as annotated in STRING 210

Figure 7.8 Pie chart summarising GO term enrichments of proteins 211

Figure 7.9 Actin cytoskeleton organisation and focal adhesion pathways are shown as in the KEGG pathway database 226

Figure 7.10 Interaction network of the 7 proteins in the biological process of actin cytoskeleton organisation is shown as annotated in STRING 227

Figure 7.11 DEF6 and CORO1A co-localised partially during IS formation 228

Figure 7.12 DEF6 and CORO1A were localised to the F-actin-rich structures and co-localised at some points of the cell protrusions 229

Figure 7.13 Spliceosome-mediated RNA splicing is shown as in the KEGG pathway database 231

Figure 7.14 Interaction network of the 28 proteins in the biological process of RNA splicing and processing is shown as annotated in STRING 232

Figure 7.15 DEF6 did not co-localise with HNRNPA2B1 during IS formation 233

Figure 7.16 Resting Jurkat T cells exhibiting the absence of co-localision between DEF6 and HNRNPA2B1 234

Figure 7.17 Aminoacyl-tRNA biosynthesis for translation is shown as in the KEGG pathway database 236

Figure 7.18 RNA transport pathway which includes the translation process and ribosomal proteins are shown as in the KEGG pathway database 237

Figure 7.19 Interaction network of the 13 proteins in the biological process of translation is shown as annotated in STRING 238

Figure 7.20 Transcription pathway is shown as in the Reactome pathway database 240

Figure 7.21 Interaction network of the 36 proteins in the biological process of transcription is shown as annotated in STRING 241

Figure 7.22 Purine metabolism is shown as in the KEGG pathway database 243

Figure 7.23 Oxidative phosphorylation which includes the components of mitochondrial membrane ATP biosynthesis is shown as in the KEGG pathway database 244

Figure 7.24 Amino acid biosynthesis/degradation metabolism is shown as in the KEGG pathway database 245

Figure 7.25 Cardiac muscle contraction pathway containing the ion homeostasis processes regulated by ATPases is shown as in the KEGG pathway database 246

Figure 7.26 Interaction network of the 17 proteins in the biological process of metabolism is shown as annotated in STRING 247

Figure 7.27 Protein processing in endoplasmic reticulum (ER) which includes both protein folding and modification processes is shown as in the KEGG pathway database 249

Figure 7.28 Proteasome complex regulating the ATP-dependent degradation of ubiquitinated proteins is shown as in the KEGG pathway database 250

Figure 7.29 Interaction network of the 15 proteins in the biological process of protein folding and modification is shown as annotated in STRING 251

Figure 8.1 The Wnt/PCP/Ca^{2+} signalling pathway model demonstrating the roles of def6a and swap70b in zebrafish gastrulation 262

Figure 8.2 Confirmed and hypothetical roles of DEF6 in T cells 267

Figure 9.1 JDS74 vector backbone of TALEN constructs of def6a and swap70b genes 315

Figure 9.2 Sizes of TALEN region after PCR amplification and digestion 316

Figure 9.3 Sizes of TALEN region after PCR amplification and digestion 317

Figure 9.4 Zebrafish Def6a and Swap70b amino acid sequences 318

Figure 9.5 Flow cytometric analysis of blood cell lineages of WT zebrafish 319

Figure 9.6 Flow cytometric analysis of blood cell lineages of $def6a^{qmc811/qmc811}$ mutant zebrafish 320

Figure 9.7 Flow cytometric analysis of blood cell lineages of $swap70b^{qmc809/qmc809}$ mutant zebrafish 321

Figure 9.8 Flow cytometric analysis of blood cell lineages of double mutant zebrafish 322

Figure 9.9 Plasmid maps of pEGFP-C2/DEF6 and pcDNA3.1 mycBioID 323

Figure 9.10 Sequence analysis confirming the in-frame insertions of FL, N-terminal, PH and C-terminal DEF6 into the pcDNA3.1 mycBioID vector 324

Figure 9.11 Scaffold-mediated identification of all biotinylated proteins 325-343

List of Tables

Table 1.1 Five genes of the SWAP70 protein family and their gene IDs in different databases 52

Table 2.1 Left and right TALEN plasmids of *def6a* and *swap70b* genes 72

Table 2.2 Left and right TALEN mRNA sequences targeting Exon-1 of *def6a* and *swap70b* loci 72

Table 2.3 StrataClone blunt PCR cloning vector 72

Table 2.4 Plasmids for biotinylation of proximal and interacting proteins of DEF6 in Jurkat T cells 72

Table 2.5 Plasmids for sense mRNA synthesis 73

Table 2.6 Prepared buffers and solutions 73

Table 2.7 Buffers, solutions and reagents 74

Table 2.8 Reaction kits 75

Table 2.9 Enzymes 76

Table 2.10 Competent cells 76

Table 2.11 Technical equipment 77

Table 2.12 Microinjection equipment and microscopes 78

Table 2.13 Whole mount *in situ* hybridisation materials 79

Table 2.14 Antisense mRNA probes synthesised from listed genes for *in situ* hybridisations 80

Table 2.15 FACS buffers 80

Table 2.16 Cell lines 81

Table 2.17 Cell culture, SDS-PAGE, Western blotting, co-immunoprecipitation and immunostaining materials 81-83

Table 2.18 Databases, software and online programmes 84

Table 2.19 Primers used for standard and colony PCR to amplify the region flanking TALEN target site for *def6a* and *swap70b* 90

Table 2.20 Primers used for standard PCR to amplify FL, N-terminal, PH and C-terminal DEF6 sequences from pEGFP-C2/DEF6 vector 90

Table 2.21 Components, used amounts and final concentrations for standard and colony PCR in a total volume of 50µl 91

Table 2.22 Standard and colony PCR cycles for amplifying the TALEN regions by using Q5 Hot Start High-Fidelity DNA polymerase 91

Table 2.23 Standard PCR cycle for cloning the def6 full-length and its truncation sequences into the pcDNA3.1 mycBioID vector by using Q5 Hot Start High-Fidelity DNA polymerase 92

Table 2.24 Solutions for 10% SDS-PAGE 99

Table 3.1 Germline transmission efficiencies for *def6a* TALEN mRNAs-injected F_0 founders 115

Table 3.2 Germline transmission efficiencies for *swap70b* TALEN mRNAs-injected F_0 founders 116

Table 3.3 The number of F_1 adults fin-clip genotyped to establish def6a$^{qmc811/amc811}$ and swap70b$^{qmc809/qmc809}$ homozygous mutant lines 119

Table 7.1 Table demonstrates the GO term enrichments of 103 proteins 212-221

CHAPTER 1
INTRODUCTION

1.1. The Wnt signalling pathways

The Wnt signalling pathway has a vital role in controlling key mechanisms in embryogenesis and diseases in vertebrates and invertebrates (Montcouquiol *et al.,* 2006). Cell fate specification, cell differentiation, rearrangement of cytoskeleton, cell migration, adhesion and dorsal-ventral axis formation are the developmental functions regulated by Wnt proteins (Miller, 2001; Logan and Nusse, 2004; Gomez-Orte *et al.,* 2013). In adults, Wnt proteins are responsible for maintaining homeostasis and altered Wnt signalling has been linked to tumorigenesis in many human tissue types such as colorectal cancer cells (Miller, 2002; Logan and Nusse, 2004; Behrens and Lustig, 2004).

Wnt genes encode cysteine-rich secreted glycoproteins that are highly conserved between vertebrates and less conserved between vertebrates and invertebrates. 19 *WNT* genes for human, 16 w*nt* genes for *Xenopus*, 12 *wnt* genes for zebrafish, 11 *Wnt* genes for chick and 7 *Wnt* genes for *Drosophila* have been identified so far (Miller, 2002). Phylogenetic analysis of *Wnt* genes revealed that some of these *Wnt* genes (e.g *Wnt5a*) are orthologues of each other within vertebrates (e.g. mouse, human, zebrafish) (Sidow, 1992).

Wnt proteins are usually 350-400 amino acids in length but their structures are unknown, as they are highly insoluble secreted proteins and all Wnt proteins contain sites for N-linked glycosylation and conserved 22-24 cysteine residues (Cadigan and Nusse, 1997; Komekado *et al.,* 2007; Willert and Nusse, 2012). The cysteine residues are responsible for forming intracellular di-sulphide bridges regulating the formation of the globular secondary structure (Willert and Nusse, 2012) **(Figure 1.1(A)).** The primary amino acid sequence of Wnt proteins revealed that they harbour a signal sequence for secretion on their N-terminus (Miller, 2002) and they are mostly detected at the cell membrane and extracellular matrix (ECM) (Reichsman *et al.,* 1996). The Wnt proteins bind directly to the cell membrane receptors like Frizzled receptors, or inhibitors like Cerberus (Cer), Frizzled related protein (Frp) and Wnt inhibitory factor (Wif) (Nusse, 2003) **(Figure 1.1(B))**.

After translation, Wnt proteins are exposed to posttranslational modifications on their journey to the ECM. Acylation and glycosylation are the most important modifications on Wnt proteins

and acylation is also the reason for the hydrophobic and high degree of insoluble structure of Wnt proteins (Willert *et al.,* 2003; Willert and Nusse, 2012). The isolation of Wnt protein (mouse Wnt3a) confirmed that palmitoylation (covalently attachment of an acyl group, palmitate) of a cysteine residue by a thioesther is essential for Wnt activity since site-directed mutagenesis of the cysteine residue or removal of palmitate caused Wnt3a to lose its activity and hydrophobic structure (Willert *et al.,* 2003) **(Figure 1.1(A))**. Similarly, the experiments on Wnt3a palmitoylation mutants and on removing palmitate from a cysteine residue also showed supressed activity of protein that is unable to bind its receptors Frizzled8 and Lrp6 (Komekado *et al.,* 2007). On the other hand, glycosylation (covalently attachment of a N-linked glycan) plays a critical role in the secretion of Wnt proteins since the glycosylation mutants of Wnt3a and Wnt5a showed impaired secretion (Komekado *et al.,* 2007; Kurayoshi *et al.,* 2007). Furthermore, studies by Komekado *et al.,* (2007) have shown that glycosylation is essential for the acylation of Wnt3a protein suggesting that both modifications work together to ensure the intact activity and secretion of Wnt proteins (Komekado *et al.,* 2007).

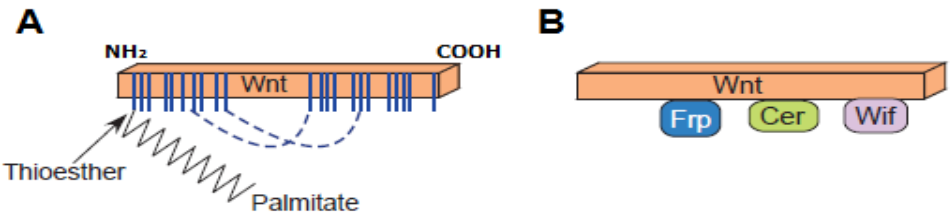


Figure 1.1 Schematic representation of Wnt proteins. (A) Schematic representation of the conserved 22 cysteine residues and palmitoylation of the Wnt protein. Dashed lines indicate the formation of di-sulphide bridges between cysteine residues. **(B)** Schematic representation exhibiting the direct interaction of Wnt proteins with antagonists like Frizzled related protein (Frp), Cerberus (Cer) and Wnt inhibitory factor (Wif) (Adapted from Nusse, 2003).

Wnt proteins directly bind to a complex that harbours a member of Frizzled (Fz) family of transmembrane receptors and a member of a co-receptor to activate its downstream effectors in Wnt signalling pathways (Miller, 2002; Cadigan and Liu, 2006; Gomez-Orte *at al.,* 2013). The *frizzled* genes were first identified in *Drosophila* (Adler, 2002) and also found in other vertebrates including humans. The Frizzled proteins are essential for the regulation of cell polarity, embryonic development, formation of neural synapses and proliferation in developing and adult organisms (Huang and Klein, 2004). Frizzled proteins are formed of 500-700 amino acids in length and contain an extracellular N-terminal cysteine rich domain (CRD) binding to ligands, a hydrophilic variable linker region and seven hydrophobic domains forming transmembrane α-helices. The C-terminal domain of the Frizzled proteins is an intracellular structure and usually contains 25-200 amino acids. (Wang *et al.,* 1996) **(Figure 1.2(A-B)).**

CRD is the ligand-binding domain where Wnt proteins bind directly and consists of ten conserved cysteines that form di-sulphide bonds (Bhanot *et al.,* 1996; Dann *et al.,* 2001). Furthermore, a motif conserved (KTXXXW) among Frizzled proteins, which is located at the two amino acids after the seventh transmembrane domain, was discovered to be essential for the activation of canonical Wnt/β-catenin signalling pathway and membrane relocalisation (Umbhauer *et al.,* 2000). Further investigations on this motif have shown that a peptide from this motif has a direct interaction with a peptide from the PDZ domain of the cytoplasmic Dishevelled (Dsh/Dvl) protein. This finding suggests that this conserved motif may be an essential regulator of signal transduction process by mediating the interaction between Fz and Dsh proteins (Wong *et al.,* 2003).

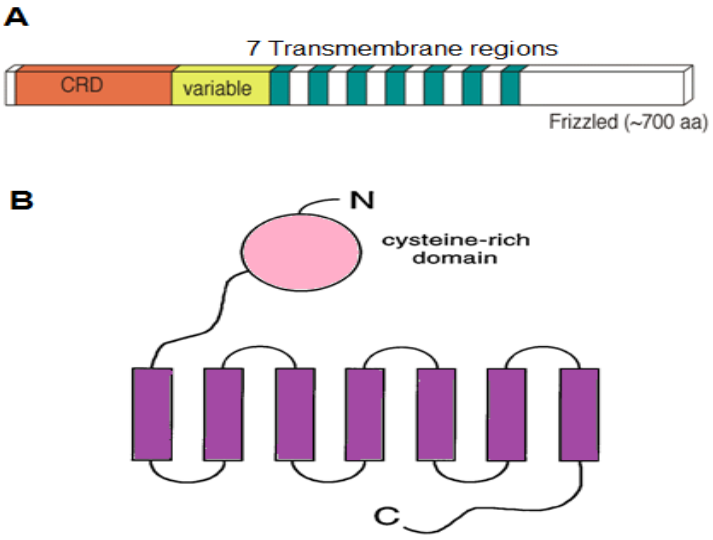


Figure 1.2 Schematic representation of Frizzled proteins. (A) Schematic representation of the domain structure of Frizzled proteins containing a N-terminal cysteine rich domain (CRD), a variable linker region and seven hydrophobic transmembrane domains (Adapted from Cadigan and Nusse, 1997). **(B)** The N-terminus is located on the extracellular part of the membrane whereas the C-terminus is located on the cytoplasmic part. The seven transmembrane domains encompass the membrane (Adapted from Wang *et al.,* 1996).

The integration of Wnt protein and Frizzled receptor results in the activation of the intracellular signal transducer, Dishevelled (Dsh/Dvl) proteins (Wharton, 2003). Dsh proteins are the significant mediators organising the pathway-specific signalling complexes like cell fate specification and cell polarity by delivering the signal to its downstream effectors (Wallingford and Habas, 2005).

Dsh proteins are composed of 500-600 amino acids and harbour a N-terminal Dishevelled/Axin (DIX) domain, a central PSD-95, DLG, ZO1 (PDZ) domain followed by a Dishevelled, EGL-10, Pleckstrin (DEP) domain (Boutros and Mlodzik, 1999; reviewed in Wallingford and Habas, 2005). In addition to the conserved domains, two additional phosphorylation regions, the serine/threonine-rich region between the DIX and PDZ domains, and the proline-rich region between the PDZ and DEP domains were also found to be conserved (Penton *et al.,* 2002) **(Figure 1.3)**.

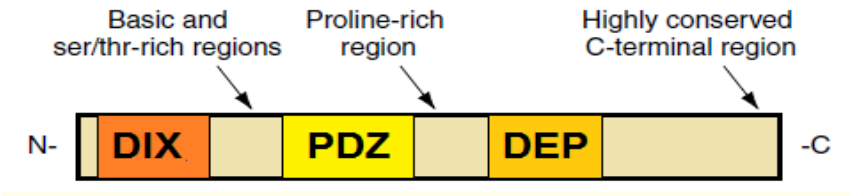


Figure 1.3 Schematic representation of the domain structure of Dishevelled (Dsh). Dsh is composed of three conserved domains of DIX, PDZ and DEP in addition to the serine/threonine-rich and proline-rich regions (Adapted from Wallingford and Habas, 2005).

1.1.1. The multiple pathways of Wnt signalling

As the intracellular receptor-generated signal is transduced to the Dsh, either of the three major Wnt signalling pathways comes into prominence (Boutros and Mlodzik, 1999). These pathways are termed canonical Wnt/β-catenin signalling, non-canonical Wnt/Planar Cell Polarity (PCP) signalling and non-canonical Wnt/Ca^{2+} signalling (Miller *et al.,* 1999; Kühl *et al.,* 2000; Adler, 2002) **(Figure 1.4)**. However, the mechanism by which pathways are selected to activate its downstream targets remains mysterious, since different domains of Dsh are required for each of the three pathways. While DIX and PDZ domains are used for canonical Wnt/β-catenin signalling pathway, the PDZ and DEP domains are used for non-canonical Wnt/PCP and Wnt/Ca^{2+} signalling pathways (Axelrod *et al.,* 1998; Boutros *et al.,* 1998; Heisenberg *et al.,* 2000; Wallingford *et al.,* 2000; Penton *et al.,* 2002; Sheldahl *et al.,* 2003; Veeman *et al.,* 2003b; reviewed in Wallingford and Habas, 2005). DIX domain is essential for canonical Wnt/β-catenin signalling since it interacts with Axin directly (Kishida *et al.,* 1999). By contrast, the DEP domain is essential for non-canonical Wnt/PCP signalling pathway and a mutation in the DEP domain results in defective membrane localisation and functional activity of Dsh (Axelrod *et al.,* 1998; Boutros *et al.,* 1998).

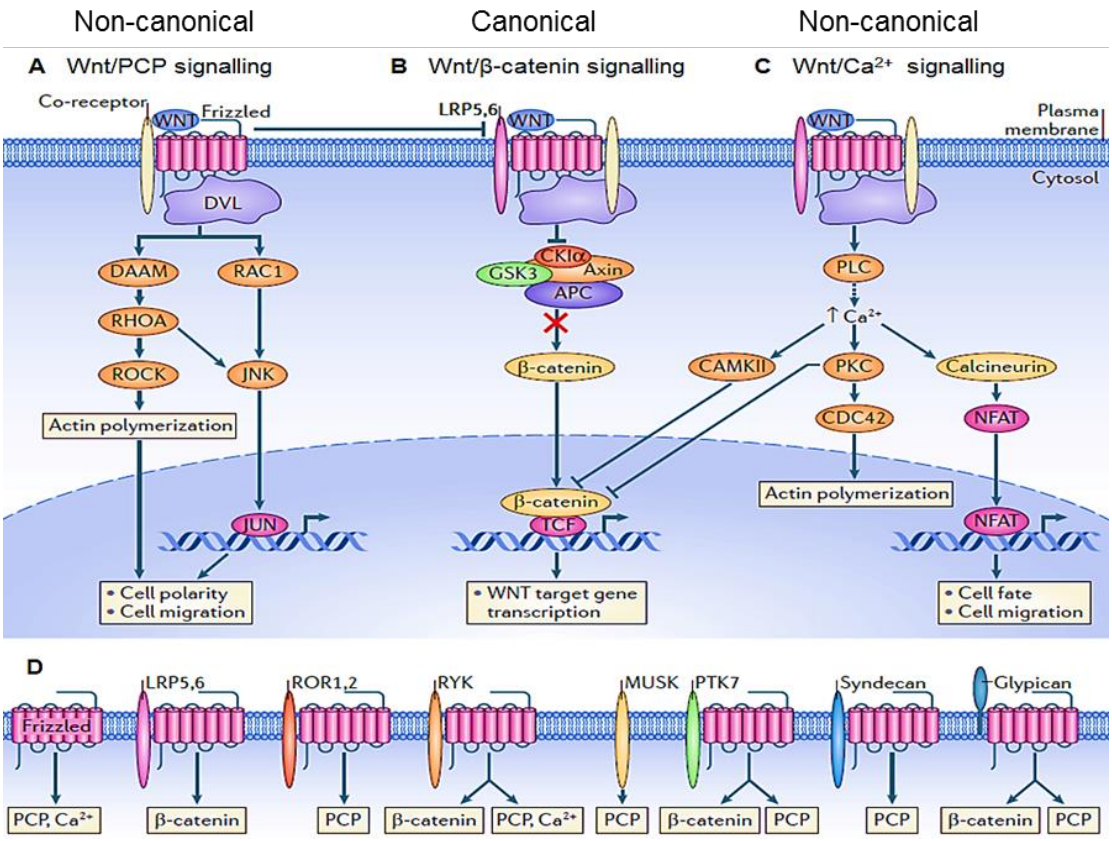


Figure 1.4 The canonical and non-canonical Wnt signalling pathways. (A) Non-canonical Wnt/PCP signalling: After the activation of FZ receptor, DVL/DSH leads to the activation of small GTPases of Rho family, RACI and RHOA. RHOA pathway activation is mediated by Dishevelled-associated activator of morphogenesis 1 (DAAM) protein unlike RACI pathway. RHOA GTPase in turn activates RHO kinase (ROCK) for the maintenance of actin cytoskeleton depolymerisation, cell polarity and the cell migration. The activation of RACI GTPase and possibly RHOA GTPase provide the activation of JUN-N-terminal kinase (JNK) pathway. JNK pathway then regulates cell polarity and cell migration (Niehrs, 2012). **(B)** Canonical Wnt/β-catenin signalling: The Wnt protein binds to the FZ receptor and its co-receptor LRP5/6. It triggers the activation of DVL and phosphorylation of LRP5/6 by CKIα and GSK3. The phosphorylation stabilizes Axin protein and prevents the formation of destruction complex. Therefore, β-catenin can accumulate in the nucleus and activate the transcription of Wnt responsive genes (Macdonald *et al.,* 2009). **(C)** Non-canonical Wnt/Ca^{2+} signalling: The signalling is separated into three branches. The activation of FZ receptor stimulates Ca^{2+} release from endoplasmic reticulum (ER) which in turn activates the calmodulin-dependent kinase II (CAMKII), protein kinase C (PKC) and calcineurin. CaMKII suppresses canonical Wnt signalling through inhibition of β-catenin dependent transcription. PKC activates CDC42 GTPase which also contributes to the rearrangement of actin polymerisation. Lastly, Ca^{2+}-calcineurin pathway mediates the activation of NFAT transcriptional factor to regulate gene expression controlling cell fate and cell migration (Wallingford and Habas, 2005). **(D)** FZ receptor and its distinct co-receptors for canonical and non-canonical pathways are illustrated. DVL: Dishevelled, LRP5/6: low-density lipoprotein receptor-related protein 5/6, MUSK: muscle skeletal receptor Tyr kinase, PLC: phospholipase C, PTK7: protein Tyr kinase 7, ROR: receptor Tyr kinase-like orphan receptor, RYK: receptor Tyr kinase (Adapted from Niehrs, 2012).

1.1.1.1. The canonical Wnt/β-catenin signalling pathway

The canonical Wnt/β-catenin is the best characterised signalling pathway in which β-catenin is the targeted key factor controlling the transcription of developmental genes (Macdonald *et al.,* 2009).

In the absence of Wnt, a 'destruction complex', which is composed of tumor suppressor Axin, tumor suppressor *adenomatous polyposis coligene* product (APC), casein kinase 1 (CK1), and glycogen synthase kinase 3 (GSK3), targets β-catenin for degradation (Macdonald, 2009). Axin is the scaffolding component of the complex as it interacts with each component and β-catenin to maintain the phosphorylation of β-catenin on its N-terminal serine and threonine residues (Kimelman and Xu, 2006). Sequential phosphorylation of N-terminal β-catenin by CK1 and GSK3 results in a recognition site for E3 ubiquitin ligase, β-TrCP. As a result, β-catenin is ubiquitinated and degraded by the proteasome (Aberle *et al.,* 1997; He *et al.,* 2004). The degradation of β-catenin prevents it from accumulating in the cell nucleus and activating the Wnt target genes **(Figure 1.4B)**. Therefore, DNA-bound T cell factor/lymphoid enhancer factor (TCF/LEF) family of transcription factors represses the expression of Wnt target genes (Macdonald *et al.,* 2009). Mutations at the phosphorylation residues of β-catenin or at the tumor suppressor APC are usually found in cancers that provide β-catenin to escape from degradation and accumulate in the cell nucleus (Korinek *et al.,* 1997; Morin *et al.,* 1997).

The presence of Wnt, Wnt binds to Fz receptor and its co-receptor low-density lipoprotein receptor-related protein 6 (LRP6) or LRP5 to activate the signalling pathway (Clevers, 2006). The formation of Wnt-Fz-LRP5/6 complex results in the phosphorylation of Dsh and subsequent recruitment to the plasma membrane to interact with Fz directly (Wong *et al.,* 2003). Following the activation of Dsh, the cytoplasmic tail of LRP harbouring a Pro-Pro-Pro (Ser/Trp)-Pro motif is phosphorylated by CK1 and GSK3 (Tamai *et al.,* 2004; Zeng *et al.,* 2005; Davidson *et al.,* 2005). The phosphorylation then ensures the interaction between Axin and cytoplasmic tail of LRP and/or Fz bound Dsh. Thus, Wnts are thought to be the key elements regulating the docking of Axin and dissolving the destruction complex away (Logan and Nusse, 2004; Clevers, 2006). The disassociation of the complex inhibits the phosphorylation of β-catenin and in turn its ubiquitination and degradation (Macdonald *et al.,* 2009). The increasing levels of β-catenin lead to its nuclear accumulation and binding to the TCF/LEF transcription factors to promote the transcription of Wnt target genes (Behrens *et al.,* 1996; Molenaar *et al.,* 1996, van de Wetering, 1997; Bienz and Clevers, 2003) **(Figure 1.4(B)).** These target genes are commonly responsible for maintenance and activation of stem cells, cell proliferation, cell fate specification in development and self-renewing of tissues in adults (Reya and Clevers, 2005; Clevers, 2006; Macdonald *et al.,* 2009). Given the critical diverse roles of Wnt/β-catenin

signalling, it is not surprise to see that various cell-specific self-regulatory loops are the central key features of Wnt pathway regulation that ensure to conduct the mechanism properly (Logan and Nusse, 2004). The expression of Wnt signalling components including Fz, Axin2, LRP, Heparin-sulfated forms of proteoglycans (HSPG), TCF/LEF, Naked, Dickkopf (DKK1) and R-spondin2 (Rspo2) are regulated negatively or positively by β-catenin/TCF/LEF transcription complex (Logan and Nusse, 2004; Kazanskaya *et al.,* 2004; Chamorro *et al.,* 2005). For instance, while Wnt induction of TCF/LEF genes induce a positive feedback loop to support Wnt signalling, Wnt induction of Axin2 gene induces a negative feedback loop to dampen Wnt signalling (Logan and Nusse, 2004; Arce *et al.,* 2006).

1.1.1.2. The non-canonical Wnt/Planar Cell Polarity (PCP) signalling pathway

The non-canonical Wnt/PCP signalling pathway is also activated by the interaction between Wnt and Fz receptors and its co-receptors such as receptor Tyr kinase‑like orphan receptor (ROR) or protein Tyr kinase 7 (PTK7) which in turn recruits Dsh to transduce the signal to its downstream targets. However, the downstream targets in non-canonical Wnt/PCP pathway do not contain β-catenin or a destruction complex (Niehrs, 2012). Instead, the small GTPases of Rho family; Ras-Related C3 Botulinum Toxin Substrate I (RacI), Ras homolog gene family member A (RhoA) and MAP kinase module; Jun proto-oncogene (JUN), JUN N-terminal kinase (JNK) and JNK kinase (JNKK) are downstream effectors regulating the rearrangement of actin cytoskeleton, tissue polarity (e.g. fish scales, bird feathers and inner ear), cell migration (convergent and extension (CE) cell movements in vertebrate development), neural tube closure and hair and stereocilia orientation by managing both transcriptional and non-transcriptional responses in cell (Strutt *et al.,* 1997; Boutros *et al.,* 1998; Weber *et al.,* 2000; Fanto *et al.,* 2000; Mlodzik, 2002; Simons and Mlodzik, 2008; Niehrs, 2012).

At the level of Dsh, two independent and parallel pathways are activated individually through PDZ and DEP domains of Dsh (Wallingford and Habas, 2005). On the one hand, the PDZ domain binds to Dishevelled-associated activator of morphogenesis 1 (DAAM1) molecule and activates the first pathway containing RhoA GTPase (Habas *et al.,* 2001). Then, RhoA GTPase leads to the activation of the Rho-associated kinase (ROCK) which regulates the rearrangement of actin cytoskeleton directly without initiating a transcriptional activation (Niehrs, 2012). Similar to DAAM1 binding factor, other factors such as *Strabismus/Van Gogh (Stbm/Vang)*, *Flamingo (Fmi)* or *Diego (Dgo)* that bind to the PDZ domain are also required to antagonise or agonise the Fz-Dsh activity in PCP signalling of vertebrates (Park and Moon, 2002; Jenny *et al.,* 2003; Das *et al.,* 2004; Wallingford and Habas, 2005; Jenny *et al.,* 2005). On the other hand, the DEP domain interacts with, and activates the RacI GTPase, which in turn induces the JUN N-terminal kinase (JNK) or related kinase pathway regulating the cell

polarity and cell migration through the transcriptional activation of JUN transcriptional factor (Boutros *et al.,* 1998) **(Figure 1.4(A))**.

1.1.1.3. The non-canonical Wnt/Ca^{2+} signalling pathway

The presence of an additional Wnt signalling pathway other than Wnt/β-catenin was first discovered in zebrafish and *Xenopus* embryos. Overexpression of Wnt1, Wnt3a, Wnt8, Wnt8b, Wnt2 and Wnt7b have been found to induce axis duplication in *Xenopus* embryos, while Wnt5a, Wnt4 and Wnt11 perturbed the morphogenetic movements and antagonised the activity of Wnt8 that induces a secondary axis (Du *et al.,* 1995; Torres *et al.,* 1996). In addition, the existence of a distinct pathway depending on both intracellular Ca^{2+} release and heterotrimetric G-proteins was confirmed when the ectopic expression of *Xenopus* Wnt-5a and rat Frizzled 2 but not *Xenopus* Wnt8 and rat Frizzled 1 induced increased intracellular Ca^{2+} levels in zebrafish embryo (Slusarski *et al.,* 1997a,b; Moon *et al.,* 1997; Sheldahl *et al.,* 1999). As the Ca^{2+} release was the first described feature of this non-canonical pathway, and possibly playing a role in the stimulation of calmodulin-dependent kinase II (CAMKII), protein kinase C (PKC) and calcineurin, this pathway was named as non-canonical Wnt/Ca^{2+} signalling pathway (Kühl *et al.,* 2000a).

The non-canonical Wnt/Ca^{2+} signalling pathway is activated through the binding of Wnt to the G-proteins linked Fz receptor which in turn recruits Dsh. The stimulation of G-proteins linked Fz receptor leads to hydrolysis of phosphatidylinositol-4,5-biphosphate ($PtdIns_{(4,5)}P_2$) into diacylglycerol (DAG) and inositol-1,4,5-trisphosphate ($InsP_3$). Diacylglycerol induces the activation of PKC, while $InsP_3$ interacts with the calcium channels on the membrane of ER to induce the release of the intracellular Ca^{2+} (Berridge and Irvine, 1989; Berridge, 1993), Ca^{2+} release stimulates the calcium responsive enzymes, CAMKII, PKC and calcineurin (Sheldahl *et al.,* 1999; Kühl *et al.,* 2000a,b; Sheldahl *et al.,* 2003; Wallingford and Habas, 2005). As a result of the activation of PKC, Cell Division Control Protein 42 homolog (Cdc42) GTPase which also reorganises the actin cytoskeleton is stimulated (Choi and Han, 2002). The activation of CAMKII antagonises the Wnt/β-catenin signalling pathway through suppressing the expression of β-catenin. In addition, in some cases both CAMKII and PKC were found to activate NFκB and CREB transcription factors (De, 2011). Lastly, activation of calcineurin induces the activation of nuclear factor of activated T cells (NFAT) transcription factor via dephosphorylation that regulates various biological processes ranging from cell fate determination and cell migration in vertebrate development, inflammatory responses and neurodegeneration (Moon *et al.,* 1997; Hogan *et al.,* 2003; De, 2011; Niehrs, 2012) **(Figure 1.4(C)).**

Additionally, even though Wnt5a, Wnt4 and Wnt11 were accepted as Wnt5a class of Wnts acting substantially in non-canonical Wnt/Ca^{2+} signalling pathway and Wnt1, Wnt3a, Wnt8a and Wnt8b were accepted as Wnt1 class of Wnts acting substantially in canonical Wnt/β-catenin signalling pathway (Du *et al.,* 1995), it has been suggested that one Wnt can activate two different pathways by using different receptors (Mikels and Nusse, 2006). A member of class Wnt5a, *XWnt1,* also participates in the Wnt/PCP pathway to regulate gastrulation cell movements in *Xenopus* (Tada and Smith, 2000). Furthermore, it has been shown that *Wnt5a* activates or inhibits the Wnt/β-catenin pathway and stimulates the JNK pathway in the Wnt/PCP pathway in the presence of Fz4 receptor and LRP5 coreceptor or in the presence of Fz2 receptor and Ror2 receptor, respectively (Mikels and Nusse, 2006; Oishi *et al.,* 2003; Sato *et al.,* 2010). Since the acting roles of Wnt proteins in a pathway vary from non-canonical to canonical and vice versa depending on different receptors and factors, further investigations are essential for understanding the complex mechanism configuring each of the Wnt signalling pathways.

Interestingly, it has been suggested that in both vertebrates and invertebrates, the non-canonical Wnt/Ca^{2+} signalling pathway overlaps with the non-canonical Wnt/PCP signalling pathway to mediate actin cytoskeleton re-modelling, cell polarity and migration while it antagonises canonical Wnt/β-catenin signalling (Torres *et al,* 1996; Ishitani *et al.,* 2003; Westfall *et al.,* 2003; Topol *et al.,* 2003; Sato *et al.,* 2010; Niehrs, 2012; reviewed in Kestler and Kühl, 2008). Even though the Wnt/PCP and Wnt/Ca^{2+} signalling pathways are illustrated separately in **Figure 1.4**, studies in mammalian cells suggested that Cdc42 can also activate the JNK pathway to regulate actin cytoskeleton dynamics and cell migration (Coso *et al.,* 1995; Minden *et al.,* 1995; Tao *et al.,* 2001). Moreover, studies in vertebrate and *Drosophila* embryonic development showed that while Dsh activates the Wnt/Ca^{2+} signalling pathway (Sheldahl *et al.,* 2003), some of the G-proteins like $G\alpha_o$ are involved in Wnt/PCP signalling pathway (Katanaev *et al.,* 2005). Cdc42 acts downstream of Frizzled receptor to activate JNK in *Drosophila* and a Wnt/PCP signalling component, *prickle* has also been shown to regulate intracellular calcium signalling in zebrafish (Schlessinger *et al.,* 2009; Veeman *et al.,* 2003a). Furthermore, experiments on homozygous *pipetail/wnt5* (*ppt*/*wnt5)* mutant embryos showed decreased release of Ca^{2+} and maternal zygotic (mz) *ppt/wnt5* mutant embryos exhibited hyper-dorsalisation and partial axis duplication phenotypes which were rescued by a CA-CamKII mutant (Westfall *et al.,* 2003). These results suggested that impairment in the Wnt/PCP signalling pathway disrupted the Wnt/Ca^{2+} signalling pathway and it's antagonising activity for Wnt/ β-catenin signalling pathway (Kühl *et al.,* 2000a; Ishitani *et al.,* 2003; Westfall *et al.,* 2003). Taken together, these results further support the idea that the non-canonical Wnt signalling pathways are highly connected.

1.2. The role of Wnt signalling in zebrafish embryonic development

1.2.1. Early zebrafish development

1.2.1.1. Zebrafish as a model organism

Zebrafish, *Danio rerio*, is a teleost fish of the cyprinid family. The zebrafish genome is 1.7 gigabases in size and composed of 25 chromosomes (1n) (Nüsslein-Volhard and Dahm, 2002). Comparative genome analysis between vertebrates and fish revealed that genome-wide duplication (up to 20% of the zebrafish genome) had occurred within teleosts before the teleost radiation (Amores *et al.,* 1998; Postlethwait *et al.,* 1998). After genome duplication, usually one paralogue becomes silenced through mutations and disappears over time. However, in some cases, both paralogues may remain active if beneficial mutations occur in one or both paralogues leading to acquire new functions or the function of ancestral gene divides up between both genes leading to both paralogues acquiring more restricted functions than the original ancestral gene. Finding divergent spatial and temporal expression patterns of the resulted paralogues in zebrafish suggested that the function of ancestral genes may be split in two genes each coding a different protein with different expression patterns (Nüsslein-Volhard and Dahm, 2002).

Zebrafish was chosen as a model organism for being easy to keep and breed. Fertilisation occurs externally and early embryonic development can be easily observed through the chorion. The embryos are transparent during the first 24 hours of development which allows the visualisation of germ layers and developing organs. After 48 hours of development, the developing parts of brain, eyes, ears, notochord and other internal organs can be observed. At 5 days of development after fertilisation, the zebrafish larvae can balance their body properly to swim and seek for food.

The most important advantage of using zebrafish as a model organism is, zebrafish can be genetically modified and the progeny can be screened in a generation time of 2-4 months to check the germline transmission efficiency. The development of genome editing tools like Transcription Activator-Like Effector Nucleases (TALENs) facilitated the investigation of genetics regulating early development of zebrafish. Transgenic lines can be generated to understand gene function and underlying causes of genetic diseases.

1.2.1.2. Embryonic developmental stages of zebrafish

Seven periods of embryogenesis were defined as the zygote, cleavage, blastula, gastrula, segmentation, pharyngula and hatching during the first three days of embryogenesis after fertilisation **(Figure 1.5)**. These broad periods were sub-divided into stages that are based on morphological developments (Kimmel *et al.,* 1995). This specification of stages is widely accepted and applied in developmental biology.

The zygote period (0-0.75hpf) comprises of four morphological stages including the newly fertilised egg until the first cleavage of the cell (Kane, 1999). The zygote, protected by a chorion which swells and lifts away from the zygote upon the fertilisation, is composed of a mixture of translucent yolk and cytoplasm. Fertilisation also activates the calcium waves inducing the contraction of actin cytoskeleton to move non-yolky cytoplasm toward the animal pole (Leung *et al.,* 1998). Cytoplasm begins to accumulate at the animal pole to separate and generate a blastodisc on top of the clear yolk cell (Kane, 1999; Kimmel *et al.,* 1995). The zygote period ends when the first mitosis occurs (Kimmel *et al.,* 1995).

The cleavage period (0.75-2.25hpf) consists of six stages of cleavage from 2 cells to 64 cells which are named as blastomeres. After the first cleavage, blastomeres divide rapidly and synchronously in approximately every 15 minutes. A cleavage furrow appears at the animal pole of the dividing cell, progresses toward the vegetal pole, and terminates at the end of the blastodisc and does not pass through the yolk cell. This cleavage is called meroblastic and only blastodisc forms the embryo. Thus, until the 8-cell stage, all of the blastomeres are interconnected to the yolk by cytoplasmic bridges (Kimmel *et al.,* 1995).

The blastula period (2.25-5.25hpf) starts at 128-cell stage and ends at the early stages of epiboly. This period harbours three broad stages known as early blastula, midblastula and late blastula stages. In early blastula, the cells continue to divide synchronously which is called metasynchronous since the mitoses do not occur all at the same time. In midblastula starting at tenth cell division, 512-cell stage (2.75h), the embryo enters the midblastula transition (MBT) characterised by asynchronous, slow and long cell cycles (Kimmel *et al.,* 1995). During the tenth cell division, the cells at the margin of blastodisc-yolk cell fuse their cytoplasm and nuclei with the yolk cell. This formation is termed as yolk syncytial layer (YSL) (Kimmel and Law, 1985). At first, the YSL looks like a ring of nuclei that is sunk into the yolk cell under the blastodisc. However, later the blastodisc expands towards the vegetal pole within two cell cycles and internal YSL (I-YSL) and external YSL (E-YSL) form by the movement of the yolk syncytial nuclei under and above the blastodisc margin, respectively (Kimmel *et al.,* 1995).

The other cell populations distinguishable in MBT are the enveloping layer (EVL) and deep cells (DEL). While the YSL cells have short cell cycles, the deep cells have longer cell cycles and the EVL cells have the longest and asynchronous cell cycles (Kane *et al.,* 1992; Kane, 1999). The EVL cells are the outer cells of blastodisc forming the epithelium (Kimmel *et al.,* 1990). The deep cells between the EVL and YSL cells play a role in the formation of embryo proper by giving rise to the epiblast and hypoblast during the gastrulation period (Warga and Kimmel, 1990; Kimmel *et al.,* 1995). The YSL leads the blastodisc to expand toward the vegetal pole (Kimmel and Law, 1985). In addition, zygotic gene transcription begins and deep cells gain their motility during the midblastula stage (Kane and Kimmel, 1993). In late blastula, epiboly, which is the first important cell movement to create the three germ layers and body axes, begins. Epiboly is characterised by thinning and spreading of the blastodisc over the yolk cell to shape the embryo properly (Kimmel *et al.,* 1995). It is suggested that cell movement of radial intercalations is the driving force of early epiboly movements (Keller, 1980; Warga and Kimmel, 1990) by mixing deep blastomeres and thinning the blastodisc. As a result, a uniform thickened blastoderm is formed and spreads over across the yolk cell. I-YSL begins to dome towards the animal pole when the radial intercalations of deep cells move upwards into the superficial cells and the doming (4.33hpf) is the sign of the start of epiboly. At 30% epiboly stage, the blastoderm is composed of a monolayer of enveloping cells and a multilayer of deep cells **(Figure 1.6A).** Epiboly also continues in gastrulation period (Kimmel *et al.,* 1995).

Gastrulation (5.25-10hpf) is the most important period of embryogenesis in which cell movements of epiboly, internalisation, convergence and extension occur to generate the three germ layers and embryonic axes (Heisenberg and Tada, 2002). This period starts at 50% epiboly (5.25hpf) and ends when the blastoderm covers the entire yolk cell (10hpf) (Kimmel *et al.,* 1995). At the onset of gastrulation period (50% epiboly), deep cells move to accumulate and internalise at the dorsal side of the blastoderm margin and a germ ring is formed **(Figure 1.6Bi)**. Epiboly temporarily stops during the internalisation period and resumes after 1.5 hours to cover the yolk cell completely (Kimmel *et al.,* 1995). It was suggested by Warga and Kimmel (1990) that, the time of internalisation is highly related to cell fate. So, the first internalised mesendodermal cells usually form endoderm whereas the later internalised mesendodermal cells usually form mesoderm except the early internalised mesodermal heart tissue. In addition, the internalising cells have different directions of movement at different times during the internalisation that determines the anterior-posterior positions of embryo. The early internalised cells change their direction after reaching the yolk cell surface and move towards the animal pole in order to form the more anterior parts (e.g. prechordal plate) of the embryo. However, the later internalised cells do not change their direction that extremely and move towards the vegetal pole, along with the epiboly in order to form more posterior parts (e.g.

somites) of the embryo. As a consequence of the internalisation of mesendordermal cells and non-internalisation of ectodermal cells, two types of cell layers are formed at the germ ring which are named as epiblast and hypoblast **(Figure 1.6Bii)** (Warga and Kimmel, 1990). The hypoblast layer will form endodermal and mesodermal tissues whereas epiblast layer will form ectodermal tissues later during the late embryogenesis (Kimmel *et al.,* 1990). Convergence and extension (CE) cell movements follow the internalisation movements. These movements begin at the dorsal side at the germ ring and form the embryonic organizer, the shield. During this period, mesendordermal and neuroectodermal cells move towards the dorsal pole of the embryo to become medio-laterally arranged (directed cell migration) and intercalate with their neighbours to elongate the anterior-posterior body axis (medio-lateral intercalation). As a consequence of medio-lateral narrowing and anterior-posterior lengthening which were referred to as convergence and extension, respectively, embryonic axis forms (Wallingford *et al.,* 2002; Montero *et al.,* 2005; Montero and Heisenberg, 2004; reviewed in Tada and Heisenberg, 2012) **(Figure 1.6C).** According to Myers *et al.,* (2002), the cells at different positions during the gastrulation period have different behaviours and extents of convergence and extension cell movements. Cells at the ventral pole (mostly mesodermal cells) move vegetally to join the formation of tail instead of converging towards the dorsal pole. On the other hand, cells at lateral positions converge towards the dorsal pole with increasing speed and show elevated intercalations. However, cells at dorsal pole have low level of convergence cell movements while they exhibit high level of extension cell movements (Myers *et al.,* 2002). Gastrulation movements are important for the cell fate specification since the positions of different germ layers during gastrulation defines their cell fate. A fate map at the onset of gastrulation **(Figure 1.7A)** demonstrates the location of different germ layers along the anteroposterior axis. While the ectodermal cells locate more animally, the mesodermal cells locate more vegetally towards margin and the endodermal cells, mixed with mesodermal cells, locate at the margin. Ectodermal cells give rise to epidermis, nervous system and sensory organs, mesodermal cells give rise to muscles, heart, bone, connective tissues, urogenital, and circulatory systems and endodermal tissues give rise to gastrointestinal organs and related systems. In addition, the location of germ layers along the dorsoventral axis also defines their fate. For example, the mesodermal cells that locate more dorsally give rise to the axial tissues like notochord and prechordal plate while cells that locate more laterally and ventrally give rise to paraxial tissues like tail, somites, blood and heart **(Figure 1.7A-C)**. As shown in **Figure 1.7A-B**, the nervous system is formed from the ectodermal cells locate more dorsally, while the epidermis is formed from the ectodermal cells locate more ventrally (Shier and Talbot, 2005). The gastrulation period ends approximately at 10hpf, when the blastoderm covers the yolk cell completely (tail-bud stage). However, the convergent and extension cell movements continue during the segmentation period (Kimmel *et al.,* 1995).

The segmentation period starts at tail bud stage (10hpf) when the tail bud becomes visible and ends at 28-somites stage (24hpf). During this period, convergence and extension cell movements still continue and elongate the anterior-posterior axis of the embryo. Separately, somites develop starting from the anterior part (1-somite) and carrying on to the posterior part of the embryo until the 28-somites stage. The developing rate of somites decreases in time; the earlier somites develop faster than the later somites. In addition, the preliminary signs of primary organs such as pronephric kidneys and neural tube become prominent due to the morphogenetic movements during this period. As segmentation proceeds, the neural keel which is the precursor of brain begins to differentiate by swelling. Ten distinct swelling named as neuromeres, become visible. The first three neuromeres are larger than the other ones that correspond to forebrain parts as telencephalon, diencephalon and midbrain part as mesencephalon. The precursors of eyes and optic primordia develop from the lateral diencephalon. The seven smaller neuromeres correspond to the rhombomeres (r1-r7) and form the parts of hindbrain. At the end of segmentation period (prim-5 stage- 24hpf), the epiphysis (diencephalon), midbrain or tectum (mesencephalon) and cerebellum (midbrain-hindbrain border) can also be distinguished easily. Initial movements of body begin (Kimmel *et al.,* 1995).

The pharyngula period starts at prim-5 stage (24hpf) and ends at the long-pec stage (48hpf). The embryo enters the pharyngula period with a well-developed notochord, somites and five lobes of brain. The most remarkable feature of this period is the rapid development of seven pharyngeal arches and therefore this period is termed as the pharyngula period. During the first few hours (until 32hpf), the embryo continues to lengthen and the tail straightens rapidly. The embryo lifts its head rapidly during this period and the rate of straightening decreases in time. This straightening of the head (head-trunk angle) is used for the determination of appropriate stage of the embryo (Kimmel *et al.,* 1995). The posterior lateral line (PLL) primordium moves along the trunk and tail starting from the postotic placode. As it moves along, it lays a group of cells that will become the neuromasts (eight sense organs) along the horizontal myoseptum (Metcalfe, 1989). After 40hpf, the primordium reaches the posterior end and becomes small. In addition, the fins begin to form during this period. Pigment cells such as melanophores patterning the embryo with stripes begin to differentiate. Another important development of this period is the formation of circulatory system and heart. The heart begins to beat and the blood begins to circulate in the body (head, trunk, tail) through the newly developed arches, veins and arteries. Lastly, tactile sensitivity develops and embryo starts to swim in bouts. Embryo lies on its side to rest after a bout of swimming. The pharyngula period ends at 48hpf and the embryo enters the hatching period (Kimmel *et al.,* 1995).

The hatching period begins at long-pec stage (48hpf) and ends at protruding mouth stage (72hpf). During the third day of the embryogenesis, individual embryos even from the same clutch hatch irregularly. However, the developmental progress still continues at the same rate independent of hatching. The morphogenesis of many organs is near completion. Pectoral fins, jaws, mouth and gills morphogenesis increases and the mouth protrudes anteriorly beyond the eye. The heart beats strongly and circulates the blood rapidly. Dechorionated embryos start to keep their dorsal-up positions while swimming in bouts. The escape response increases. The hatching period ends at 72hpf and the embryo enters the larval period (Kimmel *et al.,* 1995).

The larval period starts from 72hpf and ends at 30dpf. The embryo enters the juvenile period at 30dpf. During the early larval period, the larva continues to grow rapidly in size as well as the organs like swim bladder. The swim bladder inflates and protrusion of mouth continues. The larva continues to swim actively and moves their pectoral fins, eyes and jaws. On the fifth day of embryogenesis (120hpf), the larva exhibits intense escape response, active respiration and predatory behaviour that also corresponds to being ready for feeding (Kimmel *et al.,* 1995).

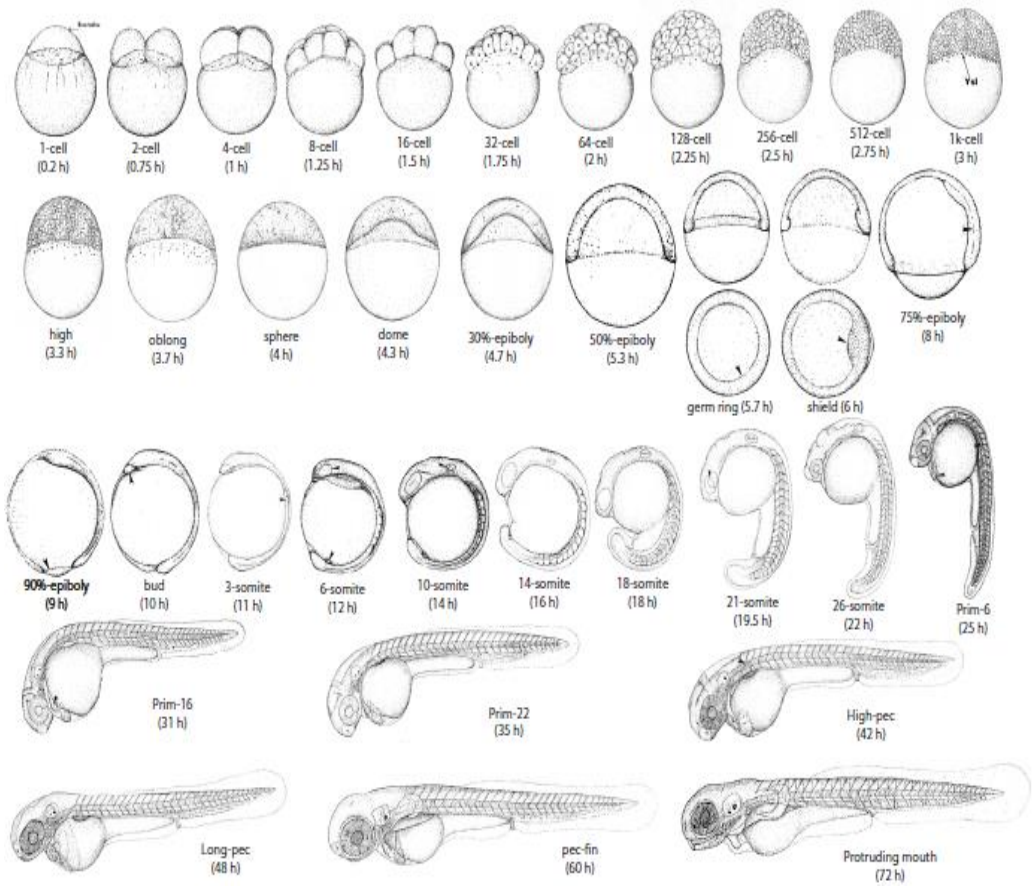


Figure 1.5 Schematic representations exhibiting the early stages of zebrafish embryonic development. The stages start from the 1-cell stage (0.2hpf) and end at the protruding mouth stage (72hpf). Embryos are grown at 28.5°C and standard specification of stages accepted by the developmental biology field is applied (Adapted from Kimmel *et al.,* 1995).

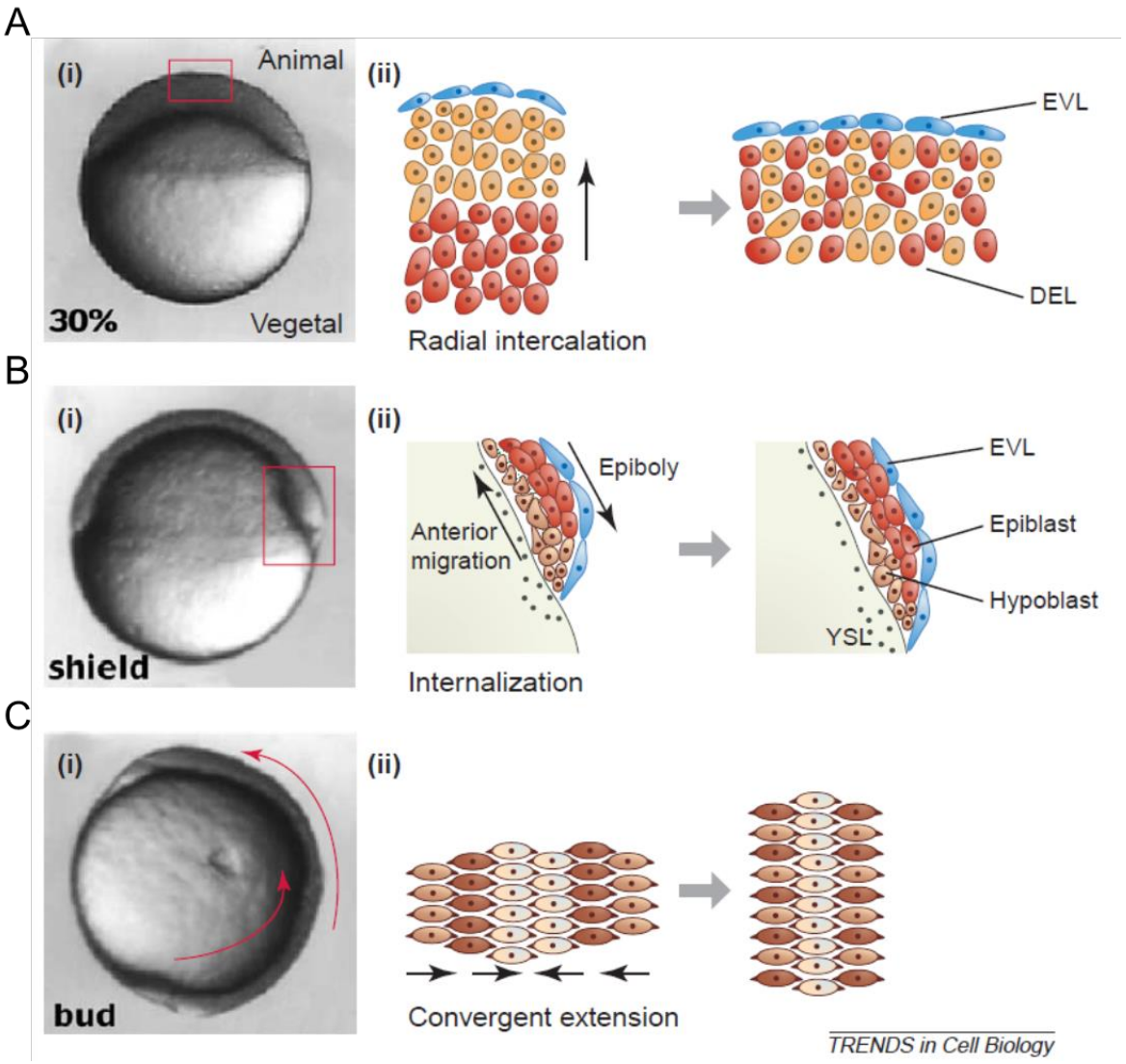


Figure 1.6 Gastrulation cell movements in zebrafish. **(A)** Radial intercalation of deep cells (DEL) that move upwards into the more superficial cells results in the thinning of the DEL cells and contributes to the epiboly. **(B)** Internalisation of the mesendodermal precursors by moving away from the shield margin and towards the anterior pole results in the formation of two different cell layers, epiblast (ectodermal) and hypoblast (mesendodermal). **(C)** Mesendordermal and neuroectodermal cells move towards the dorsal pole of the embryo to become medio-laterally arranged and intercalate with their neighbours to elongate the anterior-posterior body axis. Lateral view, dorsal to the right, animal pole to the top. Adapted from (Montero and Heisenberg, 2004).

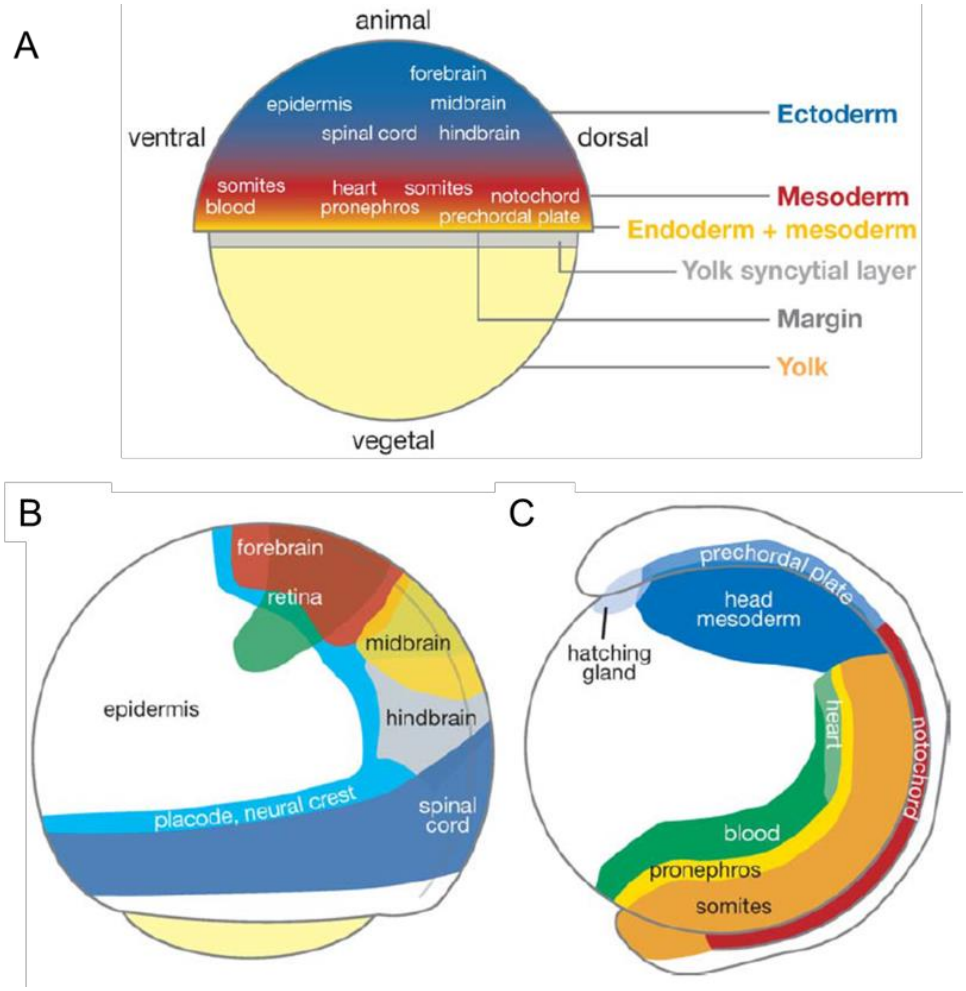


Figure 1.7 Cell fate maps of zebrafish. (A) Fate map at 50% epiboly exhibiting the arrangement of different germ layers along the anteroposterior and dorsoventral axes. **(B)** Fate map of ectoderm at 90% epiboly. **(C)** Fate map of mesoderm at early somitogenesis. Lateral view, dorsal to the right, animal pole to the top. Adapted from (Shier and Talbot, 2005).

1.2.2. The canonical Wnt/β-catenin signalling pathway regulates cell fate specification and axis formation

The development of three germ layers, cell fate specification, axis formation and cell movements of gastrulation are the processes that occur concurrently to shape a vertebrate embryo. The wnt signalling pathway is one of the key pathways that can control all these processes. While the canonical Wnt/β-catenin signalling pathway has been shown to regulate cell fate specification and axis formation rather than cell movements, the non-canonical Wnt/PCP and Wnt/Ca^{2+} signalling pathways have been shown to regulate CE cell movements rather than cell fate specification and patterning (Shier and Talbot, 2005). Nevertheless, a few exceptions have shown that both of the Wnt pathways (canonical and non-canonical) possess roles in both cell fate specification and cell movements of gastrulation (Yamashita *et al.,* 2002; Yin and Solnica-Krezel, 2007). Yamashita *et al.,* (2002) have shown that the canonical Wnt//β-catenin signalling regulates the phosphorylation and activation of *stat3* that is essential cell autonomously for the migration of the prechordal plate cells and cell non-autonomously for the convergence movements of the paraxial mesoderm. On the other hand, Yin and Solnica-Krezel (2007) have shown that impaired CE cell movements in the *knypek(kny)*;*trilobite(tri)* double mutants affected the specification and maintenance of the adaxial cell fate, suggesting that cell movements and cell fate specification are not completely independent processes.

Wnt/β-catenin signalling pathway coordinates with other signalling pathways including Bmp, Fgf, Nodal and Retinoic acid for cell fate specification and axis formation (Shier and Talbot, 2005). The accumulation of maternal β-catenin at the dorsal margin results in the activation of dorsal-specific gene expression such as anti-BMPs (*chordin (chd), noggin, follistatin),* transcription factors *(bozozok (boz),* anti-Nodal *(squint (sqt))* and anti-Wnts *(dickkopf1 (dkk1), cerberus; crescent)* (reviewed in Niehrs, 2004; Hikasa and Sokol, 2013). These genes are essential for the formation of the Speeman-Mangold organiser regulating the dorsal fate specification and dorsal-ventral axis determination. Several *wnts* (*wnt3a, wnt5a, wnt8* and *wnt11*) and *bmps (bmp2b, bmp4* and *bmp7)* are expressed in the ventral side of the embryo to induce the posterior fates by antagonising the formation of anterior structures. Therefore, organiser-derived antagonists are required to inhibit the action of ventralising factors for the precise formation of the anterior structures (reviewed in Niehrs, 2004; Kimelman and Martin, 2012; Hikasa and Sokol, 2013). Indeed, inhibiting the activity of β-catenin by overexpressing cadherin and the mutant forms of Tcf3 interfered with the expression of dorsal-specific genes, *chordin* and *goosecoid,* resulted in the formation of ventralised embryos (Pelegri and Maischein, 1998). Embryos of the maternal effect mutant of β-catenin-2, *Ichabod*, failed to form a normal embryonic shield and to develop head and notochord, but displayed extensive

development of ventral tissues like blood and ventral fin tissue. Consistent with the lack of accumulation of β-catenin at the dorsal side, the expression of the early dorsal markers, *boz* and *sqt*, was also missing during the mid-blastula stage. The embryos showed significant ventralisation during gastrulation characterised by defective expression of dorsal fates and increased expression of ventral fates. Injection of *β-catenin* or their downstream effector RNAs (*boz* and *sqt*) rescued the *ichabod* phenotype completely, indicating the essential role of *β-catenin* in the formation of organiser and dorsoventral patterning (Kelly *et al.,* 2000; Bellipanni *et al.,* 2006). In addition, the identification of *headless/tcf3* and *mastermind/axin1* mutants has shown the key role of canonical Wnt signalling in anteroposterior axis specification due to the presence of posteriorisation phenotype. *headless/tcf3* mutant embryos exhibited loss of forebrain and eyes and expansion of ventral mesoderm while *mastermind/axin1* mutant embryos showed fate transformation of telencephalon and eyes to diencephalon (Kim *et al.,* 2000; Heisenberg *et al.,* 2001). Moreover, the posteriorising activity of zygotic *wnt8* has also been shown in various studies as the *wnt8* morphants and mutants displayed loss of ventro-posterior structures and severe expansion in dorsal fates (Erter *et al.,* 2001; Lekven *et al.,* 2001). Consistently, the transcriptional targets of Wnt/β-catenin pathway such as the *cdx* group and the *vent/vox/ved/xom* group genes have been shown to be essential for ventro-posterior fates and posterior development (Melby *et al.,* 2000; Imai *et al.,* 2001; Davidson *et al.,* 2003; Shimizu *et al.,* 2004; Shimizu *et al.,* 2005).

Taken together, the dual role of Wnt/β-catenin signalling determines the zebrafish axis specification and cell fate determination. While the maternal Wnt pathway induces the formation of dorsoventral axis and anterior structures, zygotic Wnt pathway induces the anteroposterior axis specification and also the posterior structures via its downstream transcriptional targets.

1.2.3. The non-canonical Wnt/PCP signalling pathway regulates cell movements during gastrulation

The non-canonical Wnt/PCP signalling pathway is the key regulator of CE cell movements by regulating cell polarity-mediated directed cell migration and medial-lateral cell intercalation through activating RhoA, Rac and Cdc42 GTPases (Heisenberg *et al.,* 2000, Tada and Smith, 2000; Wallingford *et al.,* 2000; Wallingford *et al.,* 2002; Habas *et al.,* 2003). Zebrafish embryos carrying mutations in the Wnt/PCP signalling pathway components, such as Wnt ligands, transmembrane proteins, membrane-associated proteins, Frizzled receptors and Wnt co-factors, exhibited impaired CE cell movements but normal cell fate specification during gastrulation. These mutants/morphants include *silberblick/wnt11* (Heisenberg and Nüsslein-Volhard, 1997; Heisenberg *et al.,* 2000), *pipetail/wnt5* (Hammerschmidt *et al.,* 1996; Rauch *et*

al., 1997; Kilian *et al.,* 2003), *trilobite/vangl2* (Solnica-Krezel *et al.,* 1996; Sepich *et al.,* 2000; Jessen *et al.,* 2002), *prickle/pk1* (Carreira-Barbosa *et al.,* 2003), *frizzled/fz2* (Sumanas *et al.,* 2001; Kilian *et al.,* 2003) and *kynpek/gpc4* (Solnica-Krezel *et al.,* 1996; Topczewski *et al.,* 2001).

1.2.3.1. Wnt ligand mutants

The *pipetail* locus encodes *wnt5* and the *ppt/wnt5* mutants showed defective CE cell movements of posterior paraxial mesendodermal and ectodermal cells resulting in shortened and broadened body axis at tail-bud stage **(Figure 1.8B)** and defects in tail elongation (Hammerschmidt *et al.,* 1996; Rauch *et al.,* 1997; Kilian *et al.,* 2003). In *ppt/wnt5* mutants, the prechordal plate was not significantly affected **(Figure 1.8F)** whereas the notochord was shortened and broadened **(Figure 1.8J).** This result suggests that in contrast to *slb/wnt11* that regulates CE cell movements predominantly in the anterior regions, *ppt/wnt5* regulates CE cell movements predominantly in the posterior regions (Hammerschmidt *et al.,* 1996; Rauch *et al.,* 1997; Heisenberg *et al.,* 2000; Heisenberg and Tada, 2002; Kilian *et al.,* 2003). To test the requirement of *ppt/wnt5* in cell movement and shape of posterior paraxial ectoderm cells, cell elongation along the medio-lateral axis was measured in WT and *ppt/wnt5* mutants. WT ectodermal cells were found less rounded than the cells in *ppt/wnt5* mutants. Two-photon confocal imaging of individual ectodermal and mesendodermal cells revealed that while ectodermal and mesendodermal cells in WT were more elongated with long protrusions oriented in the direction of movements, ectodermal and mesendodermal cells in *ppt/wnt5* morphants were less elongated with short protrusions oriented randomly. These results suggested that *ppt/wnt5* is required for the medio-lateral elongation and orientation of both ectodermal and mesendodermal cells during gastrulation (Kilian *et al.,* 2003).

The *silberblick(slb)* locus encodes *wnt11* and the *slb/wnt11* mutants exhibit defective CE cell movements of anterior and posterior mesendodermal and ventral central nervous system (CNS) midline cells resulting in shortened and broadened body axis at the tail-bud stage (**Figure 1.8C**) and cyclopia at later stages (Heisenberg *et al.,* 2000). In *slb/wnt11* mutants, the axial mesendoderm forming the prechordal plate and notochord was also affected. The anterior-most end of the prechordal plate, polster, marked by *hgg1* (*hatching gland gene 1*) was more elongated, narrowed and shifted posteriorly (**Figure 1.8G**; po). The notochord marked by *ntl* (*no tail*) was shortened and broadened (**Figure 1.8K**; no) and the anterior edge of the neural plate marked by *dlx3* (*distal-less*) was expanded (**Figure 1.8G**; np) compared to wild type (WT) (**Figure 1.8E-I**; po, np and no). In addition, the anterior migration of the ventral CNS midline cells was impaired (Heisenberg and Nüsslein-Volhard, 1997; Heisenberg *et al.,* 2000). Overexpression of Slb/Wnt11 and the mutant form of Dsh (Dsh-ΔN), which can function

only in the Wnt/PCP pathway, rescued the CE cell movement phenotype in *slb/wnt11* mutants. Moreover, axial and non-axial mesodermal cell transplantation analyses revealed the requirement of *wnt11* expression in paraxial mesodermal cells to regulate the medio-lateral cell intercalation along the anteroposterior axis (Heisenberg *et al.,* 2000). The movement and morphology of the individual cells in *slb* mutants were investigated during gastrulation using two-photon confocal imaging. During the formation of germ ring, hypoblast cells showed less and slower directional movements accompanied with defective orientation in their directions. Ubiquitous overexpression of Wnt11 rescued the observed phenotype of *slb* mutants (Ulrich *et al.,* 2003).

In addition, establishing *slb;ppt* double mutants revealed an additive phenotype characterised by more severe CE cell movement defects and shortened body axis at the end of gastrulation **(Figure 1.8D)**. In *slb;ppt* double mutants the notochord was significantly shortened and expanded as expected since both *slb* and *ppt* mutants exhibited posterior mesendoderm defects **(Figure 1.8J-K)**. In contrast, the prechordal plate was found more elongated and narrowed **(Figure 1.8H)** than the expected additive phenotype (because *ppt* did not display significant defects in prechordal plate), indicating that *slb/wnt11* and *ppt/wnt5* possess functional redundancy only in the anterior mesendoderm. Consistently, injection of *ppt/wnt5* RNA rescued the prechordal plate phenotype in *slb* mutants suggests that *ppt/wnt5* can partially replace the function of *slb/wnt11* in the anterior mesendoderm (Kilian *et al.,* 2003).

1.2.3.2. Transmembrane and membrane-associated protein mutants

The *trilobite (tri)* locus encodes a four-pass transmembrane protein, *van gogh-like 2* (*vangl2,* also known as *strabismus)* and *tri/vangl2* mutants have been shown to regulate tissue polarity in *Drosophila* and cell polarity-mediated CE cell movements in vertebrate gastrulation (Taylor *et al.,* 1998; Sepich *et al.,* 2000; Jessen *et al.,* 2002; Darken *et al.,* 2002; Park and Moon, 2002). Jessen *et al.,* (2002) demonstrated that mediolateral cell elongation and alignment of paraxial ectodermal cells were reduced in *tri/vangl2* mutants compared to WT. Using time-lapse Nomarski imaging also showed less directed and slower convergence movements of mesodermal and ectodermal cells in *tri/vangl2* mutants. These results indicate that *tri/vangl2* as a core modulator of PCP signalling is required for both directed cell migration and mediolateral cell intercalation that underlie CE cell movements. The migration of branchiomotor neurons was also found disrupted in *tri/vangl2* mutants, however since other Wnt/PCP mutants like *slb/wnt11* and *ppt/wnt5* have not shown this defect, it was suggested that this process is regulated independent from the Wnt/PCP signalling pathway (Jessen *et al.,* 2002).

The *prickle (pk)* locus encodes an intracellular protein, *prickle1 (pk1)*, which mediates the subcellular localisation of Fz/Dsh complex in the non-canonical Wnt/PCP signalling pathway (Tree *et al.,* 2002). The *pk1* morphants exhibited disruption in mesendodermal and ectodermal CE cell movements during gastrulation. Injection of *pk1*-MO enhanced the *slb/wnt11* and *ppt/wnt5* phenotypes while it blocked the rescue ability of *wnt11* in *slb/wnt11* mutants, all indicating that *pk1* functions with *slb/wnt11* and *ppt/wnt5* to regulate the CE cell movements. In addition, *pk1* was found to interact with *tri/vangl2* to regulate the migration of branchiomotor neurons (Carreira-Barbosa *et al.,* 2003).

1.2.3.3. Frizzled receptor mutants

As mentioned earlier in Section 1.1, *Frizzled (Fz)* encode seven-pass transmembrane receptors (Bhanot *et al.,* 1996). Studies in *Xenopus*, mice and zebrafish suggested that *frizzled-2 (fz2)* and *frizzled-7 (fz-7)* receptors function in the non-canonical Wnt/PCP signalling pathway to regulate CE cell movements (Djiane *et al.,* 2000; Sumanas *et al.,* 2001; Kilian *et al.,* 2003; Kim *et al.,* 2008; Yu *et al.,* 2012). Specifically, it was suggested that *fz2* and *fz7* function downstream of *wnt5* and *wnt11*, respectively (Habas *et al.,* 2001; Habas *et al.,* 2003; Kilian *et al.,* 2003; Kim *et al.,* 2008; Kraft *et al.,* 2012).

1.2.3.4. Wnt co-factor mutant

The *knypek (kny)* locus encodes *heparan sulfate proteoglycan (HSPG), glypican,* which functions as a co-factor to promote the activity of ligands in the non-canonical Wnt/PCP signalling pathway. The *kny/gpc4* mutants exhibited CE cell movement defects as well as less cell elongation and orientation of mesodermal and ectodermal cells compared to WT. Specifically, *kynpek/gpc4* has been shown to functionally interact with *wnt11* and promote its activity for CE cell movements (Solnica Krezel *et al.,* 1996; Topczewski *et al.,* 2001).

Taken together, the existing body of evidence suggests that CE cell movements during gastrulation are regulated predominantly by the Wnt/PCP signalling pathway.

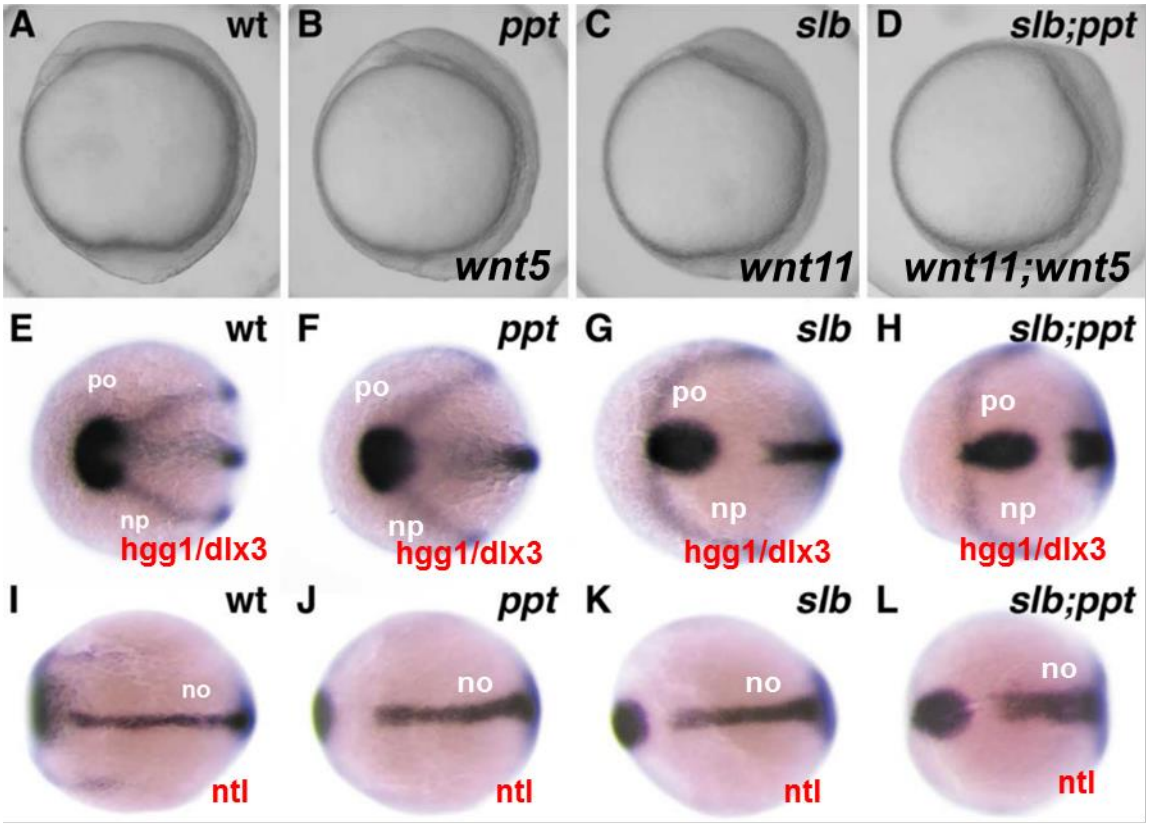


Figure 1.8 *ppt/wnt5*, *slb/wnt11 and slb;ppt* double mutants exhibited CE cell movement defects at tail-bud stage. Live images showing WT **(A)**, *ppt* **(B)**, slb **(C)** and *slb;ppt* double **(D)** embryos at tail-bud stage (Lateral views anterior to the top, dorsal to the right). Expression of *hgg1* marking polster (po) and *dlx3* marking neural plate (np) was shown at tail-bud stage in **(E)** WT**,** *ppt* **(F)**, *slb* **(G)** and **(H)** *slb;ppt* embryos. Length of the notochord (no) marked by *ntl* in WT **(I)**, *ppt* **(J)**, *slb* **(K)** and *slb;ppt* embryos **(L)**. Dorsal views anterior to the left. Adapted from (Kilian *et al.,* 2003).

1.3. Rho GTPases and their role in the regulation of actin cytoskeleton

GTP-binding proteins (GTPases) act as molecular switches by looping between guanosine diphosphate (GDP)-bound-inactive and guanosine triphosphate (GTP)-bound-active states (Hall, 1994; Schmitz *et al.,* 2000). Five major subfamilies of GTPases are known as Ras, Rho, Rab, Arf and Ran (Etienne-Manneville and Hall, 2002). Ras homologous (Rho) GTPases, which is the best characterised family of GTPases, contain 22 members and can be subdivided into ten different classes as RhoA, RacI, Cdc42, RhoD Rif/RhoF, Rnd3/RhoE, Chp/RhoV, TTF/RhoH, Miro1/RhoT1 and RhoBTB (Rossman *et al.,* 2005). As a result of the downstream activation of specific Rho GTPases, Rho, Rac and Cdc42, the specific structures of actin cytoskeleton are regulated to provide cell polarity, membrane protrusions in the direction of movement, contraction of the actin-myosin filaments, cell adhesion and cell movement (Ridley and Hall, 1992; Nobes and Hall, 1995; Van Aelst and D'Souza-Schorey, 1997; Nobes and Hall, 1999; d'Enfert, 1999; Etienne-Manneville and Hall, 2002).

RhoA, RacI and Cdc42 GTPases have distinct roles in regulating three major components of the actin cytoskeleton. The components; lamellipodia, cross-linked meshwork of actin filaments and filopodia, thin bundles of actin filaments are protrusive structures appearing at the leading edge of the moving cells. These two actin filaments allow cell motility. The third component, stress fibres, are composed of actin-myosin filaments providing the contractile function of the cell allowing forward movement of the rear (Nobes and Hall, 1995; Nobes and Hall, 1999). The primary function of Rho GTPase is to regulate the assembly of functional integrin and focal adhesion complexes which link stress fibres to the extracellular matrix and as a matter of course the formation of actin-myosin stress fibres (Ridley and Hall, 1992; Hall, 1994; Etienne-Manneville and Hall, 2002). In addition, Rac GTPase triggers membrane ruffles and protrusive actin-rich lamellipodia formation whereas Cdc42 GTPase triggers protrusive actin-rich filopodia formation (Ridley *et al.,* 1992; Kozma *et al.,* 1995; Etienne-Manneville and Hall 2002; Jaffe and Hall, 2005) **(Figure 1.9)**. Interestingly, it has been suggested that the formation of these three structures of actin cytoskeleton occurs in a hierarchical manner in fibroblasts due to the activation order between Rho, Rac and Cdc42 GTPases. The primary activation of Rac GTPase by Cdc42 GTPase leads to the association of filopodia and lamellipodia during their formation. The secondary activation of Rho GTPase by Rac GTPase leads to the formation of focal adhesions and stress fibres (Nobes and Hall, 1995). The activation and rearrangement of these cytoskeletal components are essential for morphogenesis during vertebrate embryogenesis where Rho GTPases are involved for

mediating the planar cell polarity, cell adhesion and cell movements of gastrulation by participating in the non-canonical Wnt signalling pathways.

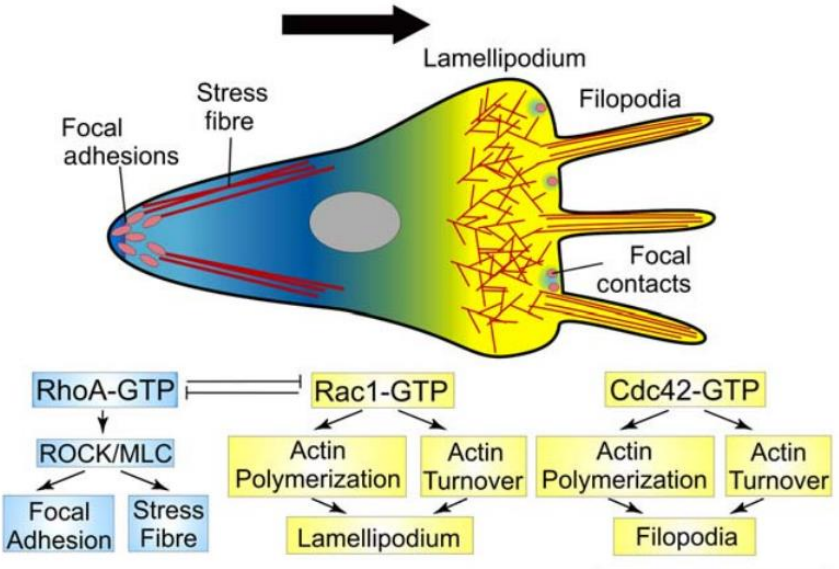


Figure 1.9 Arrangement of actin cytoskeleton components and cell migration. Actin-rich lamellipodium and filopodia are the protrusive components providing the cell migration. In addition, actin-myosin stress fibres are the contractile filaments promoting the rear to move forward. The formation of stress fibres and focal adhesions are regulated by RhoA whereas the formation of filopodia and lamellipodia are regulated by Cdc42 and RacI, respectively. Rho-kinase (ROCK), myosin light chain (MLC). Adapted from (Mayor and Carmona-Fontaine, 2010).

The role of Rho GTPses in morphogenesis has been studied widely in both *Drosophila* and *Xenopus* but less in zebrafish. Before studying loss of function mutations, dominant negative (DN) and constitutively active (CA) versions of Rho GTPases which are unable to release GDP and hydrolyse GTP, respectively, were generated (primarily in *Drosophila*) to reveal the role of Rho GTPases in an organismal context. Seven Rho family members have been identified in *Drosophila*, one Rho gene (*Rho1*), three Rac genes (*RacI, Rac2* and *Mtl*), one Cdc42 gene (*Cdc42*) and two other Rho family members (*RhoI, Rhobtb*). Ectopic expression of DN and CA versions of Rho GTPases revealed defects in the actin cytoskeleton remodelling during *Drosophila* oogenesis, early embryogenesis, gastrulation, neural morphogenesis and polarity-mediated orientation of hair and ommatidia (reviewed in Johndrow *et al.,* 2004). During oogenesis, expression of DN-Rac and CA-DN-Cdc42 in germline resulted in failure of border cell migration and of nurse cell dumping, respectively, suggesting that both Rac and Cdc42 have crucial roles in actin remodelling responsible for the migration of follicle cells and nurse cell dumping (Murphy and Montell, 1996). In contrast to DN- and CA-Cdc42 expression in the germline causing complete failure of nurse cell dumping, loss of Cdc42 function caused only delayed nurse cell dumping (Genova *et al.,* 2000). Furthermore, the maternal phenotype of loss of *Rho1* function includes disorganised actin cytoskeleton structures in ovaries and defective segmentation gene expression (Magie *et al.,* 1999).

During early embryogenesis, expression of DN-Rho1 and also the loss of *rho1* function resulted in completely blocked cytokinesis which lead to polyploidy of cells indicating that *Rho1* is required for actin-myosin mediated cytokinesis in early embryogenesis (Prokopenko *et al.,* 1999). During gastrulation, expression of DN-Rho1 resulted in failure in internalisation of some mesodermal cells and delay in ventral furrow formation. In addition, expression of DN-Rho1, Rac and Cdc42 resulted in a 'dorsal open' phenotype caused by defects in migration of the leading edge cells over the amnioserosa that in turn results in failure of dorsal closure (Harden *et al.,* 1999). In addition to DN and CA constructs of Rho GTPases, the embryos homozygous for *Rho1* exhibited a zygotic phenotype showing severe defects in both head involution and dorsal closure (Magie *et al.,* 1999). Similar to embryos expressing DN-RacI, loss of *Rac* (all three genes) function also exhibited dorsal closure defects (Hakeda-Suzuki *et al.,* 2002). However, in contrast to embryos expressing DN-Cdc42, loss of *Cdc42* function did not show failure of dorsal closure (Magie *et al.,* 1999; Genova *et al.,* 2000). Since the responsible pathway regulating the dorsal closure process, is JNK pathway; Rho GTPases have been proposed to act upstream of the Jnk pathway during dorsal closure (Sluss *et al.,* 1996; Kockel *et al.,* 1997; Harden *et al.,* 1999).

Other development processes of *Drosophila* that require Rho GTPases are neural morphogenesis, Wnt/PCP signalling pathway-mediated polarity and orientation of hairs on wings and of the ommatidia in the eye (Luo *et al.,* 1994; Adler, 2002). During neurogenesis, expression of CA-RacI and DN-RacI caused defects in axon outgrowth in peripheral neurons (Luo *et al.,* 1994). In addition to DN and CA constructs of Rac, loss of *Rac* (all three genes) function, revealed defects in myoblast fusion, epithelial morphogenesis, axon growth, guidance and branching. Each of these processes involves its own characteristic rearrangement of the cytoskeleton (Hakeda-Suzuki *et al.,* 2002; Ng *et al.,* 2002).

In Wnt/PCP signalling pathway, overexpression of DN-Cdc42 caused defects in distal hair formation of wings (Eaton *et al.,* 1996). Expression of DN- or CA-Rac constructs and overexpression RacI led to impairment in eye polarity (Fanto *et al.,* 2000). However, loss of *rac* (all three genes) function did not lead to impairment in polarity of the eye (Hakeda-Suzuki *et al.,* 2002). In addition, loss of *Rho1* function caused disruption of normal eye development exhibiting missing pigment cells, reduction in the number of photoreceptor cells and severe morphological change in rhabdomeres (Hariharan *et al.,* 1995). Similarly, loss of *RhoA* (or *Rho1*) function revealed a phenotype called 'anterior open', which is characterised by defects in cell polarity and failure of movements in epidermis. Genetic analysis demonstrated that Rho1 and RacI act downstream of Fz receptor to regulate the tissue polarity during the development of *Drosophila* wings and eyes (Strutt *et al.,* 1997; Fanto *et al.,* 2000; Strutt, 2003).

On the other hand, studies on *Xenopus* have suggested that *rhoa* and *racI* act in parallel in order to regulate convergent extension movements of axial mesoderm during gastrulation. The role of *rhoa* in the formation of head structures was first proposed after the expression of DN-*rhoa* leading to reduction in the formation of head structures (Wunnenberg-Stapleton, *et al.,* 1999). Similarly, expression of DN or CA forms of Rhoa and Rac in the marginal zone of the embryos revealed multiple anterior and axial gastrulation defects. While the anterior defects were reduced or the head formation was absent, the axial gastrulation defects were failure of the proctodaeum to close, spina bifida, and shortening of the anterior-posterior axis (Tahinci and Symes, 2003). Defects in axial gastrulation were led by the failure of convergent extension movements of the axial and paraxial mesoderm (Wallingford and Harland, 2001). Besides acting parallel to regulate cell polarity and migration, *rhoa* and *rac* were suggested to act separately but collectively for maintaining the polarity and stability of cytoplasmic protrusions during *Xenopus* gastrulation (Tahinci and Symes, 2003). Regulating the cell adhesion in ectoderm was suggested as the other role of *rac* and *rho* (Wunnenberg-Stapleton *et al.,* 1999; Hens *et al.,* 2002). Additionaly, *cdc42* was shown to be involved in Wnt/Ca^{2+} signalling pathway to regulate CE cell movements (Djiane *et al.,* 2000; Choi and Han, 2002).

As mentioned earlier, studies on *Xenopus* revealed that *rho* and *rac* act in parallel pathways downstream of Wnt11/Fz7 in the non-canonical Wnt/PCP signalling pathway (Habas *et al.,* 2001; Wallingford *et al.,* 2002; Habas *et al.,* 2003).

Studies on zebrafish have also shown that knock-down of *rhoa* expression resulted in CE cell movement defects reminiscent of the *wnt* mutants. Rescuing the phenotypes of *wnt5* and *wnt11* mutants by the ectopic expression of RhoA, Rock and diaphanous (mDia) clearly indicated that RhoA acts downstream of Wnt5 and Wnt11 via its downstream effectors Rock and mDia (Zhu *et al.,* 2006). Marlow *et al.,* (2002) have shown that overexpression of DN-Rock2 resulted in impaired CE cell movements and overexpression of Rock2 rescued the *slb/wnt11* phenotype. In addition, cell morphology analysis of WT and DN-Rock2-expressing ectodermal and mesodermal cells revealed that DN-Rock2 expressing cells exhibit less cell elongation, less orientation and slower migration (Marlow *et al.,* 2002). Another group studying the role of *rho* revealed that the use of *Clostridium botulinum* C3-exoenzyme (C3) and Y27632 inhibitors, which block cytokinesis and Rock respectively, resulted in disruption in actin and β-catenin assembly, epiboly and gastrulation. These results suggested that Rho GTPase regulates cytokinesis, epiboly and gastrulation via its downstream effector Rock (Lai *et al.,* 2005).

Taken together, studies to identify the specific roles of Rho GTPases in vertebrates have shown that Rho GTPases are essential for several biological processes and act downstream of the non-canonical Wnt signalling pathways, which rely on the remodelling of actin cytoskeleton and gastrulation cell movements.

1.3.1. The regulators of Rho GTPases

Rho GTPases are molecular switches that cycle between GTP-bound active state and GDP-bound inactive state. The activation process of Rho GTPases is essential for their activity, since they can only recognise their targets in the active state to generate a response until the hydrolysis of GTP to GDP (Etienne-Manneville and Hall, 2002). The cycling between active and inactive states is regulated by different cellular proteins known as guanine nucleotide exchange factors (GEFs), GTPase activating proteins (GAPs) and guanine nucleotide dissociation inhibitors (GDIs) (Boguski and McCormick, 1993; Kjoller and Hall, 1999). While the activation process is controlled by GEFs catalysing the exchange of GDP to GTP (Schmidt and Hall, 2002), the inactivation process is controlled by GAPs which induce the hydrolysis of GTP to GDP and phosphate (P_i) (Bernards, 2003). Lastly, GDIs are responsible for extracting inactive GTPases from cell membrane to prevent their spontaneous activation, misfolding and degradation (Garcia-Mata *et al.,* 2011) **(Figure 1.10)**. In mammalians, 85 GEFs, 80 GAPs and

3 GDIs have been identified as regulator proteins of Rho GTPases (Jaffe and Hall, 2005). The multiple functions that the same Rho GTPases manage depending on cellular basis have shown that the regulators of Rho GTPases not only dominate the Rho GTPase activity, but also decide on the specific downstream pathway (Iden and Collard, 2008).

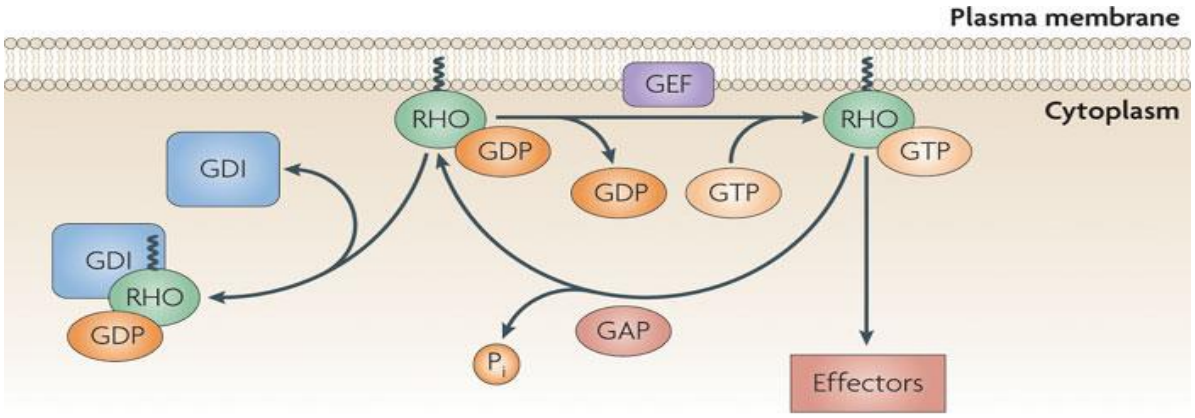


Figure 1.10 Regulators of Rho GTPases. The figure exhibits a Rho GTPase that binds to the plasma membrane through its prenylated C terminus and its regulators. Guanine nucleotide exchange factors (GEFs) are activators catalysing the disassociation of GDP from inactive GDP-bound Rho GTPases allowing it to bind GTP. Binding of GTP induces the activation of Rho GTPases providing its interaction with its effector proteins. In contrast, GTPase activating proteins (GAPs) are in-activators catalysing the hydrolysis of GTP to GDP and phosphate (P_i). The third regulator of Rho GTPases, guanine nucleotide dissociation inhibitors (GDIs) bind to the prenyl group of GDP-bound inactive Rho GTPases to arrest them in the cytoplasm and avoid the membrane binding. Adapted from (Tybulewicz and Henderson, 2009).

1.3.1.1. GTPase activating proteins (GAPs)

The GTPase activating proteins (GAPs) are the first negative regulators of Rho GTPases whose role is to catalyse the deactivation of Rho GTPases through cleaving the phospho-monoester bond on a GTP substrate by hydrolysis. As a result of this chemical reaction, a GDP substrate and an inorganic phosphate are formed and the activity of Rho GTPases is supressed (Mishra and Lambright, 2016). The molecular characterisation of the first identified GAP for Ras superfamily, p120GAP, has shown that it is composed of a hydrophobic N terminus, two SH2 domains, one SH3 domain, a pleckstrin homology (PH) domain, a putative CalB motif and a catalytic domain formed of three highly conserved sequences (Bollag and McCormick, 1991; Gawler *et al.,* 1995; Boguski and McCormick, 2003).

1.3.1.2. Guanine nucleotide dissociation inhibitors (GDIs)

The guanine nucleotide dissociation inhibitors (GDIs) are the second negative regulators of Rho GTPases and three different activities have been suggested for Rho GDIs (Olofsson, 1999; reviewed in DerMardirossian and Bokoch, 2005). The first role of Rho GDIs is to inhibit the release of GDP and subsequent binding of GTP to GTPases (Ueda *et al.,* 1990). This first inhibitor activity is essential for sequestering the GDP-bound GTPases in the inactive state to prevent its redundant activation and interaction with its downstream effectors (Garcia-Mata *et al.,* 2011). The second role of Rho GDIs is to inhibit the hydrolysis of GTP by interacting with GTP-bound active Rho GTPase. This activity also has crucial importance since it prevents both intrinsic and GAP-stimulated hydrolysis of GTP (Hart *et al.,* 1992). Lastly, the third role of Rho GDIs is to regulate the cycling of Rho GTPases between cytoplasm and membrane to maintain the cytosolic pool of inactive GTPases as a reservoir and to protect them from degradation. This reservoir allows inactive GTPases to be translocated to the lipid membranes through their prenylated C-terminus for subsequent activation and activity (Hori *et al.,* 1991; Olofsson, 1999; Robbe *et al.,* 2003; Boulter *et al.,* 2010).

Three Rho GDIs have been identified in mammals which are RhoGDI1 (also known as RhoGDIα), RhoGDI2 (also known as RhoGDIβ, LY-GDI and D4‑GDI) and RhoGDI3 (also known as RhoGDIγ) (Olofsson, 1999; reviewed in DerMardirossian and Bokoch, 2005; Garcia-Mata *et al.,* 2011). RhoGDI1 is a ubiquitously expressed member that was found to interact with several Rho GTPases including RhoA, RacI and Cdc42 (Fukumoto *et al.,* 1990; Leonard *et al.,* 1992). The crystal structure of RhoGDI1-RhoA, RhoGDI1-RacI and RHOGDI1-Cdc42 complexes have also been solved and described in detail (Longenecker *et al.,* 1999; Hoffman *et al.,* 2000; Grizot *et al.,* 2001). The RhoGDI2 is expressed in haematopoietic tissues and predominantly in B and T lymphocyte cell lines (Lelias *et al.,* 1993; Scherle *et al.,* 1993) whereas RhoGDI3 is specifically expressed at low levels in lung, brain and testis to interact predominantly with RhoB and RhoG (Zalcman *et al.,* 1996; Adra *et al.,* 1997).

1.3.1.3. Guanine nucleotide exchange factors (GEFs)

The guanine nucleotide exchange factors (GEFs) are the positive regulators that directly interact and activate the inactive GDP-bound GTPases in response to the upstream signals (Quilliam *et al.,* 1995). The activation process is composed of several steps. The first step is binding of the GEF to the GDP-bound inactive GTPase and forming a low-affinity complex of GDP-GTPase-GEF for disassociating the GDP from GTPase allowing the GTP to bind. Then, GDP disassociates from this complex and a high-affinity protein complex of GTPase-GEF is derived. The high intracellular concentration of GTP comparing to GDP leads to the rapid association of GTP-GTPase-GEF. Lastly, the GEF disassociates from this complex resulting

in the structural changes and interaction of GTP-bound active GTPase with its downstream effectors (Cherfils and Chardin, 1999). In addition to the activator role of GEFs by catalysing the destabilisation of GDP-bound GTPse, another regulatory role has been suggested as to stabilise the nucleotide free GTPase during the exchange of GDP for GTP, since the nucleotide-free GTPase is unstable (Lai *et al.,* 1993).

Different subfamilies of Ras-superfamily GTPases are regulated by structurally distinct GEFs and even for the same subfamily, they are composed of diverse multi-domains responsible for different biochemical roles, apart from the conserved specific catalytic domains (e.g. Dbl homology (DH)- pleckstrin homology (PH) domains for Rho GTPases or Cdc25 homology domain for Ras GTPases) (Zheng and Quilliam, 2003). Rho GTPases are activated by three distinct families of GEFs; either a Dbl family (at least 70 members), a Dock family (11 members) or a DEF6/SWAP70 family GEFs (2 members) (Mavrakis *et al.,* 2004; Rossman *et al.,* 2005; Cote and Vuori, 2007; Vigil *et al.,* 2010).

Dbl is a mammalian oncogenic protein that was initially isolated from diffuse B-cell lymphoma and it has been shown that the *Dbl* oncogene product acts upstream of Cdc42 GTPase to catalyse the disassociation of GDP, thereby regulating cytoskeletal-mediated cell polarity, cytokinesis and cell migration (Eva and Aaronson, 1985; Hart *et al.,* 1991; reviewed in Hoffman and Cerione, 2002). Since the first classification of Dbl as a GEF, more of the Dbl-family oncogenic products such as Tiam1, Ost, Vav1, etc. have been identified to contain a conserved region responsible for the Rho GTPases-specific catalytic activity (Horii *et al.,* 1994; Cerione and Zheng, 1996; Aghazadeh *et al.,* 2000; Worthylake *et al.,* 2000) **(Figure 1.11)**. This conserved region in almost all Dbl-family GEFs is composed of a Dbl homology (DH) domain (~180-amino acids), and an adjacent C terminal pleckstrin homology (PH) domain (~100-amino acids) (Cerione and Zheng, 1996; Whitehead *et al.,* 1997). The DH domain which is responsible for catalysing the exchange of GDP for GTP, is an oblong helical bundle, reminiscent of a ‘chaise longue’ shape (Whitehead *et al.,* 1997; Worthylake *et al.,* 2000). However, the functions of PH domain are less well-understood and may mediate binding to phosphoinositides ($PI_{(3,4,5)}P_3$) to localise the Dbl-family proteins to the plasma membrane and in some cases supporting the DH domain for a better GEF activity by also interacting with the bound-GTPases (Liu *et al.,* 1998; Hoffman and Cerione, 2002; Rossman *et al.,* 2005). Except this tandem DH-PH cassette, Dbl-family GEFs show high diversity and contain other protein domains suggesting variable biochemical functions controlled by the different family members (Zheng, 2001; Rossman *et al.,* 2005).

The DOCK family GEFs, containing 11 members, are characterised by two highly conserved domains; a regulatory Dock-homology region (DHR-1) domain and a catalytic C-terminal DHR-2 domain. Similar to PH domain of Dbl family GEFs, DHR-1 domain was shown to play a critical role in interacting with PtdIns$(_{3,4,5})P_3$ and positioning and promoting the activation of Rac, thereby regulating the biological functions including cell polarity, cell migration (Kobayashi *et al.,* 2001). Moreover, similar to DH domain of Dbl family GEFs, the DHR-2 domain was shown to interact with the GTPases to catalyse the activation process (Brugnera *et al.,* 2002; Cote and Vuori, 2002; Hiramoto *et al.,* 2006).

Lastly, the DEF6/SWAP70 family GEFs contain two members termed as Differentially Expressed in FDCP cells (DEF6) and Switch Associated Protein-70kDa (SWAP70). Although they both harbour the conserved DH-like and PH domains, they were separated from Dbl-family GEFs and classified as novel GEFs due to their unique domain arrangement which is PH domain followed by C-terminal DH-like domain (Mavrakis *et al.,* 2004). The identification of DEF6 and SWAP70, their unique structure and their roles in signal transduction, immune system, and embryogenesis of zebrafish will be explained in detail in Section 1.4 and 1.5.

In contrast to the abundant information about the role of Rho GTPases in vertebrate gastrulation, less is known about its upstream effectors, GEFs. Investigation on GEFs in *Xenopus* has suggested that *weak-similarity gef* (*wgef*) regulates the activation of RhoA downstream of Wnt11 in the Wnt/PCP signalling pathway (Tanegashima *et al.,* 2008). In addition, studies on zebrafish revealed that knock-down of *synectin-binding rhoa exchange factor* (*syx*) GEF resulted in disruption in the migration of intersegmental vessels and gastrulation defects (Ernkvist *et al.,* 2009; Goh and Manser. 2010).

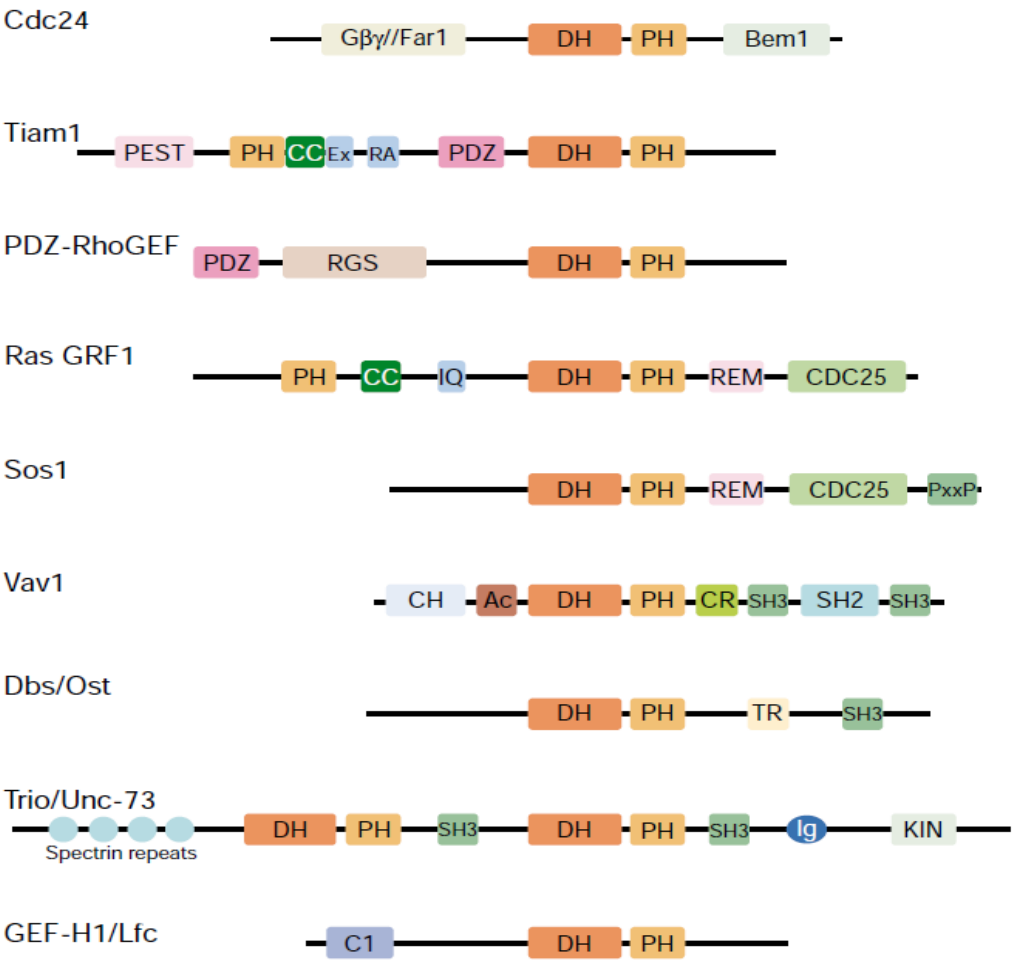


Figure 1.11 Domain structures of some Dbl-family GEFs exhibiting a conserved DH-PH cassette and multifunctional domains regulating distinct biological functions. The GEFs are aligned according to the Dbl homology (DH) and pleckstrin homology (PH) domains. *Ac*, acidic amino-acid-rich motif; *Bem1*, Bem1- binding domain; *CC*, coiled coil; *CDC25*, Ras GEF catalytic domain; *CH*, calponin homology; *CR*, cysteine-rich zinc butterfly motif; *C1*, EF-hand calcium binding motif; *Ex*, an uncharacterized region that co-operates with the PH and CC regions of Tiam1; *Gβγ/Far-1*, G protein Gβγ-subunit /Far1-binding domain; *Ig*, immunoglobulin-like domain; *IQ*, calmodulin-binding motif; *KIN*, serine/threonine protein kinase domain; *PDZ*, PSD95/Dlg/ZO1 domain; *PEST*, amino-acid P-, E-, S- and T-rich degradation motif; *RA*, Ras association domain; *REM*, Ras exchange motif; *RGS*, regulator of G-protein signalling domain; *SH2*, Src homology 2; *SH3*, Src homology 3. Adapted from (Zheng and Quilliam, 2003).

1.4. DEF6 and SWAP70 are novel GEFs

1.4.1. The isolation and identification of DEF6 and SWAP70

1.4.1.1. The isolation and identification of DEF6

Differentially Expressed in FDCP cells-6 (*Def6*) was first identified within murine haematopoietic precursor cells while investigating the developmentally regulated genes during myeloid differentiation (Hotfilder *et al.,* 1999). A retro-viral gene trap vector carrying a 5' splice acceptor, β-galactosidase and neomycin (*SA-lacZ-neo*) fusion gene was used to infect the FDCP-Mix A4 progenitor cells. Thereby, 37 G418-resistant and β-galactosidase-positive cell lines (gene-trap integration (GTI)) were generated and induced to differentiate into predominantly macrophages or granulocytes *in vitro*. The gene expression during the differentiation was screened according to the levels of β-gal$^+$ activity in the different lineages. All 37 GTI clones exhibited down-regulation upon either granulocyte or both granulocyte and macrophage differentiation. The sequence analysis from cDNAs of the eight differentially expressed genes in FDCP-A4 (*Def*) precursor cells revealed that half of them (*Def2, Def3, Def6* and *Def8*) had not been previously described, whereas the other half (*Def1, Def4, Def5* and *Def7*) had been previously described (Hotfilder *et al.,* 1999). *Def1, Def4*, and *Def7* were described as the mouse homologues of the rat *Hexokinase type II* (Ichihara *et al,* 1995), the human *Lasp-1/MLN50* (Schreiber *et al,* 1998; Tomasetto *et al,* 1995) and the human *IKBL* (Albertella and Campbell, 1994) genes, respectively. *Def5* was proposed as the mouse *TAZ4/Tex2* gene (Lemaire *et al,* 1994). *Def2, Def3, Def6* and *Def8* were proposed as novel mouse genes (Hotfilder *et al.,* 1999).

In addition to the GTI clone results, novel Def cDNA probes were used in Northern blot analysis in order to test the developmentally regulated expression of *Def* genes in undifferentiated FDCP-Mix A4 progenitor cells and differentiated macrophages, granulocytes and erythrocytes. More specifically, *Def2* was expressed in both myeloid progenitor cells and macrophages. *Def3* was expressed in both myeloid progenitor cells and macrophages but down-regulated during granulocyte differentiation. Consistent with the GTI clone result, the down-regulation of *Def6* expression was observed not only upon the macrophage and granulocyte differentiation which was the case for *Def8*, but also upon erythrocyte differentiation.

Furthermore, the expression pattern analysis of novel *DEF* genes in human haematopoietic tissues revealed that all four genes have differential expression patterns. The expression of *DEF2* was detected in primary haematopoietic cells; human foetal liver and bone marrow, but

not in mature haematopoietic cells; lymph node, thymus, appendix and peripheral blood leucocytes. The expression of *DEF3* was detected in all haematopoietic tissues. However, the expression of *DEF3* was highest in lymphoid tissues; lymph node and thymus, but lower in bone marrow. Lastly, the expression of *DEF8* was predominantly detected in peripheral leucocytes, whereas the expression of *DEF6* was observed in human lymph node, thymus and peripheral leucocytes (Hotfilder *et al.,* 1999). Interestingly, *DEF6* cDNA was found to display high degree of homology to *SWAP70* cDNA, which was isolated from B-cell nucleus complex catalysing DNA recombination between immunoglobulin heavy chain switch regions (Borggrefe *et al.,* 1998). Taken together, developmentally regulation and expression patterns of novel *DEF* genes have suggested that, while *DEF2* and *DEF3* might have a role in macrophage development, *DEF6* and *DEF8* might play a critical role in lymphoid development or function (Hotfilder *et al.,* 1999).

In addition to the identification of *DEF6* within the haematopoietic precursor cells, it was also isolated during a yeast two-hybrid interaction analysis aiming to determine the interaction partners of lymphoid-restricted transcription factor, IRF-4. The identified 2.3kb cDNA, which was predicted to encode a protein formed of 631 amino acid residues (~74kDa), was termed as *IRF-4 binding protein (IBP)*. The comparison between 5' fragment of human *IBP* cDNA and murine *Def6* cDNA revealed a high sequence homology suggesting that *IBP* is the human orthologue of *Def6* (Gupta *et al.,* 2003b). On the other hand, *DEF6* was also termed as *SWAP70-like adaptor of T-cells* (*SLAT*) on account of displaying high homology to *SWAP70* and playing a critical role in T-cell receptor (TCR)-mediated Th2 cell development or activation (Tanaka *et al.,* 2003; Borggrefe *et al.,* 1998).

1.4.1.2. The isolation and identification of SWAP70

Switch Associated Protein-70kDa (Swap70) was first isolated from a mouse B-cell specific protein complex (Swap) which is responsible for recombining the DNA sequences from immunoglobulin (Ig) heavy chain switch regions in switching B-cells. The other three proteins building up the complex, B23 (nucleophosmin), C23 (nucleolin), poly (ADP-ribose) polymerase (PARP) had been previously sequenced and were known to be expressed in most cells. After cloning and sequencing of *Swap70*, it was proposed that it encodes a novel protein formed of 585 amino acids containing three nuclear localisation signals (NLS) (Borggrefe *et al.,* 1998). Further experiments on the expression patterns revealed that *Swap70* was found to be expressed only in switch activated B-cells, but not in T-cells, activated T-cells or macrophages (Borggrefe *et al.,* 1998; Borggrefe *et al.,* 1999).

Swap70 was thought to be a key factor of the Swap complex since it was found as the component providing specificity for the switch region DNA. It was also suggested that, while Swap70 is present in the cytoplasm of resting B-cells, it localises to the nucleus upon the activation of B-cells to strongly interact with the other components of the Swap complex and weakly interact with the DNA. Taken together, consistent with its expression pattern in switch activated B-cells, taking part in the activation of B-cells and in Ig heavy chain class switching were determined as the two critical roles of Swap70 (Borggrefe *et al.,* 1998; Borggrefe *et al.,* 1999).

1.4.2. The structures of DEF6 and SWAP70 proteins

DEF6 and SWAP70 represent a novel class of GEFs for Rho GTPases because both harbour an unusual PH-DH domain arrangement and a DH domain that displays low degree homology (11% identity and 25% similarity at the amino acid level) to the DH domain of Dbl-family GEFs (Gupta *et al.,* 2003b; Mavrakis *et al.,* 2004; Rossman *et al.,* 2005). The DH domain of DEF6 and SWAP70 is therefore termed as DH-like domain (Mavrakis *et al.,* 2004).

DEF6 and SWAP70 are composed of N-terminal two calcium binding EF-hand motifs followed by a highly conserved DEF6/SWAP70 homology (DSH) domain with unknown function containing Immunoreceptor Tyrosine-based Activation Motif (ITAM). In contrast to typical DH-PH domain arrangement of Dbl-family GEFs, DEF6 and SWAP70 contain their Dbl homology-like (DHL) domain located immediately C-terminal to the PH domain **(Figure 1.12).** The amino acid sequence comparison revealed that full length DEF6 and SWAP70 share 45% identity and 65% similarity. The N-terminal domains share 55% identity and 74% similarity, PH domains share 56% identity and 76% similarity and DHL domains share 34% identity and 56% similarity at the amino acid level (Gupta *et al.,* 2003b; Mavrakis *et al.,* 2004).

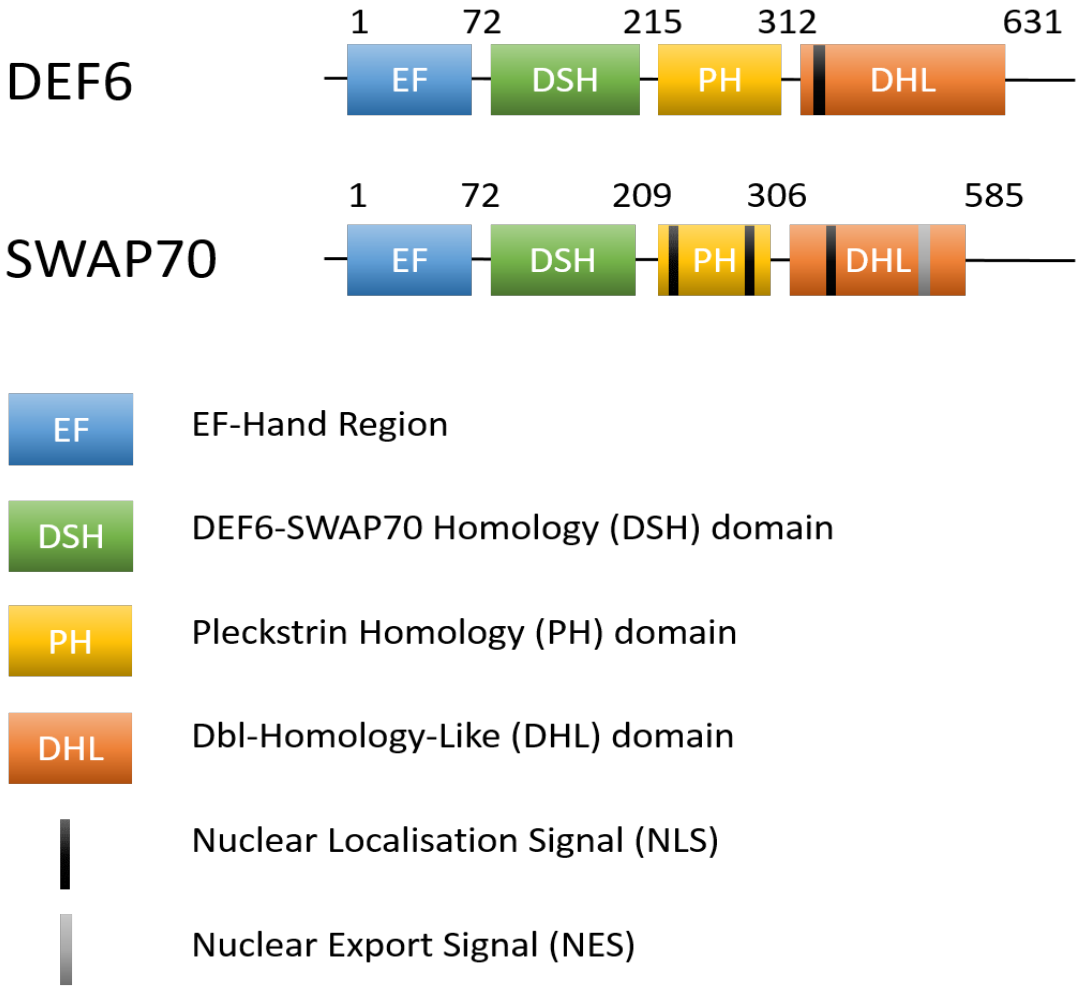


Figure 1.12 Domain structures of DEF6 and SWAP70 proteins exhibiting the unusual PH-DH domain arrangement. DEF6 and SWAP70 are composed of N-terminal EF-hand region followed by a DEF6-SWAP70 homology (DSH) domain, a pleckstrin homology (PH) domain at the centre and C-terminal Dbl homology-like (DHL) domain. In addition, DEF6 contains one nuclear localisation signal (NLS), whereas SWAP70 contains three NLS and an additional nuclear export signal (NES). The number of amino acids for each domain is shown on top of the domains. Adapted from (Gupta *et al.,* 2003b; Shuen, MRes thesis, 2010).

EF-Hand region: The N-terminal end of both proteins is highly conserved encompassing the amino acids from 1 to 72. This conserved area is composed of two putative EF-hand motifs (amino acids from 19 to 30 and 57 to 68) (Mavrakis *et al.,* 2004) The EF-hand motifs function in pairs and are known for binding calcium (Ca^{2+}) ions by using its helix-loop-helix structure to regulate structural or regulatory roles in organisms (Lewit-Bentley and Rety, 2000). EF-hand containing proteins can be divided into two groups as Ca^{2+} sensors and Ca^{2+} buffers. While Ca^{2+} sensors bind to the Ca^{2+} ions, the chemical signal is transmitted into the various biological responses, mostly through conformational changes (Gifford *et al.,* 2007). In the case of Calmodulin (CaM) as an example, the Ca^{2+}-bound form undergoes a conformational change that provides binding of CaM to its target protein and subsequent removal of the enzymatic autoinhibitory domain from the target protein to activate it (Skelton *et al.,* 1994; Grabarek, 2006; Gifford *et al.,* 2007). On the other hand, Ca^{2+} buffers adjust the Ca^{2+} signal levels in the cytoplasm by binding to the free Ca^{2+} and removing it from the cell to remove the potential harmful levels of ions (Gifford *et al.,* 2007).

Further investigation on the role of DEF6 in Ca^{2+} signalling and T cells revealed that the EF-hand motif binding to Ca^{2+} ions may mediate the interaction of DEF6-IP_3R1 (inositol 1,4,5-trisphosphate receptor type 1). Therefore, DEF6 was suggested as a Ca^{2+} sensor for promoting the activation of IP_3R1 through affecting the Ca^{2+} release from channels leading to the subsequent NFAT-dependent T-cell activation (Fos *et al.,* 2014).

DEF6-SWAP70 Homology (DSH) domain: This domain is highly conserved between DEF6 and SWAP70 and encompasses the amino acids 73 to 215 for DEF6, and 73 to 209 for SWAP70. Interestingly, this domain has been considered as specific to DEF6-SWAP70 family GEFs, because it does not horbour any sequence homology within other proteins. Thus, the domain was referred to as DEF6-SWAP70 Homology (DSH) domain (Mavrakis *et al.,* 2004). Even though the exact function of this region has not been characterised yet, an Immunoreceptor tyrosine-based activation motif (ITAM)-like sequence was identified (Tanaka *et al.,* 2003). ITAMs are critical phosphorylation sequences found in the tails of the cell surface proteins of the immune system such as T-cell receptor (TCR), B-cell receptor (BCR) or macrophages (Hayes and Love, 2002). This motif is formed of 4 residues that are repeated twice and separated by spacer residues (6-8), making the conserved signature of (tyrosine (Y) separated from a leucine (L) or isoleucine (I)); YxxL/I $x_{(6-8)}$ YxxL/I (Reth, 1989). Yet, in the case of DEF6, a lysine (K) residue replaces the second leucine (L) or isoleucine (I). Hence, the motif was referred as ITAM-like motif (Tanaka *et al.,* 2003; Bécart *et al.,* 2008).

ITAMs are critical for signal transduction in the immune system, since most of the signalling (e.g. TCR or BCR) cascades are initiated by the phosphorylation of ITAMs. (Hayes and Love, 2002). Upon the engagement of TCR, the tyrosine residues within ITAMs found in TCR ζ and co-receptor CD3 (δ, ε, γ) are phosphorylated by Src-family of tyrosine kinases, predominantly Lymphocyte-specific protein tyrosine kinase (LCK) and Zeta-chain-associated protein kinase 70 (ZAP-70) (Straus and Weiss, 1992; Straus and Weiss, 1993) or Fgr/Yes related novel protein (FYN) (Samelson *et al.,* 1990; Gauen *et al.,* 1994). In addition, it has been suggested that the association between kinases and CD4 or CD8 co-receptors is essential for the activation of T cells and optimal antigen stimulation (Veilette *et al.,* 1988; Zamoyska *et al.,* 1989; Glaichenhaus *et al.,* 1991; Clahupny *et al.,* 1991; Xu and Littman, 1993). As a consequence of the ITAM phosphorylation, a Syk-family of tyrosine kinase, ZAP-70 is directly recruited to the TCR to interact with the two-phosphorylated ITAMs through its tandem SH2 domains (Wange *et al.,* 1993; Iwashima *et al.,* 1994). Subsequent phosphorylation of ZAP-70 by LCK or ZAP-70 itself leads to its activation which is essential for the stimulation of downstream signalling pathways (i.g. rearrangement of actin cytoskeleton dynamics) and predominantly T-cell activation, differentiation and effector responses (i.g. antigen receptor-mediated secretion of interleukin-2 (IL-2) in lymphocytes (Chan *et al.,* 1995; Duplay *et al.,* 1994; Hayes and Love, 2002; Samelson *et al.,* 2002; Wang *et al.,* 2010). Similar to LCK/ZAP-70-mediated activation of T cell responses, Gauen *et al.,* (1994) suggested that, FYN can also lead to the ZAP-70 activation and in turn stimulate the effective T-cell responses (Gauen *et al.,* 1994). It has been proved that all of the ITAM-based signalling cascades utilise this two-step activation model requiring Src and then Syk-family kinases (Latour and Veillette, 2001).

Both DEF6 and SWAP70 contain an ITAM-like structure in their DSH domain, therefore it is not surprising to see that the phosphorylation of tyrosine residues might play a critical role in the signal transduction of the immune system. Indeed, LCK has been identified as a critical regulator for DEF6 in the formation of immunological synapse (IS) between antigen presenting cells (APC) and T-cells, which in turn activates the lymphocyte activation. The phosphorylation at tyr^{210} by LCK provides the translocation of DEF6 to the IS region through the interaction between $PI(3,4,5)P_3$ and the PH domain of DEF6 (Gupta *et al.,* 2003a). Furthermore, the TCR-induced translocation of DEF6 to the IS and activation of NFAT signalling-dependent T cell responses have been shown to be dependent upon the LCK-phosphorylation at tyr^{133} and tyr^{144} (Bécart *et al.,* 2008).

In addition to the kinases, LCK and ZAP-70, the Tec family kinase, Interleukin-2 inducible T-cell Kinase (ITK) has also been shown to regulate T cell signalling by controlling the spatiotemporal organisation of T cell activation (Andreotti *et al.,* 2010; Singleton *et al.,* 2011).

Singleton *et al.,* (2011) showed impaired Cdc42 localisation and defects in actin accumulation at the IS in Itk-deficient mice. Consistent with its role as a GEF for Cdc42, the accumulation of Def6 at the IS was also defective upon Itk-deficiency. Therefore, the regulation of T-cell actin dynamics and spatiotemporal patterning of T cell signalling are also Itk-dependent (Singleton *et al.,* 2011).

Upon the engagement of TCR, Itk is recruited to the membrane where it is activated via the phosphorylation by Lck and Itk itself at tyr^{511} and tyr^{180}, respectively. The activation of Itk leads to the elevation in intracellular Ca^{2+} and diacylglycerol concentrations which in turn activates the phospholipase C-λ (Plc-λ) (Singleton *et al.,* 2011). Lastly, DEF6 was found to be phosphorylated at tyr^{210} and tyr^{222} by ITK to be recruited to the IS (Hey *et al.,* 2012). In summary, tyrosine phosphorylation of ITAM may be the key mechanism that initiates the T-cell activation and response cascades therefore both DEF6 and SWAP70 come into more prominence in the ITAM-based immunological mechanisms.

Pleckstrin Homology (PH) domain: The pleckstrin homology (PH) domain encompasses amino acids 216 to 312 for DEF6, and 210 to 306 for SWAP70. This domain can be found in a large variety of signalling proteins and are best known for their functions as relocating its host protein to the cellular membrane or regulatory roles that facilitates the functional activity of its adjacent domains by binding to the specific phosphoinositides (Harlan *et al.,* 1994; Hyvonen *et al,* 1995; Hoffmann and Cerione, 2002; Cozier *et al.,* 2004; Lemmon, 2007). It has been suggested that the weak affinity between PH domain and phosphoinositides in some of the Dbl-family GEFs is important because after the PH-phosphoinositide interaction, the conformational changes occur at the membrane surface that facilitates and supports the GEF activity (Baumeister *et al.,* 2003; Worthylake *et al.,* 2004; Lemmon, 2007).

As mentioned, the tyr^{210} phosphorylation of DEF6 by LCK leads to a conformational change that induces the binding of PH-domain to phosphatidylinositol 3,4,5 triphosphate, ($PI(_{3,4,5})P_3$) and enables the entire activation of DEF6 for GEF activity and also the relocation of DEF6 to a specific cellular location like the IS (Gupta *et al.,* 2003a).

Considering the high sequence similarity (76%) and identity (56%) between PH domains of DEF6 and SWAP70 at the amino acid level (Gupta *et al.,* 2003b; Mavrakis *et al.,* 2004), it is not surprising to see that the PH domain of SWAP70 has the same binding function as DEF6. The PH domain of SWAP70 has been suggested to bind to $PtdIns(_{3,4,5})P_3$ for its translocation to the membrane that may facilitate its GEF activity for Rac and thus regulate the F-actin reorganisation during membrane ruffling (Shinohara *et al.,* 2002; Wakamatsu *et al.,* 2006).

Dbl-homology-like (DHL) domain: The Dbl-homology-like (DHL) domain encompasses the amino acids 313 to 631 for DEF6, and 307 to 585 for SWAP70. The Dbl-homology (DH) domains are known to undertake the GEF function to activate the Rho GTPases in both Dbl and DEF6-SWAP70-family proteins (Whitehead *et al.,* 1997; Mavrakis *et al.,* 2004; Rossman *et al.,* 2005). In addition, the DHL domains of DEF6 and SWAP70 have been shown to contain coiled coil regions (Shuen, MRes thesis, 2010; Hey *et al.,* 2012; Cheng, PhD thesis, 2017).

The GEF activity of the DHL domain of DEF6 was shown by expressing a truncated protein lacking all domains apart from DHL domain fused to GFP in NIH3T3 cells. Similar to the outcome when expressing full-length DEF6-GFP fusion, the expression of DHL-GFP fusion in NIH 3T3 cells also induced the formation of lamellipodia/membrane ruffles, filopodia and stress fibers. This data suggests that the DHL domain alone is sufficient enough to activate Rho GTPases that regulate the actin cytoskeleton dynamics (Mavrakis *et al.,* 2004). On the other hand, the DHL domain of SWAP70 was shown to interact with RacI to induce membrane ruffling after the observation of an impaired membrane ruffling in *SWAP70* knock-out cells (Shinohara *et al.,* 2002). More recently, the C terminal of SWAP70 has been shown to bind specifically to non-muscle F-actin and induces the formation of membrane ruffling (Ihara *et al.,* 2006).

Nuclear localisation and export signals: Nuclear localisation signal (NLS) and nuclear export signal (NES) are short amino acid sequences that imports or exports the protein to the cell nucleus by using nuclear transport, respectively (Kalderon *et al.,* 1984; Lange *et al.,* 2007; Wen *et al.,* 1995). While DEF6 contains one NLS in its DHL domain, SWAP70 contains two NLS in its PH domain and one NLS in its DHL domain. In addition, SWAP70 contains a NES in its DHL domain (Shuen, MRes thesis, 2010). In this case, the PH domain of SWAP70 plays a critical trans-locational role that localises it to plasma membrane and nucleus (Tokuda *et al.,* 2012).

1.5. The proposed roles of DEF6 and SWAP70

1.5.1. DEF6 and SWAP70 act as GEFs

1.5.1.1. The role of DEF6 as a GEF

As discussed in Section 1.4.2, the DHL domain of DEF6 has GEF activity for Rho GTPases to induce the formation of lamellipodia/membrane ruffles, filopodia and stress fibres. Indeed, a DEF6-GFP fusion expression in NIH 3T3 cells resulted in the translocation of DEF6-GFP fusion to the cell membrane and induced the formation of lamellipodia and filopodia after the treatment with H_2O_2 or platelet-derived growth factor (PDGF) (Mavrakis *et al.,* 2004). In addition, the expression of a DHL-GFP fusion lacking all other domains also induced the formation of actin cytoskeleton dynamics without any treatment in COS-7 cells. This finding suggests that the DHL domain is constitutively active for GEF activity. To understand whether DEF6 acts upstream of one of the main Rho GTPases, the constitutively active DHL-GFP fusion and the dominant-negative mutants of either RacI (N17RacI), Cdc42 (N17Cdc42), or RhoA (N19RhoA) were co-expressed in COS-7 cells. The presence of N17RacI, N17Cdc42 and N19RhoA resulted in disruption of lamellipodia/membrane ruffles, filopodia and stress fibers, respectively. These findings indicated that the formation of lamellipodia/membrane ruffling, filopodia and stress fibres are mediated through DEF6-dependent activation of RacI, Cdc42 and RhoA GTPases. Consistent with these results, GST-pull-down assays confirmed the direct interaction of DEF6 with RacI, Rac2, Cdc42 and RhoA, indicating that DEF6 interacts with these proteins to activate them (Mavrakis *et al.,* 2004).

In contrast to the findings of Mavrakis *et al.,* (2004), Gupta *et al.,* (2003a) have suggested that DEF6 exhibits GEF activity for only RacI and Cdc42 but not RhoA. DEF6 deletion mutants lacking either the N terminal (DEF6 ΔN) or the C terminal DHL domain (DEF6 Δ313-631) and containing only the C terminal DHL domain (DEF6 313-631) were expressed in COS-7 cells. While the expression of DEF6 ΔN and DEF6 313-631 mutants induced the activation of RacI and Cdc42 activation, the expression of DEF6 Δ313-631 did not lead to the activation of these GTPases. In addition, while the DEF6 313-631 mutant stimulated the GDP dissociation from RacI and Cdc42 but not from RhoA, the DEF6 Δ313-631 mutant did not stimulate any GEF activity (Gupta *et al.,* 2003a).

In addition to its GEF activity, DEF6 was also proposed to interact with filamentous (F)-actin and activated RacI to regulate the actin cytoskeleton dynamics and morphological change of cells, respectively (Mavrakis *et al.,* 2004; Oka *et al.,* 2007). *In vivo* assays of the activated GFP-full-length DEF6 and GFP-DHL have shown the co-localisation with F-actin whereas *in*

vitro assays have only shown the direct interaction between F-actin and GFP-FL-DEF6 but not between F-actin and GFP-DHL (Mavrakis *et al.,* 2004). On the other hand, overexpression of DEF6 together with the activated Rac1 in COS7 cells have shown significant morphological change whereas in the absence of activated Rac1, no morphological change was observed. The point mutations in the N terminal region of DEF6 that abolished the binding to activated Rac1 and also the morphological change, suggested that the N terminal region and central parts of DEF6 are essential for the binding (Oka *et al.,* 2007).

Taken together, DEF6 acts as a GEF for Rac1, Cdc42 and possibly for RhoA in order to regulate the actin cytoskeleton dynamics (Mavrakis *et al.,* 2004) which is essential for the function of IS in T cells (Gupta *et al.,* 2003a). In addition to its GEF role, DEF6 also interacts with F-actin and activated Rac1 in order to regulate the morphological and cytoskeletal changes (Mavrakis *et al.,* 2004; Oka *et al.,* 2007).

1.5.1.2. The role of SWAP70 as a GEF

SWAP70 has been shown to regulate actin polymerisation through activating Rho GTPases in NIH 3T3 cells (Shinohara *et al.,* 2002), dendritic cells (Oberbanscheidt *et al.,* 2007, Ocana-Morgner *et al.,* 2009; 2011; 2013; Baranov *et al.,* 2016), mast cells (Sivalenka and Jessberger, 2004; Sivalenka *et al.,* 2008) and macrophages (Hilpela *et al.,* 2003).

As discussed in Section 1.4.2, the DHL domain of SWAP70 has GEF activity for Rac1 to induce the formation of membrane ruffling. Specifically, cytoplasmic SWAP70 was found to bind to PtdIns$_{(3,4,5)}$P$_3$ upon the stimulation by several growth factors like PDGF and translocate to the membrane ruffles together with actin filaments in both NIH 3T3 and COS7 cells. However mutant forms of SWAP70 that do not have either the binding ability to PtdIns$_{(3,4,5)}$P$_3$ or the C-terminal region, failed to localise with actin filaments and also the formation of membrane ruffles were found to be prevented (Shinohara *et al.,* 2002). In addition, to determine the further activity of SWAP70, *in vitro* release of [^{3}H] GDP from purified glutathione S-transferase (GST) of several GTPases were monitored in the presence of SWAP70 and PtdIns$_{(3,4,5)}$P$_3$. The GEF activity of SWAP70 was detected only on Rac1 but not on Cdc42 or RhoA. Moreover while mutant form of SWAP70 lacking N terminal region have shown enhanced GEF activity, the other mutant form lacking C terminal region have shown inhibited Rac1 activation and membrane ruffling (Shinohara *et al.,* 2002).

However, SWAP70 does not only perform its GEF activity to regulate the actin cytoskeleton dynamics, but also interacts with F-actin and activated Rac1. Expression of C terminal SWAP70 in COS7 cells (GFP-SWAP70 (448-585)) led to the co-localisation with F-actin while

the expression of the mutant forms of SWAP70 lacking the C terminal region (GFP–SWAP70 (Δ448-564)] or the PH domain (GFP–SWAP-70 ΔPH) did not. In addition, co-localisation of full-length SWAP70 with F-actin was only detected upon the stimulation by growth factors suggesting that the binding activity of the C-terminal region may be masked in the unstimulated condition and may need to be activated that; may lead to a conformational change regulated by binding to PtdIns$_{(3,4,5)}$P$_3$. Besides, the expression of a mutant form of SWAP70 lacking the actin binding region (SWAP70 (Δ1-564) failed to form membrane ruffling in COS7 cells stimulated by epidermal growth factor (EGF), indicating that the binding activity of SWAP70 to non-muscle F-actin is crucial for the formation of membrane ruffling. Similar to the interaction between DEF6 and activated RacI, the interaction between SWAP70 and activated RacI was also detected (Ihara *et al.,* 2006).

Binding of the C-terminal SWAP70 to F-actin to regulate the actin cytoskeleton dynamics was also supported by Chacón-Martínez *et al.,* (2013). The cross-linking of actin filaments by SWAP70 were increased in low-speed pelleting assays whereas the mutant form of SWAP70 that contains the actin binding region and part of the coiled-coil region (His6- SWAP-70(444 – 585)) was even more efficient to bundle the actin filaments (Chacón-Martínez *et al.,* 2013). This finding also supports the previous finding of Ihara *et al.,* (2006), who suggested the higher binding capacity of SWAP70 C terminal (448-585) for F-actin compared with the full-length SWAP70 due to the masked condition of F-actin binding C terminal region in the folded form of full-length protein (Ihara *et al.,* 2006; Chacón-Martínez *et al.,* 2013). Furthermore, it has been suggested that the coiled-coil region of SWAP70 spanning amino acids 312-529, has the self-association capacity (oligomerisation) to bundle the actin filaments. Binding to PtdIns$_{(3,4,5)}$P$_3$, RacI or other proteins or phosphorylation may change the tertiary structure of SWAP70 and thus enables it to oligomerise for bundling filaments or performing its functions (Chacón-Martínez *et al.,* 2013).

Taken together, SWAP70 acts as a GEF for RacI in order to regulate stimulation-dependent membrane ruffling (Shinohara *et al.,* 2002). In addition to its GEF activity, it interacts with F-actin and activated RacI to regulate the actin dynamics (Ihara *et al.,* 2006). The oligomerisation of the C terminal region of SWAP70 to bundle F-actin filaments and delay their depolymerisation was also suggested as an essential feature of SWAP70 for regulating the cell polarity, adhesion and motility (Chacón-Martínez *et al.,* 2013).

1.5.2. The roles of Def6 and Swap70 in the immune system

1.5.2.1. The role of Def6 in the immune system

Considering the expression pattern of Def6 that includes lymph node, thymus, and peripheral leucocytes (Hotfilder *et al.,* 1999), in detail thymocytes and differentiated T helper 2 (Th2) cells (Tanaka *et al.,* 2003), it is not surprising to see that DEF6 might actually play an essential role in the adaptive immune system. Indeed, Def6 has been shown to control the T-cell receptor (TCR)-mediated NFAT activation regulating T cell differentiation, activation, expansion and inflammatory responses in mice (Tanaka *et al.,* 2003; Bécart *et al.,* 2007; 2008; 2009). Upregulation of *Def6* in primary differentiating Th2 cells after 3-4 days of culture but not in Th1 cells has suggested that *Def6* may be responsible for regulating the differentiation and expansion of Th1 and Th2 cells, possibly by decreasing the expansion of Th1 and increasing the expansion of Th2. The later findings displaying the decrease of IFNγ-producing Th1 cells and the increase of IL-4-producing Th2 cells induced by Def6 retrovirus infection are also consistent with the selective effects of Def6 on T cell differentiation and response. Moreover, following its recruitment to the IS upon stimulation, Def6 was found to interact with ZAP-70 kinase, resulting in the inhibition of the phosphorylation of linker for activation of T cells (LAT) and the stimulation of Th2 differentiation (Tanaka *et al.,* 2003; Madrenas, 2003). In contrast, according to the studies of Bécart *et al.,* (2007; 2008 and 2009), Def6 regulates the development of both Th1 and Th2 cell inflammatory responses by controlling the Ca^{2+}-NFAT signalling pathway. By using homologous recombination in embryonic stem cells, *Def6*$^{-/-}$ mice on a homogenous C57BL/6 background were generated. Despite being viable and fertile, *Def6*$^{-/-}$ mice displayed defects in thymocyte differentiation and impaired expansion of the double negative-1 (DN1) population. In addition, *Def6*$^{-/-}$ peripheral $CD4^+$ T cells exhibited impaired TCR/CD28-induced proliferation and IL-2 production, which could be rescued by exogenous *IL-2*. While *Def6*$^{-/-}$ $CD4^+$ T cells displayed normal activation of early signalling processes like activation of ZAP-70, LAT or Akt upon TCR-CD28 ligation, the duration of extracellular signal-regulated kinase (ERK)1/2 and p38 MAPK activation was mostly reduced. Furthermore, a sharp reduction of intracellular Ca^{2+} influx was observed in *Def6*-deficient T cells leading to defective TCR-CD28-induced translocation of NFAT to the nucleus, indicating that Def6 is involved in the Ca^{2+}-NFAT signalling pathway (Bécart *et al.,* 2007). In addition, dominant-negative forms of Cdc42 and Racl were found to diminish TCR-mediated NFAT activation, which was overcome by transduction of the constitutively active form of Cdc42 in *Def6*$^{-/-}$ $CD4^+$ T cells, suggesting that Def6 may exert its GEF role on Cdc42 and, to a lesser extent on Racl, to induce Ca^{2+}-NFAT activation (Bécart *et al.,* 2008). Wiskott-Aldrich syndrome protein (WASP) and WASP-family verprolin homologous protein (WAVE) are two of the downstream effectors of Cdc42/Racl regulating not only the reorganisation of actin

cytoskeleton, but also the Ca^{2+}-NFAT signalling by affecting the intracellular Ca^{2+} levels and CRAC-mediated Ca^{2+} entry (Huang *et al.,* 2005; Nolz *et al.,* 2006).

Def6 has been shown to participate in the formation and maintenance of the IS upon LCK-dependent phosphorylation at tyr^{210} or tyr^{133} and tyr^{144} which in turn results in the activation of NFAT and differentiation of Th1/Th2 cells (Gupta *et al.,* 2003a; Bécart *et al.,* 2008). Due to the complex structure of IS that requires F-actin reorganisation, Def6-mediated regulation of actin polymerisation may be critical for the formation of IS and T cell responses. Fanzo *et al.,* (2006) have shown that *Def6*$^{-/-}$ T cells resulted in a defective T cell response characterised by reduced ERK1/2 activation, decreased c-Fos induction, disrupted immunological synapse formation and defective actin polymerisation. The constitutively active form of *Rac2* rescued the actin polymerisation defect in *Def6*$^{-/-}$ T cells, indicating the defects in the cytoskeletal organisation and thus in the IS are dependent on the ability of Def6 to activate Rho GTPases (Fanzo *et al.,* 2006).

Consistent with the role of Def6 in regulating T cell inflammatory responses, defective Th1 and Th2 inflammatory responses were detected in *Def6*$^{-/-}$ mice on a homogenous C57BL/6 background. The defects were characterised by reduced numbers of neutrophils and eosinophils in the Broncho alveolar lavage (BAL) liquid of the mutant mice as well as a reduction in IFN and IL-4/5 cytokines, respectively, for Th1 and Th2 cell subsets (Bécart *et al.,* 2007). In contrast, on a mixed C57BL/6 x 129 background, *Def6*$^{-/-}$ mice (mostly females and aged more than 5 months old) were found to develop a lupus-like autoimmune syndrome, spontaneously (Fanzo *et al.,* 2006). However, on a C57BL/6 background, only double knockout (DKO; *Def6*$^{-/-}$/*Swap70*$^{-/-}$) female mice have been shown to develop lupus-like syndrome (splenomegaly, lymphadenopathy and aberrant autoantibody production) compared to WT, *Def6*$^{-/-}$ or *Swap70*$^{-/-}$ female/male mice. Furthermore, female DKO mice showed increased number of B cells, expansion of germinal center (GC) B cells, switched $IgG1^{+}$ B cells and plasma cells in the spleen. They have also suggested that Def6 interacts with IRF4 to regulate the induction of activation-induced cytidine deaminase (AID) in B cells that controls B cell differentiation (Biswas *et al.,* 2012).

Additionally, a third subset, Th17 cells, was shown to play critical roles in the development of organ-specific autoimmune and inflammatory diseases including experimental autoimmune encephalomyelitis (EAE) (Park *et al.,* 2005; Langrish *et al.,* 2005). Recently, *Def6*$^{-/-}$ mice on a homogenous C57BL/6 background were found resistant to EAE development, while WT mice developed acute EAE upon the induction by injecting encephalitogenic MOG_{35-55} peptide. Also, consistent with the lack of clinical EAE signs, defective $CD4^{+}$ T cell infiltration into the

central nervous system (CNS), lack of demyelination of the spinal cord's white matter and impaired Th1/Th17 inflammatory responses (defective IFNγ and IL-17 production in CNS and lymphoid organs) were observed in *Def6*-deficient mice compared to WT. Lastly, *Def6*-deficient $CD4^+$ T cells failed to differentiate into Th17 cells *in vivo* and *in vitro* indicating that Def6 is a positive regulator of Th17 inflammatory responses and is responsible for triggering the development of autoimmune and inflammatory diseases like EAE (Canonigo-Balancio *et al.,* 2009). In contrast, on a mixed background (BALB/c x DO11.10), *Def6*$^{-/-}$ mice developed rheumatoid arthritis-like joint disease and large vessel vasculitis spontaneously as a result of increased production of IL-17 and IL-21 (Chen *et al.,* 2008), whereas on a BALB/c background, young *Def6*-deficient mice did not develop the arthritis (Altman and Bécart, 2009). This discrepancy may be explained by studying on a DO11.10 TCR transgenic background; harbouring an MHC class-II restricted ovalbumin-specific TCR (Chen *et al.,* 2008). However, according to the letter written by Chen *et al.,* (2009) as a response to the letter from Altman and Bécart, (2009), deregulated expression of IL-17 and IL-21 was observed in both transgenic (DO11.10) and nontransgenic *Def6*$^{-/-}$ cells, indicating that the outcome was not due to the transgenic background. The same group has suggested that, aberrant production of IL-17 and IL-21 and consequent development of the autoimmune disease depend on Def6-mediated control of the transcription factor, Interferon-regulatory factor-4 (IRF4) that regulates the Th17 differentiation and the production of the cytokines IL-17 and IL-21 (Chen *et al.,* 2008; Biswas *et al.,* 2010a; Biswas *et al.,* 2010b).

In addition, *Def6*$^{-/-}$ mice were immunized with interphotoreceptor retinoid-binding protein (IRBP) to determine the development of experimental autoimmune uveitis (EAU) disease on a C57BL/6 background. *Def6*$^{-/-}$ mice were found more resistant to the EAU as well as exhibiting less lymphocyte responsiveness and low levels of IFN-γ and IL17 comparing to WT C57BL/6 controls. This data was also consistent with that of Canonigo-Balancio *et al.,* (2009), in which *Def6*$^{-/-}$ mice were also resistant to the development of EAE, both indicating that Def6 plays a critical role in the development of diseases like EAE or EAU, possibly by inducing the activation or migration of lymphocytes (Vistika *et al.,* 2012).

Def6 has also been suggested as a regulator of Rap1 dependent leukocyte function-associated antigen-1 (LCA-1) activation and intercellular adhesion molecule-1 (ICAM-1) adhesion upon TCR-engagement (Cote *et al.,* 2015). Rap1 is a critical regulator of TCR-dependent integrin adhesion in lymphocytes, *Rap1A*$^{-/-}$ T cells have deficient cell adhesion, polarisation and migration to secondary lymphoid organs (Duchniewicz *et al.,* 2006). The studies on the role of Def6 in integrin activation and adhesiveness revealed defective adhesion to ICAM-1 upon TCR engagement in *Def6*$^{-/-}$ $CD4^+$ T cells comparing to WT $CD4^+$ cells. Further

experiments have shown the interaction of Def6 with Rap1 by its PH domain and the interdependent localisation of both to the IS for the subsequent LFA-1 activation and adhesion to ICAM-1 (Cote *et al.,* 2015).

1.5.2.2. The role of Swap70 in the immune system

Swap70, which is predominantly expressed in mature B-lymphocytes and to a lesser extent, in immature mast cells, was identified as one of the component of an enzyme complex responsible for the DNA recombination of Ig switch regions in B cells (Borggrefe *et al.,* 1998; Borggrefe *et al.,* 1999). Swap70 localises in the cytoplasm in mast cells and in resting B cells. However, upon stimulation it relocates to the nucleus to induce the Ig class switching in B cells (Masat *et al.,* 2000).

Swap70$^{-/-}$ mice were generated on a 129SvJ background in order to address its role in B cell activation, Ig class switching and DNA repair. Although being phenotypically healthy and producing same numbers of B cells expressing IgM or IgD antibodies compared to WT mice, LPS-activated *Swap70*$^{-/-}$ B-lymphocytes showed more radiation sensitivity than WT. Moreover, Swap70 is important for CD40-dependent switching to IgE isotype antibody since the CD40-dependent response was altered in *Swap70*$^{-/-}$ mice and the levels of IgE were detected as six to seven-fold less than in WT mice before immunisation and three to four-fold less after immunisation. These findings have demonstrated that Swap70 might play an active role in CD40-dependent activation of B cells and in producing IgE antibody, essential for allergic responses (Borggrefe *et al.,* 2001).

Since the only two cell types expressing Swap70 are B cells and mast cells, the potential role of Swap70 in mast cells was also studied in *Swap70*$^{-/-}$ mice (Gross *et al.,* 2002; Sivalenka and Jessberger, 2004). Consistent with the role of Swap70 in actin cytoskeleton remodelling, cultured bone marrow mast cells (BMMC) of *Swap70*$^{-/-}$ mice have shown impaired actin rearrangement and migration *in vivo* and *in vitro.* Furthermore, high-affinity IgE receptor (FcERI)-mediated degranulation (Gross *et al.,* 2002), c-kit receptor signalling-mediated translocation of Racl and Rac2, Ca^{2+} flux and Akt kinase activity were defective in *Swap70*$^{-/-}$ BMMC, indicating that Swap70 plays an effective role in c-kit signalling regulating the mast cell activation, adhesion and migration (Sivalenka and Jessberger, 2004).

In addition to its role in B cell activation, Ig class switching and c-kit signalling-induced development of mast cells, Swap70 was also found to play a role in B cell adhesion and migration into secondary lymphoid organs. The study by Pearce *et al.,* (2006) has suggested that on a 129/Sv background, *Swap70*$^{-/-}$ B cells showed normal adhesion and accumulation in

lymph node (LN) high endothelial venules, however they failed to enter into the LNs. This defect was due to high amount of integrin-mediated adhesion leading to lack of lamellipodia stabilisation, uropod formation and thereby an impaired B cell polarisation preventing the entry of B cells into the LNs (Pearce *et al.,* 2006).

Lastly, Biswas *et al.,* (2012) have shown that double knock-out (DKO) female mice (*Def6*$^{-/-}$ */Swap70*$^{-/-}$) developed a lupus-like syndrome while *Swap70*-deficient female/male mice did not on a C57BL/6 background (Biswas *et al.,* 2012). They have also shown the plasma cell accumulation in DKO and *Swap70*$^{-/-}$ B cells, consistent with previous findings suggesting that Swap70 fine-tunes IRF4 expression for controlling the plasma cell development (Quemeneur *et al*., 2008; Chopin *et al.,* 2011).

1.5.3. The roles of Def6 and Swap70 in embryogenesis

Even though majority of the studies have focused on the functions of Def6 and Swap70 in the immune system, studies on murine and zebrafish revealed broad expression patterns of Def6 and Swap70 in embryonic development (Mavrakis *et al.,* 2004; Martin, PhD thesis, 2007; Shuen, MRes thesis, 2010). Further experiments have suggested that, the zebrafish orthologous *def6a* and *swap70b* act downstream of *wnt5b* and *wnt11*, respectively, in the non-canonical Wnt signalling pathway to regulate the CE cell movements during zebrafish gastrulation (Goudevenou *et al.,* 2011; Xu, PhD thesis, 2015). However, little is known about the underlying molecular mechanisms and direct downstream targets of Def6a and Swap70b during zebrafish embryogenesis.

1.5.3.1. The identification of Def6 and Swap70 within the zebrafish genome

The genome duplication occurred within teleost resulted in the formation of Def6 and Swap70 paralogues in zebrafish. The zebrafish genome contains five genes similar to DEF6 and SWAP70 belonging to the SWAP70 family (protein family ID; PTHR14383) according to the Ensembl database. The detailed gene IDs of these five paralogous in different databases are shown in **Table 1.1.** The amino acid sequences of these genes were compared with sequences of mouse and human proteins to generate a phylogenetic neighbour-joining tree. Phylogenetic analysis of these paralogues revealed that *def6a* (NCBI accession number; zgc:63721) is the most likely zebrafish orthologue of mouse and human *DEF6*, as the domains of zebrafish Def6a share 63-72% identity and 78-85% similarity with human and mouse DEF6 at the amino acid level. Similarly, *swap70b* (NCBI accession number; si:dkey-8I13.4) is the most likely zebrafish orthologue of human and mouse *SWAP70,* as the domains of zebrafish Swap70b share 72-88% identity and 84-96% similarity with human and mouse SWAP70 at

the amino acid level **(Figure 1.13).** The preliminary expression analyses of these five paralogous have shown that all five genes are expressed diversely during the early zebrafish embryonic development. While *def6a* and *swap70b* are maternally and ubiquitously expressed from 1hpf to 72hpf, *def6b, def6c* and *swap70a* are expressed only at specific time points (Shuen, MRes thesis, 2010) **(Figure 1.14).**

Since *def6a* (zgc:63721) and *swap70b* (si:dkey-8I13.4) are the likely zebrafish orthologues of mouse and human *DEF6* and *SWAP70*, respectively, only *def6a* and *swap70b* are targeted in this present study. The following sections will summarise the expression patterns of *def6a* and *swap70b* during zebrafish embryonic development and preliminary loss of function analyses by using *def6a* and *swap70b* morpholinos (MOs).

Name	NCBI Symbol	NCBI Gene ID	Ensembl Gene ID	ZFIN Gene ID	UniProt Gene ID	Chr
def6a	Zgc:63721	394015	ENSDARG00000012247	ZDB-GENE-040426-1246	Q7SYB5	8
def6b	LOC570940	570940	ENSDARG00000044524	ZDB-GENE-110408-59	-	22
def6c	si:dkeyp15g12.1	563690	ENSDARG00000034717	ZDB-GENE-060503-87	Q1L978	4
swap70a	zgc:63599	393645	ENSDARG00000051819	ZDB-GENE-040426-1182	Q6PEH7	7
swap70b	si:dkey-8l13.4	562490	ENSDARG00000057286	ZDB-GENE-030131-3587	Q1LYE0	18

Table 1.1 Five genes of the SWAP70 protein family and their gene IDs in different databases. The zebrafish orthologous of *DEF6* and *SWAP70* are indicated in red and bold, co-orthologous are indicated in black.

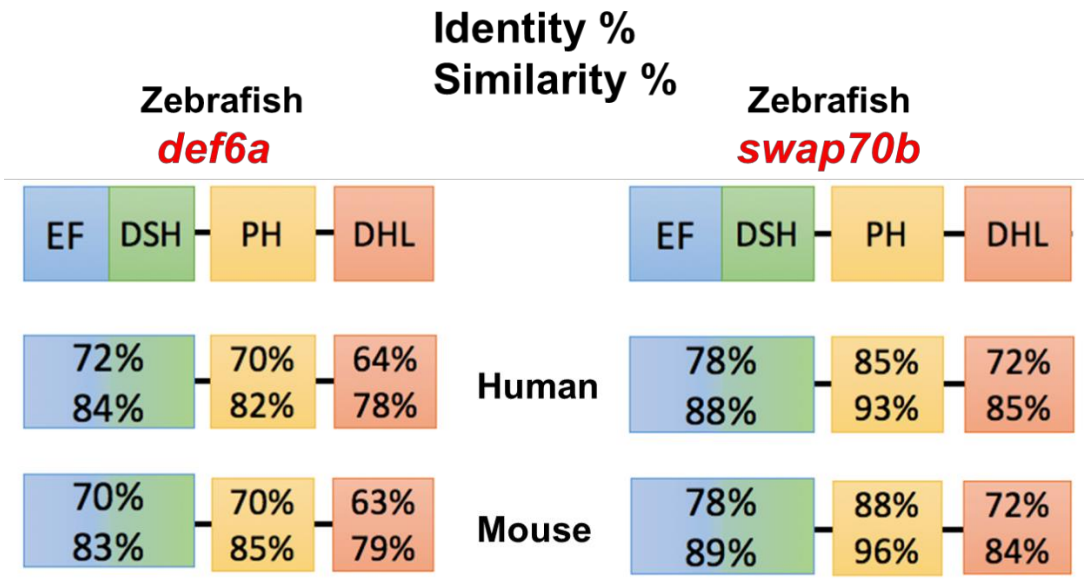


Figure 1.13 Amino acid comparison of Def6a and Swap70b to human and mouse DEF6 and SWAP70. The figure shows the schematic representation of DEF6 and SWAP70 domains. The numbers on each domain represents the identities and similarities that zebrafish and human/mouse share at the amino acid level. EF; EF-hand, DSH; DEF6-SWAP70-homology domain, PH; pleckstrin homology domain, DHL; Dbl-homology-like domain. Adapted from (Goudevenou *et al.,* 2011 and Shuen, MRes thesis, 2010).

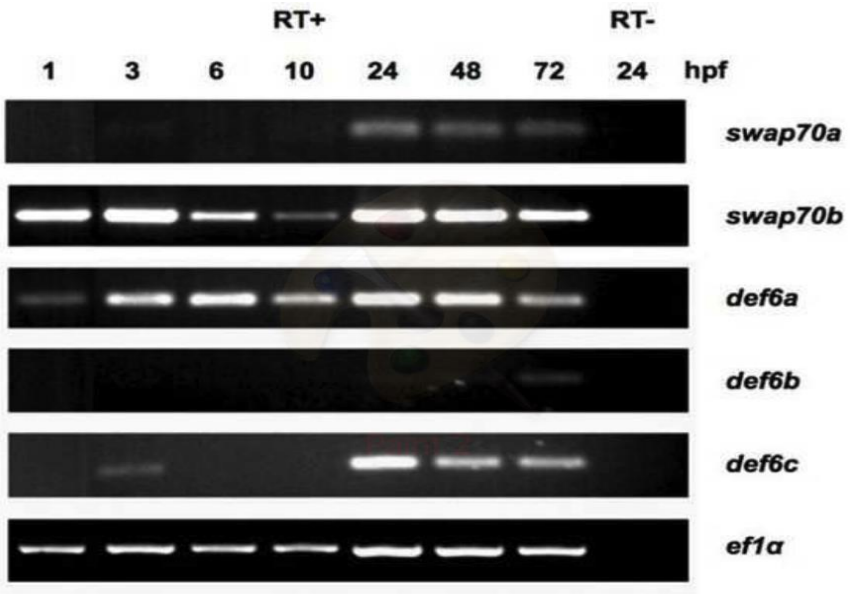


Figure 1.14 Developmental expression levels of *def6* paralogous at different time points. RT-PCR analysis of the five paralogous have shown that *def6a* and *swap70b* are expressed from 1hpf to 72hpf (RT+) indicating that both are maternally expressed. Strong zygotic expression can be easily observed for *def6a* and *swap70b* during the gastrulation and segmentation periods whereas their co-orthologous *def6c* and *swap70a* are weakly expressed or not expressed until 24hpf. Additionally, the expression of *def6b* can not be detected until 72hpf. Reverse transcription (RT-) represents the negative control at 24hpf and *ef1*α represents the positive control as a housekeeping gene. Adapted from (Shuen, MRes thesis, 2010).

1.5.3.2. The role of *def6a* in the zebrafish embryonic development

1.5.3.2.1. Expression of *def6a* during zebrafish embryonic development

Whole mount *in situ* hybridisation of zebrafish embryos using *def6a*-specific antisense RNA probe has revealed the expression pattern of *def6a* during zebrafish early embryonic development. The ubiquitous expression of *def6a* was detected throughout the cleavage, blastula, gastrulation and early segmentation stages (1hpf to 24hpf) **(Figure 1.15 (A-H))**. Since the zygotic transcription starts at mid-blastula transition period (2.45hpf), the expression earlier than this period indicates the maternal expression of *def6a* (Martin, PhD thesis, 2007), which was also confirmed by RT-PCR analysis (Figure 1.14; Shuen, MRes thesis, 2010). In addition, from the beginning of late segmentation (from 24hpf to 4dpf), the expression of *def6a* was detected more restricted, specifically at the developing nervous system, brain, somite boundaries, otic vesicle, ventral and caudal fins, pharyngeal arches and neuromasts of anterior and posterior lateral line **(Figure 1.15)**. The anterior part of the embryos at 24hpf has shown the expression in the midbrain-hindbrain boundaries and around the developing brain ventricles whereas the posterior part has shown the expression in somite boundaries **(Figure 1.15 (I-K))**. Furthermore, the anterior part of the embryos at 48hpf has shown the expression in brain boundaries as well as the otic vesicle, the pectoral fins and the developing musculature. The posterior part of the embryos at 48hpf has shown the expression in somites, caudal fin and the lateral line primordium **(Figure 1.15 (L-N))**. At 72hpf and 4dpf, the expressions were restricted to the neuromasts of anterior and posterior lateral line, pectoral fins and the pharyngeal arches **(Figure 1.15 (O-S))** (Martin, PhD thesis, 2007).

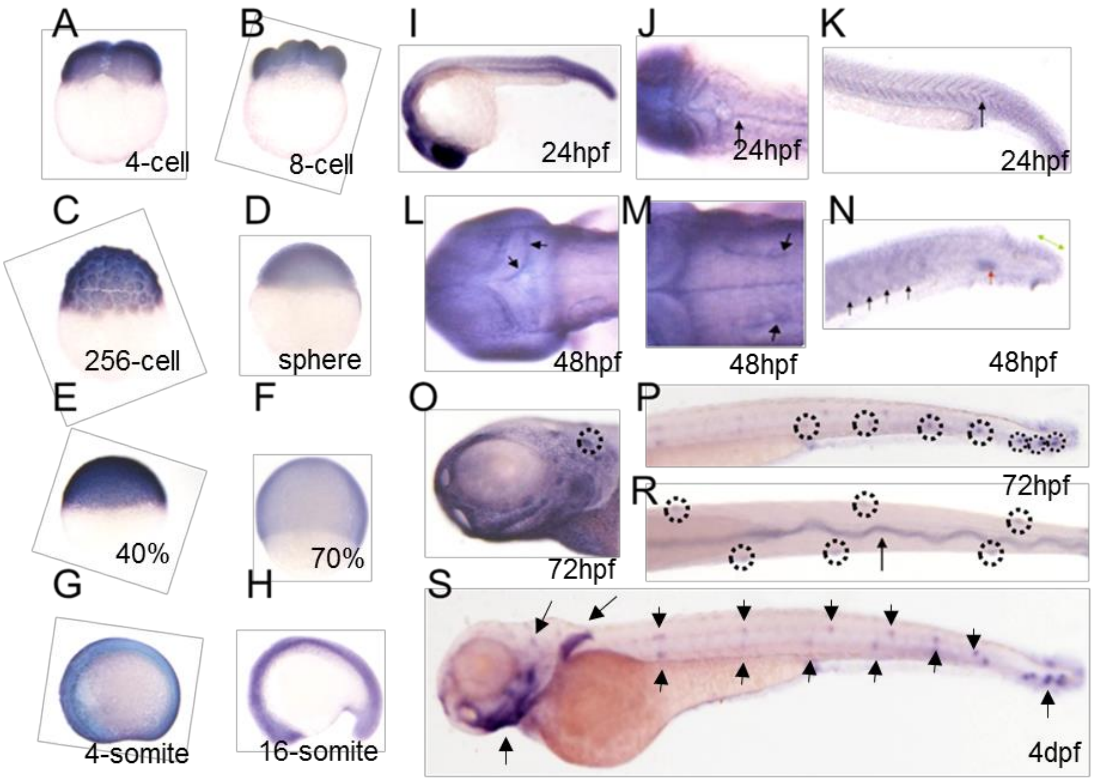


Figure 1.15 Expression pattern of *def6a* during zebrafish embryonic development. Lateral views of **(A)** 4-cell **(B)** 8-cells **(C)** 256-cells **(D)** sphere stage **(E)** 40% epiboly, **(F)** 70% epiboly, **(G)** 4-somites and **(H)** 16-somites stages showing the ubiquitous expression of *def6a* throughout the cleavage, blastula, gastrula and early segmentation periods. **(I)** Lateral view of an embryo at 24hpf, **(J)** dorsal view of the anterior region and **(K)** posterior region of embryos at 24hpf showing intense expression of *def6a* in the brain boundaries (black arrow in **(J)**) and somites (black arrow in **(K)**). **(L-M)** Dorsal views of the anterior region at 48hpf show the expression at the brain boundaries and otic vesicle (black arrows), while **(N)** lateral view of the posterior region at 48hpf shows the expression in somites (black arrows), caudal fin (green arrow) and lateral line primordium (red arrow). **(O-S)** Lateral views and **(P-R)** ventral views of an embryo at 72hpf reveal expressions in neuromasts of anterior **(O)** and posterior **(P-R)** lateral line (circled), caudal fin, ventral fin (black arrow), pharyngeal arches. Adapted from (Martin, PhD thesis, 2007).

1.5.3.2.2. Functional analysis of *def6a* during zebrafish embryonic development

The spatial and temporal expression of *def6a* in both zebrafish and mouse embryos have suggested a potential role of *def6a* in vertebrate embryonic development. Therefore, a loss-of-function analysis by morpholino (MO)-mediated knock-down of *def6a* expression, rescue experiments and gain-of-function analysis by over-expressing *def6a* were carried out to understand the function of *def6a* and the signalling pathway that *def6a* is involved during zebrafish embryonic development (Goudevenou *et al.,* 2011).

MO-mediated knock-down of *def6a* in zebrafish embryos revealed morphological defects at the end of gastrulation period characterised by shorter and broader anterior-posterior axis and reduced body length at 3dpf. Whole mount *in situ* hybridisation experiments using dorsal, ventral and mesendodermal markers confirmed that the cell fate specification was not affected by the *def6a* MO-mediated knock-down. Rescue experiments co-injecting *gfp*-tagged *def6a* RNA and *def6a* MO revealed the increase in the body length at tail-bud stage comparing to *def6a* morphants. The increased angle between the most anterior and posterior end of *def6a* morphants, was decreased upon the co-injection with *gfp*-tagged *def6a* RNA.

Since the morphological defects of *def6*a morphants were reminiscent of the mutants (*pipetail/wnt5b* and *silberblick/wnt11*) showing CE cell movement defects and the dorsoventral patterning was not affected by the MO-mediated knock-down, double *in situ* hybridisation experiments were carried out to determine whether the *def6a* MO-mediated phenotype was due to defective CE cell movements during gastrulation. Expression of *dlx3, hgg1* and *ntl* markers revealed an enlarged neural plate, posterior shift of prechordal plate and medio-laterally broader and anterior-posteriorly shorter notochord in *def6a* morphants at tail-bud stage, suggesting impaired CE cell movement defects. In addition, the expression of *myoD* revealed the medio-lateral expansion and anterior-posterior shortening of the two stripes of adaxial cells in *def6a* morphants at tail-bud stage,

Furthermore, rescue experiments to check whether *gfp-def6a* RNA could rescue the *wnt5b* MO-induced phenotype revealed that Def6a acts downstream of Wnt5b signalling pathway as the *wnt5b* MO-induced convergence and extension defects were rescued by *gfp-def6a* RNA. The number of severely affected embryos at 24hpf were decreased from 50% to 10% upon co-injecting *wnt5b* MO and *gfp-def6a* RNA. Similar rescue experiments co-injecting *wnt11* MO and *gfp-def6a* RNA showed that *gfp-def6a* RNA failed to rescue the *wnt11* MO-induced phenotype, suggesting that *def6a* does not act downstream of *wnt11* signalling pathway. However, mild phenotypes that was observed when only *def6a* MO or *wnt11* MO were

injected, were turned into the severe phenotypes upon co-injecting both MOs at the same concentrations.

Taken together, these results demonstrated that *def6a* functions in parallel or overlapping pathway with *wnt11*, whereas it functions downstream of *wnt5b* in Wnt/PCP signalling pathway to regulate the CE cell movements during zebrafish gastrulation (Goudevenou *et al.,* 2011).

1.5.3.3. The role of *swap70b* in the zebrafish embryonic development

1.5.3.3.1. Expression of *swap70b* during zebrafish embryonic development

Whole mount *in situ* hybridisation of zebrafish embryos using *swap70b*-specific antisense RNA probe has revealed that the expression of *swap70b* is temporarily and spatially regulated during zebrafish early embryonic development. The ubiquitous expression of *swap70b* can be observed from cleavage period (4-cell stage) to late gastrulation period (10hpf) **(Figure 1.16(A-F))**. The detection of *swap70b* before the zygotic transcription, which starts at the mid-blastula stage (2.45hpf), indicates the presence of maternally expressed *swap70b*. At the onset of segmentation period (10.6hpf), the expression becomes restricted to the optic primordium **(Figure 1.16(G))**, whereas at the late segmentation period the expression is found at optic primordium, otic vesicle and ventral mesoderm **(Figure 1.16(H-I))**. At the pharyngula period, the expression was detected at the caudal vein **(Figure 1.16(J-K))** and lastly at the hatching period the expression of *swap70b* was detected in pharyngeal arches and pectoral fins **(Figure 1.16(L))** (Shuen, MRes thesis, 2010).

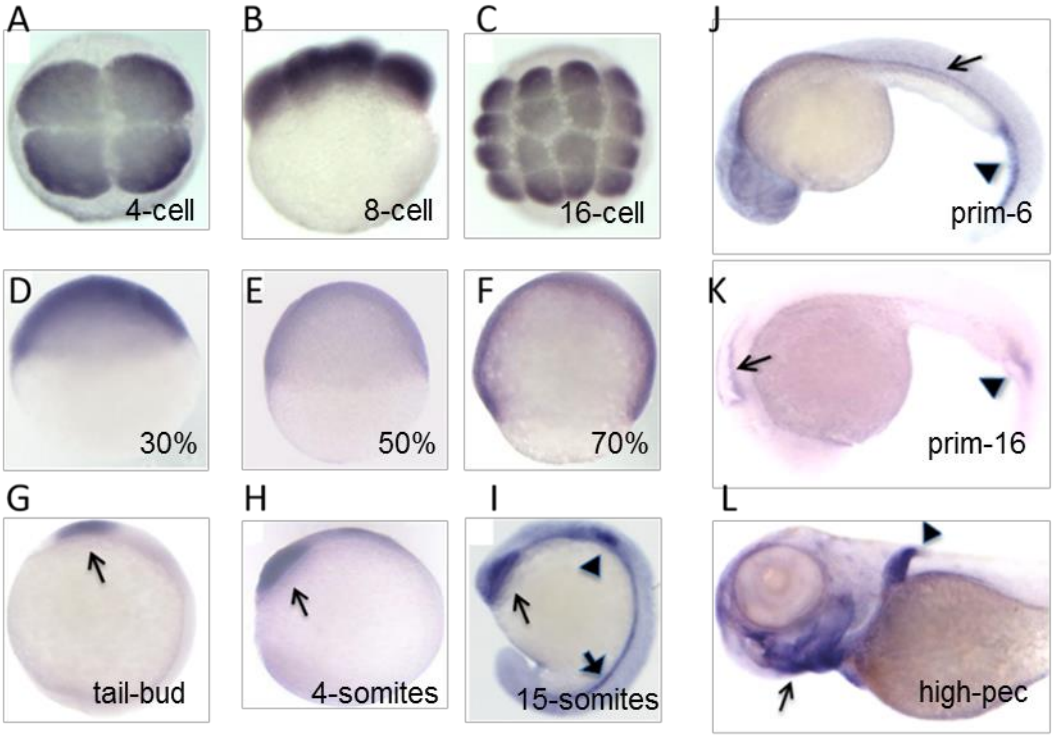


Figure 1.16 Expression pattern of *swap70b* during zebrafish embryonic development. Dorsal views of **(A)** 4-cell, **(C)** 16-cell, and lateral views of **(B)** 8-cell, **(D)** 30% epiboly **(E)** 50% epiboly **(F)** 70% epiboly stages showing the ubiquitous expression of *swap70b*. Lateral views of **(G)** tail-bud, **(H)** 4-somites and **(I)** 15-somites stages have shown the expression at optic primordium, otic vesicle and ventral mesoderm (black arrows). Lateral views of **(J)** prim-6 and **(K)** prim-16 stages have shown the expression at the caudal vein. Lastly, the lateral view of **(L)** high-pectoral stage demonstrates the expression at pectoral fins and pharyngeal arches (black arrows). Adapted from (Shuen, MRes thesis, 2010).

1.5.3.3.2. Functional analysis of *swap70b* during zebrafish embryonic development

The high sequence homology between *def6a* and *swap70b* and the spatial and temporal expression pattern of *swap70b* during zebrafish embryonic development have suggested that *swap70b* may also have a rolein CE cell movements during the zebrafish embryonic development. Therefore, preliminary functional analyses including the gain-of-function analysis by overexpressing Gfp-tagged Swap70b, loss-of-function analysis by *swap70b* MO-mediated knock-down of *swap70b* expression and rescue experiments were carried out by Shuen (MRes thesis, 2010) and Xu (PhD thesis, 2015) to understand the role of *swap70b* and the pathway it is involved during the zebrafish embryonic development. This section will summarise these analyses.

MO-mediated knock-down of *swap70b* (AUG MO; binding to the start codon and splice MO1; binding to the exon1-intron1 junction) revealed normal development throughout cleavage, blastula and gastrulation periods. However, during the segmentation period from tail-bud stage (10hpf) to 24hpf, the embryos displayed reduced body length and curved tails. Depending on the MO type and injected amount, the severity and the mortality rates were increased comparing to uninjected WT embryos. The severe phenotype, which was especially observed upon the injection of AUG MO, was characterised by shortened body length, twisted tail, disruption in the development of eyes, somites, brain and increased mortality. At 48hpf, 31% of splice MO1 injected-embryos survived with curved tail and shortened body axis and at 72hpf, 7% of these embryos have shown no formation of red blood cells (Shuen, MRes thesis, 2010). Injection of *gfp*-tagged *swap70b* RNA was sufficient to rescue the *swap70b* splice MO1-induced phenotype since the numbers of moderate and severe phenotypes were decreased whereas the numbers of normal and mild phenotypes were increased (Shuen, MRes thesis, 2010; Xu, PhD thesis, 2015).

Whole mount *in situ* hybridisation of *swap70b* MO injected and WT embryos using specific markers revealed that knock-down of *swap70b* did not affect the cell fate specification but resulted in CE cell movement defects. The neural plate edges marked by *dlx3*, were broadened in *swap70b* MO-injected embryos comparing to WT controls. The ratio of the width of *dlx3* staining to the embryo width showed a remarkable increase in the MO-injected embryos, suggesting defects in convergence movements. Separately, the shortened body length, which was quantified as the distance between the *hgg1* and *ntl* markers, was increased in injected embryos, suggesting defects in extension movements. In addition, the ratio of the distance between *hgg1* and *ntl* markers to the embryo width has also suggested extension movement defects (Xu, PhD thesis, 2015).

The paraxial mesoderm, marked by *myoD,* was also tested in tail-bud and 10-somite stage embryos. While the WT embryos at tail-bud stage showed the *myoD* expression in adaxial cells extending along the anterior-posterior axis and converging towards the midline, the *swap70b* MO-injected embryos displayed the failed extension and convergence of the adaxial cells that result in a shorter and wider *myoD* expression pattern. In addition, *swap70b* MO-injected embryos showed thinner and wider somites as well as down-regulation of *myoD* expression and slightly disorganised somites at 10-somite stage (Xu, PhD thesis, 2015).

In addition, injecting *gfp-swap70b* RNA rescued the CE cell movement phenotype of *wnt11* morphants while it failed to rescue the phenotype of *wnt5* morphants, indicating that Swap70b acts downstream of Wnt11 signalling pathway. Lastly, functional redundancy between *def6a and swap70b* was observed as ectopic expression of Def6a and Swap70b could rescue *swap70b* and *def6a* morphants, respectively. Also, co-injection of *def6a* and *swap70b* MOs revealed more severe phenotype than the single mutants (Xu, PhD thesis, 2015).

Taken together, these preliminary results suggested that *swap70b* regulates CE cell movements without affecting the cell fate specification downstream of *wnt11* in the Wnt/PCP signalling pathway. Rescue experiments indicated a functional redundancy between *swap70b* and *def6a*.

1.6. Targeted genome editing to study gene functions

Reverse genetics is the approach being utilised to discover the functions of genes by analysing the phenotypic effects of targeted or non-targeted gene sequences. The aim of reverse genetics is to understand the exact biological function of a known gene by exploring the effect leading to a phenotype. Gene silencing using RNA interference (RNAi), knock-down using morpholino (MO) oligos, chemical mutagenesis using ethyl methane sulfonate (EMS) or targeting induced local lesions in genomes (TILLING) were some of the methods used as reverse genetics approaches (Adams and Sekelsky, 2002; Tierney and Lamour, 2005). More recently, engineered nucleases; Zinc-finger nucleases (ZFNs), Transcription activator-like effector nucleases (TALENs) and Clustered regulatory interspaced short palindromic repeats (CRISPR)/ CRISPR-associated (Cas) system, have been used as targeted genome editing methods in various organisms to investigate gene functions (Gaj *et al.,* 2013; Cong *et al.,* 2013).

The precise genome engineering of higher vertebrates is achievable by cleaving a chromosome at specific site and promoting the repair of targeted locus. These engineered nucleases enable gene editing, gene addition or gene deletions by generating double strand breaks (DSBs) at the desired locus (Galetto *et al.,* 2009). One of the two major DNA repair mechanisms, non-homologous end joining (NHEJ) or homology-directed repair (HDR), can repair these DSBs (Gaj *et al.,* 2013).

The NHEJ mechanism can re-ligate broken DNA ends without the requirement of a homologous template. Therefore, it can occur at any phase of cell cycle. The repair by the NHEJ starts with the recognition of the DNA ends and stabilisation of the essential NHEJ factors to protect the DNA ends from nonspecific processing. Then, recruitment of the DNA-PKcs enables holding the two ends together and bridging them before the end processing. DNA end processing requires different enzymes to generate ligatable ends, if it is necessary. Lastly, the final step is ligation of the broken ends by DNA ligase IV and dissolution of the NHEJ complex (Davis and Chen, 2013). The NHEJ repair mechanism is evolutionary conserved in mammalian cells to maintain the genome stability after DSBs. However, it leads to the introduction of small insertions or deletions that result in frameshift mutations and so, gene disruptions and null phenotypes (Sander *et al.,* 2011; Gupta *et al.,* 2013). In addition, the simultaneous cleavage by two nucleases has also been shown to lead to large chromosomal inversions and translocations (Brunet *et al.,* 2009; Lee *et al.,* 2012; Gupta *et al.,* 2013) (**Figure 1.17A**).

Unlike NHEJ, the HDR mechanism requires a homologous template and it only occurs during S and G2 phases of the cell cycle utilising the sister chromatid as a homologous template (Sonoda *et al.,* 2006).The repair by HDR mechanism starts with the resection of ends to generate a 3' single-stranded DNA which is essential for the homologous strand invasion. The invading 3' end serves as a primer to synthesise the new DNA strand using the intact duplex as a template. The strand invasion (D loop) dissolves in a number of different ways leading either crossover or noncrossover products (Jasin and Rothstein, 2013). Repairing by HDR pathway requires an exogenous DNA donor carrying desired genetic modifications and this exogenous DNA fragment can be replaced or inserted into the target gene locus (Jasin, 1996; Mussolino and Cathomen, 2012). Gene targeting by homology-directed repair has been successfully achieved in various organisms including zebrafish, using a single-stranded-DNA or double-stranded-DNA donors for targeted gene addition or correction (Bedell *et al.,* 2012; Zu *et al.,* 2013; Auer *et al,* 2014) (**Figure 1.17B**).

1.6.1. Zinc-Finger Nuclease (ZFN) based genome editing

Zinc-finger nucleases (ZFN) are engineered nucleases composed of a DNA-cleavage domain and a zinc-finger DNA-binding domain (Durai *et al.,* 2005; Porteus and Carroll, 2005). Zinc fingers are responsible for coordinating zinc ions with a combination of zinc ligands to stabilise folding and binding to DNA, RNA or other small molecules. Cys_2-His_2 zinc finger consists of approximately 30 amino acids in a conserved ββα structure and a single zinc finger recognises 3bp sequence by the several amino acids on its α-helix structure (Pavletich and Pabo, 1991; Porteus and Carroll, 2005). ZFNs are usually formed of 3 to 6 zinc-fingers, which can recognise 9 to 18 bp in length (Gaj *et al.,* 2013). In addition, the type IIS restriction endonuclease *FokI* is used as the cleavage domain. It cleaves DNA non-specifically and binds to DNA separately from the zinc-finger domain (Li *et al.,* 1992). However, dimerisation is necessary for the cleavage; therefore, a pair of ZFNs, which bind to the target sequences on opposite strands of DNA are required (Smith *et al.,* 2000). Hence, the *FokI* nuclease is typically fused to the C-terminus of zinc-finger domain with the requirement of 5-7 bp of a spacer region between the binding sites of zinc-finger domains for the cleavage of DNA spacer region (Carroll, 2011; Gaj *et al.,* 2013).

ZFN-mediated gene targeting has been reported for many organisms and *in vitro* cells including zebrafish, fruit fly, mouse, rat and human cells (Bibikova *et al.,* 2002; Bibikova *et al.,* 2003; Doyon *et al.,* 2008; Meyer *et al.,* 2010; Cui *et al.,* 2011; Mashimo *et al.,* 2010; Urnov *et al.,* 2005; DeKelver *et al.,* 2010; Kim and Kim, 2014). However, low specificity and efficiency, limited number of target regions, high off-target effects and time consuming design have reduced the use of ZFNs, significantly (DeFrancesco, 2011; Kim and Kim, 2014).

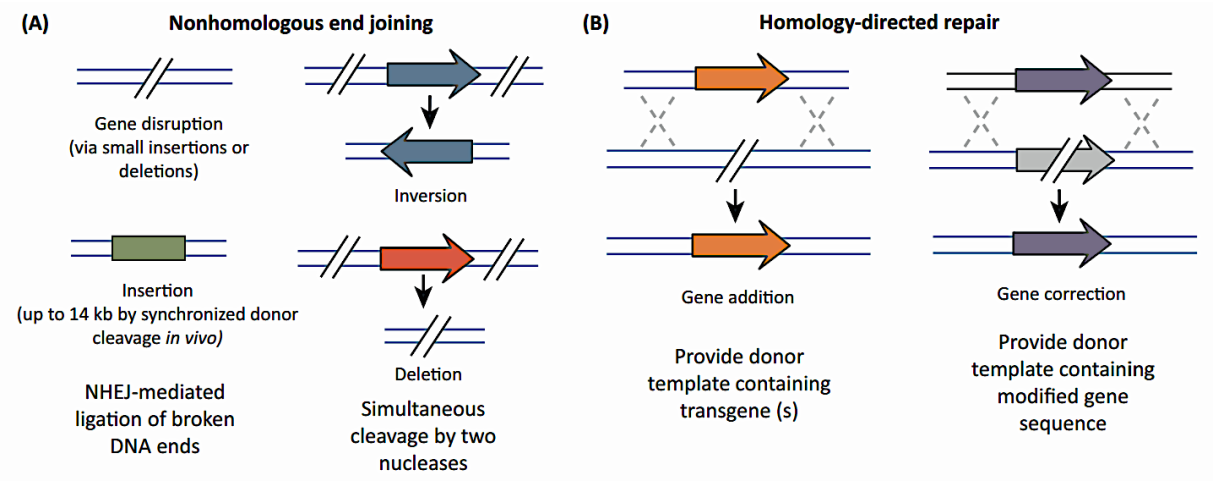


Figure 1.17 Possible genome editing pathways using locus-specific engineered nucleases or CRISPR/Cas system. Non-homologous end joining (NHEJ) or homology-directed repair (HDR) mechanisms can repair nuclease-induced DSBs at the targeted locus. **(A)** NHEJ repair mechanism can be used for gene disruptions, insertions, inversions or deletions, in a homology-independent manner. **(B)** HDR mechanism can be used for gene additions or corrections in a homology-dependent manner using a donor DNA as a template. Adapted from (Gaj *et al.,* 2013).

1.6.2. Transcription Activator-Like Effector Nuclease (TALEN) based genome editing

Recently, a novel approach based upon transcription activator-like effectors (TALEs) from *Xanthomonas* plant pathogen has been suggested (Boch *et al.,* 2009; Moscou *et al.,* 2009). TALEs are transcriptional activators regulating plant genes to facilitate pathogenesis of the plants (Bogdanove *et al.,* 2010). TALE structure is composed of a N terminal translocation domain, C terminal activation domain and a central DNA binding domain which is formed of 33-35 amino acid repeat domains, each recognising one target base (Miller *et al.,* 2011). The specificity of TALE structures is determined by two adjacent amino acids at positions 12 and 13 which are known as the repeat variable di-residue (RVD). The RVD harbours a simple code allowing each repeat to recognise its target base (Wei *et al.,* 2013). The TALEs can be generated through the addition of repeat domains together for recognising target sequences specifically by this code (Boch *et al.,* 2009).

Fusion of TALE and non-specific *FokI* endonuclease is referred to as TALE nucleases (TALENs) (Li *et al*., 2010). TALENs are designed as pairs to bind to the adjacent target sequences and the spacer sequence of varying length (12-20bp) exists between these target sequences. The active *FokI* endonuclease performs as a dimer and cleaves the DNA spacer region which in turn generates DSBs (Ding *et al.,* 2013). Gene targeting using TALENs has been adopted for various organisms such as zebrafish (Sander *et al.,* 2011, Huang *et al.,* 2011; Bedell *et al.,* 2012; Dahlem *et al.,* 2012; Gupta *et al.,* 2013), fruit fly (Liu *et al.,* 2012), rat (Tesson *et al.,* 2011) and human cells (Hockemeyer *et al.,* 2011). Comparing to ZFNs, TALENs are more specific and efficient in generating mutations since low off-target effects were reported for TALENs. Golden Gate cloning (Zhang *et al.,* 2011; Weber *et al.,* 2011; Cermak *et al.,* 2011) and PCR based TALE toolbox (Sanjana *et al.,* 2012) construction methods facilitated rapid and specific design of TALEs which makes it more useful than ZFNs (Kim and Kim, 2014).

1.6.3. Clustered Regularly Interspaced Short Palindromic Repeats (CRISPR)/ CRISPR-associated (CRISPR-Cas) based genome editing

Type II clustered regularly interspaced short palindromic repeats (CRISPR) and CRISPR-associated (Cas) system is the newest engineered nuclease method for targeted genome editing. CRISPR sequences and Cas proteins are the components of the prokaryotic adaptive defence mechanism of bacterial and archeal genomes (Horvath and Barrangou, 2010; Garneau *et al*., 2010). CRISPR sequences are inheritable DNA-encoded memory mechanism of the immune system, formed of short DNA repeats separated by unique spacer sequences that are acquired from previous infections (Bolotin *et al.,* 2005). Cas proteins are encoded by

the gene clusters located close to the CRISPR locus (Jansen *et al.,* 2002). Cas proteins are the endonucleases that process CRISPR sequences into small RNAs (crRNAs) and form a Cas-crRNA complex to cleave the infectious DNA sequences which are complementary to the crRNA (Jore *et al.,* 2011; Gasiunas *et al.,* 2012).

To use this prokaryotic defence mechanism as a genome editing tool, the crRNA and the tracrRNA (trans-activating CRISPR crRNA) are fused into a guide RNA (sgRNA). This sgRNA can be complementary to any genomic locus followed by a 5' NGG protospacer-adjacent motif (PAM) (Jinek *et al.,* 2012). Cas9 nuclease is the final effector cleaving both strands of DNA after recognising the homologous base pair matching between the target sequence and the 20 nucleotide sequence within the sgRNA (Gasiunas *et al.,* 2012; Jinek *et al.,* 2012; Charpentier and Doudna, 2013).

The CRISPR-Cas system has been adopted for many organisms and *in vivo* cells including zebrafish, mice and human or bacterial cells (Charpentier and Doudna, 2013; Wu *et al.,* 2013; Auer *et al,* 2014; Yang *et al.,* 2014). Compared with ZFNs and TALENs, CRISPR-Cas system is cheaper, easier to design, less time-consuming, more efficient and more precise (Seruggia and Montoliu, 2014; Kim and Kim, 2014). However, minimal off-target reports interrogating the specificity have prompted the scientists into a research to find a safer approach of CRISPR-Cas system (Fu *et al.,* 2013). In this case, alternative design of sgRNAs such as two offset gRNAs together or a truncated sgRNA were suggested by different research groups which will improve the specificity of genome editing (Ran *et al.,* 2013; Fu *et al.,* 2014).

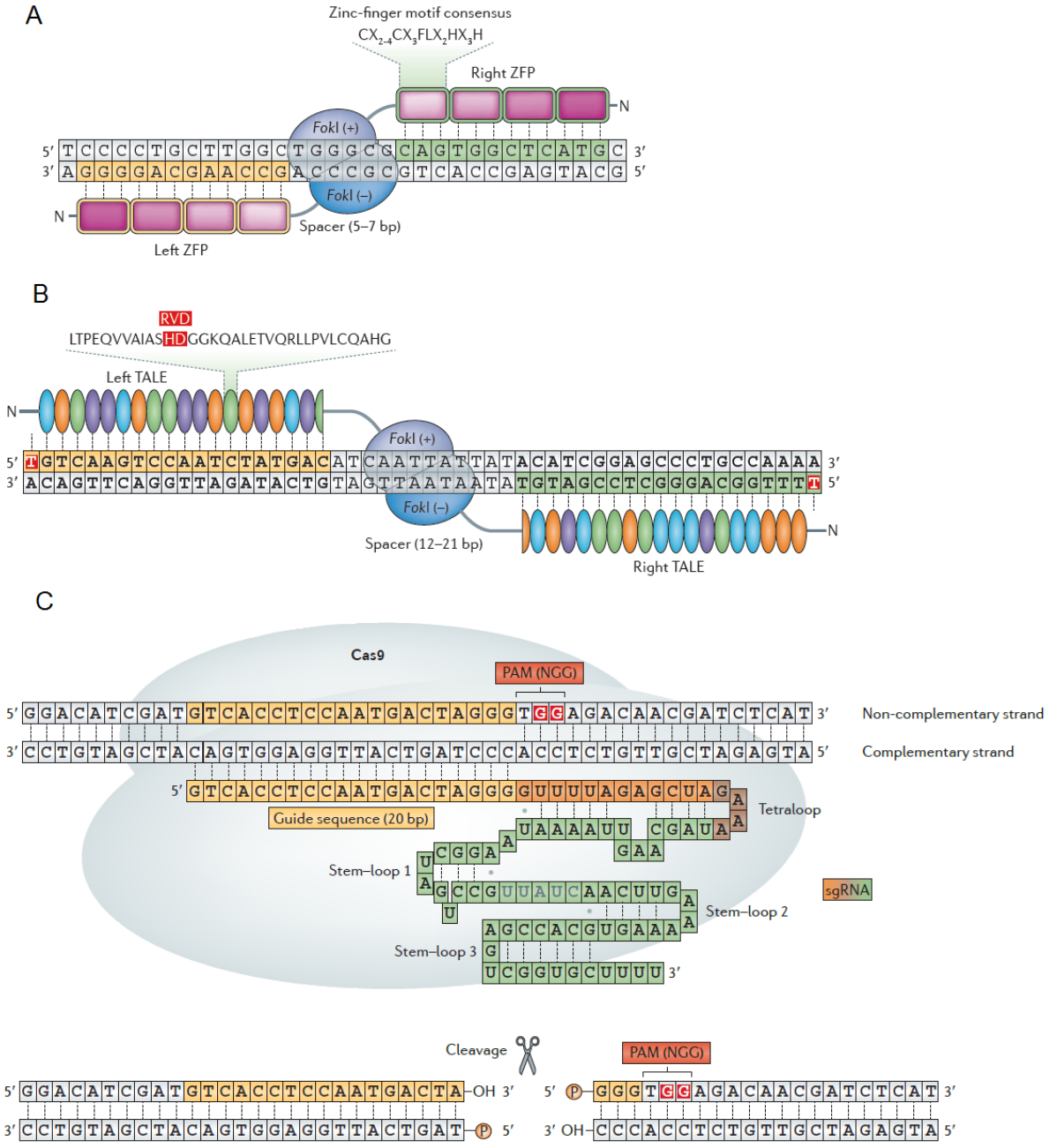


Figure 1.18 Schematic representations of engineered nucleases. (A) Each zinc-finger nuclease (ZFN) contains an N-terminal zinc-finger protein and a C-terminal *FokI* nuclease that recognises 18-36bp target sequences in length. In the zinc-finger motif consensus, X represents any amino acid and each zinc-finger recognises 3bp sequence. **(B)** Each Transcription Activator-Like Effector Nuclease (TALEN) contains an N-terminal TALE and a C-terminal *FokI* nuclease that targets 30-40bp in length. Each TALE repeat is formed of 33-35 amino acids that recognises a single base pair through the amino acids at positions of 12 and 13. **(C)** Clustered Regularly Interspaced Short Palindromic Repeats (CRISPR)-Cas system is composed of a guide RNA (sgRNA) that recognises a 20bp target sequence followed by a protospacer adjacent motif (PAM); 5' NGG 3' and a Cas9 nuclease that recognises the PAM sequence to cleave the DNA at the target region. Adapted from (Kim and Kim, 2014).

1.7. Identification of proximal and interacting proteins in mammalian cells by using BioID technique

Recently, a new technique, proximity-dependent **bio**tin **id**entification, BioID, was developed to study *in vivo* protein-protein interactions in mammalian cells and to unravel the complex biological processes. BioID is based on the biotin-labelling of interacting or proximal proteins of a target protein and subsequent identification of these biotin-labelled proteins by mass spectrometry. Introduction of the fusion, formed of a promiscuous *Escherichia coli* biotin ligase, BirA R118G and a bait protein, into the mammalian cell will biotinylate the proximal and interacting proteins of the target protein. The biotinylated proteins can then be isolated by streptavidin-based affinity purification and identified by mass spectrometry (MS) (Roux *et al.,* 2012) **(Figure 1.19)**.

The BioID method has been attested as an efficient method to study protein-protein interactions since it has been used in various studies ranging from cancer development (Dingar *et al.,* 2015) to signalling pathway mechanisms (Zhou *et al.,* 2015). Considering the suggested roles of DEF6 in T cells (Section 1.5.2.1), human DEF6 protein and its truncated domains were fused to BirA R118G to understand its interactions and possible roles in Jurkat T cells (Chapter 7).

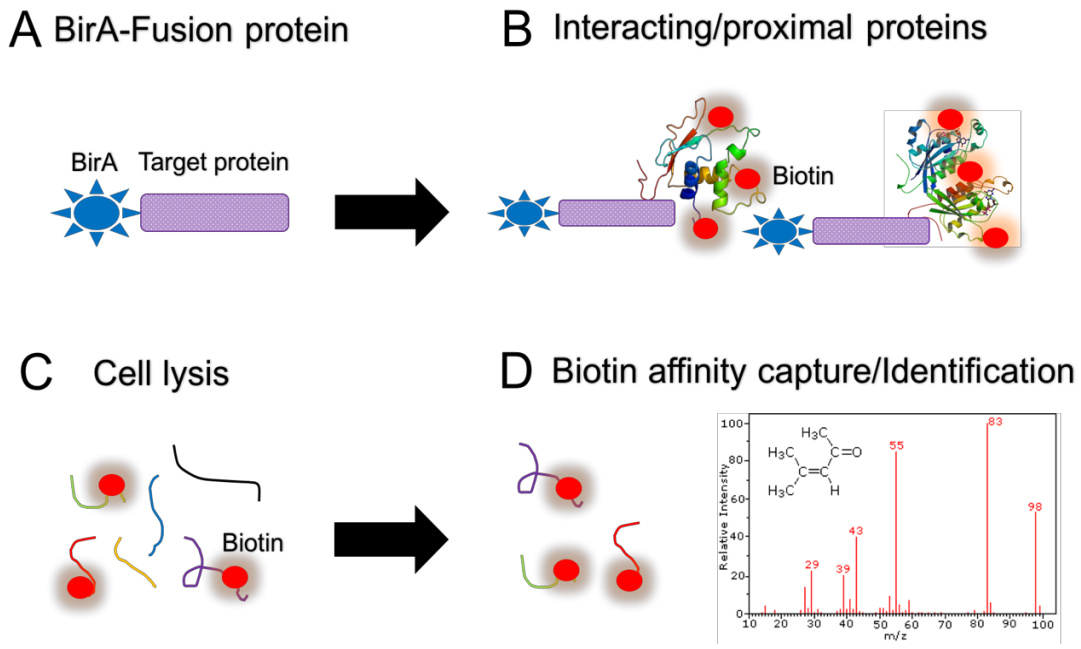


Figure 1.19 Schematic representation demonstrating the application of BioID method. **(A)** The fusion protein composed of a BirA biotin ligase and a target protein is generated to understand the possible interaction in mammalian cells. **(B)** The expression of the fusion protein in live mammalian cells to biotinylate the interacting and proximal proteins. **(C)** Cell lysis and protein denaturation are carried out to facilitate the affinity capture. **(D)** Streptavidin beads-mediated isolation and mass spectrometry based identification of the biotinylated proteins will reveal the indirect or direct protein interactions and vicinal proteins.

1.8. Research aims and objectives

Research aims

DEF6 and SWAP70 act as GEFs for Rho GTPases to regulate the actin cytoskeleton and cell polarity in various cell types. However, the spatial and temporal expression pattern of their zebrafish orthologous, *def6a and swap70b,* during zebrafish embryogenesis suggested additional roles in vertebrate development. Preliminary analyses by MO-mediated knock-down of *def6a* and *swap70b* revealed that Def6a and Swap70b regulate CE cell movements of gastrulation acting downstream of Wnt5b and Wnt11, respectively, in the Wnt/PCP signalling pathway. As MOs often show off-target effects causing false phenotypes it is important to establish mutant zebrafish using genome editing. TALEN-mediated establishment of single *def6a, swap70b* and double *def6a; swap70b* homozygous mutant lines enabled the analysis not only during embryogenesis but also in the adult fish. In addition to its role in actin cytoskeleton and embryogenesis, various distinct roles of DEF6 in the immune system, cancer and mRNA translation have been reported. Therefore, the aims of this study are (i) to understand the functions of *def6a* and *swap70b* in zebrafish embryonic development, (ii) to determine the putative roles of *def6a* and *swap70b* in adult haematopoiesis and (iii) to reveal the biological processes that DEF6 may be involved in Jurkat T cells by analysing BioID-mediated identification of DEF6 interactome.

Research objectives

- To generate single (*def6a*$^{qmc811/qmc811}$, *swap70b*$^{qmc809/qmc809}$) and double knock-out mutant lines (*def6a*$^{qmc811/qmc811}$; *swap70b*$^{qmc809/qmc809}$) by injecting TALENs into *def6a* and *swap70b* loci

- To investigate the loss of function effects of *def6a* and/or *swap70b* during early embryogenesis by phenotypic and whole mount *in situ* hybridisation analyses on single and double homozygous mutant lines

- To determine the downstream effectors of Def6a and Swap70b were in the non-canonical Wnt/PCP signalling pathway by overexpressing Rho GTPases in single mutant lines

- To determine the loss of function effects of *def6a* and/or *swap70b* on the transcriptional control of *wnt5b* and *wnt11*

- To determine the potential roles of *def6a* and *swap70b* in adult zebrafish haematopoiesis by FACS sorting of kidney marrow cells

- To understand the potential roles of DEF6 in Jurkat T cells by analysing BioID-identifed DEF6 interactome

CHAPTER 2

MATERIALS & METHODS

2.1. Materials

2.1.1. Molecular biology and microbiological materials

2.1.1.1. Plasmids

Genes	TALEN plasmids		Source
	Left	**Right**	
def6a	Plasmid #47139: TAL3420	Plasmid #47140: TAL3421	Dr. J. Keith Joung Obtained from Addgene
swap70b	Plasmid #47285: TAL3566	Plasmid #47286: TAL3567	Dr. J. Keith Joung Obtained from Addgene

Table 2.1 Left and right TALEN plasmids of *def6a* and *swap70b* genes.

Gene locus	Left TALEN (5'→3')	Right TALEN (5'→3')	Spacer (5'→3')	Restriction site (5'→3')
def6a	TCAGAACTGCTCAAGTCC (18bp)	CAGCTCTGGATGTGGAGA (18bp)	ATTTG**GTAC**GCTTTCA (16bp)	*RsaI* GTAC
swap70b	TAAGGGACGAGCTTCTC (17bp)	CCTTCACAGCCCTGGA (16bp)	AAGGCAATCTGG**CA****TG** (16bp)	*NlaIII* CATG

Table 2.2 Left and right TALEN mRNA sequences targeting Exon-1 of *def6a* and *swap70b* loci. *RsaI* restriction site (GTAC) for *def6a* and *NlaIII* restriction site (CATG) for *swap70b* were selected for genotyping.

Plasmid for blunt PCR cloning	Source
pSC-B-amp/kan	Agilent Technologies (#240207)

Table 2.3 StrataClone blunt PCR cloning vector.

Plasmids for biotinylation	Source
pEGFP-C2/DEF6 Full-length	Dr. K. J. Mavrakis From laboratory stock
pcDNA3.1 mycBioID	Dr. Kyle J. Roux Obtained from Addgene (#35700)

Table 2.4 Plasmids for biotinylation of proximal and interacting proteins of DEF6 in Jurkat T cells.

Gene	Plasmids	Restriction Endonuclease	RNA Polymerase
cdc42	*GFP*/pβUT3	*EcoRI*	T3
gfp	*GFP*/pβUT3	*SfiI*	T3
racI	*GFP*/pβUT3	*EcoRI*	T3
rhoA	*GFP*/pβUT3	*EcoRI*	T3

Table 2.5 Plasmids for sense mRNA synthesis

2.1.1.2. Solutions, buffers and reagents

Solutions and Buffers	Composition
50x Base Solution for HotShot DNA Preparation from caudal fin or embryo	1.25M NaOH 10mM EDTA 50g of NaOH crystals and 20ml 0.5M EDTA, up to 1L with dH_2O. (~pH 12) Autoclave sterilised. Working concentration is 1x Base solution.
60x E3 Zebrafish Medium	17.4g NaCl 0.8g KCl 2.9g $CaCl_2 \cdot 2H_2O$ 4.89g $MgCl_2 \cdot 6H_2O$ Up to 1L of dH_2O. pH 7.2 Autoclave sterilised. Working solution is 1X medium (1L). 100 µL of 1% methylene blue (Sigma-Aldrich)
Luria-Bertani (LB) Agar	3g NaCl 3g Bacto-tryptone 1.5g Yeast Extract 4.5g Agar Add dH_2O up to 300ml. Autoclave sterilised.
LB Medium	10g Bacto-tryptone 5g Yeast Extract 10g NaCl Add dH_2O up to 1L. pH 7.5 Autoclave sterilised.
MS222 (Tricaine Methanesulfonate)	4g MS222 in 1L dH_2O pH 7.0
50x Neutralisation Solution for HotShot DNA Preparation from caudal fin or embryo	2M Tris-HCl 315.2g TRIS-HCl in 1L dH_2O. (~pH 5) Autoclave sterilised. Working concentration is 1x Neutralisation solution.
SOC medium	0.5% Yeast Extract 2% Tryptone 10 mM NaCl 2.5 mM KCl 10 mM $MgCl_2$ 10 mM $MgSO_4$ 20 mM Glucose Add dH_2O up to 1L.

3M Sodium acetate	40.8g $CH_3COONa.3H_2O$ 100ml dH_2O pH 5.2
10x TBE (Tris-Borate-EDTA) Buffer	108g Tris base 55g Boric acid 40ml 0.5M EDTA (pH 8.0) Up to 1L with dH_2O. Working concentration is 1x TBE buffer.

Table 2.6 Prepared buffers and solutions

Solutions, Buffers and Reagents	Composition	Company
Agarose powder	**1.5% agarose gel** 1.5% (w/v) agarose powder in 1X TBE buffer, 10% (v/v) SafeView stain	Sigma-Aldrich (#A9539)
Alexa Fluor 568 Phalloidin	-	Life Technologies (#1320997)
Antibiotics (Ampicillin/Kanamycin)	**Ampicillin** stock; 100mg/ml in dH_2O. Working concentration is 100µg/ml. **Kanamycin** stock; 60mg/ml in dH_2O. Working concentration is 30µg/ml.	Sigma-Aldrich (#A9518) Sigma-Aldrich (#B5264)
BSA (Bovine Serum Albumin)	20 mM Tris-HCl 100 mM KCl 0.1 mM EDTA 50% Glycerol pH 8.0	New England Biolabs (NEB)
Chloroform	100%	Fisher Scientific
10x CutSmart Buffer	**1x Buffer Components** 50mM Potassium Acetate 20mM Tris-acetate 10mM Magnesium Acetate 100µg/ml BSA pH 7.9	New England Biolabs (NEB) (#B7204S)
1kb DNA Ladder	(500bp to 10,002bp) 10 mM Tris-HCl 1 mM EDTA pH 8.0	New England Biolabs (NEB) (#N3232S)
100bp DNA Ladder	(100bp to 1,517bp) 10 mM Tris-HCl 1 mM EDTA pH 8.0	New England Biolabs (NEB) (#N3231S)
6x DNA Loading Dye (Purple)	**1x Dye Components** 2.5% Ficoll-400 10mM EDTA 3.3mM Tris-HCl 0.08% SDS 0.02% Dye 1 (purple/pink) 0.001% Dye 2 (blue) pH 8.0	New England Biolabs (NEB) (#B7024S)

DNaseZap	-	Ambion (#9890)
dNTP Mix	10mM of dATP, dCTP, dGTP and dTTP in water.	Promega (#U151A)
10x *EcoRI* Buffer	**1x Buffer Components** 100mM Tris-HCl 50mM NaCl 10mM $MgCl_2$ 0.025% Triton X-100 pH 7.5	New England Biolabs (NEB) (#R0101S)
Ethanol	100% Ethanol diluted with dH_2O for lower concentrations (70%)	Sigma-Aldrich
Isopropanol	100%	Sigma-Aldrich
Methanol	100%	Sigma-Aldrich
Phenol:Chloroform:Isoamylalcohol (25:24:1)	-	VWR Chemicals (#101174-118)
RNaseZap	-	Ambion (#AM9780)
2x RNA Loading Dye	**1X Dye Components** 47.5% Formamide 0.01% SDS 0.01% bromophenol blue 0.005% Xylene Cyanol 0.5mM EDTA	New England Biolabs (NEB) (#B0363S)
SafeView Nucleic Acid Stain	10% (v/v) in 1x agarose gel before pouring	NBS Biologicals (#NBS-SV1)
10x T4 DNA Ligase Buffer	**1x Buffer Components** 50mM Tris-HCl 10mM $MgCl_2$ 1mM ATP 10mM DTT pH 7.5	New England Biolabs (NEB) (#M0202)
5x Q5 Reaction Buffer	**-**	New England Biolabs (NEB) (#B9027S)

Table 2.7 Buffers, solutions and reagents

2.1.1.3. Reaction kits

Reaction kits	Company
GenElute Plasmid Mini-Prep Kit	Sigma-Aldrich (#PLN70-1KT)
Maxi-prep Kit (Tip-500)	Qiagen (#12963)
mMESSAGE mMACHINE T7/T3 Transcription Kit	Ambion (#AM1344)/ (#AM1348)
Nucleospin Gel and PCR Clean-up Kit	Macherey-Nagel (#740609.50)
StrataClone Blunt PCR Cloning Kit	Agilent Technologies (#240207)
Superscript II Reverse Transcriptase (RT)	Invitrogen (#18064014)

Table 2.8 Reaction kits

2.1.1.4. Enzymes

Enzymes	Company
***AflII* Restriction Endonuclease**	New England Biolabs (NEB) (#R0520)
***BamHI* Restriction Endonuclease**	New England Biolabs (NEB) (#R3136)
***EcoRI* Restriction Endonuclease**	New England Biolabs (NEB) (#R3101)
***EcoRV* Restriction Endonuclease**	New England Biolabs (NEB) (#R3195)
***HindIII* Restriction Endonuclease**	New England Biolabs (NEB) (#R0104)
***NlaIII* Restriction Endonuclease**	New England Biolabs (NEB) (#R0125)
***NotI* Restriction Endonuclease**	New England Biolabs (NEB) (#R0189)
***PmeI* Restriction Endonuclease**	New England Biolabs (NEB) (#R0560)
***PstI* Restriction Endonuclease**	New England Biolabs (NEB) (#R0140)
***RsaI* Restriction Endonuclease**	New England Biolabs (NEB) (#R0167)
***SfiI* Restriction Endonuclease**	New England Biolabs (NEB) (#R0123)
***XhoI* Restriction Endonuclease**	New England Biolabs (NEB) (#R0146)
DNaseI	Ambion (#AM2222)
SP6 RNA Polymerase	New England Biolabs (NEB) (#M0207)
T4 DNA Ligase	New England Biolabs (NEB) (#M0202)
T3 RNA Polymerase	New England Biolabs (NEB) (#M0378)
T7 RNA Polymerase	New England Biolabs (NEB) (#M0251)
Q5 Hot Start High-Fidelity DNA Polymerase	New England Biolabs (NEB) (#M0493)

Table 2.9 Enzymes

2.1.1.5. Competent cells

Competent Cells	Company
NEB-5-alpha Competent *E.coli* Cells	New England Biolabs (NEB) (#C2688J)
StrataClone SoloPack Competent Cells	Agilent Technologies (#240207)

Table 2.10 Competent cells

2.1.2. Technical equipment

Equipment Name	Company
Autoradiography Film Cassette	Harmer
Balance DP-300 (300 x 0.01g)	Fisherbrand
BTXECM 830 Electroporator	Harvard Apparatus Inc
Class II Microbiological Safety Cabinet	Walker Safety Cabinet Limited
CO_2 Air-Jacketed Incubator	Nuaine DH Autoflow
Coverslips (0.13-0.17mm)	Cover Glass
Discovery Bioscience Rotary Mixer Cell	Stuart Scientific
Dri-block DB-2A Heating Block	Techne
Dual-intensity UV transilluminator	UVP, LLC
Electrophoresis Power Supply-EPS 300	Pharmacia Biotech
Gibco BRL Horizontal Gel Electrophoresis Apparatus	Life Technologies
Hybond-P PVDF Membranes	Amersham/Millipore
Medical X-ray Blue Film	Scientific Laboratory Supplies; Carestream
Microfuge	Sigma
Micromax RF Centrifuge	International Equipment Company (IEC)
Microscope Slides (1.2mm)	VWR
Mini Protean 3 System Short Glass Plates	Bio-Rad
Mini Protean 3 System Spacer Glass Plates with 1.5mm spacers	Bio-Rad
Miximatic Vortex	Jencons
Molecular Imager Gel Doc XR System	Bio-Rad
Nanodrop Spectrophotometer ND1000	Nanodrop
Orbital Incubator SI50	Stuart Scientific
PCR Thermal Cycler	Takara
pH210 Microprocessor pH Meter	Hanna Instruments
Pipettes (0.2-2 µl, 2-20 µl, 50-200 µl, 200-1000 µl, 1000-5000 µl)	Gilson
Power-Pac 300 Power Supply	Bio-Rad
Sponges	GE Healthcare; Whatman
Transblot SD Semi-Dry Transfer Cell	Bio-Rad
Vibra-Cell Sonicator	Jencons
Video Graphic Printer UP-890CE	Sony

Water Bath	Jencons

Table 2.11 Technical equipment

2.1.3. Zebrafish and microinjection equipment

Wild-type (WT) zebrafish, *Danio rerio,* are maintained at 28.5^{0}C in a cycle of 14 hours light, 10 hours dark in system water (Westerfield, 2000).

Microinjection Equipment Name	**Company**
Flamming/brown Micropipette Puller Model P-97	Sutter Instrument Company
Glass Capillaries (1.0 mm OD x 0.58 mm)	Harvard apparatus
Incubators (28.5^{0}C; 22°C; 31°C)	Griffin
Microinjection pipette	Drummond Nanoject II Automatic Nanolitre Injector
Microloader (0.1 µl – 20 µl)	Eppendorf
Nitrogen (oxygen free)	BOC
Parafin Oil (Mineral Oil)	Eppendorf
Picospritzer Micro Injector	Intracel
Microscopes for Microinjection and Visualisation	**Company**
Camera DS-5MC	Nikon
Cold Light Sources KL1500 LCD	Zeiss
Digital sight DS-U1	Nikon
Eyepieces C-W10X A/22	Nikon
Eyepieces W-PI10x/23 Br. Foc	Zeiss
Lsm710 Confocal Microscope	Zeiss
Lsm Exciter Confocal Microscope	Zeiss
Stereomicroscope SMZ1500	Nikon
Stereomicroscope Stemi 2000-C	Zeiss
Stereomicroscope Stemi SV 6	Zeiss

Table 2.12 Microinjection equipment and microscopes

2.1.4. Whole mount *in situ* hybridisation materials

Solutions, Buffers and Reagents	Composition	Company
Anti-Digoxigenin-AP Fab fragments Antibody	-	Roche (#11093274910)
BCL Buffer III	0.1M Tris-HCl pH 9.5 0.1M NaCl 50mM MgCl2 0.1% Tween 20	-
Blocking Reagent	2% blocking reagent dissolved in MABT	Roche (#11096176001)
BM-Purple Staining	1:1 dilution with BCL Buffer III	Roche (#11442074001)
DIG RNA Labelling Mix	-	Roche (#11277065910)
Formamide	-	Sigma-Aldrich (#F9037)
Glycerol	90% Glycerol 50% Glycerol in PBST 30% Glycerol in PBST	-
Hybridisation Buffer (Hybe+)	50% Deionised Formamide 5x SSC 0.5mg/ml Yeast tRNA 50mg/ml Heparin 9.2mM Citric acid 0.1% Tween 20	-
Maleic acid Buffer (MAB)	0.1M Maleic acid 0.15M NaCl pH 7.5	Sigma-Aldrich
Maleic acid buffer-Tween (MABT)	0.1% Tween 20 in MAB	-
Methanol	100% Methanol 75% Methanol in PBST 50% Methanol in PBST 25% Methanol in PBST	Sigma-Aldrich
Phosphate Buffered Saline (PBS)	8g of NaCl 0.2g of KCl 1.44g of Na_2HPO_4 0.24g of KH_2PO_4 Add dH_2O up to 1L pH 7.4 Autoclave sterilised	-
Phosphate Buffered Saline- Tween (PBST)	0.1% Tween 20 in PBS	-
Paraformaldehyde (PFA)	4% PFA (w/v) in 1x PBS	Sigma-Aldrich (#P6148)
Proteinase K	10mg/ml stock solution in PBST in 100µl aliquots. Final concentration for embryo permeabilisation is 10µg/ml	Roche (#P2308)

PTU (1-phenyl-2-thiouria)	0.03% 1-phenyl-2-thiourea in 1xPBS Diluted to 0.003% in system water or 1x E3 fish medium	Sigma-Aldrich (#P7629)
Sodium Sulphate Saline (SSC)	**20x SSC** 3M NaCl 300mM Sodium Citrate Diluted to 1x SSC with dH_2O	-
Sodium Sulphate Saline-Tween (SSCT)	0.1% Tween 20 in SSC	-
tRNA from Baker's yeast	-	Roche (#10109495001)

Table 2.13 Whole mount *in situ* hybridisation materials

Gene	Restriction Endonuclease	RNA Polymerase	Source
bmp2b	*EcoRI*	T3	Paul Scotting
chordin	*NotI*	T7	Martin Gering
cdx4	*BamHI*	T7	Martin Gering
dlx3	*EcoRV*	T7	Steve Wilson
fgf8a	*EcoRV*	SP6	Simon Hughes
hgg1	*XhoI*	T3	Steve Wilson
hoxb1a	*NcoI*	SP6	Project students
krox20	*PstI*	T7	Paul Scotting
myoD	*BamHI*	T7	Simon Hughes
ntl	*XhoI*	T7	Martin Gering
pax2	*BamHI*	T7	Martin Gering
shh	*HindIII*	T7	Martin Gering
wnt5b	*ApaI*	SP6	Project students
wnt11	*NcoI*	SP6	Project students

Table 2.14 Antisense mRNA probes synthesised from listed genes for *in situ* hybridisations

2.1.5. Fluorescence activated cell sorting (FACS) materials

Solutions, Buffers and Reagents	Composition	Company
Hank's Balanced Salt Solution (HBSS)	**1x HBSS** 10ml of 10x HBSS 90ml of dH_2O	-
FCS/PBS	4.5ml of 10x PBS 2.5ml of FCS 43ml of dH_2O	-

Table 2.15 FACS buffers

2.1.6. Cell culture, Western blotting, co-immunoprecipitation and immunostaining materials

Cell Lines	Source
Jurkat E6.1 human leukemic T cell lymphoblast line	The European Collection of Cell Cultures (ECACC) #88042803
Raji human B cell line	Raji human B cell lymphoblasts (Sigma #85011429)

Table 2.16 Cell lines

Solutions, Buffers and Reagents	Composition	Company
Cell Culture and Transfection		
Biotin Powder	-	Sigma-Aldrich (#B4639)
10x Foetal Bovine Serum (FBS)	-	Sigma-Aldrich (#F9665)
Penicillin-Streptomycin	10.000 U/ml penicillin and 10.000 µg/ml streptomycin diluted 1:9 in 1XPBS	Gibco (Life Technologies) (#15140122)
Roswell Park Memorial Institute 1640 (RPMI) medium	with sodium bicarbonate and L-glutamine	Sigma-Aldrich (#R8758)
SDS-PAGE and Western blotting		
Albumin fraction V from Bovine Serum (BSA)	-	VMR Chemicals (#441555J)
Anti-biotin, HRP linked Antibody	10Mm Sodium HEPES (Ph 7.5) 150Mm NaCl 2mg/ml BSA 50% Glycerol	Cell Signaling Technology (CST) (#7075P5)
Anti-mouse IgG, HRP-linked antibody	-	Cell signalling Technology (CST)(#7076S)
Anti-rabbit polyclonal to myc tag	-	Abcam (#ab13836)
Anti-rabbit IgG, HRP-linked antibody	-	Cell 81pprox.81ng Technology (CST)(#7074S)
β-actin (8H10D10) mouse ab	-	Cell 81pprox.81ng Technology (CST) (#3700S)
Biotinylated Protein Ladder	62.5M TRIS-HCl (Ph 6.8) 2% SDS(w/v) 40Mm Dithiothreitol (DTT) 0.01% (w/v) Phenol Red 10% Glycerol	Cell Signalling Technology (CST) (#7727)
Butanol	100% Butanol	Sigma-Aldrich
Enhanced ChemiLuminescence (ECL) Reagents	-	ECL, Amersham (#RPN2232)
2x Laemmli Sample Buffer	4% SDS 20% glycerol	

	10% 2-mercaptoethanol, 0.004% bromphenol blue 0.125 M Tris HCl, pH approx. 6.8	Sigma-Aldrich (#S3401)
PageRuler Prestained Protein Ladder	10 to 180kDa	Fermentas (#26616)
Paper Developer	-	Ilford PQ Universal (#1155091)
10x PBS (Phosphate Buffer Saline)	80g of NaCl 2.0g of KCl 14.4g of Na_2HPO_4 2.4g of KH_2PO_4 Add dH_2O up to 1L Ph 7.4 Autoclave sterilised	-
PBST	PBS+ 0.01% Tween-20 (10µl Tween 20 in 100ml) PBS+0.1% Tween 20 (100µl Tween 20 in 100ml)	-
Resolving Solution for 10% SDS-PAGE	30% Acrylamide mix 1.5M Tris (8.8) 10% SDS (Sodium dodecyl sulfate) 10% APS (Ammonium persulfate) TEMED dH_2O	-
10x RIPA buffer	20 Mm Tris-HCl (Ph 7.5), 150 Mm NaCl, 1 Mm Na_2EDTA, 1 Mm EGTA, 1% NP-40, 1% sodium deoxycholate, 2.5 Mm sodium pyrophosphate, 1 Mm beta-glycerophosphate, 1 Mm Na_3VO_4, 1 µg/ml leupeptin, 1Mm PMSF Diluted to 1X with dH_2O	Cell Signalling Technology (CST) (#9806)
Stacking Solution for 10% SDS-PAGE	30% Acrylamide mix 1.0M Tris (6.8) 10% SDS 10% APS TEMED H_2O	-
10x SDS Running Buffer	1.87M glycine, 250Mm Tris and 0.1% (w/v) SDS diluted 1:9 to give a 1x working buffer.	-
Streptavidin, Alkaline Phosphatase (AP)	Streptavidin Alkaline Phosphatase in PBS, 1mg/ml BSA, 1Mm MgCl2, 0.1Mm ZnCl2 and 0.02% sodium azide	Promega (#V559C)
Streptavidin, HRP	136Mm NaCl, 2.6Mm KCl, 12Mm sodium phosphate	Cell Signalling Technology (CST) (#3999)

	(Ph 7.4) dibasic, 2mg/ml BSA, 50% glycerol	
Transfer Buffer	7.57g Tris 36.02g Glycine in 1500ml of dH_2O 500ml Methanol	-
Western Blue Stabilized Substrate for Alkaline Phosphatase	Mixture of 5-bromo-4-chloro-3-indolyl-phosphate (BCIP) and nitro blue tetrazolium (NBT) in a proprietary stabilizing buffer	Promega (#S3841)
Affinity Capture for MS		
50Mm ammonium bicarbonate	0.040g NH_4HCO_3 to 10 Ml of dH_2O. Ph 7.8 Filter sterilised	Sigma-Aldrich
Dynabeads MyOne Streptavidin C1	Dynabeads are supplied in PBS, Ph 7.4 with 0.01% Tween-20 and 0.09% NaN_3.	Invitrogen (#65001)
Immunostaining and IS formation		
Anti-CORO1A Antibody Mouse Monoclonal	1:250 dilution in blocking solution	Abcam (#ab56820)
Anti-DEF6 Antibody Rabbit Monoclonal	1:250 dilution in blocking solution	Abcam (#126792)
Anti-HNRNPA2B1 Antibody Mouse Monoclonal	1:250 dilution in blocking solution	Abcam (#ab6102)
Anti-Mouse IgG (H+L), Alexa Fluor 488	1:500 dilution in blocking solution	Life Technologies (#A-11008)
Anti-Rabbit IgG (H+L), Alexa Fluor 568	1:500 dilution in blocking solution	Life technologies (#A-11011)
Blocking Solution	3% (w/v) BSA in 1x PBS	-
Calcein Blue	1μg/ml in 1 ml RPMI medium	Life Technologies (#C1429)
Fixing Solution	4% (w/v) PFA in 1x PBS	-
Mounting Solution	FluoroGel Mounting Medium	GeneTex (#821701106)
Permeabilisation Solution	0.02% (v/v) Triton X-100 in 1x PBS	-
Poly-L-Lysine Solution	0.1% (w/v) in H_2O	Sigma-Aldrich (#P8920)
***Staphylococcus aureus* enterotoxin A-*Staphylococcus aureus* enterotoxin B**	1.5μg/μl in full RPMI	Sigma-Aldrich (#S9399)-(#S4881)

Table 2.17 Cell culture, SDS-PAGE, Western blotting, co-immunoprecipitation and immunostaining materials

2.1.7. Databases, software and online programmes

Databases	Website
BioGrid	https://thebiogrid.org/
Ensembl	http://www.ensembl.org/index.html
Database for Annotation, Visualization and Integrated Discovery (DAVID)	https://david.ncifcrf.gov/
IntAct	http://www.ebi.ac.uk/intact/
KEGG pathway	http://www.genome.jp/kegg/pathway.html
NCBI	https://www.ncbi.nlm.nih.gov/
Uniprot	http://www.uniprot.org/
Reactome pathway	https://reactome.org/
STRING	http://string-db.org/
Software	**Usage**
Cytoscape	A software for protein network
FinchTV	DNA sequencer chromatogram
GrandPad Prism 7	Statistical analysis
ImageJ	Analysing the images
Kaluza Analysis 1.5a	FACS
Microsoft Excel 2013	Statistical analysis
Microsoft Powerpoint 2013	Figure alignments and labels
Bio-Rad Quantity One	A software for image acquisition and analysis
SnapGene Viewer 3.3.3	A software for molecular biology
Scaffold	A visualisation software for proteomics data
Nikon ACT-2U 1.40 software	A microscope software for image acquisition
ZEN 2009 (Zeiss Exciter and LSM710 confocal)	A microscope software for image acquisition
Online Programmes	**Usage/ Website**
ClustalW2	Multiple Sequence Alignment http://www.ebi.ac.uk/Tools/msa/clustalo/
ExPASy	Translate tool to translate DNA sequence to protein sequence https://www.expasy.org/
IDT OligoAnalyzer 3.1	Identifies oligonucleotide properties, including melting temperature and GC contents https://www.idtdna.com/calc/analyzer
Gene Ontology Consortium	Gene ontology analysis http://geneontology.org/

Table 2.18 Databases, software and online programmes

2.2. Methods

2.2.1. Molecular biology and microbiological techniques

2.2.1.1. Streaking the bacterial stab for purification of the plasmid DNA

TALEN plasmid DNAs (TAL3420, TAL3421, TAL3566, TAL3567) and BirA plasmid DNA (pcDNA3.1 mycBioID) were obtained in bacterial stabs from Addgene. In order to purify the plasmid DNAs, the bacteria had to be streaked on agar plates containing appropriate antibiotics (100µg/ml Ampicillin). Therefore, sterile inoculating loop was used to gather bacteria from the stabs. Bacteria were spread on agar plates and streaked for single colonies. The agar plates were incubated at 37°C overnight. Additionally, for long-term storage of the plasmid DNAs, bacterial glycerol stocks (500µl of the overnight culture and 500µl of 80% glycerol) were prepared and kept at -80°C.

2.2.1.2. Small and large scale preparation of plasmid DNA

The plasmid DNAs were extracted with GenElute Plasmid Mini-Prep kit (Sigma-Aldrich) for small scale purification when small amount of plasmid DNA required or Maxi-prep Tip-500 kit (Qiagen) for large scale purification when high amount of plasmid DNA required.

GenElute Plasmid Mini-Prep:

Bacterial cultures was prepared in a 5ml fresh LB medium containing 100µg/ml ampicillin by picking a single colony from the agar plate and inoculating at 37°C overnight (14-18 hours) with agitation at 220rpm. 2-3ml of overnight *E.coli* culture was pelleted by centrifugation at 12,000rpm for 1 minute. The supernatant and rest of the overnight culture were discarded into 2% Trigene. The bacterial pellet was resuspended completely with 200µl of the Resuspension solution by vortexing. The resuspended cells were lysed with 200µl of Lysis solution by gentle mixing not vortexing. The cell debris was precipitated with 350µl of Neutralisation solution by inverting. The precipitated cell debris was then pelleted by centrifugation at 12,000rpm for 10 minutes. GenElute Miniprep binding column was prepared by adding 500µl of Column Preparation solution and centrifugation at 12,000rpm for 1 minute. The flow-through liquid was discarded. The cleared lysate containing the plasmid DNA was loaded into the prepared column and centrifuged at 12,000rpm for 1 minute. 500µl of Optional Wash solution was added and centrifuged at 12,000rpm for 1 minute. The flow-through liquid was discarded. The column was washed lastly with 750µl Wash solution and centrifuged at 12,000rpm for 1 minute. The flow-through liquid was discarded and the column was centrifuged again at 12,000rpm for 1 minute without additional wash solution. The column was transferred into a clean collection tube and 50µl of Elution solution was added in order to elute the plasmid DNA. The tube was

centrifuged at 12,000rpm for 1 minute and the eluted plasmid DNA was stored at -20°C for further experiments.

Qiagen Tip-500 Maxi-prep:

A single colony was picked for the starter bacterial culture of 5 ml LB medium (with 100µg/ml ampicillin) and the culture was inoculated at 37^0C in a shaking incubator for 8 hours. 100µl of starter culture was diluted in 100ml of LB medium and inoculated at 37°C overnight (12-16 hours) with agitation at 300rpm. The bacterial cells were pelleted by centrifugation at 6,000g for 15 minutes at 4°C. The supernatant and rest of the overnight culture were discarded into 2% Trigene. The bacterial pellet was re-suspended with 10ml of Buffer P1. 10ml of Buffer P2 was added and inverted for several times to lyse the cells. After 5 minutes of incubation at room temperature, 10ml of chilled Buffer 3 was added and inverted for several times to neutralise the mix. The tube was incubated on ice for 20 minutes and centrifuged at 20,000g for 30 minutes at 4°C. The QIAGEN-tip 500 was equilibrated by adding 10ml Buffer QBT and letting to be emptied by gravity flow. The supernatant containing plasmid DNA from the centrifugation step was loaded to the QIAGEN-tip and letting the supernatant to enter the resin by gravity flow. QIAGEN-tip was washed two times with 30ml of Buffer QC by gravity flow. The plasmid DNA was eluted by adding 15ml of Buffer QF in a 50ml Falcon tube. The plasmid DNA was precipitated by adding 10.5ml isopropanol, mixing and centrifuging at 15,000g for 30 minutes at 4°C. The supernatant was carefully discarded. The DNA pellet was washed with 5ml of 70% Ethanol and centrifuged at 15,000g for 10 minutes. The supernatant was carefully discarded and the pellet was air-dried for 10 minutes. Lastly, the plasmid DNA was re-dissolved in TE buffer. The plasmid DNA was stored at -20°C for further experiments.

2.2.1.3. Quantification of nucleic acid concentrations and purity

Nanodrop spectrophotometer ND1000 was used to quantify the concentrations of DNA and RNA samples. The nanodrop area was cleaned with 70% ethanol, followed by dH_2O. After initiating the spectrophotometer with nuclease-free water, 1.5µl of blank sample (elution buffer or nuclease-free water) was loaded for calibration. To measure the concentration and purity, 1.5µl of nucleic acid sample was loaded. The ratio of absorbance at 260/280nm and 260/230nm were assessed for measuring the purity. The absorbance ratios at 260/280 of ~1.8 and ~2.0 are generally accepted as pure for DNA and RNA, respectively. Expected 260/230 values are commonly in the range of 2.0-2.2 for purity.

2.2.1.4. Restriction endonuclease digestion

Restriction endonucleases and the supplied buffers were obtained from New England Biolabs (NEB). In order to linearise the plasmid DNAs for *in vitro* transcription of mRNAs, 10µg plasmid

DNA was digested with 3µl of *PmeI* restriction endonuclease, 8µl of 10x Buffer-4, 1µl of 100x BSA and nuclease-free water for 3 hours at 37°C in a volume of 80µl. Phenol-Chloroform extraction and ethanol precipitation of DNA (Section 2.2.1.5) was carried out for digested plasmid DNAs and digested products were tested by running samples on a 1-1.5% agarose gel in TBE buffer. Undigested plasmid DNAs were loaded as controls. The sizes of digested fragments were confirmed with 1kb ladder (NEB).

For cloning and checking the presence of a target insert, 1µg of plasmid DNA was digested with appropriate enzymes and supplied buffers in a volume of 20µl. Specifically, for cloning DEF6 (Full-length or its truncated versions) into the pcDNA3.1 mycBioID vector, 1µg of plasmid DNAs (pcDNA3.1 mycBioID vector and pEGFP-C2/DEF6 Full-length) were double digested with 1µl of *EcoRI* and *AflII* restriction endonucleases, 2µl of *EcoRI* and CutSmart buffers and nuclease-free water in a volume of 20µl. The samples were incubated for 1.5 hours for each enzyme at 37°C. The sizes of digested fragments were confirmed with 1kb ladder on a 1-1.5% agarose gel.

For genotyping zebrafish embryos or fin clips and checking the presence of genome-edited sequences, 10µl of PCR products were digested with 1µl of *RsaI* (for *def6a*) or *NlaIII* (for *swap70b*) restriction endonucleases, 2µl of CutSmart buffer and nuclease-free water in a volume of 20µl. The reactions were incubated at 37°C for 1.5 hours. Digested products were tested by running a sample on 1.5-2.5% agarose gel in TBE buffer. The sizes of digested fragments were confirmed with 100bp DNA ladder (NEB).

2.2.1.5. Phenol-Chloroform extraction and ethanol precipitation of DNA

In order to purify digested or undigested plasmid DNAs, nuclease-free water was added up to the volume of 100µl. An equal volume of phenol: chloroform: isoamyalcohol (25:24:1) was added and the sample was vortexed for 10 seconds. The sample was then centrifuged at 14000rpm for 5 minutes. The bottom aqueous layer, which contains proteins, was discarded and the top aqueous layer which contains plasmid DNA was transferred to an Eppendorf tube. Equal volume of chloroform was added onto the transferred plasmid DNA sample, inverted several times and spun down at 14000rpm for 5 minutes. The top aqueous layer was transferred to an Eppendorf tube. Plasmid DNA was precipitated by adding 1/10 volume of 3M sodium acetate (pH 5.2) and followed by adding 2.5 volumes of ice-cold 100% ethanol. The sample was left at -20^{0}C for 30-60 minutes. Then, the sample was spun at 13000rpm for 30 minutes at 4^{0}C. The supernatant was discarded and the tiny pellet was washed with ice-cold 70% ethanol. The sample was spun at 13000rpm for 5 minutes at 4^{0}C again and after removing of ethanol, the pellet was air-dried for 5-10 minutes at room temperature. Lastly, the

sample was dissolved in 15-30 µl of nuclease-free water and stored at -20°C for further experiments.

2.2.1.6. Agarose gel electrophoresis

Agarose gel electrophoresis was performed for checking DNA and mRNA samples. 1-2.5% (w/v) agarose was resolved in TBE buffer by heating and after cooling down, 10% (v/v) SafeView staining dye was added before pouring the gel into the comb inserted gel tray. 6X loading dye was diluted into 1X and added to each DNA sample with nuclease-free water. 1kb or 100bp DNA ladders were used depending on the sizes of DNA samples. Gels were run at 120V for 1 hour and visualised by UV illumination. Gel photographs were taken on a Biorad gel-doc system.

2.2.1.7. DNA extraction from agarose gels and purification of PCR products

Extraction of DNAs from agarose gels as a part of cloning process and purification of PCR products were carried out by using Nucleospin Gel and PCR Clean-up Kit (Macherey-Nagel). For gel extraction, the DNA to be extracted was loaded on 1.5% agarose gel and run at 120V for 1 hour. After a short time UV exposure, the target fragment of DNA was cut with a scalpel and put in an eppendorf tube. The gel slice was weighed and 200µl of NTI binding buffer per 100mg of gel was added to dissolve the gel at 50°C for 10 minutes. After complete dissolving of gel, the mixture was loaded into a column and centrifuged at 11,000g for 30 seconds to bind DNA to the column. The column was washed two times with 700µl of NT3 wash buffer and centrifuged at 11,000 for 30 seconds. To dry the silica membrane, the column was centrifuged at 11,000g for 1 minute and the flow-through was discarded. Lastly, for the elution of DNA, 30µl of NE elution buffer was added and centrifuged at 11,000g for 1 minute.

Similarly, the same protocol with only one exception, which was loading the nuclease-free water added PCR product into the column, was followed. 200µl of NTI binding buffer was added into the column and centrifuged at 11,000g for 30 seconds. From this step, the protocol was followed like as the gel extraction process. The concentration and purity of DNAs were measured by using Nanodrop (Section 2.2.1.3).

2.2.1.8. DNA ligation

For cohesive end ligation, 40-50ng of vector was mixed with 3-5 fold mass of insert, 2µl of 10x T4 ligation buffer, 1µl of T4 DNA ligase (NEB) and nuclease-free water up to 20µl. The reaction was kept at room temperature overnight and the reaction was stopped by keeping the reaction at 65^0C for 15 minutes. The sample was then transformed into NEB-5-alpha competent *E.coli* cells (Section 2.2.1.9).

For the insertion of PCR-amplified fragment into a StrataClone blunt vector, a StrataClone Blunt PCR Cloning Kit was used (Agilent Technologies). The PCR reaction was diluted in 1:10 in nuclease free water. 3µl of StrataClone blunt cloning buffer, 2µl of diluted PCR reaction, 1µl of StrataClone Blunt Vector Mix amp/kan was mixed and incubated at room temperature for 5 minutes. Then, the sample was incubated on ice prior to transformation into StrataClone solo pack competent cells (Section 2.2.1.9).

2.2.1.9. Transformation

NEB-5-alpha Transformation

The NEB-5-alpha competent *E.coli* cells were obtained from NEB and 50µl of aliquots for each reaction was stored at -80^{0}C. 50µl of aliquot was thawed on ice and 5µl of plasmid DNA (10pg-100ng) was added into the tube, mixed gently. The mix was placed on ice for 30 minutes and subsequently heat-shocked for 45 seconds in 42^{0}C water bath. The mix then placed on ice for 5 minutes. 950µl of SOC medium was added to the cells and incubated at 37^{0}C for 60 minutes. Agar plate containing 100µg/ml ampicillin was taken out from 4^{0}C fridge and warmed up in 37^{0}C incubator. Finally, 100-200µl of sample was spread on plate and incubated overnight in 37^{0}C incubator.

StrataClone Blunt PCR Cloning Transformation

50µl of StrataClone Solo Pack competent cells were thawed on ice and 1µl of PCR ligation mix was added into the competent cells. The reaction was kept on ice for 20 minutes followed by heat shock in 42°C for 45 seconds. The reaction was put on ice for 2 minutes and 250µl of pre-warmed SOC medium was added into the reaction for later incubation at 37°C with agitation for 1 hour. While the reaction is in the incubation process, agar plate containing 100µg/ml ampicillin was prepared by spreading 40µl of X-gal. 100µl of the competent cells were spread on the plate and the plate was incubated at 37°C overnight. Only white colonies were picked for colony PCR or mini-prep.

2.2.1.10. DNA sequencing

The purified colony PCR samples were sequenced for confirming the mutation in the TALEN targeting region. In addition, plasmid DNA samples were sequenced for confirming the insertion of the target DNA into the vector. The PCR samples were diluted to 1ng/µl per 100bp and sent together with sequencing primers (diluted into 3.2pmol/µl) for Sanger sequencing, Source Bioscience (Nottingham, UK). The plasmid DNA samples were diluted to 100ng/µl and sent together with sequencing primers. Multiple sequence alignment was performed by using Clustal-W2 multiple sequence alignment program (EMBL-EBI) according to the results

received from Source Bioscience. For mutation analysis, ExPASy translate tool was used to translate the DNA sequence to the protein sequence.

2.2.2. Polymerase Chain Reaction (PCR)

Primer Design

Primers were designed by IDT OligoAnalyzer 3.1 tool and synthesised by Invitrogen. Melting temperatures and GC% content were taken into account. Different amount of nuclease-free water was added to the desalted primers to make a 100μM stock solution. Primers were diluted to 10μM working solution to use in the reactions.

Primers	Sequence (5'-3')	Product size (bp)
***def6a* Forward**	CTTCTGGTTTCAGTTCAGGTGT	350bp
***def6a* Reverse**	AAGCCTAATTTTCAGCCTCTCTC	
***swap70b* Forward**	GAAAACAGTCCACATCAAGTGC	243bp
***swap70b* Reverse**	TGTCTTCAGTGAAGCGTTAAAAAC	

Table 2.19 Primers used for standard and colony PCR to amplify the region flanking TALEN target site for *def6a* and *swap70b.*

Primers	Sequence (5'-3')	Product size (bp)
Full length DEF6 Forward	CAAGCTTCGAATTCTGCAGTC	1988bp
Full length DEF6 Reverse (+AflII)	AGGCTTAAGGTCCTGGTGGATATGACATTGG	
N-terminal DEF6 Forward	CAAGCTTCGAATTCTGCAGTC	370bp
N-terminal DEF6 108 Reverse (+AflII)	TATCTTAAGCCCCTAGCTATCTGCCC	
PH DEF6 214 Forward (+EcoRI)	GGCCCGCCGCGAGGAATTCCAGGAGATGATCCAAGATGTCC	432bp
PH DEF6 341 Reverse (+AflII)	ATTCAGCTCCTCCTTAAGGGCCTACCGGCGCCGCTC	
C-terminal 312 DEF6 Forward (+EcoRI)	ACATCTGAATTCCAGATCGCGATGCGGCTG	1088bp
C-terminal DEF6 Reverse (+AflII)	AGGCTTAAGGTCCTGGTGGATATGACATTGG	

Table 2.20 Primers used for standard PCR to amplify FL, N-terminal, PH and C-terminal DEF6 sequences from pEGFP-C2/DEF6 vector.

Standard and Colony PCR

Standard polymerase chain reactions (PCR) were carried out for cloning or checking the mutagenic effects of TALEN injections, whereas colony PCRs were performed for confirming the presence of an insert. The reactions were set up and carried out in Takara PCR thermocycler machine. Q5 hot start high-fidelity DNA polymerase was used (NEB). The amount and final concentrations of the components in a 50µl reaction are listed in Table 2.21. The standard and colony PCR reactions were cycled as in Table 2.22 for amplifying the TALEN region, while the standard PCR reaction was cycled as in Table 2.23 for cloning the *def6* full length and its truncation sequences into the pcDNA3.1 mycBioID vector.

	Standard PCR		Colony PCR	
Component	**Amount**	**Final concentration**	**Amount**	**Final concentration**
5X Q5 Reaction Buffer (NEB)	10µl	1X	10µl	1X
10 mM dNTPs (Promega)	1µl	200µM	1µl	200µM
10 µM Forward Primer (Invitrogen)	1µl	0.5µM	1µl	0.5µM
10 µM Reverse Primer (Invitrogen)	1µl	0.5µM	1µl	0.5µM
Template DNA	Variable (typically 2µl)	Variable	Pick a single colony	-
Q5 Hot Start High-Fidelity DNA polymerase (NEB)	0.5µl	0.02U/µl	0.5µl	0.02U/µl
Nuclease-free water	Up to 50µl	-	Up to 50µl	-
Total	50µl		50µl	

Table 2.21 Components, used amounts and final concentrations for standard and colony PCR in a total volume of 50µl.

Step	Temperature (^{0}C)	Time	Number of cycles
Initial denaturation	98^{0}C	2 min	-
Denaturation	98^{0}C	30 secs	30
Primer Annealing	55^{0}C	30 secs	
Template Extension	72^{0}C	30 secs	
Final Extension	72^{0}C	4 min	-
Hold	4^{0}C	∞	

Table 2.22 Standard and colony PCR cycles for amplifying the TALEN regions by using Q5 Hot Start High-Fidelity DNA polymerase.

Step	Temperature (^{0}C)	Time	Number of cycles
Initial denaturation	95^{0}C	2 min	-
Denaturation	95^{0}C	30 secs	35
Primer Annealing	55^{0}C	30 secs	
Template Extension	72^{0}C	1 min	
Final Extension	72^{0}C	4 min	-
Hold	4^{0}C	∞	

Table 2.23 Standard PCR cycle for cloning the *def6* full-length and its truncation sequences into the pcDNA3.1 mycBioID vector by using Q5 Hot Start High-Fidelity DNA polymerase.

2.2.3. *In vitro* transcription of mRNAs for microinjection and whole mount *in situ* hybridisation

2.2.3.1. *In vitro* transcription and phenol-chloroform extraction of TALEN mRNAs and mRNAs for microinjections into embryos

mMessage mMachine T7 or T3 transcription kit (Ambion, UK) were used for transcribing mRNAs (Table 2.8). 1µg of linearised and phenol/chloroform extracted DNA was mixed with 10µl of 2X NTP/CAP, 2µl of 10X reaction buffer, 2µl of T7 or T3 enzyme mix and nuclease-free water in a total volume of 20µl reaction. The reaction was incubated for 2 hours at 37^{0}C. Residual plasmid DNA was removed by adding 1µl of Turbo DNase and incubated at 37^{0}C for 15 minutes. The transcription reaction was stopped by adding 15µl of (final concentration of 0.5M) ammonium acetate solution and 115µl of nuclease-free water. The mRNA was extracted by adding 1 volume of phenol/chloroform, vortexing and centrifuging at 13,000rpm for 5 minutes. The top layer was extracted and 1 volume of chloroform was added to centrifuge at 13,000rpm for 5 minutes. The top layer containing the mRNA was precipitated with an equal volume of isopropanol and incubated at -20°C for 30 minutes. The mRNA was pelleted by centrifuging (4°C) at 13,000rpm for 10 minutes. After removing isopropanol, air-dried mRNA was resuspended in 30µl of nuclease-free water. For checking the purity, 5µl of mRNA was mixed with 6µl of 6X RNA loading dye and the sample was heated at 65^{0}C for 5 minutes for removing hairpins. Then, the sample was run on a 1.5% agarose gel. The concentration and purity were checked with a Nanodrop spectrophotometer and aliquots were prepared for storing at -80^{0}C.

2.2.3.2. *In vitro* transcription of mRNA probes for whole mount *in situ* hybridisation

For antisense mRNA probe synthesis, 2.5µg of linearised and phenol-chloroform extracted template DNA was transcribed with 2µl of Digoxigenin (DIG) labelled NTP mix, 4µl of 5x Transcription buffer, 2µl of DTT, 1µl RNAseout, 2µl of T7, T3 or SP6 RNA polymerase and dH_2O in a total volume of 20µl at 37°C for at least 3 hours. 5µl of DNAseI was added to remove excess DNA in the tube and incubated at 37°C for 20 minutes. To stop the reaction, 1µl of 0.5M EDTA and 80µl of H_2O were added. To clean and extract the mRNA product, 33µl (1:3 v/v) of 10M ammonium acetate was added. 250µl (2.5 v/v) of ice-cold 100% Ethanol was added and incubated at -20°C for 30 minutes. The samples were then centrifuged for 10 minutes at 13000rpm at 4°C. The pellet was washed with 70% Ethanol and centrifuged for 10 minutes at 13000rpm at 4°C. The pellet was air-dried for 5 minutes and re-suspended in DEPC treated H_2O. 2µl of sample was run on a 1.5% agarose gel to check the successful transcription and purity.

For whole mount *in situ* hybridisation experiments typically 1:200 dilution of probe in Hybridisation mix ($Hybe^+$) was applied. The probes were stored at -20°C and re-used several times.

Table 2.14 (Section 2.1.4) summarises the genes for antisense mRNA probes, the enzymes for digestion of template DNA and RNA polymerases for *in vitro* transcription.

2.2.4. Zebrafish techniques

All experiments on zebrafish were conducted under the project licences (PPL) of **30/3356 19b1** and **30/3378 19b1** and the personal licence (PIL) of **IDA196950.**

2.2.4.1. Embryo culture, crosses and zebrafish stock maintenance

Zebrafish (*Danio rerio*) are maintained at 28.5°C in system water on a cycle of 14 hours light and 10 hours dark. Wild type and mutant embryos were collected after spawning and raised at 28.5^0C in E3 zebrafish medium containing 1% methylene blue, according to the standard procedures for zebrafish (Westerfield, 2000). A small plastic container which has larger holes at the bottom than the diameter of embryos was placed into a larger container for separating the pair from embryos. The containers were filled with system water and a pair of zebrafish (female and male) was placed into the containers, usually separating them with a plastic divider until next day. Several hours after the lights are turned on next day, the divider was removed and the embryos were collected with a mesh net. The pair was returned to their tanks. The embryos were grown at 28.5°C in E3 medium until 5 days post fertilisation (dpf) and if they were needed to be grown to adulthood, the larvae were moved to the tanks in the

nursery (BSU, aquarium). The tanks were named with the breeding numbers and after 28dpf, zebrafish were counted and replaced in a bigger tank for breeding.

The specification of stages by Kimmel *et al.,* (1995) was accepted and applied.

2.2.4.2. TALEN mRNAs microinjection into one-cell stage embryos

2.2.4.2.1. Preparation of microinjection needle

The needles for microinjections were prepared from glass capillaries by using needle puller (Sutter Instrument CO). 3µl of TALEN mRNAs or mRNAs were loaded into the needle and the needle was adjusted into micropipette holder. The micropipette holder was linked to a pico pump for injecting with pressure. Under a microscope at the highest magnification, the tip of the needle was cut with a sterile forceps. The amount of injected mRNA was adjusted according to the concentration of mRNA. The drop size was measured through injection into air and calculated with scale bar. The size of injection was calibrated by adjusting the pulse duration of the pressure.

2.2.4.2.2. TALEN mRNAs microinjections

After the digestion of TALEN DNAs with *PmeI* restriction enzyme, purification by phenol-chloroform extraction was carried out prior to *in vitro* transcriptions of TAL3420, TAL3421, TAL3566, TAL3567 TALEN plasmids. The newly synthesised mRNAs were checked for purity. Right and left TALEN mRNAs of *def6a* and *swap70b* were diluted into 250ng/µl and 500ng/µl, respectively, and mixed in a single tube to inject. Once 3µl of TALEN mRNAs was loaded onto the needle, the drop size was calibrated to 0.5-1 nl. 1-cell stage embryos were lined up on an edge of a slide placed in a petri dish lid. The cells of the embryos were arranged touching the edge of the slide. A defined drop size (0.5-1 nl) of equal amounts of right and left TALEN mRNAs were injected together into the cytoplasm of 1-cell stage embryos. Injected embryos were moved to a clean petri dish containing E3 buffer and methylene blue. Wild type embryos were also collected as controls and incubated together with injected embryos at 28.5^{0}C until the desired stage, typically 2 days for checking the mutation efficiency.

Similar to TALEN mRNAs microinjections, *gfp, gfp-racI*, gfp-rhoA and *gfp-cdc42* vectors were linearised with *SfiI* and *EcoRI* restriction enzymes for *in vitro* transcription. After phenol-chloroform extraction, DNAs were transcribed into sense mRNAs by T3 RNA polymerase. mRNAs were diluted to 400ng/µl and 500ng/µl. 3µl of mRNAs was loaded onto the needle, the drop size was calibrated to 0.5 nl. 1-cell stage embryos were lined up on an edge of a slide which placed in a petri dish lid. The cells of the embryos were arranged touching the edge of the slide. A defined drop size (0.5 nl) of mRNAs were injected together into the cytoplasm of 1-cell stage embryos. Injected embryos were moved to a clean petri dish containing E3 buffer

and methylene blue. Wild type and un-injected qmc811 *def6a*$^{-/-}$ and qmc809 *swap70b*$^{-/-}$ embryos were also collected as controls and incubated together with injected embryos at 28.5^{0}C until the desired stage.

2.2.4.3. Genomic DNA extraction from embryos

To prepare genomic DNA from embryos, HOTSHOT DNA extraction method was carried out (Moens lab, Fred Hutchinson Cancer Research Center, Seattle, USA). Individual 2dpf embryos were incubated in 50µl of 1X Base solution (Alkaline-lysis reagent) containing 5M NaOH and 0.5M EDTA at 95^{0}C for 30 minutes. The tube was cooled to room temperature and 50µl of 1X Neutralisation solution containing 1M TRIS-HCl in water was added to the samples. The DNAs were kept at 4^{0}C. The tubes were vortexed and spun down for 5 minutes at 3000rpm before using for PCR. 2µl of this solution was sufficient for PCR reactions to analyse the mutations.

2.2.4.4. Fin clipping genotyping

To obtain samples for genotyping, fish are anesthetized in 3% (v/v) Tricaine (MS-222; Sigma) solution. Sterile scissors were used to clip the fin tails which were placed on ice in a tube containing a 50µl Base solution. Then, genomic DNA extraction protocol (Section 2.2.4.3) was applied to genotype the DNAs by PCR and subsequent digestion.

2.2.4.5. Fixation and storage of zebrafish embryos for whole mount *in situ* hybridisation

The dechorionated embryos of the required developmental stages were fixed in 4% (w/v) PFA in 1x PBS overnight at 4°C. The embryos were washed for 3 times in 1x PBST for 5 minutes. The embryos before 18hpf were dechorionated after the fixation in 4% PFA overnight and washing in 1x PBST for 3 times. Embryos were dehydrated for 5 minutes in each of 25%, 50% and 75% (v/v) Methanol in PBST. Lastly, the embryos were washed in 100% Methanol for 5 minutes and stored in 100% Methanol at -20°C for at least two hours to several months.

2.2.4.6. Whole mount *in situ* hybridisation of zebrafish embryos

All washes were carried out in a 500µl total volume, shaking at room temperature unless it is stated. Embryos stored in methanol at -20°C were rehydrated through 75%, 50% and 25% (v/v) methanol in PBST and washed four times in 1x PBST for 5 minutes each. For embryos older than 18hpf, proteinase K treatment (10µg/ml) was applied for 5 minutes or more which depends on the age of the embryos. After treatment, embryos were refixed in 4% PFA for 20 minutes and washed five times with 1x PBST for 5 minutes each. Embryos were washed in 50% PBST, 50% Hybridisation mix (without tRNA) for 5 minutes before washing in

prehybridisation mix (Hybe$^+$) for at least 1 hour at 68°C. After removing the prehybridisation mix, probe (generally 1:200 dilution in Hybe$^+$) was added to incubate overnight at 68°C.

Next day, the probe was removed and saved for reuse in later *in situ* experiments. The excess probe was removed by successive washing steps at 68°C for 10 minutes each. The embryos were washed through 100% Hybe$^-$ (without tRNA and heparin), 75% Hybe$^-$/25% 2xSSC, 50% Hybe$^-$/50% 2xSSC, 25% Hybe$^-$/ 75% 2xSSC and 100% 2x SSC. The last washing steps at 68°C were washing three times in 100% 0.2x SSC for 15 minutes. Then, at room temperature, 75% 0.2x SSC/25% MABT, 50% 0.2x SSC/50% MABT, 25% 0.2x SSC/75% MABT and 100% MABT solutions were used to wash the embryos for 5 minutes. To block the embryos for at least 1 hour, 2% Boehringer blocking reagent diluted in MAB was used. The blocking reagent was replaced with anti-digoxigenin antibody (1:5000 dilution) in 2% blocking reagent in MAB and incubated for 3 hours at room temperature. To reduce the background, the embryos were not incubated with the antibody overnight. After 3 hours of incubation, the embryos were washed three times with MABT for 15 minutes each and kept in MABT overnight at 4°C.

Next day, the embryos were washed three more times in MABT for 15 minutes. Then, fresh prepared BCL buffer III was used to wash embryos three times for 5 minutes. For colouration, BM Purple was diluted 1:1 in BCL buffer III to stain the embryos. This process was carried out in dark at room temperature or 37°C to increase the colouration process until the colour had developed. The colouring reaction was stopped by washing the embryos three times in 20mM EDTA for 5 minutes.

For long-term storage or stopping the colouring reaction permanently, the embryos were re-fixed in 4% PFA for 20 minutes at room temperature. The embryos were then washed three times in PBST for 5 minutes. The embryos were dehydrated through 50% Methanol in dH_2O, 100% Methanol and 50% Methanol/50% PBST for 5 minutes each. 30%, 50% and 90% glycerol in PBST were used successively to prepare the embryos for long term storage and visualisation. The embryos were then stored at 4°C for long-term.

2.2.4.7. Genotyping after whole mount *in situ* hybridisation

After imaging the embryos, every single embryo was transferred into an eppendorf tube and the tubes were named after the used probe and image number. 90% glycerol was removed as much as possible and the embryos were washed through 70% and 30% glycerol in PBST for 5 minutes each at room temperature. PBST was used to wash the embryos three times for 5 minutes each prior to adding 100µl 300mM NaCl. The samples were incubated in NaCl for 4 hours at 65°C. After removing the excess NaCl, HotShot DNA extraction method (Section

2.2.4.3) was proceeded and extracted DNA (2µl) was directly used in PCR reaction as mentioned earlier.

2.2.4.8. Actin staining of zebrafish embryos

Wild type and mutant embryos at the desired stage were fixed in 4% PFA at 4°C overnight after dechorionation. Embryos were rinsed in 1x PBST (0.1% Tween-20) for 3 times for 5 minutes. After removing the last PBST, embryos were permeabilised in 1x PBS; 2% TritonX-100 for 1.5 hours at room temperature. After removing the PBS; Triton mixture, Alexa Fluor 568 Phalloidin (Life Technologies) diluted 1:20 in PBS; 2% TritonX-100 was added into the each tube laying down and shaking at 4°C overnight. The tubes were kept in dark. To remove the excess staining, the embryos were washed in PBST (0.1%) 3 times for 5 minutes at room temperature. Lastly, the embryos were washed in 30:70 (glycerol: PBS), 60:40 (glycerol: PBS) and 80:20 (glycerol: PBS) for 5 minutes. The embryos were transferred to the microscope glass, oriented with a tool and mounted in 80:20 (glycerol: PBS). Cover slips were placed onto the embryos and the corners were sealed with a nail polisher. Slides were kept in dark at 4°C until they were imaged. Zeiss Exciter Confocal microscope was used for image acquisition.

2.2.4.9. Imaging of zebrafish embryos

Live or *in situ* hybridised embryos were imaged using Nikon SMZ1500 microscope, Nikon-DS-5M camera, Nikon DS-1 control unit and Nikon ACT-2U 1.40 software. Images were edited in Adobe Photoshop and Microsoft Powerpoint programmes. For actin stained embryos, LSM710 confocal microscopes and Zeiss ZEN 2009 software were used to take images. 40x Plan-Apochromat Ph3 (NA 1.3) oil immersion objective was used. Channel images were obtained using only 561nm laser. Pinhole diameter was set to 1 Airy unit. ImageJ software was used to analyse the Z-stack images and compressed to a single images at maximum intensity. The intensity of fluorescence in actin stained samples was measured with ImageJ and a comparative analysis was made using Microsoft Excel.

2.2.4.10. Flow cytometry analysis of cells isolated from adult kidney marrow

WT and mutant fish were culled in MS222 and placed on ice. The dissection protocol suggested by Gerlach *et al.,* (2011) was followed. The body of fish was opened from the caudal and the internal organs and eggs were removed. As the kidney was localised to the dorsal body wall, the dorsal body wall was not disturbed. The kidney was detached using a pair of forceps and placed into 10mm tissue culture dish containing 2 ml of cold 1x HBSS and kept on ice. Cells of the kidney were dissociated by pipetting various times. 5 ml of FCS/PBS was added into each dish and the kidney solution was strained into 50 ml falcon tubes on ice using 40µm cell strainers. The tubes were centrifuged at 4°C at 1500 rpm for 5 minutes. The supernatant was discarded and the pellets were re-suspended in 300µl of FCS/PBS. The

kidney solutions were transferred into 15ml tubes and the tubes were taken to the FACS sorter on ice. The samples were sorted by flow cytometry, which is a laser-based method to examine fluorescently labelled cells. The results were analysed on Kaluza Analysis 1.5a software and four different gates showing the blood cell populations were added manually. While the forward scatter (FSC) is directly related to the cell size, the side scatter (SSC) is directly related to the cell granularity.

2.2.4.11. Data quantification and statistical analysis

Microsoft Excel and GraphPad Prism 7 were used for data quantification and statistical analysis. One-way ANOVA and two tailed Student's t-test were used to analyse the significant difference between the groups. P values were calculated by using GraphPad Prism software and while $p<0.05$ indicates significant difference, $p>0.05$ indicates no significant difference between the groups.

2.2.5. Cell culture techniques

2.2.5.1. Maintenance and passaging of suspension cells

Jurkat T cells and Raji B cells were maintained in 75cm^2 flasks in Roswell Park Memorial Institute 1640 (RPMI) medium containing 10% (v/v) FBS and 1% (v/v) penicillin/streptomycin in an incubator at 37°C and 5% CO_2. Cultures were maintained at 5-8x10^5 cells/ml. The cells were passaged when they reached 5-8x10^5 cells/ml density. For passaging, cells were transferred to a new 75cm^2 flask in a dilution of 1:8 with fresh RPMI 1640 medium. The plate then was agitated slowly and incubated at 37°C and %5 CO_2.

2.2.5.2. Cell counting using a haemocytometer

To calculate the cell density, both counting chambers of a haemocytometer were loaded with 20µl of cells and covered with coverslip. Cells were counted in a 5 of 1mm^2 areas counting the upper and left borders but not lower and right borders under a light microscope. After counting, cells were diluted to correct density and plated into the flasks.

2.2.5.3. Precipitation of DNA for the transfection of cells

50µg of DNA was precipitated for Jurkat T cells. 0.1 volume of NaCl buffer and 2 volumes of ice-cold 100% Ethanol were added to the DNA sample. The sample was placed in -20°C for 1 hour and centrifuged at 14000rpm for 15 minutes at 4°C. The supernatant was removed and the precipitated DNA was washed with ice-cold 70% Ethanol. Lastly, the sample was centrifuged at 14000rpm for 15 minutes at 4°C. The precipitated DNA, which is sterile, was used for the transfection of cells under the fume hood.

2.2.5.4. Transient transfection of Jurkat T cell lines

In the logarithmic growing phase, Jurkat T cells were transfected by square-wave electroporation. Jurkat T cells were re-suspended in RPMI medium at a density of $2x10^7$/ml. 50µg of previously precipitated DNA was mixed with 250µl of cell suspension in a 4-mm gap electroporation cuvette. The cuvette was exposed to a single pulse at 310V for 10 ms from the BTX ECM 830 electroporator (Harvard Apparatus Inc). Cells were then removed from the cuvette and re-suspended in 10ml pre-warmed medium containing 50µM excess Biotin (Sigma-Aldrich). The flask was incubated at 37°C and 5% CO_2 for 24-48 hours prior to cell harvesting for western blotting or co-immunoprecipitation.

2.2.6. Protein techniques

2.2.6.1. Cell lysis and SDS-PAGE

After 24 or 48 hours of transfection, cells were washed with PBS and lysed with 1X RIPA lysis buffer on ice. Lysates were sonicated for 30 seconds and mixed with 2x Laemmli sample buffer and heated at 95-100^0C for 5 minutes prior to loading on polyacrylamide gel. Protein samples were visualised on 10% SDS-Polyacrylamide Gel Electrophoresis (SDS-PAGE) **(Table 2.24)** by using a Mini-Protean 3 system (Biorad) which is composed of a spacer glass plate with 1.5mm spacer and a short glass plate. The resolving solution was prepared and TEMED was added just before pouring the gel between the plates. Butanol was poured onto the 10% resolving solution to prevent the formation of bubbles and the gel was left to set for 30 minutes. After the setting of resolving gel, the 5% stacking solution was prepared by adding TEMED and poured onto the resolving gel. 1.5mm well comb was placed before leaving the stacking gel to set for a further 20 minutes. The gel was placed into the tank by using inner chamber assembly and the tank was filled up with 1x SDS-PAGE running buffer. The comb was removed and firstly, PageRuler protein ladder as a protein size indicator, secondly biotinylated protein ladder as a positive control and lastly 20µl of samples were loaded into the wells. The proteins were resolved at a constant current of 35mA for at least 1 hour.

Resolving and Stacking solutions for 10% SDS-PAGE			
Resolving solution		**Stacking solution**	
H_2O	4.0 ml	**H_2O**	3.4 ml
30% Acrylamide mix*	3.3 ml	**30% Acrylamide mix**	0.83 ml
1.5M Tris (8.8)	2.5 ml	**1.0M Tris (6.8)**	0.63 ml
10% Sodium dodecyl sulfate (SDS)	100 µl	**10% SDS**	50 µl
10% Ammonium persulfate (APS)	100 µl	**10% APS**	50 µl
TEMED**	8 µl	**TEMED**	8 µl

Table 2.24 Solutions for Tris/Glycine 10% SDS-PAGE. * 29.2% acrylamide and 0.8% N,N'-methylene-bis-acrylamide, ** dN,N,N'N'- Tetramethylethylenediamine.

2.2.6.2. Western blotting and immunodetection

After resolving the proteins by SDS-PAGE, the proteins were transferred to Hybond-P Polyvinylidene Fluoride (PVDF) membrane (Amersham, Millipore). Before the transfer, the PVDF membrane was activated in 100% Methanol for 10 seconds and washed in dH_2O and transfer buffer for 10 minutes with agitation. The proteins were then transferred to the membrane using Transblot SD Semi-Dry Transfer Cell (Bio-rad) transfer machine at a constant current of 15V for 1 hour. After transfer, the membrane was blocked in blocking solution (5% BSA in PBS with 0.1% Tween 20) for 1 hour at room temperature with agitation. The membrane was then incubated in alkaline phosphatase (AP)-conjugated streptavidin (3% BSA in PBS and 6µl substrate in 15ml; Promega) for 1 hour at room temperature with agitation to detect the *in vivo* biotinylated proteins. The membrane was then washed for three times in PBS with 0.1% Tween-20 for 5 minutes, dried and incubated with Western Blue stabilised substrate for alkaline phosphatase for 2-4 minutes at room temperature. Excess reagent was removed and the membrane was washed in dH_2O for 2 minutes and left to air-dry in dark.

2.2.6.3. PVDF membrane antibody stripping and re-probing

In order to re-probe the membrane, membrane was stripped of antibodies by incubating in antibody stripping buffer for 45 minutes at room temperature. The membrane was then washed for two times in PBS with 0.01 Tween-20 for 20 minutes at room temperature with agitation. The membrane was blocked in blocking solution (5% BSA in PBS with 0.1% Tween 20) for 2 hours at room temperature before re-probed with primary antibody (1:500; 1:2,000) overnight at 4°C and secondary antibody (1:1,000; 1:2,000) for 40 minutes at room temperature.

2.2.6.4. Affinity capture of the biotinylated proteins

Dynabeads MyOne Streptavidin C1 (Invitrogen) was used to capture the biotinylated proteins. Appropriate amount of beads (50-100µl) were transferred to a tube. 1 ml PBS (pH 7.4) was added onto the beads for re-suspending. The tube was placed on a magnet for 1 minute and the supernatant was discarded. The tube was removed from the magnet and re-suspended in 1 ml PBS. These washing steps were repeated twice, for a total of 3 washes. After discarding the supernatant, the biotinylated proteins were added to the washed Dynabeads. The tube was incubated for 30 minutes at room temperature with gentle rotation. Then, the tube was placed in a magnet for 2 minutes and the supernatant was discarded. The beads were washed in PBS for 4 times prior to re-suspending in 50mM ammonium bicarbonate buffer. To check the biotinylation level on gel, the beads were re-suspended in 1x Laemmli buffer and heated to 95°C for 5 minutes before loading onto the polyacrylamide gel. On the other hand, for mass

spectrometry analysis, the beads were re-suspended in 50mM ammonium bicarbonate buffer and sent for mass spectrometry analysis on dry ice.

2.2.6.5. Mass spectrometry (MS)

After using Dynabeads MyOne Streptavidin C1, the beads containing the biotinylated proteins were re-suspended in 50mM ammonium bicarbonate buffer and sent to Dr Andrew Bottrill, Protein and Nucleic Acid Chemistry Laboratory (PNACL), University of Leicester for mass-spectrometry analysis. The results were analysed using Scaffold Proteomics software.

2.2.6.6. Immunological synapse formation

The immunological synapse forms between antigen presenting B cells and T cells. In order to form synapses, antigen-loaded Raji B cells had to be incubated with Jurkat T cells. Therefore, 6.6x 10^6 Raji B cells were stained in the dark with 1μg/ml calcein blue at 37°C and 5% CO_2 for 20 minutes. Cells were washed three times with 1x PBS and were incubated in full RPMI containing 1.5μg/μl *Staphylococcus aureus* enterotoxin A and 1.5μg/μl *Staphylococcus aureus* enterotoxin B for 30 minutes at 37°C, 5% CO_2. Before incubating with Jurkat T cells, Raji B cells were re-suspended in 250μl of RPMI. 3.3x 10^6 Jurkat T cells were re-suspended in 250μl of RPMI and mixed with Raji B cells to incubate for 1 hour at 37°C, 5% CO_2. Cells were diluted 1:2 in 3% BSA in 1x PBS. 250μl cells from this dilution were added onto the Poly-L-Lysine coated cover slips and settled for 10 minutes. Cells were washed with 1x PBS, 3% BSA and fixed with 250μl 4% PFA for 10 minutes. Cells were washed with 3% BSA in 1xPBS before and after the permeabilisation with 200μl of 0.2% Triton X-100 in 1x PBS for 10 minutes. Fluorescent immunostaining of the immunological synapses was described in detail in Section 2.2.6.6.

2.2.6.7. Immunofluorescence

200μl Poly-L-Lysine solution was spread onto the cover slips and left to dry for 1 hour. All the excess solution was aspirated and the cover slips were washed with 200μl 1x PBS. After drying, suspension cells were added onto the cover slips and settled for 10 minutes. Cells were washed with 3% BSA in 1xPBS and fixed with 4% PFA for 10 minutes. After washing with 3% BSA in 1x PBS, the cells were permeabilised in 0.2% Triton X-100 in 1x PBS for 10 minutes. 3% BSA in 1x PBS was added onto the cells and incubated for 1 hour at room temperature for blocking. Primary antibodies were diluted (usually 1:250) in 3% BSA in 1x PBS and incubated with cells for 1 hour at room temperature. Cells were washed three times in 3% BSA in 1x PBS and secondary antibodies were diluted (usually 1:500) in 3% BSA in 1x PBS to incubate with cells for 1 hour at room temperature in dark. Cells were washed three times with 3% BSA in 1x PBS for 2 minutes followed by mounting the cover-slip with FluoroGel

mounting medium. Slides were kept at 4°C in dark until the imaging by LSM710 Confocal microscope.

2.2.6.8. Confocal microscopy and analysis of images

Confocal images were taken using a Zeiss LSM Exciter and LSM710 laser confocal microscopes with a 63x Plan-Apochromat Ph3 (NA 1.4) oil immersion objective. Channel images were obtained sequentially using 488nm and 561nm lasers. Pinhole diameter was set to 1 Airy unit.

Images were analysed using Fiji-ImageJ software. The channels were split to present each colour individually and merged to indicate the presence or absence of co-localisation. Colour intensity was adjusted using the features of brightness and contrast equally in both channels. Scale bars were added onto the images, usually set to 1μm-10μm. Z- stack images were taken in 1024x1024 pixels and compressed to single images to present the entire cell.

CHAPTER 3

RESULTS

Establishment of *def6a* and *swap70b* mutant zebrafish

3.1. TALEN-mediated mutagenesis of *def6a* and *swap70b* loci

After microinjection of mRNAs encoding *def6a* and *swap70b* TALENs into 1-cell stage zebrafish embryos (**Figure 3.1Ai**), in-del mutations in somatic tissues were determined by genotyping (**Figure 3.1Aii; Section 3.3.3**). TALEN mRNAs-injected embryos (F_0) were grown to adulthood and mated with wild type (WT) zebrafish to analyse the germline transmission efficiency of mutations in offspring (F_1) (**Figure 3.1Bi; Section 3.3.4**). F_1 generations were then grown to adulthood to identify heterozygous carriers by fin-clip genotyping (**Figure 3.1Ci-ii**). Homozygous zebrafish (F_2) mutant lines were established by in-crossing heterozygous F_1 carriers (**Figure 3.1Di-Ei-ii; Section 3.3.5**) and homozygous mutant lines (F_3) were generated by in-crossing homozygous carriers (**Figure 3.1Fi-Gi; Section 3.3.5)**. Furthermore, double homozygous mutant line lacking both *def6a* and *swap70b*, were established by crossing single homozygous mutants. Double heterozygous mutants were then in-crossed to generate double homozygous mutants (**Section 3.3.6**). Phenotypic analysis, whole mount *in situ* hybridisations and rescue experiments by injecting mRNAs encoding the potential downstream targets were carried out on single (*def6a*$^{qmc811/qmc811}$, *swap70b*$^{qmc809/qmc809}$) and double homozygous mutant (*def6*$^{qmc811/qmc811}$*;swap70b*$^{qmc809/qmc809}$) lines (**Figure 3.1Gii**).

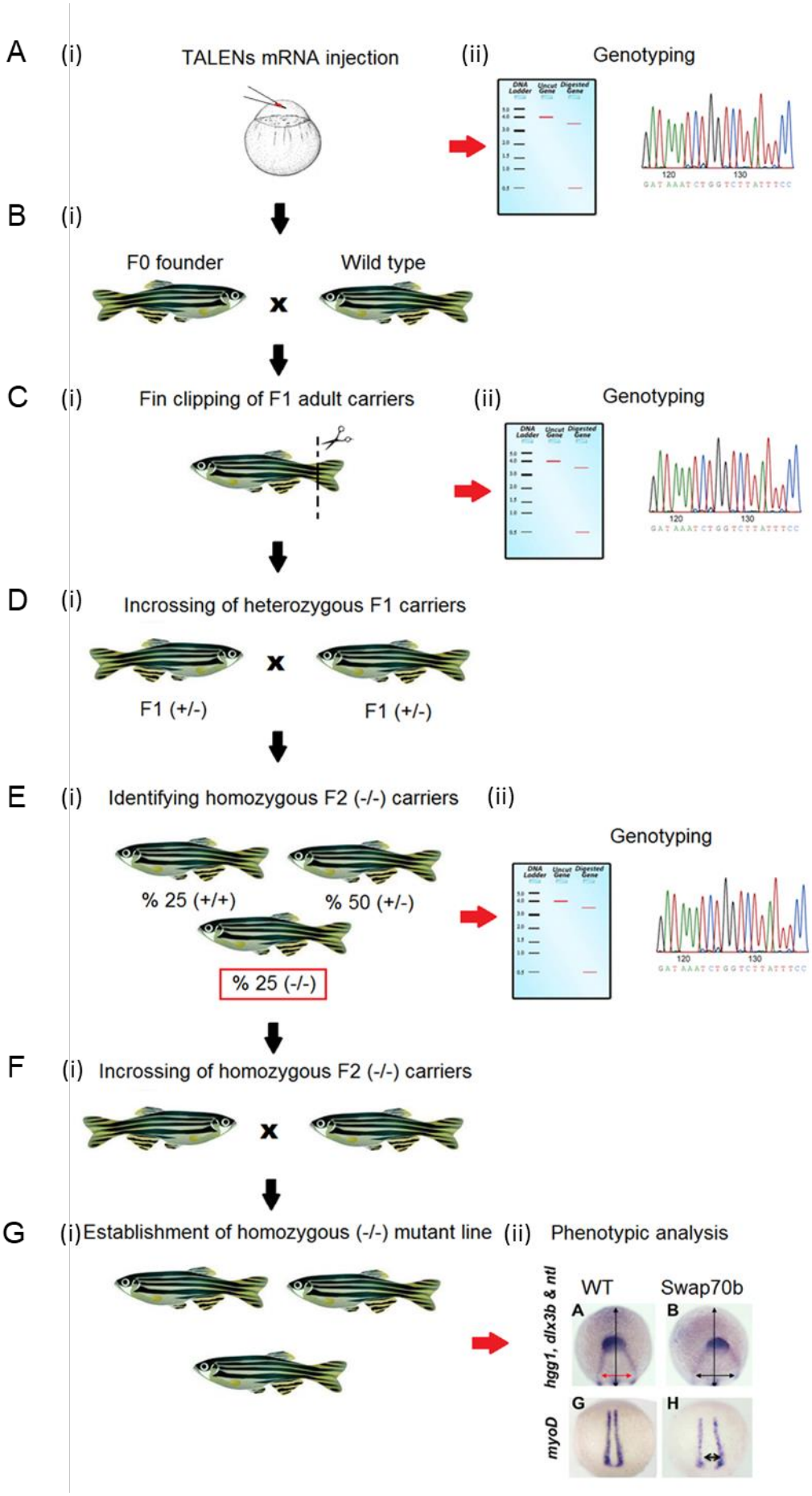

A
(i)
TALENs mRNA injection
(ii)
Genotyping
B
(i)
F0 founder
Wild type
x
C
(i)
Fin clipping of F1 adult carriers
(ii)
Genotyping
D
(i)
Incrossing of heterozygous F1 carriers
x
F1 (+/-)
F1 (+/-)
E
(i)
Identifying homozygous F2 (-/-) carriers
(ii)
Genotyping
% 25 (+/+)
% 50 (+/-)
% 25 (-/-)
F
(i)
Incrossing of homozygous F2 (-/-) carriers
x
G
(i)
Establishment of homozygous (-/-) mutant line
(ii)
Phenotypic analysis
WT
Swap70b
hgg1, dlx3b & ntl
myoD
A
B
G
H

Figure 3.1 Overview of the TALEN-mediated establishment of the *def6a* and *swap70b* homozygous mutant lines. (A)(i) After TALEN mRNAs were injected, **(ii)** the mutation efficiency was evaluated by genotyping. **(B)(i)** F_0 mosaic embryos were raised to adulthood to generate F_1 carriers and to evaluate the germline transmission efficiency. **(C)(i)** After fin clipping of F_1 adult carriers, **(ii)** heterozygous F_1 (+/-) carriers were identified for **(D)(i)** in-crossing and **(E)(i-ii)** identifying F_2 (-/-) homozygous carriers by genotyping. **(F-G)(i)** Homozygous mutant line was established by in-crossing F_2 (-/-) homozygous carriers. **(G)(ii)** Phenotypic analysis by observing the development of mutant embryos and whole mount *in situ* hybridisation-mediated gene expression analysis were carried out on mutant lines and WT embryos as control.

3.2. Construction and design of TALENs targeting *def6a* and *swap70b* loci

The zebrafish *def6a* gene (zgc:63721; ENSDARG00000012247) is located on chromosome 8:14,147,590-14,172,147 and has 11 exons encoding a 612-amino acid protein (www.ensemble.org). The zebrafish *swap70b* gene (si:dkey-8l13.4; ENSDARG00000057286) is located on chromosome 18:16,887,767-16,927,774 and has 12 exons encoding a 588-amino acid protein (www.ensembl.org). **Exon-1** encodes the EF-hand region for both *def6a* and *swap70b* genes and was targeted specifically in both cases by TALEN mRNAs immediately downstream of the start codon to generate knock-out zebrafish lines by creating a premature stop codon or possible truncated proteins. TALEN plasmids for both *def6a* and *swap70b* were generated by Keith Joung's research group and obtained from Addgene (www.addgene.com). All TALENs were synthesised with Golden Gate Assembly method on a JDS74 vector backbone. The plasmid maps are illustrated in **Appendix I**. TALEN mRNA sequences targeting *def6a* and *swap70b* loci and restriction sites are listed in **Section 2.1.1.1; Table 2.2.** The mutagenesis of *def6a* and *swap70b* loci is illustrated in **Figure 3.2**.

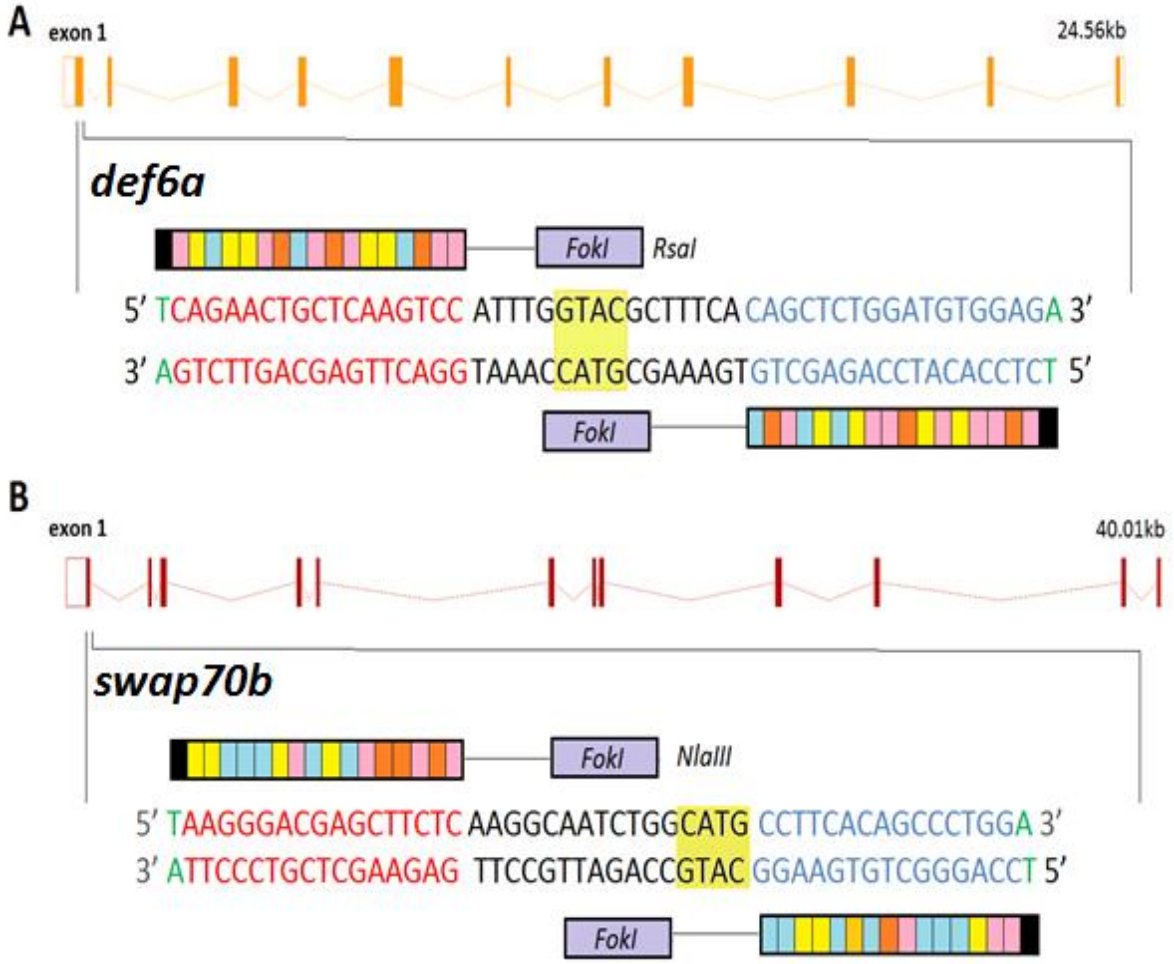


Figure 3.2 Left and right TALEN binding sequences targeting exon-1 of *def6a* (A) and *swap70b* (B) loci to generate knock-out zebrafish lines (A) Figure illustrates the left and right TALEN binding sequences targeting exon-1 of *def6a* locus. The spacer region contains the restriction site, *RsaI,* for diagnosing the mutations. Forward and reverse primers (FP' and RP') were designed to amplify a 350bp sequence for *def6a* locus including the TALEN-binding regions. **(B)** Figure illustrates the left and right TALEN binding sequences targeting exon-1 of *swap70b* locus. The spacer region contains the restriction site, *NlaIII* for diagnosing the mutations. Forward and reverse primers (FP' and RP') were designed to amplify a 243bp sequence for *swap70b* locus including the TALEN-binding regions. Red and blue colours indicate left and right TALEN sequences (5'-3'), respectively, and the spacer regions are indicated by black colour. The restriction sites for *RsaI* and *NlaIII* are highlighted in yellow. Adenine (A), guanine (G), cytosine (C) and thymine (T) bases are illustrated in yellow, blue, pink and orange, respectively.

3.3. TALEN-mediated targeted mutations at *def6a* and *swap70b* loci

3.3.1. *In vitro* transcription of *def6a* and *swap70b* TALEN mRNAs

In vitro transcription of mRNAs requires a purified linear DNA template as the transcription proceeds to the end of the DNA template and linearisation is essential for a defined length of RNA transcripts. Therefore, TALEN vectors of *def6a* (TAL3420 and TAL3421) and *swap70b* (TAL3566 and TAL3567) were linearised with *PmeI* restriction enzyme **(Section 2.2.1.4; Figure 3.3A-B)** and TALEN mRNAs were synthesised by *in vitro* transcription **(Section 2.2.3.1; Figure 3.3C-D)**. Left and right TALEN mRNAs were mixed in a 1:1 ratio at a concentration of 500ng/µl for microinjections.

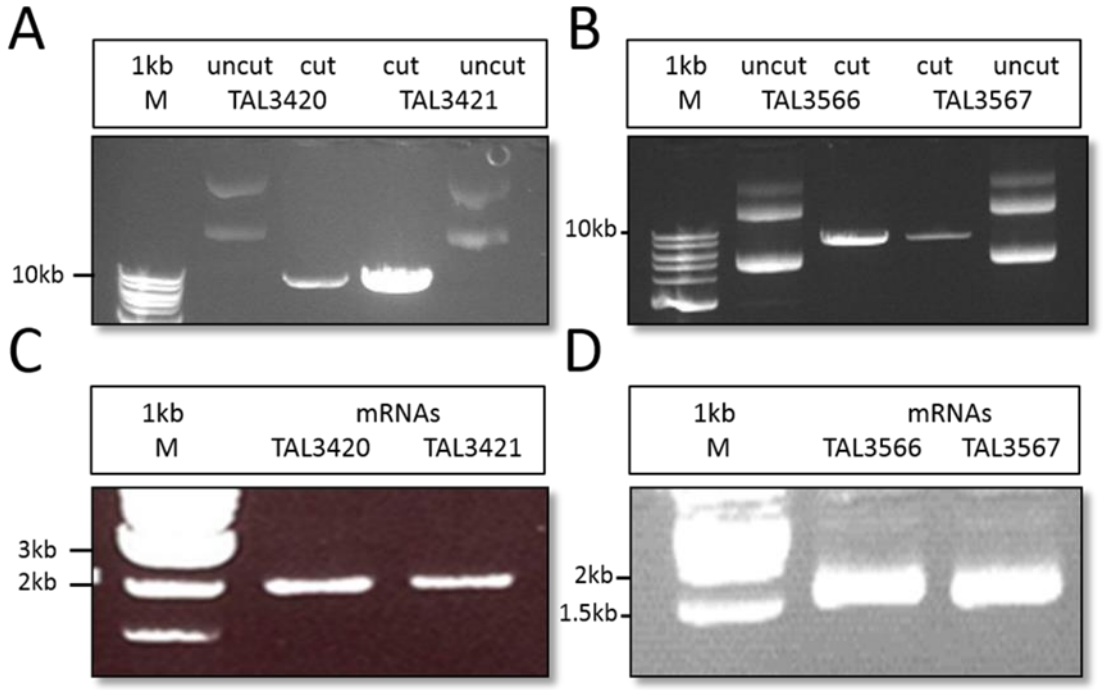


Figure 3.3 Linearisation of *def6a* and *swap70b* TALEN plasmids and *in vitro* transcription of *def6a* (TAL3420-TAL3421) and *swap70b* (TAL3566-TAL3567) TALEN mRNAs. (A) Linearised plasmids of *def6a* are shown as cut TAL3420, cut TAL3421 whereas, **(B)** Linearised plasmids of *swap70b* are shown as cut TAL3566, cut TAL3567. Supercoiled and nicked circle of undigested plasmids were observed for uncut TALEN 3420, TALEN 3421, TALEN 3566 and TALEN3567, whereas linearised plasmids exhibited a single fragment. *In vitro* transcription of **(C)** *def6a* (TAL3420 and TAL3421) and **(D)** *swap70b* (TAL3566 and TAL3567) TALEN mRNAs demonstrated that mRNAs were not degraded and suitable for microinjection. (M: DNA molecular weight marker, 1 kb. Molecular weights of 1kb ladder are pointed in the figure.

3.3.2. Optimising the amount of TALEN mRNAs injected for efficient mutagenesis

Injection of high amount of TALEN mRNAs can be toxic and low amount might not result in efficient mutagenesis. Therefore, TALEN mRNAs were diluted to 500ng/µl. Two distinct amounts of *def6a* TALEN mRNAs; 125pg and 250pg were injected. Similarly, two distinct amounts of *swap70b* TALEN mRNAs; 250pg and 500pg were injected. The efficiency of the TALEN-mediated mutations was tested by analysing the genomic DNA isolated from WT and injected embryos at 48hpf. Using primers flanking the target sites of the TALENs (see **Section 2.2.2; Table 2.19**), the amplified products were subsequently digested with diagnostic restriction enzymes *RsaI* for *def6a* and *NlaIII* for *swap70b* (**Figure 3.2**). The amplified products that were not digested by either *RsaI* or *NlaIII* were subcloned and sequenced (see **Sections 2.2.1.9** and **2.2.1.10**) to determine TALEN-mediated mutations.

3.3.2.1. Genotyping and analysing the mutation efficiency in *def6a* locus

After amplification of the *def6a* TALEN region, the expected fragment size is 350bp. Digestion with *RsaI* endonuclease may reveal different outcomes. WT embryos are un-injected controls which contain the sequence of intact spacer region and the restriction site allowing the complete digestion of DNA. **(Appendix II)**:

1. WT control shows two fragment sizes of 226bp and 124bp.
2. Embryo which does not carry any mutation shows two fragment sizes of 226bp and 124bp.
3. Embryo which carries mutation, is partially digested and shows three fragment sizes of 350bp, 226bp and 124bp.

Exceptionally, the heterozygous *def6a*$^{+/qmc811}$ mutants showed four fragments including the undigested *qmc811* mutant allele, 339bp. The homozygous *def6a*$^{qmc811/qmc811}$ mutants were not digested showing an intact fragment of 339bp.

3.3.2.2. Genotyping and analysing the mutation efficiency in *swap70b* locus

Similar to the *def6a* locus, amplification of the *swap70b* TALEN region reveals the expected fragment size of 243bp. After the digestion with *NlaIII*, different outcomes may be come across (**Appendix II**):

1. WT control shows two fragment sizes of 145bp and 98bp.
2. Embryo which does not carry any mutation shows two fragment sizes of 145bp and 98bp.
3. Embryo which carries mutation, is partially digested and shows three fragment sizes of 243bp, 145bp and 98bp.

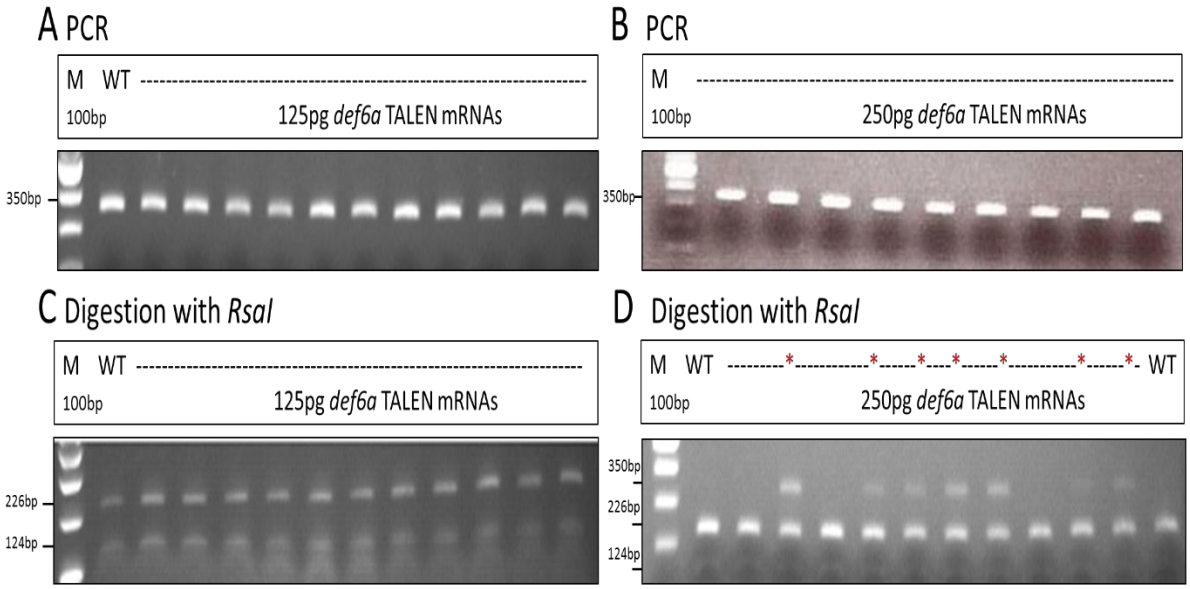
Exceptionally, the heterozygous *swap70b*$^{+/qmc809}$ mutants showed four fragments including the undigested *qmc809* mutant allele, 189bp. The homozygous *swap70b*$^{qmc809/qmc809}$ mutants were not digested showing an intact fragment of 189bp.

3.3.3. TALEN mRNAs-induced somatic mutations at *def6a* and *swap70b* loci

As illustrated in **Figure 3.4**, amplification and digestion of the TALEN region of 125pg *def6a* TALEN mRNAs-injected embryos demonstrated two fragments of 226bp and 124bp indicating that there is no mutation at the restriction site of the spacer region **(Figure 3.4C)**. In contrast, 7 out of 10 of the 250pg *def6a* TALEN mRNAs-injected embryos were partially digested showing an additional fragment of 350bp in addition to the digested fragments of 226bp and 124bp, indicating mutations at the restriction site **(Figure 3.4D)**. The sequencing analysis confirmed that 250pg *def6a* TALEN mRNAs injection generated deletions of 5bp and 11bp and insertions of 11bp, 17bp and 27bp at *def6a* loci **(Figure 3.4E)**.

As illustrated in **Figure 3.5**, amplification and digestion of the TALEN region of 250pg and 500pg *swap70b* TALEN mRNAs-injected embryos revealed that 2 out of 5 250pg *swap70b* TALEN mRNAs-injected embryos and 8 out of 10 500pg *swap70b* TALEN mRNAs-injected embryos were not completely digested showing three fragments of 243bp, 145bp and 98bp indicating the mutations at the targeted site. The sequencing analysis confirmed the deletions of 7bp and 13bp and insertions of 96bp for 250pg *swap70b* TALEN mRNAs injection **(Figure 3.5E)** and also the deletions of 12bp, 43bp and 23bp and insertions of 46bp for 500pg *swap70b* TALEN mRNAs injection **(Figure 3.5F)**.

To calculate the mutation efficiency **(Figure 3.6)**, two different sets of injections were carried out for each concentration of *def6a* and *swap70b* TALEN mRNAs. While 60% (13 samples out of 22) and 70% (7 samples out of 10) **(Figure 3.4D)** of mutation efficiency were calculated for 250pg *def6a* TALEN mRNAs, 0% (0 samples out of 14 and 0 samples out of 9) of mutation efficiency was calculated for 125pg *def6a* TALEN mRNAs. 15% (2 samples out of 13) and 40% (2 samples out of 5) **(Figure 3.5C)** mutation efficiencies for 250pg *swap70b* TALEN mRNAs and 60% (6 samples out of 10) and 80% (8 samples out of 10) **(Figure 3.5D)** mutation efficiencies were calculated for 500pg *swap70b* TALEN mRNAs. Average mutation efficiencies for each concentration was also indicated in **Figure 3.6.** These results indicate that *def6a* and *swap70b* TALEN mRNA injections successfully induced somatic mutations and increasing the amount of injected TALEN mRNAs induced more mutations for both targeted loci.



E 250pg *def6a* TALEN mRNAs induced somatic indel mutations

```
                LEFT TALEN              SPACER            RIGHT TALEN
WT 5′ TCAGAACTGCTCAAGTCCATTTGGTACGCTTTCACAGCTCTGGATGTGGAGA 3′ 52
   5′ TCAGAACTGCTCAAGTCC----------TTTCACAGCTCTGGATGTGGAGA 3′ 41 Δ11
   5′ TCAGAACTGCTCAAGTCCATTTG-----CTTTCACAGCTCTGGATGTGGAGA 3′ 47 Δ5
   5′ TCAGAACTGCTCAAGTCCATTTGGTACGCTTTCTTTCCTCTGGNTGGGGGA 3′ 52 Δ17 +17
   5′ TCAGAACTGCTCAAGTCCATTTGTCACACTTCTGCATGTGTGGATGAGTGGA 3′ 52 Δ27 +27
      ******************          **       * *** ** *  **

WT 5′ TCAGAACTGCTCAAGTCCATTTGGTACG--------CTTTCACAGCTCTGGATGTGGAGA 3′52
   5′ TCAGAACTGCTCAAGTCCATTTGGTCCTTTCAAGTCCTTTCACAGCTCTGGATGTGGAGA 3′60Δ11 +11
      ************************          ************************
```

Figure 3.4 Induction of somatic mutations at the targeted locus by injecting *def6a* TALEN mRNAs. (A-B) A 350bp DNA fragment was amplified after the injections of **(A)** 125pg and **(B)** 250pg *def6a* TALEN mRNAs. **(C-D)** Digestion of the amplified samples revealed two fragments of 226bp and 124bp for WT and samples that do not contain any mutation, whereas samples that contain the mutations at the restriction site could not be digested by *RsaI* and three fragments of 350bp, 226bp and 124bp were formed. Red asterisk (*) indicates the samples showing an additional undigested fragment of 350bp. **(E)** Sequencing of 250pg *def6a* TALEN mRNAs-injected embryos confirmed the deletions and insertions at the TALEN region. Left and right TALEN binding sequences are highlighted in yellow and grey colours, respectively. The direction of each sequence is 5' to 3'. Red dashes (-) indicate deletions and red letters indicate insertions. M: Size marker; 100bp (NEB). WT: Wild type.

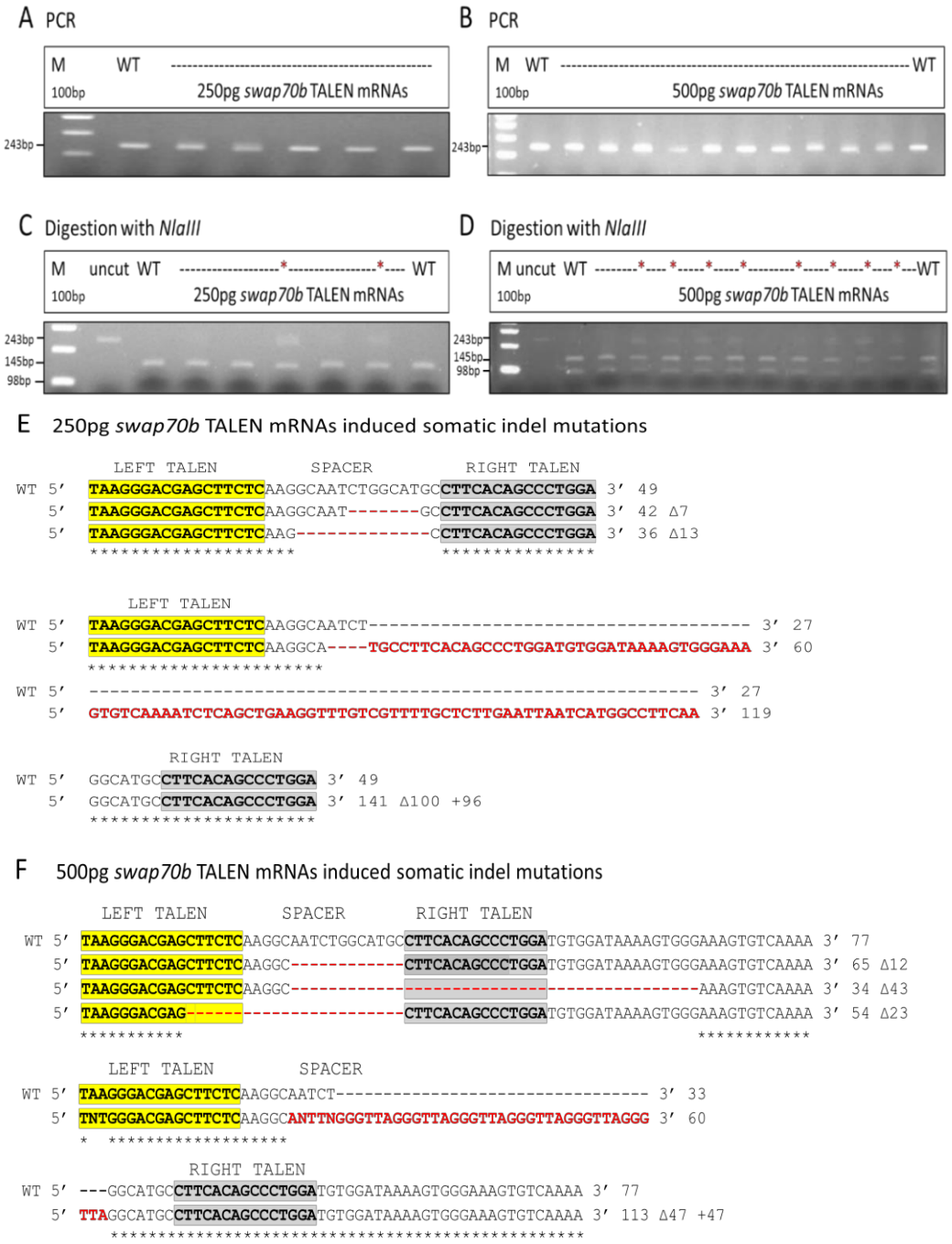


Figure 3.5 Induction of somatic mutations at the targeted locus by injecting *swap70b* TALEN mRNAs. (A-B) 243bp DNA fragment was amplified after the injections of **(A)** 250pg and **(B)** 500pg *swap70b* TALEN mRNAs. **(C-D)** Digestion of the amplified samples revealed two fragments of 145bp and 98bp for WT and samples that do not contain any mutation, whereas *NlaIII* could not digest the samples that contain mutations at the restriction site and three fragments of 243bp, 245bp and 98bp were formed. Red asterisk (*) indicates the samples showing an additional undigested fragment of 243bp. Sequencing of **(E)** 250pg and **(F)** 500pg *swap70b* TALEN mRNAs-injected embryos confirmed the deletions and insertions at the TALEN region. Left and right TALEN binding sequences are highlighted in yellow and grey colours, respectively. The direction of each sequence is 5' to 3'. Red dashes (-) indicate deletions and red letters indicate insertions. M: Size marker; 100bp (NEB). WT: Wild type.

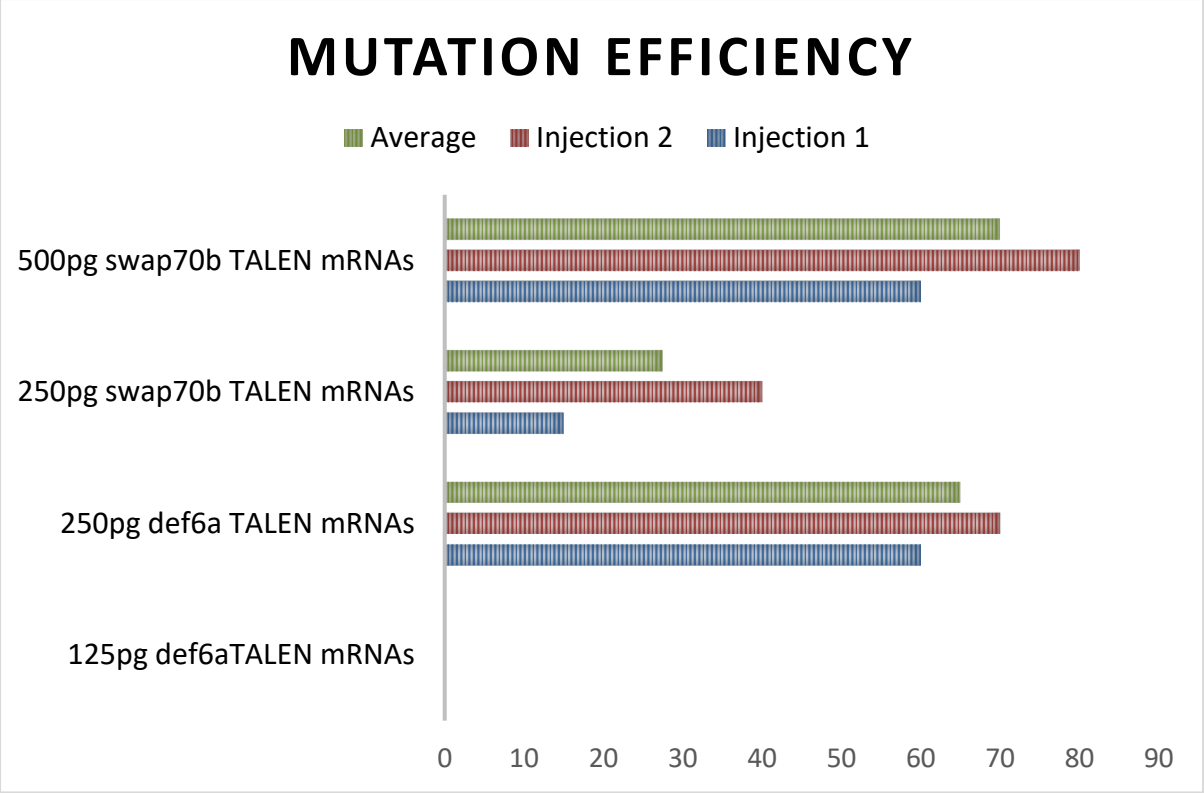


Figure 3.6 Chart indicates the mutation efficiencies after two sets of *def6a* and *swap70b* TALEN mRNAs injection. Average mutation efficiencies were calculated as 0% for 125pg *def6a*, 65% for 250pg *def6a* TALEN mRNAs, 27% for 250pg *swap70b* and 70% for 500pg *swap70b* TALEN mRNAs.

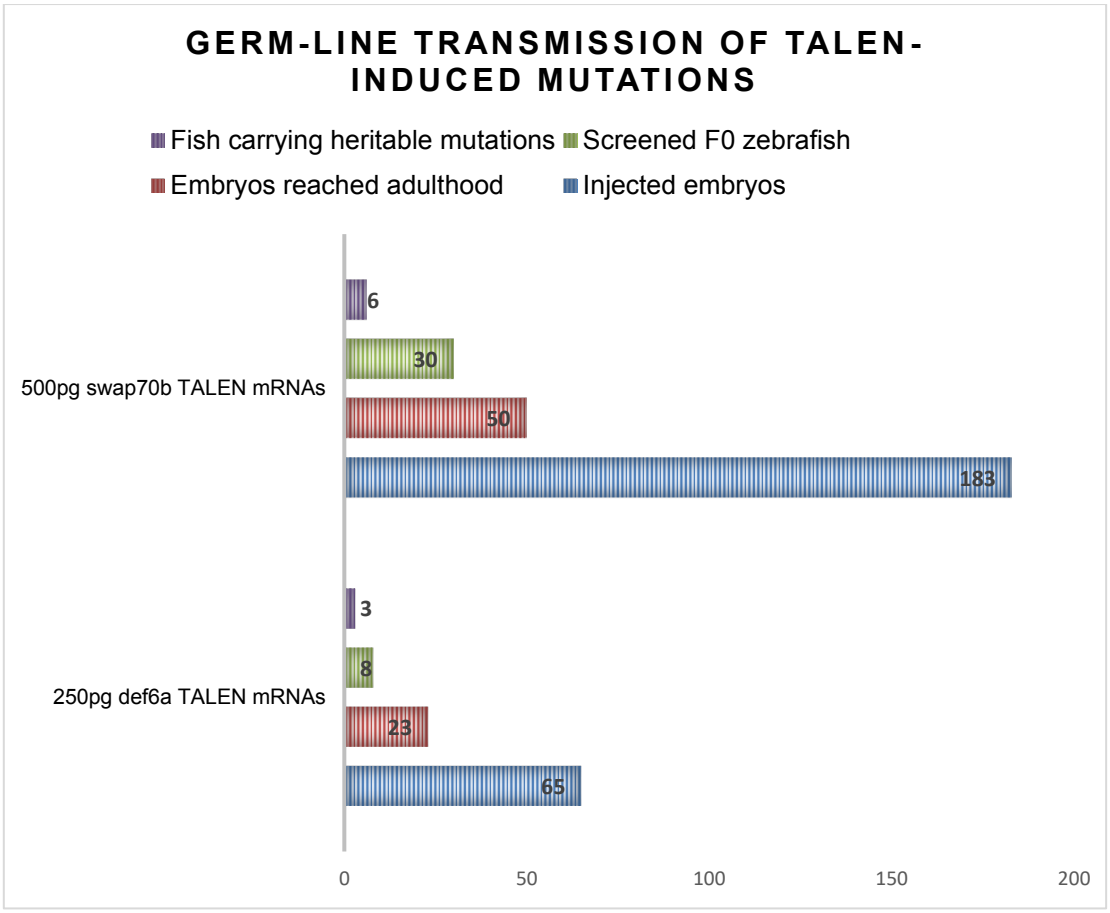
3.3.4. Germline transmission of TALEN-induced mutations

To generate a homozygous mutant line, the mutations must be transmitted to offspring through the germline. Therefore, as discussed earlier in this chapter **(Figure 3.1Bi)**, 250pg *def6a* and 500pg *swap70b* TALEN mRNAs-injected embryos were grown to adulthood and out-crossed with WT. The offspring (F_1) was genotyped for assessing the germline transmission efficiency.

As illustrated in **Figure 3.7**, 250pg *def6a* TALEN mRNAs were injected into 62 embryos and only 23 zebrafish were able to grow to adulthood. 8 fish were out-crossed with WT fish to check the germline transmission of mutations and 3 of them were found to carry heritable mutations. The germline transmission efficiency was calculated as 37.5% (3 fish out of 8).

500pg *swap70b* TALEN mRNAs were injected into 183 embryos and only 50 zebrafish were able to grow to adulthood. 30 fish were out-crossed with WT fish and only 6 of them were found to carry heritable mutations. The germline transmission efficiency was calculated as 20% (6 fish out of 30) **(Figure 3.7)**.

3 *def6a* F_0 founders and 6 *swap70b* F_0 founders were found to be carrying the heritable mutations to transfer into the offspring (F_1). In-frame and frameshift mutations are listed in **Figure 3.8** and **Figure 3.9** for *def6a* and *swap70b*, respectively. Specifically, 2 out of 3 *def6a* F_0 founders were found to be carrying frameshift mutations. While the mutations (-9bp) in founder 1 did not lead a frameshift, the mutations (-28bp; -2bp and +19bp) in founders 2 and 3 led to frameshifts. Therefore founders 2 and 3 were selected for generating *def6a* F_1 fish. The germline transmission efficiency of mutations was ranging from 10% to 20% for *def6a* founders **(Table 3.1)**. Furthermore, 3 out of 6 *swap70b* F_0 founders were found to be carrying frameshift deletions. Founders 1 and 2 were selected for generating *swap70b* F_1 fish, since the mutations (-54bp) in founder 1 include the 5' untranslated region (UTR) and start codon (ATG) of translation and the mutations (-82bp) in founder 2 resulted in frameshifts mutations. The mutations in founders 3, 4 and 5 did not lead frameshifts (-12bp, -18bp, -9bp) and the germline transmission efficiency of the mutations was low (3.3%) for founder 6, therefore, these founders were not selected for the generation of F_1 fish. The germline transmission efficiency of mutations was ranging from 3.3% to 90% for *swap70b* founders **(Table 3.2)**.



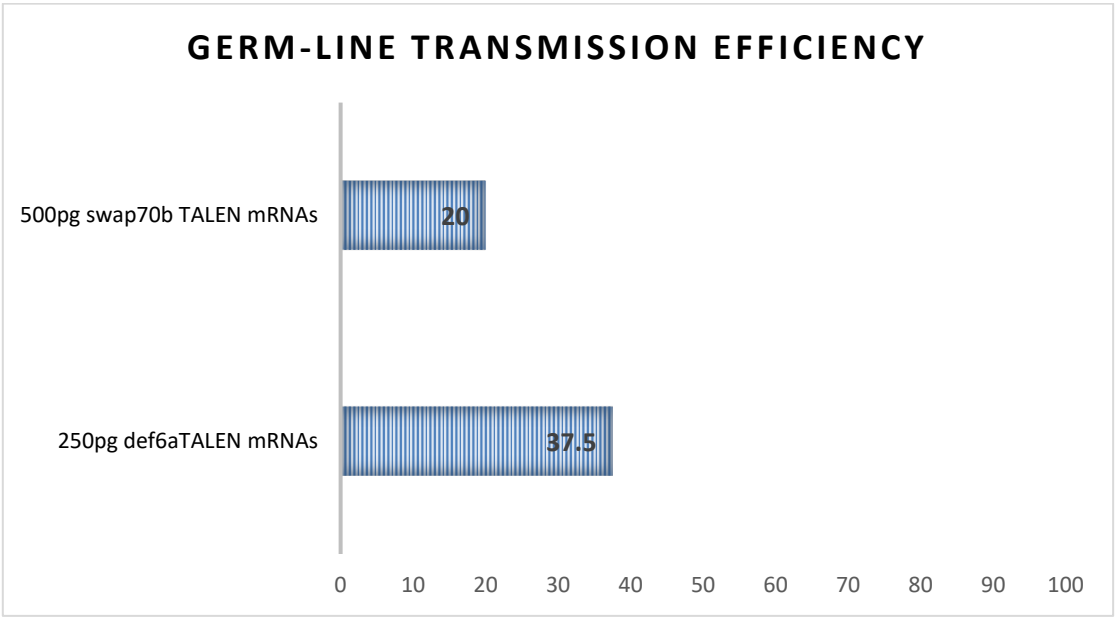


Figure 3.7 Charts illustrate the germline transmission of TALEN-induced mutations and germline transmission efficiency for both *def6a* and *swap70b* TALEN mRNAs-injected F_0 embryos.

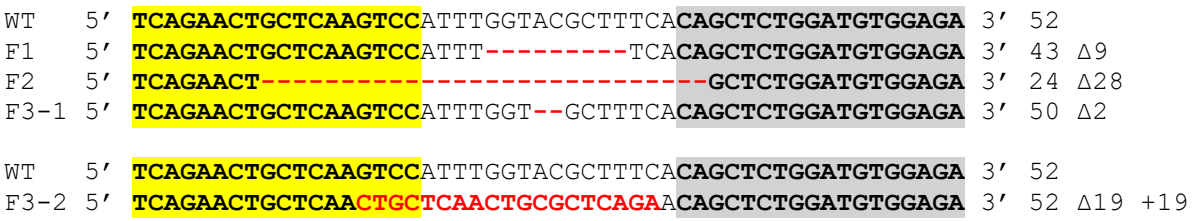


Figure 3.8 In frame and out of frame mutations were inherited from 250pg *def6a* TALEN mRNAs-injected F_0 founders. TALEN mRNAs injected-F_0 founders were grown to adulthood and crossed with WT. Embryos from each cross were genotyped by PCR, restriction digestion and sequencing. Sequencing results confirmed the in frame mutation (-9bp) for founder 1 and out of frame mutations (-28bp, -2bp and +19bp) for founders 2 and 3, respectively. Left and right TALEN binding sequences are highlighted in yellow and grey colours, respectively. The direction of each sequence is 5' to 3'. Red dashes (-) indicate deletions and red letters indicate insertions. WT: Wild type, F1: Founder 1, F2: Founder 2, F3: Founder 3; F3-1 and F3-2 indicate the two independent sequences observed for founder 3.

def6a F_0 Founders	Embryos screened	Embryos with heritable mutations	Germline transmission efficiency	Mutations
Founder 1	10	2	20%	**-9bp**
Founder 2	10	2	20%	**-28bp**
Founder 3 1	40	4	10%	**-2bp**
Founder 3 2				**-19/+19bp**

Table 3.1 Germline transmission efficiencies for *def6a* TALEN mRNAs-injected F_0 founders. The germline transmission efficiency was ranging from 10% to 20%.

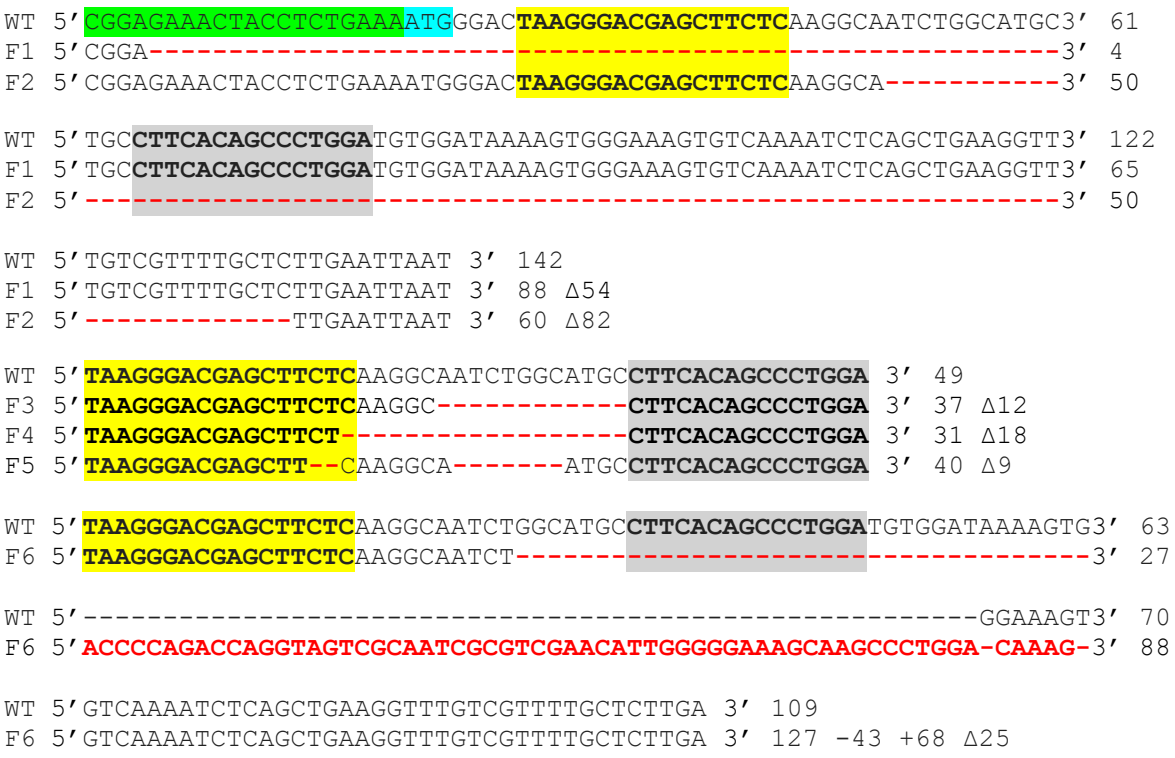


Figure 3.9 In frame and out of frame mutations were inherited from 500pg *swap70b* TALEN mRNAs-injected F_0 founders. TALEN mRNAs injected-F_0 founders were grown to adulthood and crossed with WT. Embryos from each cross were genotyped by PCR, restriction digestion and sequencing. Sequencing results confirmed the in frame mutations (-12bp, -18bp and -9bp) for founders 3, 4 and 5 and frameshift mutations, -54bp (containing 5' UTR and ATG), -82bp and -43/ +68bp for founders 1, 2 and 6, respectively. Left and right TALEN binding sequences are highlighted in yellow and grey colours, respectively. The 5' untranslated region (UTR) and the start codon (ATG) which are missing for founder 1 are highlighted in green and blue colour, respectively. The direction of each sequence is 5' to 3'. Red dashes (-) indicate deletions and red letters indicate insertions. WT: Wild type, F1: Founder 1, F2: Founder 2, F3: Founder 3, F4: Founder 4, F5: Founder 5, F6: Founder 6.

swap70b F_0 Founders	Embryos screened	Embryos with heritable mutations	Germline transmission efficiency	Mutations
Founder 1	24	13	54%	**-54bp**
Founder 2	20	8	40%	**-82bp**
Founder 3	25	14	56%	**-12bp**
Founder 4	20	2	10%	**-18bp**
Founder 5	22	20	90%	**-9bp**
Founder 6	30	1	3.3%	**-43/+68bp**

Table 3.2 Germline transmission efficiencies for *swap70b* TALEN mRNAs-injected F_0 founders. The germline transmission efficiency was ranging from 3.3% to 90%.

3.3.5. Establishment of *def6a*$^{qmc811/qmc811}$ and *swap70b*$^{qmc809/qmc809}$ mutant lines

For the *def6a*$^{qmc811/qmc811}$ mutant line, *def6a* founders 2 and 3 for were crossed with WT fish and 50 F_1 fish were selected to raise to adulthood for both founders 2 and 3. However, only 13 and 11 F_1 fish survived until adulthood for founders 2 and 3, respectively. As illustrated in **Figure 3.1C (i-ii)**, fin-clip genotyping of these fish revealed that none of the fish were carrying frameshift mutations for founder 2 and only 1 fish was carrying a frameshift mutation (-20/+9bp) in one allele for founder 3 **(Table 3.3 and Figure 3.10)**. Specifically, a 350bp DNA region was amplified after DNA extraction from fins **(Figure 3.10A)**. Digestion with *RsaI* nuclease revealed that only 1 F_1 fish was a carrier of the mutant allele since it also showed the undigested fragment of 339bp **(Figure 3.10C)**. The sequencing analysis confirmed that the heterozygous F_1 fish was carrying 20bp deletion and 9bp addition resulting in 11bp deletion **(Figure 3.10E)**. The 11bp deletion was predicted to result in a premature stop codon in the transcribed mRNA and only a truncated, non-functional or incomplete protein will be produced if any **(Figure 3.11A)**. Heterozygous F_1 fish was used for generating the homozygous mutant line which was named as ***qmc811*** (-20/+9bp; Δ11bp). The heterozygous fish was out-crossed with wild type to generate a line containing heterozygous mutants (*def6a*$^{+/qmc811}$) since there was only one mutant fish and a heterozygous line containing both female and male mutants was needed to be generated. As illustrated in **Figure 3.1D(i)**, two *def6a*$^{+/qmc811}$heterozygous mutants were in-crossed to identify the *def6a*$^{qmc811/qmc811}$ homozygous mutants and to analyse the Mendelian inheritance rate of the mutant allele. After genotyping 20 individual embryos, the *qmc811* mutant allele was found to be inherited at the expected Mendelian rate (~25%) **(Figure 3.12A)**. As shown in **Figure 3.1E (i-ii)**, fin-clip genotyping of the F_2 generation to find homozygous mutants revealed that 6 out of 30 (20%) fish were *def6a*$^{qmc811/qmc811}$ homozygous mutants (Only 3 of them are shown in **Figure 3.13A-C**). Therefore, two of these fish were in-crossed to establish a homozygous mutant line (**Figure 3.1Fi-Gi**) and the homozygosity was confirmed by genotyping **(Figure 3.14A-C)**. The *def6a*$^{qmc811/qmc811}$ mutant line was used for phenotypic analysis and also for establishing a double homozygous mutant line (**Figure 3.1Gii**).

For the *swap70b*$^{qmc809/qmc809}$ mutant line, *swap70b* founders 1 and 2 were crossed with WT fish and 100 F_1 fish were selected to grow for both founders 1 and 2. Only 40 and 90 F_1 fish survived until adulthood for founders 1 and 2, respectively. As illustrated in **Figure 3.1C (i-ii)**, fin-clip genotyping of 10 F_1 fish of founder 1 revealed that 2 fish carrying the same mutation (-54bp) in one allele **(Table 3.3 and Figure 3.10)**. A 243bp DNA region was amplified after DNA extraction from fins. However, not only the wild type allele fragment of 243bp, but also the mutant allele fragment of 189bp was observed due to the large deletion (54bp) **(Figure 3.10B)**. Digestion with *NlaIII* nuclease confirmed that 2 F_1 fish were carriers of the mutant allele since an undigested fragment of 189bp was also visible **(Figure 3.10D)**. Sequencing analysis confirmed that heterozygous F_1 fish were carrying the same 54bp deletion inherited from *swap70b* F_0 founder 1 **(Figure 3.10E)**. The 54bp deletion was predicted to block the translation of Swap70b protein by preventing the binding of the translational machinery to 5'UTR sequence since the deletions include both 5' UTR and start codon (AUG) of *swap70b* or the translation might start from the next AUG which would result in a N-terminally-truncated protein formed of 547 amino acids missing the first 41 amino acids **(Figure 3.11B)**. Heterozygous F_1 fish was used for generating the homozygous mutant line which was named as ***qmc809*** (-54bp). F_1 adults from Founder 2 were kept as a back-up since only one homozygous mutant line is enough for the phenotypic analysis. Therefore, fin-clip genotyping was not applied on these fish. As illustrated in **Figure 3.1D(i)**, two *swap70b*$^{+/qmc809}$heterozygous mutants were in-crossed to identify *swap70b*$^{qmc809/qmc809}$ homozygous mutants and to analyse the Mendelian inheritance rate of the mutant allele**.** Genotyping 50 individual embryos revealed that the mutant allele was found to be inherited at the expected Mendelian rate (~25-30%) **(Figure 3.12B)**. As shown in **Figure 3.1E (i-ii),** fin-clip genotyping of the F_2 generation to identify homozygous mutants revealed that 12 out of 44 (27%) fish were homozygous (*swap70b*$^{qmc809/qmc809}$) (Only 4 of them are shown in **Figure 3.13B-D**). Two of these fish were in-crossed to establish *swap70b*$^{qmc809/qmc809}$ homozygous mutant line (**Figure 3.1Fi-Gi**). Genotyping of homozygous mutant line (*swap70b*$^{qmc809/qmc809}$) confirmed the homozygosity for all fish **(Figure 3.14B-D)**. *swap70b*$^{qmc809/qmc809}$ mutant line was used for the phenotypic analysis and also for establishing a double homozygous mutant line (**Figure 3.1Gii**).

F1 Heterozygous carriers	Number of embryos selected for growing	Survived fish until adulthood	Fin-clip genotyping	F_1 fish carrying frameshift mutation
def6a **F_1 carriers from Founder 2**	50	13	13	0
def6a **F_1 carries from Founder 3**	50	11	11	1 -20 /+9bp
swap70b **F_1 carries from Founder 1**	100	40	10	2 -54bp

Table 3.3 The number of F_1 adults fin-clip genotyped to establish *def6a*$^{qmc811/qmc811}$ and *swap70b*$^{qmc809/qmc809}$ homozygous mutant lines

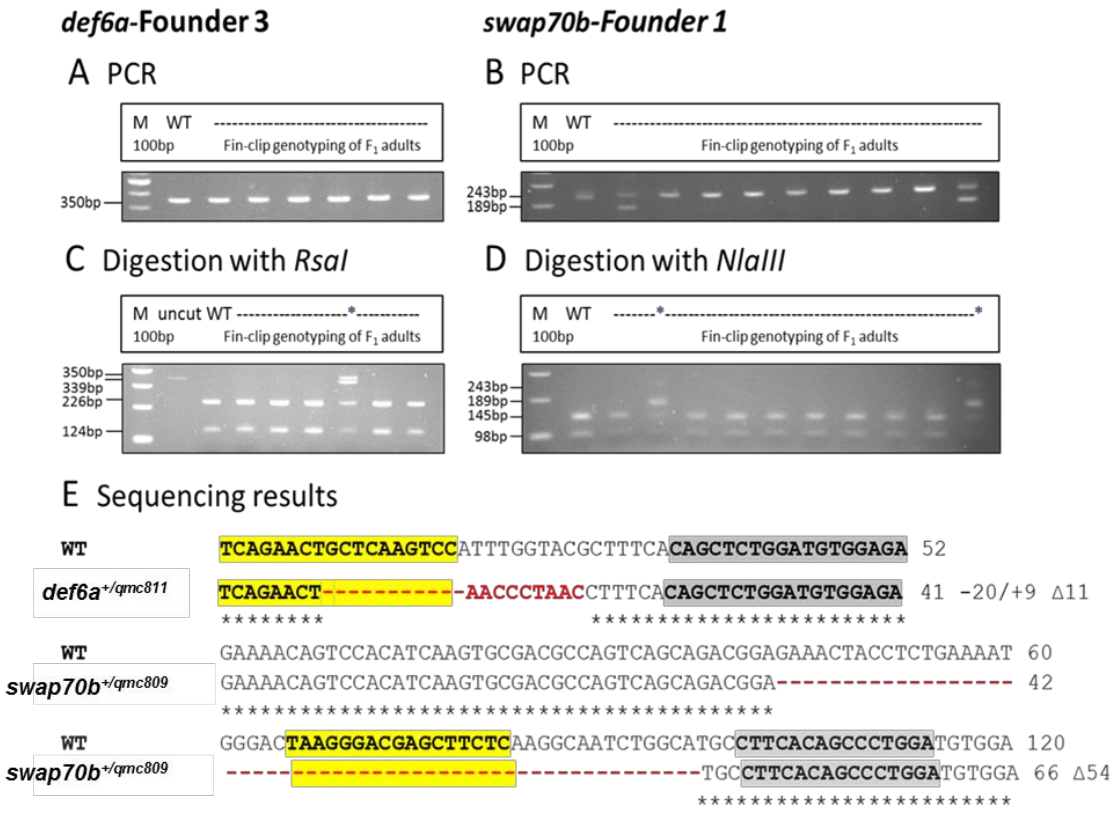


Figure 3.10 Fin-clip genotyping to find heterozygous F_1 carriers. Amplification of the TALEN regions by PCR and subsequent digestion with *RsaI* and *NlaIII* nucleases revealed that 1 F_1 fish from *def6a* founder 3 and 2 F_1 fish from *swap70b* founder 1 were carrying the mutations in one allele. **(A)** A 350bp and **(B)** a 243bp DNA fragments were amplified after the DNA extraction from fins. Due to the large deletion (54bp) in *swap70b* heterozygous F_1 carriers (*swap70b*$^{+/qmc809}$), an additional fragment of 189bp was also visible after PCR in contrast to the amplified fragments of *def6a* heterozygous F_1 carriers (*def6a*$^{+/qmc811}$) which were overlapped and not visible due to the small deletion (11bp). **(C)** Digestion of the amplified samples with *RsaI* nuclease revealed that only 1 fish was carrying the mutant allele (*qmc811*) exhibiting also the undigested fragment of 339bp. WT control was completely digested showing the fragments of 226bp and 124bp as expected. **(D)** Digestion of the amplified samples with *NlaIII* nuclease revealed that 2 fish were carrying the mutant allele (*qmc809*) exhibiting also the undigested fragment of 189bp. WT control was digested showing the fragments of 145bp and 98bp as expected. **(E)** The sequencing results confirmed that *def6a* F_1 and *swap70b* F_1 heterozygous fish were carriers of mutations. Left and right TALEN binding sequences are highlighted in yellow and grey colours, respectively. The direction of each sequence is 5' to 3'. Red dashes (-) indicate deletions and red letters indicate insertions. Purple asterisk (*) indicates heterozygous F_1 adults carrying the mutant allele since they exhibited the undigested fragments of 339bp and 189bp for *def6a* and *swap70b*, respectively. M: Size marker; 100bp (NEB). WT: Wild type, uncut: undigested control of WT sample, F_1: F_1 heterozygous carries.

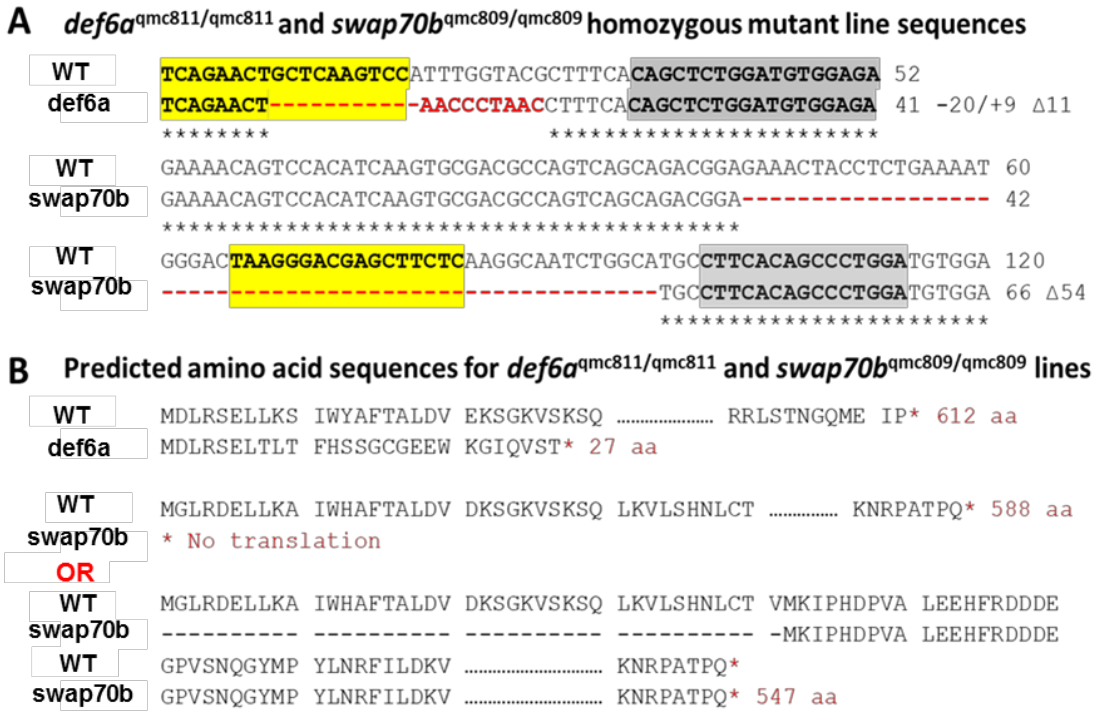


Figure 3.11 Mutated DNA and predicted protein sequences of *def6a*$^{qmc811/qmc811}$ and *swap70b*$^{qmc809/qmc809}$ mutant lines. (A-B) Nucleotide and amino acid sequence alignments of WT-def6a and mutated-def6a suggested the production of a truncated protein of def6a due to the premature stop codon after 27 amino acids. Nucleotide and amino acid sequence alignments of wild type-swap70b and mutated swap70b suggested that either a truncated protein formed of 547 amino acids will be produced or the translation will not occur. Left and right TALEN binding sequences are highlighted in yellow and grey colours, respectively. The direction of each sequence is 5' to 3'. Red dashes (-) indicate deletions and red letters indicate insertions. Red asterisk (*) indicates the premature stop codon. WT: wild type, aa: amino acid. The amino acid sequences of def6a and swap70b are shown in Appendix III.

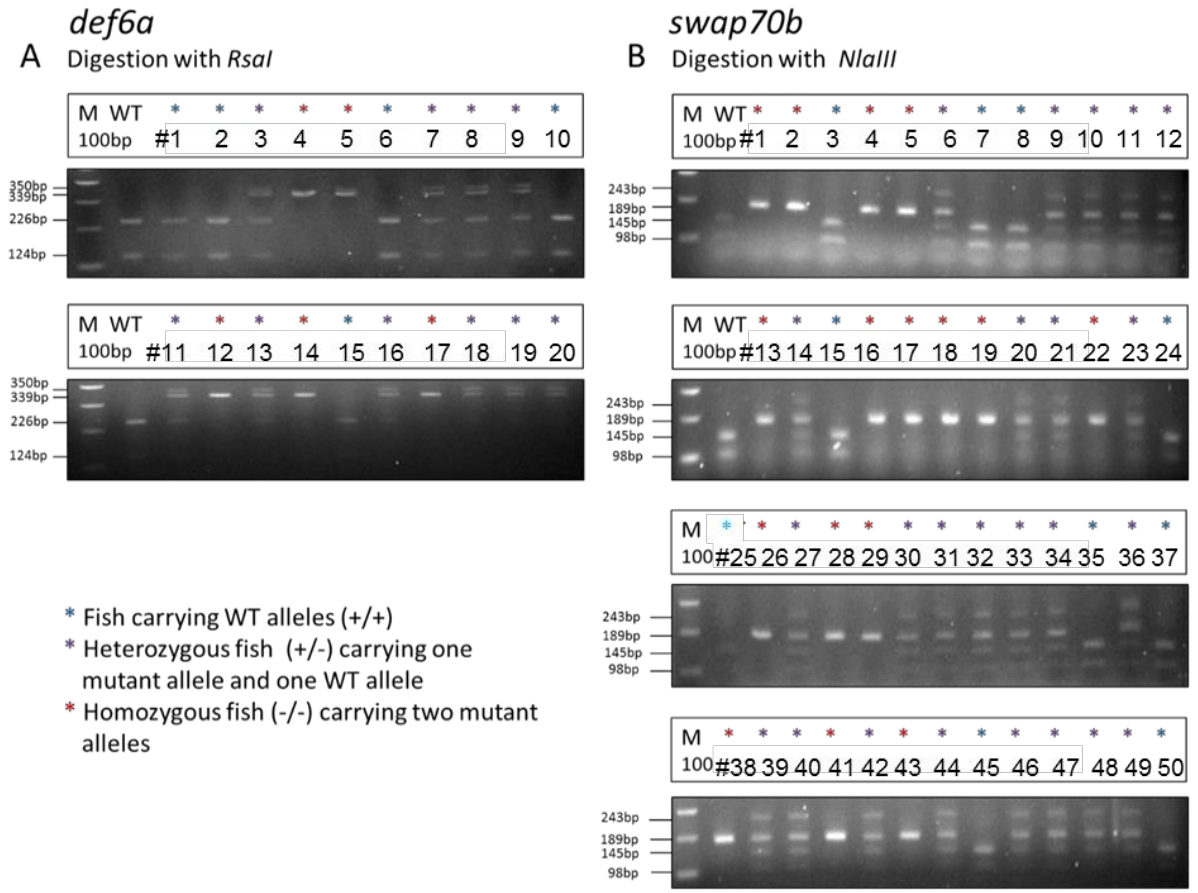


Figure 3.12 Distribution of *qmc811*^{def6a} and *qmc809*^{swap70b} mutant alleles were found at the expected Mendelian rate. (A) Two heterozygous mutants (*def6a*$^{+/qmc811}$) were in-crossed to establish homozygous mutants (*def6a*$^{qmc811/qmc811}$) and the expected Mendelian rate for *qmc811* allele was 25%. Digesting 20 samples with *RsaI* revealed that, the distribution of the *qmc811*^{def6a} mutant allele was consistent with the expected Mendelian rate since 5 homozygous mutants (*def6a*$^{qmc811/qmc811}$) (25%), 5 wild types (*def6a*$^{+/+}$) (25%) and 10 heterozygous mutants (*def6a*$^{+/qmc811}$) (50%) were found. WT controls (+/+) (indicated with WT) and WT fish (*def6a*$^{+/+}$) (indicated with blue asterisks) were completely digested exhibiting two fragments of 226bp and 124bp. Heterozygous mutants (*def6a*$^{+/qmc811}$) (indicated with purple asterisks) were partially digested exhibiting fragments of 350bp, 339bp, 226bp and 124bp. Homozygous mutants (*def6a*$^{qmc811/qmc811}$)(indicated with red asterisks) were not digested exhibiting a fragment of 339bp. **(B)** The expected Mendelian rate for *qmc809*^{swap70b} allele was 25% since two heterozygous mutants (*swap70b*$^{+/qmc809}$) were in-crossed to establish homozygous mutants (*swap70b*$^{qmc809/qmc809}$). Digestion of 50 samples with *NlaIII* revealed that, the distribution of *qmc809*^{swap70b} mutant allele was compatible with the expected mendelian rate since 24 heterozygous mutants (*swap70b*$^{+/qmc809}$) (~50%), 10 wild types (*swap70b*$^{+/+}$) (~20%) and 16 homozygous mutants (*swap70b*$^{qmc809/qmc809}$) (~30%) were found. WT controls (+/+) (indicated with WT) and WT fish (*swap70b*$^{+/+}$) (indicated with blue asterisks) were completely digested exhibiting two fragments of 145bp and 98bp. Heterozygous mutants (*swap70b*$^{+/qmc809}$) (indicated with purple asterisks) were partially digested exhibiting fragments of 243bp, 189bp, 145bp and 98bp. Homozygous mutants (*swap70b*$^{qmc809/qmc809}$) (indicated with red asterisks) were not digested exhibiting a fragment of 189bp. Blue asterisk (*) indicates fish carrying two wild type alleles, red asterisk (*) indicates homozygous mutants carrying two mutant alleles and purple asterisk (*) indicates heterozygous mutants carrying one mutant allele and one wild type allele. M: Size marker; 100bp (NEB). WT: Wild type.

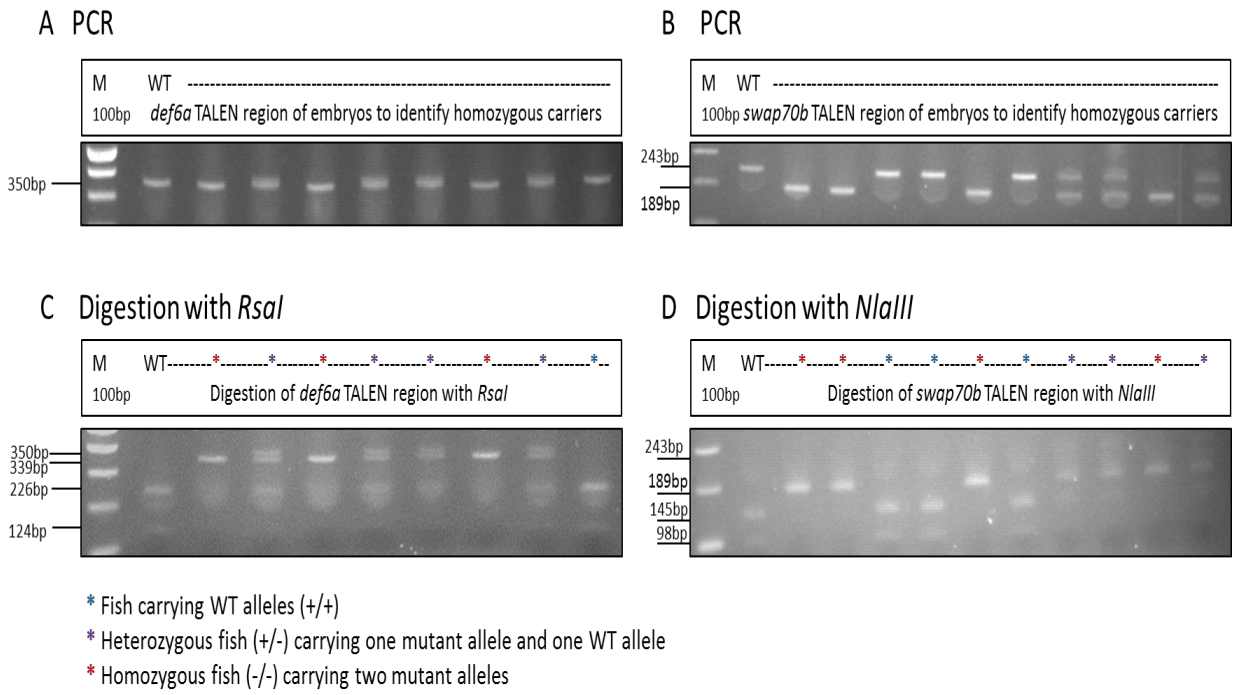


Figure 3.13 Fin-clip genotyping to find F_2 homozygous carriers. After in-crossing F_1 heterozygous mutants (*def6a*$^{+/qmc811}$ and *swap70b*$^{+/qmc809}$), F_2 generation was grown to adulthood and homozygous mutants were identified by fin-clip genotyping. **(A-B)** Amplification of the TALEN regions and **(C-D)** digestion of the PCR products revealed the homozygous mutants (*def6a*$^{qmc811/qmc811}$ and *swap70b*$^{qmc809/qmc809}$) as they demonstrate undigested fragments of 339bp and 189bp. Blue asterisk (*) indicates fish carrying two wild type alleles, red asterisk (*) indicates homozygous mutants carrying two mutant alleles and purple asterisk (*) indicates heterozygous mutants carrying one mutant allele and one wild type allele. M: Size marker; 100bp (NEB). WT: Wild type.

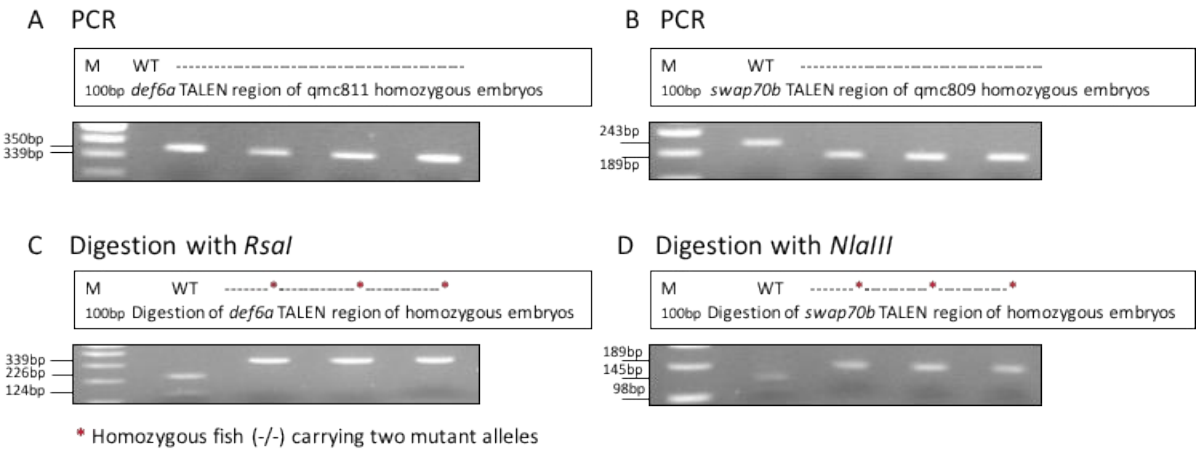


Figure 3.14 Genotyping of *def6a*$^{qmc811/qmc811}$ and *swap70b*$^{qmc809/qmc809}$ lines to confirm their homozygosity. Three homozygous mutant embryos for both mutant lines (*def6a*$^{qmc811/qmc811}$ and *swap70b*$^{qmc809/qmc809}$) were genotyped. **(A-B)** Amplification of *def6a* and *swap70b* TALEN regions revealed that while WT embryos showed fragments of 350bp and 243bp, *def6a*$^{qmc811/qmc811}$ and *swap70b*$^{qmc809/qmc809}$ mutants showed fragments of 339bp and 189bp for *def6a* and *swap70b*, respectively. **(C-D)** After digestion of PCR products, WT samples were digested showing two fragments of 224bp and 124bp for *def6a* locus and two fragments of 145bp and 98bp for *swap70b* locus. However, *def6a*$^{qmc811/qmc811}$ and *swap70b*$^{qmc809/qmc809}$ mutants were not digested showing the intact fragments of 339bp and 189bp, respectively. These results confirmed the homozygosity of both mutant lines. Red asterisk (*) indicates homozygous mutants carrying two mutant alleles. M: Size marker; 100bp (NEB). WT: Wild type.

3.3.6. Establishment of double knock-out mutant line, *qmc813*, lacking both *def6a* and *swap70b*

def6a$^{qmc811/qmc811}$ and *swap70b*$^{qmc809/qmc809}$ mutants were crossed to establish a double knock-out mutant line (*def6a*$^{qmc811/qmc811}$*; swap70b*$^{qmc809/qmc809}$). Since the parents were single homozygous mutants (*def6a*$^{qmc811/qmc811}$*; swap70b*$^{+/+}$) and (*def6a*$^{+/+}$*; swap70b*$^{qmc809/qmc809}$), the expected mendelian rate was 100% heterozygous for both alleles (*def6a*$^{+/qmc811}$*; swap70b*$^{+/qmc809}$). 19 out of 50 fish survived until adulthood and 7 of them were genotyped to confirm the double heterozygosity. Amplification of the *def6a* TALEN region of double heterozygous mutants revealed a fragment of 350bp similar to WT control, whereas amplification of *swap70b* TALEN region of double heterozygous mutants revealed two fragments of 243bp and 189bp due to 54bp deletion. WT control revealed only the fragment of 243bp as expected **(Figure 3.15A-B)**. Digestion of the *def6a* PCR products with *RsaI* nuclease revealed fragments of 350bp, 339bp, 226bp and 124bp for the double heterozygous mutants and two fragments of 226bp and 124bp for WT control. Digestion of *swap70b* PCR products with *NlaIII* nuclease revealed fragments of 243bp, 189bp, 145bp and 98bp for double heterozygous mutants and two fragments of 145bp and 98bp for WT control. Consistent with the previous results of single heterozygous mutants, in addition to the *qmc811* and *qmc809* mutant alleles (339bp and 189bp; respectively), an intact undigested fragments (350bp and 243bp) were also visible after digestion **(3.15C-D)**. In summary, these results confirmed that all fish were double heterozygous mutants (*def6a*$^{+/qmc811}$*; swap70b*$^{+/qmc809}$) fitting to the expected mendelian rate (100%).

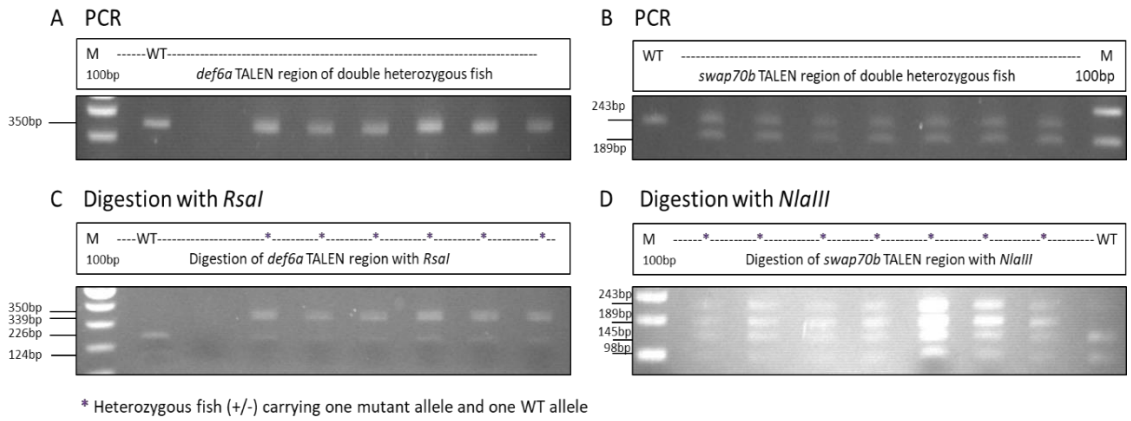


Figure 3.15 Fin clip genotyping confirmed the double heterozygosity for both *def6a* and *swap70b* genes. Single homozygous mutants were crossed to generate double heterozygous mutants. Fin clip genotyping of 7 fish showed that **(A-C)** 6 fish were carrying one *qmc811*^{def6a} mutant allele and one WT allele. **(B-D)** 7 fish were carrying one *qmc809*^{swap70b} mutant allele and one WT allele. These results confirmed that 6 fish (1 sample failed to amplify for *def6a*) were double heterozygous and suitable for in-crossing. Purple asterisk (*) indicates heterozygous mutants carrying one mutant allele and one wild type allele. M: Size marker; 100bp (NEB). WT: Wild type.

Double heterozygous fish (*def6a*$^{+/qmc811}$*; swap70b*$^{+/qmc809}$) were in-crossed to identify double homozygous mutant fish (*def6a*$^{qmc811/qmc811}$*; swap70b*$^{qmc809/qmc809}$). 110 out of 150 were survived until adulthood and 81 of them were subjected to the fin-clipping. *def6a* and *swap70b* loci were amplified for all samples **(Figure 3.16A-B-E-F)** and digested with *RsaI* and *NlaIII*, respectively **(Figure 3.16C-D-G-H)**. 5 fish (2 female, 3 males) were found as double homozygous mutants **(Figure 3.16C-D-G-H**; only 1 female and 2 males are shown in the figure). The distribution of the mutant alleles (1:16) correlated with the expected mendelian rate (6.3%).

Sequencing analysis revealed that all 5 fish contained both of the *qmc811* mutant alleles in their *def6a* locus **(Figure 3.17A)** and both of the *qmc809* mutant alleles in their *swap70b* locus **(Figure 3.17B)**, confirming double homozygosity. Double homozygous mutant line was named as *qmc813 def6a*$^{qmc811/qmc811}$*; swap70b*$^{qmc809/qmc809}$. Fish were viable and fertile thereby this line was used to generate mutant embryos for phenotypic and whole mount *in situ* hybridisation analyses.

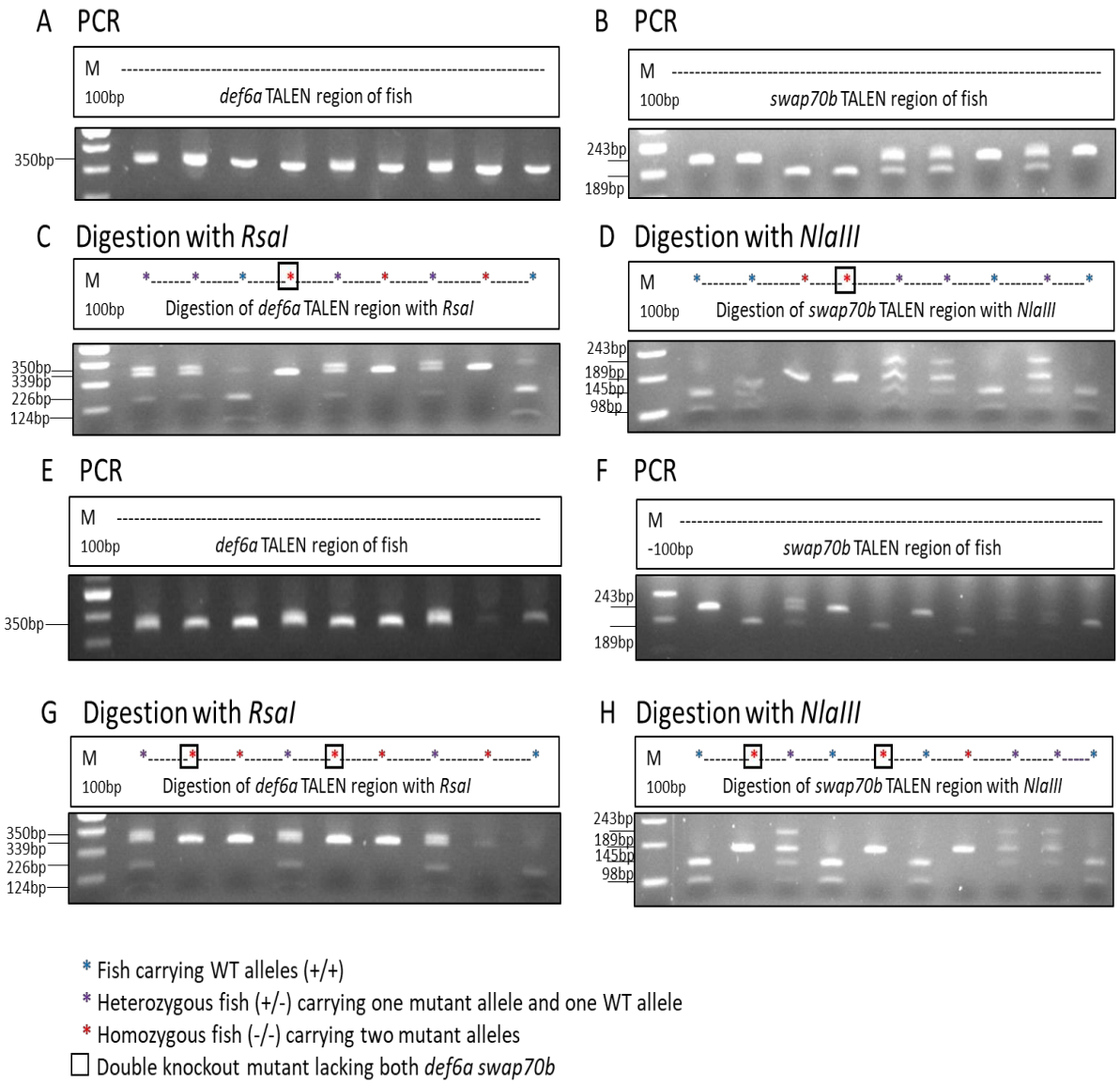


Figure 3.16 Fin-clip genotyping to identify double homozygous mutants. Only 18 and 19 zebrafish out of 81 were presented for *def6a* and *swap70b* loci, respectively, to point out double homozygous mutants (*def6a*$^{qmc811/qmc811}$*:swap70b*$^{qmc809/qmc809}$) specifically. **(A-B-E-F)** Amplification and **(C-D-G-H)** digestion of *def6a* and *swap70b* loci showed that 3 out of 51 (6%) were not digested with both enzymes clearly indicates that they are double homozygous mutants. Blue asterisk (*) indicates fish carrying two wild type alleles, red asterisk (*) indicates homozygous mutants carrying two mutant alleles and purple asterisk (*) indicates heterozygous mutants carrying one mutant allele and one wild type allele. Black square (□) demonstrates double homozygous mutants (*def6a*$^{qmc811/qmc811}$*: swap70b*$^{qmc809/qmc809}$). M: Size marker; 100bp (NEB).

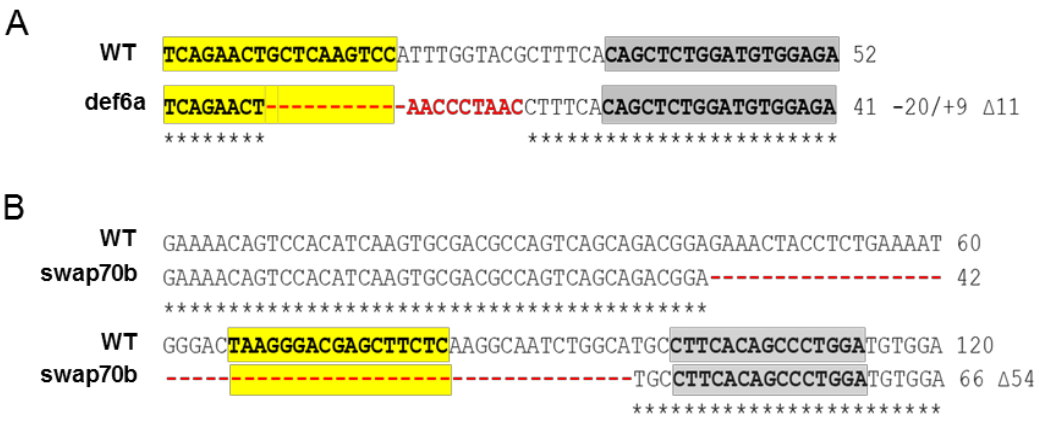


Figure 3.17 Sequencing analysis confirmed the double homozygosity of the *qmc813 def6a; swap70b* mutant line. Sequencing of **(A)** *def6a* and **(B)** *swap70b* locus of the *def6a; swap70b* double mutant line confirmed the deletions and insertions as observed in *def6a*$^{qmc811/qmc811}$ and *swap70b*$^{qmc809/qmc809}$ mutant lines before (section 3.3.5). Left and right TALEN binding sequences are highlighted in yellow and grey colours, respectively. The direction of each sequence is 5' to 3'. Red dashes (-) indicate deletions and red letters indicate insertions.

3.4. Summary

- Injection of 250pg *def6a* and 500pg *swap70b* TALEN mRNAs generated in-del somatic mutations at exon-1 for both gene loci.
- Genotyping of the F_1 offspring revealed that 3 *def6a a*nd 6 *swap70b* F_0 founders transferred the mutations through their germlines.
- F_1 heterozygous mutants carrying the frameshift mutations for *def6a* (-11bp) and *swap70b* (-54bp including 5'UTR and AUG) were in-crossed to establish homozygous mutants.
- Homozygous mutant lines were established and named as *qmc811* and *qmc809* for *def6a* and *swap70b*, respectively.
- Double homozygous mutant line, $def6a^{qmc811/qmc811};swap70b^{qmc809/qmc809}$, was generated by crossing $def6a^{qmc811/qmc811}$ and $swap70b^{qmc809/qmc809}$ homozygous lines.
- $def6a^{qmc811/qmc811}$, $swap70b^{qmc809/qmc809}$ and double $def6a^{qmc811/1mc811}$; $swap70b^{qmc809/qmc809}$ homozygous lines were viable and fertile and used for phenotypic and whole mount *in situ* hybridisation analyses.

CHAPTER 4

RESULTS

def6a and/or *swap70b*-deficiency results in CE cell movement defects during zebrafish gastrulation

4.1. Loss of *def6a* and/or *swap70b* resulted in shortened body axis and developmental delay during gastrulation

Single (*def6a*$^{qmc811/qmc811}$ and *swap70b*$^{qmc809/qmc809}$) and double (*def6a*$^{qmc811/qmc811}$; *swap70b*$^{qmc809/qmc809}$) homozygous mutant embryos were observed at early developmental stages and their morphology compared with wild type (WT) embryos (**Figure 4.1**). Seven cycles of cleavage occurred normally and the mutant embryos entered the blastula stage without a delay in development. The blastula stage includes the midblastula transition (MBT), yolk syncytial layer formation and the start of epiboly movements (Kimmel *et al.,* 1995). No obvious defects and delays were observed in mutants during these early developmental stages (data not shown). Gastrulation starts with the involution of cells at 50% epiboly, and is followed by the formation of the germ ring around the blastoderm cells (5.25hpf). Convergence movements of both the hypoblast and epiblast cells result in the accumulation of cells at the dorsal side referred to as the embryonic shield (6hpf) (Kimmel *et al.,* 1995). The formation of embryonic shield was normal in single (*def6a*$^{qmc811/qmc811}$ and *swap70b*$^{qmc809/qmc809}$) and double homozygous mutant embryos (*def6a*$^{qmc811/qmc811}$; *swap70b*$^{qmc809/qmc809}$) (**Figure 4.1A-D**; black arrows) and there was no delay in development during 50% epiboly and shield stages. Epiboly movements continue until the blastoderm covers the yolk, while convergence and extension (CE) cell movements form the body axis through narrowing the cells medio-laterally and extending the body axis anterior-posteriorly during the gastrulation period (Kimmel *et al.,* 1995). No obvious epiboly defects were observed during 50%, 75% and 90% epiboly stages, but a slight delay in development was apparent in single as well as double homozygous mutants compared to WT embryos during the gastrulation period (data not shown). At the end of gastrulation however (tail-bud stage; 10hpf), a consistent delay in development (1-2 hours lag) with reduced body axis was observed in the mutants (**Figure 4.1E-H**), a hall mark of impaired CE cell movements.

To further verify the reduction of body axis in single and double homozygous mutants, the angle between the lines defining the anterior and posterior embryonic structures was measured at tail-bud stage (10hpf; **Figures 4.1** and **4.2**). Single and double homozygous mutant embryos exhibited a clear increase of the angle (θ) indicating reduced extension of the body axis (**Figure 4.2A-D)**. Two-tailed student's t-test and one-way ANOVA statistical analyses confirmed the significant increase (****; $p<0.0001$) in the angle between the anterior and posterior parts in single (*def6a*$^{qmc811/qmc811}$ and *swap70b*$^{qmc809/qmc809}$) and double (*def6a*$^{qmc811/qmc811}$; *swap70b*$^{qmc809/qmc809}$) homozygous mutants compared to the WT embryos. Two-tailed student's t-test indicated no significant (N.S) difference ($p=0.1223$) between single *def6a*$^{qmc811/qmc811}$ and *swap70b*$^{qmc809/qmc809}$ mutants. Moreover, double homozygous mutants did not display a more severe phenotype than single homozygous mutants, as no significant differences were identified between the single (*def6a*$^{qmc811/qmc811}$: $p=0.545$; *swap70b*$^{qmc809/qmc809}$: $p=0.6959$) and double mutants (**Figure 4.2E**).

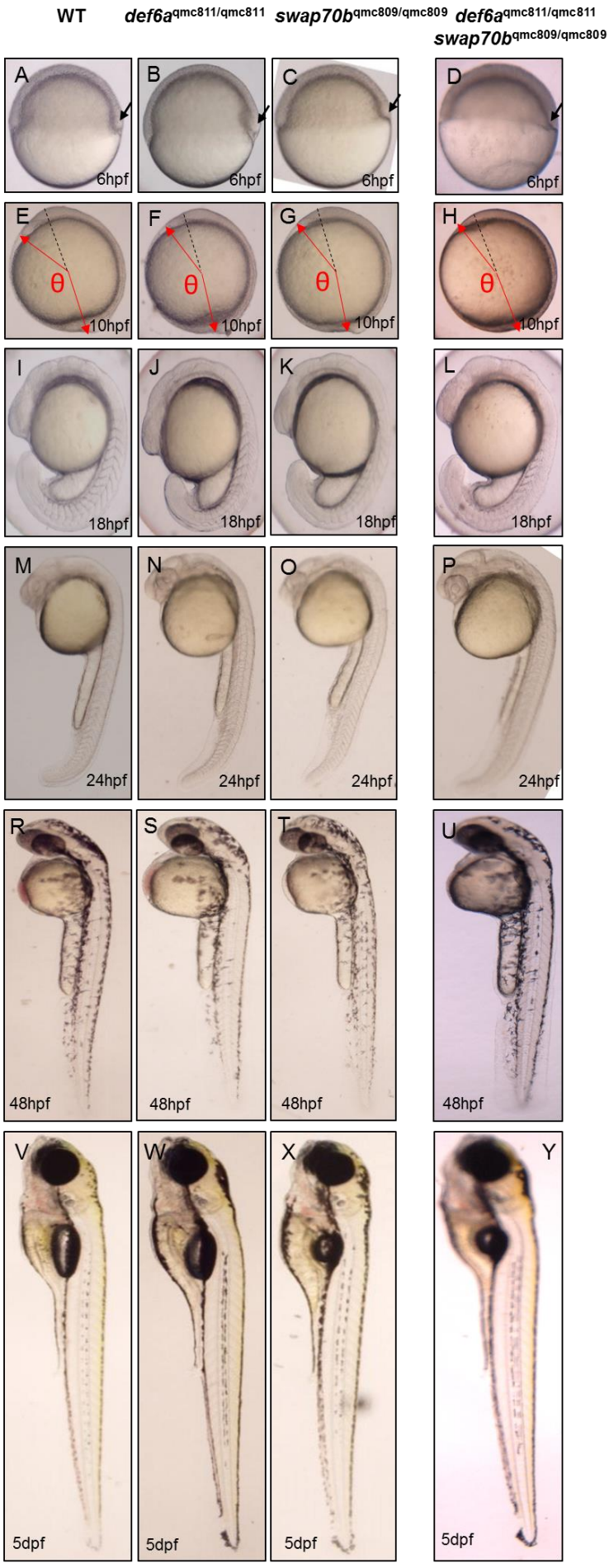

WT
def6a qmc811/qmc811
swap70b qmc809/qmc809
def6a qmc811/qmc811
swap70b qmc809/qmc809
A
6hpf
B
6hpf
C
6hpf
D
6hpf
E
θ
10hpf
F
θ
10hpf
G
θ
10hpf
H
θ
10hpf
I
18hpf
J
18hpf
K
18hpf
L
18hpf
M
24hpf
N
24hpf
O
24hpf
P
24hpf
R
48hpf
S
48hpf
T
48hpf
U
48hpf
V
5dpf
W
5dpf
X
5dpf
Y
5dpf

Figure 4.1 Morphological analysis of WT, single (*def6a*$^{qmc811/qmc811}$ and *swap70b*$^{qmc809/qmc809}$) and double (*def6a*$^{qmc811/qmc811}$; *swap70b*$^{qmc809/}$qmc809) homozygous mutants. Single and double homozygous mutants exhibited reduced body axis and developmental delay, but no other observable morphological defects during their development until 5dpf. Wild type (WT) (left column), *def6a*$^{qmc811/qmc811}$ (middle left column), *swap70b*$^{qmc809/qmc809}$ (middle right column) and double *def6a*$^{qmc811/qmc811}$; *swap70b*$^{qmc809/qmc809}$ mutants (right column) are stated on top the figures. **(A-B-C-D)** Embryos developed normally until the shield stage (6hpf), no obvious defect was observed for the mutant embryos **(B-C-D)** compared to WT embryos **(A)**. Black arrows indicate the embryonic shield formation at the dorsal side. **(E-F-G-H)** *def6a*$^{qmc811/qmc811}$ **(F)**, *swap70b*$^{qmc809/qmc809}$ **(G)** and double *def6a*$^{qmc811/qmc811}$; *swap70b*$^{qmc809/qmc809}$ mutants **(H)** exhibited shortened anterior-posterior body axis at the tail-bud stage (10hpf) compared to the WT embryos **(E)**. The increased angle (θ) indicates the shortening of the body axis in mutants. **(I-J-K-L)** WT, single and double mutants exhibited normal development of somites and well-shaped brain subdivisions at 18hpf. **(M-N-O-P)** WT, single and double mutants at 24hpf demonstrated normal development of brain and tail, no cyclopia was observed. **(R-S-T-U)** WT, single and double mutants at 48hpf developed normally, no heart defects observed and melanogenesis was also normal. **(V-W-X-Y)** Normally developed WT, single and double mutants at the early larva stage (5dpf). No defects were observed in brain, tail, eye, notochord, heart and swim bladder. All embryos are illustrated in lateral view with anterior at the top, dorsal at the right.

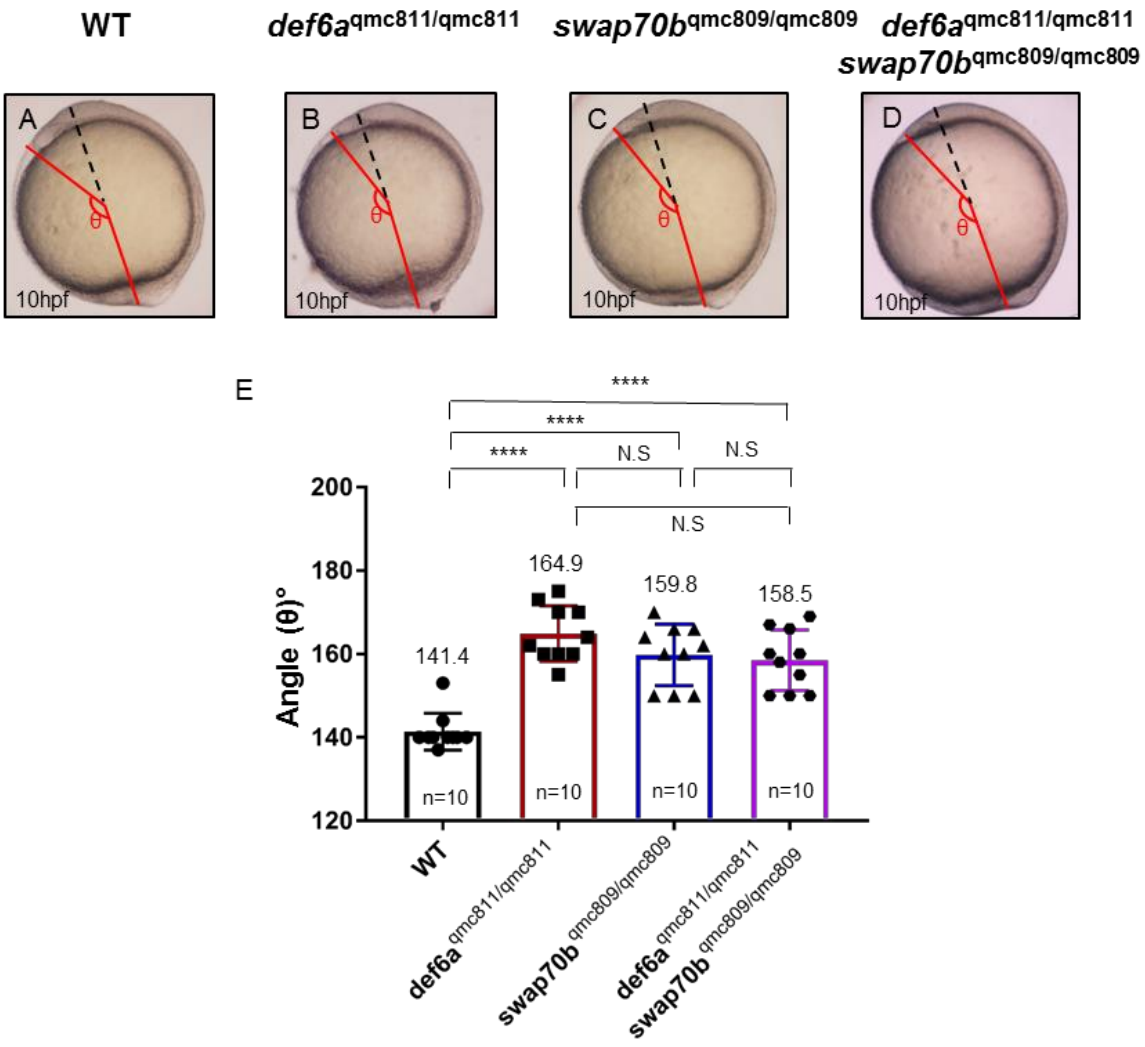


Figure 4.2 Single *def6a*$^{qmc811/qmc811}$, *swap70b*$^{qmc809/qmc809}$ and double *def6a*$^{qmc811/qmc811}$; *swap70b*$^{qmc809/qmc809}$ homozygous mutants showed reduced extension of the body axis at tail bud stage (10hpf) compared to WT controls. Representative embryos from each category are shown. **(A-B-C-D)** The prechordal plates and tail buds were defined by red lines and the angle (θ) at the centre of the yolk between these structures was measured for WT, single *def6a*$^{qmc811/qmc811}$, *swap70b*$^{qmc809/qmc809}$ and double *def6a*$^{qmc811/qmc811}$; *swap70b*$^{qmc809/qmc809}$ mutants (Lateral view, anterior at the top). **(E)** One-way ANOVA and two-tailed student's t-test analyses confirmed the significant ($p<0.0001$(****)) increase in the angle (θ) between the anterior and posterior embryonic structures in both single and double mutants, however double mutants did not display a more severe phenotype than single mutants. N.S indicates no significant ($p>0.05$) difference between single (*def6a*$^{qmc811/qmc811}$ and *swap70b*$^{qmc809/qmc809}$) and double (*def6a*$^{qmc811/qmc811}$; *swap70b*$^{qmc809/qmc809}$) mutants. The scatter plots indicate the mean with standart deviation (SD) and the number of tested embryos.

Remarkably, the mutant embryos did not exhibit any apparent morphological abnormalities during segmentation (normal somite and brain morphology at 18hpf; **Figure 4.1I-L**), the pharyngula period that starts with the prim-5 stage (24hpf) and results in elongation and straightening out of the tail, establishment of early pigmentation and onset of heart beat (**Figure 4.1M-P**) or hatching period that starts with the long-pec stage at 48hpf. At this stage, dorsal and ventral stripes converge at the tail, 6 melanophores in lateral stripe and iridophores in the retina become clear. The beating of the heart is obvious and the bending of the heart tube brings the atrium dorsal to the ventricle. Dechorionated embryos can rest in a dorsal-up position (Kimmel *et al.,* 1995). Comparison of WT embryos with single and double mutant embryos at the long-pec stage (48hpf) did not reveal any obvious defects in the mutants (**Figure 4.1R-U**). By 72hpf, the hatched larva completes most of its development such as organogenesis or blood circulation, however it continues to grow. At the early larva period (5dpf), the protrusion of mouth continues, the swim bladder inflates and the larva start to swim (Kimmel *et al.,* 1995). The mutant larva were normal and viable at 5dpf (**Figure 4.1 W-Y**), grew to adulthood and were fertile.

Taken together, TALEN-mediated *def6a* and *swap70b* mutant embryos exhibited a developmental delay and a reduction of the body axis at tail-bud stage (10hpf) indicative of impaired CE cell movement during gastrulation. Single and double homozygous mutants exhibited a similar phenotype suggesting a non-redundant function of *def6a* and *swap70b* during gastrulation.

4.2. Normal cell fate specification in single and double homozygous *def6a* and *swap70b* mutants

Cell fate specification and movements are key factors working co-ordinately to establish a normal animal body plan formed of dorsoventral and anteroposterior axes. The interaction between cell movements and cell fate specification has been revealed using *spadetail* mutant embryos. The mutation in the *spadetail* gene resulted in mismigration of mesodermal cells during gastrulation, consequently the mismigrated cells expressed the fate of their new position, clearly indicating that cell movements affect cell fate specification by placing them in the correct positions to receive the signal for determination of future cell fate during gastrulation (Ho, 1992). Similarly, impaired CE cell movements and altered cell fate specification was also observed in *chordino* mutants (Sepich *et al.,* 2000). Several signalling pathways, such as Wnt, BMP, FGF, Nodal and Retinoic acid, have been identified as the regulators of the dorsoventral patterning by regulating both cell fate specification and movements (Ciruna and Rossant, 2001; Myers *et al.,* 2002; Branford and Yost, 2002; Yamashita *et al.,* 2002; Schier and Talbot, 2005; Tucker *et al.,* 2008; reviewed in Kimelman and Martin, 2012).

Caudal homeobox transcription factors* (*cdx1a, cdx1b and ***cdx4*)** are caudal-related homeodomain-containing transcription factors for the regulation of *hox* genes, which are expressed in the posterior part of the embryo and required for the normal development of anteroposterior patterning (Charite *et al.,* 1998). The regulation of the *cdx* genes depends on multiple signalling pathways such as Wnt, FGF and Retinoic acid (Northrop and Kimelman, 1994; Houle *et al.,* 2000; Lickert *et al.,* 2000; Prinos *et al.,* 2001).

Bone Morphogenetic Proteins (such as **Bmp2b)** are extracellular ligands of the TGF-β superfamily of growth factors and trigger the BMP signalling pathway by binding to the type I and II membrane receptors. The activated receptors phosphorylate two serines in the C-terminus of Smad transcription factors resulting in their accumulation in the nucleus and activation of target genes (Plouhinec *et al.,* 2011). The activation of BMP signalling is regulated by extracellular antagonists such as Chordin and Noggin that bind to the Bmps directly to prevent their binding to the receptors (Sasai *et al.,* 1994; Zimmerman *et al.,* 1996).

***Chordin* (*chd*)** is a zygotic dorsal gene acting as an inhibitor for the ventral fates (*bmps*) and an activator for the dorsal fates. The accumulation of β-catenin at the organiser activates the expression of zygotic dorsal genes, such as *bozozok (boz), chordin (chd), dickkopf1 (dkk1), squint (sqt)* and *fgfs* (Schulte-Merker *et al.,* 1997; Yamanaka *et al.,* 1998; Feldman *et al.,* 1998; Shimizu *et al.,* 2000; Hashimoto *et al.,* 2000; Ryu *et al.,* 2001; Furthauer *et al.,* 2004; reviewed

in Schier and Talbot, 2005 and Maegawa *et al.,* 2006). Expression of *chordin* directs the development of dorso-lateral mesoderm and ectoderm by inhibiting the activity of ventral fates and thus inducing the development of dorsal fates (Sasai *et al.,* 1994; Piccolo *et al.,* 1996; reviewed in Miller-Bertoglio *et al.,* 1997; Schier and Talbot, 2005).

No tail (ntl) is the homologue of the mouse *T* (*Brachyury*) gene and is essential for normal development of mesoderm and extension of the body axis (Schulte-Merker *et al.,* 1994). While *ntl* is transiently expressed in endoderm and mesoderm, it is constantly expressed in the future notochord (Schulte-Merker *et al.,* 1992; Schulte-Merker, 1995). The *ntl* mutants cannot survive because of lack of a differentiated notochord and the posterior parts of their somites (Halpern *et al.,* 1993).

To test whether lack of *def6a* and/or *swap70b* resulted in impaired cell specification, *in situ* hybridisation was carried out to determine the expression patterns of key marker genes during early development. WT, single *def6a*$^{qmc811/qmc811}$ and *swap70b*$^{qmc809/qmc809}$ and double mutant embryos were assessed for expression of *cdx4, bmp2b, chordin* and *ntl* at shield stage (**Figure 4.3**).

As illustrated in **Figure 4.3**, expression patterns of the genes tested were indistinguishable between WT and mutant embryos. Normal expression of *cdx4* in the margin region (**Figure 4.3A-D**) indicated cell fate specification affecting the posterior body formation is normal in the mutant embryos. Ventral cell fate specification appeared normal as indicated by the unaltered expression pattern of *bmp2b* (**Figure 4.3 E-H**) and *chd* expression indicated normal dorsal cell specification at shield stage (**Figure 4.3 I-L**) as well as 75% and 90% epiboly stages (**Figure 4.4**). Expression of *ntl* in the axial mesendoderm region was also not changed in single (**Figure 4.3N-N'-O-O'**) or double homozygous mutants (**Figure 4.3P-P'**) compared to the WT controls (**Figure 4.3M-M'**), suggesting that both *def6a* and *swap70b* have no potential roles in the process of mesoderm development and somite formation.

Thus, neither *def6a* nor *swap70b* plays a role in cell fate specification determining posterior and dorsal-ventral body axes.

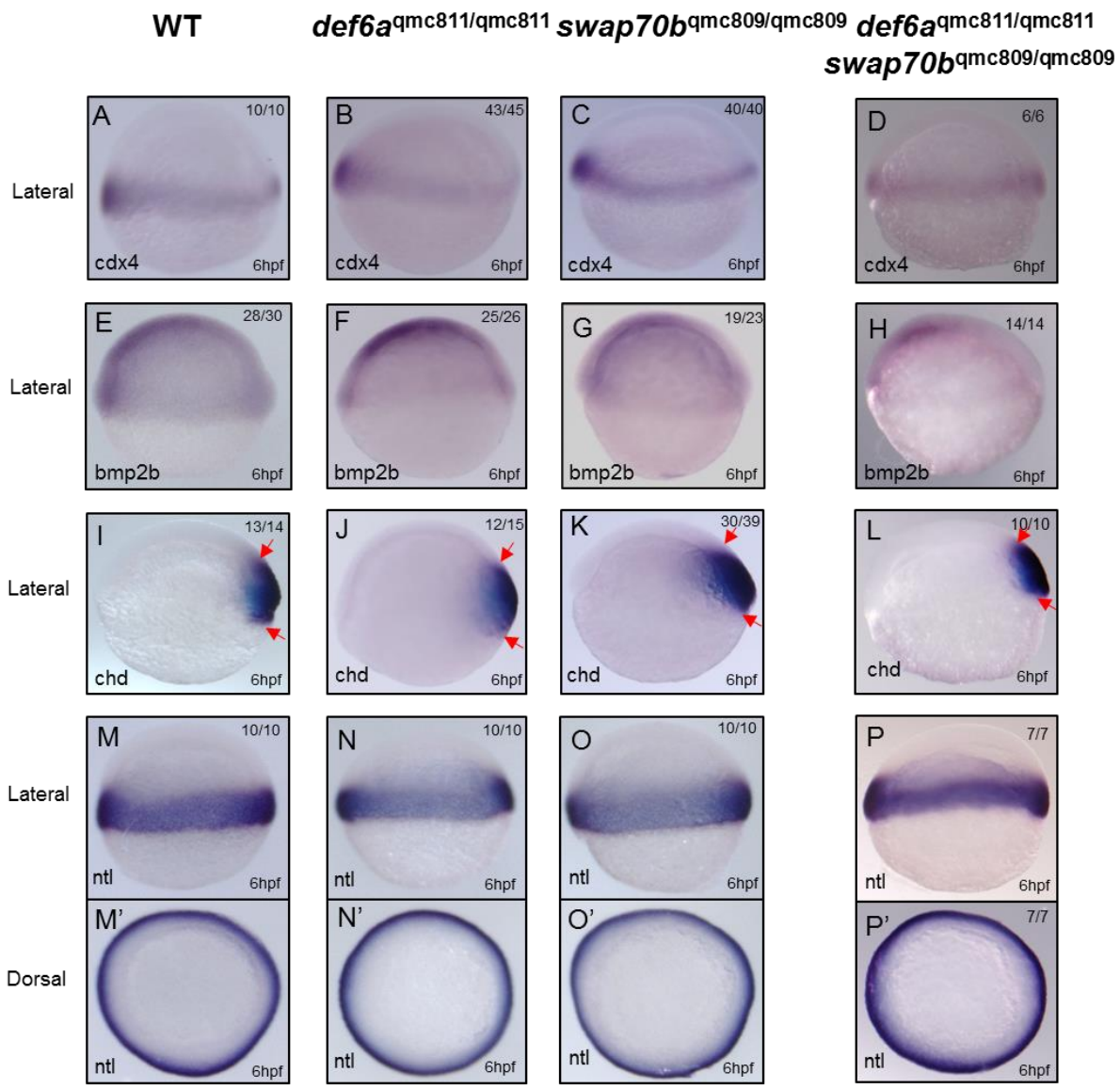


Figure 4.3 Cell specification was not altered in single *def6a*$^{qmc811/qmc811}$, *swap70b*$^{qmc809/qmc809}$ and double *def6a*$^{qmc811/}$qmc811; *swap70b*$^{qmc809/qmc809}$ homozygous mutants. WT (left column), *def6a*$^{qmc811/qmc811}$ mutants (middle left column), *swap70b*$^{qmc809/qmc809}$ mutants (middle right column) and *def6a*$^{qmc811/}$qmc811; *swap70b*$^{qmc809/qmc809}$ double mutants (right column) were fixed at shield stage (6hpf) and subjected to WISH using *cdx4* **(A-B-C-D,** lateral view, dorsal right**)**, *bmp2b* **(E-F-G-H,** lateral view, dorsal right**)**, *chd* **(I-J-K-L,** lateral view, dorsal right**)** *and ntl* (**M-N-O-P,** lateral view, dorsal right and **M'-N'-O'-P',** animal view**)** riboprobes. The expressions of *cdx4, bmp, chd* and *ntl* markers were not altered in single and double mutants. Red arrows specify the starting and ending parts of *chd* expression. The number of embryos tested for each probe is indicated at the top of the figures, the stage is indicated at the bottom of the figures.

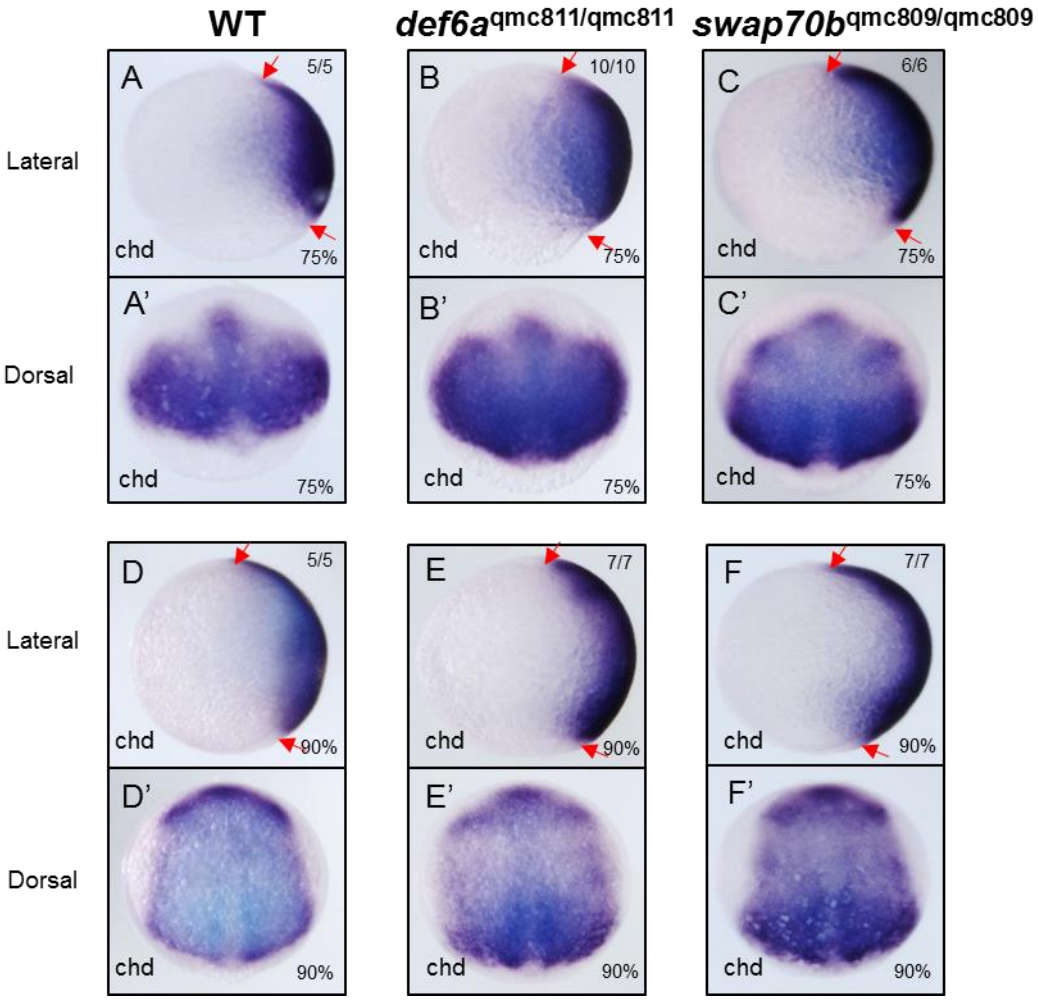


Figure 4.4 *chd* expression was not altered in *def6a*$^{qmc811/qmc811}$ and *swap70b*$^{qmc809/qmc809}$ mutants during gastrulation. WT (left column), *def6a*$^{qmc811/qmc811}$ mutants (middle column) and *swap70b*$^{qmc809/qmc809}$ mutants (right column) were fixed 75% (8hpf) (**A-B-C,** lateral view, dorsal right and **A'-B'-C',** dorsal view, anterior top) and 90% (9hpf) epiboly (**D-E-F,** lateral view, dorsal right and **D'-E'-F',** dorsal view, anterior top) stages and subjected to WISH using *chd* riboprobe. No obvious change in *chd* expression was observed for both homozygous mutants during the 75% and 90% epiboly stages. Red arrows indicate the starting and ending parts of *chd* expression. The number of embryos tested for each probe is indicated at the top of the figures, the stages are indicated at the bottom of the figures.

4.3. Single *def6a*$^{qmc811/qmc811}$ and *swap70b*$^{qmc809/qmc809}$ and double *def6a*$^{qmc811/qmc811}$; *swap70b*$^{qmc809/qmc809}$ homozygous mutants displayed posterior shift, reduction and expansion in neuroectoderm markers

To establish whether dorsal ectoderm and posterior mesoderm fates, which regulate brain patterning, were altered, expression of *pax2a*, *krox20, hoxb1a* and *fgf8a* was determined.

Paired box (pax) genes encode transcription factors regulating the important developmental events including kidney organogenesis and brain regionalisation during zebrafish embryonic development (Krauss *et al.,* 1991; Majumdar *et al.,* 2000). It has been proposed that *pax2a* coordinates with *wnt1* and *fgf8* signals to form the midbrain-hindbrain organiser (Lun and Brand, 1998; Reifers *et al.,* 1998). The two *pax2* genes, *pax2.1 (pax2a)* and *pax2.2,* are both expressed in mid-hindbrain boundary, neural tube, ears and optic tracts. However, *pax2a* is also expressed in the pronephros suggesting an additional role in nephrogenesis (Drummond, 2002; reviewed in Majumdar *et al.,* 2000). Solnica-Krezel *et al.,* (1996) have shown that *pax2a* can also be used as a marker to analyse CE cell movement defects as the defects in convergence and extension cause an expansion and a posterior shift, respectively. *In situ* hybridisation at tail-bud stage (10hpf) revealed that the expression of *pax2a* in the midbrain-hindbrain boundary was posteriorly shifted and expanded and the expression signal was slightly reduced in *def6a*$^{qmc811/qmc811}$ (**Figure 4.5B-B'**), *swap70b*$^{qmc809/qmc809}$ (**Figure 4.5C-C'**) and double *def6a*$^{qmc811/}$qmc811; *swap70b*$^{qmc809/qmc809}$ mutants **(Figure 4.5D-D')** compared to the WT controls (**Figure 4.5A-A'**). Therefore, while the posterior shift is most probably the consequence of reduced body length caused by defective extension movements (**Figure 4.1** and **4.2**), the expansion is most probably the consequence of reduced convergence (**Figure 4.6B-C-D**).

Fibroblast growth factors (Fgfs) are the growth factors binding to the tyrosine-kinase class receptors to activate the FGF signalling pathway, which then activates other signalling pathways including the Ras-MAP kinase pathway (Bottcher and Niehrs, 2005; Thisse and Thisse, 2005). The FGF signalling pathway has been shown to regulate various developmental processes such as dorsoventral patterning (Furthauer *et al.,* 2004), cell migration (Ciruna and Rossant, 2001), morphogenesis (Martin, 1998), neural induction (Streit *et al.,* 2000) or midbrain-hindbrain patterning (Liu and Joyner, 2001; reviewed in Thisse and Thisse, 2005). The zebrafish *fgf* family contains 27 members which can be subdivided into seven subfamilies (Itoh and Konishi, 2007). Of these zebrafish genes, *fgf8* is expressed in mesodermal precursors and required for the development of midbrain-hindbrain boundary

organiser and mesoderm-derived posterior structures (Amaya *et al.,* 1991; Draper *et al.,* 2003; Wiellette and Sive, 2004). The *acerebellar (ace/fgf8)* mutants display defects in the cerebellum and the midbrain-hindbrain boundary organiser development (Brand *et al.,* 1996; Reifers *et al.,* 1998). Like *pax2a*, the expression of *fgf8* in hindbrain was posteriorly shifted, expanded and reduced in *def6a*$^{qmc811/qmc811}$ (**Figure 4.5F-F'**), *swap70b*$^{qmc809/qmc809}$ (**Figure 4.5G-G'**) and double *def6a*$^{qmc811/}$qmc811; *swap70b*$^{qmc809/qmc809}$ mutants (**Figure 4.5H-H'**) compared to WT (**Figure 4.5E-E'**). The posterior shift and the expansion are most probably the consequence of impaired CE cell movements (**Figure 4.6**).

Early growth response (egr, also termed krox) genes encode zinc finger-containing transcription factors regulating hindbrain development. *krox20,* which is specifically expressed in rhombomeres (r) 3 and 5, controls the transcriptional activation or inhibition of other regulatory genes including several *homeobox-containing* genes (*hox)* (Schneider-Maunoury *et al.,* 1997; Seitanidou *et al.,* 1997; Sham *et al.,* 1993; Nonchev *et al.,* 1996; reviewed in Oxtoby and Jowett, 1993). Mice homozygous mutants for *krox20* showed loss of rhombomeres 3 and 5 and cranial sensory ganglia defects (Swiatek and Gridley, 1993). It has been suggested that the roles of *krox20* in hindbrain segmentation are evolutionary conserved in various organisms including mice, chick and fish (Nonchev *et al.,* 1996). Indeed, like in other organisms, zebrafish *krox20* is expressed in r3 and r5 and it is the most conserved gene among the other zebrafish *krox* genes, *krox-24, egr-3* and *ngfi-c* (Reviewed in Oxtoby and Jowett, 1993). *krox20* expression at tail-bud stage was altered in the mutant embryos exhibiting a posterior shift and expansion as well as a loss of expression in r5 (**Figure 4.5I-L'**). Posterior shift and expansion of *pax2a* and *fgf8* expression clearly indicates CE cell movement defects. However, the loss of *krox20* expression in r5 (**Figure 4.5J-K-L**) might be the consequence of reduced *fgf8* expression given that *fgf* signalling is also important for hindbrain patterning (Liu and Joyner, 2001) and in zebrafish and chick embryos *fgf* signalling controls *krox20* expression (Aragon and Pujades, 2009; Marin and Charnay, 2000; Walshe *et al.,* 2002; Wiellette and Sive, 2004).

homeobox (hox) genes encode homeodomain-containing transcription factors to specify the anterior-posterior identity in different tissues, especially regulating the segmentation of hindbrain during development (Nolte and Krumlauf, 2007). While mammals have four *hox* clusters (A-D) with 39 genes, zebrafish have seven *hox* clusters with 48 genes due to whole chromosome duplication and multiple gene losses during evolution (Amores *et al.,* 1998; Hurley *et al.,* 2005). Among these genes, zebrafish *hoxb1a* is required for the normal development of r4 and most importantly is crucial for the migration of r4-derived facial (VIIth nerve) branchiomotor neurons (BMNs) into the posterior hindbrain (r6 and r7) (Chandrasekhar *et al.,* 1997). *hoxb1a* expression also exhibited a posterior shift and expansion in

def6a$^{qmc811/qmc811}$ **(Figure 4.5N-N')**, *swap70b*$^{qmc809/qmc809}$ **(Figure 4.5O-O')** and double *def6a*$^{qmc811/}$qmc811; *swap70b*$^{qmc809/qmc809}$ mutants (**Figure 4.5P-P'**) compared to WT controls **(Figure 4.5M-M').** However, single and double mutants also displayed the loss of *hoxb1a* expression in the neural keel suggesting a shortened hindbrain and neural keel (**Figure 4.5M'-P';** black arrow). The posterior shift and expansion of *hoxb1a* as well as *pax2a, fgf8, krox20* expression was more severe in *swap70b*$^{qmc809/qmc809}$ and double *def6a*$^{qmc811/}$qmc811; *swap70b*$^{qmc809/qmc809}$ mutants than *def6a*$^{qmc811/qmc811}$ mutants **(Figure 4.5)**.

Taken together, these results indicate that loss of *def6a* and *swap70b* does not affect cell specification of the brain structures since the cells continue to express the genes despite the reduction in the expression patterns. However, posterior shift and expansion in the expression patterns observed in *def6a*$^{qmc811/qmc811}$ mutants, *swap70b*$^{qmc809/qmc809}$ mutants and *def6a*$^{qmc811/}$qmc811; *swap70b*$^{qmc809/qmc809}$ double mutants strongly indicate CE cell movement defects.

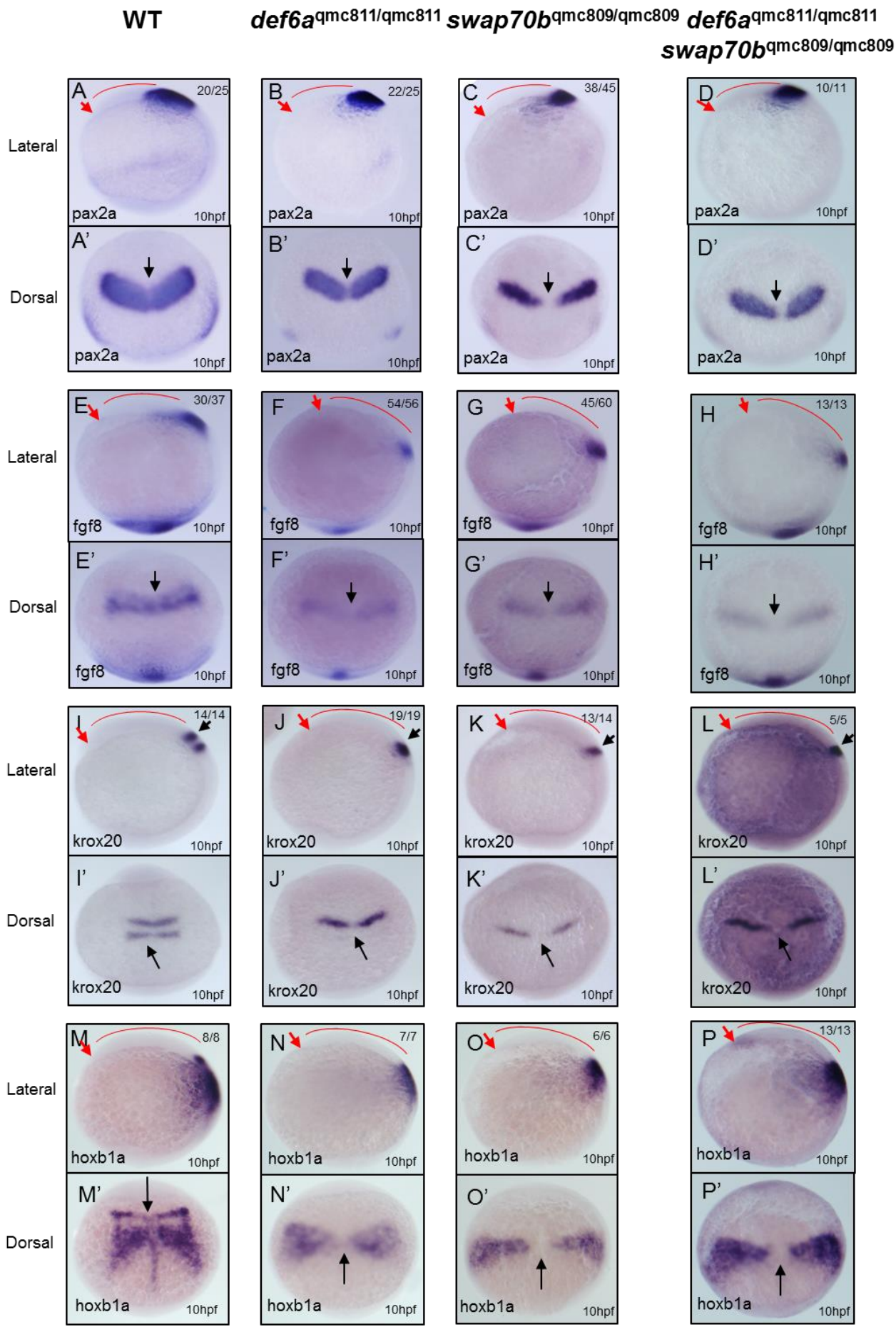

WT
def6a qmc811/qmc811 swap70b qmc809/qmc809
def6a qmc811/qmc811 swap70b qmc809/qmc809
Lateral
Dorsal
A 20/25
B 22/25
C 38/45
D 10/11
A' B' C' D'
pax2a 10hpf
E 30/37
F 54/56
G 45/60
H 13/13
E' F' G' H'
fgf8 10hpf
I 14/14
J 19/19
K 13/14
L 5/5
I' J' K' L'
krox20 10hpf
M 8/8
N 7/7
O 6/6
P 13/13
M' N' O' P'
hoxb1a 10hpf

Figure 4.5 Posterior shift, reduction and expansion in the neuroectoderm markers, *pax2a, fgf8*, *krox20* and *hoxb1a* were observed in single *def6a*$^{qmc811/qmc811}$ and *swap70b*$^{qmc809/qmc809}$ and double *def6a*$^{qmc811/}$qmc811; *swap70b*$^{qmc809/qmc809}$ homozygous mutants during gastrulation. WT (left column), *def6a*$^{qmc811/qmc811}$ (middle left column), *swap70b*$^{qmc809/qmc809}$ (middle right column) and double *def6a*$^{qmc811/}$qmc811; *swap70b*$^{qmc809/qmc809}$ mutants (right column) were fixed at tail-bud (10hpf) stage and subjected to WISH using *pax2a* **(A-B-C-D,** lateral view, dorsal right; **A'-B'-C'-D',** dorsal view**)**, *fgf8* **(E-F-G-H,** lateral view, dorsal right; **E'-F'-G'-H',** dorsal view**)**, *krox20* (**I-J-K-L,** lateral view, dorsal right and **I-'J'-K'-L',** dorsal view**)** and *hoxb1a* **(M-N-O-P,** lateral view and **M'-N'-O'-P',** dorsal view**)** riboprobes. Expansion and posterior shift of expression patterns and reduction of expression signals were observed in *def6*$^{qmc811/qmc811}$, *swap70b*$^{qmc809/qmc809}$ and double *def6a*$^{qmc811/}$qmc811; *swap70b*$^{qmc809/qmc809}$ mutants for all tested probes. Loss of *krox20* and *hoxb1a* expressions in r5 and neural keel, respectively, was also observed in single **(J-J'; K-K'; N-N'; O-O';** black arrow**)** and double mutants **(L-L'-P-P';** black arrow). Posterior shifts are specified by the red arrows and arcs, whereas, expansions in the area are specified by the black arrows. The number of embryos tested for each probe is indicated at the top of the figures, the stage is indicated at the bottom of the figures.

4.4. *def6a* and *swap70b* are required for convergence and extension (CE) cell movements during gastrulation

Normal cell specification and patterning of the body axes but reduced body elongation, posterior shift and expansion of anterior markers in *def6a*$^{qmc811/qmc811}$, *swap70b*$^{qmc809/qmc809}$ mutants and the double mutants are characteristic features of mutants and morphants that exhibit CE cell movement defects during gastrulation. These include *silberblick/wnt11*, *pipetail/wnt5b*, *knypek/gpc4* and *trilobite/vangl2; prickle1/prickle1a*. (Heisenberg *et al.,* 2000; Kilian *et al.,* 2003; Jessen *et al.,* 2002; Topczewski *et al.,* 2001; Carreira-Barbosa *et al.,* 2003; reviewed in Solnica-Krezel *et al.,* 1996). Therefore, expression of neuroectodermal and mesodermal markers, *hgg1, dlx3, ntl*, *otx2* and *myoD*, was determined at tail-bud stage to analyse CE cell movements during gastrulation.

hatching gland (hgg) is a set of unicellular glands secreting an enzyme that facilitates hatching during pharyngula period. *hgg1* forms the anterior half of the prechordal plate and is expressed in the presumptive hatching gland cells located on top of the neural plate boundary during zebrafish gastrulation (Thisse *et al.,* 1994). However, *hgg1* expression pattern was found to be elongated posteriorly in the CE mutants/morphants due to reduced cell migration and mediolateral intercalation (Heisenberg *et al.,* 2000; Kilian *et al.,* 2003; Jessen *et al.,* 2002; Topczewski *et al.,* 2001; Carreira-Barbosa *et al.,* 2003; Solnica-Krezel *et al.,* 1996). Consistent with the CE mutants/morphants phenotype, *def6a*$^{qmc811/qmc811}$ (**Figure 4.6B**; red arrow), *swap70b*$^{qmc809/qmc809}$ (**Figure 4.6C**; red arrow) and double *def6a*$^{qmc811/qmc811}$; *swap70b*$^{qmc809/qmc809}$ mutants (**Figure 4.6D**; red arrow) exhibited the same result as the prechordal plate (*hgg1*) was posteriorly elongated and slightly located beneath the neural plate (*dlx3*) compared to the WT control (**Figure 4.6A**; red arrow). These results indicate defective CE cell movements in both single and double mutants.

The ***distal-less homeobox (dlx)*** gene family is the vertebrate homologue of *distal-less (dll)* gene of *drosophila,* encoding homeodomain-containing transcription factors to regulate various developmental events including forebrain and limb/fin development (Panganiban and Rubenstein, 2002; Stock *et al.,* 1996; Akimenko *et al.,* 1994). The zebrafish *dlx* gene family contains eight members and six of them form two gene clusters (*dlx1/dlx2, dlx3/dlx7 and dlx4/dlx6)* as a result of the genome duplication. Among these genes, only *dlx3/dlx7* genes are expressed in the presumptive neural plate during zebrafish gastrulation (Akimenko *et al.,* 1994; Ellies *et al.,* 1997). As a consequence of CE cell movement defects, the neural plate marked by *dlx3* is enlarged mediolaterally in CE mutants/morphants (Heisenberg *et al.,* 2000; Kilian *et al.,* 2003; Jessen *et al.,* 2002; Topczewski *et al.,* 2001; Carreira-Barbosa *et al.,* 2003; Solnica-Krezel *et al.,* 1996). Consistent with this, the neural plate in *def6a*$^{qmc811/qmc811}$ (**Figure**

4.6B; black arrow, **4.6B''**; red arrow), *swap70b*$^{qmc809/qmc809}$ (**Figure 4.6C**; black arrow, **4.6C''**; red arrow) and double *def6a*$^{qmc811/qmc811}$; *swap70b*$^{qmc809/qmc809}$ mutants (**Figure 4.6D**; black arrow, **4.6D''**; red arrow) were expanded mediolaterally compared to the WT controls (**Figure 4.6A**, black arrow, **4.6A''**; red arrow), indicating that *def6a* and *swap70b* are required for the convergence movements during gastrulation.

***no-tail* (*ntl*)** is expressed in posterior axial mesoderm marking the presumptive notochord during gastrulation. Wider and shorter notochord was one of the characteristic phenotypes of the CE mutants (Heisenberg *et al.,* 2000; Kilian *et al.,* 2003) since the axial mesoderm tissues fail to converge and extend properly. Like the CE mutants/morphants, *def6a*$^{qmc811/qmc811}$ (**Figure 4.6B'**; red and yellow lines), *swap70b*$^{qmc809/qmc809}$ (**Figure 4.6C'**; red and yellow lines) and double *def6a*$^{qmc811/qmc811}$; *swap70b*$^{qmc809/qmc809}$ mutants (**Figure 4.6D'**; red and yellow lines) exhibited wider and shorter notochord during gastrulation, compared to the WT controls (**Figure 4.6A'**; red and yellow lines), clearly indicating that *def6a* and *swap70b* are required for the CE cell movements of mesodermal and ectodermal tissues during gastrulation.

orthodenticle homeobox (otx) genes encode homeodomain-containing transcription factors regulating the anterior neural patterning and brain morphogenesis (Acampora *et al.,* 2001). The zebrafish *otx* genes, including *otx1a (also referred to as otx3), otx1b, otx2* are expressed in anterior neuroectoderm forming the presumptive forebrain and midbrain during zebrafish gastrulation (Li *et al.,* 1994; Mercier *et al.,* 1995). The expression pattern of *otx2* marking the forebrain/midbrain neural plate during the tail-bud stage was tested to reveal whether mutations in *def6a* and *swap70b* interfered with the convergence movements of the neural tissues. Consistent with the expansion of the neural plate (*dlx3*), the forebrain/midbrain neural plate was expanded medio-laterally in *def6a*$^{qmc811/qmc811}$ (**Figure 4.6F-F'**; red arc) *swap70b*$^{qmc809/qmc809}$ (**Figure 4.6G-G'**; red arc) and double *def6a*$^{qmc811/qmc811}$; *swap70b*$^{qmc809/qmc809}$ mutants (**Figure 4.6H-H'**; red arc) compared to the WT controls (**Figure 4.6E-E'**; red arc). This result also indicates the disruption in CE cell movements during gastrulation.

myogenic differentiation* (*myoD) is a member of myogenic regulatory transcription factors (MRFs) gene family and encodes a helix-loop-helix transcription factor regulating myogenic proliferation and differentiation (Hinits *et al.,* 2011). It is expressed in adaxial cells and forms somites. It is used as a marker of paraxial mesodermal tissues during zebrafish gastrulation (Weinberg *et al.,* 1996). While in WT embryos, the adaxial cells expressing *myoD* elongate anterior-posteriorly and converge dorsally (**Figure 4.6I;** black line and red arrow), the adaxial cells were shortened anterior-posteriorly and expanded medio-laterally in *def6a*$^{qmc811/qmc811}$ (**Figure 4.6J;** black line and red arrow), *swap70b*$^{qmc809/qmc809}$ (**Figure 4.6K;**

black line and red arrow) and double *def6a*$^{qmc811/qmc811}$; *swap70b*$^{qmc809/qmc809}$ mutants (**Figure 4.6L;** black line and red arrow). Interestingly, the shortening and expansion of *myoD* pattern was more severe in *swap70b*$^{qmc809/qmc809}$ and double *def6a*$^{qmc811/qmc811}$; *swap70b*$^{qmc809/qmc809}$ mutants than *def6a*$^{qmc811/qmc811}$ mutants.

Taken together, the defects observed in single *def6a*$^{qmc811/qmc811}$ and *swap70b*$^{qmc809/qmc809}$ and double *def6a*$^{qmc811/qmc811}$; *swap70b*$^{qmc809/qmc809}$ mutants are reminiscent of the CE cell movement defects in the CE mutants/morphants (Hammmerschmidt *et al.,* 1996; Heisenberg *et al.,* 2000; Kilian *et al.,* 2003; Jessen *et al.,* 2002; Topczewski *et al.,* 2001; Carreira-Barbosa *et al.,* 2003; Solnica-Krezel *et al.,* 1996), suggesting that *def6a* and *swap70b* are required for CE cell movements of mesodermal and ectodermal tissues during zebrafish gastrulation.

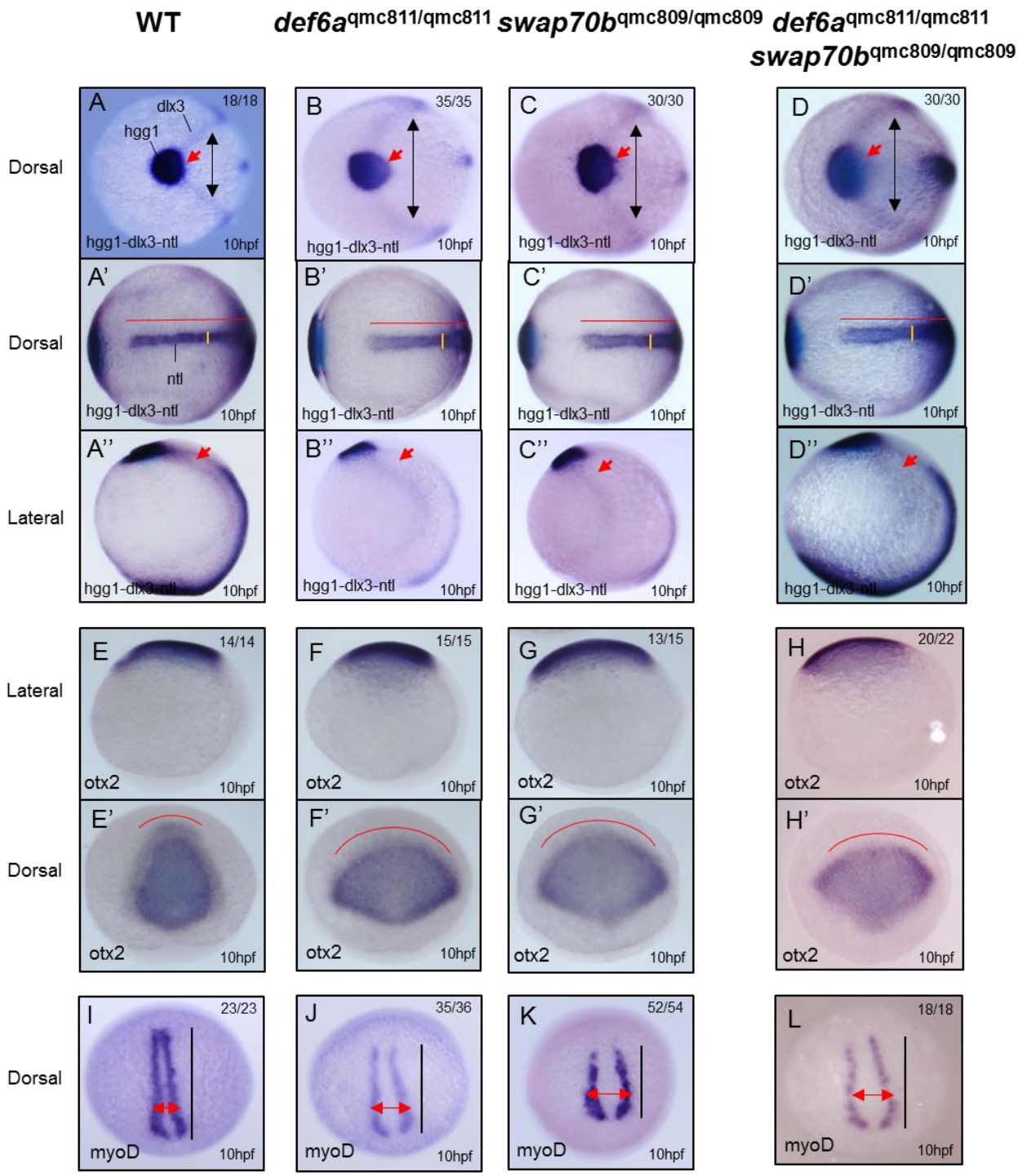

WT
def6a qmc811/qmc811 swap70b qmc809/qmc809
def6a qmc811/qmc811 swap70b qmc809/qmc809
Dorsal
Dorsal
Lateral
Lateral
Dorsal
Dorsal
A
dlx3
hgg1
18/18
hgg1-dlx3-ntl
10hpf
B
35/35
C
30/30
D
30/30
A'
ntl
B'
C'
D'
A''
B''
C''
D''
E
14/14
otx2
F
15/15
G
13/15
H
20/22
E'
F'
G'
H'
I
23/23
myoD
J
35/36
K
52/54
L
18/18

Figure 4.6 Single *def6a*$^{qmc811/qmc811}$ and *swap70b*$^{qmc809/qmc809}$ and double *def6a*$^{qmc811/qmc811}$; *swap70b*$^{qmc809/qmc809}$ mutants displayed impaired convergence and extension (CE) cell movements during gastrulation. WT (left column), *def6a*$^{qmc811/qmc811}$ mutants (middle left column), *swap70b*$^{qmc809/qmc809}$ mutants (middle right column) and double *def6a*$^{qmc811/qmc811}$; *swap70b*$^{qmc809/qmc809}$ mutants (right column) were fixed at tail-bud stage (10hpf) and subjected to WISH using *hgg1* (**A-B-C-D**; red arrow, dorsal view), *dlx3* (**A-B-C-D**; black arrow, dorsal view and **A''-B''C''-D''**; red arrow, lateral view, dorsal right), *ntl* (**A'-B'C'-D'**; red line, dorsal view, anterior left), *otx2* (**E-F-G-H**; lateral view, dorsal right and **E'-F'-G'-H'**; red arc, dorsal view, anterior top) and *myoD* (**I-J-K-L**; black line, dorsal view, anterior top) riboprobes. (**A-B-C-D**) The posterior shift of the prechordal plate (*hgg1)*, the medio-lateral expansion of neural plate (*dlx3*), the shortening and expansion of notochord (*ntl*) were observed in *def6a*$^{qmc811/qmc811}$ (**B**), *swap70b*$^{qmc809/qmc809}$ (**C**) and double *def6a*$^{qmc811/qmc811}$; *swap70b*$^{qmc809/qmc809}$ mutants (**D**) compared to the WT controls (**A**). (**E-F-G-H**) The expansion of the forebrain-midbrain neural plate marked by *otx2* in *def6a*$^{qmc811/qmc811}$ **(F')**, *swap70b*$^{qmc809/qmc809}$ **(G')** and double *def6a*$^{qmc811/qmc811}$; *swap70b*$^{qmc809/qmc809}$ mutants **(H')** confirmed the expansion of the neural plate. (**I-J-K-L**) The adaxial cells (*myoD*) were expanded mediolaterally and shortened anterior-posteriorly in *def6a*$^{qmc811/qmc811}$ **(J)**, *swap70b*$^{qmc809/qmc809}$ **(K)** and double *def6a*$^{qmc811/qmc811}$; *swap70b*$^{qmc809/qmc809}$ mutants **(L)**, with a greater extent in *swap70b*$^{qmc809/qmc809}$ and double *def6a*$^{qmc811/qmc811}$; *swap70b*$^{qmc809/qmc809}$ mutants. The number of embryos tested for each probe is indicated at the top of the figures, the stage is indicated at the bottom of the figures.

To quantify the CE cell movement defects, WT, *def6a*$^{qmc811/qmc811}$, *swap70b*$^{qmc809/qmc809}$ and double *def6a*$^{qmc811/qmc811}$; *swap70b*$^{qmc809/qmc809}$ mutants were fixed at the tail-bud stage and subjected to the WISH using *hgg1, dlx3* and *ntl* probes (**Figure 4.7A-B-C-D**). Two statistical analyses, one-way ANOVA and two-tailed student's t-test were used to determine the significant differences in the angle between the borders of the neural plate (**Figure 4.7E**) and in the posterior elongation of the prechordal plate (**Figure 4.7F**). The prechordal plate marked by *hgg1* was posteriorly elongated and slightly positioned bottom of the neural plate in *def6a*$^{qmc811/qmc811}$ (**Figure 4.7B'**) and *swap70b*$^{qmc809/qmc809}$ (**Figure 4.7C'**) and double *def6a*$^{qmc811/qmc811}$; *swap70b*$^{qmc809/qmc809}$ mutants (**Figure 4.7D')** compared to WT controls (**Figure 4.7A'**). The connection point between the neural plate (*dlx3*) and prechordal plate (*hgg1*) was marked with a border (yellow line) and the ratio (α/β) of the prechordal plate length was calculated. α indicates the top part of the prechordal plate and β indicates the bottom part of the prechordal plate separated by a yellow line (**Figure 4.7A'-B'-C'-D'**).

The angle (θ) between the borders of neural plate marked by *dlx3* (red lines) was increased in *def6a*$^{qmc811/qmc811}$ (**Figure 4.7B**), *swap70b*$^{qmc809/qmc809}$ (**Figure 4.7C**) and double *def6a*$^{qmc811/qmc811}$; *swap70b*$^{qmc809/qmc809}$ mutants (**Figure 4.7D**) compared to WT controls (**Figure 4.7A**). The mean angle was calculated as 74.9 for WT, 94.4 for *def6a*$^{qmc811/qmc811}$ mutants, 96.8 for *swap70b*$^{qmc809/qmc809}$ mutants and 95.1 for double *def6a*$^{qmc811/qmc811}$; *swap70b*$^{qmc809/qmc809}$ mutants (**Figure 4.7G**). One-way ANOVA and two-tailed student's t-test analyses confirmed the significant ($p<0.0001$(****) increase in the angle between WT and single (*def6a*$^{qmc811/qmc811}$ and *swap70b*$^{qmc809/qmc809}$) or double (*def6a*$^{qmc811/qmc811}$; *swap70b*$^{qmc809/qmc809}$) mutants, while no significant (N.S) differences were detected between single and double mutants (**Figure 4.7E**). These results confirmed the defects in convergence movements in mutants and also absence of increased severity in double *def6a*$^{qmc811/qmc811}$; *swap70b*$^{qmc809/qmc809}$ mutants compared to the single mutants.

The mean ratio (α/β) calculated as 2.20 for WT decreased to 1.04, 0.95 and 1.03 for *def6a*$^{qmc811/qmc811}$, *swap70b*$^{qmc809/qmc809}$ and double *def6a*$^{qmc811/qmc811}$; *swap70b*$^{qmc809/qmc809}$ mutants, respectively, thereby indicating that the bottom (β) length of the prechordal plate is more than the top (α) length in the mutants. One-way ANOVA and two-tailed student's t-test analyses confirmed the significant ($p<0.0001$(****) decrease in the ratio of single (*def6a*$^{qmc811/qmc811}$ and *swap70b*$^{qmc809/qmc809}$) and double (*def6a*$^{qmc811/qmc811}$; *swap70b*$^{qmc809/qmc809}$) mutants compared to WT controls. No significant (N.S) difference was detected between single and double mutants (**Figure 4.7F**). These findings suggest that double *def6a*$^{qmc811/qmc811}$; *swap70b*$^{qmc809/qmc809}$ mutants do not display severe CE cell movement defects compared with both *def6a*$^{qmc811/qmc811}$ and *swap70b*$^{qmc809/qmc809}$ mutants. These results

confirmed the posterior elongation of the prechordal plate in mutants which is the consequence of defects in convergent and extension movements.

The increased angle of the neural plate and the decreased ratio of the prechordal plate in single *def6a*$^{qmc811/qmc811}$, *swap70b*$^{qmc809/qmc809}$ and double *def6a*$^{qmc811/qmc811}$; *swap70b*$^{qmc809/qmc809}$ mutants indicated that both convergence and extension cell movements are impaired in the *def6a*$^{qmc811/qmc811}$ and *swap70b*$^{qmc809/qmc809}$ mutants and *def6a* and *swap70b* are not functionally redundant during gastrulation.

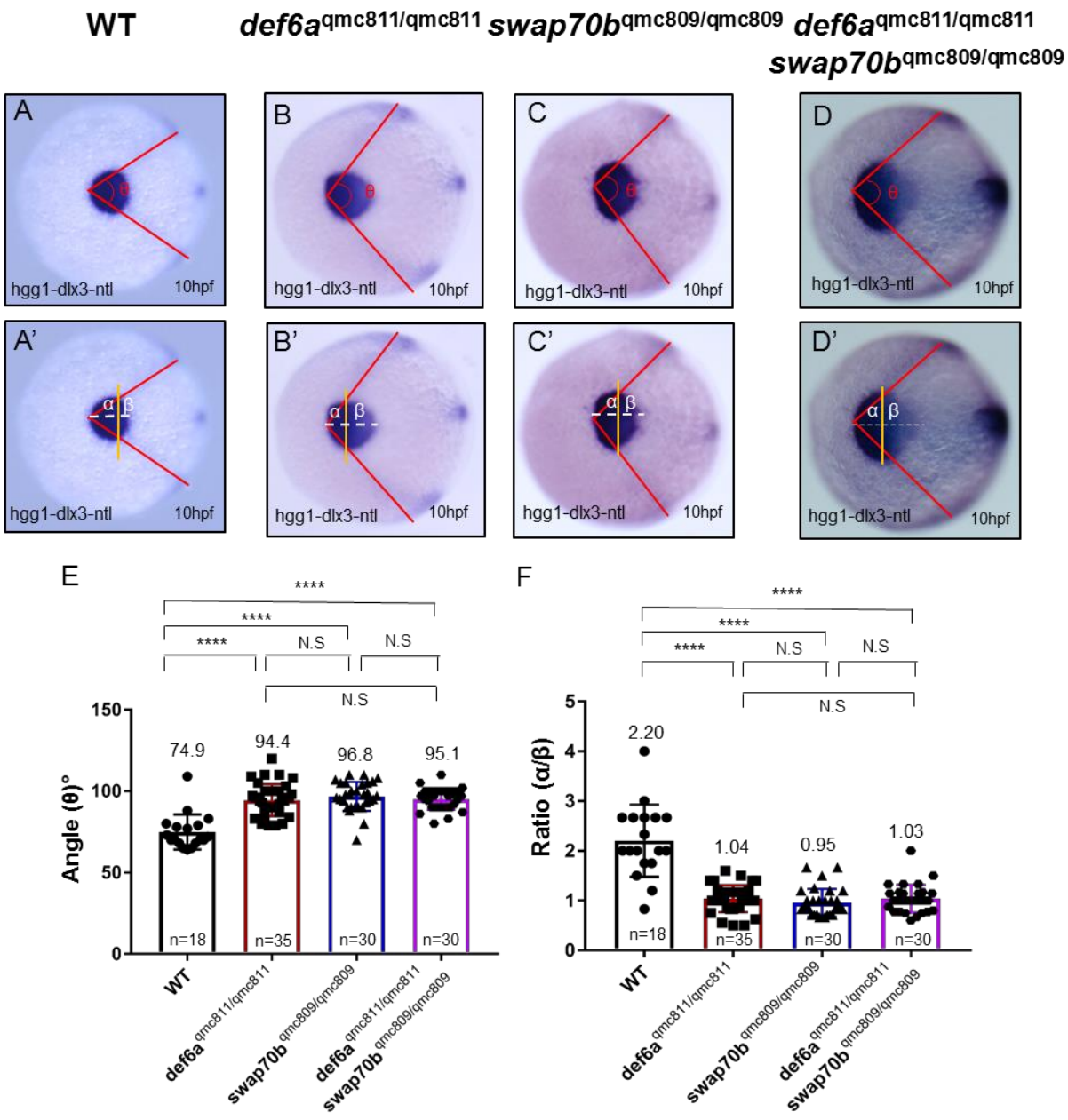

WT
def6a qmc811/qmc811 swap70b qmc809/qmc809
def6a qmc811/qmc811 swap70b qmc809/qmc809
A
B
C
D
A'
B'
C'
D'
hgg1-dlx3-ntl
10hpf
θ
α
β
E
F
Angle (θ)°
Ratio (α/β)
74.9
94.4
96.8
95.1
2.20
1.04
0.95
1.03
n=18
n=35
n=30
n=30
****
N.S
WT
def6a qmc811/qmc811
swap70b qmc809/qmc809
def6a qmc811/qmc811 swap70b qmc809/qmc809

Figure 4.7 Impaired CE cell movements in single *def6a*$^{qmc811/qmc811}$ and *swap70b*$^{qmc809/qmc809}$ and double *def6a*$^{qmc811/}$qmc811; *swap70b*$^{qmc809/qmc809}$ mutants were confirmed by statistical analyses. Representative embryos from each category are illustrated. WT (left column), *def6a*$^{qmc811/qmc811}$ mutants (middle left column), *swap70b*$^{qmc809/qmc809}$ mutants (middle right column) and double *def6a*$^{qmc811/qmc811}$; *swap70b*$^{qmc809/qmc809}$ mutants (right column) were fixed at the tail-bud stage and WISH was carried out using *hgg1, dlx3* and *ntl* probes. **(A-B-C-D;** dorsal view, anterior left**)** The neural plate marked by *dlx3* (red line) was expanded in *def6a*$^{qmc811/qmc811}$ **(B)** *swap70b*$^{qmc809/qmc809}$ **(C)** and double *def6a*$^{qmc811/qmc811}$; *swap70b*$^{qmc809/qmc809}$ mutants **(D)**, compared to WT controls **(A)**. The angle (θ) between the neural plate borders was calculated and **(E)** one-way ANOVA and two-tailed student's t-test analyses confirmed the significant ($p<0.0001$) increase in the angle between WT and the mutants (**A'-B'-C'-D';** dorsal view, anterior left) ($p=0.3189$; *def6a*$^{qmc811/qmc811}$ and *swap70b*$^{qmc809/qmc809}$ mutants), $p=0.7717$; *def6a*$^{qmc811/qmc811}$ and double *def6a*$^{qmc811/qmc811}$; *swap70b*$^{qmc809/qmc809}$ mutants, $p=0.3943$; *swap70b*$^{qmc809/qmc809}$ and double *def6a*$^{qmc811/qmc811}$; *swap70b*$^{qmc809/qmc809}$ mutants). The connection of the neural plate and prechordal plate was bordered (yellow line) and the ratio of the top (α) to the bottom (β) parts of the prechordal plate was measured. The ratio (α/β) was found to be decreased in single **(B'-C')** and double mutants **(D')**, compared to WT controls **(A')**. **(F)** One-way ANOVA and two-tailed student's t-test analyses confirmed the significant ($p<0.0001$) decrease in the ratio in the mutants. N.S indicates no significant ($p>0.05$) difference among *def6a*$^{qmc811/qmc811}$, *swap70b*$^{qmc809/qmc809}$ and double *def6a*$^{qmc811/qmc811}$; *swap70b*$^{qmc809/qmc809}$ mutants ($p=0.2120$; *def6a*$^{qmc811/qmc811}$ and *swap70b*$^{qmc809/qmc809}$ mutants, $p=0.9804$; *def6a*$^{qmc811/qmc811}$ and double *def6a*$^{qmc811/qmc811}$; *swap70b*$^{qmc809/qmc809}$ mutants, $p=0.2472$; *swap70b*$^{qmc809/qmc809}$ and double *def6a*$^{qmc811/qmc811}$; *swap70b*$^{qmc809/qmc809}$ mutants). The scatter plots indicate the mean with standart deviation (SD). The graphs present the mean angle (θ), the mean ratio (α/β) for WT and the mutants and the number (n) of tested embryos.

4.5. Single and double homozygous mutants displayed normal development of anterior and posterior body parts after gastrulation

4.5.1. Single *def6a*$^{qmc811/qmc811}$ and *swap70b*$^{qmc809/qmc809}$ and double *def6a*$^{qmc811/qmc811}$*; swap70b*$^{qmc809/qmc809}$ homozygous mutants displayed normal neural patterning and brain morphogenesis during segmentation

As shown in section 4.1, the morphology of mutant embryos following gastrulation appeared normal. To further verify normal patterning of the developing brain, expression of *otx2, pax2a, krox20* and *hoxb1a* was determined at segmentation stage (22hpf; **Figure 4.8**). *otx2* expression in the midbrain (**Figure 4.8A-D**), *pax2a* expression in the hindbrain-midbrain boundary, neural tube, optic stalk, otic vesicle and pronephric duct (**Figure 4.8E-H**), *krox20* expression in r3 and r5 (**Figure 4.8I-L**) and *hoxb1a* expression in r4 (**Figure 4.8M-P)** appeared normal in single and double homozygous mutants. These results suggest that the CE cell movement defects during gastrulation observed in the mutant embryos have no significant effect on the later development of the brain. However, the paralogues genes of *def6a* and *swap70b* are expressed in later stages (**Figure 1.14**) and could possibly compensate for loss-of-function of *def6a* and *swap70b.*

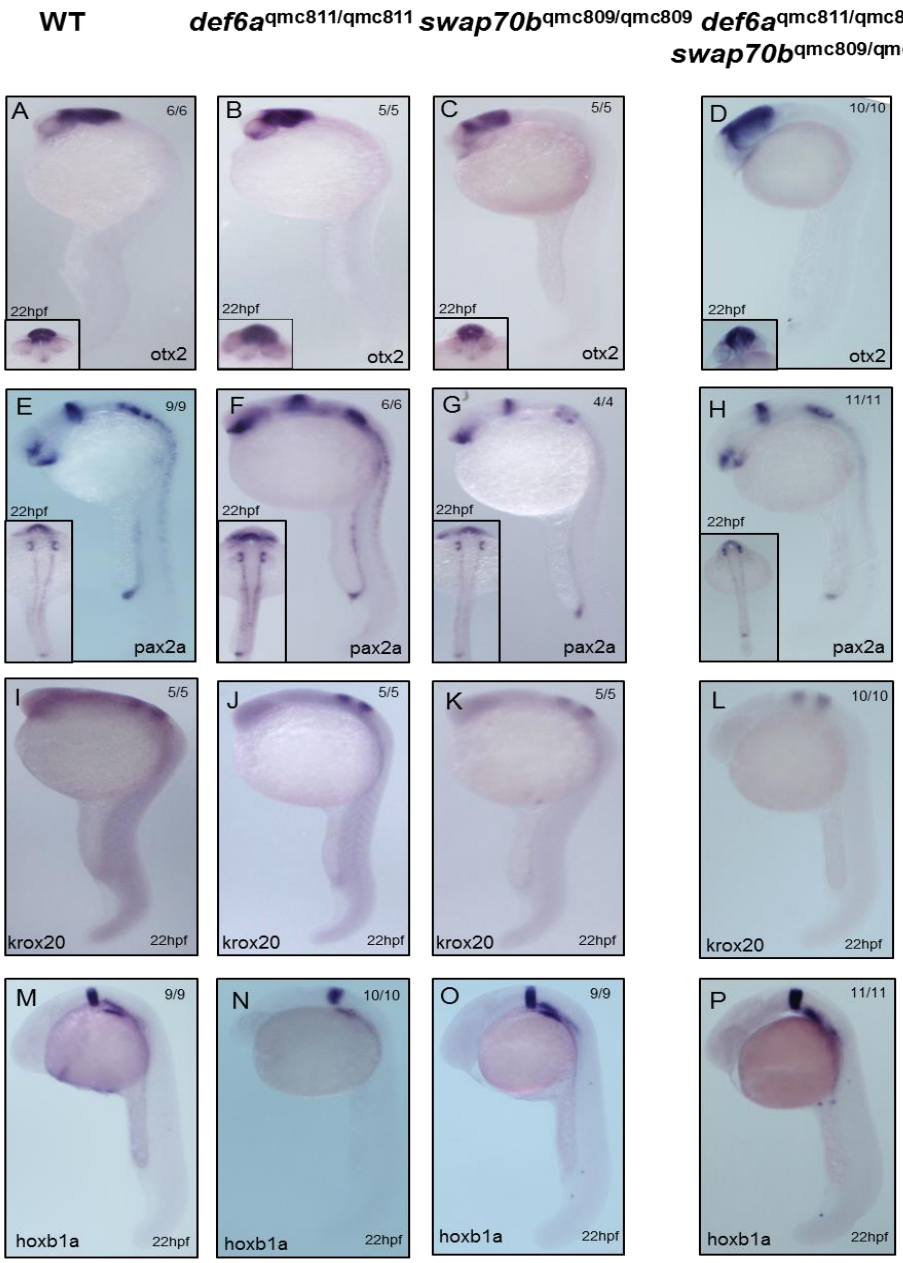


Figure 4.8 Single *def6a*$^{qmc811/qmc811}$ and *swap70b*$^{qmc809/qmc809}$ and double *def6a*$^{qmc811/qmc811}$; *swap70b*$^{qmc809/qmc809}$ mutants displayed normal neural patterning and brain morphogenesis during segmentation. WT (left column), *def6a*$^{qmc811/qmc811}$ mutants (middle left column), *swap70b*$^{qmc809/qmc809}$ mutants (middle right column) and double *def6a*$^{qmc811/qmc811}$; *swap70b*$^{qmc809/qmc809}$ mutants (right column) were fixed at segmentation (22hpf) stage and subjected to WISH using *otx2* **(A-B-C-D;** lateral view, anterior top**)**, *pax2a* **(E-F-G-H;** lateral view, anterior top**)**, *krox20* **(I-J-K-L;** lateral view, anterior top**)** and *hoxb1a* **(M-N-O-P;** lateral view, anterior top**)** riboprobes. None of the expression patterns of *otx2, pax2a, krox20* and *hoxb1a* was changed in *def6a*$^{qmc811/qmc811}$, *swap70b*$^{qmc809/qmc809}$ and double *def6a*$^{qmc811/qmc811}$; *swap70b*$^{qmc809/qmc809}$ mutants. The number of embryos tested for each probe is indicated at the top of the figures, the stage is indicated at the bottom of the figures.

4.5.2. Single *def6a*$^{qmc811/qmc811}$ and *swap70b*$^{qmc809/qmc809}$ and double *def6a*$^{qmc811/qmc811}$*; swap70b*$^{qmc809/qmc809}$ homozygous mutants displayed normal development of somite and tail structures during segmentation

To verify whether development of posterior structures such as somites and tail was normal, we determined expression of *myoD, fgf8*, *ntl* and *shh* expression at segmentation stage (22hpf). As illustrated in **Figure 4.9**, expression of *myoD* in the somites **(4.9A-D)**, expression of *fgf8* in the midbrain hindbrain boundary and posterior somites **(4.9E-H)**, expression of *ntl* in the notochord **(4.9I-K)** and expression of shh in notochord, hypothalamus and floor plate **(Figure 4.9M-P)** was indistinguishable between WT and mutant embryos.

Although single *def6a*$^{qmc811/qmc811}$ and *swap70b*$^{qmc809/qmc809}$ mutants and double *def6a*$^{qmc811/qmc811}$; *swap70b*$^{qmc809/qmc809}$ mutants exhibited CE cell movement defects during gastrulation, confirmed by reduced body axis (**Figure 4.2B-D**) and *in situ* hybridisation analysis using *ntl* probe (**Figure 4.6B'-D'**), the reduced length of the body axis was rescued during segmentation since the tail length in *def6a*$^{qmc811/qmc811}$ mutants (**Figure 4.9J**) and *swap70b*$^{qmc809/qmc809}$ mutants (**Figure 4.9K**) was not shorter than the WT controls (**Figure 4.9I**) during segmentation (22hpf).

Taken together, single *def6a*$^{qmc811/qmc811}$ and *swap70b*$^{qmc809/qmc809}$ mutants and double *def6a*$^{qmc811/qmc811}$; *swap70b*$^{qmc809/qmc809}$ mutants displayed no obvious defects in the development of somite and tail structures following gastrulation. Moreover, the extension of tail was also not shorter than the WT controls. This suggests that the CE cell movement defects observed during gastrulation might be rescued by compensation from other paralogues genes of *def6a* and *swap70b* during segmentation.

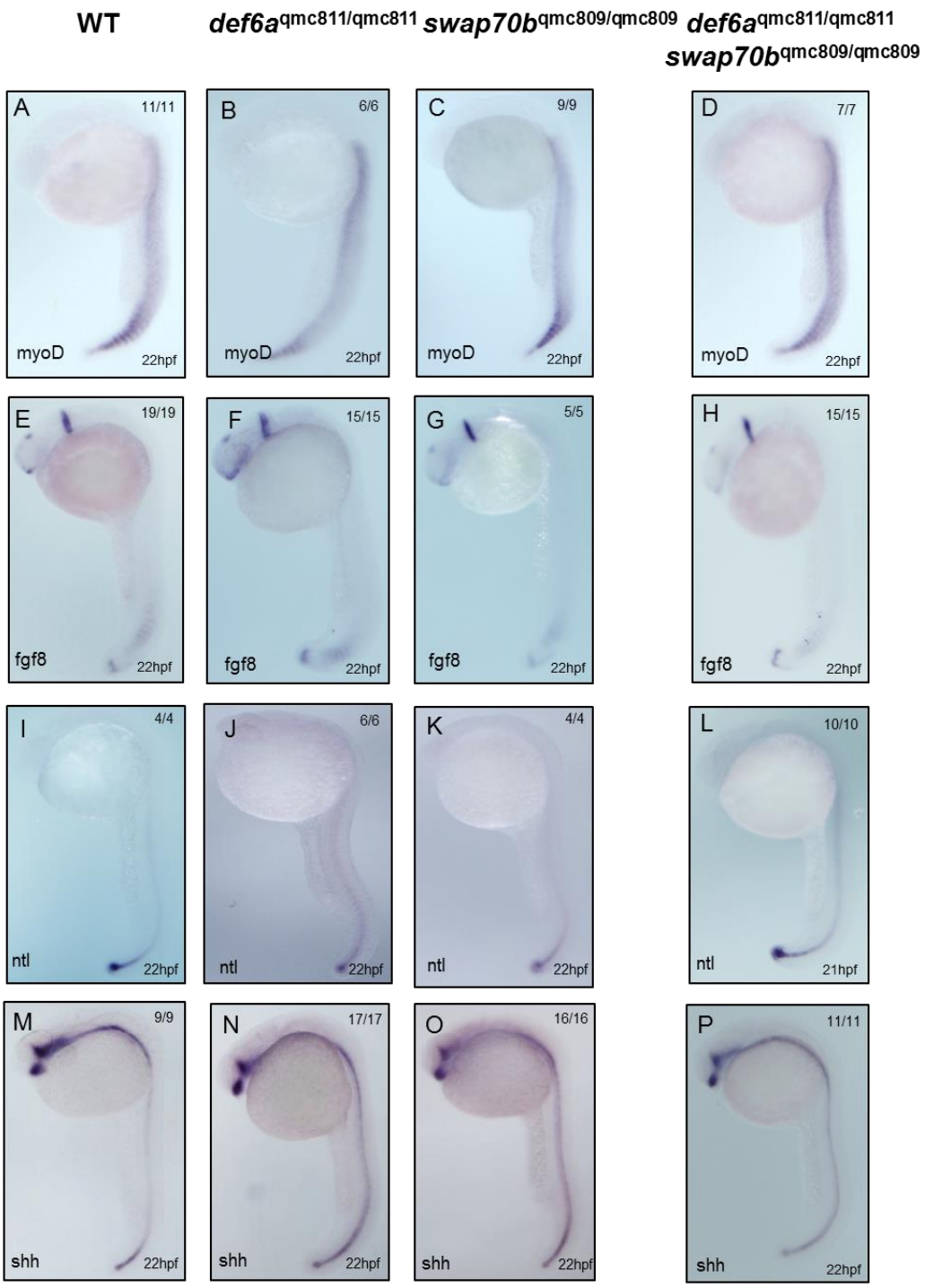


Figure 4.9 Single *def6a*$^{qmc811/qmc811}$, *swap70b*$^{qmc809/qmc809}$ and double *def6a*$^{qmc811/qmc811}$; *swap70b*$^{qmc809/qmc809}$ mutants displayed normal development of somite and tail structures during segmentation. WT (left column), *def6a*$^{qmc811/qmc811}$ mutants (middle left column) and *swap70b*$^{qmc809/qmc809}$ mutants (middle right column) and double *def6a*$^{qmc811/qmc811}$; *swap70b*$^{qmc809/qmc809}$ mutants (right column) were fixed at segmentation (21-22hpf) stage and subjected to WISH using *myoD* **(A-B-C-D;** lateral view, anterior top**)**, *fgf8* **(E-F-G-H;** lateral view, anterior top**)**, *ntl* **(I-J-K-L;** lateral view, anterior top**)** and *shh* **(M-N-O-P;** lateral view, anterior top) riboprobes. None of the expression patterns of *myoD, fgf8, ntl* and *shh* was changed in single and double mutants. The number of embryos tested for each probe is indicated at the top of the figures and the stages are indicated at the bottom of the figures.

4.6. Summary

- Phenotypic analysis revealed that single *def6a*$^{qmc811/qmc811}$, *swap70b*$^{qmc809/qmc809}$ and double *def6a*$^{qmc811/qmc811}$; *swap70b*$^{qmc809/qmc809}$ homozygous mutants displayed reduced body axis at the tail-bud stage. This is a characteristic of CE cell movement defects.
- Analysis of *cdx4, bmp2b, chd* and *ntl* gene expression at the shield stage revealed that cell fate specification determining posterior and dorsoventral development was not affected by the loss of *def6a* or *swap70b* or both.
- Analysis of *pax2a, fgf8, krox20* and *hoxb1a* gene expression at the tail-bud stage revealed a posterior shift and expansion of the expression patterns of all neuroectoderm markers, thus, indicating CE cell movement defects.
- Analysis of *hgg1, dlx3, ntl, otx2* and *myoD* gene expression at the tail-bud stage revealed that both *def6a* and *swap70b* are required for CE cell movements during gastrulation. However, CE cell movement defects in double homozygous *def6a*$^{qmc811/qmc811}$; *swap70b*$^{qmc809/qmc809}$ mutants did not demonstrate increased severity compared to single homozygous mutants, suggesting that *def6a* and *swap70b* are not redundant during gastrulation.
- Analysis of *otx2, pax2a* and *krox20* gene expression after gastrulation at the segmentation stage (22hpf) revealed that neural patterning and brain morphogenesis were normal in single as well as double homozygous mutants.
- Analysis of *myoD, fgf8, ntl* and *shh* gene expression at the segmentation stage (22hpf) revealed that development of somites and tail was normal.
- Despite a developmental delay during gastrulation, single and double homozygous mutant zebrafish recovered from the apparent CE cell movement defects, grew to adulthood and were fertile.

CHAPTER 5
RESULTS
def6a and *swap70b* regulate actin cytoskeleton and *wnt5b/wnt11* expression through Cdc42 and Racl in the non-canonical Wnt/PCP/Ca^{2+} signalling pathways

5.1. CE cell movement defects in *def6a*$^{qmc811/qmc811}$ mutants were robustly rescued by overexpression of Cdc42, while overexpression of either Cdc42 or Racl rescued *swap70b*$^{qmc809/qmc809}$ mutants

To investigate whether *def6a and/*or *swap70b* regulates CE cell movements during gastrulation via Rho GTPases, Gfp-tagged Cdc42, RhoA and Racl were overexpressed in *def6a*$^{qmc811/qmc811}$ and *swap70b*$^{qmc809/qmc809}$ mutants. Overexpression of Gfp alone served as a negative control. Expression of *hgg1, dlx3* and *ntl* was determined in control and experimental embryos at tail-bud stage by *in situ* hybridisation and CE cell movement defects which are characterised by the increased angle in the neural plate (*dlx3*) and the elongation in the prechordal plate (*hgg1*) were measured and analysed by one-way ANOVA and two-tailed student's t-test statistical analyses as previously demonstrated (Section 4.4 / Figure 4.7). WT embryos served as a control thereby the same samples were used for the statistical analyses of all injections.

5.1.1. Overexpression of Cdc42 robustly rescued CE cell movement defects in *def6a*$^{qmc811/qmc811}$ mutants

As illustrated in **Figure 5.1**, injection of 200pg of *gfp-cdc42* mRNA was sufficient to robustly rescue the CE cell movement defects in *def6a*$^{qmc811/qmc811}$ mutants. *def6a*$^{qmc811/qmc811}$ mutants exhibited the characteristic medio-lateral expansion of the neural plate marked by *dlx3* (**Figure 5.1A-B**), elongation of the prechordal plate marked by *hgg1* **(Figure 5.1A'-B')** and the shortened and broadened notochord marked by *ntl* compared to WT **(Figure 5.1A''-B'')**. Overexpression of Gfp-Cdc42 in *def6a*$^{qmc811/qmc811}$ mutants reverted the observed CE cell movement defects **(Figure 5.1C-C''')**. The prechordal plate was less elongated and shifted **(Figure 5.1C-C')**, the neural plate was less expanded **(Figure 5.1C'-C''')** and the notochord was not shortened and expanded **(Figure 5.1C'')** in *def6a*$^{qmc811/qmc811}$ mutants injected with *gfp-cdc42* mRNA. The mean angle (θ) between the borders of the neural plate was determined

as 72, 91.4 and 74.7 for WT, *def6a*$^{qmc811/qmc811}$ mutants and *def6a*$^{qmc811/qmc811}$ mutants injected with *gfp-cdc42* mRNA, respectively (**Figure 5.1D**). One-way-ANOVA and two-tailed student's t-test statistical analyses confirmed the significant ($p<0.0001$ (****)) increase in the angle between un-injected *def6a*$^{qmc811/qmc811}$ mutants and WT controls **(Figure 5.1D)**. On the other hand, *def6a*$^{qmc811/qmc811}$ mutants injected with *gfp-cdc42* mRNA did not exhibit a significant difference to WT **(Figure 5.1D; N.S:** $p=0.3358$**)** but exhibited a significant difference to un-injected *def6a*$^{qmc811/qmc811}$ mutants **(Figure 5.1D;** ****: $p<0.0001$). Similarly, the ratio (α/β=top/bottom) of the prechordal plate length was determined using the connection point between the neural plate (*dlx3*) and prechordal plate (*hgg1*) as a marker dividing the prechordal plate **(Figure 5.1A'-C';** yellow line). The mean ratio was calculated as 2.91, 1.24 and 2.49 for WT, *def6a*$^{qmc811/qmc811}$ mutants and *def6a*$^{qmc811/qmc811}$ mutants injected with *gfp-cdc42* mRNA, respectively (**Figure 5.1E**). One-way ANOVA and two-tailed student's t-test statistical analyses confirmed the significant ($p<0.0001$ (****)) decrease in the ratio between the un-injected *def6a*$^{qmc811/qmc811}$ mutants and WT controls **(Figure 5.1E)** and indicated that overexpression of Gfp-Cdc42 in *def6a*$^{qmc811/qmc811}$ mutants rescued the CE cell movement phenotype. There was no significant difference between WT and *def6a*$^{qmc811/qmc811}$ mutants injected with *gfp-cdc42* mRNA (**Figure 5.1E; N.S:** $p=0.1163$), however, a significant difference did exist between *def6a*$^{qmc811/qmc811}$ mutants and *def6a*$^{qmc811/qmc811}$ mutants injected with *gfp-cdc42* mRNA **(Figure 5.1E;** ****: $p<0.0001$).

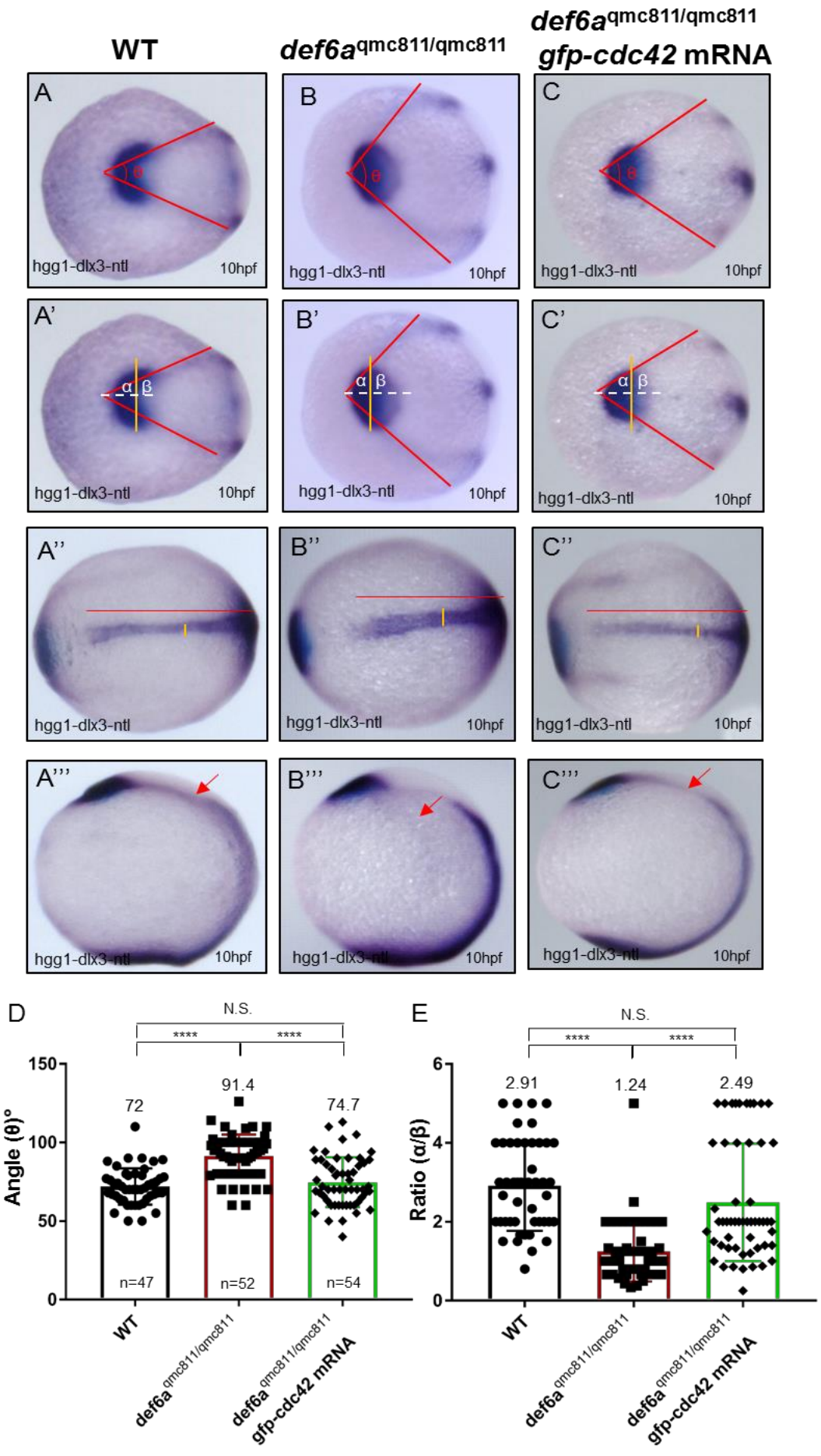

WT
def6a qmc811/qmc811
def6a qmc811/qmc811
gfp-cdc42 mRNA
A
B
C
A'
B'
C'
A''
B''
C''
A'''
B'''
C'''
θ
α β
hgg1-dlx3-ntl
10hpf
D
N.S.
****
****
Angle (θ)°
150
100
50
0
72
91.4
74.7
n=47
n=52
n=54
WT
def6a qmc811/qmc811
def6a qmc811/qmc811 gfp-cdc42 mRNA
E
N.S.
****
****
Ratio (α/β)
6
4
2
0
2.91
1.24
2.49
WT
def6a qmc811/qmc811
def6a qmc811/qmc811 gfp-cdc42 mRNA

Figure 5.1 Injection of *gfp-cdc42* mRNA robustly rescued the CE cell movement defects in *def6a*$^{qmc811/qmc811}$ mutants. Representative embryos from each category are illustrated. WT (left column), un-injected *def6a*$^{qmc811/qmc811}$ (middle column), *def6a*$^{qmc811/qmc811}$ mutants injected with *gfp-cdc42* mRNA (right column) were fixed at the tail-bud stage and WISH was carried out using *hgg1, dlx3* and *ntl* probes. **(A-B-C;** dorsal view, anterior left**)** The neural plate marked by *dlx3* (red line) was expanded in *def6a*$^{qmc811/qmc811}$ mutants **(B-B'''),** compared to WT controls **(A-A''')**. The notochord marked by *ntl* was expanded and shortened in the un-injected *def6a*$^{qmc811/qmc811}$ mutants **(B'')**, compared to WT controls **(A'')** and *def6a*$^{qmc811/qmc811}$ mutants injected with *gfp-cdc42* mRNA **(C'')**. The angle (θ) between the neural plate borders was calculated. (**D**) One-way ANOVA and two-tailed student's t-test analyses confirmed the significant ($p<0.0001$;****) increase in the angle between WT and the un-injected *def6a*$^{qmc811/qmc811}$ mutants **(A-B;** dorsal view, anterior left**)** and the significant ($p<0.0001$;****) decrease in the angle between the un-injected *def6a*$^{qmc811/qmc811}$ mutants and *def6a*$^{qmc811/qmc811}$ mutants injected with *gfp-cdc42* mRNA **(B-C;** dorsal view, anterior left). The connection of neural plate and prechordal plate was bordered (yellow line) and the ratio of the top (α) to the bottom (β) parts of the prechordal plate was measured. The ratio (α/β) was found to have decreased in *def6a*$^{qmc811/qmc811}$ mutants **(B')** while it was robustly restored in the *def6a*$^{qmc811/qmc811}$ mutants injected with *gfp-cdc42* mRNA **(C')**, compared to WT controls **(A')**. **(E)** One-way ANOVA and two-tailed t-test analyses confirmed the significant ($p<0.0001$;****) decrease in the ratio between the un-injected *def6a*$^{qmc811/qmc811}$ mutants and WT controls and also the significant ($p<0.0001$;****) increase in the ratio between the un-injected *def6a*$^{qmc811/qmc811}$ mutants and *def6a*$^{qmc811/qmc811}$ mutants injected with *gfp-cdc42* mRNA. N.S indicates no significant ($p>0.05$) difference between WT and *def6a*$^{qmc811/qmc811}$ mutants injected with *gfp-cdc42* mRNA, the scatter plots indicate the mean with standart deviation (SD). The graphs present the mean angle (θ) and mean ratio (α/β) for WT, un-injected *def6a*$^{qmc811/qmc811}$ mutants and *def6a*$^{qmc811/qmc811}$ mutants injected with *gfp-cdc42* mRNA. The number (n) of tested embryos is also indicated.

5.1.2. Overexpression of either Racl, RhoA or Gfp in *def6a*$^{qmc811/qmc811}$ mutants had no effect on CE cell movement defects

To test whether *def6a* is not only acting upstream of Cdc42 as previously shown **(Section 5.1.1)**, Gfp-tagged Racl and RhoA or Gfp alone were overexpressed in *def6a*$^{qmc811/qmc811}$ mutants **(Figures 5.2-5.4 A-C''')**. Quantitative analysis of the mean angle and ratio as previously described (**Section 5.1.1**) revealed that neither Racl, RhoA nor Gfp overexpression resulted in a significant rescue of the CE cell movement defects observed in *def6a*$^{qmc811/qmc811}$ mutants (**Figures 5.2-5.4 D-E; 5.5)**.

Elongation and shift in the prechordal plate **(Figure 5.2C-C')**, expansion in the neural plate **(Figure 5.2C-C''')** and shortening and expansion in the notochord **(Figure 5.2C'')** were not altered in *def6a*$^{qmc811/qmc811}$ mutants injected with 200pg *gfp-racl* mRNA. The mean angle (θ) was 72, 85.8 and 90.2 for WT, *def6a*$^{qmc811/qmc811}$ mutants and *def6a*$^{qmc811/qmc811}$ mutants injected with *gfp-racl* mRNA, respectively **(Figure 5.2D-E)**. One-way-ANOVA and two-tailed student's t-test statistical analyses confirmed the significant ($p<0.0001$ (****)) increase in the angle (θ) in both injected and un-injected *def6a*$^{qmc811/qmc811}$ mutants relative to WT controls **(Figure 5.2D)**. A slight difference (*) of the mean angle (θ) was detected between un-injected *def6a*$^{qmc811/qmc811}$ mutants **(Figure 5.2B-D)** and *def6a*$^{qmc811/qmc811}$ mutants injected with *gfp-racl* mRNA **(Figure 5.2C-D)**. However, no significant (N.S) difference of the mean ratio (α/β) was detected between un-injected *def6a*$^{qmc811/qmc811}$ mutants **(Figure 5.2B'-E)** and *def6a*$^{qmc811/qmc811}$ mutants injected with *gfp-racl* mRNA **(Figure 5.2C'-E)** indicating lack of rescue.

Injection of 200pg *gfp-rhoA* mRNA did also not rescue the CE cell movement defects in *def6a*$^{qmc811/qmc811}$ mutants since elongation and shift in the prechordal plate **(Figure 5.3C-C')**, expansion in the neural plate **(Figure 5.3C-C''')** and shortening and expansion of the notochord **(Figure 5.3C'')** were not altered. No significant (N.S) difference of the mean angle (θ) and the mean ratio (α/β) was detected between the un-injected *def6a*$^{qmc811/qmc811}$ mutants and *def6a*$^{qmc811/qmc811}$ mutants injected with *gfp-rhoA* mRNA **(Figure 5.3B-E)**.

Similarly, injection of 200pg *gfp* mRNA did not result in any rescue of the CE cell movement defect observed in *def6a*$^{qmc811/qmc811}$ mutants **(Figure 5.4)**. No significant (N.S) difference of the mean angle (θ) and the mean ratio (α/β) was detected between the un-injected *def6a*$^{qmc811/qmc811}$ mutants **(Figure 5.4B-D-E)** and *def6a*$^{qmc811/qmc811}$ mutants injected with *gfp* mRNA **(Figure 5.4C-E)**.

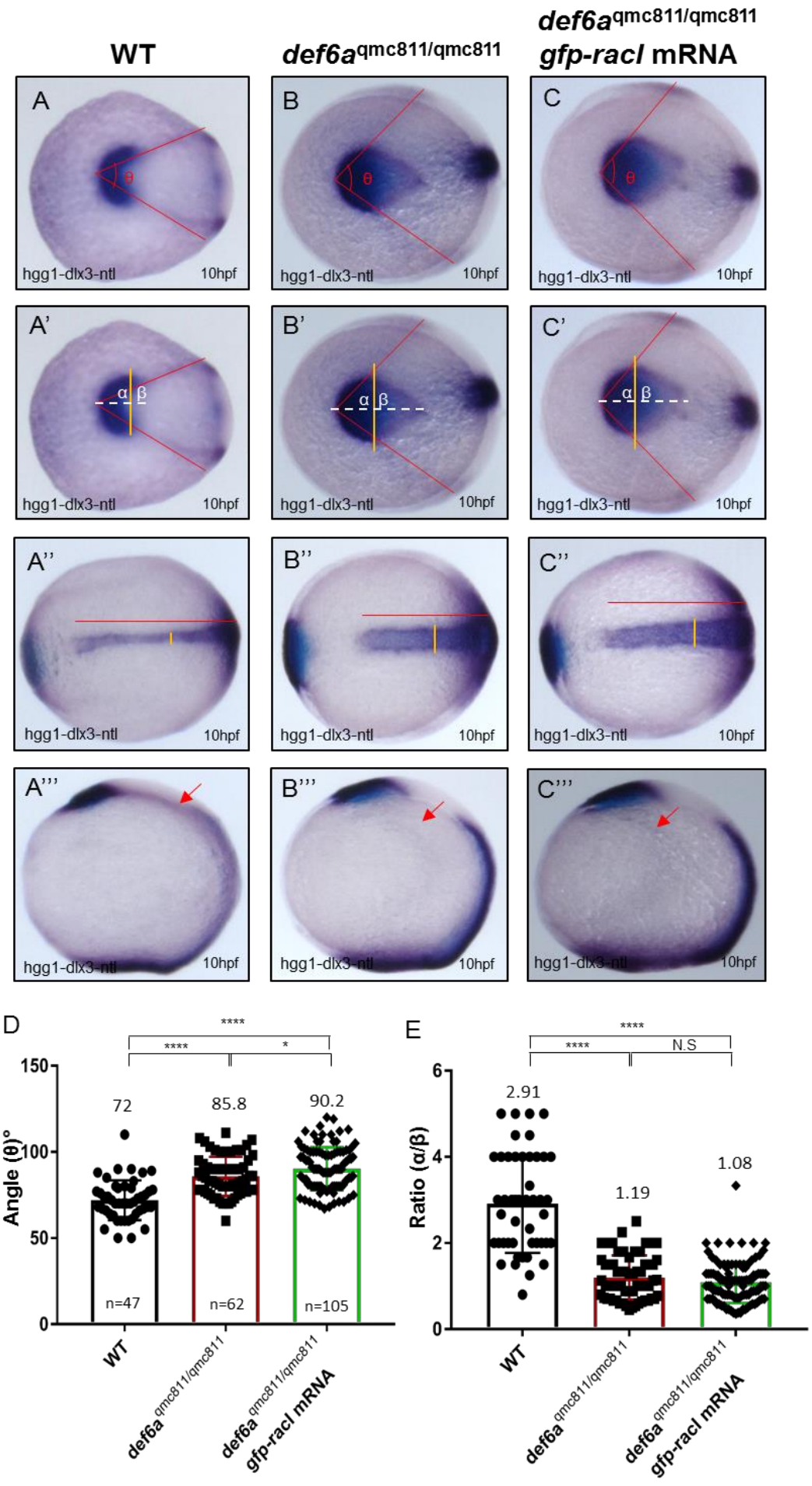
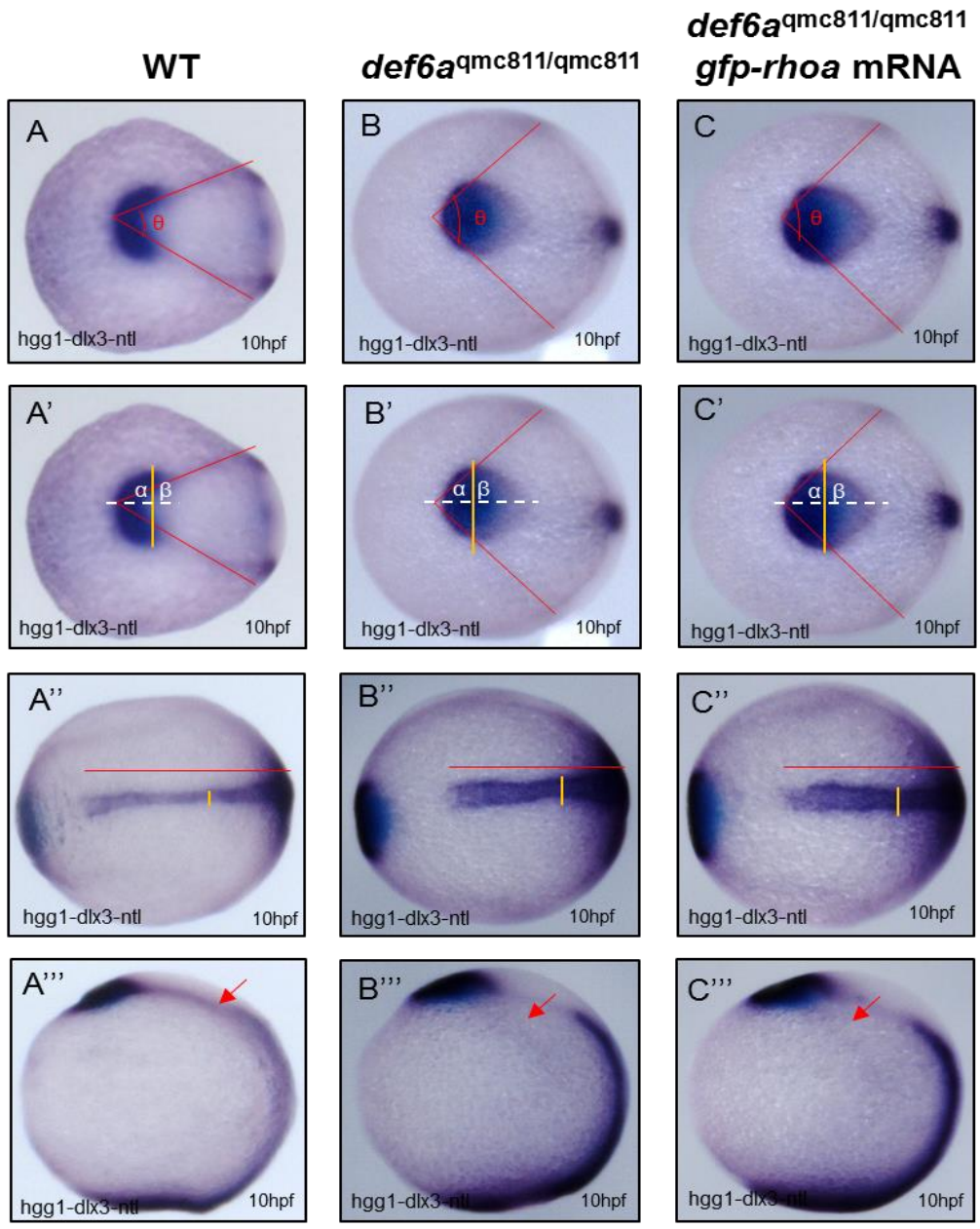

WT
def6a qmc811/qmc811
def6a qmc811/qmc811
gfp-racl mRNA
A
B
C
A'
B'
C'
A''
B''
C''
A'''
B'''
C'''
θ
α
β
hgg1-dlx3-ntl
10hpf
D
Angle (θ)°
150
100
50
0
72
85.8
90.2
n=47
n=62
n=105
****
****
*
WT
def6a qmc811/qmc811
def6a qmc811/qmc811
gfp-racl mRNA
E
Ratio (α/β)
6
4
2
0
2.91
1.19
1.08
****
****
N.S
WT
def6a qmc811/qmc811
def6a qmc811/qmc811
gfp-racl mRNA

Figure 5.2 Injection of *gfp-racl* mRNA did not rescue the CE cell movement defects in *def6a*$^{qmc811/qmc811}$ mutants. Representative embryos from each category are illustrated. WT (left column), un-injected *def6a*$^{qmc811/qmc811}$ (middle column), *def6a*$^{qmc811/qmc811}$ mutants injected with *gfp-racl* mRNA (right column) were fixed at the tail-bud stage and WISH was carried out using *hgg1, dlx3* and *ntl* probes. **(A-B-C;** dorsal view, anterior left**)** The neural plate marked by *dlx3* (red line) was expanded in *def6a*$^{qmc811/qmc811}$ mutants **(B-B'')** and *def6a*$^{qmc811/qmc811}$ mutants injected with *gfp-racl* mRNA **(C-C'')**, compared to WT controls **(A-A'')**. The notochord marked by *ntl* was expanded and shortened in *def6a*$^{qmc811/qmc811}$ mutants **(B'')** and *def6a*$^{qmc811/qmc811}$ mutants injected with *gfp-racl* mRNA **(C'')**, compared to WT controls **(A'')**. The angle (θ) between the neural plate borders was calculated and (**D**) one-way ANOVA and two-tailed t-test analyses confirmed the significant (p<0.0001;****) increase in the angle between WT and un-injected and injected *def6a*$^{qmc811/qmc811}$ mutants **(A-B-C;** dorsal view, anterior left**)**. The connection of neural plate and prechordal plate was bordered (yellow line) and the ratio of the top (α) to the bottom (β) parts of the prechordal plate was measured. The ratio (α/β) was confirmed to be decreased in *def6a*$^{qmc811/qmc811}$ mutants **(B')** and *def6a*$^{qmc811/qmc811}$ mutants injected with *gfp-racl* mRNA **(C')**, compared to WT controls **(A')**. **(E)** One-way ANOVA and two-tailed t-test analyses confirmed the significant (p<0.0001;****) decrease in the ratio in un-injected *def6a*$^{qmc811/qmc811}$ mutants and *def6a*$^{qmc811/qmc811}$ mutants injected with *gfp-racl* mRNA, compared to WT. N.S indicates no significant)difference between un-injected *def6a*$^{qmc811/qmc811}$ mutants and *def6a*$^{qmc811/qmc811}$ mutants injected with *gfp-racl* mRNA (p=0.0231; ratio, (p=0.1556 (*); angle). The scatter plots indicate the mean with standart deviation (SD). The graphs list the mean angle (θ) and mean ratio (α/β) for WT, un-injected *def6a*$^{qmc811/qmc811}$ mutants and *def6a*$^{qmc811/qmc811}$ mutants injected with *gfp-racl* mRNA. The number (n) of tested embryos is also indicated.


WT
def6a qmc811/qmc811
def6a qmc811/qmc811
gfp-rhoa mRNA
A
B
C
θ
hgg1-dlx3-ntl
10hpf
A'
B'
C'
α
β
A''
B''
C''
A'''
B'''
C'''

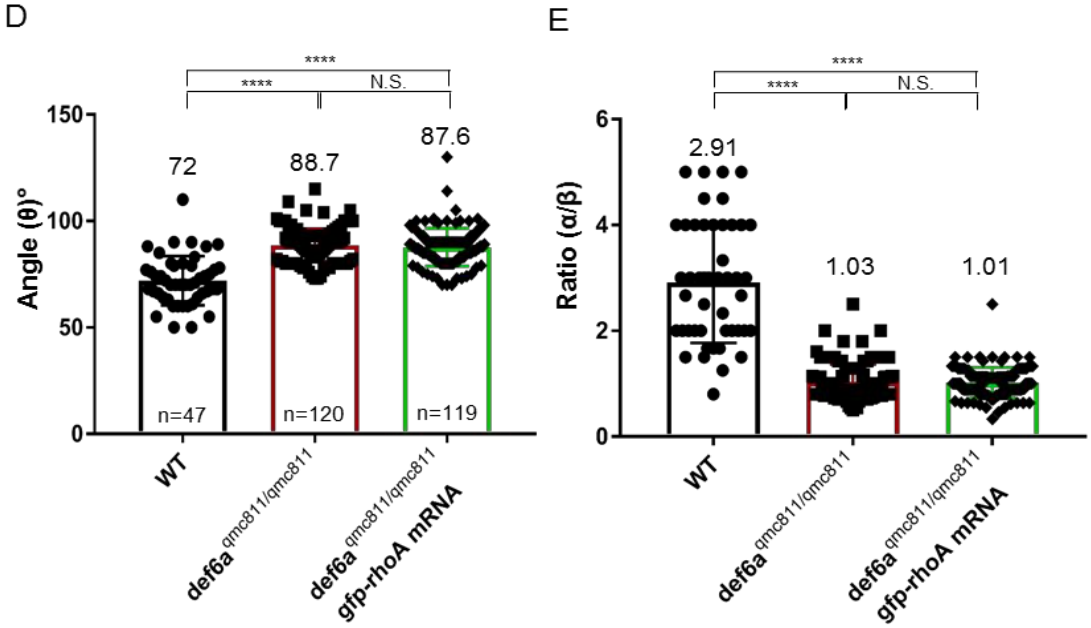

D
E
****
N.S.
Angle (θ)°
Ratio (α/β)
72
88.7
87.6
2.91
1.03
1.01
n=47
n=120
n=119
WT
def6a qmc811/qmc811
def6a qmc811/qmc811
gfp-rhoA mRNA

Figure 5.3 Injection of *gfp-rhoA* mRNA did not rescue the CE cell movement defects in *def6a*$^{qmc811/qmc811}$ mutants. Representative embryos from each category are illustrated. WT (left column), un-injected *def6a*$^{qmc811/qmc811}$ (middle column), *def6a*$^{qmc811/qmc811}$ mutants injected with *gfp-rhoA* mRNA (right column) were fixed at the tail-bud stage and WISH was carried out using *hgg1, dlx3* and *ntl* probes. **(A-B-C;** dorsal view, anterior left**)** The neural plate marked by *dlx3* (red line) was expanded in *def6a*$^{qmc811/qmc811}$ mutants **(B-B'')** and *def6a*$^{qmc811/qmc811}$ mutants injected with *gfp-rhoA* mRNA **(C-C'')**, compared to WT controls **(A-A'')**. The notochord marked by *ntl* was expanded and shortened in *def6a*$^{qmc811/qmc811}$ mutants **(B'')** and *def6a*$^{qmc811/qmc811}$ mutants injected with *gfp-rhoA* mRNA **(C'')**, compared to WT controls **(A'')**. The angle (θ) between the neural plate borders was calculated and (**D**) one-way ANOVA and two-tailed t-test analyses confirmed the significant ($p<0.0001$;****) increase in the angle between WT and un-injected and injected *def6a*$^{qmc811/qmc811}$ mutants **(A-B-C;** dorsal view, anterior left**)**. The connection of neural plate and prechordal plate was bordered (yellow line) and the ratio of the top (α) to the bottom (β) parts of the prechordal plate was measured. The ratio (α/β) was confirmed to be decreased in *def6a*$^{qmc811/qmc811}$ mutants **(B')** and *def6a*$^{qmc811/qmc811}$ mutants injected with *gfp-rhoA* mRNA **(C')**, compared to WT controls **(A')**. **(E)** One-way ANOVA and two-tailed t-test analyses confirmed the significant ($p<0.0001$;****) decrease in the ratio in un-injected *def6a*$^{qmc811/qmc811}$ mutants and *def6a*$^{qmc811/qmc811}$ mutants injected with *gfp-rhoA* mRNA, compared to WT. N.S indicates no significant ($p>0.05$) difference between un-injected *def6a*$^{qmc811/qmc811}$ mutants and *def6a*$^{qmc811/qmc811}$ mutants injected with *gfp-rhoA* mRNA ($p=0.3389$; angle, $p=0.6698$; ratio). The scatter plots indicate the mean with standard deviatiation (SD). The graphs list the mean angle (θ) and the mean ratio (α/β) for WT, un-injected and *def6a*$^{qmc811/qmc811}$ mutants injected with *gfp-rhoA* mRNA, as well as the number (n) of tested embryos.

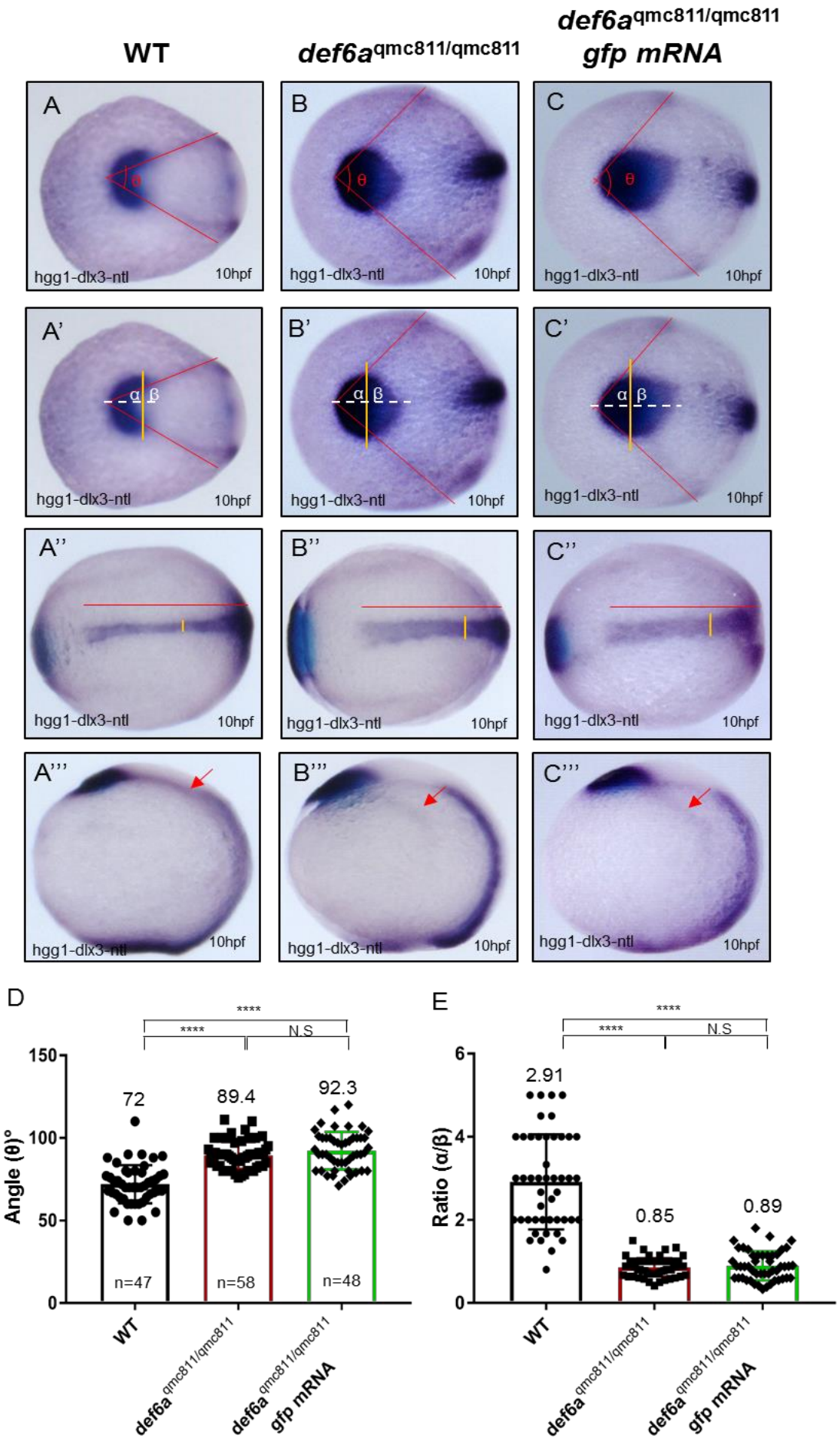

WT
def6a qmc811/qmc811
def6a qmc811/qmc811
gfp mRNA
A
B
C
A'
B'
C'
A''
B''
C''
A'''
B'''
C'''
θ
α
β
hgg1-dlx3-ntl
10hpf
D
E
****
N.S
Angle (θ)°
Ratio (α/β)
72
89.4
92.3
2.91
0.85
0.89
n=47
n=58
n=48
WT
def6a qmc811/qmc811
def6a qmc811/qmc811 gfp mRNA

Figure 5.4 Injection of *gfp* mRNA did not rescue the CE cell movement defects in *def6a*$^{qmc811/qmc811}$ mutants. Representative embryos from each category are depicted. WT (left column), un-injected *def6a*$^{qmc811/qmc811}$ (middle column), *def6a*$^{qmc811/qmc811}$ mutants injected with *gfp* mRNA (right column) were fixed at the tail-bud stage and WISH was completed using *hgg1, dlx3* and *ntl* probes. **(A-B-C;** dorsal view, anterior left**)** The neural plate marked by *dlx3* (red line) was expanded in *def6a*$^{qmc811/qmc811}$ mutants **(B-B'''')** and *def6a*$^{qmc811/qmc811}$ mutants injected with *gfp* mRNA **(C-C'''')**, compared to WT controls **(A-A'''')**. The notochord marked by *ntl* was expanded and shortened in *def6a*$^{qmc811/qmc811}$ mutants **(B'')** and *def6a*$^{qmc811/qmc811}$ mutants injected with *gfp* mRNA **(C'')**, compared to WT controls **(A'')**. The angle (θ) between the neural plate borders was calculated and (**D**) one-way ANOVA and two-tailed t-test analyses confirmed the significant ($p<0.0001$;****) increase in the angle between WT and the un-injected and injected *def6a*$^{qmc811/qmc811}$ mutants **(A-B-C;** dorsal view, anterior left**)**. The connection of the neural plate and prechordal plate was bordered (yellow line) and the ratio of the top (α) to the bottom (β) parts of the prechordal plate was measured. The ratio (α/β) was found to have decreased in *def6a*$^{qmc811/qmc811}$ mutants **(B')** and *def6a*$^{qmc811/qmc811}$ mutants injected with *gfp* mRNA **(C')**, compared to WT controls **(A')**. **(E)** One-way ANOVA and two-tailed student's t-test analyses confirmed the significant ($p<0.0001$;****) decrease in the ratio in un-injected *def6a*$^{qmc811/qmc811}$ mutants and *def6a*$^{qmc811/qmc811}$ mutants injected with *gfp* mRNA, compared to WT. N.S indicates no significant difference between un-injected *def6a*$^{qmc811/qmc811}$ mutants and *def6a*$^{qmc811/qmc811}$ mutants injected with *gfp* mRNA ($p=0.1320$; angle, $p=0.5357$; ratio). The scatter plots indicate the mean with standard deviation (SD). The graphs present the mean angle (θ) and mean ratio (α/β) for WT, un-injected *def6a*$^{qmc811/qmc811}$ mutants and *def6a*$^{qmc811/qmc811}$ mutants injected with *gfp* mRNA, and the number (n) of tested embryos is also indicated.

The quantitative analyses of the mean angle and ratio are summarised in **Figure 5.5** to illustrate that overexpression of Gfp-Cdc42 specifically rescued the CE cell movement defects in *def6a*$^{qmc811/qmc811}$ mutants.

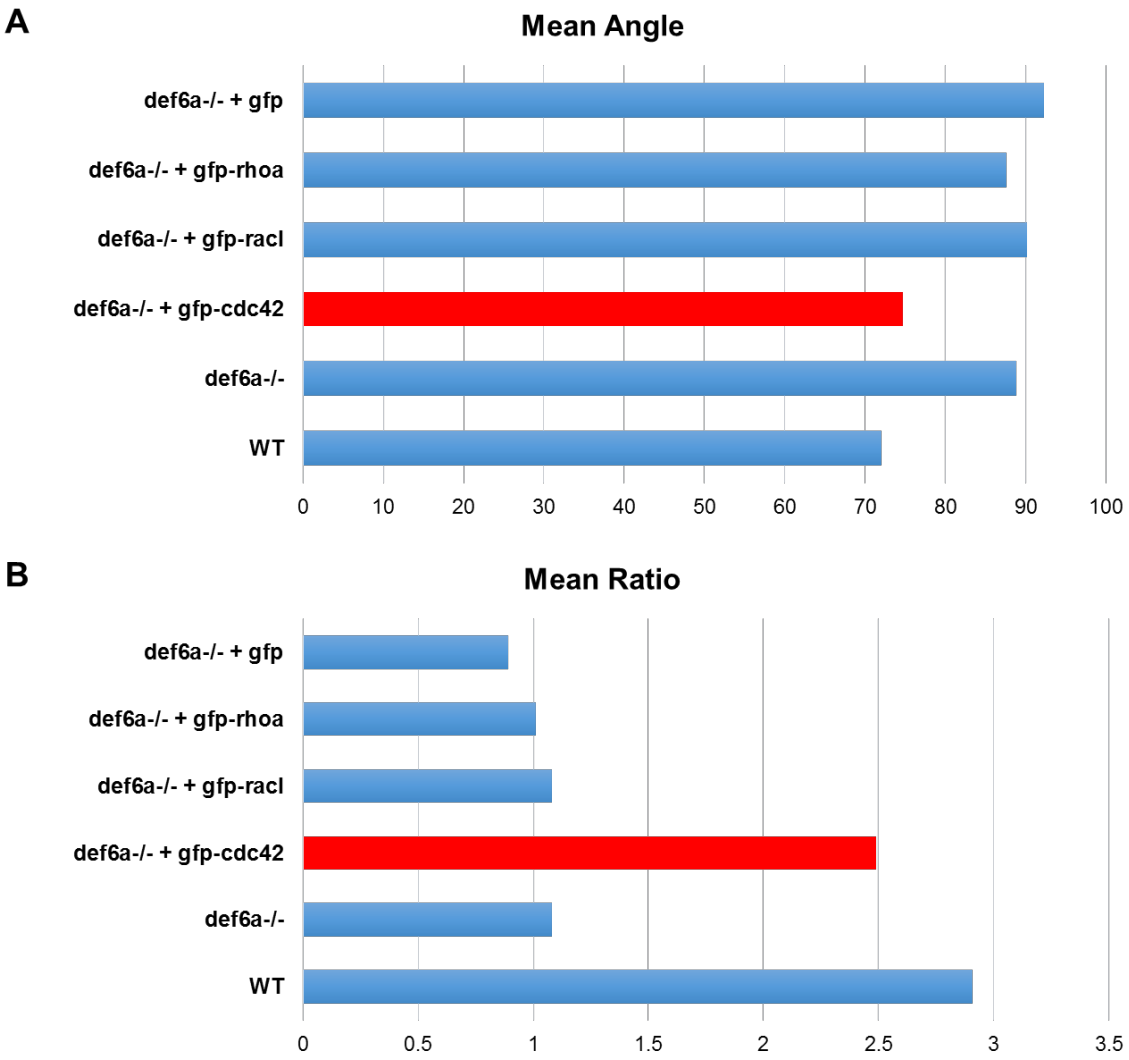


Figure 5.5 Summary of the quantitative analysis indicating robust rescue of the CE cell movement defects by overexpression of Gfp-Cdc42 in *def6a*$^{qmc811/qmc811}$ mutants. (A) The mean angle between the neural borders and **(B)** the mean ratio of the prechordal plate are illustrated for WT, un-injected *def6a*$^{qmc811/qmc811}$ (*def6a*$^{-/-}$) and *def6a*$^{qmc811/qmc811}$ (*def6a*$^{-/-}$) mutants injected with *gfp-cdc42* (indicated with red bar), *gfp-racl*, *gfp-rhoA* and *gfp* mRNAs.

5.1.3. Overexpression of either Cdc42 or Racl rescued CE cell movement defects in *swap70b*$^{qmc809/qmc809}$ mutants

To determine whether *swap70b* is an upstream activator of Rho GTPases, *swap70b*$^{qmc809/qmc809}$ mutants were also injected with 200pg of either *gfp*-tagged *cdc42*, *racl*, *rhoA* mRNA or *gfp* mRNA as control and the mean angle (θ) and the mean ratio (α/β) were calculated as previously described (**Section 5.1.1** and **Figures 5.6-5.9**).

As shown in **Figure 5.6**, overexpression of Gfp-Cdc42 restored the CE cell movement defects in *swap70b*$^{qmc809/qmc809}$ mutants. The mean angle (θ) was 96.9 for *swap70b*$^{qmc809/qmc809}$ mutants but 74.2 for *swap70b*$^{qmc809/qmc809}$ mutants injected with *gfp-cdc42* mRNA similar to WT (72; **Figure 5.6D**). One-way-ANOVA and two-tailed student's t-test statistical analyses confirmed the significant ($p<0.0001$ (****)) increase in the angle between un-injected *swap70b*$^{qmc809/qmc809}$ mutants and WT controls **(Figure 5.6D)**. The mean angle (θ) between WT **(Figure 5.6A-D)** and *swap70b*$^{qmc809/qmc809}$ mutants injected with *gfp-cdc42* mRNA were not significantly (N.S) different **(Figure 5.6C-D).** However**,** a significant ($p<0.0001$ (****)) decrease in the angle was observed in *swap70b*$^{qmc809/qmc809}$ mutants injected with *gfp-cdc42* mRNA **(Figure 5.6C-D)** compared to un-injected *swap70b*$^{qmc809/qmc809}$ mutants **(Figure 5.6B-D)** thereby, indicating a robust rescue of the convergent cell movements of neural plate.

The mean ratio for *swap70b*$^{qmc809/qmc809}$ mutants was 0.85 and for *swap70b*$^{qmc809/qmc809}$ mutants injected with *gfp-cdc42* mRNA, 2.66 that was similar to WT (2.91; **Figure 5.6E**). One-way ANOVA and two-tailed t-test statistical analyses confirmed the significant ($p<0.0001$ (****)) decrease in the ratio between the un-injected *swap70b*$^{qmc809/qmc809}$ mutants and WT controls **(Figure 5.6E)**. No significant (N.S) difference in the mean ratio (α/β) was detected between WT **(Figure 5.6A'-E)** and *swap70b*$^{qmc809/qmc809}$ mutants injected with *gfp-cdc42* mRNA **(Figure 5.6C'-E)**, but a significant ($p<0.0001$ (****)) increase in the mean ratio was observed after *gfp-cdc42* mRNA injection into *swap70b*$^{qmc809/qmc809}$ mutants **(Figure 5.6C'-E)**, compared to un-injected *swap70b*$^{qmc809/qmc809}$ mutants **(Figure 5.6B'-E)** thereby, indicating rescue of the prechordal plate elongation.

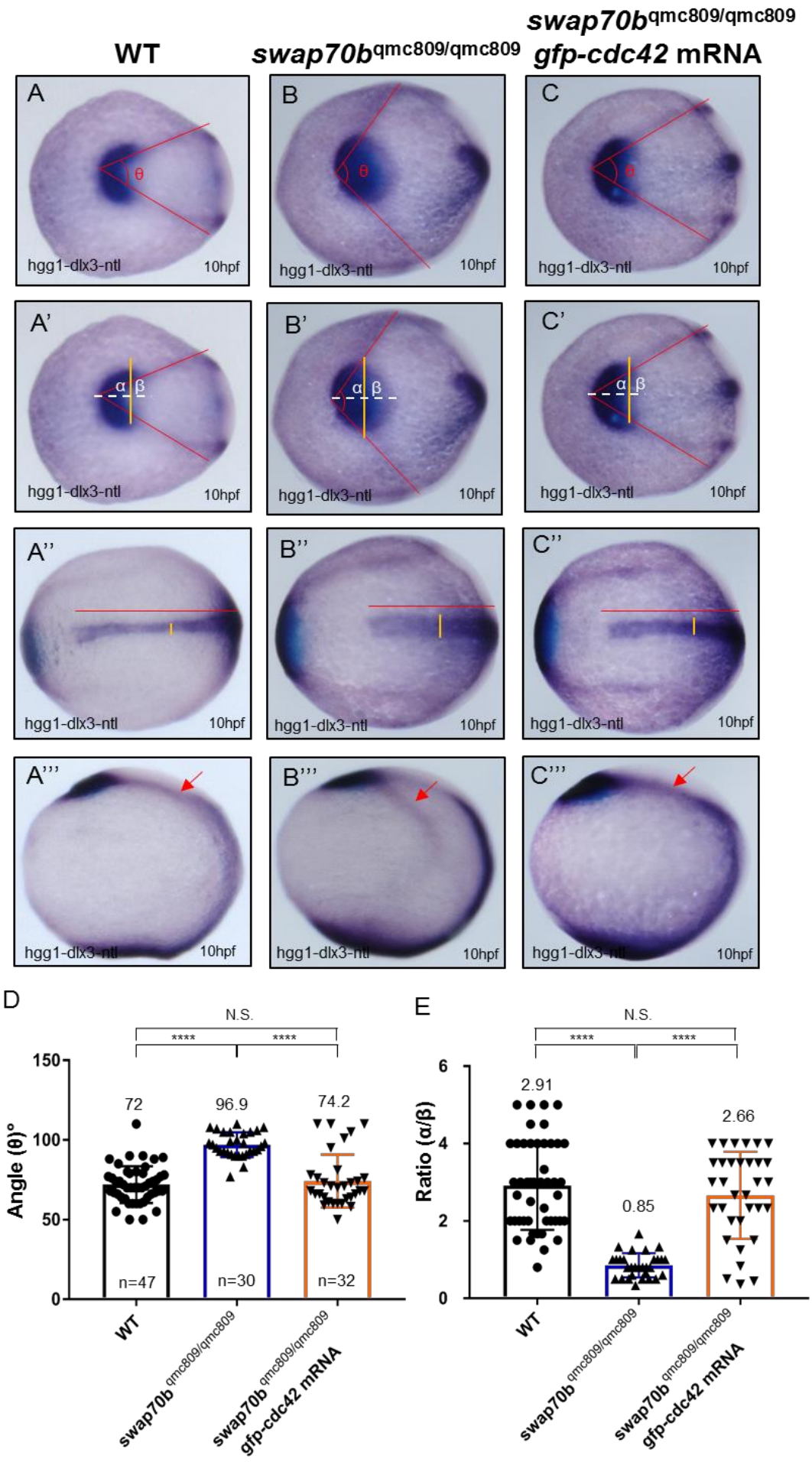

WT
swap70b qmc809/qmc809
swap70b qmc809/qmc809 gfp-cdc42 mRNA
A
B
C
A'
B'
C'
A''
B''
C''
A'''
B'''
C'''
θ
α
β
hgg1-dlx3-ntl
10hpf
D
Angle (θ)°
150
100
50
0
N.S.
****
****
72
96.9
74.2
n=47
n=30
n=32
WT
swap70b qmc809/qmc809
swap70b qmc809/qmc809 gfp-cdc42 mRNA
E
Ratio (α/β)
6
4
2
0
2.91
0.85
2.66

Figure 5.6 Injection of *gfp-cdc42* mRNA robustly rescued the CE cell movement defects in *swap70b*$^{qmc809/qmc809}$ mutants. Representative embryos from each category are illustrated. WT (left column), un-injected *swap70b*$^{qmc809/qmc809}$ (middle column), *swap70b*$^{qmc809/qmc809}$ mutants injected with *gfp-cdc42* mRNA (right column) were fixed at the tail-bud stage and WISH was performed using *hgg1, dlx3* and *ntl* probes. **(A-B-C;** dorsal view, anterior left**)** The neural plate marked by *dlx3* (red line) was expanded in *swap70b*$^{qmc809/qmc809}$ mutants **(B-B'''')** and *swap70b*$^{qmc809/qmc809}$ mutants injected with *gfp-cdc42* mRNA **(C-C'''')**, compared to WT controls **(A-A'''')**. The notochord marked by *ntl* was expanded and shortened in the un-injected *swap70b*$^{qmc809/qmc809}$ mutants **(B'')**, compared to WT controls **(A'')** and *swap70b*$^{qmc809/qmc809}$ mutants injected with *gfp-cdc42* mRNA **(C'')**. The angle (θ) between the neural plate borders was calculated. (**D**) One-way ANOVA and two-tailed t-test analyses confirmed the significant ($p<0.0001$;****) increase in the angle between WT and the un-injected *swap70b*$^{qmc809/qmc809}$ mutants **(A-B;** dorsal view, anterior left**)** and the significant ($p<0.0001$;****) decrease in the angle between un-injected *swap70b*$^{qmc809/qmc809}$ mutants and *swap70b*$^{qmc809/qmc809}$ mutants injected with *gfp-cdc42* mRNA **(B-C;** dorsal view, anterior left). The connection of the neural plate and prechordal plate was bordered (yellow line) and the ratio of the top (α) to the bottom (β) parts of the prechordal plate was measured. The ratio (α/β) was found to be decreased in *swap70b*$^{qmc809/qmc809}$ mutants **(B'),** compared to WT controls **(A')**, while it was robustly restored in *swap70b*$^{qmc809/qmc809}$ mutants injected with *gfp-cdc42* mRNA **(C')**. **(E)** One-way ANOVA and two-tailed t-test analyses confirmed the significant ($p<0.0001$;****) decrease in the ratio between un-injected *swap70b*$^{qmc809/qmc809}$ mutants and WT controls and also the significant ($p<0.0001$;****) increase in the ratio between un-injected *swap70b*$^{qmc809/qmc809}$ mutants and *swap70b*$^{qmc809/qmc809}$ mutants injected with *gfp-cdc42* mRNA. N.S indicates no significant ($p>0.05$) difference between WT and *swap70b*$^{qmc809/qmc809}$ mutants injected with *gfp-cdc42* mRNA ($p=0.4862$; angle, $p=0.3305$; ratio). The mean with standard deviation is illustrated by the scatter plots. The graphs list the mean angle (θ) and mean ratio (α/β) for WT, un-injected *swap70b*$^{qmc809/qmc809}$ mutants and *swap70b*$^{qmc809/qmc809}$ mutants injected with *gfp-cdc42* mRNA, and the number (n) of tested embryos is also indicated.

Like *gfp-cdc42*, 200pg *gfp-racI* mRNA injection could also rescue the CE cell movement defects in *swap70b*$^{qmc809\text{-}qmc809}$ mutants **(Figure 5.7)** as elongation in the prechordal plate **(Figure 5.7C-C'-D)**, expansion in the neural plate borders **(Figure 5.7C-C''')** and shortening and expansion of the notochord **(Figure 5.7C'')** were robustly restored in *swap70b*$^{qmc809\text{-}qmc809}$ mutants injected with *gfp-racI* mRNA.

The mean angle (θ) was 81.9 for *swap70b*$^{qmc809/qmc809}$ mutants (slightly lower than in the experimental group described in **Figure 5.6**) but 75.7 for *swap70b*$^{qmc809/qmc809}$ mutants injected with *gfp-racI* mRNA which was similar to WT (72; **Figure 5.7D**). One-way-ANOVA and two-tailed student's t-test statistical analyses confirmed the significant (p=0.0005 (***)) increase in the angle (θ) between un-injected *swap70b*$^{qmc809/qmc809}$ mutants and WT controls **(Figure 5.7D)**. The mean angle (θ) between WT **(Figure 5.7A-D)** and *swap70b*$^{qmc809/qmc809}$ mutants injected with *gfp-racI* mRNA were not significantly (N.S) different **(Figure 5.7C-D)** but a significant (p=0.0086 (**)) decrease in the angle was observed in *swap70b*$^{qmc809/qmc809}$ mutants injected with *gfp-racI* mRNA **(Figure 5.7C-D)** compared to un-injected *swap70b*$^{qmc809/qmc809}$ mutants **(Figure 5.7B-D)**, confirming a rescue of the convergent cell movements of neural plate.

The mean ratio for *swap70b*$^{qmc809/qmc809}$ mutants was 1.67 (again slightly different from the value determined in the experimental group in **Figure 5.6**) and for *swap70b*$^{qmc809/qmc809}$ mutants injected with *gfp-racI* mRNA 2.66 that was similar to WT (2.91; **Figure 5.7E**). One-way ANOVA and two-tailed t-test statistical analyses confirmed the significant (p<0.0001 (****)) decrease in the ratio between un-injected *swap70b*$^{qmc809/qmc809}$ mutants and WT controls **(Figure 5.7E)**. No significant (N.S) difference in the mean ratio (α/β) was detected between WT **(Figure 5.7A'-E)** and *swap70b*$^{qmc809/qmc809}$ mutants injected with *gfp-racI* mRNA **(Figure 5.7C'-E)**. However, a significant (p=0.0012 (**)) increase in the mean ratio (α/β) was observed after *gfp-racI* mRNA injection into *swap70b*$^{qmc809/qmc809}$ mutants **(Figure 5.7C'-E)** relative to un-injected *swap70b*$^{qmc809/qmc809}$ mutants **(Figure 5.7B'-E)**, indicating notable rescue of the prechordal plate elongation.

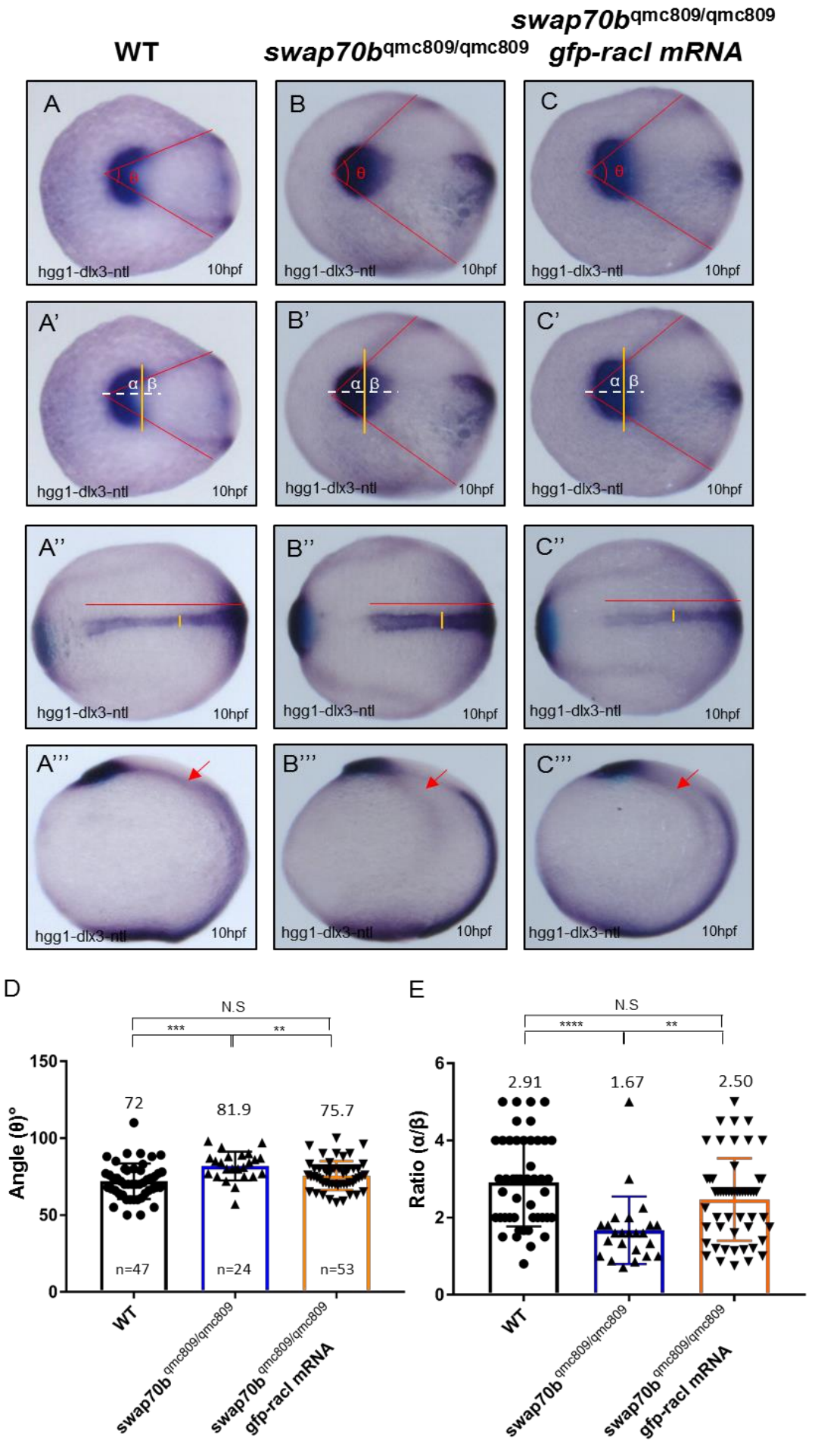

WT
swap70b qmc809/qmc809
swap70b qmc809/qmc809 gfp-racI mRNA
A
B
C
A'
B'
C'
A''
B''
C''
A'''
B'''
C'''
θ
α
β
hgg1-dlx3-ntl
10hpf
D
N.S
***
**
Angle (θ)°
150
100
50
0
72
81.9
75.7
n=47
n=24
n=53
WT
swap70b qmc809/qmc809
swap70b qmc809/qmc809 gfp-racI mRNA
E
N.S
****
**
Ratio (α/β)
6
4
2
0
2.91
1.67
2.50
WT
swap70b qmc809/qmc809
swap70b qmc809/qmc809 gfp-racI mRNA

Figure 5.7 Injection of *gfp-racI* mRNA robustly rescued the CE cell movement defects in *swap70b*$^{qmc809/qmc809}$ mutants. Representative embryos from each category are illustrated. WT (left column), un-injected *swap70b*$^{qmc809/qmc809}$ (middle column), *swap70b*$^{qmc809/qmc809}$ mutants injected with *gfp-racI* mRNA (right column) were fixed at the tail-bud stage and WISH was carried out using *hgg1, dlx3* and *ntl* probes. **(A-B-C;** dorsal view, anterior left**)** The neural plate marked by *dlx3* (red line) was expanded in *swap70b*$^{qmc809/qmc809}$ mutants **(B-B'')**, compared to WT controls **(A-A'')** and *swap70b*$^{qmc809/qmc809}$ mutants injected with *gfp-racI* mRNA **(C-C'')**. The notochord marked by *ntl* showed a greater degree of expansion and shortening in the un-injected *swap70b*$^{qmc809/qmc809}$ mutants **(B'')**, than WT controls **(A'')** and *swap70b*$^{qmc809/qmc809}$ mutants injected with *gfp-racI* mRNA **(C'')**. The angle (θ) between the neural plate borders was calculated and (**D**) one-way ANOVA and two-tailed t-test analyses confirmed the significant ($p<0.001$;***) increase in the angle between WT and un-injected *swap70b*$^{qmc809/qmc809}$ mutants **(A-B;** dorsal view, anterior left**)** and the notable ($p<0.01$;**) decrease in the angle between un-injected *swap70b*$^{qmc809/qmc809}$ mutants and *swap70b*$^{qmc809/qmc809}$ mutants injected with *gfp-racI* mRNA **(B-C;** dorsal view, anterior left). The connection of neural plate and prechordal plate was bordered (yellow line) and the ratio of the top (α) to the bottom (β) parts of the prechordal plate was measured. The ratio (α/β) was determined as decreased in *swap70b*$^{qmc809/qmc809}$ mutants **(B'),** compared to WT controls **(A')**, while it was robustly restored in *swap70b*$^{qmc809/qmc809}$ mutants injected with *gfp-racI* mRNA **(C')**. **(E)** One-way ANOVA and two-tailed t-test analyses confirmed the significant ($p<0.0001$;****) decrease in the ratio between un-injected *swap70b*$^{qmc809/qmc809}$ mutants and WT controls and also the notable ($p<0.01$;**) increase in the ratio between un-injected *swap70b*$^{qmc809/qmc809}$ mutants and *swap70b*$^{qmc809/qmc809}$ mutants injected with *gfp-racI* mRNA. N.S indicates no significant ($p>0.05$) difference in the angle of neural plate between WT and *swap70b*$^{qmc809/qmc809}$ mutants injected with *gfp-racI* mRNA ($p=0.0793$; angle, $p=0.0623$; ratio), The scatter plots indicate the mean with standard deviation (SD). The graphs list the mean angle (θ) and mean ratio (α/β) for WT, un-injected *swap70b*$^{qmc809/qmc809}$ mutants and *swap70b*$^{qmc809/qmc809}$ mutants injected with *gfp-racI* mRNA, and the number (n) of tested embryos.

5.1.4. Overexpression of either RhoA or Gfp in *swap70b*$^{qmc809/qmc809}$ mutants did not restore CE cell movement defects

To test whether *swap70b* is not only acting upstream of Cdc42 and Racl as previously demonstrated (**Section 5.1.3**), Gfp-tagged RhoA or Gfp alone were overexpressed in *swap70b*$^{qmc809/qmc809}$ mutants (**Figures 5.8-5.9 A-C'''**). Quantitative analysis of the mean angle (θ) and mean ratio (α/β) as previously described (**Section 5.1.1**) revealed that neither RhoA nor Gfp overexpression resulted in a significant change of the CE cell movement defects observed in *swap70b*$^{qmc809/qmc809}$ mutants **(Figures 5.8-5.9 D-E; 5.10).**

Elongation and shift in the prechordal plate **(Figure 5.8C-C')**, expansion in the neural plate **(Figure 5.8C-C''')** and shortening and expansion in the notochord **(Figure 5.8C'')** were not altered in *swap70b*$^{qmc809/qmc809}$ mutants injected with 200pg *gfp-rhoA* mRNA. The mean angle (θ) was 95.1 for *swap70b*$^{qmc809/qmc809}$ mutants and 95.7 for *swap70b*$^{qmc809/qmc809}$ mutants injected with *gfp-rhoA* mRNA, relative to WT (72; **Figure 5.8D**). One-way-ANOVA and two-tailed t-test statistical analyses confirmed the significant ($p<0.0001$ (****)) increase in the mean angle (θ) in both un-injected *swap70b*$^{qmc809/qmc809}$ mutants and *swap70b*$^{qmc809/qmc809}$ mutants injected with *gfp-rhoA* mRNA **(Figure 5.8D)**, compared to WT controls. No significant (N.S) difference of the mean angle (θ) was detected between un-injected *swap70b*$^{qmc809/qmc809}$ mutants **(Figure 5.8B-D)** and *swap70b*$^{qmc809/qmc809}$ mutants injected with *gfp-rhoA* mRNA **(Figure 5.8C-D)**.

The mean ratio (α/β) was 2.91, 1.10 and 0.87 for WT, *swap70b*$^{qmc809/qmc809}$ mutants and *swap70b*$^{qmc809/qmc809}$ mutants injected with *gfp-rhoA* mRNA, respectively (**Figure 5.8F**). One-way ANOVA and two-tailed t-test statistical analyses confirmed the significant ($p<0.0001$ (****)) decrease in the mean ratio (α/β) in both un-injected and injected *swap70b*$^{qmc811/qmc811}$ mutants compared to WT controls **(Figure 5.8E)**. No significant (N.S) difference of the mean ratio (α/β) was detected between un-injected *swap70b*$^{qmc809/qmc809}$ mutants **(Figure 5.8B'-E)** and *swap70b*$^{qmc809/qmc809}$ mutants injected with *gfp-rhoA* mRNA **(Figure 5.8C'-E)**

Similarly, injection of 200pg *gfp* mRNA did not result in any rescue of the CE cell movement defect observed in *swap70b*$^{qmc809/qmc809}$ mutants (**Figure 5.9**). The mean angle (θ) was 92.6 for *swap70b*$^{qmc809/qmc809}$ mutants and 88.05 for *swap70b*$^{qmc809/qmc809}$ mutants injected with *gfp* mRNA (**Figure 5.9D**). Even though the two-tailed student's t-test analysis revealed a slight difference ($p=0.0478$ (*)) between un-injected *swap70b*$^{qmc809/qmc809}$ mutants **(Figure 5.9B-D)** and *swap70b*$^{qmc809/qmc809}$ mutants injected with *gfp* mRNA **(Figure 5.9C-D)**, a significant ($p<0.0001$ (****)) increase in the mean angle (θ) in both un-injected and injected *swap70b*$^{qmc809/qmc809}$ mutants **(Figure 5.9D)** compared to WT controls was observed, thus indicating a failure of convergent cell movements.

Furthermore, the mean ratio (α/β) was 1.42 for *swap70b*$^{qmc809/qmc809}$ mutants and 1.18 for *swap70b*$^{qmc809/qmc809}$ mutants injected with *gfp* mRNA (**Figure 5.9E**). One-way ANOVA and two-tailed t-test statistical analyses confirmed the significant ($p<0.0001$ (****)) decrease in the mean ratio (α/β) in both un-injected and injected *swap70b*$^{qmc809/qmc809}$ mutants **(Figure 5.9E)**, compared to WT controls. No significant (N.S) difference of the mean ratio (α/β) was detected between the un-injected *swap70b*$^{qmc809/qmc809}$ mutants **(Figure 5.9B'-E)** and *swap70b*$^{qmc809/qmc809}$ mutants injected with *gfp* mRNA **(Figure 5.9C'-E)**.

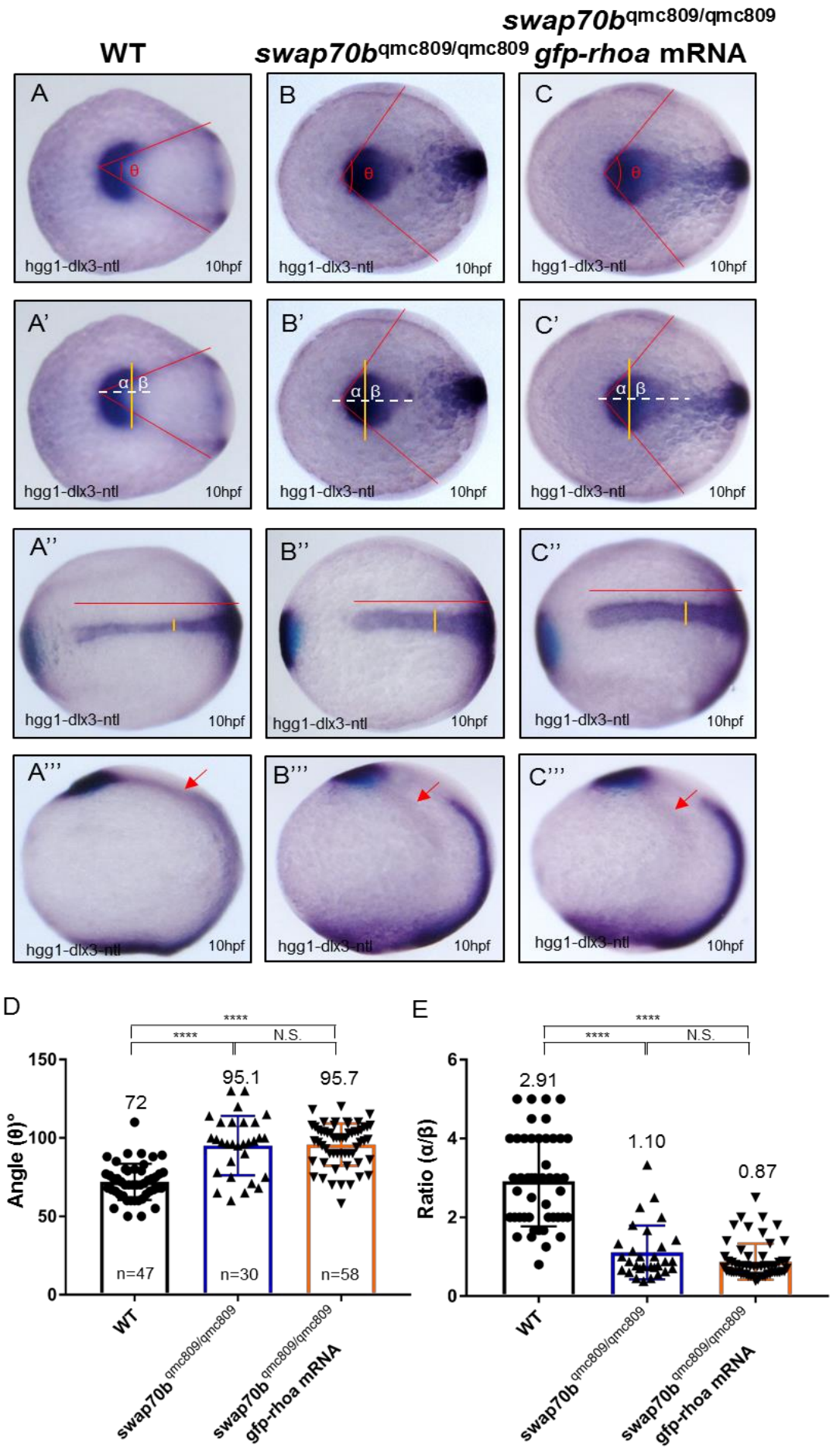

WT
swap70b qmc809/qmc809
swap70b qmc809/qmc809 gfp-rhoa mRNA
A
B
C
A'
B'
C'
A''
B''
C''
A'''
B'''
C'''
θ
α β
hgg1-dlx3-ntl
10hpf
D
Angle (θ)°
150
100
50
0
****
N.S.
72
95.1
95.7
n=47
n=30
n=58
WT
swap70b qmc809/qmc809
swap70b qmc809/qmc809 gfp-rhoa mRNA
E
Ratio (α/β)
6
4
2
0
2.91
1.10
0.87

Figure 5.8 Injection of *gfp-rhoA* mRNA did not rescue the CE cell movement defects in *swap70b*$^{qmc809/qmc809}$ mutants. Representative embryos from each category are depicted. WT (left column), un-injected *swap70b*$^{qmc809/qmc809}$ (middle column), *swap70b*$^{qmc809/qmc809}$ mutants injected with *gfp-rhoA* mRNA (right column) were fixed at the tail-bud stage and WISH was carried out using *hgg1, dlx3* and *ntl* probes. **(A-B-C;** dorsal view, anterior left**)** The neural plate marked by *dlx3* (red line) was expanded in *swap70b*$^{qmc809/qmc809}$ mutants **(B-B'''')** and *swap70b*$^{qmc809/qmc809}$ mutants injected with *gfp-rhoA* mRNA **(C-C'''')**, compared to WT controls **(A-A'''')**. The notochord marked by *ntl* was expanded and shortened in *swap70b*$^{qmc809/qmc809}$ mutants **(B'')** and *swap70b*$^{qmc809/qmc809}$ mutants injected with *gfp-rhoA* mRNA **(C'')**, compared to WT controls **(A'')**. The angle (θ) between the neural plate borders was calculated and (**D**) one-way ANOVA and two-tailed student's t-test analyses confirmed the significant ($p<0.0001$; ****) increase in the angle between WT and un-injected *swap70b*$^{qmc809/qmc809}$ mutants and *swap70b*$^{qmc809/qmc809}$ mutants injected with *gfp-rhoA* mRNA. **(A-B-C;** dorsal view, anterior left**)**. The connection of neural plate and prechordal plate was bordered (yellow line) and the ratio of the top (α) to the bottom (β) parts of the prechordal plate was measured. The ratio (α/β) was found to be decreased in *swap70b*$^{qmc809/qmc809}$ mutants **(B')** and *swap70b*$^{qmc809/qmc809}$ mutants injected with *gfp-rhoA* mRNA **(C')**, compared to WT controls **(A')**. **(E)** One-way ANOVA and two-tailed t-test analyses confirmed the significant ($p<0.0001$;****) decrease in the ratio in un-injected *swap70b*$^{qmc809/qmc809}$ mutants and *swap70b*$^{qmc809/qmc809}$ mutants injected with *gfp-rhoA* mRNA, compared to WT. N.S indicates no significant ($p>0.05$) difference between un-injected *swap70b*$^{qmc809/qmc809}$ mutants and *swap70b*$^{qmc809/qmc809}$ mutants injected with *gfp-rhoA* mRNA ($p=0.8619$; angle, $p=0.0579$; ratio). The means with standard deviation (SD) are depicted on the scatter plots. The graphs list the mean angle (θ) and mean ratio (α/β) for WT, un-injected *swap70b*$^{qmc809/qmc809}$ mutants and *swap70b*$^{qmc809/qmc809}$ mutants injected with *gfp-rhoA* mRNA, number (n) of tested embryos is also indicated.

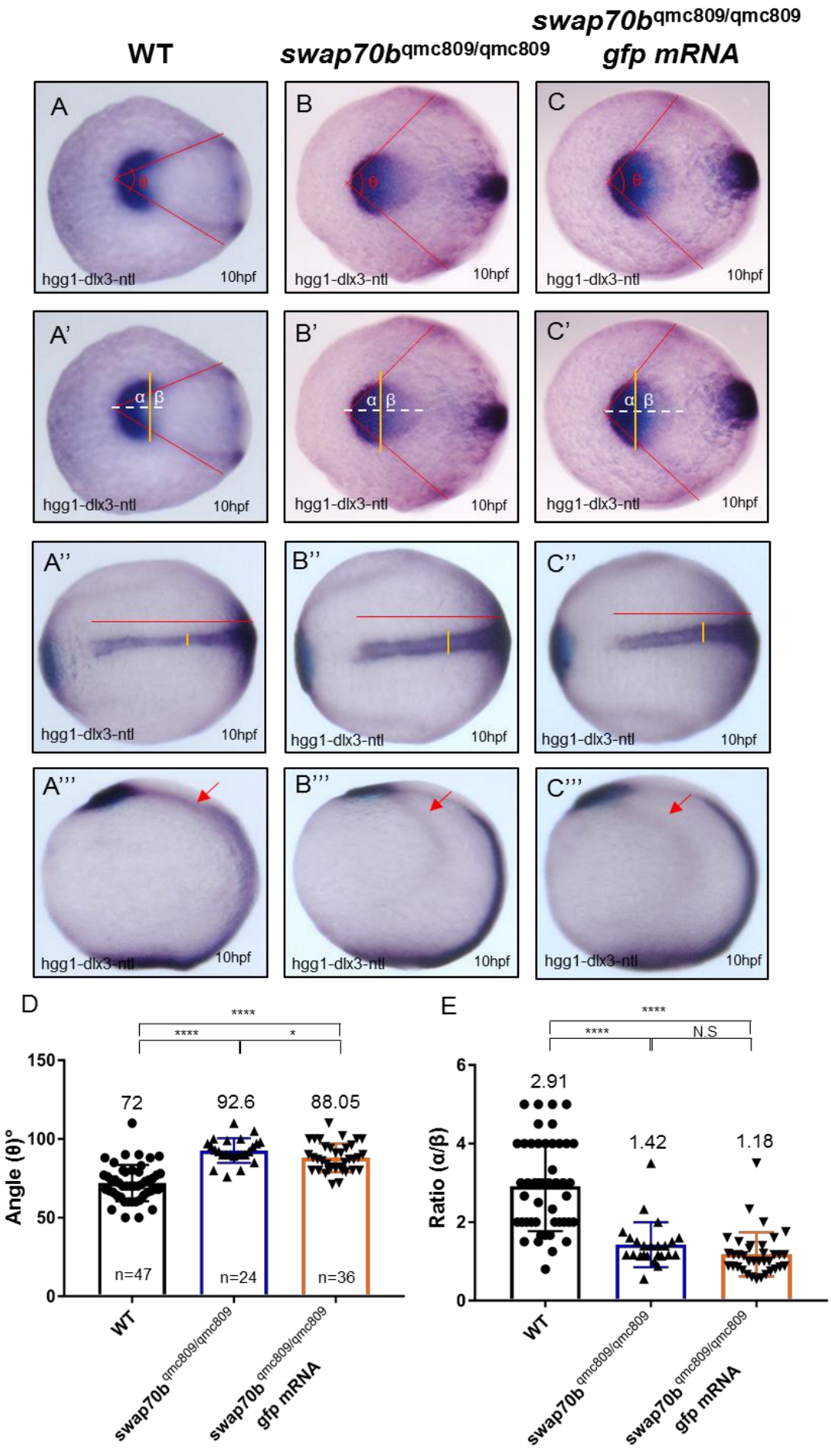

WT
swap70b qmc809/qmc809
swap70b qmc809/qmc809 gfp mRNA
A
B
C
A'
B'
C'
A''
B''
C''
A'''
B'''
C'''
θ
α β
hgg1-dlx3-ntl
10hpf
D
E
Angle (θ)°
Ratio (α/β)
72
92.6
88.05
2.91
1.42
1.18
n=47
n=24
n=36
****
*
N.S
WT
swap70b qmc809/qmc809
swap70b qmc809/qmc809 gfp mRNA

Figure 5.9 Injection of *gfp* mRNA did not rescue the CE cell movement defects in *swap70b*$^{qmc809/qmc809}$ mutants. Representative embryos from each category are illustrated. WT (left column), un-injected *swap70b*$^{qmc809/qmc809}$ (middle column), *swap70b*$^{qmc809/qmc809}$ mutants injected with *gfp* mRNA (right column) were fixed at the tail-bud stage and WISH was carried out using *hgg1, dlx3* and *ntl* probes. **(A-B-C;** dorsal view, anterior left**)** The neural plate marked by *dlx3* (red line) was expanded in *swap70b*$^{qmc809/qmc809}$ mutants **(B-B'''')** and *swap70b*$^{qmc809/qmc809}$ mutants injected with *gfp* mRNA **(C-C'''')**, compared to WT controls **(A-A'''')**. The notochord marked by *ntl* was expanded and shortened in *swap70b*$^{qmc809/qmc809}$ mutants **(B'')** and *swap70b*$^{qmc809/qmc809}$ mutants injected with *gfp* mRNA **(C'')**, compared to WT controls **(A'')**. The angle (θ) between the neural plate borders was calculated. (**D**) One-way ANOVA and two-tailed student's t-test analyses confirmed the significant ($p<0.0001$;****) increase in the angle between WT and un-injected and injected *swap70b*$^{qmc809/qmc809}$ mutants. **(A-B-C;** dorsal view, anterior left**)**. The connection of neural plate and prechordal plate was bordered (yellow line) and the ratio of the top (α) to the bottom (β) parts of the prechordal plate was measured. The ratio (α/β) was confirmed as decreased in *swap70b*$^{qmc809/qmc809}$ mutants **(B')** and *swap70b*$^{qmc809/qmc809}$ mutants injected with *gfp* mRNA **(C')**, compared to WT controls **(A')**. **(E)** One-way ANOVA and two-tailed student's t-test analyses confirmed the significant ($p<0.0001$;****) decrease in the ratio in un-injected *swap70b*$^{qmc809/qmc809}$ mutants and *swap70b*$^{qmc809/qmc809}$ mutants injected with *gfp* mRNA, compared to WT. N.S indicates no significant ($p>0.05$) difference between the un-injected *swap70b*$^{qmc809/qmc809}$ mutants and *swap70b*$^{qmc809/qmc809}$ mutants injected with *gfp* mRNA ($p=0.1054$; ratio). The scatter plots indicate the mean with standard deviation (SD). The graphs present the mean angle (θ) and mean ratio (α/β) for WT, un-injected *swap70b*$^{qmc809/qmc809}$ mutants and *swap70b*$^{qmc809/qmc809}$ mutants injected with *gfp* mRNA. The number (n) of tested embryos is also indicated.

The quantitative analyses of the mean angle and ratio are summarised in **Figure 5.10** to illustrate that overexpression of either Gfp-Cdc42 or Gfp-RacI robustly rescued the CE cell movement defects in *swap70b*$^{qmc809/qmc809}$ mutants.

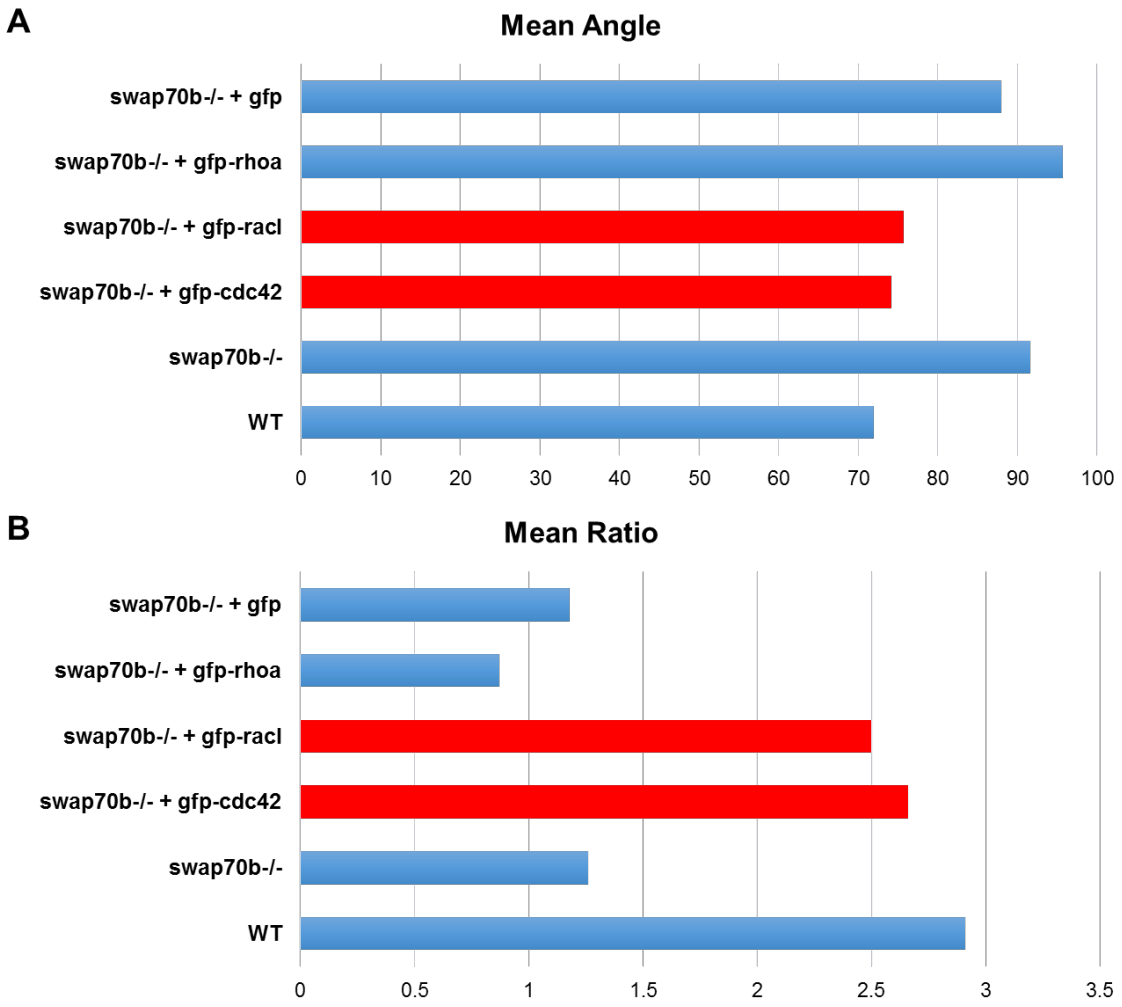


Figure 5.10 Summary of the quantitative analysis demonstrating robust rescue of the CE cell movement defects by overexpression of either Gfp-Cdc42 or Gfp-RacI in *swap70b*$^{qmc809/qmc809}$ mutants. (A) The mean angle between the neural borders and **(B)** the mean ratio of the prechordal plate are illustrated for WT, un-injected *swap70b*$^{qmc809/qmc809}$ (*swap70b*$^{-/-}$) and *swap70b*$^{qmc809/qmc809}$ (*swap70b*$^{-/-}$) mutants injected with *gfp-cdc42* (indicated with red bar), *gfp-racl* (indicated with red bar), *gfp-rhoA* and *gfp* mRNAs.

5.2. *def6a*$^{qmc811/qmc811}$ and *swap70b*$^{qmc809/qmc809}$ mutants displayed fewer cell protrusions and fewer polarised cell shape during gastrulation

To further analyse the loss of function effects of *def6a* and *swap70b* on the morphology of cells, WT, *def6a*$^{qmc811/qmc811}$ mutants and *swap70b*$^{qmc809/qmc809}$ mutants were fixed during gastrulation (shield and tail-bud) and actin staining was performed to visualise filamentous actin (F-actin) and cell shape. Ectodermal cells were selected for the analysis as their morphologies are easier to analyse and to compare than the underlying mesodermal cells. Alexa Fluor 568 Phalloidin was used to stain F-actin and embryos were visualised using confocal microscopy. Three different dorsal positions per embryo were visualised and length and width values were measured using Fiji ImageJ software. The length-width ratio was calculated for each cell and the data was compared using one-way ANOVA and two-tailed student's t-test statistical analyses.

As illustrated in **Figure 5.11**, F-actin was localised to the membrane and cell protrusions in WT, *def6a*$^{qmc811/qmc811}$ and *swap70b*$^{qmc809/qmc809}$ mutants. However, the number of protrusions in the mutants was less than the WT controls at shield stage (**Figure 5.11A-B-C;** white arrows, enlarged in **5.11A'-B'-C'**). Moreover, the cell morphology appeared altered in the mutants. Therefore, the degree of elongation was measured and the length-width ratio was determined in WT, *def6a*$^{qmc811/qmc811}$ and *swap70b*$^{qmc809/qmc809}$ mutants. The dorsal ectodermal cells in *def6a*$^{qmc811/qmc811}$ and *swap70b*$^{qmc809/qmc809}$ mutants were confirmed to be less elongated compared to WT at tail-bud stage (**Figure 5.11A''-B''-C'';** round cells indicated with white arrowheads). A more rounded cell shape was confirmed by one-way ANOVA and two-tailed student's t-test analyses exhibiting the decrease in the length-width ratio of ectodermal cells in *def6a*$^{qmc811/qmc811}$ mutants and *swap70b*$^{qmc809/qmc809}$ mutants at tail-bud stage (**Figure 5.11D**). The mean values of the length-width ratio was determined as 2.65, 1.42 and 1.32 for WT, *def6a*$^{qmc811/qmc811}$ mutants and *swap70b*$^{qmc809/qmc809}$ mutants, respectively. While a significant decrease ($p<0.0001$; ****) was apparent between WT and the mutants, no significant (N.S.; $p=0.1601$) difference was detected between *def6a*$^{qmc811/qmc811}$ and *swap70b*$^{qmc809/qmc809}$ mutants. This result indicates that *def6a* and *swap70b* are required for the elongation of ectodermal cells during gastrulation.

In conclusion, cell protrusions and cell morphology were clearly affected by the loss of *def6a* and *swap70b.* It therefore follows that *def6a* and *swap70b* regulate the CE cell movements of gastrulation through arranging actin dynamics and cell polarity.

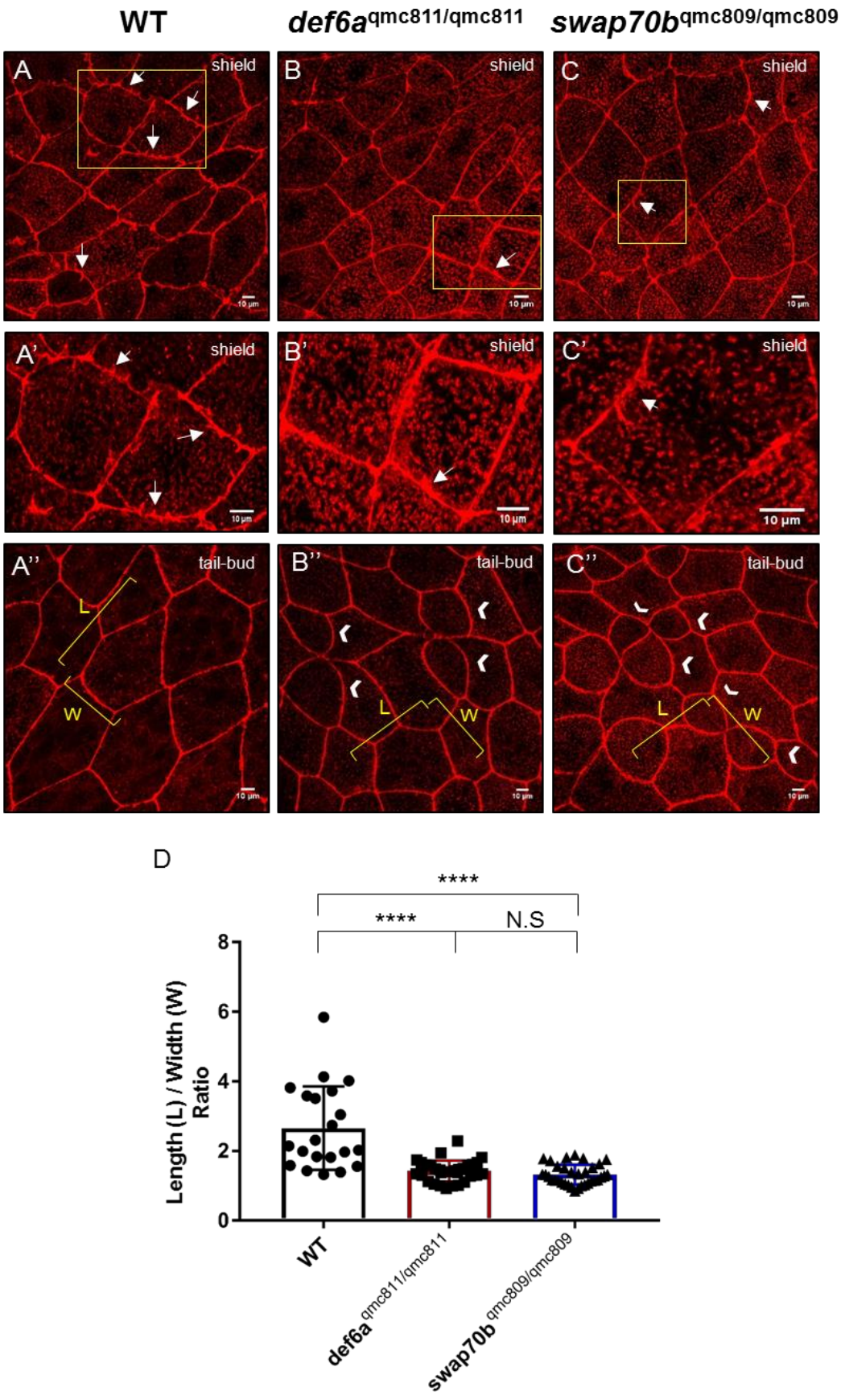

WT
def6a qmc811/qmc811
swap70b qmc809/qmc809
A
shield
B
shield
C
shield
A'
shield
B'
shield
C'
shield
10 µm
A''
tail-bud
B''
tail-bud
C''
tail-bud
L
W
D
****
****
N.S
Length (L) / Width (W) Ratio
0
2
4
6
8
WT
def6a qmc811/qmc811
swap70b qmc809/qmc809

Figure 5.11 *def6a*$^{qmc811/qmc811}$ and *swap70b*$^{qmc809/qmc809}$ mutants displayed fewer cell protrusions and fewer elongation of actin stained dorsal ectodermal cells than the WT controls. WT (left column), *def6a*$^{qmc811/qmc811}$ mutants (middle column) and *swap70b*$^{qmc809/qmc809}$ mutants (right column) were fixed at shield and tail-bud stages and subjected to the actin staining using Alexa Fluor 568 Phalloidin. Less protrusion activity was observed in *def6a*$^{qmc811/qmc811}$ mutants (**B-B'**) and *swap70b*$^{qmc809/qmc809}$ mutants (**C-C'**), compared to WT controls (**A-A'**) during shield stage. White arrows indicate the cell protrusions, yellow rectangles indicate the selected area for enlargements (**A'-B'-C'**). Less polarised ectodermal cells as indicated by white arrowheads were observed in *def6a*$^{qmc811/qmc811}$ mutants and *swap70b*$^{qmc809/qmc809}$ mutants at tail-bud stage (**A''-B''-C''**). **(D)** One-way ANOVA and two-tailed student t-test statistical analyses confirmed the reduced length-width (L/W) ratio of the dorsal ectodermal cells at tail-bud stage (**A''-B''-C''**). The statistical analysis and images were obtained from one embryo per group. Scale bar:10 μm.

5.3. Expression of *wnt5b* and *wnt11* are upregulated in single def6a$^{qmc811/qmc811}$, *swap70b*$^{qmc809/qmc809}$ and double *def6a*$^{qmc811/qmc811}$; *swap70b*$^{qmc809/qmc809}$ homozygous mutants

MO-mediated knock-down of *def6a* and *swap70b* indicated that while Def6a acts downstream of Wnt5b and synergises with Wnt11 in the non-canonical Wnt/PCP signalling pathway (Goudevenou *et al.,* 2011), Swap70b acts downstream of Wnt11 in the non-canonical Wnt/PCP signalling pathway (Xu, PhD thesis, 2015).

To examine whether loss of function of *def6a* and/or *swap70b* affected transcriptional regulation of *wnt5b* and *wnt11,* WT, single *def6a*$^{qmc811/qmc81}$ and *swap70b*$^{qmc809/qmc809}$ and double homozygous *def6a*$^{qmc811/qmc811}$*; swap70b*$^{qmc809/qmc809}$ mutants were fixed at shield stage and subjected to WISH using *wnt5b* or *wnt11* ribo-probes. Expression of *wnt5b* and *wnt11* was detected at the margin region for WT **(Figure 5.1A-A'-E-E')**, *def6a*$^{qmc811/qmc811}$ mutants **(Figure 5.1B-B'-F-F')**, *swap70b*$^{qmc809/qmc809}$ mutants **(Figure 5.1C-C'-G-G')** and double *def6a*$^{qmc811/qmc811}$*; swap70b*$^{qmc809/qmc809}$ mutants **(Figure 5.1D-D'-H-H')** as expected. Strikingly, expression of both, *wnt5b* and *wnt11* was upregulated in single and double mutants compared to WT. However, upregulation of *wnt11* expression was more pronounced in single and double mutant embryos than *wnt5b* expression.

These results suggest that *def6a* and *swap70b* are both acting as negative regulators of *wnt5b* and *wnt11* expression. However, upregulation of *wnt5b* and *wnt11* expression was more pronounced in *swap70b*$^{qmc809/qmc809}$ mutants and *def6a*$^{qmc811/qmc811}$*; swap70b*$^{qmc809/qmc809}$ double mutants compared to *def6a*$^{qmc811/qmc811}$ mutants suggesting a dominant effect of *swap70b* function. Seo *et al*., (2010) have suggested that *wnt11* expression is negatively regulated by JNK in the non-canonical Wnt/PCP signalling pathway during zebrafish gastrulation (Section 1.1.1; Figure 1.4). Therefore it is likely that *def6a* and *swap70b* function is required in the Wnt/PCP/Ca^{2+} signalling pathway upstream of Cdc42 and/or RacI that activate Jnk which negatively regulates *wnt11* (and perhaps *wnt5b*) expression and positively regulates actin cytoskeleton arrangements and cell shape.

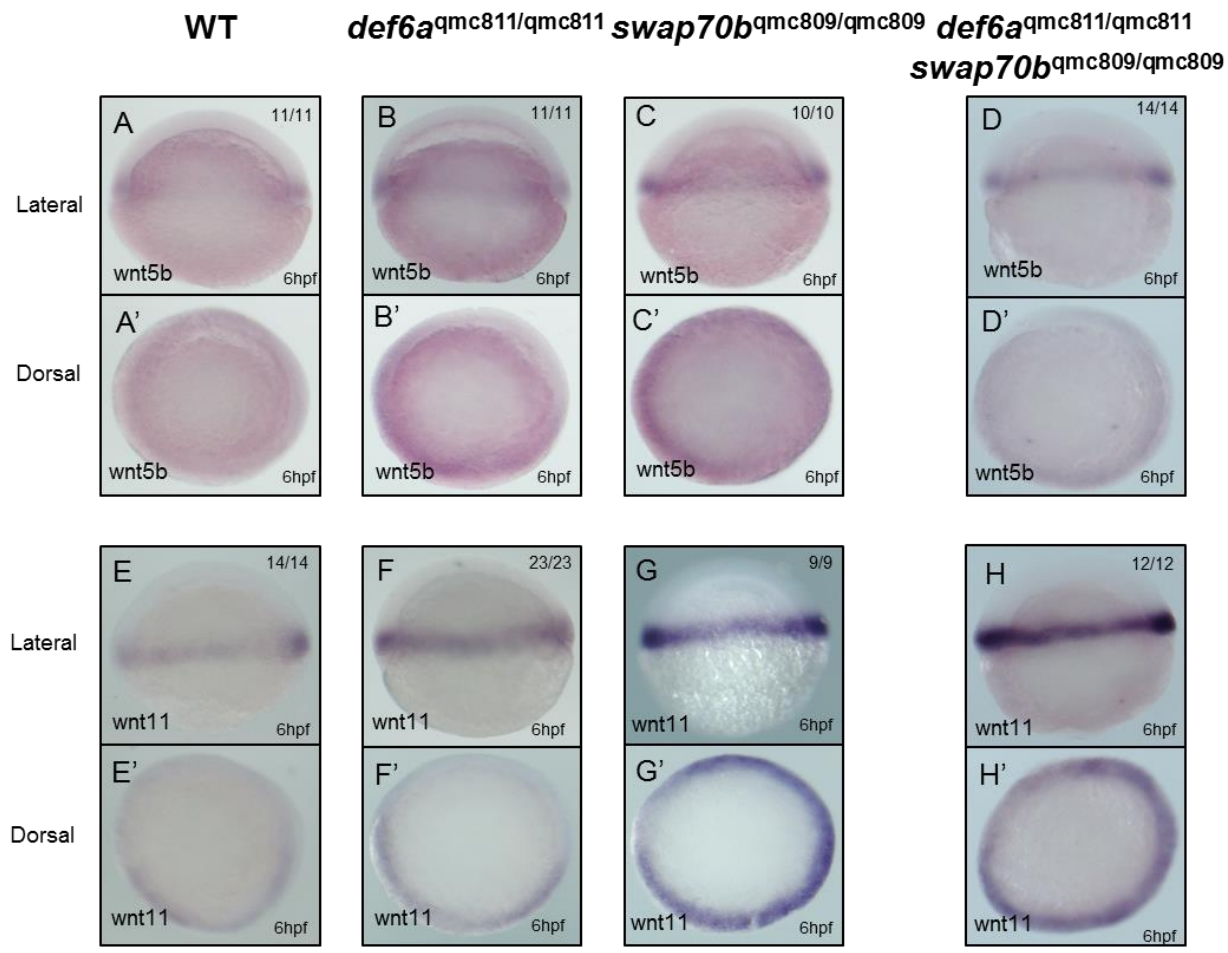


Figure 5.12 *wnt5b* and *wnt11* expression were upregulated in single *def6a*$^{qmc811/qmc811}$, *swap70b*$^{qmc809/qmc809}$ and double *def6a*$^{qmc811/qmc811}$; *swap70b*$^{qmc809/qmc809}$ mutants. Representative embryos from each category are depicted. WT (left column), *def6a*$^{qmc811/qmc811}$ mutants (middle left column), *swap70b*$^{qmc809/qmc809}$ mutants (middle right column) and *def6a*$^{qmc811/qmc811}$; *swap70b*$^{qmc809/qmc809}$ double mutants (right column) were fixed at shield stage and WISH was carried out using *wnt5b* **(A-B-C-D;** lateral view, dorsal right, **A'-B'-C'-D';** anterior view**)** *and wnt11* **(E-F-G-H;** lateral view, dorsal right, **E'-F'-G'H';** anterior view**)** probes. Expression of *wnt5b* at the margin was increased in *def6a*$^{qmc811/qmc811}$ **(B-B')**, *swap70b*$^{qmc809/qmc809}$ **(C-C')** and double *def6a*$^{qmc811/qmc811}$; *swap70b*$^{qmc809/qmc809}$ mutants (**D-D'**). Highest expression levels were recorded in *swap70b*$^{qmc809/qmc809}$ and double *def6a*$^{qmc811/qmc811}$; *swap70b*$^{qmc809/qmc809}$ mutants, compared to WT controls **(A-A')**. Similarly, elevated expression of *wnt11* was observed in single *def6a*$^{qmc811/qmc811}$ **(F-F')**, *swap70b*$^{qmc809/qmc809}$ **(G-G')** and double *def6a*$^{qmc811/qmc811}$; *swap70b*$^{qmc809/qmc809}$ mutants **(H-H')**, with the highest expression in *swap70b*$^{qmc809/qmc809}$ and double *def6a*$^{qmc811/qmc811}$; *swap70b*$^{qmc809/qmc809}$ mutants, compared to WT controls **(E-E')**. The number (n) of tested embryos is indicated on top of the figures.

5.4. Summary

- Impaired CE cell movements during gastrulation of *def6a*$^{qmc811/qmc811}$ embryos was specifically rescued through overexpression of Gfp-Cdc42, thereby indicating that Def6a acts upstream of Cdc42.
- Impaired CE cell movements during gastrulation of *swap70b*$^{qmc809/qmc809}$ embryos was restored through overexpression of either Gfp-Cdc42 or Gfp-RacI. This indicates that Swap70b acts upstream of both Cdc42 and RacI.
- CE cell movement defects in both *def6a*$^{qmc811/qmc811}$ and *swap70b*$^{qmc809/qmc809}$ embryos is likely due to aberrant actin organisation, loss of cell polarisation and altered cell shape during gastrulation.
- Lack of *def6a*, *swap70b* or both resulted in elevated expression of *wnt5b and wnt11* at the onset of gastrulation confirming the negative regulation of *wnt5b and wnt11* expression by *def6a* and *swap70b.*
- Upregulation of *wnt5b and wnt11* was more pronounced in *swap70b*$^{qmc809/qmc809}$ single and *def6a*$^{qmc811/qmc811}$*; swap70b*$^{qmc809/qmc809}$ double mutants suggesting that negative regulation of *wnt5b and wnt11* expression via *swap70b* is dominant.
- *def6a* and *swap70b* are required in the non-canonical Wnt/PCP/Ca^{2+} signalling pathway regulating CE cell movements during zebrafish gastrulation.

CHAPTER 6

RESULTS

Myelopoiesis is impaired in adult zebrafish lacking either *def6a*, *swap70b* or both

6.1. Introduction

In mouse, Def6 and Swap70 are expressed predominantly in T and B cells, respectively, and both proteins have been shown to regulate many processes in the immune system as outlined in Chapter 1. However, their expression and function in haematopoietic stem and precursor cells (HSPCs) have not been studied in zebrafish. Swap70, found to be expressed in haematopoietic stem cells and myeloid-erythroid precursors, was required for integrin-dependent development and differentiation of erythrocytes in mice (Ripich and Jessberger, 2011). To further determine the putative roles of both Def6 and Swap70 in HSPCs, Ripich *et al.,* (2016) analysed *Def6*$^{-/-}$*, Swap70*$^{-/-}$ and double knock-out (DKO: *Def6*$^{-/-}$*; Swap70*$^{-/-}$) mice on the C57BL/6 genetic background. Flow cytometry analysis of bone marrow cells showed that both *Def6* and *Swap70* are expressed in the lineage-negative, Sca1-positive, c-Kit positive (LSK) HSPC fraction of WT mice. To understand whether the deficiencies of *Def6* and *Swap70* affect the frequencies and numbers of HSPCs and mature hematopoietic cell types, WT and mutant mice at different ages (4 to 12 weeks after birth) were analysed. A significant increase was observed in the absolute and relative number of LSK cells in the absence of *Swap70* and both proteins, the increase was more in 8-week and 12-week old mice than 4-week old mice, suggesting that DKO mice revealed a dominant *Swap70*-dependent phenotype. In contrast, this increase in LSK was only observed in 4-week old but not in 8-week and 12-week old *Def6*-deficient mice. These results suggest a specific role of *Swap70* in the further development of HSPCs as LSK population accumulated in the bone marrow in the absence of *Swap70*. Moreover, further analysis on apoptosis revealed that low numbers of *Swap70*-deficient LSK cells and high numbers of *Def6*-deficient LSK cells were undergoing apoptosis, which also contributes to the accumulation of these cells in the bone marrow in *Swap70*-deficient mice.

Furthermore, analyses of blood cell lineages demonstrated that common myeloid progenitors (CMPs), granulocyte-monocyte precursors (GMPs), megakaryocyte-erythrocyte progenitors (MEPs) and common lymphoid progenitors (CLPs) were differently affected by the loss of *Swap70, Def6* or both. GMPs were strongly affected by *Def6*-deficiency as *Def6*-deficient mice showed 3-fold increase in the numbers of GMPs at all age groups, while *Swap70*-deficient

mice only showed 2-fold increase in the 4-weeks of age. Similar to the previous results, DKO mice did not significantly show an increase in GMP numbers at all age groups, suggesting a dominant effect of *Swap70*-deficiency. In contrast, the numbers of MEPs were slightly reduced in *Def6* and *Swap70*-deficient 4 week old mice. The synergistic effect was suggested as the absence of both *Def6* and *Swap70* caused 2-fold decrease in the numbers of MEPs. Lastly, CLP cells were decreased by 2-fold in 4-weeks old DKO mice, while the lack of *Swap70* did not significantly affect the CLP numbers at all age groups, the lack of *Def6* caused a slight decrease. These results suggest that *Def6* and *Swap70* play antagonistic roles in GMP development and agonistic roles in MEP differentiation. Additionally, all age groups of single and double mutant mice showed significantly decreased numbers of CD3e-positive T cells in the bone marrow. The transplantation of sorted HSC/HSP cells of single and double mutant mice into lethally irradiated WT recipients showed that haematopoiesis was rescued in *Def6*$^{-/-}$ mice but not in *Swap70*$^{-/-}$ and DKO mice. Specifically, *Def6* deficiency was shown to rescue some of the reconstitution effect of *Swap70*-deficiency, suggesting a clear antagonistic effects of *Def6* and *Swap70*. Taken together, analysis of *Def6* and *Swap70*-deficient mice revealed that Def6 and Swap70 regulate the hematopoietic stem and precursor cell homeostasis in a distinct and predominantly antagonistic manner (Ripich et al., 2016).

In zebrafish, haematopoiesis occurs in three waves referred to as the primitive, pro-definitive and definitive (reviewed in Ciau-Uitz *et al.,* 2014) **(Figure 6.1)**. Primitive haematopoiesis occurs in a ventral mesoderm tissue termed the intermediate cell mass (ICM). During this wave, the anterior lateral mesoderm (ALM) which is the anterior part of the embryo produces myeloid cells and the posterior lateral mesoderm (PLM) that is the posterior part of the embryo produces predominantly erythrocytes and some myeloid cells. The prodefinitive wave is composed of a population of multipotent erythromyeloid progenitors (EMPs) derived from posterior blood islands (Ciau-Uitz *et al.,* 2014). The differentiation of EMPs into erythroid (Ery) and myeloid (Myel) progeny has been shown *in vitro* (Bertrand *et al.,* 2007). The definitive haematopoietic stem cells (HSCs) are derived from the hemogenic endothelium localised to the ventral wall of the dorsal aorta which corresponds to the aorta-gonad-mesonephros (AGM) by the endothelial-to-hematopoietic transition (EHT) (Bertrand *et al.,* 2010, Kissa and Herbomel, 2010). In zebrafish, EHT occurs into the space between the dorsal aorta and the posterior cardinal vein (Murayama *et al.,* 2006). From 48hpf, these definitive blood cells then migrate to the posterior region of the tail referred to as caudal hematopoietic tissue (CHT). From 3dpf, the generation of lymphocytes begins in the thymus and lastly from 4dpf the HSCs seed the kidney which is the main hematopoietic site in adult zebrafish. Thymus and kidney marrow generate adult hematopoietic cells throughout the life of a zebrafish (Reviewed in Davidson and Zon, 2004; Paik and Zon, 2010; Ciau-Uitz *et al.,* 2014).

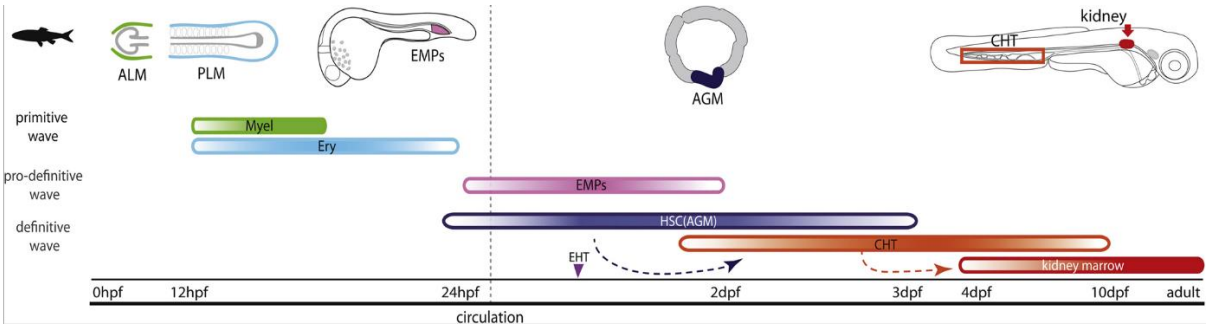


Figure 6.1 Overview of zebrafish haematopoiesis. The timeline summarises the primitive, prodefinitive and definitive waves of zebrafish haematopoiesis. The timing of hematopoietic activity is shown by bars, the color gradient represents a peak in activity. Broken arrows represent migration and seeding of hematopoietic sites by HSPCs. While the primitive wave starts at the gastrulation stage with the development of three germ layers, the prodefinitive wave starts at 24hpf and the definitive wave starts at ALM: anterior lateral mesoderm (green), PLM: posterior lateral mesoderm (blue), EMPs: Erythromyeloid progenitors (pink), EHT: endothelial-to-hematopoietic transition, AGM: aorta-gonad-mesonephros region (ventral wall of dorsal aorta) (purple), CHT: caudal hematopoietic tissue (orange), hpf: hours post-fertilisation, dpf: days post-fertilisation. Adapted from (Ciau-Uitz *et al.,* 2014).

6.2. Development of myelomonocytes in adult zebrafish is significantly affected in the absence of *def6a, swap70b* or both

To determine whether *def6a* or *swap70b* play a role in adult zebrafish, cells from whole kidney marrow isolated from adult 12 and 15-months old WT, 18-months old *def6a*$^{qmc811/qmc811}$, 12-months old *swap70b*$^{qmc809/qmc809}$ and 7-months old *def6a*$^{qmc811/qmc811}$*; swap70b*$^{qmc809/qmc809}$ double mutants were analysed by flow cytometry. Kaluza Analysis 1.5a software was employed to generate density plots using 355-488 Forward Scatter (FSC1) Height and 355-488 Side Scatter (SSC) Height scatters. Blood cell populations were gated and sub-divided into four cell populations: erythrocytes, myelomonocytes, precursor cells and lymphocytes according to Traver *et al.,* 2003 (**Figure 6.2**). One-way ANOVA and unpaired student's t-test analyses were applied to determine whether blood cell populations isolated from single or double mutant zebrafish were altered compared to WT. In total, 4 samples from each genotype were analysed (**Figure 6.2** and **appendix IV**). While the mean percentage of erythrocytes **(Figure 6.2E)**, immature progenitors **(Figure 6.2G)** and lymphocytes **(Figure 6.2H)** was slightly increased in *def6a*$^{qmc811/qmc811}$ **(Figure 6.2B-B'-B'')**, *swap70b*$^{qmc809/qmc809}$ **(Figure 6.2C-C'-C'')** and *def6a*$^{qmc811/qmc811}$; *swap70b*$^{qmc809/qmc809}$ double mutants **(Figure 6.2D-D'-D'')** compared to WT controls **(Figure 6.2A-A'-A'')**, the differences were not significant (N.S). In contrast, the myelomonocyte population was significantly decreased in the mutant zebrafish **(Figure 6.2F;** **P<0.01, ***P<0.05**).** The mean percentage of the myelomonocytes in WT controls was 28.26% **(Figure 6.2A'')**. A 2-fold decrease to 12.45% was apparent in *def6a*$^{qmc811/qmc811}$ mutants **(Figure 6.2B'')**, and a 3-fold decrease to 8.56% in *swap70b*$^{qmc809/qmc809}$ mutants **(Figure 6.2C'')** and to 8.71% in *def6a*$^{qmc811/qmc811}$; *swap70b*$^{qmc809/qmc809}$ double mutants **(Figure 6.2D'')** was observed. It therefore appears that both, *def6a* and *swap70b* are required for myelomonocyte differentiation in adult zebrafish. Furthermore, reduced myelomonocytes and the cumulative increase in erythrocytes, progenitors and lymphocytes in the mutants could reflect a shift in HSPC fate and lineage choice.

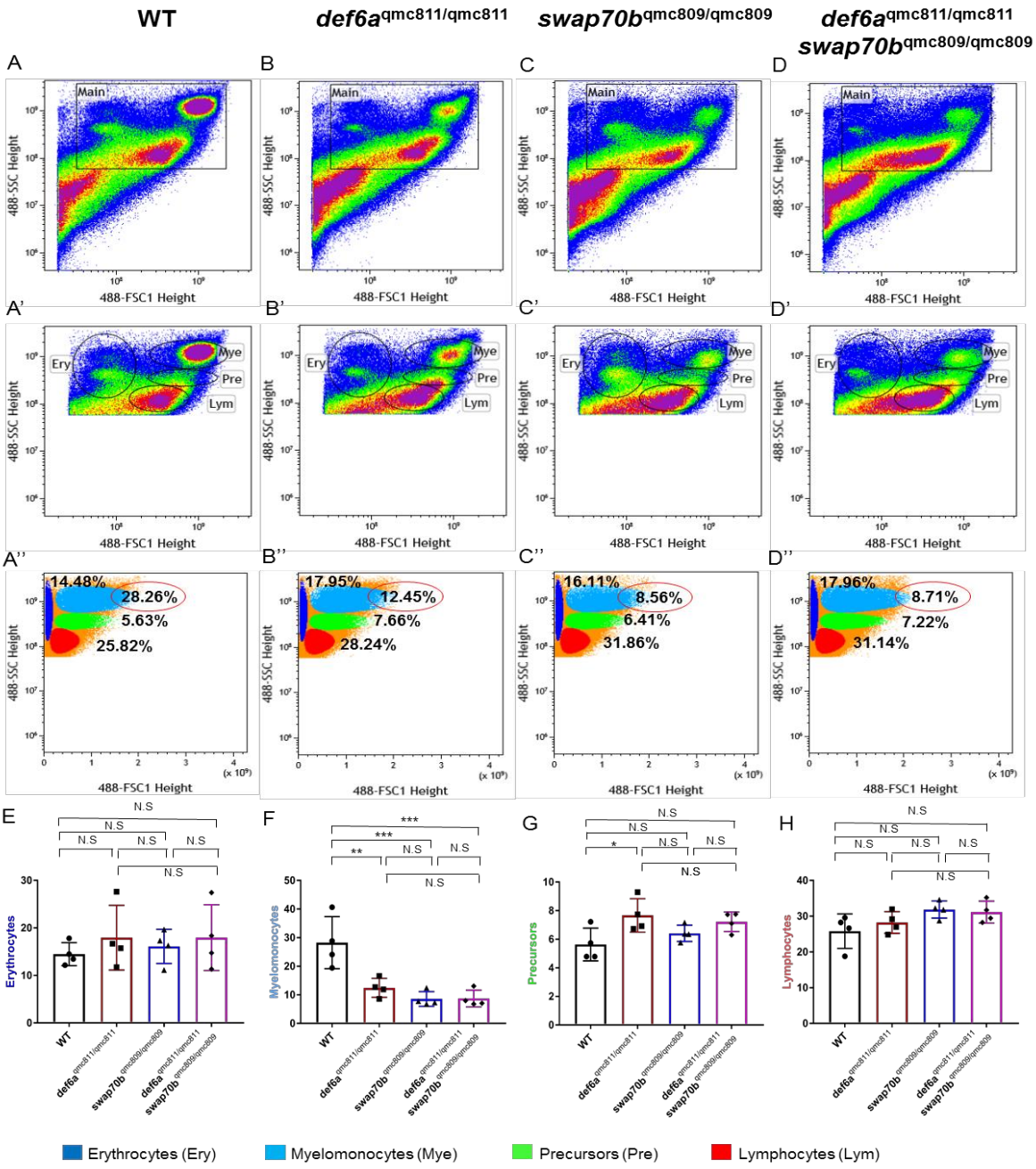

WT
def6a qmc811/qmc811
swap70b qmc809/qmc809
def6a qmc811/qmc811 swap70b qmc809/qmc809
A
B
C
D
Main
488-SSC Height
488-FSC1 Height
A'
B'
C'
D'
Ery
Mye
Pre
Lym
A''
B''
C''
D''
14.48%
28.26%
5.63%
25.82%
17.95%
12.45%
7.66%
28.24%
16.11%
8.56%
6.41%
31.86%
17.96%
8.71%
7.22%
31.14%
(x 10⁹)
E
F
G
H
N.S
Erythrocytes
Myelomonocytes
Precursors
Lymphocytes
WT
def6a qmc811/qmc811
swap70b qmc809/qmc809
def6a qmc811/qmc811 swap70b qmc809/qmc809
Erythrocytes (Ery)
Myelomonocytes (Mye)
Precursors (Pre)
Lymphocytes (Lym)

Figure 6.2 Flow cytometric analysis of the blood cell lineages of WT, single *def6a*$^{qmc811/qmc811}$ and *swap70b*$^{qmc809/qmc809}$ and double *def6a*$^{qmc811/qmc811}$*; swap70b*$^{qmc809/qmc809}$ mutants revealed that the development of myelomonocytes was significantly reduced in all mutants. Representative FACS plots of freshly isolated kidney marrow cells from WT **(A-A'')**, *def6a*$^{qmc811/qmc811}$ **(B-B'')**, *swap70b*$^{qmc809/qmc809}$ **(C-C'')** and *def6a*$^{qmc811/qmc811}$*; swap70b*$^{qmc809/qmc809}$ double mutants **(D-D'')**. For more examples please see **Appendix IV**. **(A-B-C-D)** A main gate was produced for all plots to focus only the blood cell lineages. **(A'-B'-C'-D')** The major blood cell lineages were further separated by four additional sub-gates which are erythrocytes (ery), myelomonocytes (mye), precursors (pre) and lymphocytes (lym). **(A'''-B'''-C'''-D''')** Mean percentages of each population, which were obtained from 4 adult fish per genotype, revealed a reduction in the myelomonocyte population in all mutants compared to WT. **(E-F-G-H)** Comparison of relative percentages of each population among WT and all mutants indicated that while the myelomonocyte population was significantly affected **(F)**, the erythrocyte **(E)**, precursor **(G)** and lymphocyte **(H)** populations were not significantly affected by the loss of *def6a* and *swap70b.* FSC: Forward scatter, SSC: Side Scatter. Gates; Main gate, erythrocytes (dark blue), myelomonocytes (light blue), immature precursors (green) and lymphocytes (red). *P<0.05, **P<0.001, ***P<0.005, N.S: No significant statistical difference.

6.3. Summary

- *def6a* and *swap70b* are required for myelomonocyte differentiation in adult zebrafish and they may both control HSPC fate and lineage choice.

CHAPTER 7

RESULTS

BioID-mediated identification of proximal and interacting proteins of DEF6 in Jurkat T cells

7.1. BioID-mediated identification of protein-protein interactions in mammalian cells

Biotin is an essential cofactor for biotin carboxylase and decarboxylases and it is biologically inactive when it is not bound to proteins or not covalently-attached to carboxylases or decarboxylases (Chapman-Smith and Cronan, 1999c). Biotinylation is the process of labelling proteins with biotin either chemically or enzymatically. Enzymatic biotinylation of proteins by biotin protein ligase (BPL) is adding biotin to specific lysine residues of the newly synthesised carboxylase enzymes. The best characterised BPL is the biotin ligase, BirA from *E.coli,* responsible for biotinylating a single lysine residue within the biotin carboxyl carrier protein (BCCP) subunit of acetyl-CoA carboxylase (Chapman-Smith and Cronan, 1999a; 1999b).

Biotinylation by BirA is a two-step process that the activated biotin; biotinoyl-5′-AMP (bioAMP), forms after biotin reacts with ATP in the first step and bioAMP reacts with a specific lysine residue in the second step (Lane *et al.,* 1964). Because of the high selectivity of BirA, a mutant form of BirA (R118G; also BirA*) which promiscuously biotinylates proteins in close proximity, has been developed as a general biotinylating enzyme (Kwon and Beckett, 2000; Choi-Rhee *et al.,* 2004). The R118G mutation results in weaker binding of biotin and bioAMP compared to wild type BirA. Therefore, chemically active bioAMP can react with the amine groups on lysine residues of proximal proteins (Kwon and Beckett, 2000). Indeed, R118G BirA was shown to act as a promiscuous biotin ligase and possess also a self-biotinylation activity (Choi-Rhee *et al.,* 2004).

Since biotin demonstrates high affinity interaction with streptavidin and avidin, analysing the streptavidin/avidin-mediated purified biotinylated proteins has been widely used to understand complex biological processes by identifying protein-protein interactions (Fairhead and Howarth, 2015). A new method, BioID, combining *in vivo* promiscuous biotinylation of interacting/proximal proteins and subsequent selective isolation of these biotinylated proteins, was developed to understand the role of a protein of interest. *In vivo* expression of the fusion protein in mammalian cells, containing the mutant BirA ligase and a protein of interest, will

promiscuously biotinylate the direct or indirect interacting and vicinal proteins of the bait protein. Then, biotinylated proteins can be affinity-captured and identified by mass spectrometry (Roux *et al.,* 2012; **Figure 7.1**). By using the fusion of BirA and a nuclear envelope protein, lamin-A (LaA), they isolated some known interactors of LaA, as well as a novel nuclear envelope protein called SLAP75 (Roux *et al.,* 2012). Due to its feasible application, BioID has become a widely used method in protein-protein interaction analyses (Kim *et al.,* 2016). Cancer development (Elzi *et al.,* 2014, Cole *et al.,* 2015; Dingar *et al.,* 2015), mRNA decay (Nishimura *et al.,* 2015), centrosomes (Firat-Karalar *et al.,* 2014), cell-cell junctions (Ueda *et al.,* 2015), cytoskeleton (Morriswood *et al.,* 2013) and signalling pathways (Schumacher *et al.,* 2015) are some of the processes that have been studied using BioID. The effectivity of the BioID method has prompted us to investigate the role of DEF6 in T cells by analysing the direct or indirect interactors and vicinal proteins of DEF6 in Jurkat T cells.

An overview demonstrating the BioID-mediated biotinylation of DEF6 interactome is illustrated in **Figure 7.1**.

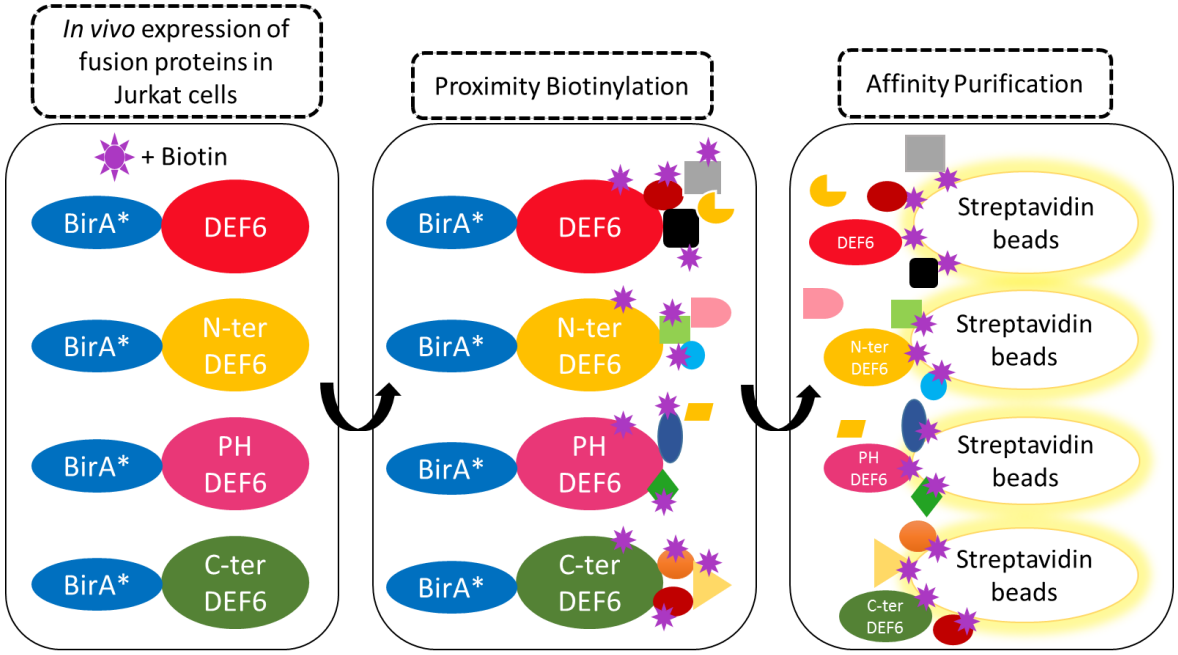


Figure 7.1 Overview of the BioID method demonstrating DEF6 and its truncations as bait proteins. DEF6 and its truncated versions, N terminal (N-ter) DEF6, PH DEF6 and C-terminal (C-ter) DEF6 are fused to the mutant BirA* (BirA R118G) and expressed in Jurkat T cells in the medium containing excess biotin. BirA* generates a cloud of activated bioAMPs, which then reacts with primary amines of the proximal lysine residues and biotinylates the proteins in close proximity. After a stringent cell lysis, streptavidin beads are used to capture the biotinylated molecules. Mass spectrometry based identification of these biotinylated molecules revealed the indirect or direct protein interactions as well as vicinal proteins which will present the interactome network of DEF6 and give us a clue about understanding the further roles of DEF6 in Jurkat T cells.

7.2. Construction of BirA-DEF6 and BirA-Truncated DEF6 fusion vectors

To establish a comprehensive interactome of DEF6 in T cells, fusion proteins of BirA* and either full-length (amino acids 1-631) or truncation mutants of DEF6 were generated. The N-terminal first 108 amino acids, the PH domain (amino acids 214 to 341) and the C-terminal domain (amino acids 312 to 631) were chosen because each of these domains facilitates different functions of DEF6 as described in Section 1.4.2 (Chapter 1). The N-terminal domain of DEF6 contains EF-hands binding Ca^{2+} and the N-terminal 45 amino acids are sufficient to target P-bodies (Cheng, PhD 2017). The PH DEF6 contains the PH domain (214-312 aa) and the N-terminal part of the Dbl-homology-like (DHL) domain (312-341 aa). The PH domain binds to phosphatidylinositol 3,4,5 triphosphate, ($PI(_{3,4,5})P_3$) to enable GEF activity and to recruit DEF6 to the immunological synapse (IS) (Gupta *et al.,* 2003a). Moreover, amino acids 312 to 341 encode a nuclear localisation signal (NLS) which will import the BirA* PH DEF6 protein into the cell nucleus (Martin, PhD 2007; Cheng, PhD 2017). The DHL domain is responsible for the GEF function and it contains a coiled-coil region that promotes formation of large aggregates when it is unmasked through phosphorylation (Hey *et al.,* 2012; Cheng, PhD 2017). Fusion proteins are schematically depicted in **Figure 7.2**. The fusion vectors of BirA*-DEF6 and BirA*-truncated DEF6 proteins were generated using the pEGFP-C2/DEF6 and pcDNA3.1-mycBioID plasmids. Plasmid maps are illustrated in **Appendix V.**

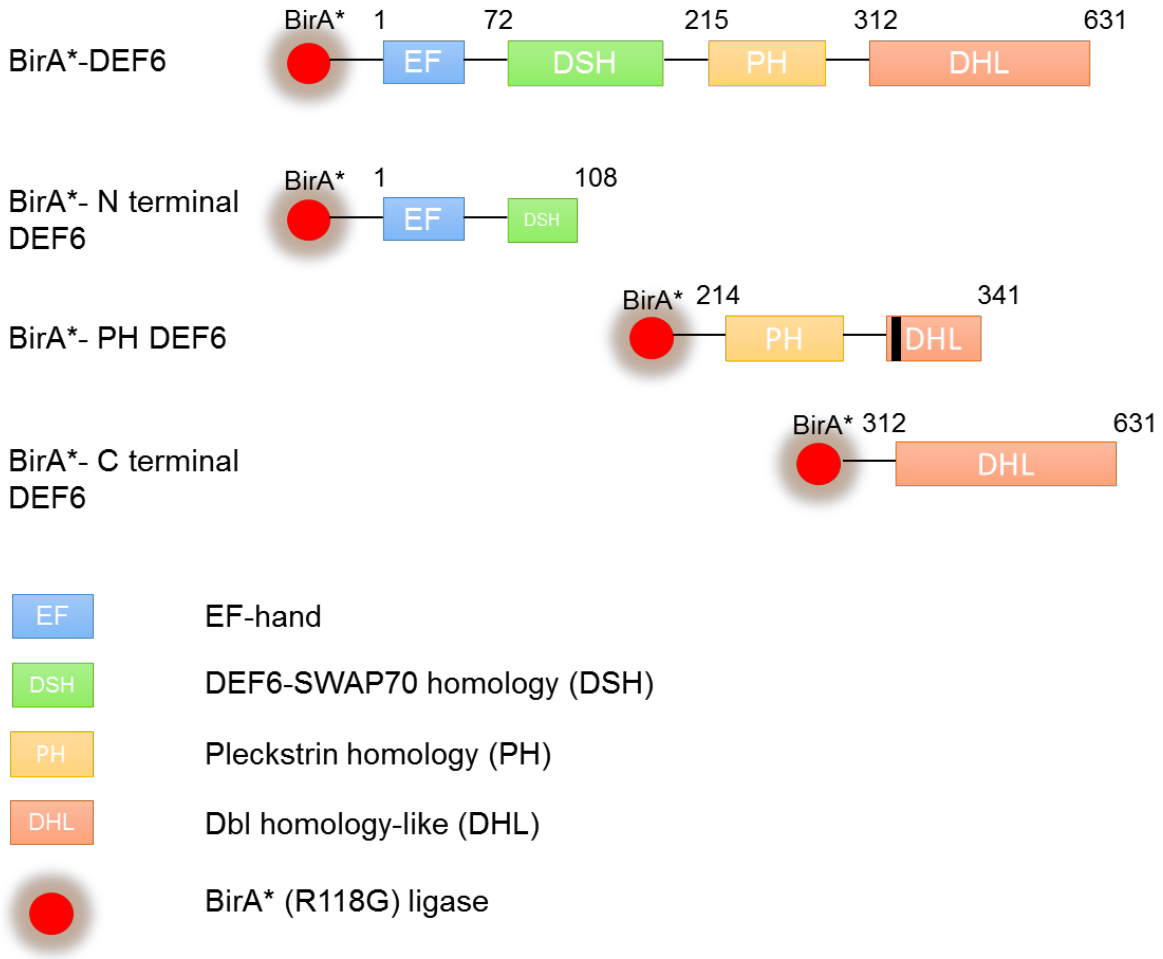


Figure 7.2 Illustration of BirA*-DEF6 and BirA*-N-terminal DEF6, BirA*-PH, BirA*-C-terminal DEF6 fusions. Full-length DEF6 encoding 631 amino acids, N-terminal DEF6 encoding 108 amino acids, PH DEF6 encoding the amino acids from 214 to 341 and C-terminal DEF6 encoding the amino acids from 312 to 631 were all fused to a mutant biotin ligase, BirA* (R118G) which promiscuously biotinylates proteins in close proximity.

7.2.1 Establishment of BirA* DEF6 fusion vectors

Human *DEF6* gene (NCBI accession number: NM_022047; Ensembl accession number: ENSG00000023892) in pEGFP-C2/DEF6 vector (Mavrakis *et al*., 2004) was amplified using specific primers containing *EcoRI* and *AflII* restriction sites for full-length (FL), N-terminal, PH and C-terminal DEF6 (for the primers used see Section 2.2.2 and Table 2.13). 1988bp, 370bp, 432bp and 1044bp fragments were amplified for full-length, N-terminal, PH and C-terminal DEF6, respectively **(Figure 7.3A)**. Amplified fragments were first subcloned into the StrataClone vector (StrataClone Blunt PCR Cloning kit (Section 2.2.1.9)) and subsequently *EcoRI* and *AflII* restriction enzyme fragments were isolated and inserted into the pcDNA3.1 mycBioID vector **(Figure 7.3B)**. Sequence analysis confirmed in-frame insertions of full-length DEF6, N-terminal DEF6, PH-DEF6 and C-terminal DEF6 into the pcDNA3.1 mycBioID vector (**Appendix VI**).

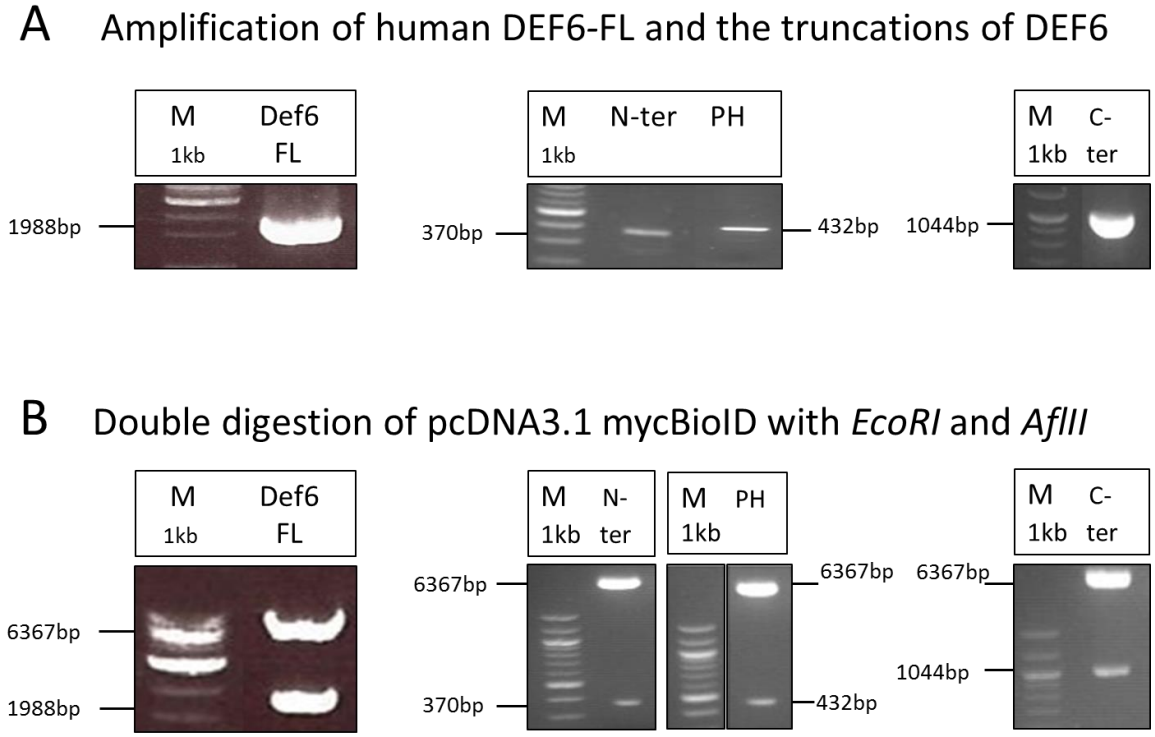


Figure 7.3 Cloning of human FL, truncated N-terminal, PH and C-terminal DEF6 into the pcDNA3.1 mycBioID vector was confirmed by agarose gel electrophoresis. (A) After the amplification of human FL-DEF6 and truncations from pEGFP-C2/DEF6 vector, expected fragment sizes; 1988bp, 370bp, 432bp and 1044bp were detected for FL DEF6, N-ter DEF6, PH DEF6, C-ter DEF6, respectively. **(B)** Cloning of the amplified fragments into a StrataClone Blunt PCR vector facilitated the cloning into pcDNA3.1 mycBioID vector since the fragments were double-digested with *EcoRI* and *AflII* and ligated with the double-digested pcDNA3.1 mycBioID vector successfully. The fragment sizes after double digestion of the pcDNA3.1 mycBioID containing the insertions were detected as expected; 1988bp and 6367bp for FL DEF6, 370bp and 6367bp for N-terminal DEF6, 432bp and 6367bp for PH DEF6 and 1044bp and 6367bp for C-terminal DEF6. The gel depicting the digestion represents of BirA*-PH DEF6 was arranged to exclude the negative result in middle. M: Size marker; 1kb (NEB); FL: Full-length DEF6; N-ter: N-terminal DEF6; PH: PH DEF6; C-ter: C-terminal DEF6.

7.2.2 *In vivo* biotinylation of DEF6 interactome in Jurkat T cells

To biotinylate the interacting and proximal proteins of DEF6 *in vivo*, Jurkat T cells were transfected with the BirA*-DEF6 fusion vectors in the presence of 50μM biotin. 24h after transfection, protein lysates were prepared from Jurkat T cells and subjected to the western blot analysis. Streptavidin-Alkaline phosphatase (AP) which binds to biotin was used to detect biotinylated proteins. As shown in **Figure 7.4,** western blotting of Jurkat T cells expressing the BirA*-DEF6 fusions revealed that their proximal and interacting proteins were biotinylated promiscuously. The negative control which is the non-transfected sample showed the presence of some biotinylated proteins in the cells. This data was used as a background signal to eliminate the proteins present in the negative control from the proteins detected for transfected samples. Enhanced biotinylation patterns were detected in the transfected samples **(Figure 7.4;** FL DEF6; lane 4, N-ter DEF6; lane 5, PH DEF6; lane 6, C-ter DEF6; lane 7**)** as compared to the negative control (**Figure 7.4**; No DNA; lane 3), indicating that endogenous proteins were biotinylated promiscuously by BirA*-DEF6 and BirA*-truncated DEF6 proteins. In addition, the distinct biotinylation pattern detected for each transfected sample suggested that FL-DEF6 and each domain of DEF6 might interact with different or additional proteins **(Figure 7.4).**

Dynabeads MyOne Streptavidin C1 were used to capture the biotinylated proteins (Chapter 2; Section 2.2.6.4). As shown in **Figure 7.5**, Western blotting analysis revealed enhanced and distinct biotinylation patterns for FL DEF6, N-ter DEF6, PH DEF6 and C-ter DEF6 samples confirming the effective capture of biotinylated proteins.

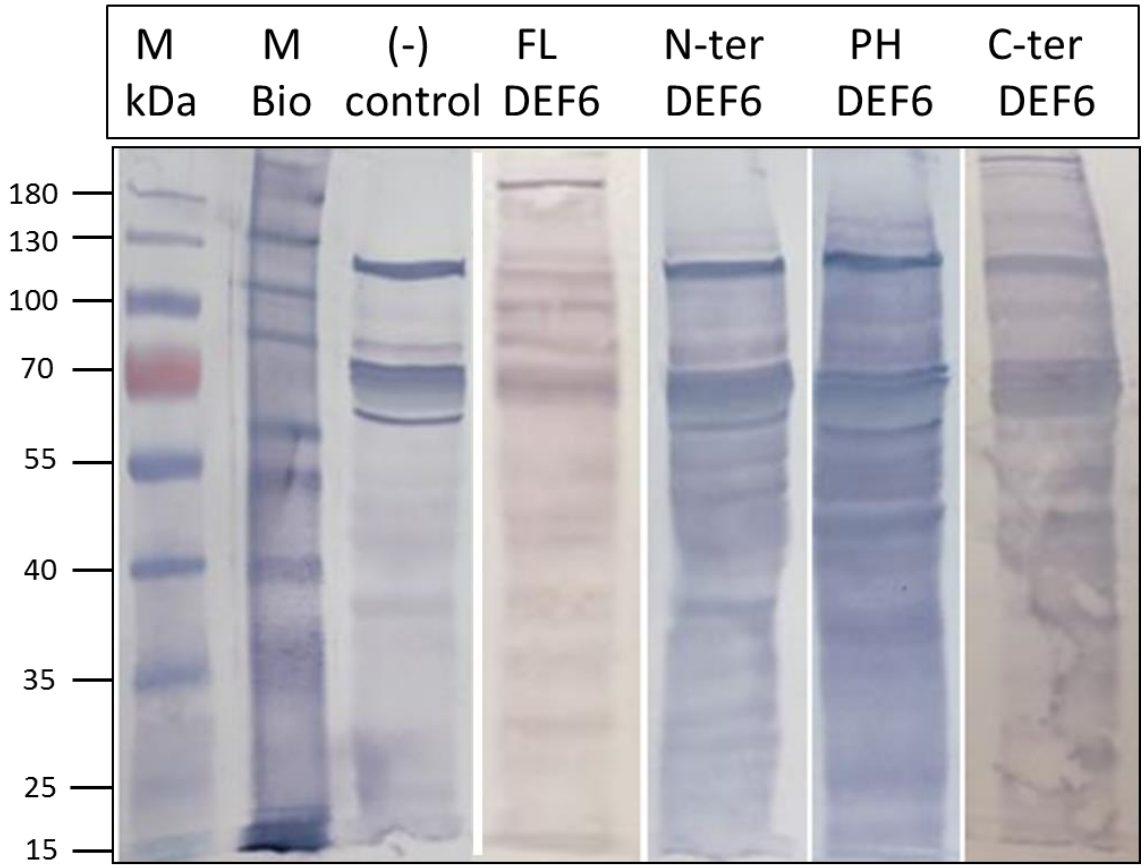


Figure 7.4 Western blot analysis demonstrating the biotinylation of interacting or proximal endogenous proteins in Jurkat T cells expressing the fusions in the presence of 50µM biotin. The blot was probed with Streptavidin- alkaline phosphatase (AP). M in lane 1 indicates the protein ladder; PageRuler, sizes (kDa) are indicated on the figure. M in lane 2 indicates the biotinylated protein ladder, which was used as a control for the biotinylation by Streptavidin-AP, thus the sizes are not indicated. (-) control in lane 3 indicates the negative control without transfection for background purpose. FL DEF6 in lane 4 indicates the biotinylation of endogenous proteins after the transfection of cells with BirA*-DEF6. N-ter DEF6 in lane 5 indicates the biotinylation of endogenous proteins after the transfection of cells with BirA*-N-terminal DEF6. PH DEF6 in lane 6 indicates the biotinylation of endogenous proteins after the transfection of cells with BirA*-PH DEF6 and lastly C-ter DEF6 in lane 7 indicates the biotinylation of endogenous proteins after the transfection of cells with BirA*-C-terminal DEF6. All transfected samples and the un-transfected sample showed distinct biotinylation patterns suggesting that each domain has a different interaction network. The gaps in between indicate the samples from different blots that are combined together to show the distinct biotinylation pattern of each sample.

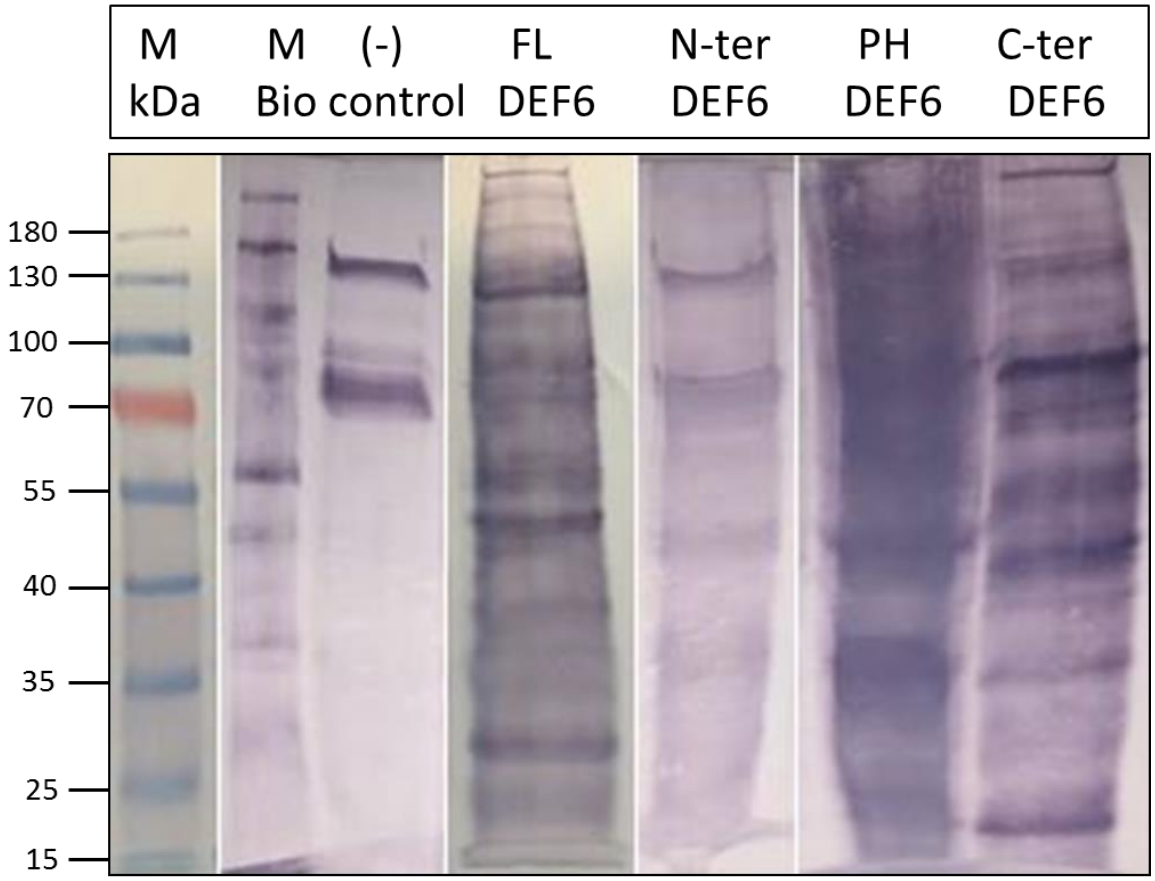


Figure 7.5 Western blot analysis after affinity capture of biotinylated proteins. The blot was probed with Streptavidin- alkaline phosphatase (AP). M in lane 1 indicates the protein ladder; PageRuler, sizes (kDa) are indicated on the figure. M in lane 2 indicates the biotinylated protein ladder, which was used as a control for the biotinylation by Streptavidin-AP, thus the sizes are not indicated. (-) control in lane 3 indicates the negative control without transfection for background purpose. FL DEF6 in lane 4 indicates the capture of biotinylated proteins after the transfection of cells with BirA*-DEF6. N-ter DEF6 in lane 5 indicates the capture of biotinylated proteins after the transfection of cells with BirA*-N-terminal DEF6. PH DEF6 in lane 6 indicates the capture of biotinylated of biotinylated proteins after the transfection of cells with BirA*-PH DEF6 and lastly C-ter DEF6 in lane 7 indicates the capture of biotinylated proteins after the transfection of cells with BirA*-C-terminal DEF6. All transfected samples and the un-transfected sample showed distinct biotinylation patterns. The gaps in between indicate the samples from different blots that are combined together to show the distinct biotinylation pattern of each sample.

7.2.3 Identification and classification of DEF6 interactome

Identification:

For mass spectrometry analysis, the beads with the captured biotinylated proteins were re-suspended in 50mM ammonium bicarbonate buffer and sent to Dr Andrew Bottrill, Protein and Nucleic Acid Chemistry Laboratory (PNACL), University of Leicester.

The identity of the captured proteins was determined by mass spectrometry and the results were viewed with a proteome software, Scaffold. 514 proteins in **404 clusters** were detected in total, however **277 clusters** were eliminated since they were also detected in the negative control sample. The remaining proteins in **127 clusters**, were subjected to further analysis. From the remaining 127 proteins, 87 proteins of FL DEF6, 9 proteins of N-terminal DEF6, 82 proteins of PH DEF6 and 91 proteins of C-terminal DEF6 were detected. While some of the proteins were same for all samples, some were specific to each sample **(Figure 7.6).** The identified proteins are listed in **Appendix VII**.

Classification:

The DEF6 interactome was grouped into the known protein complexes according to the gene ontology (GO) terms in Scaffold software and DAVID Bioinformatics Resources 6.8 (https://david.ncifcrf.gov/tools.jsp). The reason for using two different bioinformatics database for GO terms was to make an accurate classification since some proteins may have various functions and be grouped into more than one biological processes. While the physical interactions were shown as annotated in STRING database (https://string-db.org/), the pathways which the proteins might be involved are shown as annotated in KEGG and Reactome pathway databases (http://www.genome.jp/kegg/pathway.html and https://reactome.org/PathwayBrowser/).

The interaction network of the 127 putative interactors of DEF6 is shown as annotated in STRING database **(Figure 7.7)**. The interaction network revealed that the majority of proteins clustered into different sections and the minority of proteins are positioned around these sections. Therefore, to gain insight into the various functions of the identified proteins, gene ontology (GO) term analysis was performed using Scaffold and DAVID. The ontologies of the identified proteins were grouped into various categories, mostly involved in transcription, RNA splicing/processing, translation, metabolic pathways, protein folding/modification and actin cytoskeleton organisation. **Table 7.1** presents the list of six categories comprising 103 proteins that were found to be associated with DEF6, the remaining 24 proteins can be found in the list containing the mass spectrometry results in Appendix VII. The table includes the related

references supporting that the proteins have a function in that biological process and the reported peptide numbers for each sample (FL-DEF6 and the domains of DEF6). In addition, a pie chart, which demonstrates the GO term enrichment of proteins, is shown in **Figure 7.8.** The majority of proteins were associated with transcription (26%; 36 proteins) and RNA splicing/processing (20%; 28 proteins). 12% were associated with metabolic processes (17 proteins) including purine biosynthesis, ATP biosynthesis, amino acid and lipid metabolisms. 9% with mRNA translation (13 proteins), 11% with protein folding/modification (15 proteins), 5% with actin cytoskeleton organisation (7 proteins) and 17% were associated with other processes (24 proteins).

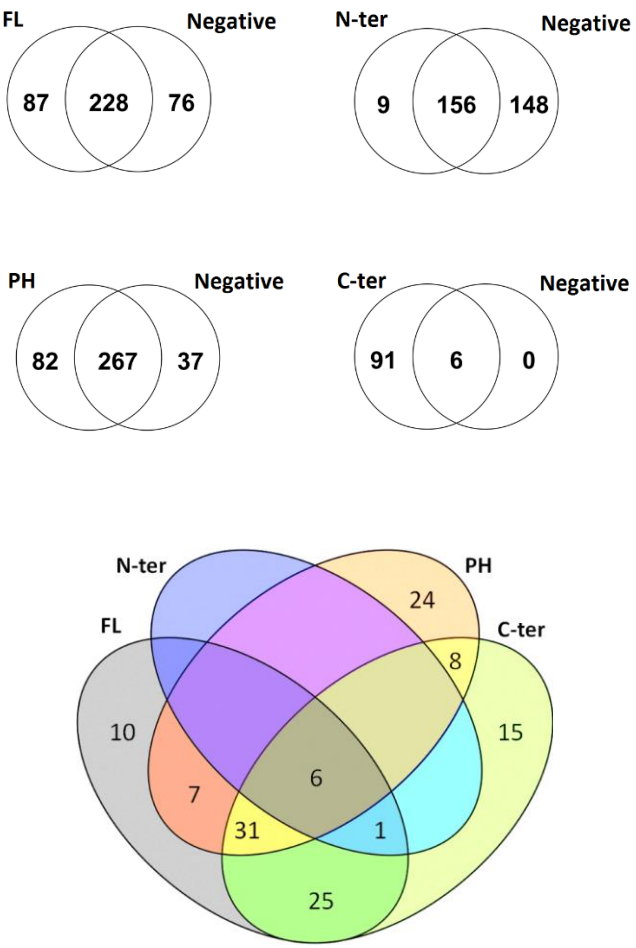


Figure 7.6 Venn diagrams demonstrating the detected protein numbers for each sample. The proteins in negative control were eliminated and the remaining proteins were considered as in close proximity or interacting with DEF6. From these proteins, only 6 of them were detected in all samples, while 10, 24 and 15 of them were specific to FL DEF6, PH DEF6 and C-terminal DEF6, respectively, as indicated.

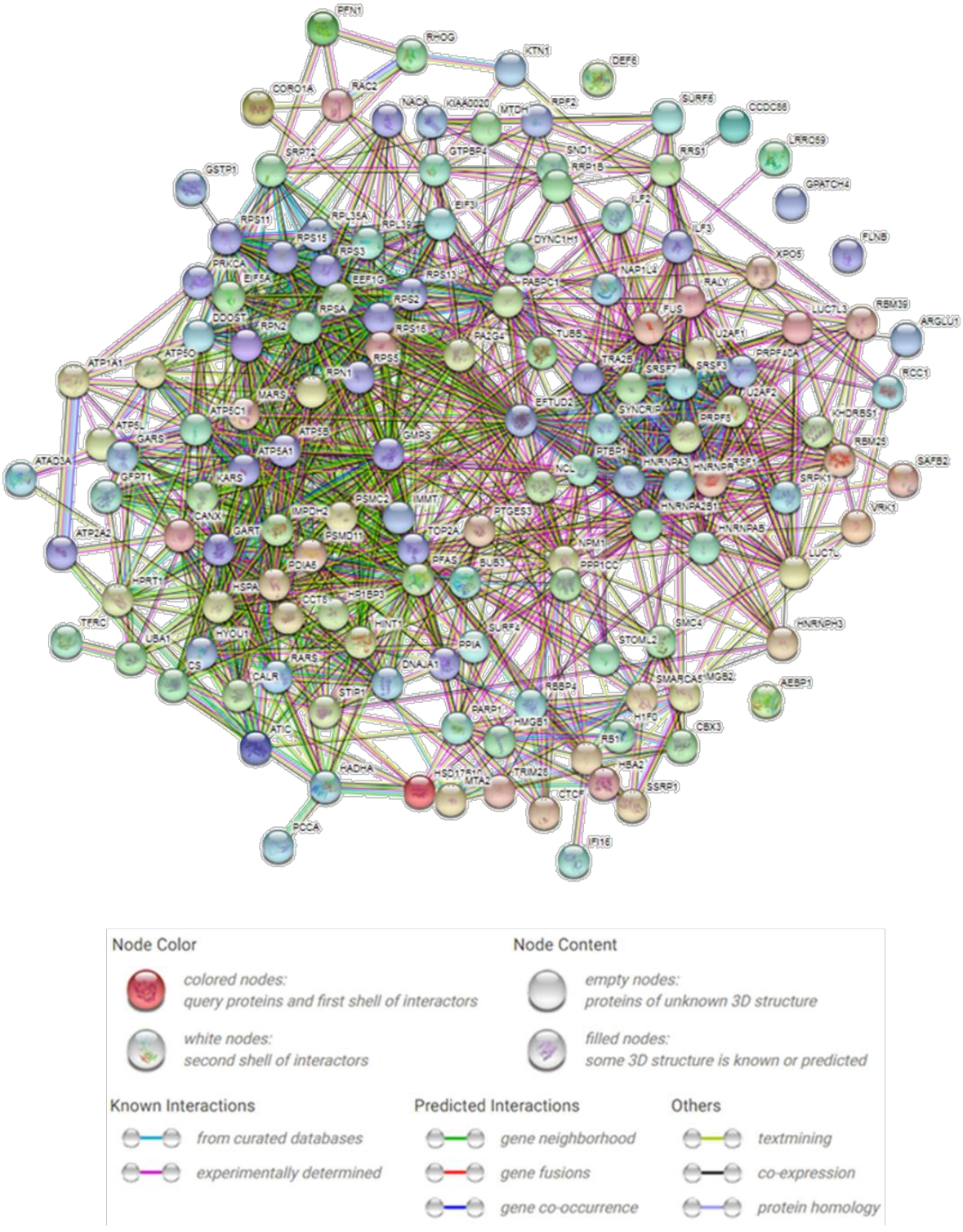


Figure 7.7 Interaction network demonstrating the interaction of 127 proteins as annotated in STRING.

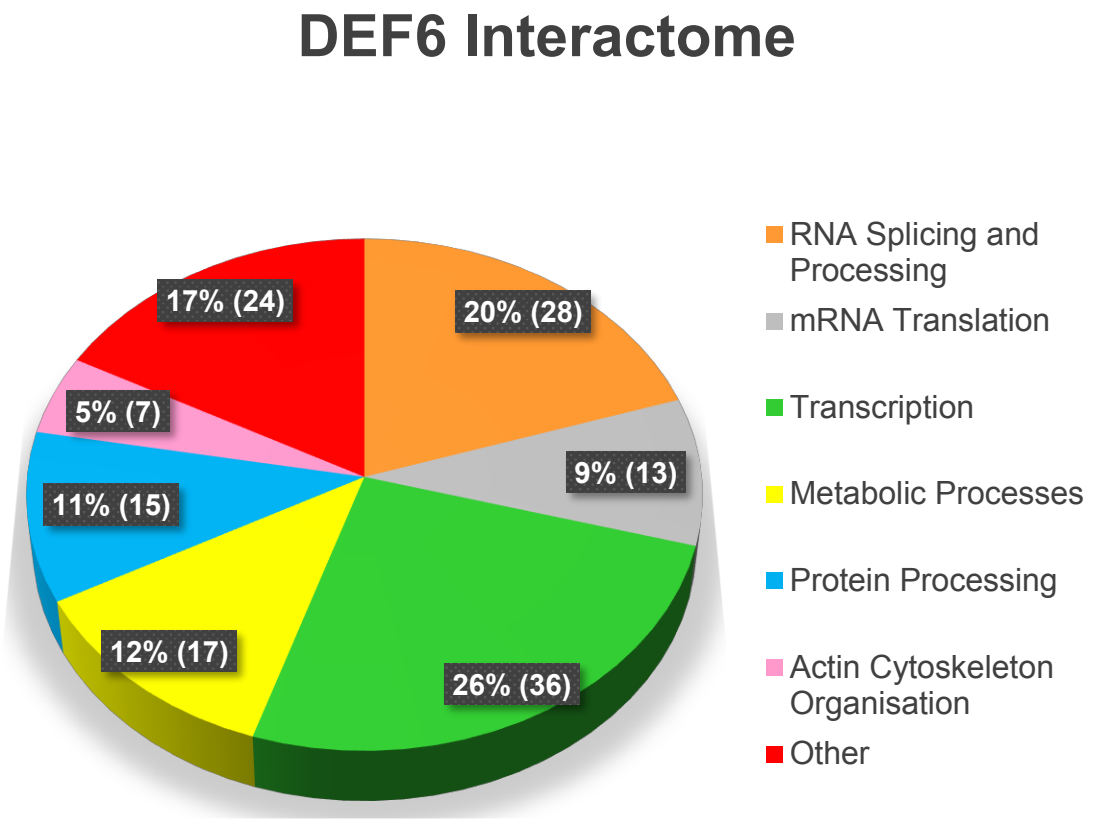


Figure 7.8 Pie chart summarising GO term enrichments of proteins. 26% represents transcription (36 proteins), 20% represents RNA splicing and processing (28 proteins), 12% represents metabolic processes (17 proteins), 9% represents translation (13 proteins), 11% represents protein processing (15 proteins), 5% represents actin cytoskeleton organisation (7 proteins) and 17% represents the other individual processes (24 proteins).

ACTIN CYTOSKELETON ORGANISATION								
Genes (7)	Accession No	Molecular Weight	Reference	FL	N-ter	PH	C-ter	Negative control
Cluster of Coronin-1A (CORO1A)	P31146	51 kDa	de Hostos, 1999; Humphries *et al.,* 2002; Ono, 2003; Föger *et al.,* 2006; Mugnier *et al.,* 2008; Castro-Castro *et al.,* 2011; Mace and Orange, 2014	3	-	8	4	-
Ras-related C3 botulinum toxin substrate 2 (RAC2)	P15153	21 kDa	Bengtsson *et al.,* 1990; Shirsat *et al.,* 1990; Reibel *et al.,* 1991; Dorseuil *et al.* 1996; Hall, 1998; Roberts *et al.,* 1999; Mavrakis *et al.,* 2004; Sun *et al.,* 2007; Rosowski *et al.,* 2016	2	-	3	-	-
Filamin-B (FLNB)	O75369	278 kDa	Hartwig *et al.,* 1980; Weihing, 1985; Cunningham *et al.,* 1992; Stossel *et al.,* 2001; Takafuta *et al.,* 2002	4	-	5	3	-
Profilin-1 (PFN1)	P07737	15kDa	Carlsson *et al.,* 1977; Bubb *et al.,* 2003; Witke, 2004; Krishnan. and Moens, 2009; Mouneimne *et al.,* 2012; Bezanilla *et al.,* 2015; Rotty *et al.,* 2015; Pernier *et al.*, 2016	-	-	3	-	-
Rho-related GTP-binding protein RhoG (RHOG)	P84095	21 kDa	Tapon and Hall, 1997; Gauthier-Rouviere *et al.,* 1998; Blangy *et al.,* 2000; Wennerberg *et al.,* 2002; Vigorito *et al.,* 2003; Ridley, 2006; Katoh *et al.,* 2006	2	-	3	-	-
Differentially expressed in FDCP 6 homolog (DEF6)	Q9H4E7	74 kDa	Gupta *et al.,* 2003a; Mavrakis *et al.,* 2004; Oka *et al.,* 2007; Bécart *et al.,* 2009	-	-	-	5	-
Protein kinase C alpha type (PRKCA)	P17252	77 kDa	Keenan and Kelleher, 1998; Brandt *et al.,* 2002; Hryciw *et al.,* 2005; Larsson, 2006; Worthmann *et al.*, 2013	-	-	3	-	-
RNA SPLICING AND PROCESSING								
Genes (28)	Accession No	Molecular Weight	Reference	FL	N-ter	PH	C-ter	Negative control
Heterogeneous nuclear ribonucleoproteins A2/B1 (HNRNPA2B1)	P22626	37 kDa	Mayeda *et al.,* 1994; Martinez-Contreras *et al.,* 2006; He and Smith, 2009; Clower *et al.,* 2010; David *et al.,* 2010; Alarcon *et al.,* 2015	6	-	8	8	-

Heterogeneous nuclear ribonucleoprotein A3 (HNRNPA3)	P51991	40 kDa	Martinez-Contreras *et al.,* 2007; Jurica *et al.,* 2002; Papadapoulou *et al.,* 2002	11	4	10	12	-
Heterogeneous nuclear ribonucleoprotein R (HNRNPR)	O43390	71 kDa	Mourelatos *et al.,* 2001; Jurica *et al.,* 2002; Martinez-Contreras *et al.,* 2007	4	-	5	5	-
Heterogeneous nuclear ribonucleoproteins A/B (HNRNPAB)	D6R9P3	30 kDa	Mayeda *et al.,* 1994; Martinez-Contreras *et al.,* 2006; He and Smith, 2009	3	-	-	-	-
Heterogeneous nuclear ribonucleoprotein H3 (HNRNPH3)	P31942	37 kDa	Mahé *et al.,* 1997; Honore, 2000; Mauger *et al.,* 2008	4	-	4	3	-
Heterogeneous nuclear ribonucleoprotein Q (SYNCRIP)	O60506	70 kDa	Neubauer *et al.,* 1998; Mourelatos *et al.,* 2001; Jurica *et al.,* 2002;	3	-	1	3	-
Ribosomal RNA processing protein 1 homolog B (RRP1B)	Q14684	84 kDa	Lee *et al.,* 2013; Lee *et al.,* 2014	3	-	-	8	-
Splicing factor U2AF 35 kDa subunit-like protein (U2AF1L5)	P0DN76	28 kDa	Das *et al.,* 2000; Jurica *et al.,* 2002; Zhang *et al.,* 1992; Wu *et al.,* 1999; Ilagan *et al.,* 2015	-	-	3	4	-
Splicing factor U2AF 65 kDa subunit (U2AF2)	P26368	54 kDa	Zamore *et al.,* 1992; Berglund *et al.,* 1998; Das *et al.,* 2000; Zhang *et al.,* 1992; Jurica *et al.,* 2002	-	-	-	3	-
RNA-binding protein Raly (RALY)	Q9UKM9	32 kDa	Rhodes *et al., 1*997; Jurica *et al.,* 2002; Tenzer *et al.,* 2013	4	-	-	5	-
Cluster of RNA-binding protein FUS (FUS)	P35637	53 kDa	Ishigaki *et al.,* 2012; Yu and Reed, 2015; Yamaguchi and Takanashi, 2016	-	-	4	-	-
116 kDa U5 small nuclear ribonucleoprotein component (EFTUD2)	Q15029	109 kDa	Fabrizio *et al.,* 1997; Lines *et al.,* 2012; De Arras *et al.,* 2014	3	-	-	-	-
Cluster of Polypyrimidine tract-binding protein 1 (PTBP1)	A0A0U1RRM4	62 kDa	Amir-Ahmady *et al.,* 2005; Spellman and Smith, 2006; Sharma *et al.,* 2008; Xue *et al.,* 2009 Llorian *et al.,* 2010; Kafasla *et al.,* 2012; Keppetipola *et al.,* 2012; Han *et al.,* 2014	3	-	-	-	-
SRSF protein kinase 1 (SRPK1)	Q96SB4	74 kDa	Gui *et al.,* 1994; Xiao and Manley, 1997; Ngo *et al.,* 2005;	-	-	-	3	-

			Ma *et al.,* 2008; Ghosh and Adams, 2011; Oltean *et al.,* 2012; Zhou and Fu, 2013; Gonçalves *et al.,* 2014					
Pre-mRNA-processing factor 40 homolog A (PRPF40A)	O75400	109 kDa	Kao and Siliciano, 1996; Abovich and Rosbash, 1997; Bedford *et al.,* 1997; Lin *et al.,* 2004; Becerra *et al.,* 2016	4	-	-	3	-
Pre-mRNA-processing-splicing factor 8 (PRPF8)	Q6P2Q9	274 kDa	Teigelkamp *et al.,* 1995; Reyes *et al.,* 1999; Collins *et al.,* 1999; McKie *et al.,* 2001; Grainger and Beggs, 2005; Tanackovic *et al.,* 2011; Wickramasinghe *et al.,* 2015 Boesler *et al.,* 2015	-	-	7	4	-
Cluster of Putative RNA-binding protein Luc7-like2 (LUC7L2)	A0A0A6YYJ8	54 kDa	Puig *et al.,* 2007; Howell *et al.,* 2007; Hosono *et al.,* 2013; Hershberger *et al.,* 2016	8	-	5	9	-
Cisplatin resistance-associated overexpressed protein, isoform CRA_b (LUC7L3)	J3KPP4	58 kDa	Nishii *et al.,* 2000; Gao *et al.,* 2011; Gao and, Dudley, 2013	-	-	-	3	-
Cluster of Transformer-2 protein homolog beta (TRA2B)	P62995	34 kDa	Hofmann *et al.,* 2000; Stoilov *et al.,* 2004; Wang *et al.,* 2005; Grellscheid *et al.,* 2011; Elliott *et al.,* 2012	4	-	3	5	-
Serine/arginine-rich-splicing factor 1 (SRSF1)	J3KTL2	28 kDa	Krainer and Maniatis, 1985; Krainer *et al.,* 1990; Zahler *et al.,* 1992; Zuo and Manley, 1993; Kohtz *et al.,* 1994; Cao *et al.,* 1997; Ghigna *et al.,* 2005; Anczuków *et al.,* 2015	4	-	-	4	-
Serine/arginine-rich-splicing factor 3 (SRSF3)	A0A087X2D0	10 kDa	Zahler *et al.,* 1992 Jia *et al.,* 2009; Sen *et al.,* 2009; Manley and Krainer, 2010; Majerciak *et al.,* 2014; Ajiro *et al.,* 2016	2	-	-	-	-
Serine/arginine-rich-splicing factor 7 (SRSF7)	A0A0B4J1Z1	16 kDa	Cavaloc *et al.,* 1994; Popielarz *et al.,* 1995; Gao *et al.,* 2007; Manley and Krainer, 2010	4	-	2	2	-
RNA-binding protein 25 (RBM25)	P49756	100 kDa	Fortes *et al.,* 2007; Zhou *et al.,* 2008; Gao *et al.,* 2011; Gao and, Dudley, 2013	3	-	-	4	-
RNA-binding protein 39	A0A0U1RQH7	27 kDa	Dowhan *et al.,* 2005; Huang *et al.,* 2012; Mai *et al.,* 2016;	3	-	-	3	-

(Fragment) (RBM39)			Stepanyuk *et al.,* 2016					
KH domain-containing, RNA-binding, signal transduction-associated protein 1 (KHDRBS1)	Q07666	48 kDa	Matter *et al.,* 2002; Paronetto *et al.,* 2010; Iijima *et al.,* 2011; Gaytan-Cervantes *et al.,* 2017	-	-	3	-	-
poly(A) binding protein cytoplasmic 1 (PABPC1)	A0A087WTT1	59 kDa	Horan *et al.,* 2015; Peng *et al.,* 2017	5	-	9	3	-
Interleukin enhancer-binding factor 2 (ILF2)	Q12905	43 kDa	Marchesini *et al.,* 2016; Marchesini *et al.,* 2017	-	-	5	-	-
Interleukin enhancer-binding factor 3 (ILF3)	Q12906	95 kDa	Chaumet *et al.,* 2013; Wu *et al.,* 2017	-	-	5	-	-
TRANSLATION								
Genes (13)	Accession No	Molecular Weight	Reference	FL	N-ter	PH	C-ter	Negative control
Cluster of 40S ribosomal protein S16 (RPS16)	P62249	16 kDa	Wagner and Perry, 1985; Wool *et al.,* 1996; Yoshihama *et al.,* 2002; Ghosh *et al.,* 2014	4	-	4	3	-
40S ribosomal protein SA (RPSA)	P08865	33 kDa	Wool *et al.,* 1996 Sato *et al.,* 1999; Yoshihama *et al.,* 2002	5	-	8	9	-
60S ribosomal protein L35a (RPL35A)	P18077	13 kDa	Kuzumaki *et al.,* 1987; Wool *et al.,* 1996; Yoshihama *et al.,* 2002	3	-	3	-	-
60S ribosomal protein L39 (RPL39)	P62891	6 kDa	Wool *et al.,* 1996; Yoshihama *et al.,* 2002	-	-	3	-	-
Eukaryotic translation initiation factor 3 subunit I (EIF3I)	Q13347	37 kDa	Verlhac *et al*., 1997; Phan *et al*., 1998; Kahvejian *et al.,* 2001; Hinnebusch 2006; Masutani *et al.,* 2007	-	-	3	-	-
Eukaryotic translation initiation factor 5A (Fragment) (EIF5A)	P63241	16 kDa	Schuller *et al.,* 2017	3	-	-	4	-
Elongation factor 1-gamma (EEF1G)	P26641	50 kDa	Carvalho *et al.,* 1984; Proud, 1994; Stapulionis and Deutscher, 1995; Negrutskii and El'skaya, 1998; Sang Lee *et al.,* 2002	5	-	8	7	-
poly(A) binding protein cytoplasmic 1 (PABPC1)	P11940	59 kDa	Imataka *et al.,* 1998; Craig *et al.,* 1998; Kahvejian *et al.,* 2001; Kühn and Wahle, 2004; Derry *et al*., 2006; Kini *et al.,* 2015	5	-	9	3	-
Nucleophosmin (NPM1)	P06748	33 kDa	Pang *et al.,* 2003	4	-	6	6	-
tRNA aminoacylation for protein translation								

Methionine--tRNA ligase, cytoplasmic (MARS)	P56192	101 kDa	Carter, 1993; Ibba and Soll, 2000; Ko *et al.,* 2000; Lee *et al.,* 2004; Kwon *et al.,* 2011	3	-	9	-	-
Glycine--tRNA ligase (GARS)	P41250	83 kDa	Carter, 1993; Ibba and Soll, 2000; Lee *et al.,* 2004; Antonellis *et al.,* 2006; Oprescu *et al.,* 2017	-	-	4	3	-
Arginine--tRNA ligase, cytoplasmic (RARS)	P54136	75 kDa	Carter, 1993; Ibba and Soll, 2000; Lee *et al.,* 2004; Ling *et al.,* 2005; Fu *et al.,* 2014	-	-	3	-	-
Lysine--tRNA ligase (KARS)	Q15046	68 kDa	Carter, 1993; Ibba and Soll, 2000; Lee *et al.,* 2004; Guzzo and Yang, 2008	3	-	-	-	-
TRANSCRIPTION								
Genes (36)	Accession No	Molecular Weight	Reference	FL	N-ter	PH	C-ter	Negative control
Interleukin enhancer-binding factor 2 (ILF2)	Q12905	43 kDa	Reichman *et al.,* 2002; Nakadai *et al.,* 2015; Higuchi *et al.,* 2016	-	-	5	-	-
Interleukin enhancer-binding factor 3 (ILF3)	Q12906	95 kDa	Reichman *et al.,* 2002; Nakadai *et al.,* 2015; Higuchi *et al.,* 2016	-	-	5	-	-
Transcription intermediary factor 1-beta (TRIM28)	Q13263	89 kDa	Friedman *et al.,* 1996; Agata *et al.,* 1999; Wang *et al.,* 2005; Suzuki *et al.,* 2008; Bunch and Calderwood, 2015	-	-	-	3	-
Transcriptional repressor CTCF (CTCF)	P49711	83 kDa	Filippova *et al.,* 1996; Yu *et al.,* 2004; Kurukuti *et al.,* 2006; Majumder *et al.,* 2008; Holwerda and de Laat, 2013; Kim *et al.,* 2015	4	-	-	8	-
FACT complex subunit SSRP1 (SSRP1)	Q08945	81 kDa	Orphanides *et al.,* 1998; Dyer *et al.,* 1998; Spencer *et al.,* 1999; Zeng *et al.,* 2002; Li *et al.,* 2007	9	-	3	10	
Heterochromatin protein 1-binding protein 3 (HP1BP3)	Q5SSJ5	61 kDa	Dutta *et al.,* 2014; Garfinkel *et al.,* 2015	3	-	4	7	-
Arginine and glutamate-rich protein 1 (ARGLU1)	Q9NWB6	33 kDa	Zhang *et al.,* 2011	3	-	-	-	-
Gamma-interferon-inducible protein 16 (IFI16)	Q16666	88 kDa	Johnstone *et al.,* 1998; Johnstone *et al.,* 2000	-	-	3	8	-
SWI/SNF-related matrix-associated actin-	O60264	122 kDa	Cavellan *et al.,* 2006; Dluhosova *et al.,* 2014	-	-	4	8	-

dependent regulator of chromatin subfamily A member 5 (SMARCA5)								
Nucleophosmin (NPM1)	P06748	33 kDa	Swaminathan *et al.,* 2005; Liu *et al.,* 2012	4	-	6	6	-
Cluster of Histone-binding protein RBBP4 (RBBP4)	Q09028	48 kDa	Qian *et al.,* 1993; Zhang *et al.,* 1999; Wolffe *et al.,* 2000; Allen *et al.,* 2013; Wang *et al.,* 2016	-	-	4	-	-
Metastasis-associated protein MTA2 (MTA2)	O94776	75 kDa	Zhang *et al.,* 1999; Yao and Yang, 2003	-	-	-	4	-
Retinoblastoma-associated protein (RB1)	P06400	106 kDa	Horowitz, 1993; Burkhart and Sage, 2008; van den Heuvel and Dyson, 2008; Dick and Rubin, 2013; Miles *et al.,* 2014	-	-	3	-	-
Proliferation-associated protein 2G4 (PA2G4)	Q9UQ80	44 kDa	Xia *et al.,* 2001; Zhang *et al.,* 2003; Zhang and Hamburger, 2004; 2005	3	-	-	3	-
Chromobox protein homolog 3 (CBX3)	Q13185	21 kDa	Lehming *et al.,* 1998; Eissenberg and Elgin, 2000; 2014; Wang *et al.,* 2017	4	-	-	3	-
Staphylococcal nuclease domain-containing protein 1 (SND1)	Q7KZF4	102 kDa	Tong *et al.,* 1995; Yu *et al.,* 2017	9	-	3	5	-
RNA-binding protein Raly (RALY)	Q9UKM9	32 kDa	Cornella *et al.,* 2017; Rossi *et al.,* 2017	4	-	-	5	-
Nascent polypeptide-associated complex subunit alpha, muscle-specific form (NACA)	E9PAV3	205 kDa	Berkholz *et al.,* 2015	3	-	3	3	-
Histidine triad nucleotide-binding protein 1 (HINT1)	P49773	14 kDa	Weiske and Huber, 2006; Motzik *et al.,* 2017	-	-	4	-	-
Cluster of RNA-binding protein FUS (FUS)	P35637	53 kDa	Wang *et al.* 2008; Tan *et al.* 2012; Schwartz *et al.,* 2012; Yu and Reed, 2015	-	-	4	-	-
Scaffold attachment factor B2 (SAFB2)	Q14151	107 kDa	Hashimoto *et al.,* 2012; Hong *et al.,* 2012	-	-	3	-	-
Profilin-1 (PFN1)	P07737	15 kDa	Lederer *et al.,* 2005	-	-	3	-	-
26S protease regulatory subunit 7	P35998	49 kDa	Shibuya *et al.,* 1992	-	-	-	3	-

(PSMC2)								
26S proteasome non-ATPase regulatory subunit 11 (PSMD11)	O00231	47 kDa	Reactome database annotated in the Gene Expression pathway	3	-	-	-	-
High mobility group protein B2 (HMGB2)	P26583	24 kDa	Thomas, 2001; Bianchi and Agresti, 2005; Malarkey and Churchill, 2012; Aird *et al.,* 2016	-	-	-	2	-
Cluster of DNA topoisomerase 2-alpha (TOP2A)	P11388	174 kDa	Wang, 2002; Ju *et al*., 2006; Haffner *et al.,* 2011	3	-	6	9	-
Cluster of High mobility group protein B1 (HMGB1)	P09429	25 kDa	Thomas, 2001; Bianchi and Agresti, 2005; Malarkey and Churchill, 2012	3	-	3	6	-
Poly [ADP-ribose] polymerase 1 (PARP1)	P09874	113 kDa	Kraus and Lis, 2003; Krishnakumar and Kraus, 2010; Schiewer and Knudsen, 2014	5	-	5	4	-
Nucleolin (NCL)	P19338	77 kDa	Ying *et al.,* 2000; Rickards *et al.,* 2007; Chen and Xu, 2016	6	-	6		-
Protein LYRIC (MTDH)	Q86UE4	64 kDa	Meng *et al.,* 2012	6	-	-	12	-
Ribosomal RNA processing protein 1 homolog B (RRP1B)	Q14684	84 kDa	Crawford *et al.,* 2009; Paik *et al.,* 2010	3	-	-	8	-
KH domain-containing, RNA-binding, signal transduction-associated protein 1 (KHDRBS1)	Q07666	48 kDa	Hong *et al.,* 2002; Rajan *et al.,* 2008; Fu *et al.,* 2013; Li and Richard, 2016	-	-	3	-	-
Heterogeneous nuclear ribonucleoproteins A2/B1 (HNRNPA2B1)	P22626	37 kDa	Xuan *et al.,* 2016	6	-	8	8	-
Adipocyte enhancer-binding protein 1 (AEBP1)	Q8IUX7	131 kDa	He *et al.,* 1995; Kim *et al.,* 2001; Lyons *et al.,* 2005; Lyons *et al.,* 2006	-	-	-	3	-
Calreticulin (CALR)	P27797	48 kDa	Dedhar *et al.,* 1994; Burns *et al.,* 1994*;* Perrone *et al.,* 1999	6	-	-	7	-
METABOLIC PROCESSES								
Genes (17)	Accession No	Molecular Weight	Reference	FL	N-ter	PH	C-ter	Negative control
Bifunctional purine biosynthesis protein PURH (ATIC)	P31939	65 kDa	Cheong *et al.,* 2004; Jimenez and Puig, 2012; Lane and Fan, 2015	6	-	6	-	-

Phosphoribosylformylglycinamidine synthase (PFAS)	O15067	145 kDa	Lane and Fan, 2015	-	-	3	-	-
Hypoxanthine-guanine phosphoribosyltransferase (HPRT1)	P00492	25 kDa	Puig *et al.,* 2001; Sculley *et al.,* 2002; Duan *et al.,* 2004; Jimenez and Puig, 2012	-	-	4	-	-
Inosine-5'-monophosphate dehydrogenase 2 (IMPDH2)	P12268	56 kDa	Natsumeda *et al.,* 1990; Pimkin and Markham, 2009; Hedstrom, 2009	3	-	3	5	-
Multifunctional protein ADE2 (Fragment) (PAICS)	P07437	46 kDa	Lane and Fan, 2015	-	-	4	4	-
ATP synthase subunit gamma, mitochondrial (ATP5C1)	P36542	33 kDa	Kinosita *et al.,* 2000; Yoshida *et al.,* 2001; Leyva *et al.,* 2003; Itoh *et al.,* 2004	6	4	4	4	-
Cluster of ATP synthase subunit O, mitochondrial (ATP5O)	P48047	23 kDa	Kinosita *et al.,* 2000; Aggeler *et al.,* 2002; Leyva *et al*., 2003; Johnson *et al.,* 2005; Wu *et al.,* 2013	3	-	-	5	-
ATP synthase subunit g, mitochondrial (ATP5L)	O75964	8 kDa	Kinosita *et al.,* 2000; Leyva *et al.,* 2003	-	-	3	-	-
Cluster of Sodium/potassium-transporting ATPase subunit alpha-1 (ATP1A1)	P05023	113 kDa	Horisberger 1994; Blanco and Mercer, 1998; Crambert *et al.,* 2000	3	-	-	3	-
Cluster of Sarcoplasmic/endoplasmic reticulum calcium ATPase 2 (ATP2A2)	P16615	115 kDa	del Monte *et al.,* 1999; Dally *et al.,* 2006; Kranias and Hajjar, 2012	3	-	-	3	-
Stomatin-like protein 2, mitochondrial (STOML2)	Q9UJZ1	39 kDa	Christie *et al.,* 2011	-	-	4	7	-
Trifunctional enzyme subunit alpha, mitochondrial (HADHA)	P40939	83 kDa	Kamijo *et al.,* 1994; Rakheja *et al.,* 2002	-	-	6	4	-
3-hydroxyacyl-CoA dehydrogenase type-2 (HSD17B10)	Q99714	27 kDa	Shafqat *et al.,* 2003; Oerum *et al.,* 2017	4	-	-	-	-
Propionyl-CoA carboxylase alpha chain, mitochondrial	P05165	44 kDa	Rosenberg, 1983; Lamhonwah *et al.,* 1986	-	-	5	-	-

(Fragment) (PCCA)								
Glutamine--fructose-6-phosphate aminotransferase [isomerizing] 1 (GFPT1)	Q06210	79 kDa	McKnight *et al.,* 1992; Sayeski *et al.,* 1994; Assrir *et al.,* 2014	-	-	7	-	-
Citrate synthase (CS)	O75390	45 kDa	Wiegand and Remington, 1986; Krebs and Weitzman, 1987	3	-	3	6	-
Prostaglandin E synthase 3 (PTGES3)	Q15185	19 kDa	Tanioka *et al.,* 2000	3	-	4	-	-
PROTEIN PROCESSING (FOLDING/UNFOLDING, MODIFICATION and DEGRADATION)								
Genes (15)	Accession No	Molecular Weight	Reference	FL	N-ter	PH	C-ter	Negative control
Calreticulin (CALR)	P27797	48 kDa``	Zapun *et al.,* 1998; Michalak *et al.,* 1999; Leach and Williams, 2003; Williams *et al.,* 2006; Ni and Lee, 2007	6	-	-	7	-
Calnexin (CANX)	P27824	68 kDa	Zapun *et al.,* 1998; Leach and Williams, 2003; Williams *et al.,* 2006; Ni and Lee, 2007	3	-	-	5	-
DnaJ homolog subfamily A member 1 (DNAJA1)	P31689	45 kDa	Davis *et al.,* 1998; Terada and Mori, 2000; Tzankov *et al.,* 2008	4	-	-	4	-
Hypoxia up-regulated protein 1 (HYOU1)	Q9Y4L1	111 kDa	Ikeda *et al.,* 1997; Bando *et al.,* 2000; Ni and Lee, 2007	15	-	4	20	-
Stress-induced-phosphoprotein 1 (STIP1)	P31948	63 kDa	Chen and Smith, 1998; Hernández *et al.,* 2002; Song and Masison, 2005	4	-	-	4	-
Protein disulfide-isomerase A6 (PDIA6)	Q15084	48 kDa	Kikuchi *et al.,* 2002; Hatahet and Ruddock, 2009; Eletto *et al.,* 2014	4	-	-	5	-
Cluster of Stress-70 protein, mitochondrial (HSPA9)	P38646	74 kDa	Liu *et al.,* 2001; Wadhwa *et al.,* 2002; Voos *et al.,* 2013	10	4	15	13	-
Peptidyl-prolyl cis-trans isomerase A (PPIA)	P62937	18 kDa	Takahashi *et al*., 1989; Kontopidis *et al.,* 2004; Obchoei *et al.,* 2009	6	-	6	6	-
Cluster of T-complex protein 1 subunit theta (CCT8)	P50990	60 kDa	Gao *et al.,* 1992; Craig *et al.,* 1994; Morimoto *et al.,* 1994; Kubota *et al.,* 1995; Frydman, 2001; Dekker *et al.,* 2008	9	3	5	11	-
Dolichyl-diphosphoolig	P39656	49 kDa	Kelleher *et al.,* 1992;	3	-	-	-	-

osaccharide--protein glycosyltransferase 48 kDa subunit (DDOST)			Kelleher and Gilmore, 2006; Roboti and High, 2012; Jones *et al.,* 2012					
Dolichyl-diphosphooligosaccharide--protein glycosyltransferase subunit 1 (RPN1)	P04843	69 kDa	Kelleher *et al.,* 1992; Kelleher and Gilmore, 2006; Wilson and High, 2007; Wilson *et al.,* 2008	8	-	-	8	-
Dolichyl-diphosphooligosaccharide--protein glycosyltransferase subunit 2 (RPN2)	P04844	69 kDa	Kelleher *et al.,* 1992; Tominaga *et al.,* 2014; Kelleher and Gilmore, 2006	8	4	8	9	-
Prostaglandin E synthase 3 (PTGES3)	Q15185	19 kDa	Bose *et al.,* 1996; Johnson and Craig, 1997; Buchner, 1999; Weaver *et al.,* 2000	3	-	4	-	-
26S protease regulatory subunit 7 (PSMC2)	P35998	49 kDa	Kanayama *et al.,* 1992; Chen *et al.,* 1997; Grune *et al.,* 2011	-	-	-	3	-
26S proteasome non-ATPase regulatory subunit 11 (PSMD11)	O00231	47 kDa	Kanayama *et al.,* 1992; Vilchez *et al.,* 2012	3	-	-	-	-

Table 7.1 Table demonstrates the GO term enrichments of 103 proteins. Actin cytoskeleton organisation, RNA splicing and processing, translation, transcription, metabolic processes and protein processing are the leading biological processes which DEF6 might be involved. FL: BirA*-Full-length DEF6, N-ter: BirA*-N terminal DEF6, PH: BirA*-PH domain DEF6, C-ter: BirA*-C terminal DEF6 and Negative control: Only BirA* plasmid. Peptide numbers were also included. Yellow highlights indicate the proteins selected for immunological synapse formation and immunofluorescence (CORO1A and HNRNPA2B1).

7.3. DEF6 might be involved in several processes in Jurkat T cells

To further explore the biological processes which DEF6 might be involved, KEGG and/or Reactome pathway databases and STRING interaction network were performed for individual biological processes.

7.3.1 Actin Cytoskeleton Organisation

7 proteins (5%) of 127 identified proteins were enriched in the actin cytoskeleton organisation category **(Figure 7.8)**. 5 proteins, Rho GTPase (RHOG), Rac GTPase (RAC2), Profilin (PFN1), Filamin (FLNB) and PKC (PRKCA) are involved in actin cytoskeleton organisation and focal adhesion pathways according to the KEGG pathway database. Despite their known function in actin cytoskeleton organisation, DEF6 and CORO1A were not annotated. **(Figure 7.9)**. In addition, the relationships among the identified proteins for actin cytoskeleton organisation are shown in **Figure 7.10** as annotated in STRING.

The role of DEF6 in the actin cytoskeleton organisation process has already been known as it exhibits a GEF activity to activate Rac1, RhoA and Cdc42 GTPases in T and NIH 3T3 cells and also Rac2 GTPase *in vitro* (Gupta *et al.,* 2003; Mavrakis *et al.,* 2004; Bécart *et al.,* 2008). DEF6-mediated activation of Rac1 and Cdc42 GTPases results in the regulation of actin cytoskeleton dynamics leading to the formation of immunological synapse (IS), NFAT activation and Th1 and Th2 inflammatory responses (Gupta *et al.,* 2003; Bécart *et al.,* 2008; 2009). Moreover, Fanzo *et al.,* (2006) have shown that $Def6^{-/-}$ T cells resulted in a defective T cell response characterised by reduced ERK1/2 activation, decreased c-Fos induction, disrupted immunological synapse formation and defective actin polymerisation. The constitutively active form of Rac2 rescued the actin polymerisation defect in $Def6^{-/-}$ T cells, indicating the defects in the cytoskeletal organisation and thus in the IS are dependent on the ability of Def6 to activate Rho GTPases (Fanzo *et al.,* 2006). Therefore, identifying RhoG and Rac2 in the DEF6 interactome (Table 7.1) was consistent with the previous studies, suggesting that DEF6 might also activate RhoG and Rac2 GTPases promoting the cytoskeleton changes and immunological responses (Gauthier-Rouvière *et al.,* 1998; Yu *et al.,* 2001; Vigorito *et al.,* 2004; Tybulewicz and Henderson, 2009).

In addition, several isoforms of PKC family of serine-threonine kinases, like PKCα, PKCθ, PKCδ, have been found to participate in many signalling cascades including actin cytoskeleton arrangement (Tang *et al.,* 1997; Harrington *et al.,* 1997; Keenan and Kelleher, 1998; Romanova *et al.,* 1999; Rojnuckarin and Kaushansky, 2001; Brandt *et al.,* 2002; Larsson, 2006), suggesting that the identified isoform of PKC, PRKCA (PKCα), (Table 7.1) might be a

downstream or upstream target of DEF6 regulating the actin cytoskeleton dynamics. Consistent with these studies, DEF6 has specifically been shown as a downstream target of atypical PKC, aPKCλ/ι, regulating Rac1, RhoA and Cdc42 as increased activation of Rho GTPases, particularly Rac1, was observed in PKCλ/ι-deficient podocytes due to the up-regulation of DEF6 (Worthmann *et al.,* 2013). Furthermore, a Bioplex 2.0 network analysis exploring the human interactome identified 56473 interactions in HEK293T cells by affinity capture-MS and PKCθ (PRKCQ) was shown as one of the interactors of DEF6 (Huttlin *et al.,* 2017 and BioGrid database).

Moreover, profilin and filamin are the known regulators of actin cytoskeleton (ref. in Table 7.1) and were found to be phosphorylated by PKC which may modulate their function in actin cytoskeleton (Kawamoto and Hidaka, 1984; Hansson *et al.,* 1988; reviewed in Keenan and Kelleher, 1998). Therefore, interaction with PKC would explain identifying Profilin-1 and Filamin-B in the DEF6 interactome.

Lastly, Coronin-1A (CORO1A) regulates cellular responses that require actin cytoskeleton organisation, including TCR-mediated signalling, phagocytosis and cell motility. As an F-actin binding protein it localises to the actin-rich structures in immune cells like leading edges of T cells and IS (de Hostos, 1999; Gandhi and Goode, 2008; Mace and Orange, 2014). A model was proposed explaining how coronin targets cofilin and Arp2/3 complex to modulate the actin dynamics (Gandhi and Goode, 2008). According to this model, while coronin recruits cofilin that disassembles the old actin filaments at the rear of actin dynamics, it recruits Arp2/3 complex that expands the actin dynamics by nucleation and branching at the front (Blanchoin and Pollard, 1999; Goley and Welch, 2006; Gandhi and Goode, 2008).

Consistent with the requirement of actin cytoskeleton organisation in T cell signalling and IS formation (Dustin and Cooper, 2000), Coro1A-deficient mice have shown T cell immunodeficiency characterised by defects in T cell survival, cell migration and TCR signalling (Foger *et al,* 2006; Shiow *et al.,* 2008; Mugnier *et al,* 2008; Mueller *et al.,* 2011; reviewed in Castro-Castro *et al.,* 2011). It has been suggested that Coro1A forms a complex with ArhGEF7, Pak1 and RhoGDIα for translocating and activating Rac1 in T lymphocytes (Castro-Castro *et al.,* 2011). Impaired activation of Rac1 was observed in Coro1A-deficient T cells upon the stimulation by the CXCL12 chemokine (Foger *et al,* 2006). Specifically, Coro1A has been shown to localise with F-actin to the natural killer (NK) cell IS for the deconstruction of F-actin, enabling effective granule secretion and NK cell cytotoxicity. Indeed, loss of Coro1A resulted in enhanced F-actin density at the IS and decreased NK cell cytotoxicity (Mace and Orange, 2014).

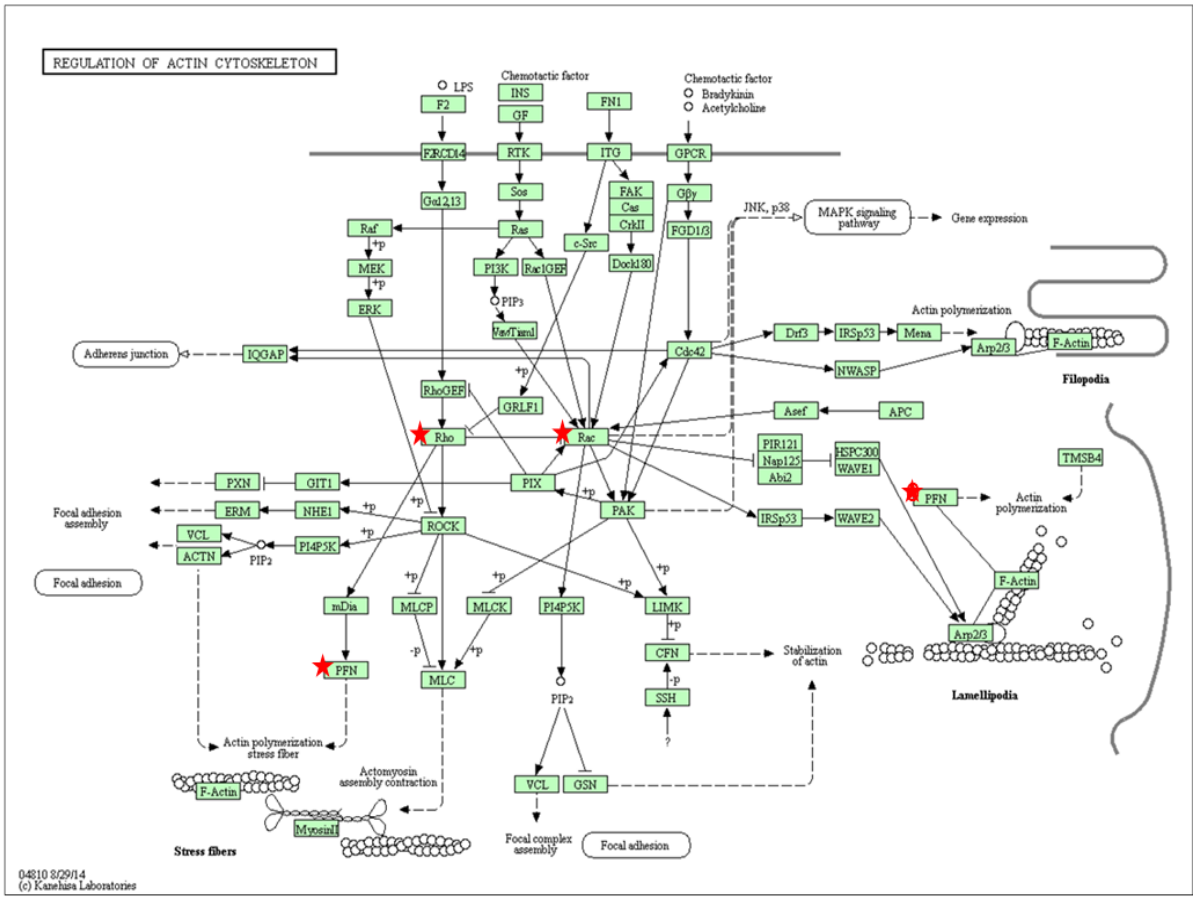
DEF6 was also found to be recruited to the IS to exhibit its GEF activity against Rac1 and Cdc42 upon the induction of TCR-mediated signalling cascades. Tyrosine-phosphorylation by Lck and binding to $PI(_{3,4,5})P_3$ via its PH domain are required for its translocation (Gupta *et al.,* 2003a). Therefore, considering the common roles of CORO1A and DEF6 in actin cytoskeleton and IS, CORO1A was chosen for further analysis. Immunohistochemistry was performed on Jurkat T cells during IS formation **(Figures 7.11)** and on resting Jurkat T cells **(Figures 7.12)** to reveal whether CORO1A co-localises with DEF6 at the IS or at the F-actin structures of resting Jurkat T cells.

To form immunological synapses, Raji B cells were stained in the dark with calcein blue and loaded with antigen by incubating in full RPMI containing *Staphylococcus aureus* enterotoxin A and *Staphylococcus aureus* enterotoxin B. Raji B cells were incubated with Jurkat T cells for 1 hour at 37°C, 5% CO_2. Cells were then diluted, applied to Poly-L-Lysine coated coverslips, fixed, and stained using rabbit anti-DEF6 and mouse anti-CORO1A. Primary antibodies were then labelled using goat anti-rabbit 568 and goat anti-mouse 488, respectively. Images were taken as a single Z plane or a Z stack at 63x magnification using a Zeiss LSM710 confocal microscope **(Figures 7.11A)** and orthogonal views from the YZ and XZ perspective were created from the Z stack images **(Figures 7.11B)**. DEF6 and CORO1A were both localised to the IS and a clear co-localisation was observed in **Figures 7.11A,** (white arrowheads). Even though DEF6 was found more in the central/peripheral regions of the IS, possibly the central supramolecular activation cluster (cSMAC) and peripheral supramolecular activation cluster (pSMAC) regions and CORO1A was found more in the distal region of the IS, possibly the distal supramolecular activation cluster (dSMAC), a partial co-localisation was observed **(Figures 7.11B)**. Orthogonal views from the YZ **(Figures 7.11Bii)** and XZ **(Figures 7.11Biii)** perspective confirmed the partial co-localisation and also the localisation of DEF6 to the cSMAC/pSMAC of IS and CORO1A to the dSMAC of IS. Consistent with its role of regulating actin cytoskeleton as mentioned above, Arp2/3 and cofilin were also found to be localised to the dSMAC (Sims *et al.,* 2007), suggesting that CORO1A regulates the actin cytoskeleton dynamics of IS in the dSMAC.

To further investigate whether DEF6 co-localises with CORO1A at the F-actin structures of resting T cells, cells were diluted, applied to Poly-L-Lysine coated coverslips, fixed, and stained using rabbit anti-DEF6 and mouse anti-CORO1A. Primary antibodies were labelled using goat anti-rabbit 568 and goat anti-mouse 488, respectively. Images were taken as a single Z plane or a Z stack at 63x magnification using a Zeiss LSM710 confocal microscope **(Figures 7.12A)** and orthogonal views from the YZ and XZ perspective were created from the

Z stack images **(Figures 7.12B)**. DEF6 and CORO1A were both localised to F-actin-rich structures like the membrane protrusions. Even though there was not a complete co-localisation, DEF6 co-localised with CORO1A at some parts of the membrane protrusions **(Figures 7.12A-B-;** white arrowheads**)**. Orthogonal views from the YZ **(Figures 7.12Bii)** and XZ **(Figures 7.12Biii)** perspective confirmed the co-localisation at some places of membrane protrusions.

Thus we concluded that, DEF6 and CORO1A co-localised partially at the IS during IS formation and at the membrane protrusions in resting Jurkat T cells.



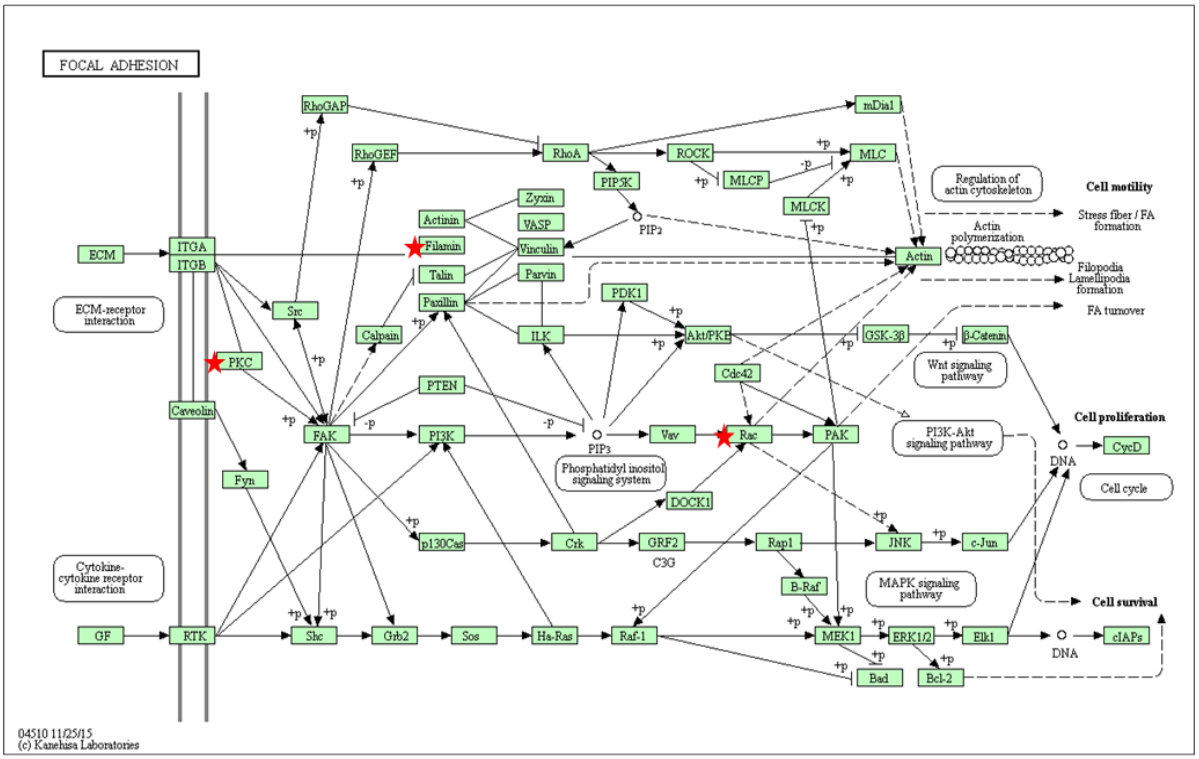


Figure 7.9 Actin cytoskeleton organisation and focal adhesion pathways are shown as in the KEGG pathway database. Rho and Rac GTPases, Profilin (PFN), Filamin and Protein kinase C (PKC) are involved in the actin cytoskeleton and focal adhesion pathways. Red stars (★) indicate the identified proteins (Table 7.1).

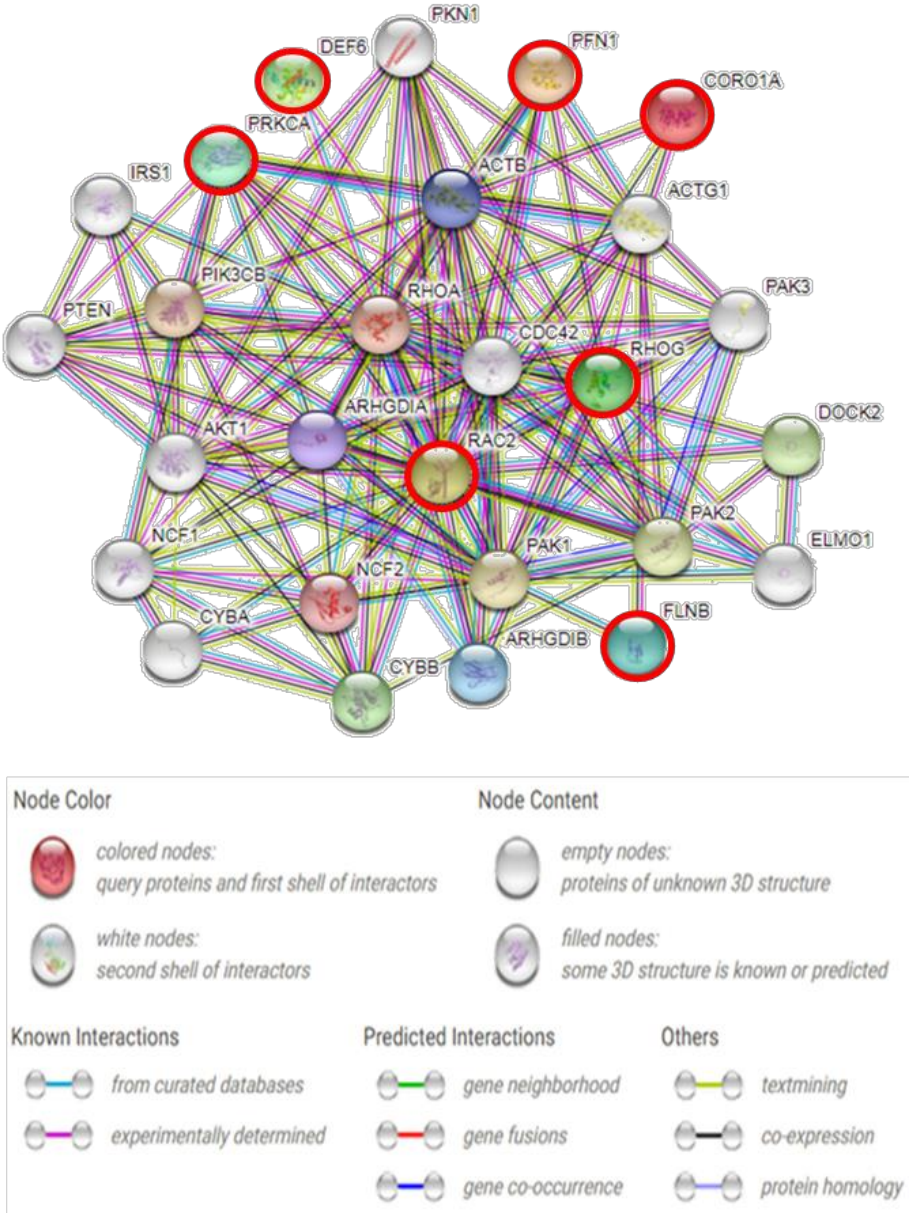


Figure 7.10 Interaction network of the 7 proteins (Table 7.1) in the biological process of actin cytoskeleton organisation is shown as annotated in STRING. Red circles (O) indicate the identified proteins.

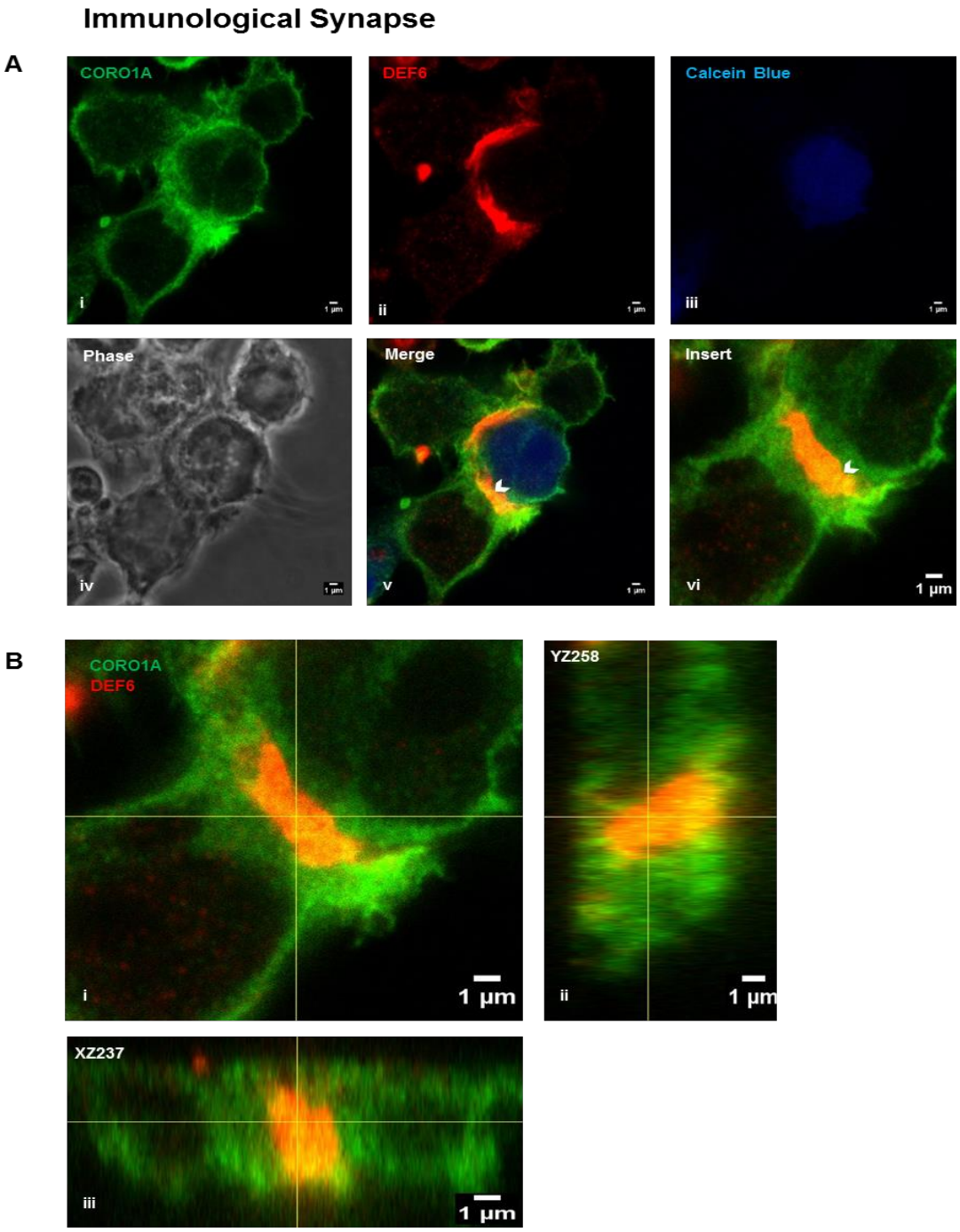


Figure 7.11 DEF6 and CORO1A co-localised partially during IS formation. Raji B cells were stained with Calcein Blue and loaded with antigens. Raji B cells were then incubated with Jurkat T cells and immunological synapses were generated. Cells were fixed and stained using rabbit anti-DEF6 and mouse anti-CORO1A primary antibodies. Goat anti-rabbit 568 and goat anti-mouse 488 antibodies were used to label primary antibodies. Cells were then loaded to Poly-L-Lysine coated coverslips and images were taken as a single Z plane **(A)** or a Z-stack **(B)** at 63x magnification using Zeiss LSM710 confocal microscope. **(A)** DEF6 and CORO1A were both localised to the IS and co-localised partially **(v-vi)**. **(B)** Orthogonal views from the YZ **(ii)** and XZ **(iii)** perspective also indicated the co-localisation and also the localisation of DEF6 to the centre of the IS, possibly cSMAC or pSMAC, and of CORO1A to the distal position of the IS, possibly dSMAC. CORO1A (green), DEF6 (red), calcein blue (blue), phase and merged images including calcein blue are shown. Scale bars indicate 1 µm.

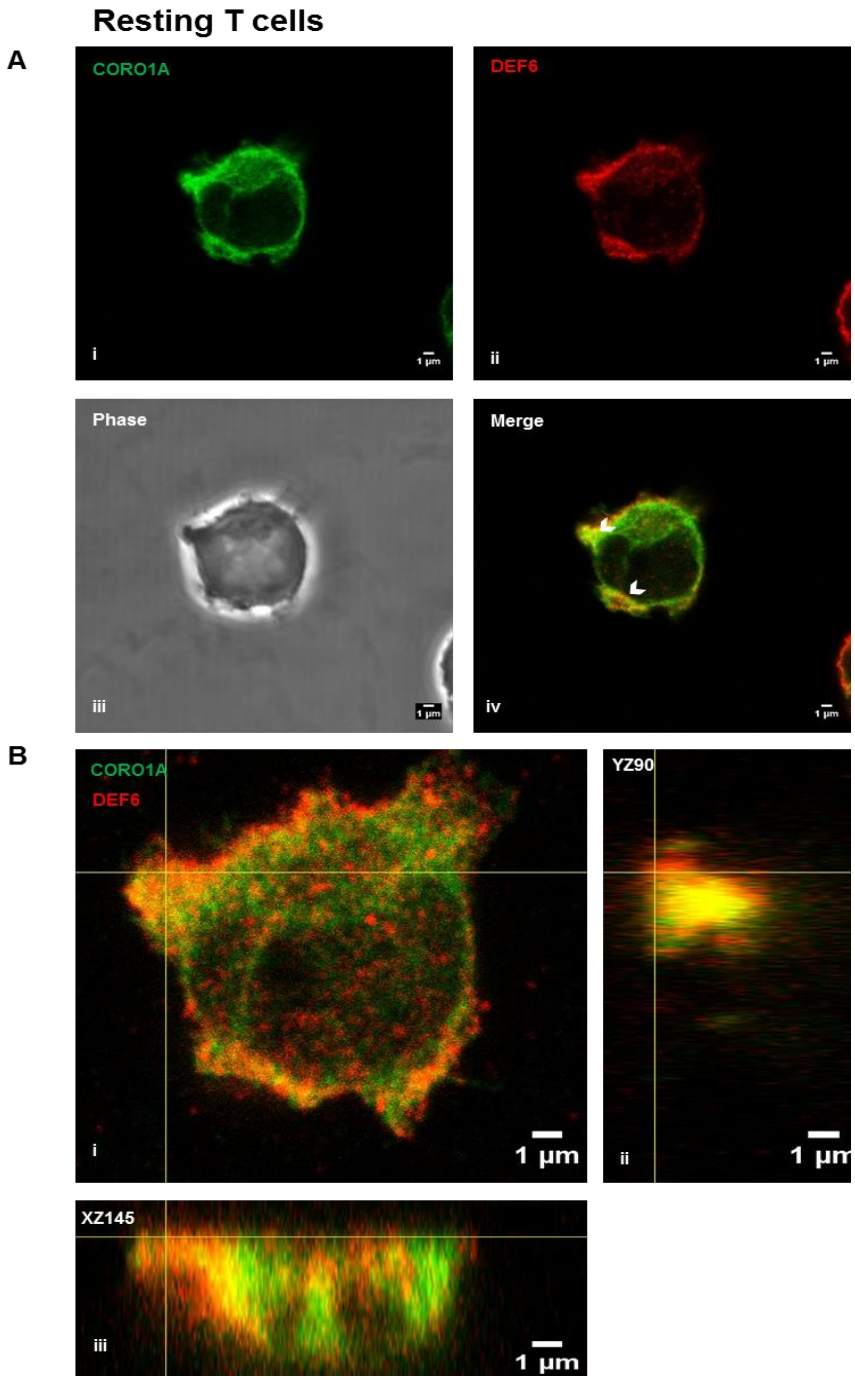


Figure 7.12 DEF6 and CORO1A were localised to the F-actin-rich structures and co-localised at some points of the cell protrusions. Cells were fixed and stained using rabbit anti-DEF6 and mouse anti-CORO1A primary antibodies. Goat anti-rabbit 568 and goat anti-mouse 488 antibodies were used to label primary antibodies. Cells were then loaded to Poly-L-Lysine coated coverslips and images were taken as a single Z plane **(A)** or a Z-stack **(B)** at 63x magnification using Zeiss LSM710 confocal microscope. **(A)** DEF6 and CORO1A were localised to F-actin rich structures, membrane and protrusions and partial co-localisation was observed at the protrusions, indicated with white arrowheads. **(B)** Orthogonal views from the YZ **(ii)** and XZ **(iii)** perspective also indicated the partial co-localisation between DEF6 and CORO1A. CORO1A (green), DEF6 (red), phase and merged images are shown. Scale bars indicate 1 µm.

7.3.2 RNA Splicing and Processing

15 proteins, FBP11 (PRPF40A), S164 (RBM25), U2AF (U2AF2/U2AF1L5), Snu114 (EFTUD2), Prp8 (PRPF8), hnRNPs (HNRNPA2/B1, HNRNPA3, HNRNPH3, HNRNPR, HNRNPAB, HNRNPQ/SYNCRIP) and SR (SRSF1, SRSF3 and SRSF7) are annotated as components of the spliceosome in the KEGG pathway database, while the remaining 13 proteins were not demonstrated since the splicing process is not illustrated in detail **(Figure 7.13).** The interaction network among the identified proteins for splicing and processing is shown in **Figure 7.14** as annotated in STRING.

This analysis implicates DEF6 in RNA splicing and processing, a potential novel function that has not been described yet (Huttlin *et al.,* 2017 and BioGrid database). To test whether DEF6 is involved in these processes, HNRNAPA2/B1 was selected to determine whether it co-localises with DEF6. HNRNAPA2/B1 was selected because (i) it plays various roles in biological processes including RNA splicing/processing, alternative splicing and transcription **(Table 7.1;** Martinez-Contreras *et al.,* 2006; He and Smith, 2009; Clower *et al.,* 2010; David *et al.,* 2010; Alarcon *et al.,* 2015; Xuan *et al.,* 2016), (ii) it represents one out of the six distinct HNRNP proteins identified and (iii) the availability and compatibility of antibodies for further analysis. Immunohistochemistry was performed on Jurkat T cells during IS formation **(Figure 7.15)** and on resting Jurkat T cells **(Figure 7.16)** to reveal whether DEF6 co-localises with HNRNPA2/B1 or active splicing sites. Confocal microscopy indicated no overlap of DEF6 and HNRNPA2B1 **(Figures 7.15A)**. DEF6 was localised to the IS **(Figures 7.15Aii)** while HNRNPA2B1 was localised to the nucleus **(Figures 7.15Ai)**. Similarly, DEF6 and HNRNPA2B1 did not co-localise in resting T cells. While DEF6 was localised to the actin-rich structures like membrane and protrusions, HNRNPA2B1 was localised to the nucleus **(Figures 7.16A)**. Orthogonal views from the YZ **(Figures 7.16Bii)** and XZ **(Figures 7.16Biii)** perspective confirmed the absence of co-localisation between DEF6 and HNRNPA2B1.

Taken together, DEF6 and HNRNPA2B1 did not co-localise during the IS formation and in resting Jurkat T cells.

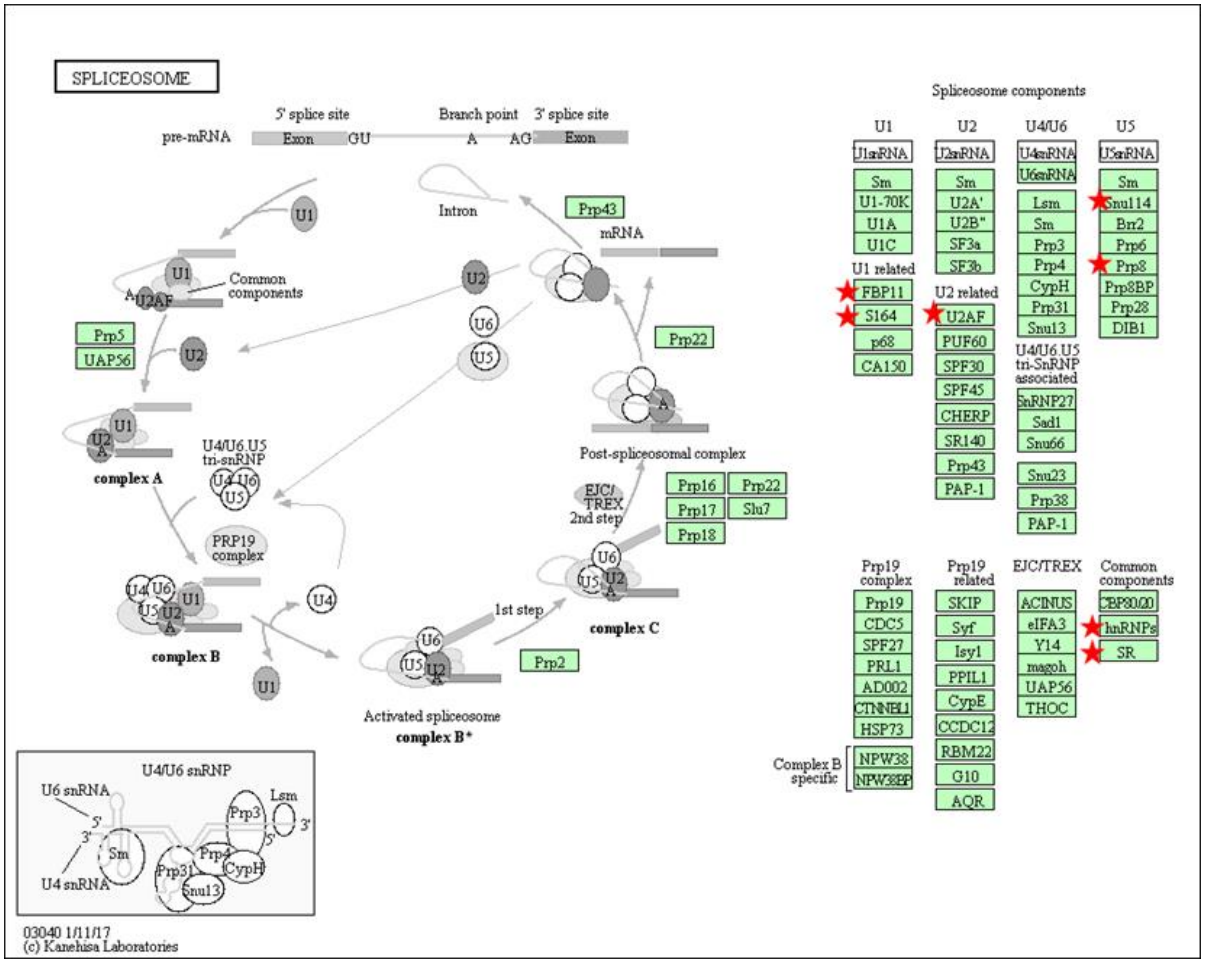


Figure 7.13 Spliceosome-mediated RNA splicing is shown as in the KEGG pathway database. FBP11 (PRPF40A), S164 (RBM25), U2AF (U2AF2 and U2AF1L5), Snu114 (EFTUD2), Prp8 (PRPF8), hnRNPs (HNRNPA2/B1, HNRNPA3, HNRNPH3, HNRNPR, HNRNPAB, HNRNPQ/SYNCRIP) and SR (SRSF1, SRSF3 and SRSF7) proteins are shown as some of the components of the spliceosome complex regulating the RNA splicing. Red stars (★) indicate the identified proteins (Table 7.1).

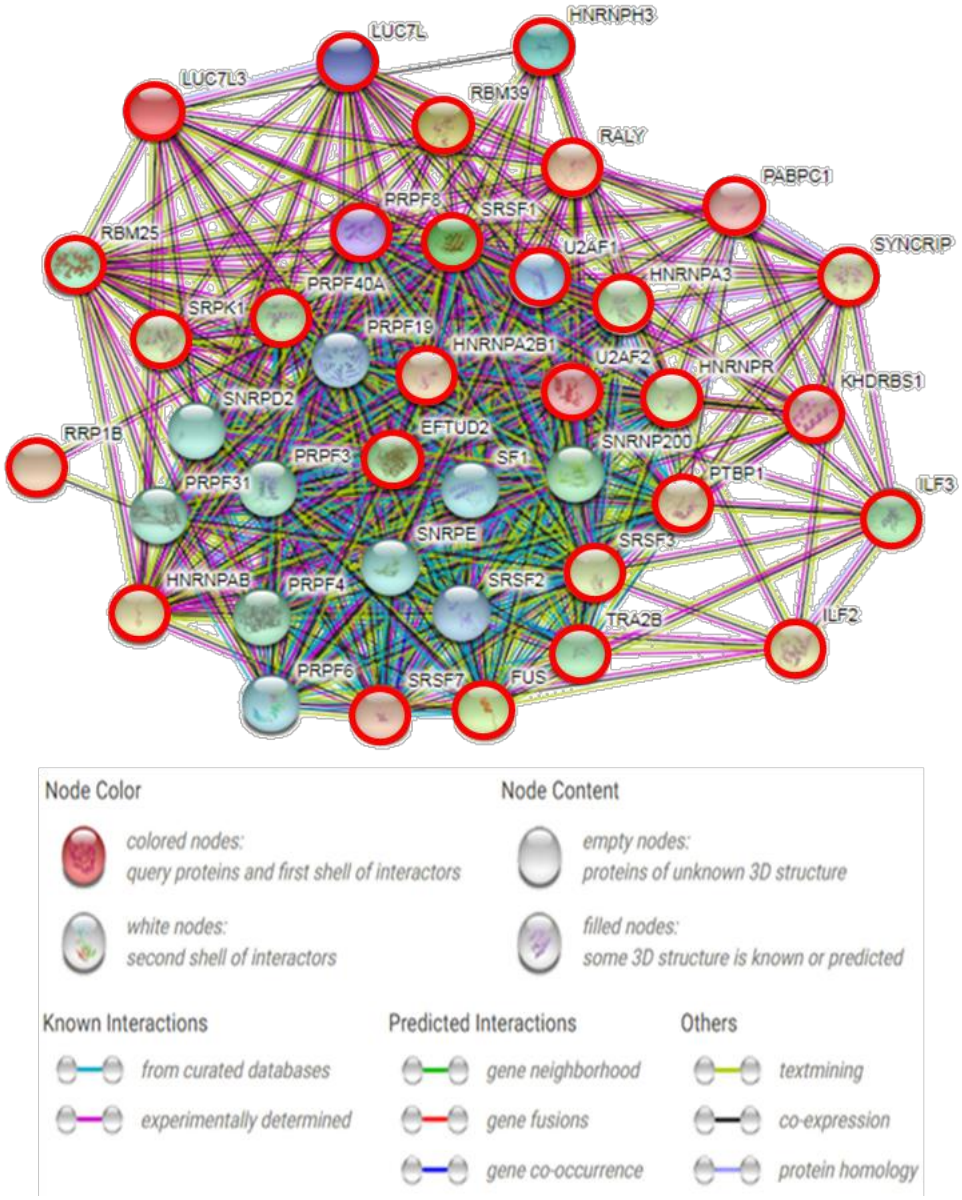


Figure 7.14 Interaction network of the 28 proteins (Table 7.1) in the biological process of RNA splicing and processing is shown as annotated in STRING. Red circles (O) indicate the identified proteins.

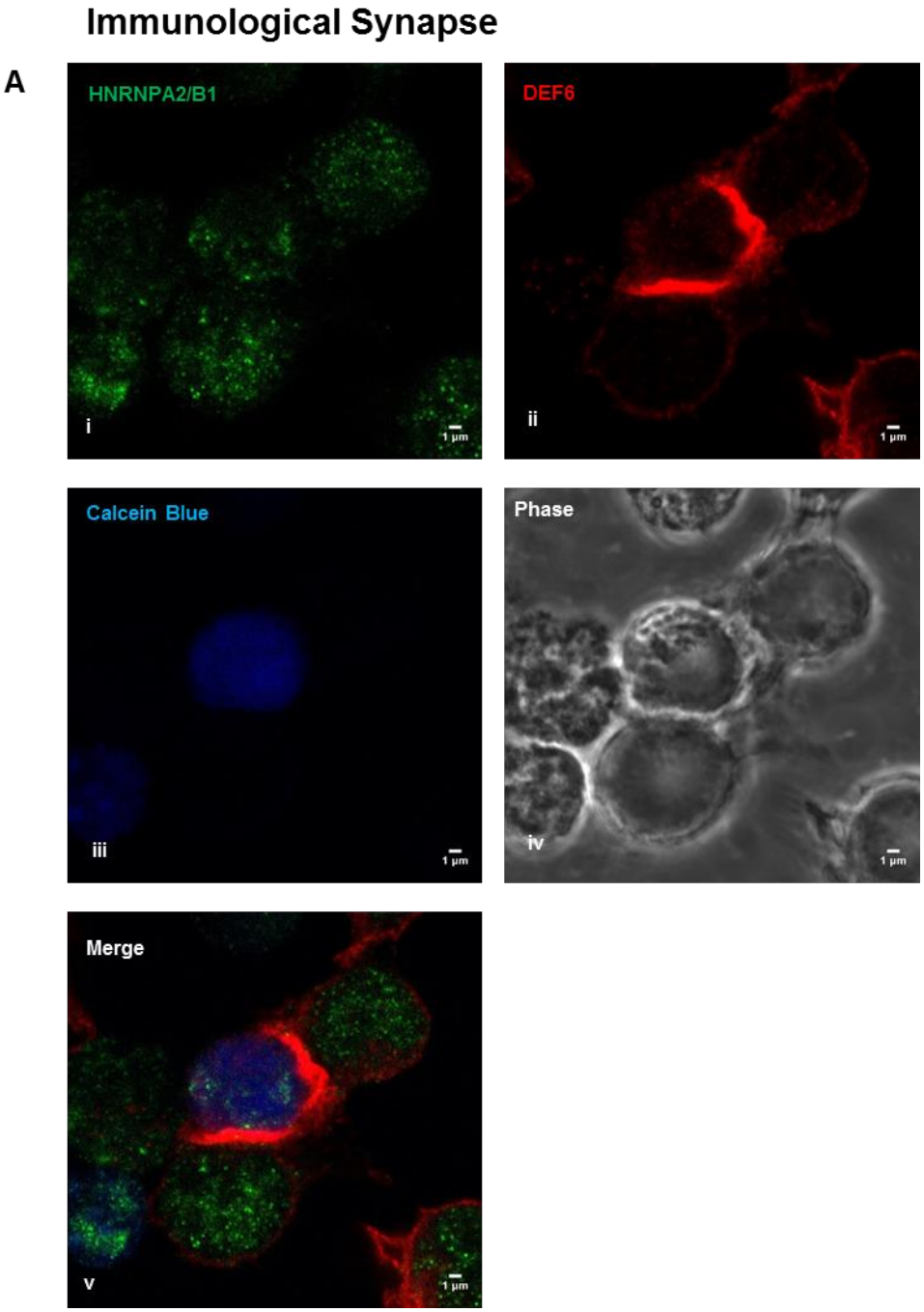


Figure 7.15 DEF6 did not co-localise with HNRNPA2B1 during IS formation. Raji B cells were stained with Calcein Blue and loaded with antigens. Raji B cells were then incubated with Jurkat T cells and immunological synapses were generated. Cells were fixed and stained using rabbit anti-DEF6 and mouse anti-HNRNPA2B1 primary antibodies. Goat anti-rabbit 568 and goat anti-mouse 488 antibodies were used to label primary antibodies. Cells were then loaded to Poly-L-Lysine coated coverslips and images were taken as a single Z plane at 63x magnification using Zeiss LSM710 confocal microscope. **(A)** DEF6 and HNRNPA2B1 were not co-localised, as DEF6 was localised to the IS **(ii,v)**, HNRNPA2B1 was localised to the nucleus **(i,v)**. HNRNPA2B1 (green), DEF6 (red), calcein blue (blue), phase and merged images including calcein blue are shown. Scale bars indicate 1 µm.

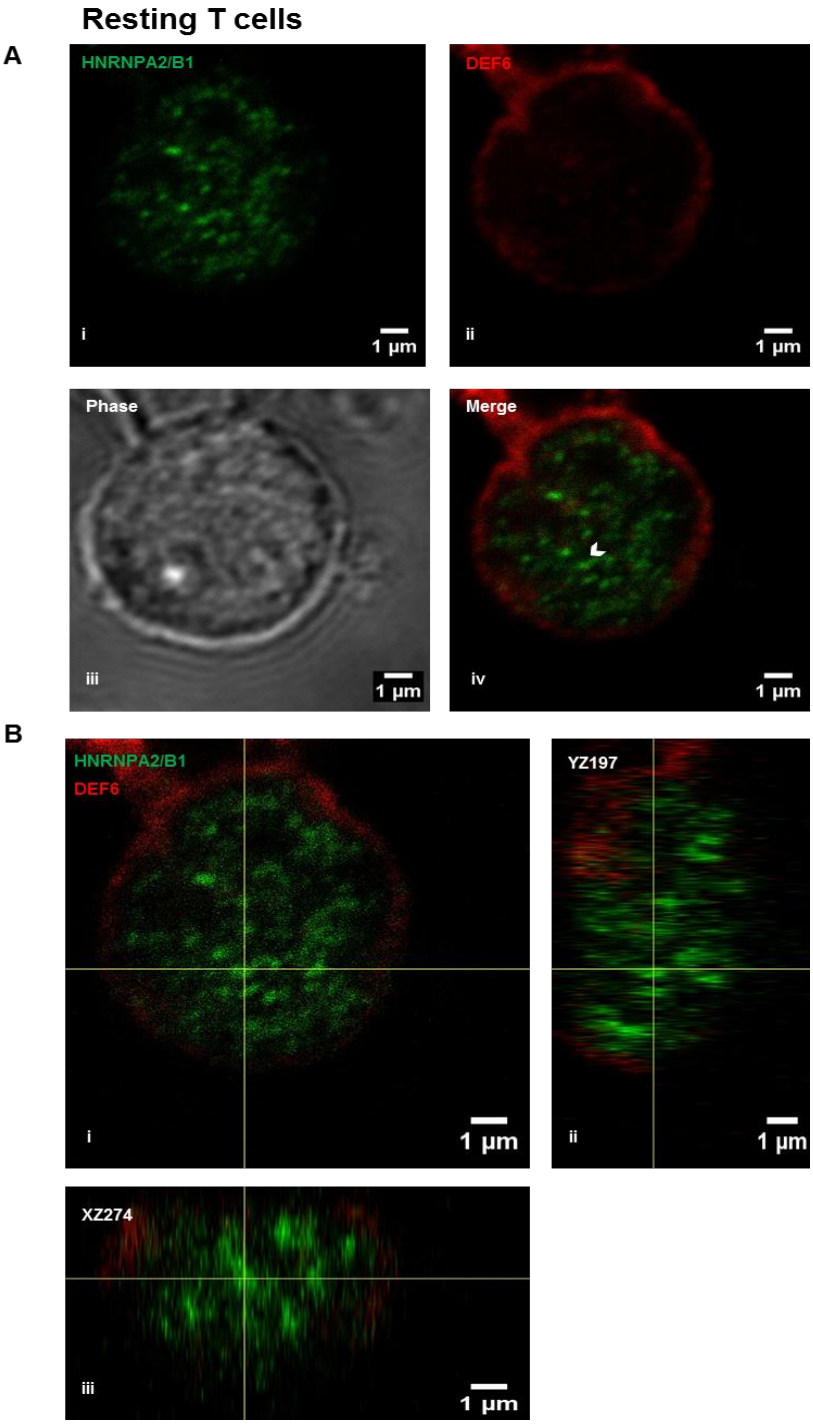


Figure 7.16 Resting Jurkat T cells exhibiting the absence of co-localision between DEF6 and HNRNPA2B1. Cells were fixed and stained using rabbit anti-DEF6 and mouse anti-HNRNPA2B1 primary antibodies. Goat anti-rabbit 568 and goat anti-mouse 488 antibodies were used to label primary antibodies. Cells were then loaded to Poly-L-Lysine coated coverslips and images were taken as a single Z plane **(A)** and a Z-stack **(B)** at 63x magnification using Zeiss LSM710 confocal microscope. **(A)** DEF6 and HNRNPA2B1 were not co-localised, as DEF6 was localised to the membrane **(ii, iv)**, HNRNPA2B1 was localised to the nucleus **(i, iv)**. **(B)** Orthogonal views from the YZ **(ii)** and XZ **(iii)** perspective also indicated the absence of co-localisation. HNRNPA2B1 (green), DEF6 (red), phase and merged images are shown. Scale bars indicate 1 µm.

7.3.3 mRNA translation

13 (9%) of the 127 identified proteins were enriched in the translation category involved in the mRNA translation process. **(Figure 7.8).** KEGG pathway database annotated 4 proteins, KARS, RARS, MARS and GARS in the tRNA aminoacylation process **(Figure 7.17)**, 3 proteins, eIF3 (EIF3I), eIF5 (EIF5A) and PABP (PABPC1) are translation initiation factors **(Figure 7.18)** and 4 proteins, SAe (RPSA), S16e (RPS16), L31e (RPL35A) and L37Ae (RPL39) are ribosomal proteins **(Figure 7.18)**. The remaining 2 proteins, EEF1G and NPM1 were not annotated by the KEGG pathway database. The interaction network among the identified proteins for mRNA translation is shown in **Figure 7.19** as annotated in STRING.

The role of DEF6 in mRNA translation has been studied by three fellow PhD students, Fiona Hey, Kerry Remon and Maha Alsayegh, in our laboratory. Hey *et al.,* (2012) demonstrated that upon the phosphorylation by ITK at tyrosines 210 and 222, DEF6 formed granules that co-localised with decapping enzyme 1 (DCP1), a P-body marker. In addition, the phosphomimic mutant of DEF6, Y210E-Y222E also formed cytoplasmic granules co-localising with DCP1. Blocking translation by treating cells with sodium arsenite or puromycin also resulted in DEF6 to form cytoplasmic granules. To test whether the aggregates of DEF6 co-localises with P-bodies, Remon (PhD thesis, 2016) used the proximity ligation assay (PLA) to identify the proximity level of DEF6 and 4E-T, specific P-body marker that regulates the transportation of specific molecules to P-bodies like eIF4E (Ferraiuolo *et al.,* 2005). The close proximity (within 40 nm) between 4E-T and DEF6 was shown in untreated and sodium arsenite-treated cells, with the increase in the number of proximal signals when treated with sodium arsenite (Remon, PhD thesis, 2016). To further investigate the interaction, co-immunoprecipitation was performed by Alsayegh (PhD thesis, 2017) and the physical interaction between 4E-T with DEF6 was observed. More importantly, while investigating the further roles of DEF6 in mRNA translation, DEF6 has been shown to be in close proximity to active translation and co-localising with the translation factors, eIF4E and PABP in resting and treated cells (Remon, PhD thesis, 2016), the interaction was detected between DEF6 and eIF4E, but not between DEF6 and PABP (Alsayegh, PhD thesis, 2017). In addition, siRNA-mediated knockdown of DEF6 expression revealed that DEF6 controls translation of eIF4E, 4E-T and PABP (Alsayegh, PhD thesis, 2017). Together with the identification of the translation initiation and elongation factors, EIF3I, EIF5A, PABPC1 and EEF1G, the proteins regulating the tRNA aminoacylation, KARS, RARS, MARS and GARS and the ribosomal proteins, RPSA, RPS16, RPL35A and RPL39 suggests therefore that DEF6 might have an important role in mRNA processing including translation initiation, elongation and decay in P-bodies.

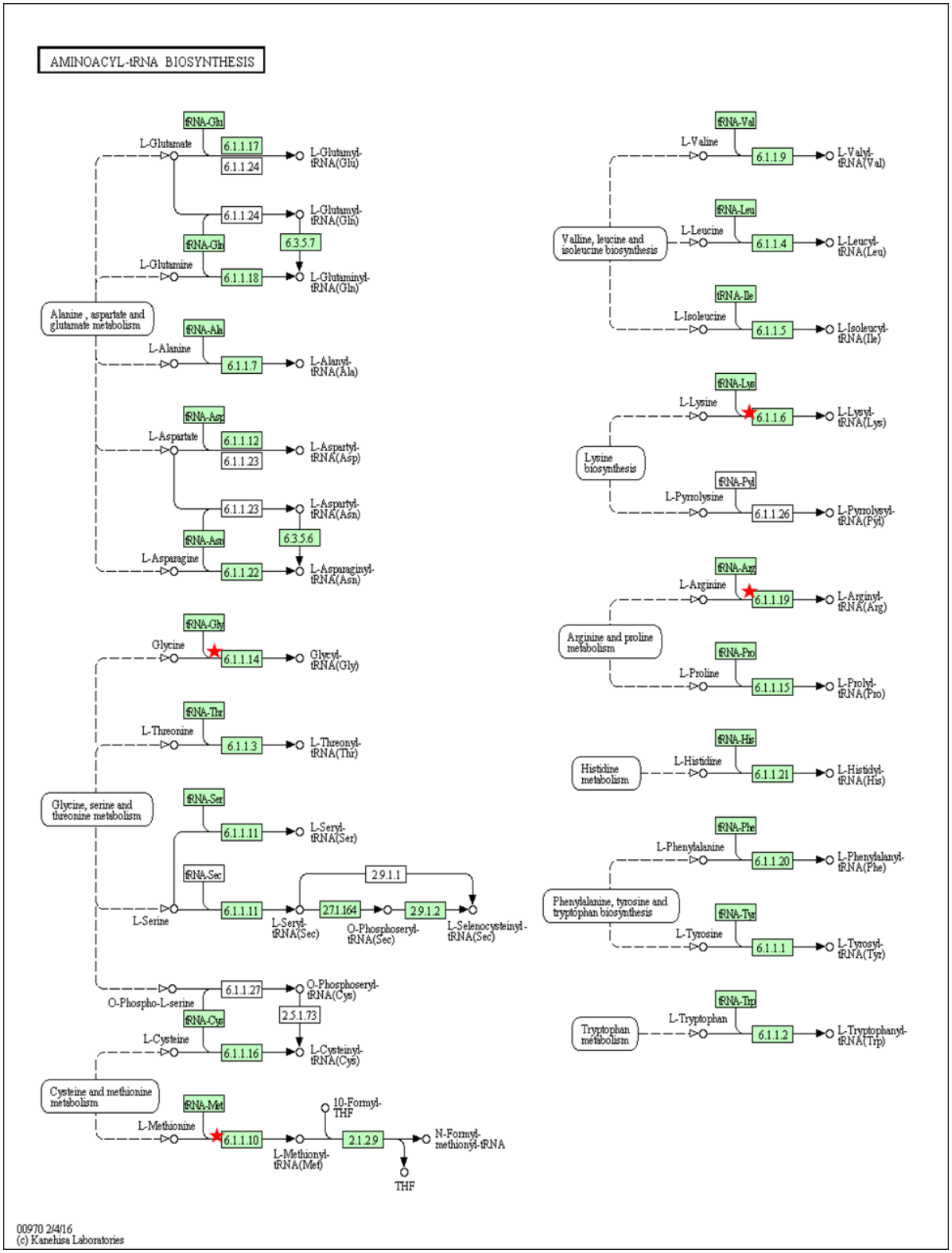
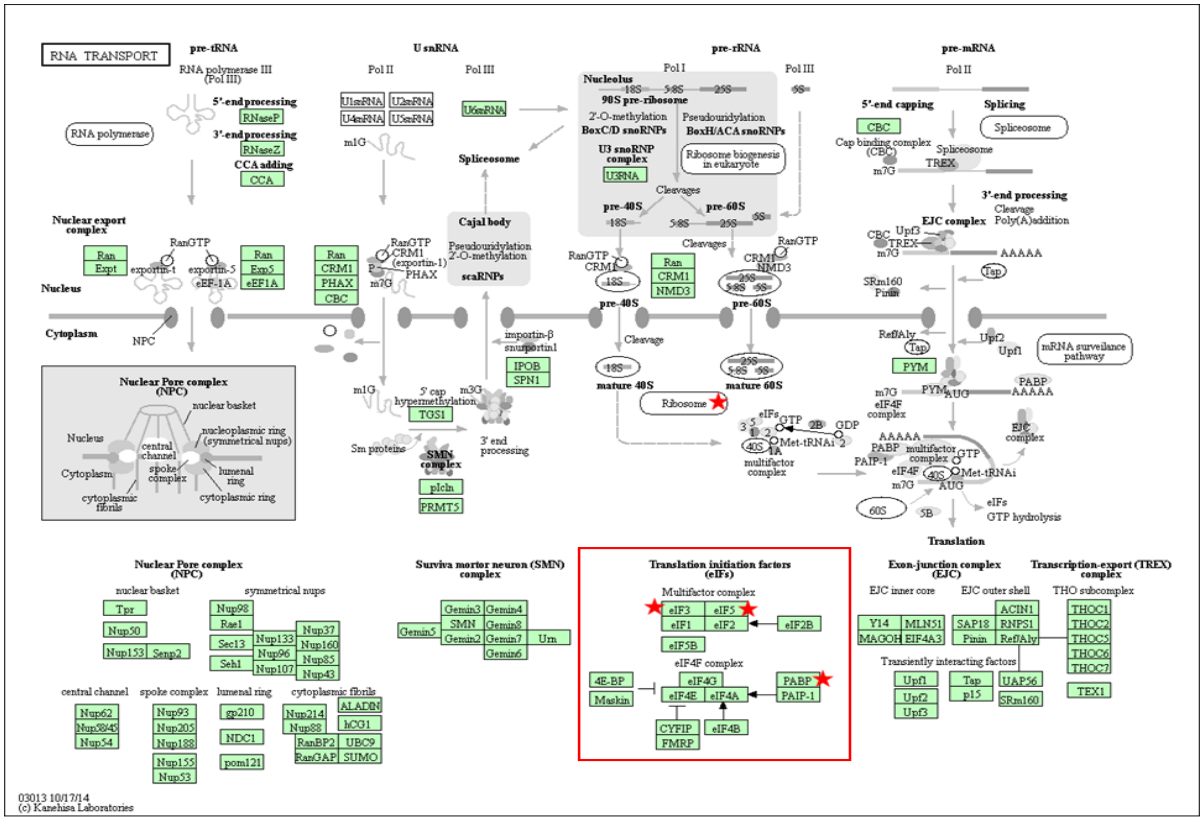


Figure 7.17 Aminoacyl-tRNA biosynthesis for translation is shown as in the KEGG pathway database. 6.1.1.6 L-Lysyl tRNA (Lys) represents KARS, 6.1.1.19 L-Arginyl tRNA (Arg) represents RARS, 6.1.1.10 L-Methionyl- tRNA (Met) represents MARS and 6.1.1.14 Glycyl tRNA (Gly) represents GARS. KARS, RARS, MARS and GARS are shown in the tRNA aminoacylation process for protein translation. Red stars (★) indicate the identified proteins (Table 7.1).



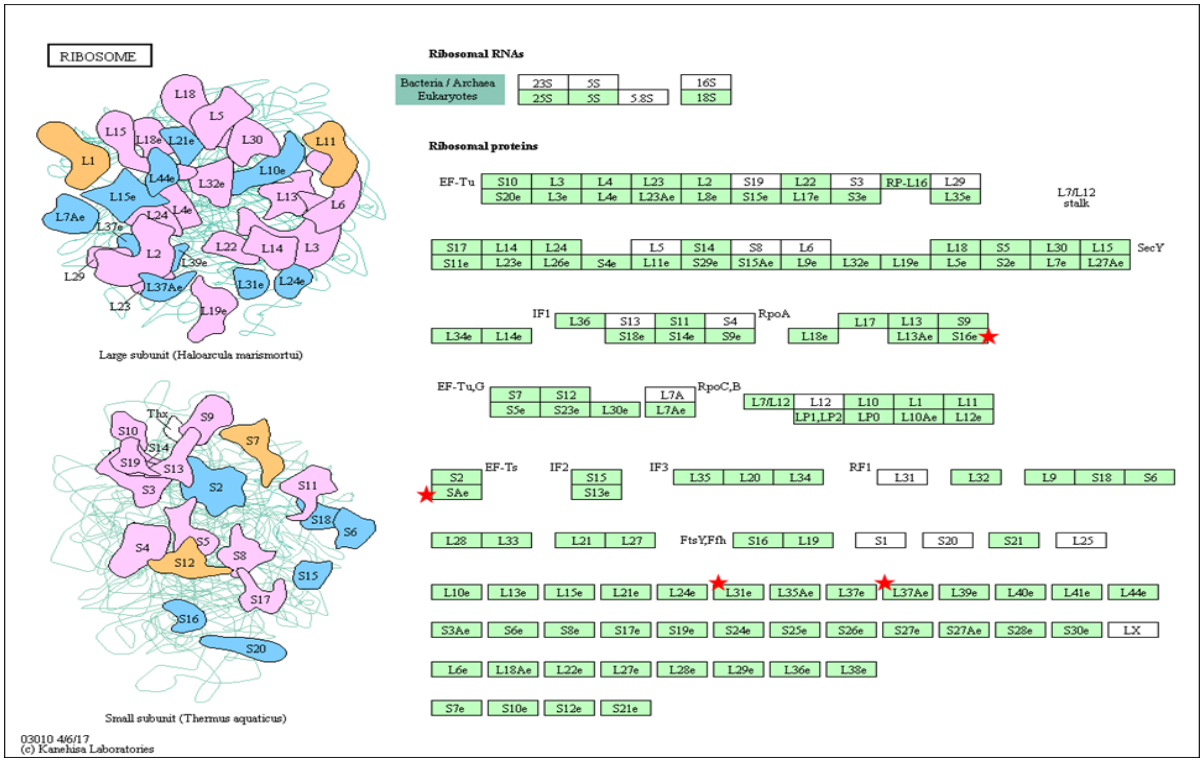


Figure 7.18 RNA transport pathway which includes the translation process and ribosomal proteins are shown as in the KEGG pathway database. eIF3 (EIF3I), eIF5 (EIF5A) and PABP (PABPC1) are shown as the translation initiation factors of translation. SAe (RPSA), S16e (RPS16), L31e (RPL35A) and L37Ae (RPL39) are shown as the ribosomal proteins. Red stars (★) indicate the identified proteins (Table 7.1). The rectangle indicates the translation factors involving in the translation process.

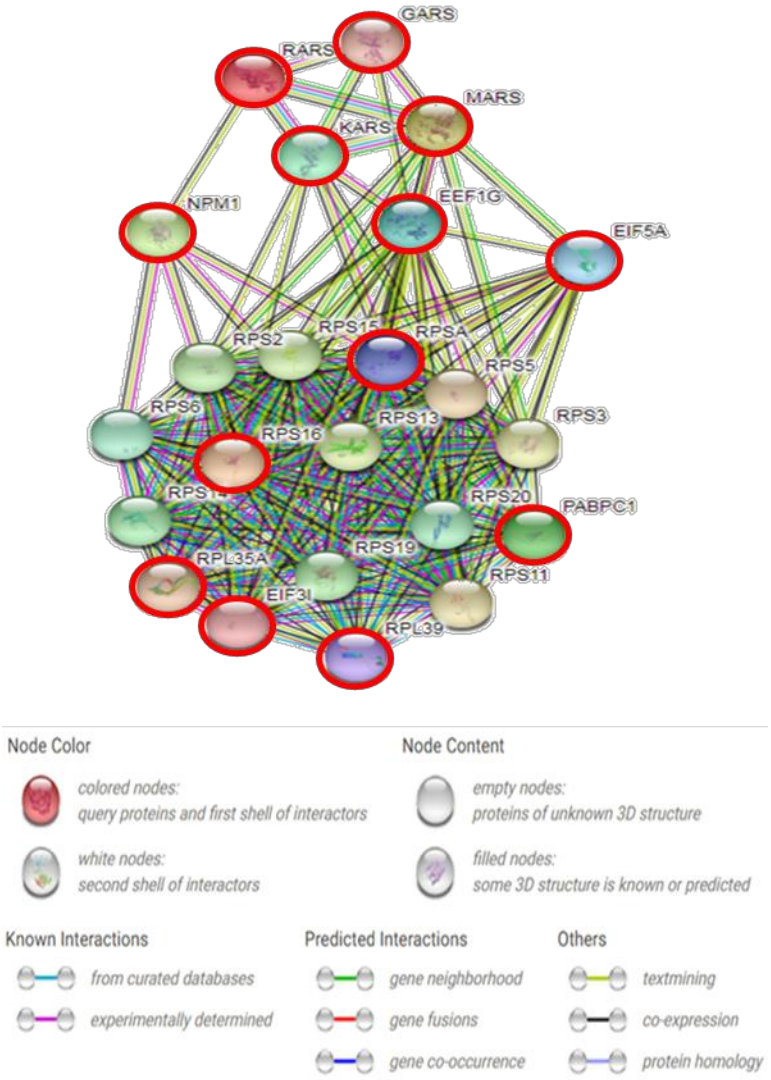


Figure 7.19 Interaction network of the 13 proteins (Table 7.1) in the biological process of translation is shown as annotated in STRING. Red circles (O) indicate the identified proteins.

7.3.4 Transcription

Given that the KEGG pathway database does not include a transcription pathway, the Reactome pathway database was utilised. 24 proteins were annotated in the transcription processes, which are MTA2, PARP1, RB1, RBBP4, NPM1, CBX3, TRIM28, PSMD11, SSRP1, PSMC2, HMBG1, FUS, IFI16, KHDRBS1, TOP2A, ILF2, ILF3, NCL, CTCF, SMARCA5, SAFB2, PA2G4, CALR and PFN1 **(Figure 7.20)**. The remaining 12 proteins were not annotated in the transcription pathways which may be the consequence of lack of detailed illustrations in the Reactome pathway database. The interaction network among the identified proteins for transcription is shown in **Figure 7.21** as annotated in STRING.

Transcriptional control has the highest percentage (26%; 36 proteins) of GO term enrichments in DEF6 interactome, suggesting that DEF6 may also play an important role in transcriptional regulation **(Figure 7.8).**

Even though none of the proteins we identified in the transcriptional control process has been shown to interact with DEF6 before, the human interactome network analysis by Huttlin *et al.,* (2017) revealed interactions between DEF6 and SMARCA1, which is a close relative of our identified protein, SMARCA5 (Barak *et al.,* 2003). SMARCA1 and SMARCA5 are the members of SWI/SNF family of proteins with helicase and ATPase activities regulating activation or repression of gene expression (Eberharter *et al.,* 2004; Lazzaro *et al.,* 2006; Dluhosova *et al.,* 2014).

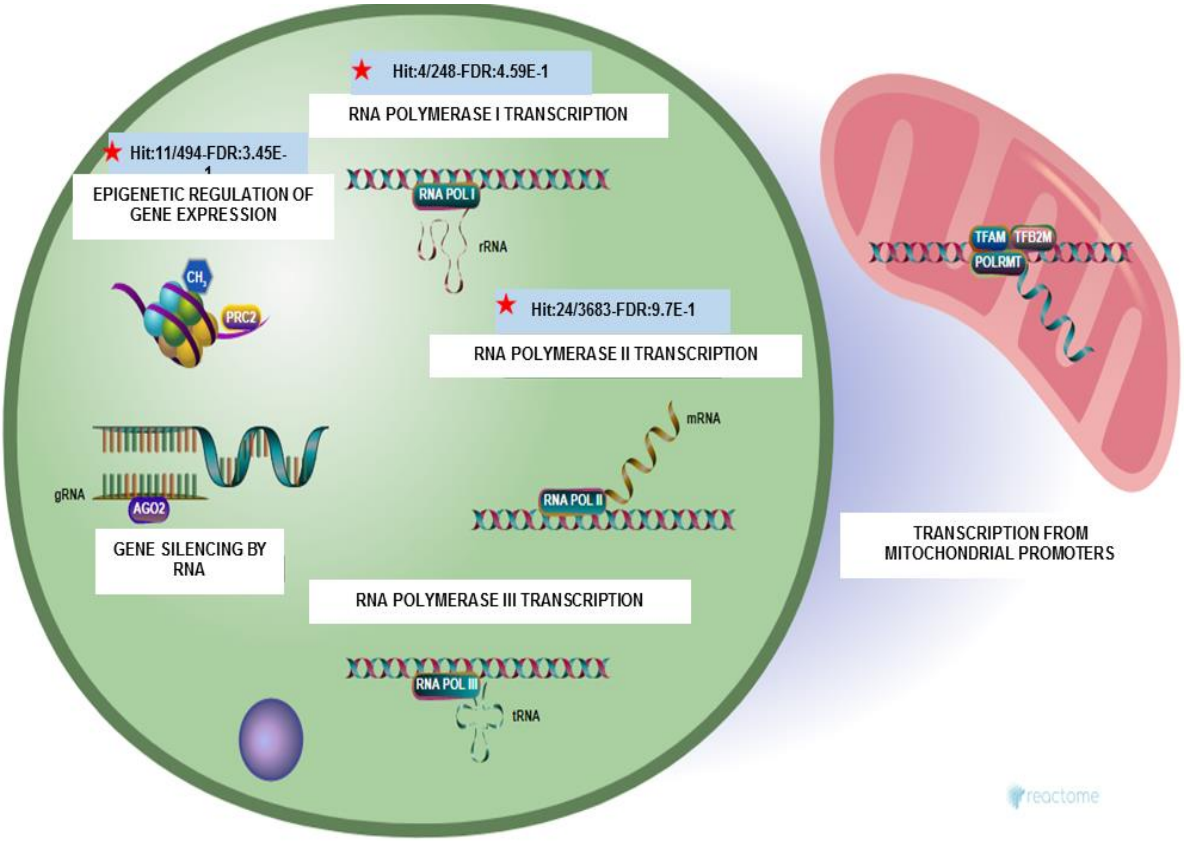


Figure 7.20 Transcription pathway is shown as in the Reactome pathway database. 11 hits of epigenetic regulation of gene expression and 4 hits of RNA polymerase I transcription were found in common with the 24 hits of RNA polymerase II transcription (Table 7.1). Red stars (★) indicate the identified proteins.

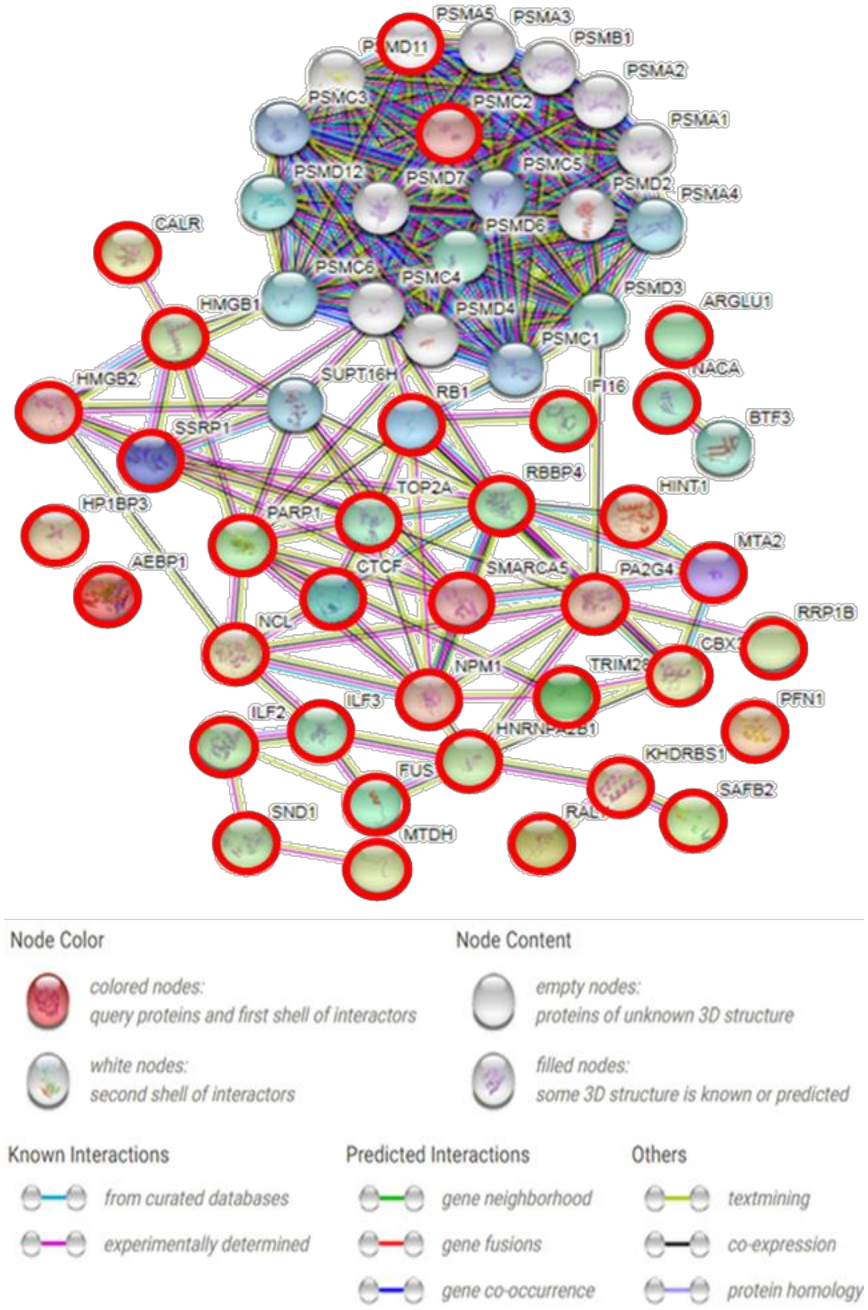


Figure 7.21 Interaction network of the 36 proteins (Table 7.1) in the biological process of transcription is shown as annotated in STRING. Red circles (O) indicate the identified proteins.

7.3.5 Metabolic Processes

17 proteins (12%) of the 127 identified proteins were specifically enriched in metabolic processes including purine metabolism, ATP biosynthesis metabolism and amino acid biosynthesis/degradation metabolism. KEGG pathway database annotated 5 proteins, PFAS, ATIC, PAICS, IMPDH2 and HPRT1 in the purine metabolism **(Figure 7.22)**, 3 proteins, ATP5C1 (gamma), ATP5O (OSCP) and ATP5I (g) in the ATP biosynthesis metabolism **(Figure 7.23)**, 3 proteins, HADHA, HSD17B10 and PCCA in the valine, leucine and isoleucine biosynthesis/degradation metabolism **(Figure 7.24),** and lastly 2 proteins, ATP1A1 and ATP2A2 in the sodium/potassium and calcium ion homeostasis of cell membrane and sarcoplasmic reticulum, respectively **(Figure 7.25)**. Due to the absence of ion pathways, cardiac muscle contraction pathway was shown to point out the roles of ATP1A1 and ATP2A2. The remaining 4 proteins were not annotated in any of the KEGG pathways. The interaction network among the identified proteins for metabolic processes is shown in **Figure 7.26** as annotated in STRING.

None of the proteins we identified in the metabolic processes has been shown to be in close proximity or to interact with DEF6, however 12% enrichment of the identified proteins in the metabolic processes suggests a role for DEF6 in the metabolic processes.

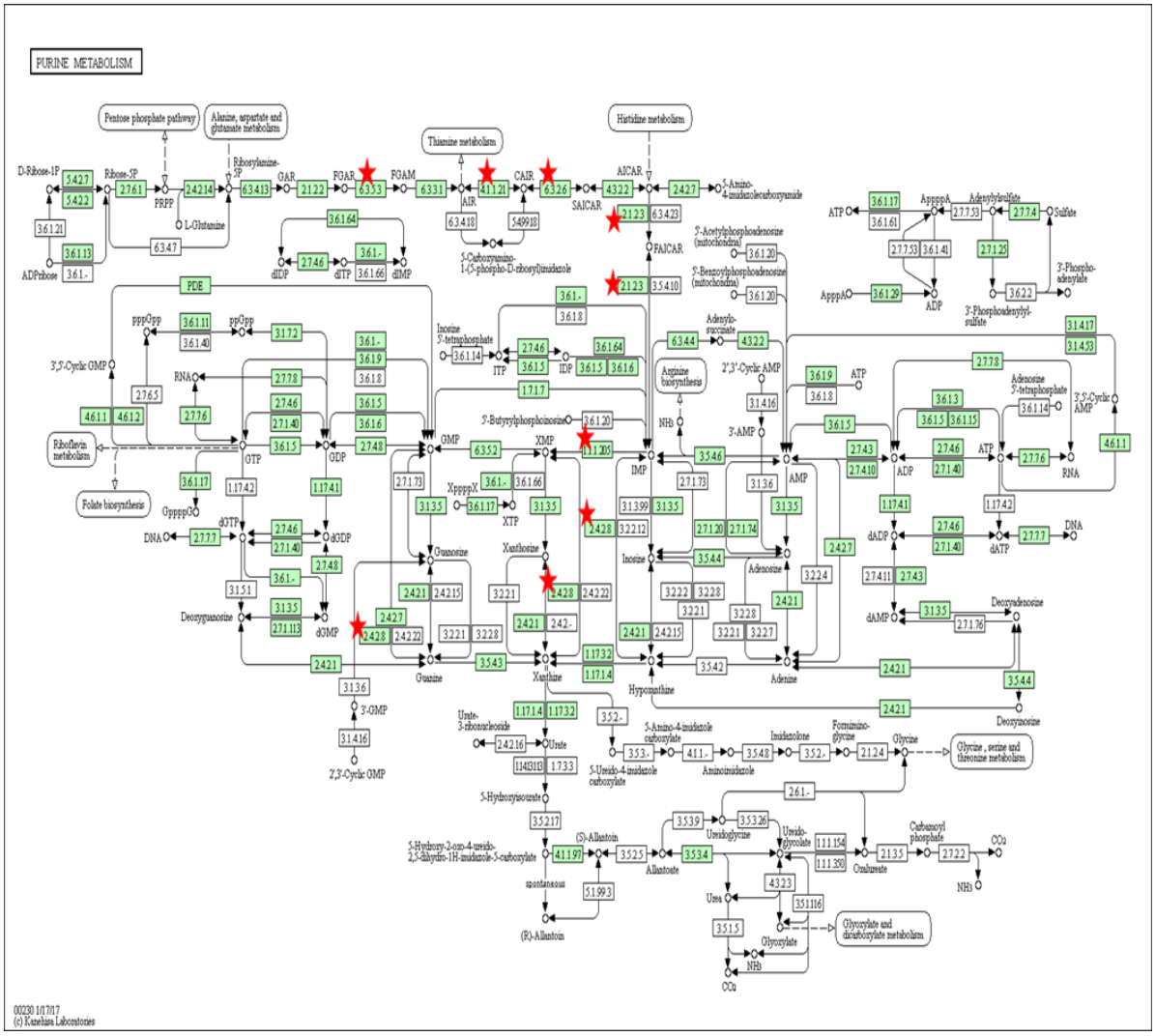


Figure 7.22 Purine metabolism is shown as in the KEGG pathway database. 6.3.5.3 represents PFAS, 2.1.2.3 represents ATIC, both 6.3.2.6 and 4.1.1.21 represent PAICS, 1.1.1.205 represents IMPDH2, 2.4.2.8 represents HPRT1. These 5 proteins (PFAS, ATIC, PAICS, IMPDH2 and HPRT1 are shown to be involved in the purine metabolism. Red stars (★) indicate the identified proteins (Table 7.1).

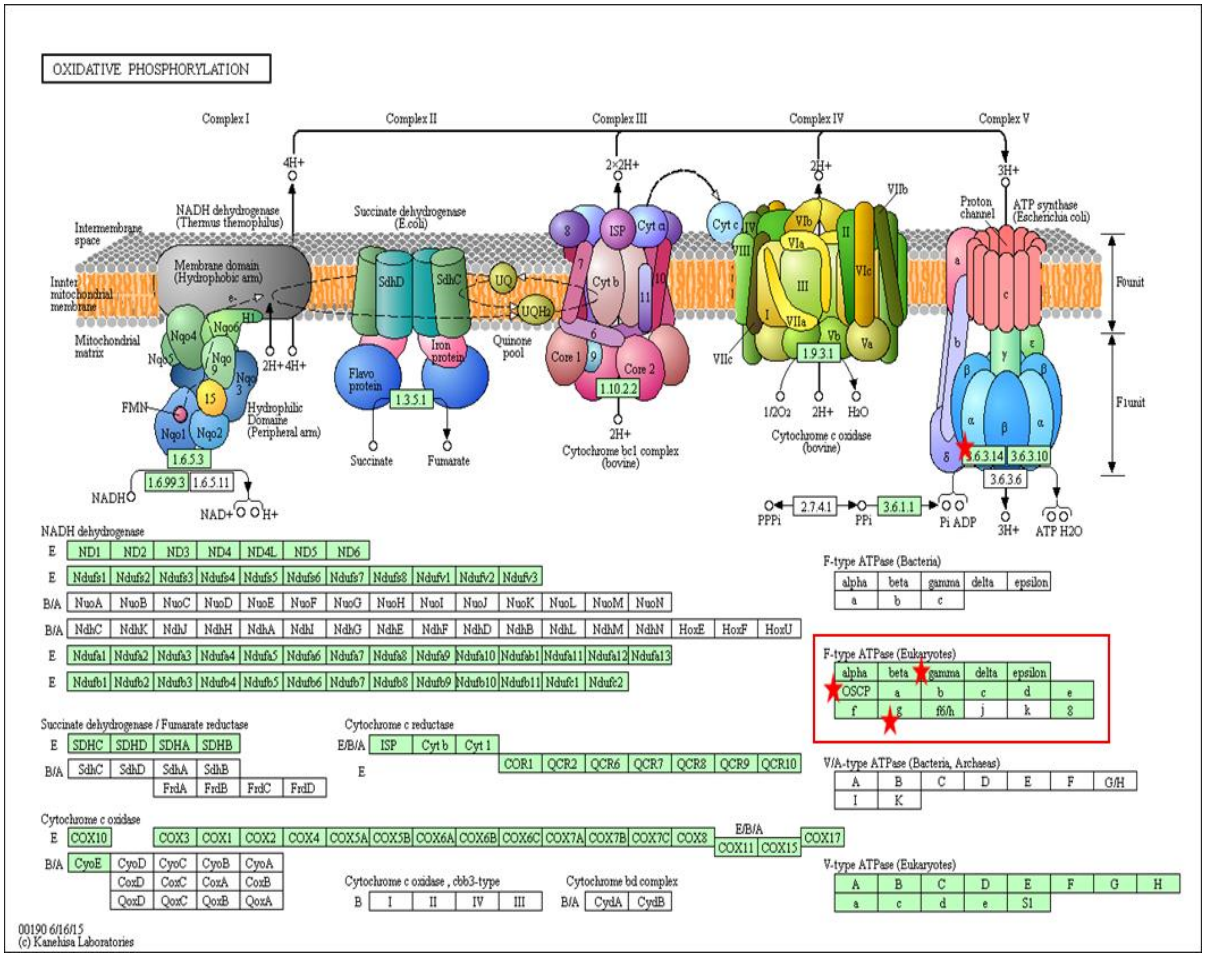


Figure 7.23 Oxidative phosphorylation which includes the components of mitochondrial membrane ATP biosynthesis is shown as in the KEGG pathway database. 3.6.3.14 represents the F-type ATP synthases which are ATP5C1 (gamma), ATP5O (OSCP) and ATP5l (g) involving in the ATP biosynthesis pathway. Red stars (★) indicate the identified proteins (Table 7.1). The rectangle indicates the subunits of ATP synthases for eukaryotes.

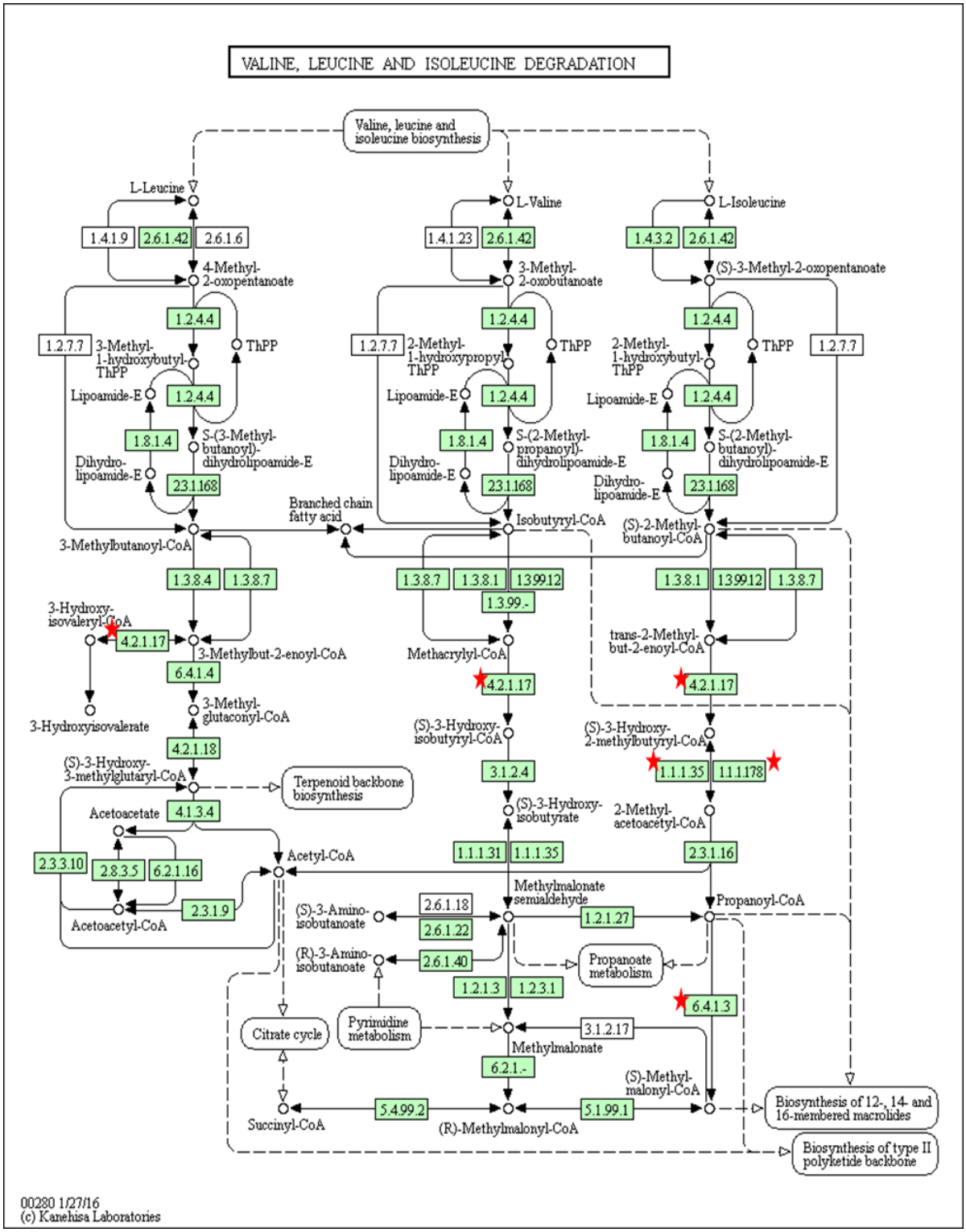


Figure 7.24 Amino acid biosynthesis/degradation metabolism is shown as in the KEGG pathway database. 4.2.1.17 represents HADHA, 1.1.1.35 and 1.1.1.178 represent HSD17B10 and 6.4.1.3 represents PCCA, all involving in the amino acid biosynthesis metabolism. Red stars (★) indicate the identified proteins (Table 7.1).

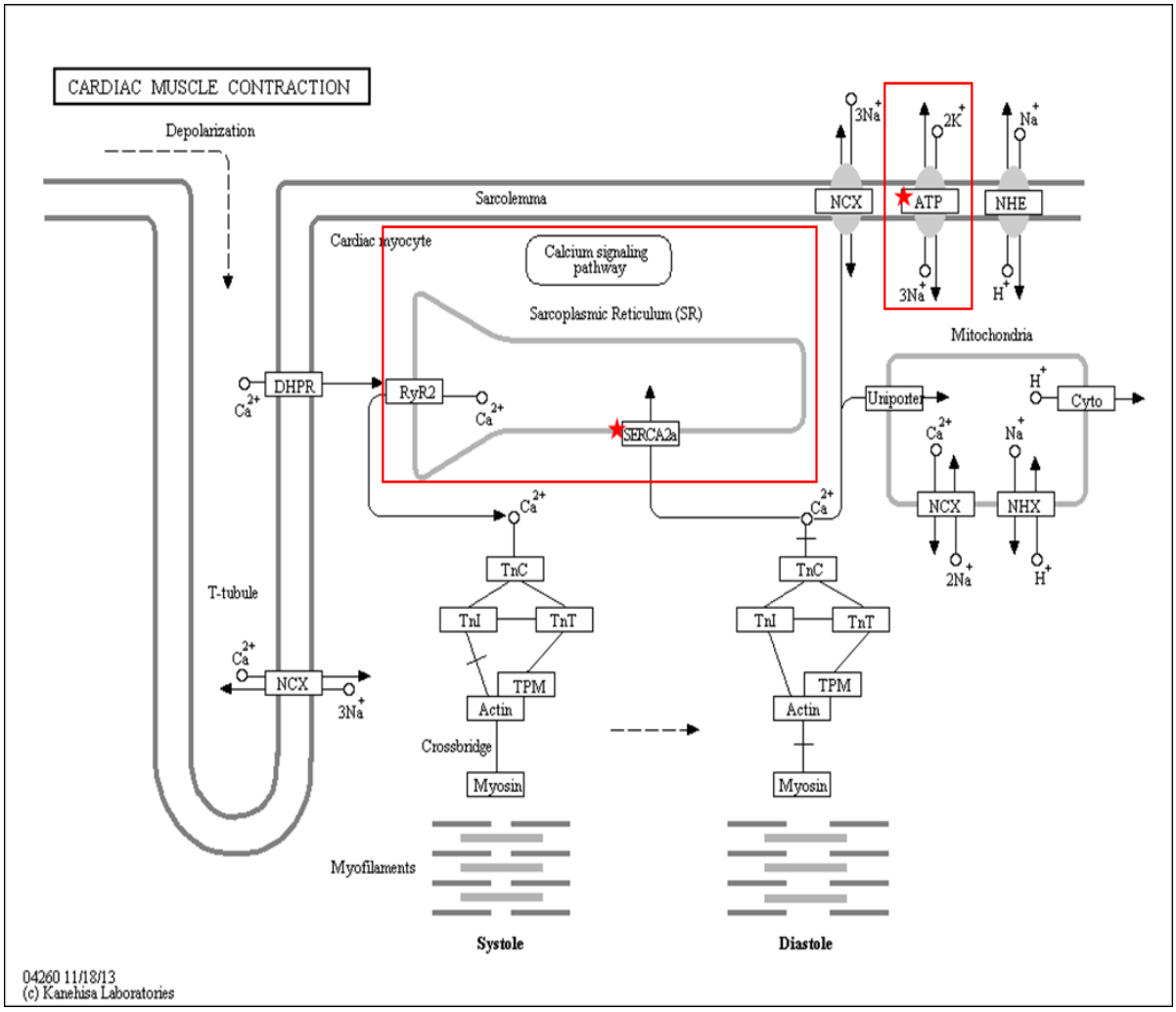


Figure 7.25 Cardiac muscle contraction pathway containing the ion homeostasis processes regulated by ATPases is shown as in the KEGG pathway database. ATP represents ATP1A1 catalysing the hydrolysis of ATP for the exchange of Na/K ions across the cell membrane and SERCA2a represents ATP2A2 catalysing the hydrolysis of ATP for taking Calcium ions into sarcoplasmic reticulum (SR). Red stars (★) indicate the identified proteins (Table 7.1). The rectangles indicate the Na/K ion exchange and Ca ion intake processes.

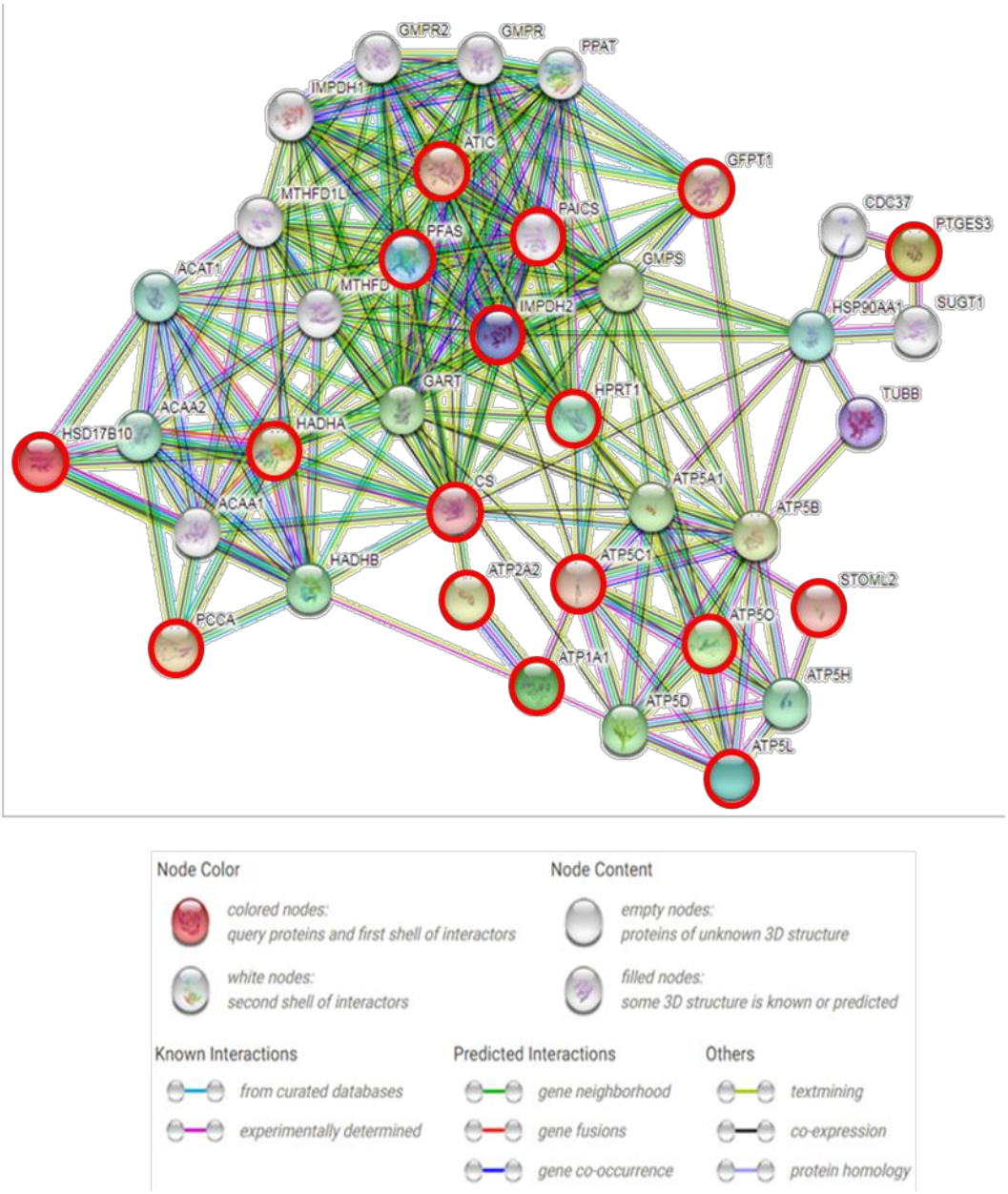


Figure 7.26 Interaction network of the 17 proteins (Table 7.1) in the biological process of metabolism is shown as annotated in STRING. Red circles (O) indicate the identified proteins.

7.3.6 Protein Processing

15 proteins (11%) of the 127 identified proteins were specifically enriched in the protein processing including folding/unfolding, modification and degradation processes. KEGG pathway database annotated 8 proteins, Hsp40 (DNAJA1), CNX (Calnexin), CRT (Calretikulin), OSTs (DDOST, Rpn1 and Rpn2), PDIs (PDIA6) and NEF (HYOU1) in the protein processing in Endoplasmic Reticulum (ER) pathway **(Figure 7.27)** and 2 proteins, PSMC2 and PSMD11 as the components of the proteasome **(Figure 7.28).** The remaining 5 proteins, PTGES3, CCT8, PPIA, HSPA9 and STIP1 were not demonstrated since the processes are not illustrated in detail. The interaction network among the identified proteins for protein folding/unfolding and modification is shown in **Figure 7.29** as annotated in STRING.

Even though none of the proteins involved in protein folding and modification processes has been shown to interact or in close proximity with DEF6, DEF6 interacts with a chaperone protein, HSP90B1 (Hong *et al.,* 2017) that regulates folding of Toll-like Receptors (TLRs) in ER (Yang *et al.*, 2007) suggesting a role for DEF6 in protein folding and modification processes.

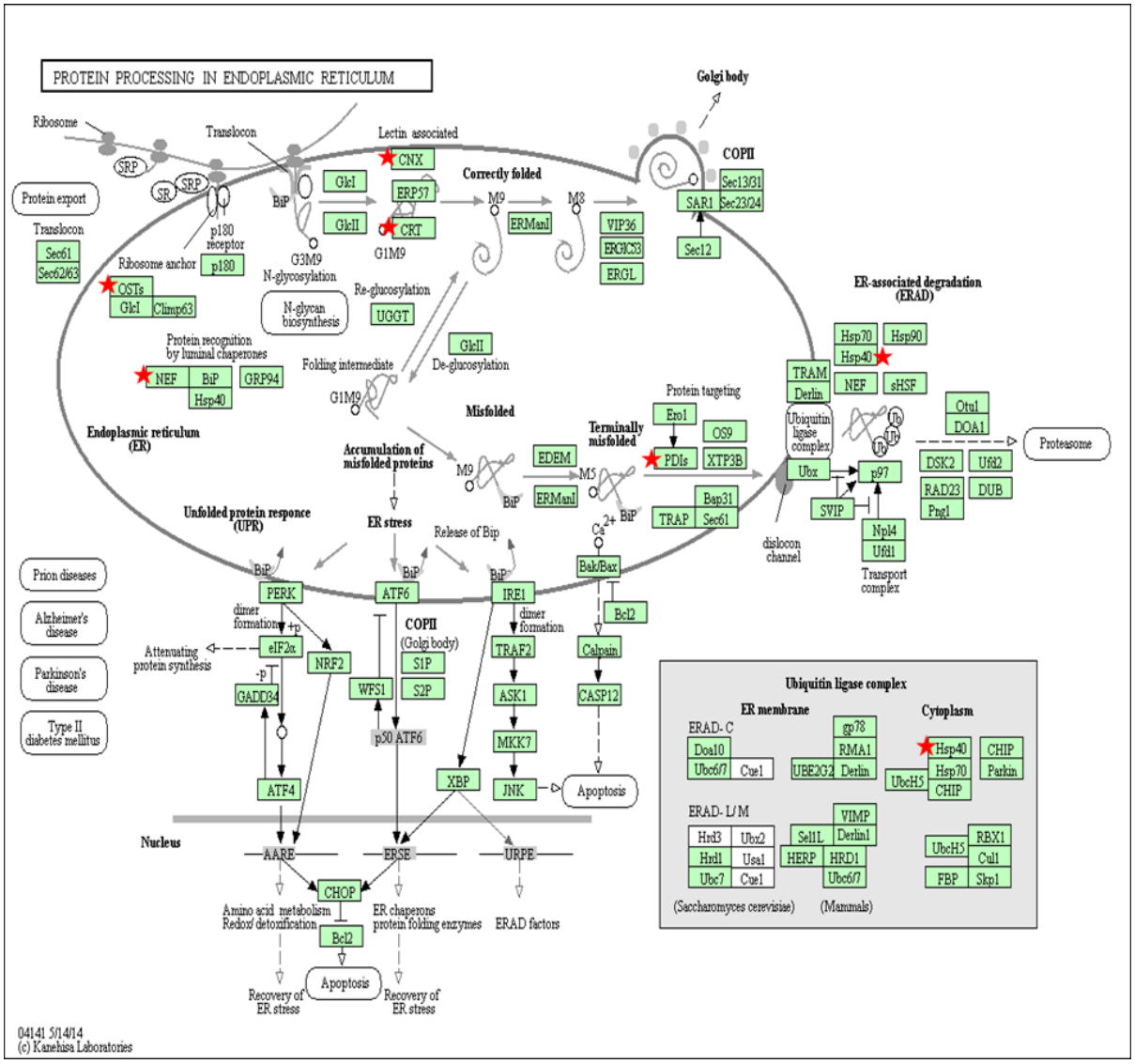


Figure 7.27 Protein processing in endoplasmic reticulum (ER) which includes both protein folding and modification processes is shown as in the KEGG pathway database. Hsp40 (DNAJA1), CNX (Calnexin), CRT (Calretikulin), OSTs (DDOST, Rpn1 and Rpn2), PDIs (PDIA6) and NEF (HYOU1) are illustrated to be involved in the protein processing in ER. Red stars (★) indicate the identified proteins (Table 7.1).

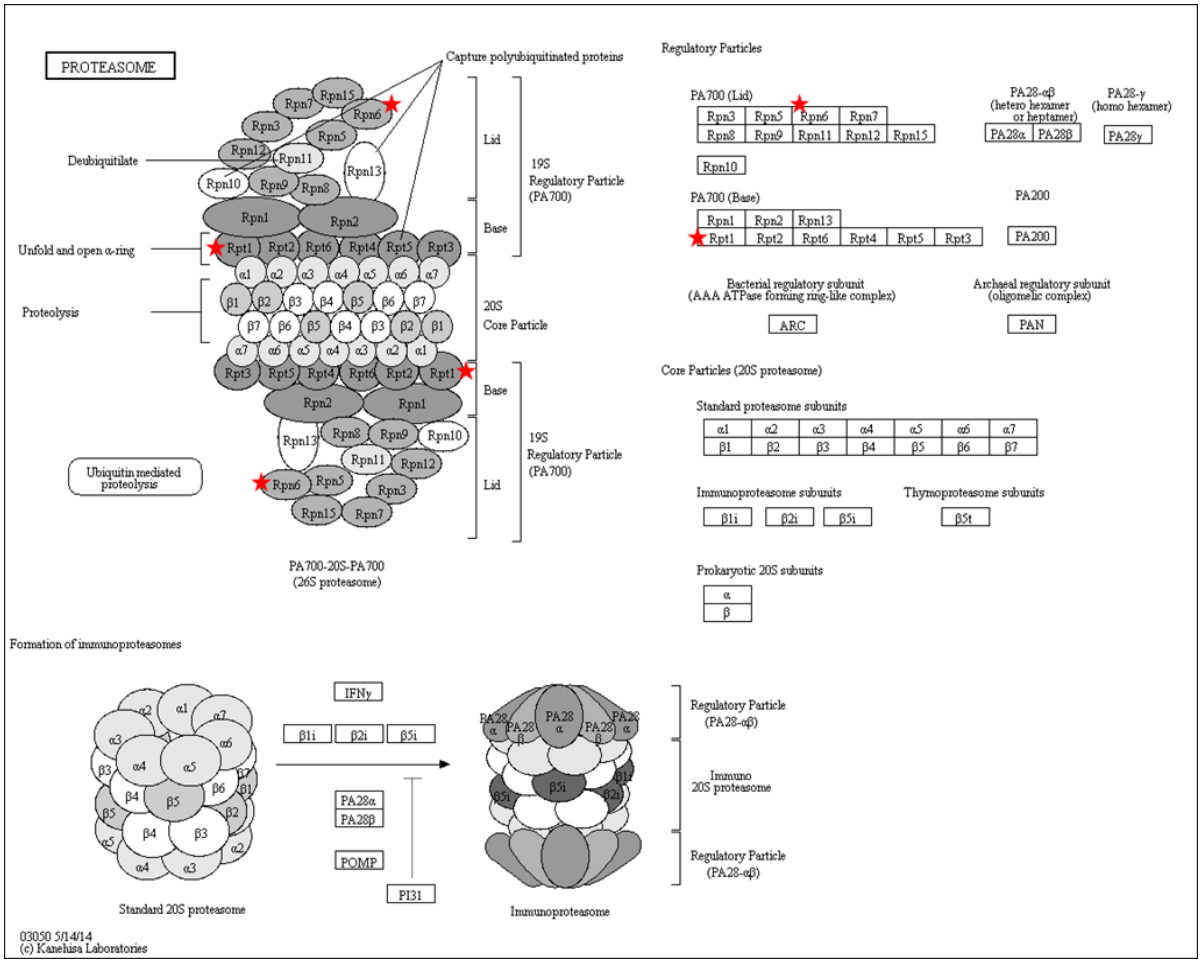


Figure 7.28 Proteasome complex regulating the ATP-dependent degradation of ubiquitinated proteins is shown as in the KEGG pathway database. Rpt1 represents PSMC2 and Rpn6 represents PSMD11. PSMC2 and PSMD11 are the components of 26S proteasome. Red stars (★) indicate the identified proteins (Table 7.1).

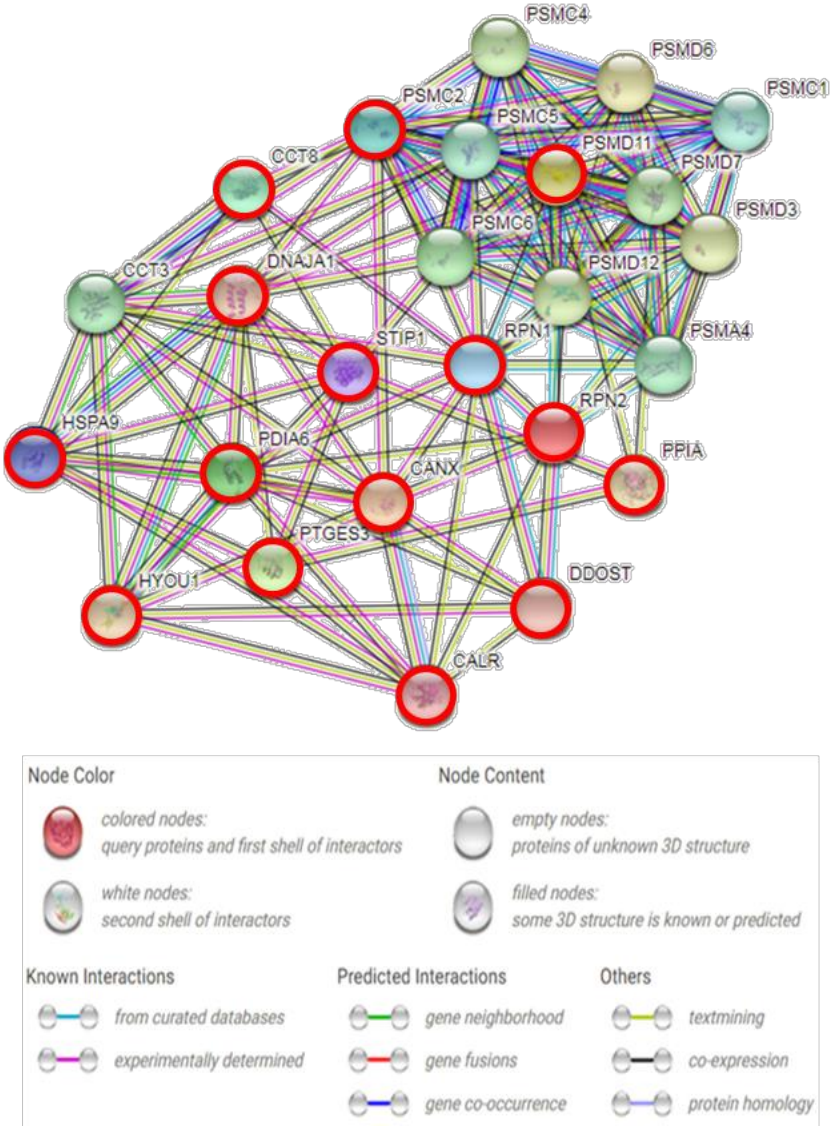


Figure 7.29 Interaction network of the 15 proteins (Table 7.1) in the biological process of protein folding and modification is shown as annotated in STRING. Red circles (O) indicate the identified proteins.

7.4. Summary

- Using BioID-mediated biotinylation *in vivo*, proteins in close proximity and/or interacting with full-length or parts of DEF6 in Jurkat T cells were affinity captured and analysed by mass spectrometry.
- Out of **404 clusters** in total, **127 clusters** were identified that specifically classified since the remaining **277 clusters** were also detected in the negative control sample.
- DEF6 interactome was grouped into the known protein complexes using the Gene Ontology (GO) system of classification in Scaffold software and DAVID Bioinformatics Resources 6.8 database. The physical interactions were shown as annotated in STRING database. KEGG or Reactome pathway databases were used to demonstrate the biological pathways which some of the identified proteins are involved.
- The proteins were enriched in 6 different biological processes, transcription (36 proteins), RNA splicing and processing (28 proteins), metabolic processes (17 proteins), mRNA translation (13 proteins), protein processing (15 proteins) and actin cytoskeleton organisation (7 proteins).
- Given that the roles of DEF6 in actin cytoskeleton and mRNA translation have already known before, suggests that DEF6 might also be involved in the other four biological processes.
- Immunohistochemistry analysis was performed to indicate whether DEF6 co-localises with some of the identified proteins. CORO1A from the actin cytoskeleton organisation and HNRNPA2B1 from the RNA splicing and processing were selected for the analysis.
- DEF6 and CORO1A were localised to the IS and co-localised partially both regulating the actin cytoskeleton dynamics of IS. Moreover, DEF6 and CORO1A were localised to the F-actin-rich structures and co-localised partially at the cell protrusions of resting T cells.
- DEF6 and HNRNPA2B1 did not co-localise during the IS formation and in resting T cells.

CHAPTER 8
DISCUSSION

8.1. TALEN-mediated targeted mutations were generated at *def6a* and *swap70b* loci and *qmc809*, *qmc811* single and *qmc813* double mutant lines were established

Transcription Activator-Like Effector Nucleases (TALENs) is are engineered nucleases that have been widely used in zebrafish to generate mutations at a specific loci (Sander *et al.,* 2011; Huang *et al.,* 2011; Bedell *et al.,* 2012; Dahlem *et al.,* 2012; Gupta *et al.,* 2013). The non-homologous end joining (NHEJ) as an error-prone repair mechanism that results in small insertions and deletions, which often lead to frame-shift mutations at the cleavage site. These frameshift mutations are inherited through the germline leading to the generation of knock-out mutants. A sequence downstream of the start codon in exon-1 was targeted for both *def6a* and *swap70b*. To increase the targeting efficiency and optimise the amount of injected TALEN mRNAs, 125pg and 250pg for *def6a* and 250pg and 500pg for *swap70b* were chosen. While injection of 125pg *def6a* TALEN mRNAs did not induce any mutations, 60-70% of the embryos injected with 250pg *def6a* TALEN mRNAs showed somatic mutations at the *def6a* locus (**Figure 3.4** and **Figure 3.6**). In addition, 15-40% and 60-80% of the embryos injected with 250pg and 500pg *swap70b* TALEN mRNAs, respectively, showed somatic mutations at the *swap70b* locus (**Figure 3.5** and **Figure 3.6**). These results indicated that TALEN mRNAs induce mutations dose-dependently as increasing the mRNA concentrations increased the mutation efficiency. Dose-dependent induction of mutations was also shown by Dahlem *et al.,* (2012) as when they increased the amount of TALEN mRNAs, the induction of mutations was also increased with up to 98.5% targeting efficiency.

Only 3 out of 8 *def6a* F_0 founders and 6 out of 30 *swap70b* F_0 founders transmitted the heritable mutations to the offspring, indicating 37% and 20% germline transmission efficiencies, respectively (**Figure 3.7**). Sequence confirmation of these 9 founders (3 for *def6a* and 6 for *swap70b*) demonstrated that 2 of the *def6a* F_0 founders contained frameshift mutations (-28bp and -2bp or +19bp) with 20% and 10% germline transmission efficiencies, respectively (**Figure 3.8; Table 3.1**) and 3 of the *swap70b* F_0 founders contained frameshift mutations (-54bp, -82bp and -43bp/+68bp) with 54%, 40% and 3% germline transmission efficiencies, respectively. (**Figure 3.9; Table 3.2**). Therefore, while both *def6a* F_0 founders containing the frameshift mutations were used to establish a knock-out *def6a* mutant line, the *swap70b* F_0 founders containing -82bp and -54bp deletions were used to establish knock-out

swap70b mutant lines since the 54bp deletions include the 5'UTR and the start codon of *swap70b* locus (**Figure 3.9** and www.ensembl.org). Fin-clipped genotyping of the adult *def6a* and *swap70b* F_1 generations and sequencing analysis revealed that only 1 *def6a* F_1 founder was carrying a frameshift mutation (-20bp/+9bp) in one allele and 2 *swap70b* F_1 founders were carrying the same (54bp) deletions in one allele lacking both 5'UTR and AUG (**Figure 3.10**). ExPasy translation tool-mediated translation of cDNA sequences containing the specific mutations into amino acid sequences demonstrated that while 54bp deletion would produce either a truncated Swap70b protein formed of 547 amino acids or the translation might not occur, -20bp/+9bp indel mutations would produce a premature stop codon after 27 amino acids resulting in the formation of a truncated Def6a protein (**Figure 3.11**). Thus, these heterozygous founders (*def6a*$^{+/qmc811}$ and *swap70b*$^{+/qmc809}$) were used to generate *qmc811 def6a* and *qmc809 swap70b* homozygous mutant lines. Identification of homozygous mutants (*def6a*$^{qmc811/qmc811}$ and *swap70b*$^{qmc809/qmc809}$) revealed that *qmc811* and *qmc809* mutant alleles were inherited at the expected mendelian rate (25%) (**Figures 3.12** and **3.13**) and these homozygous mutant lines were used for the phenotypic analysis and for establishing *qmc813* double homozygous mutant line (*def6a*$^{qmc811/qmc811}$; *swap70b*$^{qmc809/qmc809}$) since they were alive and fertile. Double homozygous mutants (*def6a*$^{qmc811/qmc811}$; *swap70b*$^{qmc809/qmc809}$) were identified and the distribution of mutant alleles correlated with the expected mendelian rate (5 in 81 fish; 6%) for double homozygous mutants (**Figure 3.16**). Sequencing analysis confirmed the single homozygosity of *qmc811* and *qmc809* mutant lines (**Figure 3.11**) and the double homozygosity of *qmc813* mutant line (**Figure 3.17**).

8.2. The roles of *def6a* and *swap70b* in zebrafish gastrulation

8.2.1. *def6a* and *swap70b* are required for CE cell movements but not for cell fate specification during gastrulation

Gastrulation is a developmental process of the embryo that establishes the three germ layers and the basic body plan. Coordinated regulation of cell fate specification and cell movements ensures the formation of dorsoventral and anteroposterior axes properly. Convergence and extension (CE) cell movements are the major driving forces, in which mesendodermal and ectodermal cells move directly towards the dorsal midline to become medio-laterally arranged (convergence) and intercalate with the neighbour cells to extend the anteroposterior body axis (extension) (Warga and Kimmel, 1990; Wallingford *et al.,* 2002; Montero and Heisenberg, 2004; Montero *et al.,* 2005). Studies have demonstrated that the non-canonical Wnt/PCP signalling pathway is the key regulator of CE cell movements during zebrafish gastrulation since disrupting some of the major components of the Wnt/PCP signalling pathway like *slb/wnt11* or *ppt/wnt5* caused CE cell movement and mediolateral cell elongation defects. The typical phenotypes observed in the CE mutants/morphants are characterised by reduced and broadened body axis, reduced CE cell movements during gastrulation with less directed and polarised cells and occasionally cyclopia but normal cell fate specification (Hammerschmidt *et al.,* 1996; Solnica-Krezel *et al.,* 1996; Heisenberg and Nüsslein-Volhard, 1997; Heisenberg *et al.,* 2000; Topczewski *et al.,* 2001; Sumanas *et al.,* 2001; Jessen *et al.,* 2002; Kilian *et al.,* 2003; Carreira-Barbosa *et al.,* 2003).

To understand the roles of *def6a* and *swap70b* in zebrafish embryogenesis, former graduate students, Katerina Goudevenou, Xiaoou Xu and Wai Ho Shuen used MOs (ATG or splice) to knock-down *def6a* and/or *swap70b* expressions and demonstrated that *def6a* and *swap70b* morphants were reminiscent of the CE mutants/morphants. Specifically, the phenotypic and whole mount i*n situ* hybridisation analyses of both *def6a* and *swap70b* morphants revealed that the morphants displayed reduced body length with a twisted tail, undulated notochord, expanded somites and CE cell movement defects but normal cell fate specification (Goudevenou *et al.,* 2011; Shuen, MRes thesis, 2010; Xu, PhD thesis, 2015). The double morphants showed more severe phenotype than single morphants suggesting a functional redundancy between *def6a* and *swap70b* (Xu, PhD thesis, 2015). Similarly, analysis of single *qmc811, qmc809* and double *qmc813* mutant lines revealed that while all mutant lines developed normally until gastrulation, a developmental delay (usually 1-2 hours lag) and a shortened body axis were observed at the end of gastrulation (tail-bud stage; 10hpf), characteristic of CE cell movements. (**Figures 4.1 and 4.2**). However, in contrast to the CE mutants/morphants and MO-induced *def6a* and *swap70b* morphants, shortening of body axis

and twisting of the tail were rescued during segmentation period in *qmc809, qmc811* and *qmc813* mutant lines resulting in normal development of somites, tail and brain compartments after gastrulation as shown in **Figure 4.1**.

In line with the CE morphant/mutant and *def6a* and/or *swap70b* morphant phenotypes, unaltered expression pattern of cell fate specification markers, *cdx4, bmp2b, chd* and *ntl,* indicated that *def6a* and/or *swap70b* are not required for cell fate specification (**Figure 4.3**). Nevertheless, posterior shift and mediolateral expansion of the *pax2a, fgf8, krox20* and *hoxb1a* expression patterns in single and mutant lines indicated the CE cell movement defects (**Figure 4.5**). Indeed, Solnica-Krezel *et al.,* (1996) and Carreira-Barbosa *et al.,* (2003) also observed posterior shift and expansion of *pax2a* expression pattern in *tri/vangl2* mutants and *pk1* morphants, respectively, and have suggested that while the extension defects resulted in the posterior shift, the convergence defects resulted in the expansion. The posterior shift and expansion in all markers were more severe in *swap70b*$^{qmc809/qmc809}$ and *def6a*$^{qmc811/qmc811}$*; swap70b*$^{qmc809/qmc809}$ double mutants than *def6a*$^{qmc811/qmc811}$ mutants, suggesting a dominant effect of *swap70b.* In addition, while slight reduction in *pax2a* and *fgf8* expressions was observed, a strong reduction in *krox20* and *hoxb1a* expression was observed that caused loss of expression in r5 and neural keel, respectively (**Figure 4.5**). As *hoxb1a*-deficient embryos have shown defective migration of the facial branchiomotor neurons (McClintock *et al.,* 2002) and some of the Wnt/PCP signalling pathway components like *pk1a/pk1b* (Carreira-Barbosa *et al.,* 2003; Rohrschneider *et al.,* 2007), *trilobite/tri* (Jessen *et al.,* 2002) and *off-limits/frizzled3a* (Wada *et al.,* 2005; 2006) have been shown to regulate facial neuron migration, the impaired expression of *hoxb1a* might be due to the Wnt/PCP signalling pathway affected by the loss of *def6a* and/or *swap70b*. However, the lack of *krox20* expression in r5 was rescued later in segmentation stages. This result suggests that the specification of r5 was probably affected by the developmental delay observed in the mutant lines.

Anterior movement and convergence of the lateral mesendodermal and ectodermal cells were found severely impaired in *def6a* and/or *swap70b*-deficient zebrafish embryos, indicating that *def6a* and *swap70b* are required for CE cell movements during gastrulation (**Figures 4.5** and **4.6**). The significance of CE cell movement defects in the *qmc809, qmc811* and *qmc813* mutant lines were confirmed by the statistical analyses and no significant (N.S) differences between single and double mutant lines indicated the absence of additive effect of both mutations in double homozygous mutants (**Figure 4.7**).

Because *fgf8* induces the development of mesodermal tissues, Reifers et *al.,* (1998) tested *myoD* expression in the *ace/fgf8* mutants. Strongly reduced expression during 80% epiboly and interruption in somite formation during somitogenesis indicated that *fgf8* is required for

the expression of *myoD* and thus for dorsoventral patterning (Reifers *et al.,* 1998). However, even though *def6a*$^{qmc811/qmc811}$, *swap70b*$^{qmc809/qmc809}$ and *def6a*$^{qmc811/qmc811}$; *swap70b*$^{qmc809/qmc809}$ double mutants also showed defects in the expression of *myoD* during tail-bud stage, these defects were most probably due to impaired CE cell movements. Because the *ace* mutants displayed reduced expression but not shorter length and expansion of adaxial cells during gastrulation and somitogenesis stages (Reifers *et al.,* 1998). Therefore, while the reduced length of *myoD* might be consequence of extension defects, the expansion of *myoD* might be the consequence of convergence defects, independently from the *fgf8* signalling. However, in contrast to the finding indicating normal development of somites in *def6a* and/or *swap70b*-deficient lines (**Figure 4.9)**, most of the CE mutants/morphants and *def6a* and *swap70b* morphants displayed shortened and expanded somites after gastrulation (Carreira-Barbosa *et al.,* 2003; Goudevenou *et al.,* 2011; Xu, PhD thesis, 2015) and even the loss of *myoD* expression in posterior somites during somitogenesis (Goudevenou *et al.,* 2011). Since Goudevenou *et al.,* (2011) also observed the lack of *fgf8* expression in posterior somites during somitogenesis, the loss of *myoD* expression in posterior somites was linked to the *fgf* signalling, because myoD expression in somites depends on the expression of *fgf8a* (Groves *et al.,* 2005).

Analysis of *otx2, pax2a, krox20, myoD, fgf8, ntl* and *shh* gene expression at segmentation stage (22hpf) confirmed that neural patterning, brain morphogenesis, development of somites and tail was normal in single as well as double homozygous mutants (**Figures 4.8** and **4.9**). These results may be the consequence of three possible reasons for maternal zygotic mutants according to Stainier *et al.,* (2017). (i) Even though some studies have shown that morphant phenotypes recapitulated the known mutant phenotypes (Draper *et al.,* 2001; Nasevicius and Ekker, 2000), recent studies have shown that there is a discrepancy between mutant and morphant phenotypes, strongly indicating MO off-target effects (Formstone *et al.,* 2005; Nourizadeh-Lillabadi *et al.,* 2010; Aman *et al.,* 2011; Aranguren *et al.,* 2011; Fleisch *et al.,* 2013; van Impel *et al.,* 2014; Su *et al.,* 2014; Kok *et al.,* 2015). Interestingly, Kok *et al.,* (2015) have shown that 10 mutant lines out of over 20 genes did not display the previously reported morphant phenotypes and these MO-induced discordant phenotypes include mostly the curved/kinked trunk. Specifically, Phosphatase and TENsin homolog, PTEN, is a tumor suppressor gene regulating normal cell proliferation, migration and survival via the phosphoinositide 3 (PI3) kinase/Akt pathway. Since blocking PI3 kinase function has been shown to induce CE cell movement defects and less directional protrusions in the leading edge of the cells during zebrafish gastrulation, knock-down effects of *ptenb* was investigated during gastrulation and later stages (Croushore *et al.,* 2005; Yeh *et al.,* 2011). While *ptenb* morphants showed impaired gastrulation movements, lagged epiboly progression and kinked

tail (Croushore *et al.,* 2005; Yeh *et al.,* 2011), *ptenb* mutants did not show any phenotypes during gastrulation (Faucherre *et al.,* 2008; Kok *et al.,* 2015). In line with these studies, Formstone *et al.,* (2005) have also shown that the *flamingo/celsr2* mutants did not exhibit a gastrulation phenotype, but *celsr2* morphants displayed mild CE cell movement defects. Thus, the discrepancy between *def6a* and/or *swap70b* morphant and mutant phenotypes may be due to MO off-target effects. (ii) The hypomorphic nature of mutant allele causes partial loss of a gene function in null mutants (Stainier *et al.,* 2017). Therefore, *def6a* and *swap70b* alleles may be hypomorphic resulting reduction in gene function but not a complete loss. (iii) Rossi *et al., (*2015) have shown that a set of extracellular matrix proteins and the paralogue of *vegfaa* gene, *vegfab*, were upregulated to compensate the loss of *egfl7* and *vegfaa* functions, respectively, in mutants but not in morphants. This suggests that the activation of genetic compensation mechanism rescues the mutant phenotype resulting in a wild-type phenotype. Indeed, the paralogues of *def6a* and *swap70b* or other GEFs may compensate their function during embryonic development. RT-PCR analysis of the paralogues have shown that while *def6a* and *swap70b* are expressed from 1hpf to 72hpf indicating maternal and zygotic expression, the expression of *def6c* and *swap70a* starts at 24hpf, (or even between 10hpf and 24hpf) (Shuen, MRes thesis, 2010), suggesting that *def6c* and *swap70a* may compensate the CE cell movement defects after gastrulation resulting in the normal development of somite, tail and brain structures. In addition, although *def6a* and *swap70b* have been shown to regulate CE cell movements during gastrulation, the extent of affecting CE cell movements during gastrulation was not as significant as other CE mutants displaying more shortened body axis, strongly reduced CE, more shortened and widened notochord and somites. This result might be due to the partial redundancy between *def6a/swap70b* and other GEFs. Considering the high numbers of human GEF members (more than 70 members in three distinct families; Dbl family, DOCK family and DEF6/SWAP70 family) all activating Rho GTPases, this possibility suggests the zebrafish orthologues of some of these GEFs may also have a role in CE cell movements and could compensate the loss of *def6a* and/or *swap70b.*

In summary, *def6a* and/or *swap70b*-deficient zebrafish embryos have shown shortened body axis and CE cell movements during gastrulation, however these phenotypes were rescued after gastrulation.

8.2.2. Def6a and Swap70b act upstream of Cdc42 and Cdc42/Racl GTPases, respectively in the non-canonical Wnt/PCP/Ca^{2+} signalling pathway to regulate CE cell movements

Investigations of molecular mechanisms underlying CE cell movements in vertebrate gastrulation have suggested that they are controlled by the non-canonical Wnt/PCP and Wnt/Ca^{2+} signalling pathways (Heisenberg *et al.,* 2000, Tada and Smith, 2000; Tada *et al.,* 2002; Choi and Han, 2002; Wallingford *et al.,* 2000; Wallingford *et al.,* 2002). In both *Drosophila* and vertebrates, Rho GTPases have been shown to regulate cell polarity and gastrulation movements through acting downstream of the non-canonical Wnt/PCP/Ca^{2+} signalling pathway (Eaton *et al.,* 1996; Strutt *et al.,* 1997; Fanto *et al.,* 2000; Habas *et al.,* 2001; Marlow *et al.,* 2002; Wallingford *et al.,* 2002; Habas *et al.,* 2003; Tahinci and Symes, 2003; Zhu *et al.,* 2006). Specifically, while Rho and Rac are regulated by the Wnt/PCP signalling pathway (Habas *et al*., 2003; Tahinci and Symes, 2003), Cdc42 is controlled by independent but parallel pathways of both Wnt/PCP and Wnt/Ca^{2+} signalling pathways (Eaton *et al.,* 1996; Harden *et al.,* 1999; Djiane *et al.,* 2000; Choi and Han, 2002; Schambony and Wedlich, 2007; reviewed in Kestler and Kühl, 2008).

To understand whether *def6a* and *swap70b* act downstream of *wnt11* or *wnt5*, rescue experiments by co-injecting *wnt5b or wnt11* MOs and *def6a or swap70b* RNAs were carried out. Interestingly, while *def6a* RNA injection rescued only *wnt5b* MO-induced CE cell movement defects, *swap70b* RNA injection rescued only *wnt11* MO-induced CE cell movement defects, indicating that Def6a acts downstream of Wnt5b and Swap70b acts downstream of Wnt11 in the non-canonical Wnt signalling pathway (Goudevenou *et al.,* 2011; Xu, PhD thesis, 2015).

To investigate whether Cdc42, RhoA and Racl GTPases are involved in the *def6a* or *swap70b*-mediated regulation of CE cell movements during zebrafish gastrulation, Gfp-tagged Cdc42, RhoA and Racl GTPases were overexpressed in *def6a*$^{qmc811/qmc811}$ and *swap70b*$^{qmc809/qmc809}$ mutants. While overexpression of Cdc42 robustly rescued CE cell movement defects in both *def6a*$^{qmc811/qmc811}$ and *swap70b*$^{qmc809/qmc809}$ mutants (**Figures 5.1** and **5.6**), overexpression of Racl robustly rescued CE cell movement defects only in *swap70b*$^{qmc809/qmc809}$ mutants (**Figures 5.2** and **5.7**). In contrast, overexpression of RhoA failed to rescue CE cell movement defects in both *def6a*$^{qmc811/qmc811}$ and *swap70b*$^{qmc809/qmc809}$ mutants (**Figures 5.3, 5.4, 5.8** and **5.9**). These results clearly suggest that Def6a and Swap70b act upstream of Cdc42 whereas Swap70b also acts upstream of Racl in the non-canonical Wnt/PCP signalling pathway.

However, some control experiments such as overexpression of Gfp and Gfp-tagged Rho GTPases in WT embryos were not included when interpretating the data. In control experiments, CE cell movement defects were not statistically quantified like all other rescue experiments. Overexpression of 200pg Gfp-tagged Rho GTPases in WT embryos caused CE cell movement phenotype suggesting that they are functional.

Moreover, actin staining of the dorsal ectodermal cells in WT, *def6a*$^{qmc811/qmc811}$ and *swap70b*$^{qmc809/qmc809}$ mutants at shield and tail-bud stages demonstrated that the mediolateral cell elongation was affected by *def6a* and *swap70b* deficiency because the protrusions and cell polarisation were less in both mutant lines relative to WT controls (**Figure 5.11**). These results indicate that the delayed and impaired CE cell movements are most likely the consequence of disrupted actin organisation and loss of cell polarisation since mediolateral cell elongation was suggested as a prerequisite for normal CE cell movements (Jessen *et al.,* 2002; Marlow *et al.,* 2002; Topczewski *et al.,* 2001; Wallingford *et al.,* 2000). In line with these findings, Roszko *et al.,* (2009) have suggested that wider notochord phenotype in CE mutants/morphants also indicates reduced mediolateral cell polarity and thus mediolateral cell intercalations.

Importantly, expression of *wnt5b* and *wnt11* was upregulated in *def6a*$^{qmc811/qmc811}$, *swap70b*$^{qmc809/qmc809}$ and *def6a*$^{qmc811/qmc811}$; *swap70b*$^{qmc809/qmc809}$ double mutants suggesting that *def6a* and/or *swap70b* functions to dampen expression of *wnt5b* and *wnt11* **(Figure 5.12)**. Interestingly, upregulation of *wnt11* was higher than *wnt5b* in all mutant lines indicating that the abrogation of *def6a* or *swap70b* affects *wnt11* expression more than *wnt5b* expression. In line with the previous hypothesis about the relation between *def6a/swap70b* and *wnt11*, even more upregulation was observed in *swap70b*$^{qmc809/qmc809}$ mutants than *def6a*$^{qmc811/qmc811}$ mutants, which strongly suggests that Swap70b acts downstream of Wnt11. The upregulation of *wnt5b* and *wnt11* in *def6a*$^{qmc811/qmc811}$; *swap70b*$^{qmc809/qmc809}$ double mutants was similar to *swap70b* mutants indicating a dominant effect of *swap70b* (**Figure 5.12**). These results suggest that the expression of *wnt5b* and *wnt11* is directly affected by the loss of *def6a and swap70b* even though they both act downstream of Wnt signalling. However, this idea still needs a support from an independent method such as qPCR.

Figure 8.1 illustrates a proposed model that summarises the roles of *def6a* and *swap70b* in the Wnt/PCP/Ca^{2+} signalling pathway during zebrafish gastrulation. In this model, Def6a acts upstream of Cdc42 and Swap70b acts upstream of Cdc42 and RacI GTPases to regulate cell polarity and CE cell movements of gastrulation in the non-canonical Wnt/PCP signalling pathway activated by Wnt5 and Wnt11. Whereas it has been thought that Cdc42 only acts downstream of the Wnt/Ca^{2+} signalling pathway, recent findings have suggested that Cdc42 is also involved in the activation of Jnk signalling to regulate the CE cell movements during vertebrate gastrulation (Schambony and Wedlich, 2007; reviewed in Kestler and Kühl, 2008). These findings in vertebrate gastrulation was also in line with the reports in mammalian cells which showed the activation of Jnk in a Cdc42-manner (Coso *et al.,* 1995; Minden *et al.,* 1995; Vogel, 2013). Thus, it is highly likely that the activation of Cdc42 and Cdc42/RacI GTPases by Def6a and Swap70b respectively, leads to the activation of Jnk signalling in the non-canonical Wnt/PCP signalling pathway. Consistent with the notion that Wnt/PCP signalling diverges into a Daam-Rho-ROCK and Rac-Jnk pathways at the Dishevelled level (Habas *et al.,* 2001; Habas *et al.,* 2003), the redundancy of RhoA in *def6a* and *swap70b*-mediated regulation of CE cell movements have suggested that Def6a and Swap70b are involved in Rac-Jnk or Cdc42-Jnk pathway but not in Daam-Rho-Rock pathway. Furthermore, Seo *et al.,* (2010) have shown that the activation of Jnk signalling represses the expression of *wnt11*, via a feedback loop. To determine the role of Jnk signalling during vertebrate gastrulation, the Jnk activators, *mkk4b* and *mkk7* were knocked-down. While *mkk4b* morphants exhibited CE cell movement defects, shortened body length and widened somites, *mkk7* morphants exhibited only shortened body length and somite defects. Similar to the results described here, they also observed the upregulation of *wnt11* in *mkk4b* morphants. Overexpression of an active form of Mkk4b that causes the ectopic activation of Jnk signalling repressed Wnt11 expression. Cell lineage tracing studies have shown that loss of mkk4b-Jnk signalling induced elevated expression of *wnt11* in a non-cell-autonomous manner (Seo *et al.,* 2010). Therefore, elevated expression of *wnt5b* and *wnt11* in *qmc811, qmc809* and *qmc813* mutant lines suggest that loss of *def6a* and *swap70b* functions interfered with the Jnk activation and thus prevented the repression of *wnt11* (and possibly *wnt5b)* inducing the CE cell movement defects, as aberrant expression of *wnt11* has been shown to induce CE cell movement defects (Seo *et al.,* 2010). In addition, checking activation states of Jnk by Western blotting in WT and mutants would support the hypothesis of *def6a* and *swap70b* leading to activated Jnk signalling. Even though Bécart *et al.,* (2008) have shown that Def6 regulates the development of both Th1 and Th2 cell inflammatory responses in mice by controlling the Ca^{2+}-NFAT signalling pathway, the upregulation of *wnt11* strongly suggests that it is a component of the Wnt/PCP signalling pathway. However, considering that *def6a* and *swap70b* act also in a non-redundant manner*, def6a* may also act downstream of Wnt/Ca^{2+} signalling pathway.

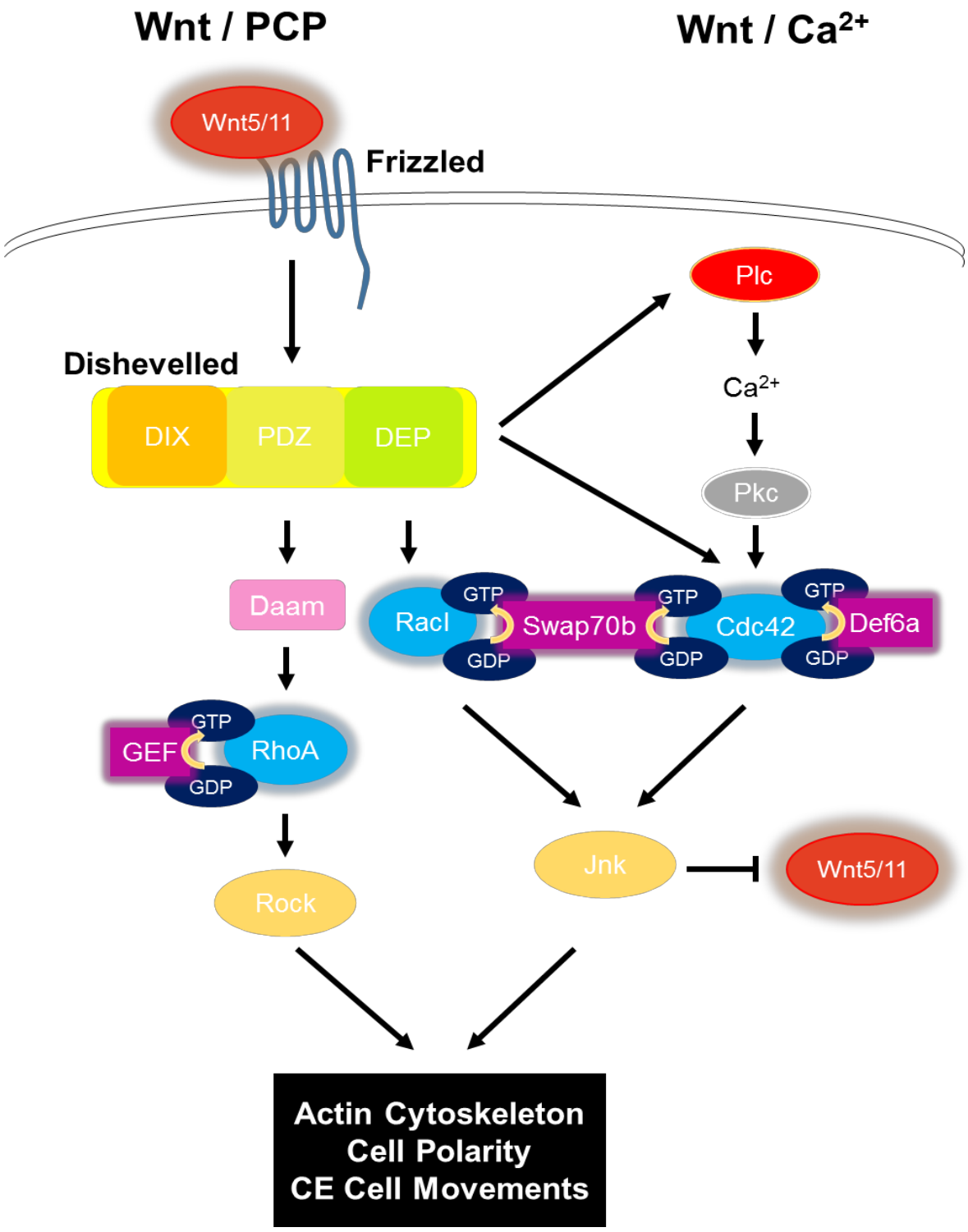


Figure 8.1 The Wnt/PCP/Ca^{2+} signalling pathway model demonstrating the roles of *def6a* and *swap70b* in zebrafish gastrulation. Def6a acts upstream of Cdc42 and Swap70b acts upstream of Cdc42 or Racl to regulate the cell polarity and CE cell movements of gastrulation in the non-canonical Wnt/PCP/Ca^{2+} signalling pathway activated by Wnt5b and Wnt11. Plc: Phospholipase C, Pkc: Protein kinase C, Rock: Rho kinase, Daam: Dishevelled-associated activator of morphogenesis, Jnk: Jun-N-terminal kinase. GDP: Guanosine diphosphate, GTP: Guanosine triphosphate, DIX: Dishevelled/Axin domain, PDZ: a central PSD-95, DLG, ZO1 domain, DEP: a Dishevelled, EGL-10, Pleckstrin domain.

8.3. *def6a* and *swap70b* play a role in the development of myeloid cells during zebrafish haematopoiesis

To address the role of *def6a* and *swap70b* in vertebrate haematopoiesis, the kidney marrow cells of WT, *def6a*$^{qmc811/qmc811}$, *swap70b*$^{qmc809/qmc809}$ mutants and *def6a*$^{qmc811/qmc811}$; *swap70b*$^{qmc809/qmc809}$ double mutants were analysed by flow cytometry. Statistical analyses revealed that the myeloid population was decreased by 2-fold in *def6a*$^{qmc811/qmc811}$ mutants and by 3-fold in both *swap70b*$^{qmc809/qmc809}$ and *def6a*$^{qmc811/qmc811}$; *swap70b*$^{qmc809/qmc809}$ double mutants (**Figure 6.2**). Additionally, even though there was a slight increase in all other cell lineages, erythrocytes, immature progenitors and lymphocytes, the difference was not significant because the lineage choice was similar for each population (**Figure 6.2**). This finding was not consistent with the hypothesis suggested by Ripich and Jessberger (2011) demonstrating that Swap70 is required for splenic and stress-induced erythropoiesis in mice as Swap70 deficiency caused disruption in α4 integrin-dependent maturation and development of erythrocytes under normal and stress conditions. Hotfilder *et al.,* (1999) showed that differentiation of myeloid and erythrocyte cells requires the downregulation of Def6, but no significant increase or decrease in the number of erythrocyte cells was observed in *def6a*$^{qmc811/qmc811}$ and *def6a*$^{qmc811/qmc811}$; *swap70b*$^{qmc809/qmc809}$ double mutants. Interestingly, the decrease in myeloid cell population was similar in *swap70b*$^{qmc809/qmc809}$ and *def6a*$^{qmc811/qmc811}$; *swap70b*$^{qmc809/qmc809}$ double mutants, indicating non-redundancy between *def6a* and *swap70b* during zebrafish haematopoiesis and a dominant effect of *swap70b*. Consistently, a dominant Swap70-dependent phenotype was also observed in double knock-out (*Def6*$^{-/-}$*; Swap70*$^{-/-}$) mice mutants (Ripich *et al.,* 2016). Additionally, since both *def6a* and *swap70b* mutants and *def6a; swap70b* double mutants have shown the similar differences relative to WT such as decrease in myeloid cell population and equal increase in other cell populations, *def6a and swap70b* do not play agonistic or antagonistic roles during zebrafish adult haematopoiesis. In contrast, Ripich *et al.,* (2016) have suggested that Def6 and Swap70 play antagonistic roles to regulate the hematopoietic stem and precursor cell homeostasis. Taken together, the preliminary results suggest that *def6a* and *swap70b* play a role in zebrafish haematopoiesis through promoting myeloid cell differentiation. As suggested by Ripich and Jessberger, (2011) that the integrin-regulatory function of Swap70 (Sivalenka and Jessberger, 2004; Pearce *et al.,* 2006) modulates erythropoiesis, it is possible that Def6 also modulates haematopoiesis in integrin-dependent manner (Samson *et al.,* 2007; Cote *et al.,* 2015). However, more experiments are required to expand our knowledge about the roles of Def6 and Swap70 in vertebrate haematopoiesis.

8.4. *def6a* and *swap70b* act in a partially redundant manner during zebrafish embryogenesis and in a non-redundant manner during haematopoiesis

Since Def6 and Swap70 are closely related, the functional redundancy was analysed through generating single and double knock-out mutant lines. Preliminary experiments using MOs revealed that *def6a; swap70b* double morphants showed more severe phenotype than single morphants. Additionally, ectopic expression of Def6a and Swap70b partially rescued the CE cell movement defects in *swap70b* and *def6a* morphants, respectively. These results clearly indicated a functional redundancy between *def6a* and *swap70b.* However, as mentioned before *def6a* was found to act downstream of *wnt5b*, whereas *swap70b* was found to act downstream of *wnt11*, suggesting distinct roles. Indeed *wnt5b; swap70b* double morphants showed more severe phenotype than single morphants, indicating that *def6a* and *swap70b* have also distinct roles in zebrafish gastrulation (Xu, PhD thesis, 2015). Consistent with these results, the lack of additive CE cell movement phenotype in *def6a*$^{qmc811/qmc811}$*; swap70b*$^{qmc809/qmc809}$ double mutants strongly indicates that *def6a* and *swap70b* don't act in a redundant manner. In contrast, rescue experiments have shown that both *def6a* and *swap70b* act upstream of *cdc42* in the non-canonical Wnt/PCP signalling pathway. Thus, these results support the hypothesis that *def6a* and *swap70b* have also overlapping roles in the zebrafish embryogenesis. In addition, the absence of additive phenotype in double mutants during haematopoiesis has also suggested that *def6a* and *swap70b* act in a non-redundant manner during haematopoiesis. Moreover, since the double mutants exactly phenocopied all phenotypes observed in *swap70b* mutants (expression patterns of all markers, upregulation of *wnt* ligands and the significant decrease in myeloid cells) (**Chapter 4, 5** and **6**), it is highly likely that *swap70b* demonstrates a dominant role over *def6a* in both embryogenesis and haematopoiesis. Taken together, *def6a* and *swap70b* possess partial overlapping roles during embryogenesis and non-overlapping roles during haematopoiesis.

Even though *def6a* and *swap70b* act partially redundant roles in zebrafish embryogenesis, the comprehensive understanding of the relationship between DEF6 and SWAP70 in the non-canonical Wnt/PCP and Wnt/Ca^{2+} signalling pathways remains elusive. Thus, overexpression of Swap70b and Def6a to rescue the CE cell movement defects in *def6a* and *swap70b* mutants respectively, might provide insight into the current knowledge about this protein family. For a deeper analysis, co-immunoprecipitation and pull-down assays can be performed to determine the direct interactions between Wnt/PCP components and Def6a/Swap70b proteins when the zebrafish antibodies are available.

8.5. Comparison of knock-out mice and knock-out zebrafish phenotypes

Def6, Swap70 knock-out and *Def6; Swap70* double knock-out mice models have been generated to study their functions in the immune system and haematopoiesis. Other than inflammatory response defects, autoimmune diseases and defective haematopoiesis, no phenotypes has been reported to date. Disrupted polarity of coat hair and of stereocilia in the cochlea and defects in neural tube closure are the PCP defects reported in the mice knock-out mutants of core Wnt/PCP mouse genes like *Fz6, Dsh1, Celsr2, Looptail/Vangl2* (Kibar *et al.,* 2001; Hamblet *et al.,* 2002; Guo *et al.,* 2004; Tissir *et al.,* 2010; Wang *et al.,* 2006; reviewed in Gray *et al*., 2011). Interestingly, none of these PCP defects have been reported before for *Def6, Swap70* and *Def6; Swap70* double mice mutants. This discrepancy between mice and zebrafish mutant phenotypes in terms of PCP defects may be the consequence of compensation of Def6 and Swap70 deficiencies by other mouse GEFs. Rescued CE cell movement phenotype after gastrulation in zebrafish embryonic development would explain the lack of PCP defects in mice mutants. Indeed, it would be interesting to see whether the loss of *Def6* and *Swap70* disrupts the tissue polarity in mammalian cells and hair follicles.

8.6. BioID-mediated identification of DEF6 interactome in Jurkat T cells

To investigate the roles of DEF6 in Jurkat T cells, BirA*-tagged full-length (1-631) and the truncated domains of DEF6 (N-terminal DEF6 (1-108), PH DEF6 (214-341) and C-terminal DEF6 (312-631)) (**Figures 7.2** and **7.3**) were expressed in Jurkat T cells to induce biotinylation of interacting and/or vicinal proteins. Streptavidin beads-mediated affinity capture of the biotinylated proteins revealed enhanced and distinct biotinylation patterns for FL DEF6, N-ter DEF6, PH DEF6 and C-ter DEF6 samples confirming the effective biotinylation and capture of biotinylated proteins (**Figure 7.5**). Mass spectrometry analysis of the biotinylated proteins identified 514 proteins in 404 different clusters in total, of which 277 were excluded since they were considered as false positives (**Appendix VII**). GO term-categorisation of the remaining 127 clusters revealed that in addition to the proteins identified as components of the previously reported biological processes that DEF6 is involved like actin cytoskeleton organisation (5%; 7 proteins) and mRNA translation (9%; 13 proteins) (Mavrakis *et al.,* 2004; Remon, PhD thesis, 2016; Alsayegh, PhD thesis, 2017), the proteins regulating different biological processes like transcription (26%; 36 proteins), RNA splicing/processing (20%; 28 proteins), metabolic processes (12%; 17 proteins) and protein folding/modification (11%; 15 proteins) were also identified in DEF6 interactome (**Table 7.1**; **Figure 7.8**). Indeed, identification of Rac2, PKC and PABP proteins, which had already been shown to be in close proximity or interact with

DEF6 (Mavrakis *et al.,* 2004; Fanzo *et al.,* 2006 Worthmann *et al.,* 2013 Huttlin *et al.,* 201; Remon, PhD thesis, 2016; Alsayegh, PhD thesis, 2017), suggested that DEF6 might play a role in additional biological processes other than actin cytoskeleton organisation and mRNA translation. Therefore, to further confirm the proof of principle, a protein regulating actin cytoskeleton, Coronin-1A (CORO1A) and a protein regulating RNA splicing/processing, Heterogeneous nuclear ribonucleoproteins A2/B1 (HNRNPA2B1) were selected for immunohistochemistry analysis. DEF6 and CORO1A co-localised partially at the immunological synapse (IS) both regulating the actin cytoskeleton dynamics of IS **(Figure 7.11)** and co-localised partially at the F-actin rich cell protrusions of resting T cells **(Figure 7.12)**. However, in contrast to CORO1A, no co-localisation or proximity was detected between DEF6 and HNRNPA2B1 during IS formation and resting cells as while DEF6 was localised to the IS and membrane protrusions, HNRNPA2B1 was localised to the nucleus (**Figures 7.15** and **7.16**). These results suggest that some of the proteins located in nucleus may be the false positives. However, it has been suggested that DEF6 also translocates to the nucleus (Peter Jones, personal comm.) and this translocation would explain the identification of proteins in the nucleus. Indeed, BirA*-DEF6 fusions *in vivo* biotinylate the proteins for 24h which is a long time period to shuttle in and out of the nucleus. In addition, most of the proteins of DEF6 interactome were found same for FL, PH and C-term DEF6 fusions suggesting that they may not be false positives (**Table 7.1**).

Taken together, even though no co-localisation was detected between HNRNPA2B1 and DEF6 to confirm the novel functions, the partial co-localisation between DEF6 and CORO1A was confirmed in resting and activated cells, indicating that DEF6 might act as a multifunctional protein to regulate actin cytoskeleton organisation, mRNA translation and possibly transcription, mRNA splicing/processing, metabolic processes and protein processing (**Figure 8.2**). The coordinated regulation of signal transduction, alternative splicing, translation and nonsense-mediated decay (NMD) has been suggested to regulate the expression of various genes in humans (Lewis *et al*., 2003; Graveley, 2005; Lareau *et al*., 2007; Soergel *et al*., 2013). Given that DEF6 regulates signal transduction, mRNA surveillance and translation (Hey *et al*., 2012; Remon, PhD thesis, 2016; Alsayegh, PhD thesis, 2017), it is tempting to speculate that DEF6 plays a role also in mRNA splicing and transcription since significant portions of the identified DEF6 interactors are implicated in transcription and mRNA splicing/processing. The serine/arginine-rich splicing factor (SRSF) family has been suggested as one of the key regulators of constitute and alternative splicing (Graveley, 2000; 2005), mRNA export (Huang and Steitz, 2001), mRNA stability (Lemaire *et al*., 2002), translation (Sanford *et al*., 2004) and NMD (Zhang and Krainer, 2004), Investigation of interaction or close proximity between SRSF proteins and DEF6 might determine whether

DEF6 can exert any role in the different steps of gene expression pathway. Moreover, consistent with the DEF6 interactome analysis showing that DEF6 interacts with or in close proximity with PKCα (PRKCA), Huttlin *et al.,* (2017) have shown that PKCθ (PRKCQ) interacts with DEF6 in HEK293T cells and Bécart *et al.,* (2008; 2009) have shown that DEF6 regulates T cell inflammatory responses perhaps through PKC which is an important component of the Ca^{2+}-NFAT signalling. Therefore, potential interaction between DEF6 and PKC during zebrafish gastrulation should be analysed to test whether Def6a also acts downstream of the Wnt/Ca^{2+} signalling pathway.

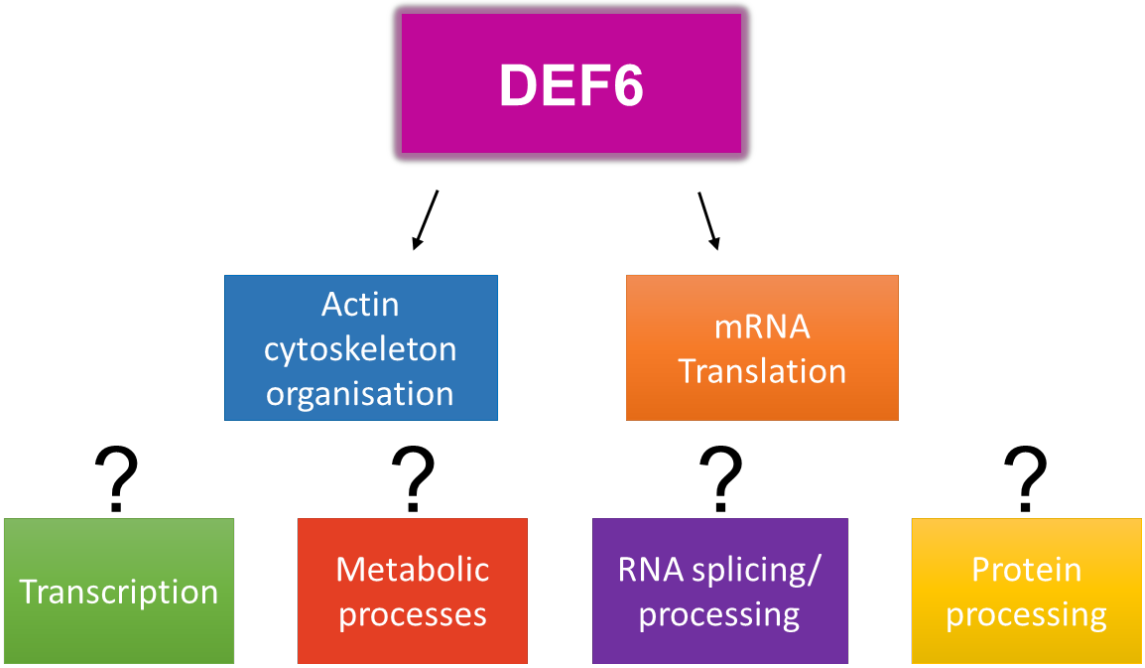


Figure 8.2 Confirmed and hypothetical roles of DEF6 in T cells. Exploring DEF6 interactome in T cells revealed that DEF6 might be involved not only in actin cytoskeleton organisation and mRNA translation but also in transcription, RNA splicing/processing, metabolic processes and protein processing.

8.7. Conclusion

In conclusion, by using TALEN-mediated genome editing technique *def6a* and *swap70b* loci were targeted and single (*def6a*$^{qmc811/qmc811}$ and *swap70b*$^{qmc809/qmc809}$) and double (*def6a*$^{qmc811/qmc811;}$ *swap70b*$^{qmc809/qmc809}$) homozygous mutant lines were established. Phenotypic, whole mount *in situ* hybridisation analyses and rescue experiments on the mutant lines revealed that *def6a* and *swap70b* act upstream of Cdc42 and Cdc42/Racl GTPases, respectively, to activate the Jnk pathway of Wnt/PCP signalling for regulating cell polarity and CE cell movements during zebrafish gastrulation. In adult zebrafish haematopoiesis, *def6a* and *swap70b* were found to regulate myeloid cell differentiation and both may play a role in HSPC fate and lineage choice. BioID-mediated identification and classification of DEF6 interactome in T cells suggested that in addition to its known roles in actin cytoskeleton organisation and mRNA translation, DEF6 may also regulate transcription, mRNA splicing/processing, protein folding/modification and metabolic pathways in mammalian T cells.

References

Aberle, H., Bauer, A., Stappert, J., Kispert, A., Kemler, R., 1997. Beta-catenin is a target for the ubiquitin-proteasome pathway. *EMBO J*; 16:3797-804.

Abovich, N., Rosbash, M., 1997. Cross-intron bridging interactions in the yeast commitment complex are conserved in mammals. *Cell*; 89:403-412.

Acampora, D., Gulisano, M., Broccoli, V., Simeone, A., 2001. Otx genes in brain morphogenesis. *Prog Neurobiol*; 64: 69–95.

Adams, M.D., Sekelsky, J.J., 2002. From sequence to phenotype: reverse genetics in *Drosophila melanogaster*. *Nat Rev Genet*; 3:189-98.

Adler, P. N., 2002. Planar signaling and morphogenesis in Drosophila. *Dev Cell*; 2:525-35.

Adra, C.N., Manor, D., Ko, J.L., Zhu, S., Horiuchi, T., Van Aelst, L., Cerione, R.A., Lim, B., 1997. RhoGDIγ: A GDP-dissociation inhibitor for Rho proteins with preferential expression in brain and pancreas. *PNAS*; 94:4279-4284.

Agata, Y., Matsuda, E., Shimizu, A., 1999. Two novel Kruppel-associated box-containing zinc-finger proteins, KRAZ1 and KRAZ2, repress transcription through functional interaction with the corepressor KAP-1 (TIF1beta/KRIP-1). *J Biol Chem*; 274:16412-16422.

Aggeler, R., Coons, J., Taylor, S.W., Ghosh, S.S., Garcia, J.J., Capaldi, R.A., Marusich, M.F., 2002. A functionally active human F1F0 ATPase can be purified by immunocapture from heart tissue and fibroblast cell lines. Subunit structure and activity studies. *J Biol Chem*; 277:33906-12.

Aghazadeh, B., Lowry, W.E., Huang, X.Y., Rosen, M.K., 2000. Structural Basis for Relief of Autoinhibition of the Dbl Homology Domain of Proto-Oncogene Vav by Tyrosine Phosphorylation. *Cell*; 102:625-633.

Aird, K.M., Iwasaki, O., Kossenkov, A.V., Tanizawa, H., Fatkhutdinov, N., Bitler, B.G., Le, L., Alicea, G., Yang, T.L., Johnson, F.B., Noma, K., Zhang, R., 2016. HMGB2 orchestrates the chromatin landscape of senescence-associated secretory phenotype gene loci. *J Cell Biol*; 215:325-334.

Ajiro, M., Jia, R., Yang, Y., Zhu, J., Zheng, Z.M., 2016. A genome landscape of SRSF3-regulated splicing events and gene expression in human osteosarcoma U2OS cells. *Nucleic Acids Res*; 44: 1854-1870.

Akimenko, M.A., Ekker, M., Wegner, J., Lin, W. and Westerfield, M., 1994. Combinatorial expression of three zebrafish genes related to distal-less: Part of a homeobox gene code for the head. *J Neurosci*; 14:3475-3486.

Alarcon, C.R., Goodarzi, H., Lee, H., Liu, X., Tavazoie, S., Tavazoie, S.F., 2015. HNRNPA2B1 is a mediator of m6A-dependent nuclear RNA processing events. *Cell*; 162:1299-1308.

Albertella, M.R., Campbell, R.D., 1994. Characterization of a novel gene in the human major histocompatibility complex that encodes a potential new member of the I kappa B family of proteins. *Hum Mol Genet*; 3:793-799.

Allen, H.F., Wade, P.A. Kutateladze, T.G., 2013. The NuRD architecture. *Cell Mol Life Sci;* 70:3513-3524.

Altman, A., Bécart, S., 2009. Does Def6 Deficiency Cause Autoimmunity? *Immunity*; 31:1-2.

Aman, A., Nguyen, M., Piotrowski, T., 2011. Wnt/beta-catenin dependent cell proliferation underlies segmented lateral line morphogenesis. *Dev Biol*; 349:470-482.

Amaya, E., Musci, T.J., Kirschner, M.W., 1991. Expression of a dominant negative mutant of the FGF receptor disrupts mesoderm formation in Xenopus embryos. *Cell*; 66:257-70.

Amir-Ahmady, B., Boutz, P.L., Markovtsov, V., Phillips, M.L., Black, D.L., 2005. Exon repression by polypyrimidine tract binding protein. *RNA*; 11:699-716.

Amores, A., Force, A., Yan, Y.L., Joly, L., Amemiya, C., Fritz, A., Ho, R.K., Langeland, J., Prince, V., Wang, Y.L., Westerfield, M., Ekker, M., Postlethwait, J.H., 1998. Zebrafish hox clusters and vertebrate genome evolution. *Science*; 282:1711-4.

Amoyel, M., Cheng, Y.C., Jiang, Y.J., Wilkinson, D.G., 2005. Wnt1 regulates neurogenesis and mediates lateral inhibition of boundary cell specification in the zebrafish hindbrain. *Development*; 132:775-85.

Anczuków, O., Akerman, M., Cléry, A., Wu, J., Shen, C., Shirole, N.H., Raimer, A., Sun, S., Jensen, M.A., Hua, Y., Allain, F.H.T., Krainer, A.R., 2015. SRSF1-Regulated Alternative Splicing in Breast Cancer. *Molecular Cell*; 60:105–117.

Ando, H., Kobayashi, M., Tsubokawa, T., Uyemura, K., Furuta, T., Okamoto, H., 2005. Lhx2 mediates the activity of Six3 in zebrafish forebrain growth. *Dev. Biol*; 287: 456-468.

Andreotti, A.H., Schwartzberg, P.L., Joseph, R.E., Berg, L.J., 2010. T-Cell Signaling Regulated by the Tec Family Kinase, Itk. *Cold Spring Harb Perspect Biol*; 2: a002287.

Antonellis, A., Lee-Lin, S.Q., Wasterlain, A., Leo, P., Quezado, M., Goldfarb, L.G., Myung,K., Burgess, S., Fischbeck, K.H., Green, E.D., 2006. Functional analyses of glycyl-tRNA synthetase mutations suggest a key role for tRNA-charging enzymes in peripheral axons. *J Neurosci*; 26:10397-406.

Aragon, F., Pujades, C., 2009. FGF signaling controls caudal hindbrain specification through Ras-ERK1/2 pathway. *BMC Dev Biol*.; 9:61.

Aranguren, X.L., Beerens, M., Vandevelde, W., Dewerchin, M., Carmeliet, P., Luttun, A., 2011. Transcription factor COUP-TFII is indispensable for venous and lymphatic development in zebrafish and *Xenopus laevis*. *Biochem Biophys Res Commun*; 410:121-126.

Arce, L., Yokoyama, N.N., Waterman, M.L., 2006. Diversity of LEF/TCF action in development and disease. *Oncogene*; 25:7492–7504.

Assrir, N., Richez, C., Durand, P., Guittet, E., Badet, B., Lescop, E., Badet-Denisot, M.A., 2014. Mapping the UDP-N-acetylglucosamine regulatory site of human glucosamine-6P synthase by saturation-transfer difference NMR and site-directed mutagenesis. *Biochimie*; 97:39-48.

Auer, T.O., Del Bene, F., 2014. CRISPR/Cas9 and TALEN-mediated knock-in approaches in zebrafish. *Methods*; 69:142-50.

Axelrod, J.D., Miller, J.R., Shulman, J.M., Moon, R.T., Perrimon, N., 1998. Differential recruitment of Dishevelled provides signaling specificity in the planar cell polarity and Wingless signaling pathways. *Genes Dev*; 12:2610-22.

Bando, Y., Ogawa, S., Yamauchi, A., Kuwabara, K., Ozawa, K., Hori, O., Yanagi, H., Tamatani, M., Tohyama, M., 2000. 150-kDa oxygen-regulated protein (ORP150) functions as a novel molecular chaperone in MDCK cells. *Am J Physiol Cell Physiol*; 278:C1172-82.

Barak, O., Lazzaro, M.A., Lane, W.S., Speicher, D.W., Picketts, D.J., Shiekhattar, R., 2003. Isolation of human NURF: a regulator of Engrailed gene expression. *EMBO J*; 22:6089-100.

Baranov, M.V., Revelo, N.H., Dingjan, I., Maraspini, R., ter Beest, M., Honigmann, A., van den Bogaart, G., 2016. SWAP70 Organizes the Actin Cytoskeleton and Is Essential for Phagocytosis. *Cell Rep*; 17: 1518-1531.

Baumeister, M.A., Martinu, L., Rossman, K.L., Sondek, J., Lemmon, M.A., Chou, M.M., 2003. Loss of phosphatidylinositol 3-phosphate binding by the C-terminal Tiam-1 pleckstrin homology domain prevents *in vivo* Rac1 activation without affecting membrane targeting. *J Biol Chem*; 278:11457-64.

Bécart, S., Charvet, C., Canonigo Balancio, A.J., De Trez, C., Tanaka, Y., Duan, W., Ware, C., Croft, M., Altman, A., 2007. SLAT regulates Th1 and Th2 inflammatory responses by controlling Ca2+/NFAT signaling. *J Clin Inves*; 117: 2164-2175.

Bécart, S., Balancio, A., Charvet, C., Feau, S., Sedwick, C., Altman, A., 2008. Tyrosine-Phosphorylation-Dependent Translocation of the SLAT Protein to the Immunological Synapse Is Required for NFAT Transcription Factor Activation. *Immunity*; 29:704-719.

Bécart, S., Altman, A. 2009. SWAP-70-like adapter of T cells: a novel Lck-regulated guanine nucleotide exchange factor coordinating actin cytoskeleton reorganization and Ca^{2+} signaling in T cells. *Immunological Reviews*; 232:319–333.

Becerra, S., Andrés-León, E., and Suñé, C., 2016. Prp40 and early events in splice site definition. *Wiley Interdiscip. Rev. RNA*; 7:17–32.

Bedell, V.M., Wang, Y., Campbell, J.M., Poshusta, T.L., Starker, C.G., Krug, R.G. 2nd, Tan, W., Penheiter, S.G., Ma, A.C., Leung, A.Y., Fahrenkrug, S.C., Carlson, D.F., Voytas, D.F., Clark, K.J., Essner, J.J., Ekker, S.C., 2012. In vivo genome editing using a high-efficiency TALEN system. *Nature*; 491:114-8.

Bedford, M.T., Chan, D.C, Leder, P., 1997. FBP WW domains and the Abl SH3 domain bind to a specific class of proline-rich ligands. *EMBO J*; 16:2376-2383.

Behrens, J., Lustig, B., 2004. The Wnt connection to tumorigenesis. *Int J Dev Biol*; 48:477-87.

Behrens, J., von Kries, J.P., Kühl, M., Bruhn, L., Wedlich, D., Grosschedl, R., Birchmeier, W., 1996. Functional interaction of beta-catenin with the transcription factor LEF-1. *Nature*; 382:638-42.

Bellipanni, G., Varga, M., Maegawa, S., Imai, Y., Kelly, C., Myers, A.P., Chu, F., Talbot, W.S., Weinberg, E.S., 2006. Essential and opposing roles of zebrafish beta-catenins in the formation of dorsal axial structures and neurectoderm. *Development*; 133:1299-309.

Bengtsson, T., Sarndahl, E., Stendahl, O., Andersson, T., 1990. Involvement of GTP-binding proteins in actin polymerization in human neutrophils. *Proc Natl Acad Sci USA*; 87:2921-2925.

Berglund, J.A., Abovich, N., Rosbash, M., 1998. A cooperative interaction between U2AF65 and mBBP/SF1 facilitates branchpoint region recognition. *Genes Dev*; 12:858–867.

Berkholz, J., Orgeur, M., Stricker, S., Munz, B., 2015. skNAC and Smyd1 in transcriptional control. *Exp Cell Res*; 336:182-91.

Bernards, A., 2003. GAPs galore! A survey of putative Ras superfamily GTPase activating proteins in man and *Drosophila*. *Biochimica et Biophysica Acta*; 1603:47-82.

Bertrand, J.Y., Kim, A.D., Violette, E.P., Stachura, D.L., Cisson, J.L., Traver, D., 2007. Definitive hematopoiesis initiates through a committed erythromyeloid progenitor in the zebrafish embryo. *Development*; 134; 4147-4156.

Bertrand, J.Y., Chi, N.C, Santoso, B., Teng, S., Stainier, D.Y., Traver, D., 2010. Haematopoietic stem cells derive directly from aortic endothelium during development. *Nature*; 464:108-111.

Bezanilla, M., Gladfelter, A.S., Kovar, D.R., Lee, W.L, 2015. Cytoskeletal dynamics: a view from the membrane. *J Cell Biol*; 209:329-337.

Bhanot, P., Brink, M., Samos, C.H., Hsieh, J.C., Wang, Y., Macke, J.P., Andrew, D., Nathans, J., Nusse, R., 1996. A new member of the frizzled family from drosophila functions as a wingless receptor. *Nature*; 382:225-230.

Bianchi, M.E., Agresti, A., 2005. HMG proteins: dynamic players in gene regulation and differentiation. *Curr Opin Genet Dev*; 15:496-506.

Bibikova, M., Golic, M., Golic, K.G., Carroll, D., 2002. Targeted chromosomal cleavage and mutagenesis in Drosophila using zinc-finger nucleases. *Genetics*; 161:1169-75.

Bibikova, M., Beumer, K., Trautman, J.K., Carroll, D., 2003. Enhancing gene targeting with designed zinc finger nucleases. *Science*; 300:764.

Bienz, M., Clevers, H., 2003. Armadillo/beta-catenin signals in the nucleus--proof beyond a reasonable doubt? *Nat Cell Biol*; 5:179-82.

Biswas, P.S., Gupta, S., Chang, E., Song, L., Stirzaker, R.A., Liao, J.K., Bhagat, G., Pernis, A.B. 2010a. Phosphorylation of IRF4 by ROCK2 regulates IL-17 and IL-21 production and the development of autoimmunity in mice. *J Clin Invest*; 120:3280–3295.

Biswas, P.S., Bhagat, G., Pernis, A.B., 2010b. IRF4 and its regulators: evolving insights into the pathogenesis of inflammatory arthritis? *Immunol Rev*; 233:79-96.

Biswas, P.S., Gupta, S., Stirzaker, R.A., Kumar, V., Jessberger, R., Lu, T.T., Bhagat, G., Pernis, A.B., 2012. Dual regulation of IRF4 function in T and B cells is required for the coordination of T-B cell interactions and the prevention of autoimmunity. *J Exp Med*; 209: 581-596.

Blanchoin, L., Pollard, T.D., 1999. Mechanism of interaction of Acanthamoeba actophorin (ADF/Cofilin) with actin filaments. *J Biol Chem*; 274:15538–15546.

Blanco, G., Mercer, R.W., 1998. Isozymes of the Na-K-ATPase: heterogeneity in structure, diversity in function. *Am J Physiol*; 275:F633–F650.

Blangy, A., Vignal, E., Schmidt, S., Debant, A., Gauthier-Rouvière, C., Fort, P., 2000. TrioGEF1 controls Rac- and Cdc42-dependent cell structures through the direct activation of RhoG. *J Cell Sci*; 113:729-39.

Boch, J., Scholze, H., Schornack, S., Landgraf, A., Hahn, S., Kay, S., Lahaye, T., Nickstadt, A., Bonas, U., 2009. Breaking the code of DNA binding specificity of TAL-type III effectors. *Science*; 326:1509-1512.

Boesler, C., Rigo, N., Agafonov, D.E., Kastner, B., Urlaub, H., Will, C.L., Lührmann, R., 2015. Stable tri-snRNP integration is accompanied by a major structural rearrangement of the spliceosome that is dependent on Prp8 interaction with the 5' splice site. *RNA*; 21:1993-2005.

Bogdanove, A.J., Schornack, S., Lahaye, T., 2010. TAL effectors: finding plant genes for disease and defense. *Curr Opin Plant Biol*; 13:394-401.

Boguski, M.S., McCormick, F., 1993. Proteins regulating Ras and its relatives. *Nature*; 366:643-54.

Bollag, G., McCormick, F., 1991. Regulators and effectors of ras proteins. *Annu Rev Cell Biol*; 7:601-32.

Bolotin, A., Quinquis, B., Sorokin, A., Ehrlich, S.D., 2005. Clustered regularly interspaced short palindrome repeats (CRISPRs) have spacers of extrachromosomal origin. *Microbiology*; 151:2551-61.

Borggrefe, T., Wabl, M., Akhmedov, A. T., Jessberger, R., 1998. A B-cell-specific DNA recombination complex. *J Biol Chem*; 273:17025-35.

Borggrefe, T., Masat, L., Wabl, M., Riwar, B., Cattoretti, G., Jessberger, R., 1999. Cellular, intracellular, and developmental expression patterns of murine SWAP-70. *Eur J Immunol*; 29:1812-22.

Borggrefe, T., Keshavarzi, S., Gross, B., Wabl, M., Jessberger, R., 2001. Impaired IgE response in SWAP-70-deficient mice. *Eur J Immunol*; 31:2467-75.

Bose, S., Weikl, T., Bügl, T., Buchner, J., 1996. Chaperone Function of Hsp90-Associated Proteins. *Science*; 274:1715-1717.

Böttcher, R.T., Niehrs, C., 2005. Fibroblast growth factor signaling during early vertebrate development. *Endocr Rev*; 26:63-77.

Boulter, E., Garcia-Mata, R., Guilluy, C., Dubash, A., Rossi, G., Brennwald, P.J., Burridge, K., 2010. Regulation of Rho GTPase crosstalk, degradation and activity by RhoGDI1. *Nat Cell Biol*; 12:477-83.

Boutros, M., Paricio, N., Strutt, D.I., Mlodzik, M., 1998. Dishevelled activates JNK and discriminates between JNK pathways in planar polarity and wingless signaling. *Cell*; 94:109-18.

Boutros, M., Mlodzik, M., 1999. Dishevelled: at the crossroads of divergent intracellular signaling pathways. *Mech Dev*; 83:27-37.

Brand, M., Heisenberg, C.P., Jiang, Y.J., Beuchle, D., Lun, K., Furutani-Seiki, M., Granato, M., Haffter, P., Hammerschmidt, M., Kane, D.A., Kelsh, R.N., Mullins, M.C., Odenthal, J., van Eeden, F.J., Nüsslein-

Volhard, C., 1996. Mutations in zebrafish genes affecting the formation of the boundary between midbrain and hindbrain. *Development*; 123:179-90.

Brandt, D., Gimona, M., Hillmann, M., Haller, H., Mischak. H., 2002. Protein Kinase C Induces Actin Reorganization via a Src- and Rho-dependent Pathway. *J Biol Chem*; 277:20903-20910.

Branford, W.W., Yost, H.J., 2002. Lefty-dependent inhibition of Nodal- and Wnt-responsive organizer gene expression is essential for normal gastrulation. *Curr Biol*; 12:2136-41.

Brugnera, E., Haney, L., Grimsley, C., Lu, M., Walk, S. F., TosselloTrampont, A. C., Macara, I. G., Madhani, H., Fink, G. R. and Ravichandran, K. S., 2002. Unconventional Rac-GEF activity is mediated through the Dock180 ELMO complex. *Nat Cell Biol*; 4: 574-582.

Brunet, E., Simsek, D., Tomishima, M., DeKelver, R., Choi, V.M., Gregory, P., Urnov, F., Weinstock, D.M., Jasin, M., 2009. Chromosomal translocations induced at specified loci in human stem cells. *Proc Natl Acad Sci USA*; 106:10620-5.

Bubb, M.R., Yarmola, E.G., Gibson, B.G., Southwick, F.S., 2003. Depolymerization of actin filaments by profilin. Effects of profilin on capping protein function. *J Biol Chem*; 278: 24629-24635.

Buchner, J., 1999. Hsp90 & Co.- a holding for folding. *Trends Biochem Sci*; 24:136-141.

Bunch, H., Calderwook, S.K., 2015. TRIM28 as a novel transcriptional elongation factor. *BMC Mol Biol*; 16:14.

Burkhart, D.L., Sage, J., 2008. Cellular mechanisms of tumour suppression by the retinoblastoma gene. *Nat Rev Cancer*; 8:671-82.

Burns, K., Duggan, B., Atkinson, E.A., Famulski, K.S., Nemer, M., Bleackley, R.C., Michalak. M., 1994. Modulation of gene expression by calreticulin binding to the glucocorticoid receptor. *Nature*; 367:476-480.

Cadigan, K. M., Nusse, R., 1997. Wnt signaling: a common theme in animal development. *Genes Dev*; 11:3286-305.

Cadigan, K.M., Liu, Y.I., 2006. Wnt signaling: complexity at the surface. *J Cell Sci*; 119:395-402.

Canonigo-Balancio, A.J., C. Fos, T. Prod'homme, S. Bécart, and A. Altman., 2009. SLAT/Def6 plays a critical role in the development of Th17 cellmediated experimental autoimmune encephalomyelitis. *J Immunol*; 183:7259–7267.

Cao, W., Jamison, S.F., Garcia-Blanco, M.A., 1997. Both phosphorylation and dephosphorylation of ASF/SF2 are required for pre-mRNA splicing *in vitro*. *RNA*; 3:1456–67.

Carlsson, L., Nyström, L.E., Sundkvist, I., Markey, F., Lindberg, U. 1977. Actin polymerizability is influenced by profilin, a low molecular weight protein in non-muscle cells. *J Mol Biol*; 115:465–483.

Carreira-Barbosa, F., Concha, M.L., Takeuchi, M., Ueno, N., Wilson, S.W., Tada, M., 2003. Prickle 1 regulates cell movements during gastrulation and neuronal migration in zebrafish. *Development*; 130:4037-46.

Carroll, D., 2011. Genome Engineering With Zinc-Finger Nucleases. *Genetics*; 188: 773-782.

Carter, C.W. Jr., 1993. Cognition, mechanism, and evolutionary relationships in aminoacyl-tRNA synthetases. *Annu Rev Biochem*; 62:715–748.

Carvalho, M. G., Carvalho, J. F., Merrick, W. C., 1984. Purification of various forms of elongation factor 1 from rabbit reticulocytes. *Arch Biochem Biophys*; 234: 603–611.

Castro-Castro, A., Ojeda, V., Barreira, M., Sauzeau, V., Navarro-Lérida, I., Muriel, O., Couceiro, J.R., Pimentel-Muíños, F.X., Del Pozo, M.A., Bustelo, X.R., 2011. Coronin 1A promotes a cytoskeletal-based feedback loop that facilitates Rac1 translocation and activation. *EMBO J*; 30:3913–3927.

Cavaloc, Y., Popielarz, M., Fuchs, J.P., Gattoni, R., Stvenin, J., 1994. Characterization and cloning of the human splicing factor 9G8: a novel 35 kDa factor of the serine/arginine protein family. *EMBO J*; 13: 2639–2649.

Cavellan, E., Asp, P., Percipalle, P., Farrants, A.K., 2006. The WSTF-SNF2h chromatin remodeling complex interacts with several nuclear proteins in transcription. *J Biol Chem*; 281:16264-16271.

Cerione, R.A., Zheng, Y., 1996. The Dbl family of oncogenes. *Curr Opin in Cell Biol*; 8:216-222.

Cermak, T., Doyle, E.L., Christian, M., Wang, L., Zhang, Y., Schmidt, C., Baller, J.A., Somia, N.V., Bogdanove, A.J., Voytas, D.F., 2011. Efficient design and assembly of custom TALEN and other TAL effector-based constructs for DNA targeting. *Nucleic Acids Res*; 39:e82.

Chacón-Martínez, C.A., Kiessling, N., Winterhoff, M., Faix, J., Müller-Reichert, T., Jessberger, R., 2013. The switch-associated protein 70 (SWAP-70) bundles actin filaments and contributes to the regulation of F-actin dynamics. *J Biol Chem*; 288:28687–28703.

Chalupny, N.J., Ledbetter, J.A., Kavathas, P., 1991. Association of CD8 with p56lCk is required for early T cell signalling events. *EMBO J*; 10:1201-1207.

Chamorro, M.N., Schwartz, D.R., Vonica, A., Brivanlou, A.H., Cho, K.R., Varmus, H.E., 2005. FGF-20 and DKK1 are transcriptional targets of beta-catenin and FGF-20 is implicated in cancer and development. *EMBO J*; 24:73-84.

Chan, A.C., Dalton, M., Johnson, R., Kong, G.H., Wang, T., Thoma, R., Kurosaki, T., 1995. Activation of ZAP-70 kinase activity by phosphorylation of tyrosine 493 is required for lymphocyte antigen receptor function. *EMBO J*; 14:2499–2508.

Chandrasekhar, A., Moens, C. B., Warren, J. T., Jr, Kimmel, C. B. and Kuwada, J.Y., 1997. Development of branchiomotor neurons in zebrafish. *Development*; 124:2633-2644.

Chapman-Smith, A., Morris, T.W., Wallace, J.C., Cronan, J.E. Jr., 1999a. Molecular recognition in a post-translational modification of exceptional specificity. Mutants of the biotinylated domain of acetyl-CoA carboxylase defective in recognition by biotin protein ligase. *J Biol Chem*; 274:1449-57.

Chapman-Smith, A., Cronan J.E. Jr., 1999b. Molecular biology of biotin attachment to proteins. *J Nutr*; 129:477S–484S.

Chapman-Smith, A., Cronan J.E. Jr., 1999c. The enzymatic biotinylation of proteins: A post-translational modification of exceptional specificity. *Trends Biochem Sci*; 24:359-363.

Charité, J., de Graaff, W., Consten, D., Reijnen, M.J., Korving, J., Deschamps, J., 1998. Transducing positional information to the Hox genes: critical interaction of cdx gene products with position-sensitive regulatory elements. *Development*; 125:4349-58.

Charpentier, E., Doudna, J.A., 2013. Biotechnology: Rewriting a genome. *Nature*; 495:50-1.

Chaumet A., Castella S., Gasmi L., Fradin A., Clodic G., Bolbach G., Poulhe R., Denoulet P., Larcher J.C. 2013. Proteomic analysis of interleukin enhancer binding factor 3 (Ilf3) and nuclear factor 90 (NF90) interactome. *Biochimie*; 95:1146-1157.

Chen, Y., Sharp, Z.D., Lee, W.H., 1997. HEC binds to the seventh regulatory subunit of the 26 S proteasome and modulates the proteolysis of mitotic cyclins. *J Biol Chem*; 272:24081-24087.

Chen, S., Smith, D.F., 1998. Hop as an adaptor in the heat shock protein 70 (Hsp70) and hsp90 chaperone machinery. *J Biol Chem*; 273:35194-200.

Chen, Q., Yang, W., Gupta, S., Biswas, P., Smith, P., Bhagat, G., 2008. IRF-4-Binding Protein Inhibits Interleukin-17 and Interleukin-21 Production by Controlling the Activity of IRF-4 Transcription Factor. *Immunity*; 29:899-911.

Chen, Q., Yang, W., Gupta, S., Biswas, P., Smith, P., Bhagat, G., Pernis, A.B., 2009. Response to Letter from Altman and Bécart. *Immunity*; 31:1-3.

Chen, Z., Med, M., Xu X.H., 2016. Roles of nucleolin. *Saudi Med J*; 37:1312-1318.

Cheng, H., 2017. Structure-Function Relationship of DEF6. University of Nottingham, PhD thesis.

Cheong, C.G., Wolan, D.W., Greasley, S.E., Horton, P.A., Beardsley, G.P., Wilson, I.A., 2004. Crystal structures of human bifunctional enzyme aminoimidazole-4-carboxamide ribonucleotide

transformylase/IMP cyclohydrolase in complex with potent sulfonyl-containing antifolates. *J Biol Chem*; 279:18034-45.

Cherfils, J., Chardin, P., 1999. GEFs: structural basis for their activation of small GTP-binding proteins. *Trends Biochem Sci*; 24:306-11.

Choi, S.C., Han, J.K., 2002. Xenopus Cdc42 regulates convergent extension movements during gastrulation through Wnt/Ca2+ signaling pathway. *Dev Biol*; 244:342-57.

Choi-Rhee, E., H. Schulman, Cronan, J.E., 2004. Promiscuous protein biotinylation by Escherichia coli biotin protein ligase. *Protein Sci*; 13:3043–3050.

Chopin, M., Chacón-Martínez, C.A., Jessberger, R., 2011. Fine tuning of IRF-4 expression by SWAP-70 controls the initiation of plasma cell development. *Eur J Immunol*; 41:3063-74.

Christie, D.A., Lemke, C.D., Elias, I.M., Chau, L.A., Kirchhof, M.G., Li, B., Ball, E.H., Dunn, S.D., Hatch, G.M., Madrenas, J., 2011. Stomatin-like protein 2 binds cardiolipin and regulates mitochondrial biogenesis and function. *Mol Cell Biol*; 31:3845-3856.

Ciau-Uitz, A., Monteiro, R., Kirmizitas, A., Patient, R., 2014. Developmental hematopoiesis: Ontogeny, genetic programming and conservation. *Exp Hem*; 42:669–683.

Ciruna, B., Rossant, J., 2001. FGF signaling regulates mesoderm cell fate specification and morphogenetic movement at the primitive streak. *Dev Cell*; 1:37-49.

Clevers, H., 2006. Wnt/beta-catenin signaling in development and disease. *Cell*; 12:469-80.

Clower, C.V., Chatterjee, D., Wang, Z., Cantley, L.C., Vander Heiden, M.G., Krainer, A.R., 2010. The alternative splicing repressors hnRNP A1/A2 and PTB influence pyruvate kinase isoform expression and cell metabolism. *Proc Natl Acad Sci USA*; 107:1894-1899.

Cole, A., Wang, Z., Coyaud, E., Voisin, V., Gronda, M., Jitkova, Y., Mattson, R., Hurren, R., Babovic, S., Maclean, N., *et al*., 2015. Inhibition of the mitochondrial protease ClpP as a therapeutic strategy for human acute myeloid leukemia. *Cancer Cell*; 27:864–876.

Collins, C.A., Guthrie, C., 1999. Allele-specific genetic interactions between Prp8 and RNA active site residues suggest a function for Prp8 at the catalytic core of the spliceosome. *Genes Dev*; 13:1970-1982.

Cong, L., Ran, F.A., Cox, D., Lin, S., Barretto, R., Habib, N., Hsu, P.D., Wu, X., Jiang, W., Marraffini, L.A., Zhang, F., 2013. Multiplex genome engineering using CRISPR/Cas systems. *Science*; 339:819-23.

Cornella, N., Tebaldi, T., Gasperini, L., Singh, J., Padgett, R.A., Rossi, A., Macchi, P., 2017. The hnRNP RALY regulates transcription and cell proliferation by modulating the expression of specific factors including the proliferation marker E2F1. *J Biol Chem*; 292:19674-19692.

Coso, O.A., Chiariello, M., Yu, J.C., Teramoto, H., Crespo, P., Xu, N., Miki, T., and Gutkind, J.S. 1995. The small GTP binding proteins Rac1 and Cdc42 regulate the activity of the JNK/SAPK signaling pathway. *Cell*; 81:1137-1146.

Cote, J.F., Vuori, K., 2002. Identification of an evolutionarily conserved superfamily of DOCK180-related proteins with guanine nucleotide exchange activity. *J Cell Sci*; 115:4901-4913.

Cote, J.F., Vuori, K., 2007. GEF what? Dock180 and related proteins help Rac to polarize cells in new ways. *Trends Cell Biol*; 17:383-93.

Cote, M., Fos, C., Canonigo-Balancio, A.J., Ley, K., Bécart, S., Altman, A., 2015. SLAT promotes TCR-mediated, Rap1-dependent LFA-1 activation and adhesion through interaction of its PH domain with Rap1. *J Cell Sci*; 128:4341-52.

Cozier, G.E., Carlton, J., Bouyoucef, D., Cullen, P.J., 2004. Membrane targeting by pleckstrin homology domains. *Curr Top Microbiol Immunol*; 282:49-88.

Craig, A.W., Haghighat, A., Yu, A.T., Sonenberg, N., 1998. Interaction of polyadenylate-binding protein with the eIF4G homologue PAIP enhances translation. *Nature*; 392:520–3.

Craig, E.A., Weissman, J.S., Hotwicht, A.L., 1994. Heat Shock Proteins and Molecular Chaperones: Mediators of Protein Conformation and Turnover in the Cell. *Cell*; 78:388-372.

Crambert, G., Hasler, U., Beggah, A.T., Yu, C., Modyanov, N.N., Horisberger, J.D., Lelievre, L., Geering, K., 2000. Transport and pharmacological properties of nine different human Na, K-ATPase isozymes. *J Biol Chem*; 275:1976-1986.

Crawford, N.P., Yang, H., Mattaini, K.R., Hunter, K.W., 2009. The metastasis efficiency modifier ribosomal RNA processing 1 homolog B (RRP1B) is a chromatin-associated factor. *J Biol Chem*; 284:28660-73.

Croushore, J.A., Blasiole, B., Riddle, R.C., Thisse, C., Thisse, B., Canfield, V.A., Robertson, G.P., Cheng, K.C., Levenson, R., 2005. Ptena and ptenb genes play distinct roles in zebrafish embryogenesis. *Dev Dyn*; 234:911–921.

Cui, X., Ji, D., Fisher, D.A., Wu, Y., Briner, D.M., Weinstein, E.J., 2011. Targeted integration in rat and mouse embryos with zinc-finger nucleases. *Nat Biotechnol*; 29:64-7.

Cunningham, C.C., Gorlin, J.B., Kwiatkowski, D.J., Hartwig, J.H., Janmey, P.A., Byers, H.R., Stossel, T.P., 1992. Actin-binding protein requirement for cortical stability and efficient locomotion.*Science*; 255:325–327.

d'Enfert, C., 1999. Rho, Rac and Cdc42. *Trends Microbiol*; 7:65.

Dahlem, T.J., Hoshijima, K., Jurynec, M.J., Gunther, D., Starker, C.G., Locke, A.S., Weis, A.M., Voytas, D.F., Grunwald, D.J., 2012. Simple methods for generating and detecting locus-specific mutations induced with TALENs in the zebrafish genome. *PLoS Genet*; 8(8):e1002861.

Dally, S., Bredoux, R., Corvazier, E., Andersen, J.P., Clausen, J.D., Dode, L., Fanchaouy, M., Gelebart, P., Monceau, V., Del Monte, F., Gwathmey, J.K., Hajjar, R., Chaabane, C., Bobe, R., Raies, A., Enouf, J., 2006. Ca2+-ATPases in non-failing and failing heart: evidence for a novel cardiac sarco/endoplasmic reticulum Ca2+-ATPase 2 isoform (SERCA2c). *Biochem J*; 395:249-258.

Dann, C.E., Hsieh, J.C., Rattner, A., Sharma, D., Nathans, J., Leahy, D.J., 2001. Insights into Wnt binding and signalling from the structures of two Frizzled cysteine-rich domains. *Nature*; 412:86-90.

Darken, R.S., Scola, A.M., Rakeman, A.S., Das, G., Mlodzik, M., Wilson, P.A., 2002. The planar polarity gene strabismus regulates convergent extension movements in *Xenopus*. *EMBO J*; 21:976-85.

Das R, Zhou Z, Reed R+ 2000+ Functional association of U2 snRNP with the ATP-independent spliceosomal complex E+ Mol Cell 5:779–787.

Das, G., Jenny, A., Klein, T.J., Eaton, S., Mlodzik, M., 2004. Diego interacts with Prickle and Strabismus/Van Gogh to localize planar cell polarity complexes. *Development*; 131:4467-76.

David, C.J., Chen, M., Assanah, M., Canoll, P., Manley, J.L., 2010. HnRNP proteins controlled by c-Myc deregulate pyruvate kinase mRNA splicing in cancer. *Nature*; 463:364–368.

Davidson, A.J., Ernst, P., Wang, Y., Dekens, M.P., Kingsley, P.D., Palis, J., Korsmeyer, S.J., Daley, G.Q., Zon, L.I., 2003. cdx4 mutants fail to specify blood progenitors and can be rescued by multiple hox genes. *Nature*; 425:300–6.

Davidson, A.J., Zon, L.I., 2004. The 'definitive' (and 'primitive') guide to zebrafish hematopoiesis. *Oncogene*; 23:7233-46.

Davidson, G., Wu, W., Shen, J., Bilic, J., Fenger, U., Stannek, P., Glinka, A., Niehrs, C., 2005. Casein kinase 1 couples Wnt receptor activation to cytoplasmic signal transduction. *Nature*; 438:867-72.

Davidson, A.J., Zon, L.I., 2006. The caudal-related homeobox genes cdx1a and cdx4 act redundantly to regulate hox gene expression and the formation of putative hematopoietic stem cells during zebrafish embryogenesis. *Dev Biol*; 292:506-18.

Davis, A.R., Alevy, Y.G., Chellaiah, A., Quinn, M.T., Mohanakumar, T., 1998. Characterization of HDJ-2, a human 40 kD heat shock protein. *Int J Biochem Cell Biol*; 30:1203-21.

Davis, A.J., Chen, D.J., 2013. DNA double strand break repair via non-homologous end-joining. *Transl Cancer Res*; 2:130-143.

De, A., 2011. Wnt/Ca2+ signaling pathway: a brief overview. *Acta Biochim Biophys Sin*; 43:745-56.

De Arras, L., Laws, R., Leach, S.M., Pontis, K., Freedman, J.H., Schwartz, D.A., Alper, S., 2014. Comparative genomics RNAi screen identifies Eftud2 as a novel regulator of innate immunity. *Genetics*; 197:485-96.

De Francesco, L., 2011. Move over ZFNs: a new technology for genome editing may put the zinc finger nuclease franchise out of business, some believe. Not so fast, say the finger people. *Nature Biotech*; 29: 681-684.

De Hostos, E.L., 1999. The coronin family of actin-associated proteins. *Trends Cell Biol*; 9:345–350.

Dedhar, S., Rennie, P.S., Shago, M., Hagesteijn, C.Y., Yang, H., Filmus, J., Hawley, R.G., Bruchovsky, N., Cheng, H., Matusik, R.J., *et al*., 1994. Inhibition of nuclear hormone receptor activity by calreticulin. *Nature*; 367:480-3.

De Kelver, R.C., Choi, V.M., Moehle, E.A., Paschon, D.E., Hockemeyer, D., Meijsing, S.H., Sancak, Y., Cui, X., Steine, E.J., Miller, J.C., *et al*., 2010. Functional genomics, proteomics, and regulatory DNA analysis in isogenic settings using zinc finger nuclease-driven transgenesis into a safe harbor locus in the human genome. *Genome Res*; 20:1133-42.

Dekker, C., Stirling, P.C., McCormack, E.A., Filmore, H., Paul, A., Brost, R.L., Costanzo, M., Boone, C., Leroux, M.R., Willison, K.R., *et al*., 2008. The interaction network of the chaperonin CCT. *EMBO J*; 27:1827-1839.

Del Monte, F., Harding, S.E., Schmidt, U., Matsui, T., Kang, Z.B., Dec, G.W., Gwathmey, J.K., Rosenzweig, A., Hajjar, R.J., 1999. Restoration of contractile function in isolated cardiomyocytes from failing human hearts by gene transfer of SERCA2a. *Circulation*; 100:2308-2311.

Der Mardirossian, C., Bokoch, G.M., 2005. GDIs: central regulatory molecules in Rho GTPase activation. *Trends Cell Biol*; 15:356-63.

Derry, M.C., Yanagiya, A., Martineau, Y., Sonenberg, N., 2006. Regulation of Poly(A)-binding Protein through PABP-interacting Proteins. *Cold Spring Harb Symp Quant Biol*; 71: 537-543.

Dick, F.A., Rubin, S.M., 2013. Molecular mechanisms underlying RB protein function. *Nat Rev Mol Cell Biol*; 14:297-306.

Ding, Q., Regan, S. N., Xıa, Y., Oostrom, L. A., Cowan, C. A., Musunuru. K., 2013. Enhanced efficiency of human pluripotent stem cell genome editing through replacing TALENs with CRISPRs. *Cell Stem Cell*; 12: 392-394.

Dingar, D., Kalkat, M., Chan, P.K., Srikumar, T., Bailey, S.D., Tu, W.B., Coyaud, E., Ponzielli, R., Kolyar, M., Jurisica, I., Huang, A., Lupien, M., Penn, L.Z., Raught, B., 2015. BioID identifies novel c-MYC interacting partners in cultured cells and xenograft tumors. *J Proteomics*; 118:95-111.

Djiane, A., Riou, J., Umbhauer, M., Boucaut, J., Shi, D., 2000. Role of frizzled 7 in the regulation of convergent extension movements during gastrulation in Xenopus laevis. *Development*; 127:3091-100.

Dluhosova, M., Curik, N., Vargova, J., Jonasova, A., Zikmund, T., Stopka, T., 2014. Epigenetic control of SPI1 gene by CTCF and ISWI ATPase SMARCA5. *PLoS One*; 9(2):e87448.

Dorseuil, O., Reibel, L., Bokoch, G.M., Camonis, J., Gacon, G., 1996. The Rac target NADPH oxidase p67phox interacts preferentially with Rac2 rather than Rac1. *J Biol Chem*; 271:83-88.

Dowhan, D.H., Hong, E.P., Auboeuf, D., Dennis, A.P., Wilson, M.M., Berget, S.M., O'Malley, B.W., 2005. Steroid hormone receptor coactivation and alternative RNA splicing by U2AF65-related proteins CAPERalpha and CAPERbeta. *Mol Cell*; 17:429–39.

Doyon, Y., McCammon, J.M., Miller, J.C., Faraji, F., Ngo, C., Katibah, G.E., Amora, R., Hocking, T.D., Zhang, L., Rebar, E.J., *et al*., 2008. Heritable targeted gene disruption in zebrafish using designed zinc-finger nucleases. *Nat Biotechnol*; 26:702-8.

Draper, B.W., Morcos, P.A., Kimmel, C.B., 2001. Inhibition of zebrafish fgf8 pre-mRNA splicing with morpholino oligos: a quantifiable method for gene knockdown. *Genesis*; 30:154-156.

Draper, B.W., Stock, D.W., Kimmel, C.B., 2003. Zebrafish fgf24 functions with fgf8 to promote posterior mesodermal development. *Development*; 130:4639-54.

Drummond, I., 2002. The pronephros. *Results Probl Cell Differ*; 40:322-45.

Du, S.J., Purcell, S. M., Christian, J.L., Mcgrew, L.L., Moon, R.T., 1995. Identification of distinct classes and functional domains of Wnts through expression of wild type and chimeric proteins in *Xenopus* embryos. *Mol Cell Biol*; 15:2625-2634.

Duan, J., Nilsson, L., Lambert, B., 2004. Structural and functional analysis of mutations at the human hypoxanthine phosphoribosyl transferase (HPRT1) locus. *Hum Mutat*; 23:599-611.

Duchniewicz, M., Zemojtel, T., Kolanczyk, M., Grossmann, S., Scheele, J.S., Zwartkruis, F.J., 2006. Rap1A-deficient T and B cells show impaired integrin-mediated cell adhesion. *Mol Cell Biol*; 26:643-53.

Duplay, P., Thome, M., Herve. F., and Acuto, O., 1994. p56lck interacts via its src homology 2 domain with the ZAP-70 kinase. *J Exp Med*; 179:1163-1172.

Durai, S., Mani, M., Kandavelou, K., Wu, J., Porteus, M.H., Chandrasegaran, S., 2005. Zinc finger nucleases: custom-designed molecular scissors for genome engineering of plant and mammalian cells. *Nucleic Acids Res*; 33:5978-90.

Dustin, M.L., Cooper, J.A., 2000. The immunological synapse and the actin cytoskeleton: molecular hardware for T cell signaling. *Nat Immunol*; 1:23-9.

Dutta, B., Ren, Y., Hao, P., Sim, K.H., Cheow, E., Adav, S., Tam, J.P., Sze, S.K., 2014. Profiling of the chromatin-associated proteome identifies HP1BP3 as a novel regulator of cell cycle progression. *Mol Cell Proteomics*; 13:2183-2197.

Dyer, M.A., Hayes, P.J., Baron, M.H., 1998. The HMG domain protein SSRP1/PREIIBF is involved in activation of the human embryonic beta-like globin gene. *Mol Cell Biol*; 18:2617-2628.

Eaton, S., Wepf, R., Simons, K., 1996. Roles for Rac1 and Cdc42 in planar polarization and hair outgrowth in the wing of *Drosophila*. *JCB*; 135:1277.

Eberharter, A., Becker, P.B., 2004. ATP-dependent nucleosome remodelling: factors and functions. *J Cell Sci*; 117:3707-11.

Eissenberg, J.C., Elgin, S.C., 2000. The HP1 protein family: getting a grip on chromatin. *Curr Opin Genet Dev*; 10:204-10.

Eissenberg, J.C., Elgin, S.C., 2014. HP1a: a structural chromosomal protein regulating transcription. *Trends Genet*; 30:103-10.

Eletto, D., Eletto, D., Dersh, D., Gidalevitz, T., 2014. Argon Y. Protein disulfide isomerase A6 controls the decay of IRE1alpha signaling via disulfide-dependent association. *Mol Cell*; 53:562-576.

Ellies, D.L., Stock, D.W., Hatch, G., Giroux, G., Weiss, K.M. and Ekker, M., 1997. Relationship between the genomic organization and the overlapping embryonic expression patterns of the zebrafish dlx genes. *Genomics*; 45:580-590.

Elliott, D.J., Best, A., Dalgliesh, C., Ehrmann, I., Grellscheid, S., 2012. How does Tra2β protein regulate tissue-specific RNA splicing? *Biochem Soc Trans*; 40:784-8.

Elzi, D.J., Song, M., Hakala, K., Weintraub, S.T., Shiio, Y., 2014. Proteomic Analysis of the EWS-Fli-1 Interactome Reveals the Role of the Lysosome in EWS-Fli-1 Turnover. *J Proteome Res*; 13:3783-91.

Ernkvist, M., Luna Persson, N., Audebert, S., Lecine, P., Sinha, I., *et al*., 2009. The Amot/Patj/Syx signaling complex spatially controls RhoA GTPase activity in migrating endothelial cells. *Blood*; 113: 244–253.

Erter, C.E., Wilm, T.P., Basler, N., Wright, C.V., Solnica-Krezel, L., 2001. Wnt8 is required in lateral mesendodermal precursors for neural posteriorization *in vivo*. *Development*; 128:3571-83.

Etienne-Manneville, S., Hall, A., 2002. Rho GTPases in cell biology. *Nature*; 420:629-35.

Eva, A., Aaronson, S.A., 1985. Isolation of a new human oncogene from a diffuse B-cell lymphoma. *Nature*; 316:273-5.

Fabrizio, P., Laggerbauer, B., Lauber, J., Lane, W.S., Lührmann, R., 1997. An evolutionarily conserved U5 snRNP-specific protein is a GTP-binding factor closely related to the ribosomal translocase EF-2. *EMBO J*; 16:4092-106.

Fairhead, M., Howarth, M., 2015. Site-specific biotinylation of purified proteins using BirA. *Methods Mol Biol*; 1266:171-84.

Fanto, M., Weber, U., Strutt, D.I., Mlodzik, M., 2000. Nuclear signaling by Rac and Rho GTPases is required in the establishment of epithelial planar polarity in the *Drosophila* eye. *Curr Biol*; 10:979-88.

Fanzo, J.C., Yang, W., Jang, S.Y., Gupta, S., Chen, Q., Siddiq, A., Greenberg, S., Pernis, A.B., 2006. Loss of IRF-4-binding protein leads to the spontaneous development of systemic autoimmunity. *J Clin Invest*; 116:703-714.

Faucherre, A., Taylor, G.S., Overvoorde, J., Dixon, J.E., Hertog, J., 2008. Zebrafish pten genes have overlapping and non-redundant functions in tumorigenesis and embryonic development. *Oncogene*; 27:1079-1086.

Feldman, B., Gates, M.A., Egan, E.S., Dougan, S.T., Rennebeck, G., Sirotkin, H.I., Schier, A.F., Talbot, W.S., 1998. Zebrafish organizer development and germ-layer formation require nodal-related signals. *Nature*; 395:181–85.

Ferraiuolo, M.A., Basak, S., Dostie, J., Murray, E.L., Schoenberg, D.R., Sonenberg, N., 2005. A role for the eIF4E-binding protein 4E-T in P-body formation and mRNA decay. *J Cell Biol*; 170:913-24.

Filippova, G.N., Fagerlie, S., Klenova, E.M., Myers, C., Dehner, Y., Goodwin, G., Neiman, P.E., Collins, S.J., Lobanenkov, V.V., 1996. An exceptionally conserved transcriptional repressor, CTCF, employs different combinations of zinc fingers to bind diverged promoter sequences of avian and mammalian c-myc oncogenes. *Mol Cell Biol*; 16:2802-2813.

Firat-Karalar, E.N., Rauniyar, N., Yates, J.R., 3rd, Stearns, T., 2014. Proximity interactions among centrosome components identify regulators of centriole duplication. *Curr Biol*; 24:664-670.

Fleisch, V.C., Leighton, P.L., Wang, H., Pillay, L.M., Ritzel, R.G., Bhinder, G., Roy, B., Tierney, K.B., Ali, D.W., Waskiewicz, A.J., *et al*., 2013. Targeted mutation of the gene encoding prion protein in zebrafish reveals a conserved role in neuron excitability. *Neurobiol Dis*; 55:11-25.

Föger, N., Rangell, L., Danilenko, D.M., Chan, A.C., 2006. Requirement for coronin 1 in T lymphocyte trafficking and cellular homeostasis. *Science*; 313:839-842.

Formstone, C.J., Mason, I., 2005. Combinatorial activity of Flamingo proteins directs convergence and extension within the early zebrafish embryo via the planar cell polarity pathway. *Dev Biol*; 282:230-35.

Fortes, P., Longman, D., McCracken, S., Ip, J.Y., Poot, R., Mattaj, I.W., Cáceres, J.F., Blencowe, B.J., 2007. Identification and characterization of RED120: a conserved PWI domain protein with links to splicing and 3'-end formation. *FEBS Lett*; 581:3087-97.

Fos, C., Bécart, S., Canonigo Balancio, A.J., Boehning, D., Altman, A., 2014. Association of the EF-hand and PH domains of the guanine nucleotide exchange factor SLAT with IP3 receptor 1 promotes Ca2+ signaling in T cells. *Sci Signal*; 7(345): ra93.

Friedman, J.R., Fredericks, W.J., Jensen, D.E., Speicher, D.W., Huang, X.P., Neilson, E.G., Rauscher, F.J., 1996. KAP-1, a novel corepressor for the highly conserved KRAB repression domain. *Genes Dev*; 10:2067-2078.

Frydman, J., 2001. Folding of newly translated proteins *in vivo*: the role of molecular chaperones. *Annu Rev Biochem*; 70:603-47.

Fu, K., Sun, X., Zheng, W., Wier, E.M., Hodgson, A., Tran, D.Q., Richard, S., Wan, F., 2013. Sam68 modulates the promoter specificity of NF-κB and mediates expression of CD25 in activated T cells. *Nat Commun*; 4:1909.

Fu, Y., Foden, J.A., Khayter, C., Maeder, M.L., Reyon, D., Joung, J.K., Sander, J.D., 2013. High-frequency off-target mutagenesis induced by CRISPR-Cas nucleases in human cells. *Nat Biotechnol*; 31:822-6.

Fu, Y., Kim, Y., Jin, K.S., Kim, H.S., Kim, J.H., Wang, D., Park, M., Jo, C.H., Kwon, N.H., Kim, D., *et al*., 2014. Structure of the ArgRS-GlnRS-AIMP1 complex and its implications for mammalian translation. *Proc Natl Acad Sci USA*; 111:15084-15089.

Fukumoto, Y., Kaibuchi, K., Hori, Y., Fujioka, H., Araki, S., Ueda, T., Kikuchi, A., Takai, Y., 1990. Molecular cloning and characterization of a novel type of regulatory protein (GDI) for the rho proteins, ras p21-like small GTP-binding proteins. *Oncogene*; 5:1321-8.

Furthauer, M., Van Celst, J., Thisse, C., Thisse, B., 2004. Fgf signalling controls the dorsoventral patterning of the zebrafish embryo. *Development*; 131:2853-64.

Gaj, T., Gersbach, C.A., Barbas III, C.F., 2013. ZFN, TALEN, and CRISPR/Cas-based methods for genome engineering. *Trends Biotech*; 31:397-405.

Galetto, R., Duchateau, P. & Paques, F. 2009. Targeted approaches for gene therapy and the emergence of engineered meganucleases. *Expert Opin Biol Ther*; 9:1289-1303.

Gandhi, M., Goode, B.L., 2008. Coronin: the double-edged sword of actin dynamics. *Subcell Biochem*; 48:72-87.

Gao, Y., Thomas, J.O, Chow, R.L., Lee, G.H., Cowan, N.J., 1992. A cytoplasmic chaperonin that catalyze β-actin folding. *Cell*; 69:1043-1050.

Gao, L., Wang, J., Wang, Y., Andreadis, A., 2007. SR protein 9G8 modulates splicing of tau exon 10 via its proximal downstream intron, a clustering region for frontotemporal dementia mutations. *Mol Cell Neurosci*; 34:48-58.

Gao, G., Xie, A., Huang, S.C., Zhou, A., Zhang, J., Herman, A.M., Ghassemzadeh, S., Jeong, E.M., Kasturirangan, S., Raicu, M., *et al*., 2011. Role of RBM25/LUC7L3 in abnormal cardiac sodium channel splicing regulation in human heart failure. *Circulation*; 124:1124-31.

Gao, G., Dudley, S.C. Jr., 2013. RBM25/LUC7L3 function in cardiac sodium channel splicing regulation of human heart failure. *Trends Cardiovasc Med*; 23:5-8.

Garcia-Mata, R., Boulter, E., Burridge, K., 2011. The invisible hand: regulation of RHO GTPases by RHOGDIs. *Nat Rev Mol Cell Biol*; 12:493–504.

Garfinkel, B.P., Arad, S., Le, P.T., Bustin, M., Rosen, C.J., Gabet, Y., Orly, J., 2015. Proportionate Dwarfism in Mice Lacking Heterochromatin Protein 1 Binding Protein 3 (HP1BP3) Is Associated With Alterations in the Endocrine IGF-1 Pathway. *Endocrinology*; 156:4558-4570.

Garneau, J.E., Dupuis, M.È., Villion, M., Romero, D.A., Barrangou, R., Boyaval, P., Fremaux, C., Horvath, P., Magadán, A.H., Moineau, S., 2010. The CRISPR/Cas bacterial immune system cleaves bacteriophage and plasmid DNA. *Nature*; 468:67-71.

Gasiunas, G., Barrangou, R., Horvath, P., Siksnys, V., 2012. Cas9-crRNA ribonucleoprotein complex mediates specific DNA cleavage for adaptive immunity in bacteria. *PNAS*; 109:E2579-E2586.

Gauen, L.K., Zhu, Y., Letourneur, F., Hu, Q., Bolen, J.B., Matis, L.A., Klausner, R.D., Shaw, A.S., 1994. Interactions of p59fyn and ZAP-70 with T-cell receptor activation motifs: defining the nature of a signalling motif. *Mol Cell Biol*; 14:3729-3741.

Gauthier-Rouviere, C., Vignal, E., Meriane, M., Roux, P., Montcourier, P., Fort, P., 1998. RhoG GTPase Controls a Pathway That Independently Activates Rac1 and Cdc42Hs. *Mol Biol Cell*; 9:1379-1394.

Gawler, D.J., Zhang, L.J., Reedijk, M., Tung, P.S., Moran, M.F., 1995. CaLBa 43 amino acid calcium-dependent membrane/phospholipid binding domain in p120 Ras GTPase-activating protein. *Oncogene*; 10:817–825.

Gaytan-Cervantes, J., Gonzalez-Torres, C., Maldonado, V., Zampedri, C., Ceballos-Cancino, G., Melendez-Zajgla, J., 2017. Protein Sam68 regulates the alternative splicing of survivin DEx3. *J Biol Chem*; 292:13745-13757.

Genova, J.L., Jong, S., Camp, J.T., Fehon, R.G., 2000. Functional analysis of cdc42 in actin filament assembly, epithelial morphogenesis, and cell signaling during *Drosophila* development. *Dev Biol*; 221:181--194.

Gerlach, G.F., Schrader, L.N., Wingert, R.A., 2011. Dissection of the adult zebrafish kidney. *J Vis Exp*; 54:2839.

Ghigna, C., Giordano, S., Shen, H., Benvenuto, F., Castiglioni, F., Comoglio, P.M., Green, M.R., Riva, S., Biamonti, G., 2005. Cell motility is controlled by SF2/ASF through alternative splicing of the Ron protooncogene. *Mol Cell*; 20:881–90.

Ghosh, G., Adams, J.A., 2011. Phosphorylation mechanism and structure of serine-arginine protein kinases. *FEBS J*; 278:587-97.

Ghosh, A., Jindal, S., Bentley, A.A., Hinnebusch, A.G., Komar, A.A., 2014. Rps5-Rps16 communication is essential for efficient translation initiation in yeast *S. cerevisiae*. *Nucleic Acids Res*; 42:8537-8555.

Gifford, J.L., Walsh, M.P., Vogel, H.J., 2007. Structures and metal-ion-binding properties of the Ca^{2+}-binding helix-loop-helix EF-hand motifs. *Biochem J*; 405:199-221.

Glaichenhaus, N., Shastri, N., Littman, D.R., and Turner, J.M., 1991. Requirement for association of p56lck with CD4 in antigen-specific signal transduction in T cells. *Cell*; 64:511–520.

Goh, L.L., Manser, E., 2010. The RhoA GEF Syx Is a Target of Rnd3 and Regulated via a Raf1-Like Ubiquitin-Related Domain. *PLoS One*; 5(8):e12409.

Goley, E.D., Welch, M.D., 2006. The ARP2/3 complex: an actin nucleator comes of age. *Nat Rev Mol Cell Biol*; 7:713–726.

Gómez-Orte, E., Sáenz-Narciso, B., Moreno, S., Cabello, J., 2013. Multiple functions of the noncanonical Wnt pathway. *Trends Genetics*; 29:545-553.

Gonçalves, V., Henriques, A.F., Pereira, J.F., Neves Costa, A., Moyer, M.P., Moita, L.F., Gama-Carvalho, M., Matos, P., Jordan, P., 2014. Phosphorylation of SRSF1 by SRPK1 regulates alternative splicing of tumor-related Rac1b in colorectal cells. *RNA*; 20:474-82.

Goudevenou, K., Martin, P., Yeh, Y., Jones, P. & Sablitzky, F., 2011. Def6 Is Required for Convergent Extension Movements during Zebrafish Gastrulation Downstream of Wnt5b Signaling. *Plos One*; 6(10): e26548.

Grabarek, Z., 2006. Structural basis for diversity of the EF-hand calcium-binding proteins. *J Mol Biol*; 359:509-25.

Grainger, R.J., Beggs, J.D., 2005. Prp8 protein: at the heart of the spliceosome. *RNA*; 11:533-57.

Graveley, B.R., 2000. Sorting out the complexity of SR protein functions. *RNA*; 6:1197-211.

Graveley, B.R., 2005. Coordinated control of splicing and translation. *Nat Struct Mol Biol*; 12:1022-1023.

Gray, R.S., Roszko, I., Solnica-Krezel, L., 2011. Planar Cell Polarity: Coordinating Morphogenetic Cell Behaviors with Embryonic Polarity. *Dev Cell*; 21:120-133.

Grellscheid, S., Dalgliesh, C., Storbeck, M., Best, A., Liu, Y., Jakubik, M., Mende, Y., Ehrmann, I., Curk, T., Rossbach, K., *et al*., 2011. Identification of evolutionarily conserved exons as regulated targets for the splicing activator tra2β in development. *PLoS Genet*; 7(12):e1002390.

Grizot, S., Fauré, J., Fieschi, F., Vignais, P.V., Dagher, M.C., Pebay-Peyroula, E., 2001. Crystal structure of the Rac1-RhoGDI complex involved in nadph oxidase activation. *Biochemistry*; 40:10007-13.

Gross, B., Borggrefe, T., Wabl, M., Sivalenka, R.R., Bennett, M., Rossi, A.B., Jessberger, R., 2002. SWAP-70-deficient mast cells are impaired in development and IgE-mediated degranulation. *Eur J Immunol*; 32:1121-8.

Groves, J.A., Hammond, C.L., Hughes, S.M., 2005. Fgf8 drives myogenic progression of a novel lateral fast muscle fibre population in zebrafish. *Development*; 132:4211-22.

Grune, T., Catalgol, B., Licht, A., Ermak, G., Pickering, A.M., Ngo, J.K., Davies, K.J., 2011. HSP70 mediates dissociation and reassociation of the 26S proteasome during adaptation to oxidative stress. *Free Radic Biol Med*; 51:1355-64.

Grunwald, D.J., 2013. A revolution coming to a classic model organism. *Nature Methods*; 10:303-306.

Gui, J.F., Lane, W.S., Fu, X.D., 1994. A serine kinase regulates intracellular localization of splicing factors in the cell cycle. *Nature*; 369:678-82.

Guo, N., Hawkins, C., Nathans, J., 2004. Frizzled6 controls hair patterning in mice. *Proc Natl Acad Sci USA*; 101:9277-9281.

Gupta, S., Fanzo, J., Hu, C., Cox, D., Jang, S., Lee, A., Greenberg, S., Pernis, A., 2003a. T cell receptor engagement leads to the recruitment of IBP, a novel guanine nucleotide exchange factor, to the immunological synapse. *J Biol Chem*; 278:43451-43459.

Gupta, S., Lee, A., Hu, C., Fanzo, J., Goldberg, I., Cattoretti, G., Pernis, A.B., 2003b. Molecular cloning of IBP, a SWAP-70 homologous GEF, which is highly expressed in the immune system. *Hum Immunol*; 64:389-401.

Gupta, A., Hall, V.L., Kok, F.O., Shin, M., McNulty, J.C., Lawson, N.D., Wolfe, S.A., 2013. Targeted chromosomal deletions and inversions in zebrafish. *Genome Res*; 23:1008–1017.

Guzzo, C.M., Yang, D.C.H., 2008. Lysyl-tRNA synthetase interacts with EF1a, aspartyl-tRNA synthetase and p38 *in vitro*. *Biochem Biophy Res Comm*; 365:718-723.

Habas, R., Kato, Y., He, X., 2001. Wnt/Frizzled activation of Rho regulates vertebrate gastrulation and requires a novel Formin homology protein Daam1. *Cell*; 107:843-54.

Habas, R., Dawid, I.B., He, X., 2003. Coactivation of Rac and Rho by Wnt/Frizzled signaling is required for vertebrate gastrulation. *Genes Dev*; 17:295–309.

Haffner, M.C., De Marzo, A.M., Meeker, A.K., Nelson, W.G., Yegnasubramanian, S., 2011. Transcription-induced DNA double strand breaks: both oncogenic force and potential therapeutic target? *Clin Cancer Res*; 17:3858–3864.

Hakeda-Suzuki, S., Ng, J., Tzu, J., Dietzl, G., Sun, Y., Harms, M., Nardine, T., Luo, L., Dickson, B.J., 2002. Rac function and regulation during Drosophila development. *Nature*; 416:438-42.

Hall, A. 1994. Small GTP-binding proteins and the regulation of the actin cytoskeleton. *Annu Rev Cell Biol*; 10:31-54.

Hall, A., 1998. Rho GTPases and the actin cytoskeleton. *Science*; 279:509-514.

Halpern, M.E., Ho., R.K., Walker, C., Kimmel, C.B., 1993. Induction of muscle pioneers and floor plate is distinguished by the zebrafish no tail mutation. *Cell*; 75:99-111.

Hamblet, N.S., Lijam, N., Ruiz-Lozano, P., Wang, J., Yang, Y., Luo, Z., Mei, L., Chien, K.R., Sussman, D.J., Wynshaw-Boris, A., 2002. Dishevelled 2 is essential for cardiac outflow tract development, somite segmentation and neural tube closure. *Development*; 129:5827-5838.

Hammerschmidt, M., Pelegri, F., Mullins, M. C., Kane, D. A., Brand, M., Van Eeden, F. J., Furutani-Seiki, M., Granato, M., Haffter, P., *et al*., 1996. Mutations affecting morphogenesis during gastrulation and tail formation in the zebrafish, *Danio rerio*. *Development*; 123:143-51.

Han, A., Stoilov, P., Linares, A.J., Zhou, Y., Fu, X.D., Black, D.L., 2014. De novo prediction of PTBP1 binding and splicing targets reveals unexpected features of its RNA recognition and function. *PLoS Comput Biol*; 10(1):e1003442.

Hansson, A., Skoglund, G., Lasing, I., Lindberg, U., Ingelman-Sundberg, M., 1988. Protein kinase C-dependent phosphorylation of profilin is specifically stimulated by phosphatidylinositol bisphosphate (PIP,). *Biochem Biophys Res Commun*; 150:526-531.

Harden, N., Ricos, M., Ong, Y.M., Chia, W., Lim, L., 1999. Participation of small GTPases in dorsal closure of the Drosophila embryo: distinct roles for Rho subfamily proteins in epithelial morphogenesis. *J Cell Sci*; 112:273-284.

Hariharan, I.K., Hu, K.Q., Asha, H., Quintanilla, A., Ezzell, R.M., Settleman, J., 1995. Characterization of rho GTPase family homologues in Drosophila melanogaster: overexpressing Rho1 in retinal cells causes a late developmental defect. *EMBO J*; 14:292-302.

Harlan, J.E., Hajduk, P.J., Yoon, H.S., Fesik, S.W., 1994. Pleckstrin homology domains bind to phosphatidylinositol-4,5-bisphosphate. *Nature*; 371:168-70.

Harrington, E.O., Loffler, J., Nelson, P.R., Kent, K.C., Simons, M., Ware, J.A., 1997. Enhancement of Migration by Protein Kinase Cα and Inhibition of Proliferation and Cell Cycle Progression by Protein Kinase Cδ in Capillary Endothelial Cells. *J Biol Chem*; 272:7390-7397.

Hart, M.J., Eva, A., Evans, T., Aaronson, S.A., Cerione, R.A., 1991. Catalysis of guanine nucleotide exchange on the CDC42Hs protein by the dbloncogene product. *Nature*; 354:311-314.

Hart, M.J., Maru, Y., Leonard, D., Witte, O.N., Evans, T., Cerione, R.A., 1992. A GDP dissociation inhibitor that serves as a GTPase inhibitor for the Ras-like protein CDC42Hs. *Science*; 258:812-5.

Hartwig, J.H., Tyler, J., Stossel, T.P., 1980. Actin-binding protein promotes the bipolar and branching polymerization of actin filaments. *J Cell Biol*; 87:841-848.

Hashimoto, H., Itoh, M., Yamanaka, Y., Yamashita, S., Shimizu, T., *et al*., 2000. Zebrafish Dkk1 functions in forebrain specification and axial mesendoderm formation. *Dev Biol*; 217:138-52.

Hashimoto, T., Matsuda, K., Kawata, M., 2012. Scaffold attachment factor B (SAFB)1 and SAFB2 cooperatively inhibit the intranuclear mobility and function of ERα. *J Cell Biochem*; 113:3039-50.

Hatahet, F., Ruddock, L.W., 2009. Protein disulfide isomerase: a critical evaluation of its function in disulfide bond formation. *Antioxid. Redox Signal*; 11:2807-2850.

Hayes, S.M., Love, P.E., 2002. Distinct structure and signaling potential of the γδ TCR complex. *Immunity*; 16:827–838.

He, G.P., Muise, A., Li, A.W., Ro, H.S., 1995. A eukaryotic transcriptional repressor with carboxypeptidase activity. *Nature*; 378:92-96.

He, X., Semenov, M., Tamai, K., Zeng, X., 2004. LDL receptor-related proteins 5 and 6 in Wnt/beta-catenin signaling: arrows point the way. *Development*; 131:1663-77.

He, Y., Smith, R., 2009. Nuclear functions of heterogeneous nuclear ribonucleoproteins A/B. *Cell Mol Life Sci*; 66:1239-56.

Hedstrom, L., 2009. IMP Dehydrogenase: Structure, Mechanism and Inhibition. *Chem Rev*; 109:2903-2928.

Heisenberg, C. P., Brand, M., Jıang, Y. J., Warga, R. M., Beuchle, D., Van Eeden, F. J., Furutani-Seiki, M., Granato, M., Haffter, P., Hammerschmidt, M., *et al*., 1996. Genes involved in forebrain development in the zebrafish, *Danio rerio. Development*; 123:191-203.

Heisenberg, C.P., Tada, M., Rauch, G.J., Saúde, L., Concha, M.L., Geisler, R., Stemple, D.L., Smith, J.C., Wilson, S.W., 2000. *Silberblick/Wnt11* mediates convergent extension movements during zebrafish gastrulation. *Nature*; 405:76-81.

Heisenberg, C.P., Houart, C., Take-uchi, M., Rauch, G.J., Young, N., Coutinho, P., Masai, I., Caneparo, L., Concha, M.L., Geisler, R., *et al*., 2001. A mutation in the Gsk3–binding domain of zebrafish Masterblind/Axin1 leads to a fate transformation of telencephalon and eyes to diencephalon. *Genes Dev*; 15:1427-1434.

Heisenberg, C.P., Tada, M., 2002. Zebrafish gastrulation movements: bridging cell and developmental biology. *Semin Cell Dev Biol*; 13:471-9.

Heisenberg, C.P., Solnica-Krezel, L., 2008. Back and forth between cell fate specification and movement during vertebrate gastrulation. *Curr Opin Genet Dev*; 18: 311-6.

Hens, M.D., Nikolic, I., Woolcock, C.M., 2002. Regulation of Xenopus embryonic cell adhesion by the small GTPase, rac. *Biochem Biophy Res Comm*; 298:364–370.

Hernández, M.P., Sullivan, W.P., Toft, D.O., 2002. The assembly and intermolecular properties of the hsp70-Hop-hsp90 molecular chaperone complex. *J Biol Chem*; 277:38294-304.

Hershberger, C.E., Hosono, N., Singh, J., Dietrich, R.C., Gu, X., Makishima, H., Saunthararajah, Y., Maciejewski, J.P., Padgett, R.A., 2016. The Role of LUC7L2 in Splicing and MDS. *Blood*; 128:5504.

Higuchi, T., Todaka, H., Sugiyama, Y., Ono, M., Tamaki, N., Hatano, E., Takezaki, Y., Hanazaki, K., Miwa, T., Lai, S., *et al*., 2016. Suppression of MicroRNA-7 (miR-7) Biogenesis by Nuclear Factor 90-Nuclear Factor 45 Complex (NF90-NF45) Controls Cell Proliferation in Hepatocellular Carcinoma. *J Biol Chem*; 291:21074-21084.

Hikasa, H., Sokol, S.Y., 2013. Wnt signaling in vertebrate axis specification. *Cold Spring Harb Perspect Biol*; 5(1):a007955.

Hilpela, P., Oberbanscheidt, P., Hahne, P., Hund, M., Kalhammer, G., Small, J.V., Bähler, M., 2003. SWAP-70 identifies a transitional subset of actin filaments in motile cells. *Mol Biol Cell*; 14:3242–3253.

Hinits, Y., Williams, V.C., Sweetman, D., Donn, T.M., Ma, T. P., Moens, C.B., Hughes, S.M., 2011. Defective cranial skeletal development, larval lethality and haploinsufficiency in Myod mutant zebrafish. *Dev Biol*; 358:102-112.

Hinnebusch, A.G., 2006. eIF3: a versatile scaffold for translation initiation complexes. *Trends Biochem Sci*; 31:553-62.

Hiramoto, K., Negishi, M. and Katoh, H., 2006. DOCK 4 is regulated by RhoG and promotes Rac-dependent cell migration. *Exp Cell Res*; 312:4205-4216.

Ho, R.K., 1992. Cell movements and cell fate during zebrafish gastrulation. *Dev Suppl*; 65-73.

Hockemeyer, D., Wang, H., Kiani, S., Lai, C.S., Gao, Q., Cassady, J.P., Cost, G.J., Zhang, L., Santiago, Y., Miller, J.C., *et al*., 2011. Genetic engineering of human ES and iPS cells using TALE nucleases. *Nat Biotechnol*; 29:731-734.

Hofmann, Y., Lorson, C. L., Stamm, S., Androphy, E. J., Wirth, B., 2000. Htra2- β1 stimulates an exonic splicing enhancer and can restore full-length SMN expression to survival motor neuron 2 (SMN2). *Proc Natl Acad Sci USA*; 97:9618–9623.

Hoffman, G.R., Nassar, N., Cerione, R.A., 2000. Structure of the Rho family GTP-binding protein Cdc42 in complex with the multifunctional regulator RhoGDI. *Cell*; 100:345-56.

Hoffman, G.R., Cerione, R.A., 2002. Signaling to the Rho GTPases: networking with the DH domain. *FEBS Letters*; 513:85-91.

Hogan, P.G., Chen, L., Nardone, J., Rao, A., 2003. Transcriptional regulation by calcium, calcineurin, and NFAT. *Genes Dev*; 17:2205-32.

Hong, W., Resnick, R.J., Rakowski, C., Shalloway, D., Taylor, S.J., Blobel, G.A., 2002. Physical and functional interaction between the transcriptional cofactor CBP and the KH domain protein Sam68. *Mol Cancer Res*; 1:48-55.

Hong, E.A., Gautrey, H.L., Elliott, D.J., Tyson-Capper, A.J., 2012. SAFB1- and SAFB2-mediated transcriptional repression: relevance to cancer. *Biochem Soc Trans*; 40:826-30.

Hong, F., Rachidi, S.M., Lundgren, D., Han, D., Huang, X., Zhao, H., Kimura, Y., Hirano, H., Ohara, O., Udono, H., *et al*., 2017. Mapping the Interactome of a Major Mammalian Endoplasmic Reticulum Heat Shock Protein 90. *PLOS ONE;* 12(1):e0169260.

Honoré, B., 2000. The hnRNP 2H9 gene, which is involved in the splicing reaction, is a multiply spliced gene. *Biochim Biophys Acta*; 1492:108-19.

Horan, L., Yasuhara, J.C., Kohlstaedt, L.A., Rio, D.C., 2015. Biochemical identification of new proteins involved in splicing repression at the Drosophila P-element exonic splicing silencer. *Genes Dev*; 29:2298-2311.

Hori, Y., Kikuchi, A., Isomura, M., Katayama, M., Miura, Y., Fujioka, H., Kaibuchi, K., and Takai, Y., 1991. Post-translational modifications of the C-terminal region of the rho protein are important for its interaction with membranes and the stimulatory and inhibitory GDP/GTP exchange proteins. *Oncogene*; 6:515–522.

Horii, Y., Beeler, J.F., Sakaguchi, K., Tachibana, M., Miki, T., 1994. A novel oncogene, ost, encodes a guanine nucleotide exchange factor that potentially links Rho and Rac signaling pathways. *EMBO J*; 13:4776-4786.

Horisberger, J.D., 1994. The Na, K-ATPase: Structure-Function Relationships. *Austin, TX:R.G. Landes.*

Horowitz, J.M., 1993. Regulation of transcription by the retinoblastoma protein. *Genes Chrom Cancer*; 6:124-31.

Horvath, P., Barrangous R., 2010. CRISPR/Cas, the immune system of bacteria and archaea. *Science*; 327:167-70.

Hosono, N., Makishima, H., Przychodzen, B., Singh, J., Padgett, R.A., Sekeres, M.A., Jerez, A., Yoshida, K., Shiraishi. Y., Miyano, S,, *et al*., 2013. Spliceosomal Gene LUC7L2 Mutation Causes Missplicing and Alteration of Gene Expression in Myeloid Neoplasms. *Blood*; 122:470.

Hotfilder, M., Baxendale, S., Cross, M. A., Sablitzky, F., 1999. Def-2, -3, -6 and -8, novel mouse genes differentially expressed in the haemopoietic system. *Br J Haematol*; 106:335-44.

Houle, M., Prinos, P., Iulianella, A., Bouchard, N., Lohnes, D., 2000. Retinoic acid regulation of Cdx1: an indirect mechanism for retinoids and vertebral specification. *Mol Cell Biol*; 20:6579-86.

Howell, V.M., Jones, J.M., Bergren, S.K., Li, L., Billi, A.C., Avenarius, M.R., Meisler, M.H., 2007. Evidence for a direct role of the disease modifier SCNM1 in splicing. *Hum Mol Genet*; 16:2506-16.

Hryciw, D.H., Pollock, C.A., Poronnik, P., 2005. PKC-α-mediated remodeling of the actin cytoskeleton is involved in constitutive albumin uptake by proximal tubule cells. *Amer Phy Soc*; 288:F1227-F1235.

Huang, Y., Steitz, J.A., 2001. Splicing factors SRp20 and 9G8 promote the nucleocytoplasmic export of mRNA. *Mol Cell*; 7:899-905.

Huang, H.C., Klein, P.S., 2004. The Frizzled family: receptors for multiple signal transduction pathways. *Genome Biol*; 5:234.

Huang, W., Ochs, H.D., Dupont, B., Vyas, Y.M., 2005. The Wiskott-Aldrich syndrome protein regulates nuclear translocation of NFAT2 and NF-kB (RelA) independently of its role in filamentous actin polymerization and actin cytoskeletal rearrangement. *J Immun*; 174:2602-2611.

Huang, P., Xiao, A., Zhou, M., Zhu, Z., Lin S., Zhang, B., 2011. Heritable gene targeting in zebrafish using customized TALENs. *Nature*; 29: 699-700.

Huang, G., Zhou, Z., Wang, H., Kleinerman, E.S., 2012. CAPER-alpha alternative splicing regulates the expression of vascular endothelial growth factor$_{165}$ in Ewing sarcoma cells. *Cancer*; 118:2106-2116.

Humphries, C.L., Balcer, H.I., D'Agostino, J.L., Winsor, B., Drubin, D.G., Barnes, G., Andrews, B.J., Goode, B.L., 2002. Direct regulation of Arp2/3 complex activity and function by the actin binding protein coronin. *J Cell Biol*; 159:993-1004.

Hurley, I., Hale, M.E., Prince, V.E., 2005. Duplication events and the evolution of segmental identity. *Evol Dev*; 7:556–567.

Huttlin, E.L., Bruckner, R.J., Paulo, J.A., Cannon, J.R., Ting, L., Baltier, K., Colby, G., Gebreab, F., Gygi, M.P., Parzen, H., *et al*., 2017. Architecture of the human interactome defines protein communities and disease networks. *Nature*; 545:505-509.

Hyvönen, M., Macias, M.J., Nilges, M., Oschkinat, H., Saraste, M., Wilmanns, M., 1995. Structure of the binding site for inositol phosphates in a PH domain. *EMBO J*; 14:4676-85.

Ibba, M., Soll, D., 2000. Aminoacyl-tRNA synthesis. *Annu Rev Biochem*; 69:617-650.

Ichihara, J., Shinohara, Y., Kogure, K., Terada, H., 1995. Nucleotide sequence of the 50'-flanking region of the rat type II hexokinase gene. *Biochimica et Biophysica Acta*; 1260:365-368.

Iden, S., Collard, J.G., 2008. Crosstalk between small GTPases and polarity proteins in cell polarization. *Nature Rev Mol Cell Biol*; 9:846-859.

Ihara, S., Oka, T., Fukui, Y., 2006. Direct binding of SWAP-70 to non-muscle actin is required for membrane ruffling. *J Cell Sci*; 119:500-7.

Iijima, T., Wu, K., Witte, H., Hanno-Iijima, Y., Glatter, T., Richard, S., Scheiffele, P., 2011. SAM68 regulates neuronal activity-dependent alternative splicing of neurexin-1. *Cell*; 147:1601-14.

Ikeda, J., Kaneda, S., Kuwabara, K., Ogawa, S., Kobayashi, T., Matsumoto, M., Yura, T., Yanagi, H., 1997. Cloning and expression of cDNA encoding the human 150 kDa oxygen-regulated protein, ORP150. *Biochem Biophys Res Commun*; 230:94-99.

Ilagan, J.O., Ramakrishnan, A., Hayes, B., Murphy, M.E., Zebari, A.S., Bradley, P., Bradley, R.K., 2015. U2AF1 mutations alter splice site recognition in hematological malignancies. *Genome Res*; 25:14-26.

Imai, Y., Gates, M.A., Melby, A.E., Kimelman, D., Schier, A.F., Talbot, W.S., 2001. The homeobox genes vox and vent are redundant repressors of dorsal fates in zebrafish. *Development*; 128:2407-20.

Imataka, H., Gradi, A., Sonenberg, N., 1998. A newly identified N-terminal amino acid sequence of human eIF4G binds poly(A)-binding protein and functions in poly(A)-dependent translation. *EMBO J*; 17:7480–9.

Ishigaki, S., Masuda, A., Fujioka, Y., Iguchi, Y., Katsuno, M., Shibata, A., Urano, F., Sobue, G., Ohno, K., 2012. Position-dependent FUS–RNA interactions regulate alternative splicing events and transcriptions. *Sci Rep*; 2:529.

Ishitani, T., Kishida, S., Hyodo-Miura, J., Ueno, N., Yasuda, J., Waterman, M., Shibuya, H., Moon, R.T., Ninomiya-Tsuji, J., Matsumoto, K., 2003. The TAK1-NLK mitogen-activated protein kinase cascade functions in the Wnt-5a/Ca2+ pathway to antagonize Wnt/β-catenin signaling. *Mol Cell Biol*; 23:131-139.

Itoh, H., Takahashi, A., Adachi, K., Noji, H., Yasuda, R., Yoshida, M., Kinosita, K., 2004. Mechanically driven ATP synthesis by F1-ATPase. *Nature*; 427:465-8.

Itoh, N., Konishi, M., 2007. The zebrafish fgf family. *Zebrafish*; 4:179-86.

Iwashima, M., Irving, B.A., van Oers, N.S., Chan, A.C., and Weiss, A., 1994. Sequential interactions of the TCR with two distinct cyto-plasmic tyrosine kinases. *Science*; 263:1136-1139.

Jaffe, A.B., Hall, A., 2005. Rho GTPases: biochemistry and biology. *Annu Rev Cell Dev Biol*; 21:247-69.

Jansen, R., Embden, J.D., Gaastra, W., Schouls, L.M., 2002. Identification of genes that are associated with DNA repeats in prokaryotes. *Mol Microbiol*; 43:1565-75.

Jasin, M., 1996. Genetic manipulation of genomes with rare-cutting endonucleases. *Trends Genet*; 12:224-8.

Jasin, M., Rothstein, R., 2013. Repair of strand breaks by homologous recombination. *Cold Spring Harb Perspect Biol*; 5(11):a012740.

Jenny, A., Darken. R.S., Wilson, P.A., Mlodzik, M., 2003. Prickle and Strabismus form a functional complex to generate a correct axis during planar cell polarity signaling. *EMBO J*; 22:4409-4420.

Jenny, A., Reynolds-Kenneally, J., Das, G., Burnett, M., Mlodzik, M., 2005. Diego and Prickle regulate frizzled planar cell polarity signalling by competing for dishevelled binding. *Nat Cell Biol*; 7:691-697.

Jessen, J.R., Topczewski, J., Bingham, S., Sepich, D.S., Marlow, F., Chandrasekhar, A., Solnica-Krezel, L., 2002. Zebrafish trilobite identifies new roles for Strabismus in gastrulation and neuronal movements. *Nat Cell Biol*; 4:610-615.

Jia, R., Li, C., McCoy, J.P., Deng, C.X., Zheng, Z.M., 2010. SRp20 is a proto-oncogene critical for cell proliferation and tumor induction and maintenance. *Int J Biol Sci*; 6:806-826.

Jiménez, R.T., Puig, J.G., 2012. Purine Metabolism in the Pathogenesis of Hyperuricemia and Inborn Errors of Purine Metabolism Associated With Disease. *Gout & Other Crystal Arthropathies*; 3:36-50.

Jinek, M., Chylinski, K., Fonfara, I., Hauer, M., Doudna, J.A., Charpentier, E., 2012. A programmable dual-RNA-guided DNA endonuclease in adaptive bacterial immunity. *Science*; 337:816-21.

Johannes, S., Holwerda, B., de Laat, W., 2013. CTCF: the protein, the binding partners, the binding sites and their chromatin loops. Philos Trans R Soc Lond B Biol Sci; 368(1620):20120369.

Johndrow, J.E., Magie, C.R., Parkhurst, S.M., 2004. Rho GTPase Function in Flies: Insights from a Developmental and Organismal Perspective. *Biochem Cell Biol*; 82:643-57.

Johnson, J.L., Craig, E.A., 1997. Protein Folding In Vivo: Unraveling Complex Pathways. *Cell*; 90:201-204.

Johnson, K.M., Chen, X., Boitano, A., Swenson, L., Opipari, A.W.Jr., Glick, G.D., 2005. Identification and validation of the mitochondrial F1F0-ATPase as the molecular target of the immunomodulatory benzodiazepine Bz-423. *Chem Biol*; 12:485-96.

Johnstone, R.W., Kerry, J.A., Trapani, J.A., 1998. The human interferon-inducible protein, IFI 16, is a repressor of transcription. *J Biol Chem*; 273:17172-17177.

Johnstone, R.W., Wei, W., Greenway, A., Trapani, J.A., 2000. Functional interaction between p53 and the interferon-inducible nucleoprotein IFI 16. *Oncogene*; 19:6033-6042.

Jones, C.M., Lyons, K.M., Lapan, P.M., Wright, C.V.E., Hogan, B.L.M., 1992. DVR-4 (bone morphogenetic protein-4) as a posteriorventralizing factor in Xenopus mesoderm induction. *Development*; 115: 639-647.

Jones, M.A., Ng, B.G., Bhide, S., Chin, E., Rhodenizer, D., He, P., Losfeld, M.E., He, M., Raymond, K., Berry, G., Freeze, H.H., Hegde, M.R., 2012. DDOST mutations identified by whole-exome sequencing are implicated in congenital disorders of glycosylation. *Am J Hum Genet*; 90:363-8.

Jopling, C., den Hertog, J., 2005. Fyn/Yes and non-canonical Wnt signalling converge on RhoA in vertebrate gastrulation cell movements. *EMBO Rep*; 6:426-31.

Jore, M.M., Lundgren, M., van Duijn, E., Bultema, J.B., Westra, E.R., Waghmare, S.P., Wiedenheft, B., Pul, U., Wurm, R., Wagner, R., *et al*., 2011. Structural basis for CRISPR RNA-guided DNA recognition by Cascade. *Nat Struct Mol Biol*; 18:529-36.

Ju, B.G., Lunyak, V.V., Perissi, V., Garcia-Bassets, I., Rose, D.W., Glass, C.K., Rosenfeld, M.G., .2006. A topoisomerase IIbeta-mediated dsDNA break required for regulated transcription. *Science*; 312:1798-802.

Jurica, M.S., Licklider, L.J., Gygi, S.P., Grigorieff, N., Moore, M.J., 2002. Purification and characterization of native spliceosomes suitable for three-dimensional structural analysis. *RNA*; 8:426-439.

Kafasla, P., Mickleburgh, I., Llorian, M., Coelho, M., Gooding, C., Cherny, D., Joshi, A., Kotik-Kogan, O., Curry, S., Eperon, I.C., *et al*., 2012. Defining the roles and interactions of PTB. *Biochem Soc Trans*; 40:815-20.

Kahvejian, A., Roy, G., Sonenberg, N., 2001. The mRNA closed-loop model: the function of PABP and PABP-interacting proteins in mRNA translation. *Cold Spring Harbor Symp Quant Biol*; 66:293-300.

Kalderon, D., Roberts, B.L., Richardson, W.D., Smith, A.E., 1984. A short amino acid sequence able to specify nuclear location. *Cell*; 39:499-509.

Kamijo, T., Aoyama, T., Komiyama, A., Hashimoto, T., 1994. Structural analysis of cDNAs for subunits of human mitochondrial fatty acid beta-oxidation trifunctional protein. *Biochem Biophys Res Commun*; 199:818-825.

Kanayama, H.O., Tamura, T., Ugai, S., Kagawa, S., Tanahashi, N., Yoshimura, T., Tanaka, K., Ichihara, A., 1992. Demonstration that a human 26S proteolytic complex consists of a proteasome and multiple associated protein components and hydrolyzes ATP and ubiquitin-ligated proteins by closely linked mechanisms. *Eur J Biochem*; 206:567-78.

Kane, D.A., Warga, R. M., Kimmel, C.B., 1992. Mitotic domains in the early embryo of the zebrafish. *Nature*; 360:735–737.

Kane, D.A., Kimmel, C.B., 1993. The zebrafish midblastula transition. *Development*; 119: 447-456.

Kane, D.A., 1999. Cell cycles and development in the embryonic zebrafish. *Methods Cell Biol*; 59:11-26.

Kao, H.Y., Siliciano, P.G., 1996. Identification of Prp40, a novel essential yeast splicing factor associated with the U1 small nuclear ribonucleoprotein particle. *Mol Cell Biol*; 16:960-7.

Katanaev, V.L, Ponzielli, R., Semeriva, M., Tomlinson, A., 2005. Trimeric G protein-dependent frizzled signaling in Drosophila. *Cell*: 120:111–122.

Katoh, H., Hiramoto, K., Negishi, M., 2006. Activation of Rac1 by RhoG regulates cell migration. *J Cell Science*; 119:56–65.

Kawamoto, S., Hidaka, H., 1984. Ca^{2+}-activated, phospholipid-dependent protein kinase catalyzes the phosphorylation of actin-binding proteins. *Biochem Biophys Res Commun*; 118:736-42.

Kazanskaya, O., Glinka, A., del Barco Barrantes, I., Stannek, P., Niehrs, C., Wu, W., 2004. R-Spondin2 is a secreted activator of Wnt/beta-catenin signaling and is required for *Xenopus* myogenesis. *Dev Cell*; 7:525-34.

Keenan, C., Kelleher, D., 1998. Protein Kinase C and the Cytoskeleton. *Cellular Signalling*; 10:225-232.

Kelleher, D.J., Gilmore, R., 2006. An evolving view of the eukaryotic oligosaccharyltransferase. *Glycobiology*; 16:47R-62R.

Kelleher, D.J., Kreibich, G., Gilmore, R., 1992. Oligosaccharyltransferase activity is associated with a protein complex composed of ribophorins I and II and a 48kd protein. *Cell*; 69:55-65.

Keller, R.E., 1980. The cellular basis of epiboly: an SEM study of deep cell rearrangement during gastrulation in *Xenopus laeuis*. *J Embryol Exp Morphol*; 60:201-234.

Kelly, C., Chin, A.J., Leatherman, J.L., Kozlowski, D.J., Weinberg, E.S., 2000. Maternally controlled (beta)-catenin-mediated signaling is required for organizer formation in the zebrafish. *Development*; 127:3899-911.

Keppetipola, N., Sharma, S., Li, Q., Black, D.L., 2012. Neuronal regulation of pre-mRNA splicing by polypyrimidine tract binding proteins, PTBP1 and PTBP2. *Critical reviews biochem mol biol*; 47:360–378.

Kestler, H.A, Kühl, M., 2008. From individual Wnt pathways towards a Wnt signalling network. *Phil Trans R Soc B*; 363:1333-1347.

Kibar, Z., Torban, E., McDearmid, J.R., Reynolds, A., Berghout, J., Mathieu, M., Kirillova, I., De Marco, P., Merello, E., Hayes, J.M., *et al*., 2007. Mutations in VANGL1 associated with neural-tube defects. *N Engl J Med*; 356:1432-1437.

Kikuchi, M., Doi. E, Tsujimoto, I., Horibe, T., Tsujimoto, Y., 2002. Functional analysis of human P5, a protein disulfide isomerase homologue. *J Biochem*; 132:451-455.

Kilian, B., Mansukoski, H., Barbosa, F.C., Ulrich, F., Tada, M., Heisenberg, C.P., 2003. The role of Ppt/Wnt5 in regulating cell shape and movement during zebrafish gastrulation. *Mech Dev*; 120: 467-76.

Kim, C.H., Oda, T., Itoh, M., Jiang, D., Artinger, K.B., Chandrasekharappa, S.C., Driever, W., Chitnis, A.B., 2000. Repressor activity of Headless/Tcf3 is essential for vertebrate head formation. *Nature*; 407:913-6.

Kim, S.W., Muise, A.M., Lyons, P.J., Ro, H.S., 2001. Regulation of adipogenesis by a transcriptional repressor that modulates MAPK activation. *J Biol Chem*; 276:10199-10206.

Kim, G.H., Her, J.H., Han, J.K., 2008. Ryk cooperates with Frizzled 7 to promote Wnt11-mediated endocytosis and is essential for Xenopus laevis convergent extension movements. *J Cell Biol*; 182: 1073-1082.

Kim, H., Kim, J.S., 2014. A guide to genome engineering with programmable nucleases. *Nat Rev Genet*; 15:321-34.

Kim, S., Yu, N.K., Kaang, B.K., 2015. CTCF as a multifunctional protein in genome regulation and gene expression. *Exp Mol Med*; 47:e166.

Kim, D.I., Jensen, S.C., Noble, K.A., Kc, B., Roux, K.H., Motamedchaboki, K., Roux, K.J., 2016. An improved smaller biotin ligase for BioID proximity labeling. *Mol Biol Cell*; 27:1188-96.

Kimelman, D., Martin, B.L., 2012. Anterior-posterior patterning in early development: three strategies. *Wiley Interdiscip Rev Dev Biol*; 1:253-66.

Kimelman, D., Xu, W., 2006. Beta-catenin destruction complex: insights and questions from a structural perspective. *Oncogene*; 25:7482-91.

Kimmel, C.B., Law, R.D., 1985. Cell lineage of zebrafish blastomeres. I. Cleavage pattern and cytoplasmic bridges between cells. *Dev Biol*; 108:78-85.

Kimmel, C.B., Warga, R.M., Schilling, T.F., 1990. Origin and organization of the zebrafish fate map. *Development*; 108:581-94.

Kimmel, C., Ballard, W., Kimmel, S., Ullmann, B., Schilling, T., 1995. Stages of embryonic-development of the zebrafish. *Dev Dyn*; 203: 253-310.

Kini, H.K., Silverman, I.M., Ji, X., Gregory, B.D., Liebhaber, S.A., 2016. Cytoplasmic poly(A) binding protein-1 binds to genomically encoded sequences within mammalian mRNAs.*RNA*; 22:1-14.

Kinosita, K.Jr, Yasuda, R., Noji, H., 2000. F1-ATPase: a highly efficient rotary ATP machine. *Essays Biochem*; 35:3-18.

Kishida, S., Yamamoto, H., Hino, S., Ikeda, S., Kishida, M., Kikuchi, A., 1999. DIX domains of Dvl and axin are necessary for protein interactions and their ability to regulate beta-catenin stability. *Mol Cell Biol*; 19:4414-22.

Kishimoto, Y., Lee, K.H., Zon, L., Hammerschmidt, M., Schulte-Merker, S., 1997. The molecular nature of zebrafish swirl: BMP2 function is essential during early dorsoventral patterning. *Development*; 124:4457-66.

Kissa, K., Herbomel, P., 2010. Blood stem cells emerge from aortic endothelium by a novel type of cell transition. *Nature;* 464: 112-115.

Kjoller, L., Hall, A., 1999. Signaling to Rho GTPases. *Exp Cell Res*; 253:166-79.

Ko, Y.G., Kang, Y.S., Kim, E.K., Park, S.G., Kim, S., 2000. Nucleolar Localization of Human Methionyl–tRNA Synthetase and Its Role in Ribosomal RNA Synthesis. *J Cell Biol*; 149:567-574.

Kobayashi, S., Shirai, T., Kiyokawa, E., Mochizuki, N., Matsuda, M,. Fukui, Y., 2001. Membrane recruitment of DOCK180 by binding to PtdIns(3,4,5)P3. *Biochem J*; 354:73-78.

Kockel, L., Zeitlinger, J., Staszewski, L.M., Mlodzik, M., Bohmann, D., 1997. Jun in Drosophila development: redundant and nonredundant functions and regulation by two MAPK signal transduction pathways. *Genes Dev*; 11:1748-1758.

Kohtz, J.D., Jamison, S.F., Will, C.L., Zuo, P., Lührmann, R., Garcia-Blanco, M.A., Manley, J.L., 1994. Protein-protein interactions and 5'-splice-site recognition in mammalian mRNA precursors. *Nature*; 368:119-24.

Kok, F.O., Shin, M., Ni, C.W., Gupta, A., Grosse, A.S., van Impel, A., Kirchmaier, B.C., Peterson-Maduro, J., Kourkoulis, G., Male, I., *et al*., 2015. Reverse genetic screening reveals poor correlation between morpholino-induced and mutant phenotypes in zebrafish. *Dev Cell*; 32:97-108.

Komekado, H., Yamamoto, H., Chiba, T., Kikuchi, A., 2007. Glycosylation and palmitoylation of Wnt-3a are coupled to produce an active form of Wnt-3a. *Genes Cells*; 12:521-34.

Kondo, M., 2007. Bone morphogenetic proteins in the early development of zebrafish. *FEBS J*; 274:2960-7.

Kontopidis G, Taylor P, Walkinshaw MD. Enzymatic and structural characterization of non-peptide ligand-cyclophilin complexes. Acta Crystallogr D Biol Crystallogr. 2004 Mar;60(Pt 3):479-85.

Korinek, V., Barker, N., Morin, P.J., van Wichen, D., de Weger, R., Kinzler, K.W., Vogelstein, B., Clevers, H., 1997. Constitutive transcriptional activation by a beta-catenin-Tcf complex in APC-/- colon carcinoma. *Science*; 275:1784-7.

Kozma, R., Ahmed, S., Best, A., Lim L., 1995. The Ras-related protein Cdc42Hs and bradykinin promote formation of peripheral actin microspikes and filopodia in Swiss 3T3 fibroblasts. *Mol Cell Biol*; 15:1942-52.

Kraft, B., Berger, C.D., Wallkamm, V., Steinbeisser, H., Wedlich, D., 2012. Wnt-11 and Fz7 reduce cell adhesion in convergent extension by sequestration of PAPC and C-cadherin. *JCB*; 198: 695-709.

Krainer, A.R., Maniatis, T., 1985. Multiple factors including the small nuclear ribonucleoproteins U1 and U2 are necessary for pre-mRNA splicing *in vitro*. *Cell*; 42:725-736.

Krainer, A.R., Conway, G.C., Kozak, D., 1990. The essential pre-mRNA splicing factor SF2 influences 5' splice site selection by activating proximal sites. *Cell*; 62:35-42.

Kranias, E.G., Hajjar. R.J., 2012. Modulation of cardiac contractility by the phospholamban/SERCA2a regulatome. *Circ Res*; 110:1646-1660.

Kraus, W.L., Lis, J.T., 2003. PARP goes transcription. *Cell*; 113: 677-683.

Krauss, S., Johansen, T., Korzh, V., Fjose, A., 1991. Expression of the zebrafish paired box gene pax[zf-b] during early neurogenesis. *Development*; 113:1193-206.

Krebs, H.A., Weitzman, P.D., 1987. Krebs' citric acid cycle: half a century and still turning. *London: Biochem Soc;* 25.

Krishnakumar, R., Kraus, W.L., 2010. PARP-1 regulates chromatin structure and transcription through a KDM5B-dependent pathway. *Mol Cell*; 39:736-49.

Krishnan, K., Moens, P.D.J., 2009. Structure and functions of profilins. *Biophys Rev*; 1:71–81.

Kubota, H., Hynes, G., Willison, K., 1995. The eighth Cct gene, Cctq, encoding the theta subunit of the cytosolic chaperonin containing TCP-1. *Gene*; 154:231-6.

Kühl, M., Sheldahl, L.C., Park, M., Miller, J.R., Moon, R.T., 2000a. The Wnt/Ca2+ pathway: a new vertebrate Wnt signaling pathway takes shape. *Trends Genet*; 16:279-83.

Kühl, M., Sheldahl, L.C., Malbon, C.C., Moon, R.T., 2000b. Ca(2+)/calmodulin-dependent protein kinase II is stimulated by Wnt and Frizzled homologs and promotes ventral cell fates in *Xenopus*. *J Biol Chem*; 275:12701-11.

Kurayoshi, M., Yamamoto, H., Izumi, S., Kikuchi, A., 2007. Post-translational palmitoylation and glycosylation of Wnt-5a are necessary for its signalling. *Biochem J*; 402:515-23.

Kurukuti, S., Tiwari, V.K., Tavoosidana, G., Pugacheva, E., Murrell, A., Zhao, Z., Lobanenkov, V., Reik, W., Ohlsson, R., 2006. CTCF binding at the H19 imprinting control region mediates maternally inherited higher-order chromatin conformation to restrict enhancer access to Igf2. *Proc Natl Acad Sci USA*; 103:10684-10689.

Kuzumaki, T., Tanaka, T., Ishikawa, K., Ogata, K., 1987. Rat ribosomal protein L35a multigene family: molecular structure and characterization of three L35a-related pseudogenes. *Biochim Biophys Acta*; 909:99-106.

Kwon, N.H., Kang, T., Lee, J.Y., Kim, H.H., Kim, H.R., Hong, J., Oh, Y.S., Han, J.M., Ku, M.J., Lee, S.Y., Kim, S., 2011. Dual role of methionyl-tRNA synthetase in the regulation of translation and tumor suppressor activity of aminoacyl-tRNA synthetase-interacting multifunctional protein-3. *Proc Natl Acad Sci USA*; 108:19635-19640.

Kwon, K., Beckett, D., 2000. Function of a conserved sequence motif in biotin holoenzyme synthetases. *Protein Sci*; 9:1530-1539.

Lai, C.C., Boguski, M., Broek, D., Powers, S., 1993. Influence of guanine nucleotides on complex formation between Ras and CDC25 proteins. *Mol Cell Biol*; 13:1345-1352.

Lai, S.L., Chang, C.N., Wang, P.J., Lee, S.J., 2005. Rho mediates cytokinesis and epiboly via ROCK in zebrafish. *Mol Reprod Dev*; 71:186-96.

Lam, S.H., Chua, H.L., Gong, Z., Lam, T.J., Sin, Y.M., 2004. Development and maturation of the immune system in zebrafish, *Danio rerio*: a gene expression profiling, *in situ* hybridization and immunological study. *Dev Comp Immunol*; 28:9-28.

Lamhonwah, A.M., Barankiewicz, T.J., Willard, H.F., Mahuran, D.J., Quan, F., Gravel, R.A., 1986. Isolation of cDNA clones coding for the alpha and beta chains of human propionyl-CoA carboxylase: chromosomal assignments and DNA polymorphisms associated with PCCA and PCCB genes. *Proc Natl Acad Sci USA*; 83:4864-4868.

Lane, A.N., Fan, T.W.M., 2015. Regulation of mammalian nucleotide metabolism and biosynthesis. *Nucleic Acids Research*; 43:2466–2485.

Lane, M.D., Rominger, K.L., Young, D.L., Lynen, F., 1964. The enzymatic synthesis of holotranscarboxylase from apotranscarboxylase and (+)-biotin. II. Investigation of the reaction mechanism. *J Biol Chem*; 239:2865–2871.

Lange, A., Mills, R.E., Lange, C.J., Stewar, M., Devine, S.E., Corbett, A.H., 2007. Classical Nuclear Localization Signals: Definition, Function, and Interaction with Importin α. *J Biol Chem*; 282:5101-5105.

Langrish, C.L., Chen, Y., Blumenschein, W.M., Mattson, J., Basham, B., Sedgwick, J.D., McClanahan, T., Kastelein, R.A., Cua, D.J., 2005. IL-23 drives a pathogenic T cell population that induces autoimmune inflammation. *J Exp Med*; 201:233–240.

Lareau, L.F., Brooks, A.N., Soergel, D.A., Meng, Q., Brenner, S.E., 2007. The coupling of alternative splicing and nonsense-mediated mRNA decay. *Adv Exp Med Biol*; 623:190-211.

Larsson, C., 2006. Protein kinase C and the regulation of the actin cytoskeleton. *Cell Signal*; 18: 276-284.

Latour, S., Veillette, A., 2001. Proximal protein tyrosine kinases in immunoreceptor signaling. *Curr Opin Immunol*; 13:299-306.

Lazzaro, M.A., Pépin, D., Pescador, N., Murphy, B.D., Vanderhyden, B.C., Picketts, D.J., 2006. The imitation switch protein SNF2L regulates steroidogenic acute regulatory protein expression during terminal differentiation of ovarian granulosa cells. *Mol Endocrinol*; 20:2406-17.

Leach, M.R., Williams, D.B., 2003. Calnexin and Calreticulin, Molecular Chaperones of the Endoplasmic Reticulum. In: Eggleton P., Michalak M. (eds) Calreticulin. *Molecular Biology Intelligence Unit. Springer,* Boston, MA.

Lederer, M., Jockusch, B.M., Rothkegel, M., 2005. Profilin regulates the activity of p42POP, a novel Myb-related transcription factor. *J Cell Science*; 118:331-341.

Lee, S.W., Cho, B.H., Park, S.G., Kim, S., 2004. Aminoacyl-tRNA synthetase complexes: beyond translation. *J Cell Sci*; 117:3725-34.

Lee, H.J., Kweon, J., Kim, E., Kim, S., Kim, J.S., 2012. Targeted chromosomal duplications and inversions in the human genome using zinc finger nucleases. *Genome Res*; 22:539–548.

Lee, M., Gildea, D., Trivedi, N.S., Wolfsberg, T.G., Crawford, N.P.S., 2013. RRP1B, a hereditary metastasis modifier, mediates transcription and splicing to regulate mRNA expression. *Cancer Res*; 72:3423-3423.

Lee, M., Dworkin, A.M., Gildea, D., Trivedi, N.S., Moorhead, G.B., Crawford, N.P.S., 2014. RRP1B is a metastasis modifier that regulates the expression of alternative mRNA isoforms through interactions with SRSF1. *Oncogene*; 33:1818–1827.

Lehming, N., Le Saux, A., Schüller, J., Ptashne, M., 1998. Chromatin components as part of a putative transcriptional repressing complex. *Proc Natl Acad Sci USA*; 95:7322-7326.

Lekven, A.C., Thorpe, C.J., Waxman, J.S., Moon, R.T., 2001. Zebrafish wnt8 encodes two wnt8 proteins on a bicistronic transcript and is required for mesoderm and neurectoderm patterning. *Dev Cell*; 1:103-14.

Lelias, J.M., Adra, C.N., Wulf, G.M., Guillemot, J.C., Khagad, M., Caput, D., Lim, B., 1993. cDNA cloning of a human mRNA preferentially expressed in hematopoietic cells and with homology to a GDP-dissociation inhibitor for the rho GTP-binding proteins. *Proc Natl Acad Sci USA*; 90:1479-1483.

Lemaire, L., Johnson, K.R., Bammer, S., Petry, P., Ruddle, F.H., Heinlein, U.A., 1994. Chromosomal assignment of three novel mouse genes expressed in testicular cells. *Genomics*; 21: 409-414.

Lemaire, R., Prasad, J., Kashima, T., Gustafson, J., Manley, J.L., Lafyatis, R., 2002. Stability of a PKCI-1-related mRNA is controlled by the splicing factor ASF/SF2: a novel function for SR proteins. *Genes Dev*; 16:594-607.

Lemmon, M.A., 2007. Pleckstrin homology (PH) domains and phosphoinositides. *Biochem Soc Symp*; 74:81-93.

Leonard, D., Hart, M.J., Platkot, J.V., Eva, A., Henzelll, W., Evansll, T., Cerione, R.A., 1992. The Identification and Characterization of a GDP-dissociation Inhibitor (GDI) for the CDC42Hs Protein. *J Biol Chem*; 267:22860-22868.

Leung, C.F., Webb, S.E., Miller, A.L., 1998. Calcium transients accompany ooplasmic segregation in zebrafish embryos. *Develop Growth Differ*; 40:313–26.

Lewis, B.P., Green, R.E., Brenner, S.E., 2003. Evidence for the widespread coupling of alternative splicing and nonsense-mediated mRNA decay in humans. *PNAS*; 100:189-192.

Lewit-Bentley, A., Réty, S., 2000. EF-hand calcium-binding proteins. *Curr Opin Struct Biol*; 10:637-43.

Leyva, J.A., Bianchet, M.A., Amzel, L.M., 2003. Understanding ATP synthesis: structure and mechanism of the F1-ATPase. *Mol Membr Biol*; 20:27-33.

Li, N., Richard, S., 2016. Sam68 functions as a transcriptional coactivator of the p53 tumor suppressor. *Nucleic Acids Res*; 44:8726-41.

Li, L., Wu, L.P., Chandrasegaran, S., 1992. Functional domains in Fok I restriction endonuclease. *Proc Natl Acad Sci USA*; 89:4275-79.

Li, Y., Allende, M.L., Finkelstein, R., Weinberg, E.S., 1994. Expression of two zebrafish orthodenticle-related genes in the embryonic forebrain. *Mech Dev*; 48:229–44.

Li, Y., Zeng, S.X., Landais, I., Lu, H., 2007. Human SSRP1 has Spt16-dependent and -independent roles in gene transcription. *J Biol Chem*; 282:6936-45.

Li, T., Huang, S., Jiang, W. Z., Wright, D., Spalding, M. H., Weeks, D. P., Yang, B., 2010. TAL nucleases (TALNs): hybrid proteins composed of TAL effectors and FokI DNA-cleavage domain. *Nucleic Acids Res*; 39:359-72.

Lickert, H., Domon, C., Huls, G., Wehrle, C., Duluc, I., Clevers, H,, Meyer, B. I., Freund, J.N., Kemler, R., 2000. Wnt/(beta)-catenin signaling regulates the expression of the homeobox gene Cdx1 in embryonic intestine. *Development*; 127:3805-13.

Lin, K.T., Lu, R.M., Tarn, W.Y., 2004. The WW domain-containing proteins interact with the early spliceosome and participate in pre-mRNA splicing *in vivo*. *Mol Cell Biol*; 24:9176-85.

Lin, F., Sepich, D.S., Chen, S., Topczewski, J., Yin, C., Solnica-Krezel, L., *et al*. 2005. Essential roles of G (alpha) 12/13 signalling in distinct cell behaviours driving zebrafish convergence and extension gastrulation movements. *J Cell Biol*; 169:777-87.

Lines, M.A., Huang, L., Schwartzentruber, J., Douglas, S.L., Lynch, D.C., Beaulieu, C., Guion-Almeida, M.L., Zechi-Ceide, R.M., Gener, B., Gillessen-Kaesbach, G., *et al*., 2012. Haploinsufficiency of a spliceosomal GTPase encoded by EFTUD2 causes mandibulofacial dysostosis with microcephaly. *Amer J Hum Genetics*; 90:369–77.

Ling, C., Yao, Y.N., Zheng, Y.G., Wei, H., Wang, L., Wu, X.F., Wang, E.D., 2005. The C-terminal appended domain of human cytosolic leucyl-tRNA synthetase is indispensable in its interaction with arginyl-tRNA synthetase in the multi-tRNA synthetase complex. *J Biol Chem*; 280:34755-63.

Liu, Q., Krzewska, J., Liberek, K., Craig, E.A., 2001. Mitochondrial hsp70 Ssc1: role in protein folding. *J Biol Chem*; 276:6112-18.

Liu, A., Joyner, A.L., 2001. Early anterior/posterior patterning of the midbrain and cerebellum. *Ann Rev Neurosci*; 24:869-896.

Liu, X., Liu, D., Qian, D., Dai, J., An, Y., Jiang, S., Stanley, B., Yang, J., Wang, B., Liu, X., Liu, D.X., 2012. Nucleophosmin (NPM1/B23) interacts with activating transcription factor 5 (ATF5) protein and promotes proteasome- and caspase-dependent ATF5 degradation in hepatocellular carcinoma cells. *J Biol Chem*; 287:19599-19609.

Liu, J., Li, C., Yu, Z., Huang, P., Wu, H., Wei, C., Zhu, N., Shen, Y., Chen, Y., Zhang, B., Deng, W.M., Jiao, R., 2012. Efficient and specific modifications of the Drosophila genome by means of an easy TALEN strategy. *J Genet Genomics*; 39:209-15.

Liu, X., Wang, H., Eberstadt, M., Schnuchel, A., Olejniczak, E.T., Meadows, R.P., Schkeryantz, J.M., Janowick, D.A., Harlan, J.E., Harris, E.A., *et al*., 1998. NMR structure and mutagenesis of the N-terminal Dbl homology domain of the nucleotide exchange factor Trio. *Cell*; 95:269–277.

Llorian, M., Schwartz, S., Clark, T.A., Hollander, D., Tan, L.Y., Spellman, R., Gordon, A., Schweitzer, A.C., de la Grange, P., Ast, G., Smith, C.W., 2010. Position-dependent alternative splicing activity revealed by global profiling of alternative splicing events regulated by PTB. *Nat Struct Mol Biol*; 17:1114-23.

Logan, C.Y., Nusse, R., 2004. The Wnt signaling pathway in development and disease. *Annu Rev Cell Dev Biol*; 20:781–810.

Longenecker, K., Read, P., Derewenda, U., Dauter, Z., Liu, X., Garrard, S., Walker, L., Somlyo, A.V., Nakamoto, R.K., Somlyo, A.P., Derewenda, Z.S., 1999. How RhoGDI binds Rho. *Acta Crystallogr D Biol Crystallogr*; 55:1503-15.

Lun, K., Brand, M., 1998. A series of no isthmus (noi) alleles of the zebrafish pax2.1 gene reveals multiple signaling events in development of the midbrain-hindbrain boundary. *Development*; 125:3049-62.

Luo, L., Liao, Y.J., Jan, L.Y., Jan, Y.N., 1994. Distinct morphogenetic functions of similar small GTPases: Drosophila Drac1 is involved in axonal outgrowth and myoblast fusion. *Genes Dev*; 8:1787-1802.

Lyons, P.J., Muise, A.M., Ro, H.S., 2005. MAPK modulates the DNA binding of adipocyte enhancer-binding protein 1. *Biochemistry*; 44:926-31.

Lyons, P.J., Mattatall, N.R., Ro, H.S., 2006. Modeling and functional analysis of AEBP1, a transcriptional repressor. *Proteins*; 63:1069-83.

Ma, C.T., Velazquez-Dones, A., Hagopian, J.C., Ghosh, G., Fu, X.D., Adams, J.A., 2008. Ordered multi-site phosphorylation of the splicing factor ASF/SF2 by SRPK1. *J Mol Biol*; 376:55-68.

MacDonald, B.T., Tamai, K., He, X., 2009. Wnt/beta-catenin signaling: components, mechanisms, and diseases. *Dev Cell*; 17:9-26.

Mace, E.M., Orange, J.S., 2014. Lytic immune synapse function requires filamentous actin deconstruction by Coronin 1A. *Proc Natl Acad Sci USA*; 111:6708-13.

Madrenas, J., 2003. A SLAT in the Th2 Signalosome. *Immunity*; 18:459-61.

Maegawa, S., Varga, M., Weinberg, E.S., 2006. FGF signaling is required for {beta}-catenin-mediated induction of the zebrafish organizer. *Development*; 133:3265-76.

Magie, C.R., Meyer, M.R., Gorsuch, M.S., Parkhurst, S.M., 1999. Mutations in the Rho1 small GTPase disrupt morphogenesis and segmentation during early Drosophila development. *Development*; 126:5353–64.

Mahé, D., Mähl, P., Gattoni, R., Fischer, N., Mattei, M.G., Stévenin, J., Fuchs, J.P., 1997. Cloning of human 2H9 heterogeneous nuclear ribonucleoproteins. Relation with splicing and early heat shock-induced splicing arrest. *J Biol Chem*; 272:1827-36.

Mai, S., Qu, X., Li, P., Ma, Q., Cao, C., Liu, X., 2016. Global regulation of alternative RNA splicing by the SR-rich protein RBM39. *Biochim Biophys Acta*; 1859:1014-24.

Majerciak, V., Lu, M., Li, X., Zheng, Z.M., 2014. Attenuation of the suppressive activity of cellular splicing factor SRSF3 by Kaposi sarcoma-associated herpesvirus ORF57 protein is required for RNA splicing *RNA*; 20:1747-58.

Majumdar, A., Lun, K., Brand, M., Drummond, I.A., 2000. Zebrafish no isthmus reveals a role for pax2.1 in tubule differentiation and patterning events in the pronephric primordia. *Development*; 12:2089-98.

Majumder, P., Gomez, J.A., Chadwick, B.P., Boss, J.M., 2008.The insulator factor CTCF controls MHC class II gene expression and is required for the formation of long-distance chromatin interactions. *J Exp Med*; 205:785-798.

Malarkey, C.S., Churchill, M.E., 2012. The high mobility group box: the ultimate utility player of a cell. *Trends Biochem Sci*; 37:553-562.

Manley, J.L., Krainer, A.R., 2010. A rational nomenclature for serine/arginine-rich protein splicing factors (SR proteins). *Genes Dev*; 24:1073-1074.

Marchesini, M., Ogoti, Y., Fiorini, E., D'anca, M., Storti, P., Nezi, L., Samur, M.K., Gañán-Gómez, I., Fulciniti, M., Bohannan, Z.S., *et al*., 2016. ILF2-YB1 Protein Interaction Modulates RNA Splicing to Induce Resistance to Chemotherapy in High Risk Multiple Myeloma. *Blood*; 128:359.

Marchesini, M., Ogoti, Y., Fiorini, E., Samur, A.A, Nezi, L., D'Anca, M., Storti, P., Samur, M.K., Ganan-Gomez, I., Fulciniti, M.T., *et al*., 2017. ILF2 Is a Regulator of RNA Splicing and DNA Damage Response in 1q21-Amplified Multiple Myeloma. *Cancer Cell*; 32:88-100.e6.

Marín, F., Charnay, P., 2000. Hindbrain patterning: FGFs regulate Krox20 and mafB/kr expression in the otic/preotic region. *Development*; 127: 4925-4935.

Marlow, F., Topczewski, J., Sepich, D., Solnica-Krezel, L., 2002. Zebrafish Rho kinase 2 acts downstream of Wnt11 to mediate cell polarity and effective convergence and extension movements. *Curr Biol*; 12:876-84.

Martin, G.R., 1998. The roles of FGFs in the early development of vertebrate limbs. *Genes Dev*; 12:1571-1586.

Martin, P., 2007. Analysis of Def6, a novel guanine nucleotide exchange factor showing dynamic regulation *in vitro* and playing an essential role in zebrafish development, University of Nottingham, PhD thesis.

Martinez-Contreras, R., Fisette, J.F., Nasim, F.U., Madden, R., Cordeau, M., Chabot, B., 2006. Intronic binding sites for hnRNP A/B and hnRNP F/H proteins stimulate pre-mRNA splicing. *PLoS Biol*; 4(2):e21.

Martinez-Contreras, R., Cloutier, P., Shkreta, L., Fisette, J.F., Revil, T., Chabot, B., 2007. HnRNP proteins and splicing control. *Adv Exp Med Biol*; 623:123-47.

Masat, L., Caldwell, J., Armstrong, R., Khoshnevisan, H., Jessberger, R., Herndier, B., Wabl, M., Ferrick, D., 2000. Association of SWAP-70 with the B cell antigen receptor complex. *Proc Natl Acad Sci USA*; 97:2180-4.

Mashimo, T., Takizawa, A., Voigt, B., Yoshimi, K., Hiai H., Kuramoto, T., Serikawa, T., 2010. Generation of knockout rats with X-linked severe combined immunodeficiency (X-SCID) using zinc-finger nucleases. *PLoS ONE*; 5:e8870.

Masutani, M., Sonenberg, N., Yokoyama, S., Imataka, H., 2007. Reconstitution reveals the functional core of mammalian eIF3. *EMBO J*; 26:3373-83.

Matter, N., Herrlich, P., König, H., 2002. Signal-dependent regulation of splicing via phosphorylation of Sam68. *Nature*; 420:691-5.

Mauger, D.M., Lin, C., Garcia-Blanco, M.A., 2008. hnRNP H and hnRNP F complex with Fox2 to silence fibroblast growth factor receptor 2 exon IIIc. *Mol Cell Biol*; 28:5403-19.

Mavrakis, K. J., Mckinlay, K. J., Jones, P., Sablitzky, F., 2004. DEF6, a novel PH-DH-like domain protein, is an upstream activator of the Rho GTPases Rac1, Cdc42, and RhoA. *Exp Cell Res*; 294:335-44.

Mayeda, A., Munroe, S.H., Cáceres, J.F., Krainer, A.R., 1994. Function of conserved domains of hnRNP A1 and other hnRNP A/B proteins. *EMBO J*; 13:5483-95.

Mayor, R., Carmona-Fontaine, C., 2010. Keeping in touch with contact inhibition of locomotion. *Trends Cell Biol*; 20:319-28.

McClintock, J.M., Kheirbek, M.A., Prince, V.E., 2002. Knockdown of duplicated zebrafish hoxb1 genes reveals distinct roles in hindbrain patterning and a novel mechanism of duplicate gene retention. *Development*; 129:2339-54.

McKie, A.B., McHale, J.C., Keen, T.J., Tarttelin, E.E., Goliath, R., van Lith-Verhoeven, J.J., Greenberg, J., Ramesar, R.S., Hoyng, C.B., Cremers, F.P.,, *et al*., 2001. Mutations in the pre-mRNA splicing factor gene PRPC8 in autosomal dominant retinitis pigmentosa (RP13). *Hum Mol Genet*; 10:1555-62.

McKnight, G.L., Mudri, S.L., Mathewes, S.L., Traxinger, R.R., Marshall, S., Sheppard, P.O., O'Hara, P.J., 1992. Molecular cloning, cDNA sequence, and bacterial expression of human glutamine:fructose-6-phosphate amidotransferase. *J Biol Chem*; 267:25208-12.

Melby, A.E., Beach, C., Mullins, M., Kimelman, D., 2000. Patterning the early zebrafish by the opposing actions of bozozok and vox/vent. *Dev Biol*; 224:275–85.

Meng, X., Zhu, D., Yang, S., Wang, X., Xiong, Z., Zhang, Y., Brachova, P., Leslie, K.K., 2012. Cytoplasmic Metadherin (MTDH) Provides Survival Advantage under Conditions of Stress by Acting as RNA-binding Protein. *J Biol Chem*; 287:4485-91.

Mercier, P., Simeone, A., Cotelli, F., Boncinelli, E., 1995. Expression patterns of two Otx genes suggest a role in specifying anterior body structures in zebrafish. *Int J Dev Biol*; 39:559–573.

Meyer, M., de Angelis, M.H., Wurst, W., Kühna, R., 2010. Gene targeting by homologous recombination in mouse zygotes mediated by zinc-finger nucleases. *Proc Natl Acad Sci USA*; 107:15022-15026.

Michalak, M., Corbett, E.F., 1999. Mesaeli N, Nakamura K and Opas M. Calreticulin: one protein, one gene, many functions. *Biochem J*; 344:281-292.

Mikels, A.J., Nusse, R., 2006. Purified Wnt5a protein activates or inhibits beta-catenin-TCF signaling depending on receptor context. *PLoS Biol*;4(4):e115.

Miles, W.O., Korenjak, M., Griffiths, L.M., Dyer, M.A., Provero, P., Dyson, N.J., 2014. Post-transcriptional gene expression control by NANOS is up-regulated and functionally important in pRb-deficient cells. *EMBO J*; 33:2201-2215.

Miller-Bertoglio, V.E., Fisher, S., Sanchez, A., Mullins, M.C., Halpern, M.E., 1997. Differential regulation of chordin expression domains in mutant zebrafish. *Dev Biol*; 192:537-550.

Miller, J.R., 2001. The Wnts. *Genome Biol*; 3:1-15.

Miller, J.F., Tan, S., Qiao, G., Barlow, K.A., Wang, J., Xia, D.F., Meng, X., Paschon, D.E., Leung, E., Hinkley, S.J., *et al*., 2011. A TALE nuclease architecture for efficient genome editing. *Nature Biotech*; 29:143-150.

Minden, A., Lin, A., Claret, F.X., Abo, A., Karin, M., 1995. Selective activation of the JNK signaling cascade and c-Jun transcriptional activity by the small GTPases Rac and Cdc42Hs. *Cell*; 81:1147-1157.

Mishra, A.K., Lambright, D.G., 2016. Small GTPases and their GAPs. *Biopolymers*; 105:431-448.

Mlodzik, M., 2002. Planar cell polarization: Do the same mechanisms regulate *Drosophila* tissue polarity and vertebrate gastrulation? *Trends Genet*; 18:564-571.

Molenaar, M., van de Wetering, M., Oosterwegel, M., Peterson-Maduro, J., Godsave, S., Korinek, V., Roose, J., Destrée, O., Clevers, H., 1996. XTcf-3 transcription factor mediates beta-catenin-induced axis formation in *Xenopus* embryos. *Cell*; 86:391-9.

Montcouquiol, M., Crenshaw, E.B., Kelley, M.W., 2006. Noncanonical Wnt signaling and neural polarity. *Annu Rev Neurosci*; 29:363–86.

Montero, J.A., Heisenberg, C.P., 2004. Gastrulation dynamics: cells move into focus. *Trends Cell Biol*; 14:620-7.

Montero, J.A., Carvalho, L., Wilsch-Bräuninger, M., Kilian, B., Mustafa, C., and Heisenberg, C.P., 2005. Shield formation at the onset of zebrafish gastrulation. *Development*; 132:1187-1198.

Moon, R.T., Brown, J.D., Torres, M., 1997. WNTs modulate cell fate and behavior during vertebrate development. *Trends Genet*; 13:157-62.

Morimoto, R.I., Tissieres, A., Georgopoulos, C., (Eds.), 1994. The Biology of Heat Shock Proteins and Molecular Chaperones. *Cold Spring Harbor*: 299-312.

Morin, P.J., Sparks, A.B., Korinek, V., Barker, N., Clevers, H., Vogelstein, B., Kinzler, K.W., 1997. Activation of beta-catenin-Tcf signaling in colon cancer by mutations in beta-catenin or APC. *Science*; 275:1787-90.

Morriswood, B., Havlicek, K., Demmel, L., Yavuz, S., Sealey-Cardona, M., Vidilaseris, K., Anrather, D., Kostan, J., Djinovic-Carugo, K., Roux, K.J., *et al*., 2013. Novel bilobe components in *Trypanosoma brucei* identified using proximity-dependent biotinylation. *Eukaryotic Cell*; 12:356-367.

Moscou, M.J., Bogdanove, A.J., 2009. A simple cipher governs DNA recognition by TAL effectors. *Science*; 326:1501.

Motzik, A., Amir, E., Erlich, T., Wang, J., Kim, B.G., Han, J.M., Kim, J.H., Nechushtan, H., Guo, M., Razin, E., Tshori, S., 2017. Post-translational modification of HINT1 mediates activation of MITF transcriptional activity in human melanoma cells. *Oncogene*; 36:4732-4738.

Mouneimne, G., Hansen, S.D., Selfors, L.M., Petrak, L., Hickey, M.M., Gallegos, L.L., Simpson, K.J., Lim, J., Gertler, F.B., Hartwig, J.H., Mullins, R.D., Brugge, J.S., 2012. Differential Remodeling of Actin Cytoskeleton Architecture by Profilin Isoforms Leads to Distinct Effects on Cell Migration and Invasion. *Cancer Cell*; 22:615-630.

Mourelatos, Z., Abel, L., Yong, J., Kataoka, N., Dreyfuss, G., 2001. SMN interacts with a novel family of hnRNP and spliceosomal proteins. *EMBO J*; 20:5443-5452.

Mueller, P., Liu, X., Pieters, J., 2011. Migration and homeostasis of naive T cells depends on coronin 1-mediated prosurvival signals and not on coronin 1-dependent filamentous actin modulation. *J Immunol*; 186:4039-50.

Mugnier, B., Nal, B., Verthuy, C., Boyer, C., Lam, D., Chasson, L., Nieoullon, V., Chazal, G., Guo, X.J., He, H.T., Rueff-Juy, D., Alcover, A., Ferrier, P., 2008. Coronin-1A links cytoskeleton dynamics to TCR alpha beta-induced cell signaling. *PLoS One*; 3(10):e3467.

Mullins, M.C., Hammerschmidt, M., Kane, D.A., Odenthal, J., Brand, M., van Eeden, F.J., Furutani-Seiki, M., Granato, M., Haffter, P., Heisenberg, C.P., Jiang, Y.J., Kelsh, R.N., Nüsslein-Volhard, C.,

1996. Genes establishing dorsoventral pattern formation in the zebrafish embryo: the ventral specifying genes. *Development*; 123:81-93.

Murayama, E., Kissa, K., Zapata, A., Mordelet, E., Briolat, V., Lin, H. F., Handin, R. I., Herbomel, P., 2006. Tracing Hematopoietic Precursor Migration to Successive Hematopoietic Organs during Zebrafish Development. Development. *Immunity*; 25: 963-975.

Murphy, A.M., Montell, D.J., 1996. Cell type-specific roles for Cdc42, Rac, and RhoL in *Drosophila* oogenesis. *J Cell Biol*; 133:617-30.

Mussolino, C., Cathomen, T., 2012. TALE nucleases: tailored genome engineering made easy. *Curr Opin Biotechnol*; 23:644-50.

Myers, D.C., Sepich, D.S., Solnica-Krezel, L., 2002. Convergence and extension in vertebrate gastrulae: cell movements according to or in search of identity? *Trends Genet*; 18:447-55.

Nakadai, T., Fukuda, A., Shimada, M., Nishimura, K., Hisatake, K., 2015. The RNA binding complexes NF45-NF90 and NF45-NF110 associate dynamically with the c-fos gene and function as transcriptional coactivators. *J Biol Chem*; 290:26832-45.

Nasevicius, A., Ekker, S.C., 2000. Effective targeted gene 'knockdown' in zebrafish. *Nat Genet*; 26:216-220.

Natsumeda, Y., Ohno, S., Kawasaki, H., Konno, Y., Weber, G., Suzuki, K., 1990. Two distinct cDNAs for human IMP dehydrogenase. *J Biol Chem*; 265:5292-5.

Negrutskii, B.S., El'skaya, A.V., 1998. Eukaryotic translation elongation factor 1 alpha: Structure, expression, functions, and possible role in aminoacyl-tRNA channeling. *Prog Nucleic Acid Res Mol Biol*; 60:47-78.

Neubauer, G., King, A., Rappsilber, J., Calvio, C., Watson, M., Ajuh, P., Sleeman, J., Lamond, A., Mann, M., 1998. Mass spectrometry and EST-database searching allows characterization of the multi-protein spliceosome complex. *Nat Genet*; 20:46-50.

Ng, J., Nardine, T., Harms, M., Tzu, J., Goldstein, A., Sun, Y., Dietzl, G., Dickson, B.J., Luo, L., 2002. Rac GTPases control axon growth, guidance and branching. *Nature*; 416:442-447.

Ngo, J.C., Chakrabarti, S., Ding, J.H., Velazquez-Dones, A., Nolen, B., Aubol, B.E., Adams, J.A., Fu, X.D., Ghosh, G., 2005. Interplay between SRPK and Clk/Sty kinases in phosphorylation of the splicing factor ASF/SF2 is regulated by a docking motif in ASF/SF2. *Mol Cell*; 20:77-89.

Ni, M., Lee, A.S., 2007. ER chaperones in mammalian development and human diseases. *FEBS Lett*; 581:3641-3651.

Niehrs, C., 2004. Regionally specific induction by the Spemann-Mangold organizer. *Nat Rev Genet*; 5:425-34.

Niehrs, C., 2012. The complex world of Wnt receptor signalling. *Nat Rev Mol Cell Biol*; 13:767-79.

Nishii, Y., Morishima, M., Kakehi, Y., Umehara, K., Kioka, N., Terano, Y., Amachi, T., Ueda, K., 2000. CROP/Luc7A, a novel serine/arginine-rich nuclear protein, isolated from cisplatin-resistant cell line. *FEBS Lett*; 465:153-156.

Nishimura, T., Padamsi, Z., Fakim, H., Milette, S., Dunham, W.H., Gingras, A.C., Fabian, M.R., 2015. The eIF4E-binding protein 4E-T is a component of the mRNA decay machinery that bridges the 5' and 3' termini of target mRNAs. *Cell Rep*; 11:1425-1436.

Nobes, C., Hall, A., 1995. Rho, Rac, and Cdc42 GTPases regulate the assembly of multimolecular focal complexes associated with actin stress fibres, lamellipodia, and filopodia. *Cell*; 81:53-62.

Nobes, C., Hall, A., 1999. Rho GTPases control polarity, protrusion, and adhesion during cell movement. *J Cell Biol*; 144:1235-1244.

Nolte, C., Krumlauf, R., 2007. Expression of Hox genes in the nervous system of vertebrates, HOX Gene Expression, ed. S. Papageorgio. *Springer Science Business Media*: 14–41.

Nolz, J.C., Gomez, T.S., Zhu, P., Li, S., Medeiros, R.B., Shimizu, Y., Burkhardt, J.K., Freedman, B.D., Billadeau, D.D., 2006. The WAVE2 complex regulates actin cytoskeletal reorganization and CRAC-mediated calcium entry during T cell activation. *Curr Biol*; 16:24-34.

Nonchev, S., Vesque, C., Maconochie, M., Seitanidou, T., Ariza-McNaughton, L., Frain, M., Marshall, H., Sham, M.H., Krumlauf, R., Charnay, P., 1996. Segmental expression of Hoxa-2 in the hindbrain is directly regulated by Krox-20. *Development*; 122:543-54.

Northrop, J.L., Kimelman, D., 1994. Dorsal-vetral differences in Xcad3 expression in response to FGF-mediated induction in *Xenopus*. *Dev Biol*; 161:490-503.

Nourizadeh-Lillabadi, R., Seilo Torgersen, J., Vestrheim, O., Konig, M., Alestrom, P., Syed, M., 2010. Early embryonic gene expression profiling of zebrafish prion protein (Prp2) morphants. *PLoS One*; 5:e13573.

Nusse, R., 2003. Wnts and Hedgehogs: lipid-modified proteins and similarities in signaling mechanisms at the cell surface. *Development*; 130:5297-305.

Nüsslein-Volhard, C., Dahm, R., 2002. Zebrafish: a practical approach. *Oxford University Press*: 303p.

Obchoei, S., Wongkhan, S., Wongkham, C., Li, M., Yao, Q., Chen, C., 2009. Cyclophilin A: potential functions and therapeutic target for human cancer. *Med Sci Mon*; 15:RA221–32.

Oberbanscheidt, P., Balkow, S., Kühnl, J., Grabbe, S., Bähler, M., 2007. SWAP-70 associates transiently with macropinosomes. *Eur J Cell Biol*; 86:13-24.

Ocana-Morgner, C., Wahren, C., Jessberger, R., 2009. SWAP-70 regulates RhoA/RhoB-dependent MHCII surface localization in dendritic cells. *Blood*; 113:1474-82.

Ocana-Morgner, C., Reichardt, P., Chopin, M., Braungart, S., Wahren, C., Gunzer, M,, Jessberger, R., 2011. Sphingosine 1-phosphate-induced motility and endocytosis of dendritic cells is regulated by SWAP-70 through RhoA. *J Immunol*; 186:5345-55.

Ocana-Morgner, C., Götz, A., Wahren, C., Jessberger, R., 2013. SWAP-70 restricts spontaneous maturation of dendritic cells. *J Immunol*; 190:5545-58.

Oerum, S., Roovers, M., Leichsenring, M., Acquaviva-Bourdain, C., Beermann, F., Gemperle-Britschgi, C., Fouilhoux, A., Korwitz-Reichelt, A., Bailey, H.J., Droogmans, L., *et al*., 2017. Novel patient missense mutations in the HSD17B10 gene affect dehydrogenase and mitochondrial tRNA modification functions of the encoded protein. *Biochim Biophys Acta*; 1863:3294-3302.

Oishi, I., Suzuki, H., Onishi, N., Takada, R., Kani, S., Ohkawara, B., Koshida, I., Suzuki, K., Yamada, G., Schwabe, G.C., *et al*., 2003. The receptor tyrosin e kinase Ror2 is involved in non-canonical Wnt5a/JNK signalling pathway. *Genes Cells*; 8:645-654.

Oka, T., Ihara, S., Fukui, Y., 2007. Cooperation of DEF6 with activated Rac in regulating cell morphology. *Biol Chem*; 282:2011-8.

Olofsson, B., 1999. Rho guanine dissociation inhibitors: pivotal molecules in cellular signalling. *Cell Signal*; 11:545-54.

Oltean, S., Gammons, M., Hulse, R., Hamdollah-Zadeh, M., Mavrou, A., Donaldson, L., Salmon, A.H., Harper, S.J., Ladomery, M.R., Bates, D.O., 2012. SRPK1 inhibition *in vivo*: modulation of VEGF splicing and potential treatment for multiple diseases. *Biochem Soc Trans*; 40:831-5.

Ono, S., 2003. Regulation of actin filament dynamics by actin depolymerizing factor/cofilin and actin-interacting protein 1: New blades for twisted filaments. *Biochem*; 42:13363-13370.

Oprescu, S.N., Chepa-Lotrea, X., Takase, R., Golas, G., Markello, T.C., Adams, D.R., Toro, C., Gropman, A.L., Hou, Y.M., Malicdan, M.C.V., *et al*., 2017. Compound heterozygosity for loss-of-function GARS variants results in a multisystem developmental syndrome that includes severe growth retardation. *Hum Mutat*; 38:1412-1420.

Orphanides, G., LeRoy, G., Chang, C.H., Luse, D.S., Reinberg, D., 1998. FACT, a factor that facilitates transcript elongation through nucleosomes. *Cell*; 92:105-116.

Oxtoby, E., Jowett, T., 1993. Cloning of the zebrafish krox-20 gene (krx-20) and its expression during hindbrain development. *Nucleic Acids Res*; 21:1087-95.

Paik, J.C., Wang, B., Liu, K., Lue, J.K., Lin, W.C., 2010. Regulation of E2F1-induced apoptosis by the nucleolar protein RRP1B. *J Biol Chem*; 285:6348-6363.

Paik, E.J., Zon, L.I., 2010. Hematopoietic development in the zebrafish. *Int J Dev Biol*; 54:1127-37.

Pang, Q., Christianson, T.A., Koretsky, T., Carlson, H., David, L., Keeble, W., Faulkner, G.R., Speckhart, A., Bagby, G.C., 2003. Nucleophosmin interacts with and inhibits the catalytic function of eukaryotic initiation factor 2 kinase PKR. *J Biol Chem*; 278:41709-41717.

Panganiban, G., Rubenstein, J.L., 2002. Developmental functions of the Distal-less/Dlx homeobox genes. *Development*; 129:4371-86.

Papadopoulou, C., Boukakis, G., Ganou, V., Patrinou-Georgoula, M., Guialis, A., 2012. Expression profile and interactions of hnRNP A3 within hnRNP/mRNP complexes in mammals. *Arch Biochem Biophys*; 523:151-60.

Park, M., Moon, R.T., 2002. The planar cell polarity gene stbm regulates cell behaviour and cell fate in vertebrate embryos. *Nat Cell Biol*; 4:20–25.

Park, H., Li, Z., Yang, X.O., Chang, S.H., Nurieva, R., Wang, Y.H., Wang, Y., Hood, L., Zhu, Z., Tian, Q., Dong, C., 2005. A distinct lineage of CD4 T cells regulates tissue inflammation by producing interleukin 17. *Nat Immunol*; 6:1133-1141.

Paronetto, M.P., Cappellari, M., Busà, R., Pedrotti, S., Vitali, R., Comstock, C., Hyslop, T., Knudsen, K.E., Sette, C., 2010. Alternative splicing of the cyclin D1 proto-oncogene is regulated by the RNA-binding protein Sam68. *Cancer Res*; 70:229-39.

Pavletich, N.P., Pabo, C.O., 1991. Zinc finger-DNA recognition: crystal structure of a Zif268-DNA complex at 2.1 A. *Science*; 252:809-17.

Pearce, G., Angeli, V., Randolph, G.J., Junt, T., Andrian, U., Schnittler, H.J., Jessberger, R., 2006. Signaling protein SWAP-70 is required for efficient B cell homing to lymphoid organs. *Nat Immunol*; 7:827–34.

Pelegri, F., Maischein, H.M., 1998. Function of zebrafish beta-catenin and TCF-3 in dorsoventral patterning. *Mech Dev*; 77:63-74.

Peng, Y., Yuan, J., Zhang, Z., Chang, X., 2017. Cytoplasmic poly(A)-binding protein 1 (PABPC1) interacts with the RNA-binding protein hnRNPLL and thereby regulates immunoglobulin secretion in plasma cells. *J Biol Chem*; 292:12285-12295.

Penton, A., Wodarz, A., Nusse, R., 2002. A mutational analysis of dishevelled in Drosophila defines novel domains in the dishevelled protein as well as novel suppressing alleles of axin. *Genetics*; 161:747-62.

Pernier, J., Shekhar, S., Jegou, A., Guichard, B., Carlier, M.F., 2016. Profilin interaction with actin filament barbed end controls dynamic instability, capping, branching, and motility. Dev Cell; 36: 201-214.

Perrone, L., Tell, G., Di Lauro, R., 1999. Calreticulin enhances the transcriptional activity of thyroid transcription factor-1 by binding to its homeodomain. *J Biol Chem*; 274:4640-5.

Phan, L., Zhang, X., Asano, K., Anderson, J., Vornlocher, H.P., Greenberg, J.R., Qin, J., Hinnebusch, A.G., 1998. Identification of a translation initiation factor 3 (eIF3) core complex, conserved in yeast and mammals, that interacts with eIF5. *Mol Cell Biol*; 18:4935-46.

Piccolo, S., Sasai, Y., Lu, B., De Robertis, E.M., 1996. Dorsoventral patterning in *Xenopus*: inhibition of ventral signals by direct binding of chordin to BMP-4. *Cell*; 86:589-98.

Pimkin, M., Markham, G.D., 2009. Inosine 5'-monophosphate dehydrogenase. *Adv Enzymol Relat Areas Mol Biol*; 76:1-53.

Plouhinec, J.L., Zakin, L., De Robertis, E.M., 2011. Systems control of BMP morphogen flow in vertebrate embryos. *Curr Opin Genet Dev*; 21:696-703.

Popielarz, M., Cavaloc, Y., Mattei, M.G., Gattoni, R., Stévenin, J., 1995. The gene encoding human splicing factor 9G8. Structure, chromosomal localization, and expression of alternatively processed transcripts. *J Biol Chem*; 270:17830-5.

Porteus, M.H., Carroll, D., 2005. Gene targeting using zinc finger nucleases. *Nat Biotechnol*; 23:967-73.

Postlethwait, J.H., Yan, Y.L., Gates, M.A., Horne, S., Amores, A., Brownlie, A., Donovan, A., Egan, E.S., Force, A., Gong, Z., *et al*., 1998. Vertebrate genome evolution and the zebrafish gene map. *Nat Genet*; 18:345-9.

Prinos, P., Joseph, S., Oh, K., Meyer, B. I., Gruss, P. and Lohnes, D., 2001. Multiple pathways governing Cdx1 expression during murine development. *Dev Biol*; 239:257-69.

Prokopenko, S.N., Brumby, A., O'Keefe, L., Prior, L., He, Y., Saint, R., Bellen, H. J., 1999. A putative exchange factor for Rho1 GTPase is required for initiation of cytokinesis in Drosophila. *Genes Dev*; 13:2301–2314.

Proud, C.G., 1994. Peptide-chain elongation in eukaryotes. *Mol Biol Rep*; 19:161-170.

Puig, J.G., Torres, R.J., Mateos, F.A., Ramos, T.H., Arcas, J.M., Buño, A.S., O'Neill, P., 2001. The spectrum of hypoxanthine-guanine phosphoribosyltransferase (HPRT) deficiency. Clinical experience based on 22 patients from 18 Spanish families. *Medicine*; 80:102-12.

Puig, O., Bragado-Nilsson, E., Koski, T., Séraphin, B., 2007. The U1 snRNP-associated factor Luc7p affects 5' splice site selection in yeast and human. *Nucleic Acids Res*; 35:5874-85.

Qian, Y.W., Wang, Y.C.J., Hollingsworth, R.E.Jr., Jones, D., Ling, N., Lee, E.Y.H.P., 1993. A retinoblastoma-binding protein related to a negative regulator of Ras in yeast. *Nature*; 364:648-652.

Quemeneur, L., Angeli, V., Chopin, M., Jessberger, R., 2008. SWAP-70 deficiency causes high-affinity plasma cell generation despite impaired germinal center formation. *Blood*; 111:2714-24.

Quilliam, L.A., Khosravi-Far, R., Huff, S.Y., Der, C.J., 1995. Guanine nucleotide exchange factors: activators of the Ras superfamily of proteins. *Bioessays*; 17:395-404.

Rajan, P., Gaughan, L., Dalgliesh, C., El-Sherif, A., Robson, C.N., Leung, H.Y., Elliott, D.J., 2008. The RNA-binding and adaptor protein Sam68 modulates signal-dependent splicing and transcriptional activity of the androgen receptor. *J Pathol*; 215:67-77.

Rakheja, D., Bennett, M.J., Rogers, B.B., 2002. Long-chain L-3-hydroxyacyl-coenzyme a dehydrogenase deficiency: a molecular and biochemical review. *Lab Invest*; 82:815-24.

Ran, F.A., Hsu, P.D., Lin, C.Y., Gootenberg, J.S., Konermann, S., Trevino, A.E., Scott, D.A., Inoue, A., Matoba, S., Zhang, Y., Zhang, F., 2013. Double nicking by RNA-guided CRISPR Cas9 for enhanced genome editing specificity. *Cell*; 154:1380-9.

Rauch, G.J., Hammerschmidt, M., Blader, P., Schauerte, H.E., Strähle, U., Ingham, P.W., McMahon, A.P., Haffter, P., 1997. Wnt5 is required for tail formation in the zebrafish embryo. *Cold Spring Harb Symp Quant Biol*; 62:227-233.

Reibel, L., Dorseuil, O., Stancou, R., Bertoglio, J., Gacon, G., 1991. A hemopoietic specific gene encoding a small GTP binding protein is overexpressed during T cell activation. *Biochem Biophys Res Commun*; 175:451–8.

Reichman, T.W., Muniz, L.C., Mathews, M.B., 2002. The RNA binding protein nuclear factor 90 functions as both a positive and negative regulator of gene expression in mammalian cells. *Mol Cell Biol*; 22:343-356.

Reichsman, F., Smith, L., Cumberledge, S., 1996. Glycosaminoglycans can modulate extracellular localization of the wingless protein and promote signal transduction. *J Cell Biol*; 135:819-827.

Reifers, F., Bohli, H., Walsh, E.C., Crossley, P.H., Stainier, D.Y.R., Brand, M., 1998. Fgf8 is mutated in zebrafish acerebellar (ace) mutants and is required for maintenance of midbrain–hindbrain boundary development and somitogenesis. *Development*; 125:2381-2395.

Reth, M., 1989. Antigen receptor tail clue. *Nature*; 338:383–384.

Reya, T., Clevers, H., 2005. Wnt signalling in stem cells and cancer. *Nature*; 434:843-50.

Reyes, J.L., Gustafson, E.H., Luo, H.R., Moore, M.J., Konarska, M.M., 1999. The C-terminal region of hPrp8 interacts with the conserved GU dinucleotide at the 5′ splice site. *RNA*; 5:167-179.

Rhodes, G.H., Valbracht, J.R., Nguyen, M.D., Vaughan, J.H., 1997. The p542 gene encodes an autoantigen that cross-reacts with EBNA-1 of the Epstein Barr virus and which may be a heterogeneous nuclear ribonucleoprotein. *J Autoimmun*; 10:447−54.

Rickards, B., Flint, S.J., Cole, M.D., LeRoy, G., 2007. Nucleolin is required for RNA polymerase I transcription *in vivo*. *Mol Cell Biol*; 27:937-948.

Ridley, A.J., Hall, A., 1992. The small GTP-binding protein rho regulates the assembly of focal adhesions and actin stress fibers in response to growth factors. *Cell*; 70:389-99.

Ridley, A.J., Paterson, H.F., Johnston, C.L., Diekmann, D., Hall, A., 1992. The small GTP-binding protein Rac regulates growth factor-induced membrane ruffling. *Cell*; 70:401-410.

Ridley, A.J., 2006. Rho GTPases and actin dynamics in membrane protrusions and vesicle trafficking. *Trends Cell Biol*; 16:522–9.

Ripich, T., Jessberger, R., 2011. SWAP-70 regulates erythropoiesis by controlling α4 integrin. *Haematologica*; 96:1743-52.

Ripich, T., Chacón-Martínez, C.A., Fischer, L., Pernis, A., Kiessling, N., Garbe, A.I., Jessberger, R., 2016. SWEF Proteins Distinctly Control Maintenance and Differentiation of Hematopoietic Stem Cells. *PLoS One*; 11(8):e0161060.

Robbe, K., Otto-Bruc, A., Chardin, P., Antonny, B., 2003. Dissociation of GDP Dissociation Inhibitor and Membrane Translocation Are Required for Efficient Activation of Rac by the Dbl Homology-Pleckstrin Homology Region of Tiam. *J Biol Chem*; 278:4756-4762.

Roberts, A.W., Kim, C., Zhen, L., Lowe, J.B., Kapur, R., Petryniak, B., Spaetti, A., Pollock, J.D., Borneo, J.B., Bradford, G.B., *et al*., 1999. Deficiency of the hematopoietic cell-specific Rho family GTPase Rac2 is characterized by abnormalities in neutrophil function and host defense. *Immunity*; 10:183-96.

Roboti P., High, S., 2012. The oligosaccharyltransferase subunits OST48, DAD1 and KCP2 function as ubiquitous and selective modulators of mammalian N-glycosylation. *J Cell Sci*; 125:3474-3484.

Robu, M.E., Larson, J.D., Nasevicius, A., Beiraghi, S., Brenner, C., Farber, S.A., Ekker, S.C., 2007. p53 activation by knockdown technologies. *PLoS Genet*; 3(5):e78.

Rohrschneider, M.R., Elsen, G.E., Prince, V.E., 2007. Zebrafish Hoxb1a regulates multiple downstream genes including prickle1b. *Dev Biol*; 309:358-372.

Rojnuckarin P., Kaushansky, K., 2001. Actin reorganization and proplatelet formation in murine megakaryocytes: the role of protein kinase Cα. *Blood*; 97:154-161.

Romanova, L.Y., Alexandrov, I.A., Blagosklonny, M.V., Nordan, R.P., Garfield, S., Acs, P., Nguyen, P., Trepel, J., Blumberg, P.M., Mushinski, J.F., 1999. Regulation of actin cytoskeleton in lymphocytes: PKC-δ disrupts IL-3–induced membrane ruffles downstream of Rac1. *J Cell Physiol*; 179:157–169.

Rosenberg, L E., 1983. The Metabolic Basis of Inherited Disease, eds. Stanbury, J.B., Wyngaarden, J.B., Frederickson, D.S., Goldstein, J.L., Brown, M.S. *McGraw-Hill, New York*: 474-497.

Rosowski, E.E., Deng, Q., Keller, N.P., Huttenlocher, A., 2016. Rac2 functions in both neutrophils and macrophages to mediate motility and host defense in larval zebrafish. *J Immunol*; 197:4780-4790.

Rossi, A., Kontarakis, Z., Gerri, C., Nolte, H., Hölper, S., Krüger, M., Stainier, D.Y., 2015. Genetic compensation induced by deleterious mutations but not gene knockdowns. *Nature*; 13:230-3.

Rossi, A., Moro, A., Tebaldi, T., Cornella, N., Gasperini, L., Lunelli, L., Quattrone, A., Viero, G., Macchi, P., 2017. Identification and dynamic changes of RNAs isolated from RALY-containing ribonucleoprotein complexes. *Nucleic Acids Res*; 45:6775-6792.

Rossman, K.L., Der, C.J., Sondek, J., 2005. GEF means go: turning on RHO GTPases with guanine nucleotide-exchange factors. *Nat Rev Mol Cell Biol*; 6:167-80.

Roszko, I., Sawada, A., Solnica-Krezel, L., 2009. Regulation of convergence and extension movements during vertebrate gastrulation by the Wnt/PCP pathway. *Semin Cell Dev Biol*; 20:986-997.

Rotty, J.D., Wu, C., Haynes, E.M., Suarez, C., Win-kelman, J.D., Johnson, H.E., Haugh, J.M., Kovar, D.R., Bear, J.E., 2015. Profilin-1 serves as a gatekeeper for actin assembly by Arp2/3-dependent and -independent pathways. *Dev Cel*; 32: 54–67.

Roux, K.J., In Kim, D., Riada, M., Burke, B. 2012. A promiscuous biotin ligase fusion protein identifies proximal and interacting proteins in mammalian cells. *J Cell Biol*; 196:801-10.

Ryu, S.L., Fujii, R., Yamanaka, Y., Shimizu, T., Yabe, T., Hirata, T., Hibi, M., Hirano, T., 2001. Regulation of dharma/bozozok by the Wnt pathway. *Dev Biol*; 231:397-409.

Samelson, L. E., Phillips, A.F., Luong, E.T., Klausner, R.D., 1990. Association of the fyn protein-tyrosine kinase with the T-cell antigen receptor. *Proc Nadl Acad Sci USA*; 87:4358-4362.

Samson, T., Will, C., Knoblauch, A., Sharek, L., von der Mark, K., Burridge, K., Wixler, V., 2007. Def-6, a Guanine Nucleotide Exchange Factor for Rac1, Interacts with the Skeletal Muscle Integrin Chain α7A and Influences Myoblast Differentiation. *J Biol Chem*; 282:15730-15742.

Sander, J.D., Cade, L., Khayter, C., Reyon, D., Peterson, R., Joung, J., Yeh, J., 2011. Targeted gene disruption in somatic zebrafish cells using engineered TALENs. *Nat Biotechnol*; 29:697-698.

Sanford, J.R., Gray, N.K., Beckmann, K., Cáceres, J.F., 2004. A novel role for shuttling SR proteins in mRNA translation. *Genes Dev*; 18:755-68.

Sang Lee, J., Gyu Park, S., Park, H., Seol, W., Lee, S., Kim, S., 2002. Interaction network of human aminoacyl-tRNA synthetases and subunits of elongation factor 1 complex. *Biochem Biophys Res Commun*; 291:158-64.

Sanjana, N.E., Cong, L., Zhou, Y., Cunniff, M.M., Feng, G., Zhang, F., 2012. A transcription activator-like effector toolbox for genome engineering. *Nat Protoc*; 7:171-92.

Sasai, Y., Lu, B., Steinbeisser, H., Geissert, D., Gont, L.K., De Robertis, E.M., 1994. *Xenopus* chordin: a novel dorsalizing factor activated by organizer-specific homeobox genes. *Cell*; 79:779-90.

Sato, M., Saeki, Y., Tanaka, K., Kaneda, Y., 1999. Ribosome-associated protein LBP/p40 binds to S21 protein of 40S ribosome: analysis using a yeast two-hybrid system. *Biochem Biophys Res Commun*; 256:385-90.

Sato, A., Yamamoto, H., Sakane, H., Koyama, H., Kikuchi, A., 2010. Wnt5a regulates distinct signalling pathways by binding to Frizzled2. *EMBO J*; 29:41–54.

Sayeski, P.P., Paterson, A.J., Kudlow, J.E., 1994. The murine glutamine: fructose-6-phosphate amidotransferase-encoding cDNA sequence. *Gene*; 140:289-290.

Schambony, A., Wedlich, D., 2007. Wnt-5A/Ror2 regulate expression of XPAPC through an alternative noncanonical signaling pathway. *Dev Cell*; 12:779–792.

Scherle, P., Behrens, T., Staudt, L.M., 1993. Ly-GDI, a GDP-dissociation inhibitor of the RhoA GTP-binding protein, is expressed preferentially in lymphocytes. *Proc Natl Acad Sci USA*; 90:7568-7572.

Schier, A.F., Talbot, W.S., 2005. Molecular genetics of axis formation in zebrafish. *Annu Rev Genet*; 39:561–613.

Schiewer, M.J., Knudsen, K.E., 2014. Transcriptional roles of PARP-1 in cancer. *Mol Cancer Res*; 12:1069–1080.

Schlessinger, K., Hall, A., Tolwinski, N., 2009. Wnt signaling pathways meet Rho GTPases. *Genes Dev*; 23:265-277.

Schmid, B., Fürthauer, M., Connors, S.A., Trout, J., Thisse, B., Thisse, C., Mullins, M.C., 2000. Equivalent genetic roles for bmp7/snailhouse and bmp2b/swirl in dorsoventral pattern formation. *Development*; 127:957-67.

Schmidt, J.E., Suzuki, A., Ueno, N. and Kimelman, D., 1995. Localized BMP-4 mediates dorsal/ventral patterning in the early *Xenopus* embryo. *Development*; 169:37-50.

Schmidt, A., Hall, A., 2002. Guanine nucleotide exchange factors for Rho GTPases: turning on the switch. *Genes Dev*; 16:1587-609.

Schmitz, A.A., Govek, E.E., Böttner, B., Van Aelst, L., 2000. Rho GTPases: signaling, migration, and invasion. *Exp Cell Res*; 261:1-12.

Schneider-Maunoury, S., Seitandou, T., Charnay, P., Lumsden, A., 1997. Segmental and neuronal architecture of the hindbrain of Krox-20 mouse mutants. *Development*; 124:1215-1226.

Schreiber, V., Masson, R., Linares, J.L., Mattei, M.G., Tomasetto, C., Rio, M.C., 1998. Chromosomal assignment and expression pattern of the murine Lasp-1 gene. *Gene*; 207:171-175.

Schuller, A.P, Wu, C.C.C., Dever, T.E., Buskirk, A.R., Green, R., 2017. eIF5A Functions Globally in Translation Elongation and Termination. *Mol Cell*; 66:194–205.e5.

Schulte-Merker, S., Ho, R.K., Herrmann, B.G., Nüsslein-Volhard, C., 1992. The protein product of the zebrafish homologue of the mouse T gene is expressed in nuclei of the germ ring and the notochord of the early embryo. *Development*; 116:1021-32.

Schulte-Merker, S., van Eeden, F.J., Halpern, M.E., Kimmel, C.B., Nüsslein-Volhard, C., 1994. no tail (ntl) is the zebrafish homologue of the mouse T (Brachyury) gene. *Development*; 120:1009-15.

Schulte-Merker, S., 1995. The zebrafish no tail gene. *Dev Biol*; 6:411-415.

Schulte-Merker, S., Lee, K.J., McMahon, A.P., Hammerschmidt, M., 1997. The zebrafish organizer requires chordino. *Nature*; 387:862-3.

Schumacher, M.M., Elsabrouty, R., Seemann, J., Jo, Y., DeBose-Boyd, R.A., 2015. The prenyltransferase UBIAD1 is the target of geranylgeraniol in degradation of HMG CoA reductase. *eLife*; 4.

Schwartz, J.C., Ebmeier, C.C., Podell, E.R., Heimiller, J., Taatjes, D.J., Cech, T.R., 2012. FUS binds the CTD of RNA polymerase II and regulates its phosphorylation at Ser2. *Genes Dev*; 26:2690-2695.

Sculley, D.G., Dawson, P.A., Emmerson, B.T., Gordon, R.B., 1992. A review of the molecular basis of hypoxanthine-guanine phosphoribosyltransferase (HPRT) deficiency. *Hum Genet*; 90:195-207.

Seitanidou, T., Schneider-Maunoury, S., Desmarquet, S., Wilkinson, D.G., Charnay, P., 1997. Krox-20 is a key regulator of rhombomere-specific gene expression in the developing hindbrain. *Mech Dev*; 65:31-42.

Sen, S., Talukdar, I., Webster, N.J., 2009. SRp20 and CUG-BP1 modulate insulin receptor exon 11 alternative splicing. *Mol Cell Biol*; 29:871–880.

Seo, J., Asaoka, Y., Nagai, Y., Hirayama, J., Yamasaki, T., Namae, M., Ohata, S., Shimizu, N., Negishi, T., Kitagawa, D., Kondoh, H., Furutani-Seiki, M., Penninger, J.M., Katada, T., Nishina, H., 2010. Negative regulation of wnt11 expression by Jnk signaling during zebrafish gastrulation. *J Cell Biochem*; 110:1022-37.

Sepich, D.S., Myers, D.C., Short, R., Topczewski, J., Marlow, F., Solnica-Krezel, L., 2000. Role of the zebrafish trilobite locus in gastrulation movements of convergence and extension. *Genesis*; 27:159-73.

Seruggia, D., Montoliu, L., 2014. The new CRISPR-Cas system: RNA-guided genome engineering to efficiently produce any desired genetic alteration in animals. *Transgenic Res*; 23:707-16.

Shafqat, N., Marschall, H.U., Filling, C., Nordling, E., Wu, X.Q., Bjork, L., Thyberg, J., Martensson, E., Salim, S., Jornvall, H., Oppermann, U., 2003. Expanded substrate screenings of human and *Drosophila* type 10 17beta-hydroxysteroid dehydrogenases (HSDs) reveal multiple specificities in bile acid and steroid hormone metabolism: characterization of multifunctional 3alpha/ 7alpha/ 7beta/ 17beta/ 20beta/ 21-HSD. *Biochem J*; 376:49-60.

Sham, M.H., Vesque, C., Nonchev, S., Marshall, H., Frain, M., Gupta, R.D., Whiting, J., Wilkinson, D., Charnay, P., Krumlauf, R., 1993. The zinc finger gene Krox20 regulates HoxB2 (Hox2.8) during hindbrain segmentation. *Cell*; 72:183-196.

Sharma, S., Kohlstaedt, L.A., Damianov, A., Rio, D.C., Black, D.L., 2008. Polypyrimidine tract binding protein controls the transition from exon definition to an intron defined spliceosome. *Nat Struct Mol Biol*; 15:183-91.

Sheldahl, L.C., Park, M., Malbon, C.C., Moon, R.T., 1999. Protein kinase C is differentially stimulated by Wnt and Frizzled homologs in a G-protein-dependent manner. *Curr Biol*; 9:695-8.

Sheldahl, L.C., Slusarski, D.C., Pandur, P., Miller, J.R., Kühl, M., Moon, R.T., 2003. Dishevelled activates Ca^{2+} flux, PKC, and CamKII in vertebrate embryos. *J Cell Biol*; 161:769-77.

Shibuya, H., Irie, K., Ninomiya-Tsuji, J., Goebl, M., Taniguchi, T., Matsumoto, K., 1992. New human gene encoding a positive modulator of HIV Tat-mediated transactivation. *Nature*; 357:700-2.

Shimizu, T., Yamanaka, Y., Nojima, H., Yabe, T., Hibi, M., Hirano, T., 2002. A novel repressortype homeobox gene, ved, is involved in dharma/bozozok-mediated dorsal organizer formation in zebrafish. *Mech Dev*; 118:125-38.

Shimizu, T., Yamanaka, Y., Ryu, S.L., Hashimoto, H., Yabe, T., *et al*. 2000. Cooperative roles of Bozozok/Dharma and Nodal-related proteins in the formation of the dorsal organizer in zebrafish. *Mech Dev*; 91:293-303.

Shimizu, T., Bae, Y.K., Muraoka, O., Hibi, M., 2005. Interaction of Wnt and caudal-related genes in zebrafish posterior body formation. *Dev Biol*; 279:125-41.

Shimizu, N., Ishitani, S., Sato, A., Shibuya, H., Ishitani, T., 2014. Hipk2 and PP1c cooperate to maintain Dvl protein levels required for Wnt signal transduction. *Cell Rep*; 8:1391-404.

Shinohara, M., Terada, Y., Iwamatsu, A., Shinohara, A., Mochizuki, N., Higuchi, M., Gotoh, Y., Ihara, S., Nagata, S., Itoh, H., Fukui, Y., Jessberger, R., 2002. SWAP-70 is a guanine-nucleotide-exchange factor that mediates signalling of membrane ruffling. *Nature*; 416:759-763.

Shiow, L.R., Roadcap, D.W., Paris, K., Watson, S.R., Grigorova, I.L., Lebet, T., An, J., Xu, Y., Jenne, C.N., Föger, N., Sorensen, R.U., Goodnow, C.C., Bear, J.E., Puck, J.M., Cyster, J.G., 2008. The actin regulator coronin 1A is mutant in a thymic egress-deficient mouse strain and in a patient with severe combined immunodeficiency. *Nat Immunol*; 9:1307-15.

Shirsat, N.V., Pignolo, R.J., Kreider, B.L., Rovera, G.A., 1990. Member of the ras gene superfamily is expressed specifically in T, B and myeloid hemopoietic cells. *Oncogene*; 5:769-772.

Shuen, W. H., 2010. Molecular evolution of the def6/swap70 gene family and functional analysis of swap70a in zebrafish embryogenesis. University of Nottingham, MRes thesis.

Sidow, A., 1992. Diversification of the Wnt gene family on the ancestral lineage of vertebrates. *Proc Natl Acad Sci USA*; 89:5098-5102.

Simons, M., Mlodzik, M., 2008. Planar cell polarity signaling: from fly development to human disease. *Annu Rev Genet*; 42:517-40.

Sims, T.N., Soos, T.J., Xenias, H.S., Dubin-Thaler, B., Hofman, J.M., Waite, J.C., Cameron, T.O., Thomas, V.K., Varma, R., Wiggins, C.H., *et al*. 2007. Opposing effects of PKCθ and WASp on symmetry breaking and relocation of the immunological synapse. *Cell*; 129:773-785.

Singleton, K.L., Gosh, M., Dandekar, R.D., Au-Yeung, B.B., Ksionda, O., Tybulewicz, V.L.J., Altman, A., Fowell, D.J., Wülfing, C., 2011. Itk controls the spatiotemporal organization of T cell activation. *Sci Signal*; 4(193): ra66.

Sivalenka, R.R., Jessberger, R., 2004. SWAP-70 regulates c-kit-induced mast cell activation, cell-cell adhesion, and migration. *Mol Cell Biol*; 24:10277-88.

Sivalenka, R.R., Sinha, M., Jessberger, R., 2008. SWAP-70 regulates mast cell FcεRI-mediated signaling and anaphylaxis. *Eur J Immunol*; 38:841–854.

Skelton, N.J., Kördel, J., Akke, M., Forsén, S., Chazin, W.J., 1994. Signal transduction versus buffering activity in Ca2+–binding proteins. *Nat Str Biol*; 1:239-245.

Slusarski, D.C., Corces, V.G., Moon, R.T., 1997a. Interaction of Wnt and a Frizzled homologue triggers G-protein-linked phosphatidylinositol signalling. *Nature*; 390:410-13.

Slusarski, D.C., Yang-Snyder, J., Busa, W.B., Moon, R.T., 1997b. Modulation of embryonic intracellular Ca2+ signaling by Wnt-5A. *Dev Biol*; 182:114-20.

Sluss, H.K., Han, Z., Barrett, T., Davis, R.J., Ip, Y.T., 1996. A JNK signal transduction pathway that mediates morphogenesis and an immune response in *Drosophila*. *Genes Dev*; 10:2745-2758.

Smith, J., Bibikova, M., Whitby, F. G., Reddy, A. R., Chandrasegaran, S., *et al*., 2000. Requirements for double-strand cleavage by chimeric restriction enzymes with zinc finger DNA-recognition domains. *Nucleic Acids Res*; 28:3361-3369.

Soergel, D.A.W., Lareau, L.F., Brenner, S.E., 2013. Regulation of Gene Expression by Coupling of Alternative Splicing and NMD. Madame Curie Bioscience Database Austin (TX): *Landes Bioscience*.

Solnica-Krezel, L., Stemple, D.L., Mountcastle-Shah, E., Rangini, Z., Neuhauss, S.C., Malicki, J., Schier, A.F., Stainier, D.Y., Zwartkruis, F., Abdelilah, S., Driever, W., 1996. Mutations affecting cell fates and cellular rearrangements during gastrulation in zebrafish. *Development*; 123:67-80.

Song, Y., Masison, D.C., 2005. Independent regulation of Hsp70 and Hsp90 chaperones by Hsp70/Hsp90-organizing protein Sti1 (Hop1). *J Biol Chem*; 280:34178-85.

Sonoda, E., Hochegger, H., Saberi, A., Taniguchi, Y., Takeda, S., 2006. Differential usage of non-homologous end-joining and homologous recombination in double strand break repair. *DNA Repair (Amst)*; 5:1021-9.

Spellman, R., Smith, C.W., 2006. Novel modes of splicing repression by PTB. *Trends Biochem Sci*; 31:73-6.

Spencer, J.A., Baron, M.H., Olson, E.N., 1999. Cooperative transcriptional activation by serum response factor and the high mobility group protein SSRP1. *J Biol Chem*; 274:15686-93.

Stainier, D.Y.R., Raz, E., Lawson, N.D., Ekker, S.C., Burdine, R.D., Eisen, J.S., Ingham, P.W., Schulte-Merker, S., Yelon, D., Weinstein, B.M., *et al.,* 2017. Guidelines for morpholino use in zebrafish. *PLoS Genet*;13(10):e1007000.

Stapulionis, R., Deutscher, M.P., 1995. A channeled tRNA cycle during mammalian protein synthesis. *Proc Natl Acad Sci USA*; 92:7158-7161.

Stepanyuk, G.A., Serrano, P., Peralta, E., Farr, C.L., Axelrod, H.L., Geralt, M., Das, D., Chiu, H.J., Jaroszewski, L., Deacon, A.M., *et al*., 2016. UHM-ULM interactions in the RBM39-U2AF65 splicing-factor complex. *Acta Crystallogr D Struct Biol*; 72:497-511.

Stock, D.W., Ellies, D.L., Zhao, Z., Ekker, M., Ruddle, F.H., Weiss, K.M., 1996. The evolution of the vertebrate dlx gene family. *Proc Natl Acad Sci USA*; 93:10858-10863.

Stoilov, P., Daoud, R., Nayler, O., Stamm, S., 2004. Human tra2-β1 autoregulates its protein concentration by influencing alternative splicing of its pre-mRNA. *Hum Mol Genet*; 13:509–524.

Stossel, T.P., Condeelis, J., Cooley, L., Hartwig, J.H., Noegel, A., Schleicher, M., Shapiro S.S., 2001. Filamins as integrators of cell mechanics and signalling. *Nat Rev Mol Cell Biol*; 2:138-145.

Straus, D.B., Weiss, A., 1992. Genetic evidence for the involvement of the lck tyrosine kinase in signal transduction through the T cell antigen receptor. *Cell*; 70:585-93.

Straus, D.B., Weiss, A., 1993. The CD3 chains of the T cell antigen receptor associate with the ZAP-70 tyrosine kinase and are tyrosine phosphorylated after receptor stimulation. *J Exp Med*; 178:1523-30.

Streit, A., Berliner, A.J., Papanayotou, C., Sirulnik, A., Stern, C.D., 2000. Initiation of neural induction by FGF signalling before gastrulation. *Nature*; 406:74-78.

Strutt, D.I., Weber, U., Mlodzik, M., 1997. The role of RhoA in tissue polarity and Frizzled signalling. *Nature*; 387:292-5.

Strutt, D., 2003. Frizzled signalling and cell polarisation in *Drosophila* and vertebrates. *Development*; 130:4501-4513.

Su, C.Y., Kemp, H.A., Moens, C.B., 2014. Cerebellar development in the absence of Gbx function in zebrafish. *Dev Biol*; 386:181-190.

Sumanas, S., Kim, H.J., Hermanson, S., Ekker, S.C., 2001. Zebrafish frizzled-2 morphant displays defects in body axis elongation. *Genesis*; 30:114-118.

Sun, C.X., Magalhães, M.A.O., Glogauer, M., 2007. Rac1 and Rac2 differentially regulate actin free barbed end formation downstream of the fMLP receptor. *J Cell Biol*; 179:239-245.

Suzuki, C., Murakumo, Y., Kawase, Y., Sato, T., Morinaga, T., Fukuda, N., Enomoto, A., Ichihara, M., Takahashi, M., 2008. A novel GDNF-inducible gene, BMZF3, encodes a transcriptional repressor associated with KAP-1. *Biochem Biophys Res Commun*; 366:226-232.

Swiatek, P.J., Gridley, T., 1993. Perinatal lethality and defects in hindbrain development in mice homozygous for a targeted mutation of the zinc finger gene Krox20. *Genes Dev*; 7:2071-84.

Tada, M., Smith, J.C., 2000. Xwnt11 is a target of *Xenopus Brachyury*: regulation of gastrulation movements via Dishevelled, but not through the canonical Wnt pathway. *Development*; 127:2227-2238.

Tada, M., Heisenberg, C.P., 2012. Convergent extension: using collective cell migration and cell intercalation to shape embryos. *Development*; 139:3897-904.

Tahinci, E., Symes, K., 2003. Distinct functions of Rho and Rac are required for convergent extension during *Xenopus* gastrulation. *Dev Biol*; 259:318-35.

Takahashi, N., Hayano, T., Suzuki, M., 1989. Peptidyl-prolyl cis-trans isomerase is the cyclosporin A-binding protein cyclophilin. *Nature*; 337:473-475.

Tamai, K., Zeng, X., Liu, C., Zhang, X., Harada, Y., Chang, Z., He, X., 2004. A mechanism for Wnt coreceptor activation. *Mol Cell*; 13:149-56.

Tan, A.Y., Riley, T.R., Coady, T., Bussemaker, H.J., Manley, J.L., 2012. TLS/FUS (translocated in liposarcoma/fused in sarcoma) regulates target gene transcription via single-stranded DNA response elements. *Proc Natl Acad Sci USA*; 109:6030–6035.

Tanackovic, G., Ransijn, A., Thibault, P., Abou Elela, S., Klinck, R., Berson, E.L., Chabot, B., Rivolta, C., 2011. PRPF mutations are associated with generalized defects in spliceosome formation and pre-mRNA splicing in patients with retinitis pigmentosa. *Hum Mol Genet*; 20:2116-30.

Tanaka, Y., Bi, K., Kitamura, R., Hong, S., Altman, Y., Matsumoto, A., Tabata, H., Lebedeva, S., Bushway, P., Altman, A., 2003. SWAP-70-like adapter of T cells, an adapter protein that regulates early TCR-initiated signaling in Th2 lineage cells. *Immunity*; 18:403-414.

Tanegashima, K., Zhao, H., Dawid, I.B., 2008. WGEF activates Rho in the Wnt/PCP pathway and controls convergent extension in *Xenopus* gastrulation. *Embo J*; 27:606-617.

Tang, S., Morgan, K.G., Parker, C., Ware, J.A., 1997. Requirement for Protein Kinase C θ for Cell Cycle Progression and Formation of Actin Stress Fibers and Filopodia in Vascular Endothelial Cells. *J Biol Chem*; 272:28704–28711.

Tanioka, T., Nakatani, Y., Semmyo, N., Murakami, M., Kudo, I., 2000. Molecular identification of cytosolic prostaglandin E2 synthase that is functionally coupled with cyclooxygenase-1 in immediate prostaglandin E2 biosynthesis. *J Biol Chem*; 275:32775-32782.

Tao, W., Pennica, D., Xu, L., Kalejta, R.F., Levine, A.J., 2001. Wrch-1, a novel member of the Rho gene family that is regulated by Wnt-1. *Genes Dev*; 15:1796–1807.

Tapon, N., Hall, A., 1997. Rho, Rac and Cdc42 GTPases regulate the organization of the actin cytoskeleton. *Curr Opin Cell Biol*; 9:86-92.

Taylor, J., Abramova, N., Charlton, J., Adler, P.N., 1998. Van Gogh: a new *Drosophila* tissue polarity gene. *Genetics*; 150:199-210.

Teigelkamp, S., Newman, A.J., Beggs, J.D., 1995. Extensive interactions of PRP8 protein with the 5′ and 3′ splice sites during splicing suggest a role in stabilization of exon alignment by U5 snRNA. *EMBO J*; 14:2602-2612.

Tenzer, S., Moro, A., Kuharev, J., Francis, A.C., Vidalino, L., Provenzani, A., Macchi, P., 2013. Proteome-Wide Characterization of the RNA-Binding Protein RALY Interactome Using the in Vivo-Biotinylation-Pulldown-Quant (iBioPQ) Approach. *J Proteome Res*; 12:2869-2884.

Terada, K., Mori, M., 2000. Human DnaJ homologs dj2 and dj3, and bag-1 are positive cochaperones of hsc70. *J Biol Chem*; 275:24728-34.

Tesson, L., Usal, C., Ménoret, S., Leung, E., Niles, B.J., Remy, S., Santiago, Y., Vincent, A.I., Meng, X., Zhang, L., *et al*., 2011. Knockout rats generated by embryo microinjection of TALENs. *Nat Biotechnol*; 29:695-696.

Thisse, C., Thisse, B., Halpern, M.E., Postlethwait, J.H., 1994. Goosecoid expression in neurectoderm and mesendoderm is disrupted in zebrafish cyclops gastrulas. *Dev Biol*; 164:420-429.

Thisse, B., Thisse, C., 2005. Functions and regulations of fibroblast growth factor signaling during embryonic development. *Dev Biol*; 287:390-402.

Thomas, J.O. 2001. HMG1 and 2: architectural DNA-binding proteins. *Biochem Soc Trans*; 29:395-401.

Tierney, M.B., Lamour, K.H., 2005. An Introduction to Reverse Genetic Tools for Investigating Gene Function. *Plant Health Instructor*; DOI: 10.1094/PHI-A-2005-1025-01.

Tissir, F., Qu, Y., Montcouquiol, M., Zhou, L., Komatsu, K., Shi, D., Fujimori, T., Labeau, J., Tyteca, D., Courtoy, P., *et al*., 2010. Lack of cadherins Celsr2 and Celsr3 impairs ependymal ciliogenesis, leading to fatal hydrocephalus. *Nat Neurosci*; 13:700-707.

Tokuda, N., Kawai, K., Lee, Y.H., Ikegami, T., Yamaguchi, S., Yagisawa, H., Fukui, Y., Tuzi, S., 2012. Membrane-induced alteration of the secondary structure in the SWAP-70 pleckstrin homology domain. *J Biochem*; 151:391-401.

Tomasetto, C., Moog-Lutz, C., Regnier, C.H., Schreiber, V., Basset, P., Rio, M.C., 1995. Lasp-1 (MLN 50) defines a new LIM protein subfamily characterized by the association of LIM and SH3 domains. *FEBS Letters*; 373:245-249.

Tominaga, N., Hagiwara, K., Kosaka, N., Honma, K., Nakagama, H., Ochiya, T., 2014. RPN2-mediated glycosylation of tetraspanin CD63 regulates breast cancer cell malignancy. *Mol Cancer*; 13:134.

Tong, X., Drapkin, R., Yalamanchili, R., Mosialos, G., Kieff, E., 1995. The Epstein-Barr virus nuclear protein 2 acidic domain forms a complex with a novel cellular coactivator that can interact with TFIIE. *Mol Cell Biol*; 15:4735-4744.

Topczewski, J., Sepich, D.S., Myers, D.C., Walker, C., Amores, A., Lele, Z., Hammerschmidt, M., Postlethwait, J., Solnica-Krezel, L., 2001. The zebrafish glypican knypek controls cell polarity during gastrulation movements of convergent extension. *Dev Cell*; 1:251-64.

Topol, L., Jiang, X., Choi, H., Garrett-Beal, L., Carolan, P.J., Yang, Y., 2003. Wnt-5a inhibits the canonical Wnt pathway by promoting GSK-3-independent β-catenin degradation. *J Cell Biol*; 162:899-908.

Torres, M.A., Yang-Snyder, J.A., Purcell, S.M., DeMarais, A.A., McGrew, L.L., Moon, R.T., 1996. Activities of the Wnt-1 class of secreted signaling factors are antagonized by the Wnt-5A class and by a dominant negative cadherin in early Xenopus development. *J Cell Biol*; 133:1123-37.

Traver, D., Paw, B.H., Poss, K.D., Penberthy, W.T., Lin, S., Zon, L.I., 2003. Transplantation and *in vivo* imaging of multilineage engraftment in zebrafish bloodless mutants. *Nat Immunol*; 4:1238-46.

Tree, D.R., Shulman, J.M., Rousset, R., Scott, M.P., Gubb, D. Axelrod, J.D., 2002. Prickle mediates feedback amplification to generate asymmetric planar cell polarity signaling. *Cell*; 109:371-381.

Tucker, J.A., Mintzer, K.A., Mullins, M.C., 2008. The BMP signaling gradient patterns dorsoventral tissues in a temporally progressive manner along the anteroposterior axis. *Dev Cell*; 14:108–119.

Tybulewicz, V.L., Henderson, R.B., 2009. Rho family GTPases and their regulators in lymphocytes. *Nat Rev Immunol*; 9:630-44.

Tzankov, S., Wong, M.J., Shi, K., Nassif, C., Young, J.C., 2008. Functional divergence between co-chaperones of Hsc70. *J Biol Chem*; 283:27100-9.

Ueda, T., Kikuchi, A., Ohga, N., Yamamoto, J., Takai, Y., 1990. Purification and Characterization from Bovine Brain Cytosol of a Novel Regulatory Protein Inhibiting the Dissociation of GDP from and the Subsequent Binding of GTP to rhoB p20, a ras p21-like GTP binding Protein. *J Biol Chem*; 265:9373-9380.

Ueda, S., Blee, A.M., Macway, K.G., Renner, D.J., Yamada, S., 2015. Force dependent biotinylation of myosin IIA by alpha-catenin tagged with a promiscuous biotin ligase. *PLoS One*; 10:e0122886.

Ulrich, F., Concha, M.L., Heid, P.J., Voss, E., Witzel, S., Roehl, H., Tada, M., Wilson, S.W., Adams, R.J., Soll, D.R., and Heisenberg, C.P., 2003. Slb/Wnt11 controls hypoblast cell migration and morphogenesis at the onset of zebrafish gastrulation. *Development*; 130:5375-5384.

Umbhauer, M., Djiane, A., Goisset, C., Penzo-Méndez, A., Riou, J.F., Boucaut, J.C., Shi, D.L., 2000. The C-terminal cytoplasmic Lys-thr-X-X-X-Trp motif in frizzled receptors mediates Wnt/beta-catenin signalling. *EMBO J*; 19:4944-54.

Urnov, F.D., Miller, J.C., Lee, Y.L., Beausejour, C.M., Rock, J.M., Augustus, S., Jamieson, A.C., Porteus, M.H., Gregory, P.D., Holmes, M.C., 2005. Highly efficient endogenous human gene correction using designed zinc-finger nucleases. *Nature*; 435:646-51.

Van Aelst, L., D'Souza-Schorey, C., 1997. Rho GTPases and signaling networks. *Genes Dev*; 11:2295-322.

Van de Wetering, M., Cavallo, R., Dooijes, D., Van Beest, M., Van Es, J., Loureiro, J., Ypma, A., Hursh, D., Jones, T., Bejsovec, A., *et al*., 1997. Armadillo coactivates transcription driven by the product of the Drosophila segment polarity gene dTCF. *Cell*; 88:789-799.

Van den Heuvel, S., Dyson, N.J., 2008. Conserved functions of the pRB and E2F families. *Nat Rev Mol Cell Biol*; 9:713-24.

Van Impel, A., Zhao, Z., Hermkens, D.M., Roukens, M.G., Fischer, J.C., Peterson-Maduro, J., Duckers, H., Ober, E.A., Ingham, P.W., Schulte-Merker, S., 2014. Divergence of zebrafish and mouse lymphatic cell fate specification pathways. *Development*; 141:1228-1238.

Veeman, M.T., Slusarski, D.C., Kaykas, A., Louie, S.H., Moon, R.T., 2003a. Zebrafish prickle, a modulator of noncanonical Wnt/Fz signaling, regulates gastrulation movements. *Curr Biol*; 13:680-5.

Veeman, M.T., Axelrod, J.D., Moon, R.T., 2003b. A second canon. Functions and mechanisms of beta-catenin-independent Wnt signaling. *Dev Cell*; 5:367-77.

Veillette, A., Bookman, M.A., Horak, E.M., Bolen, J.B., 1988. The CD4 and CD8 T cell surface antigens are associated with the internal membrane tyrosine-protein kinase p56lck. *Cell*; 55:301-8.

Verlhac, M.H., Chen, R.H., Hanachi, P., Hershey, J.W., Derynck, R., 1997. Identification of partners of TIF34, a component of the yeast eIF3 complex, required for cell proliferation and translation initiation. *EMBO J*; 16:6812-22.

Vigil, D., Cherfils, J., Rossman, K.L., Der, C.J., 2010. Ras superfamily GEFs and GAPs: validated and tractable targets for cancer therapy? *Nat Rev Cancer*; 10:842-57.

Vigorito, E., Billadeu, D.D., Savoy, D., McAdam, S., Doody, G., Fort, P., Turner, M., 2003. RhoG regulates gene expression and the actin cytoskeleton in lymphocytes. *Oncogene*; 22:330-42.

Vigorito, E., Bell, S., Hebeis, B.J., Reynolds, H., McAdam, S., Emson, P.C., McKenzie, A., Turner, M., 2004. Immunological function in mice lacking the Rac-related GTPase RhoG. *Mol Cell Biol*; 24:719-29.

Vilchez, D., Boyer, L., Morantte, I., Lutz, M., Merkwirth, C., Joyce, D., Spencer, B., Page, L., Masliah, E., Berggren, W.T., Gage, F.H., Dillin, A., 2012. Increased proteasome activity in human embryonic stem cells is regulated by PSMD11. *Nature*; 489:304-308.

Vistica, B.P., Shi, G., Nugent, L., Tan, C., Altman, A., Gery, I., 2012. SLAT/Def6 plays a critical role in the pathogenic process of experimental autoimmune uveitis (EAU). *Mol Vision*; 18:1858-1864.

Vogel, T., 2013. Insulin/IGF-Signalling in Embryonic and Adult Neural Proliferation and Differentiation in the Mammalian Central Nervous System. DOI: 10.5772/54946.

Voos, W., 2013. Chaperone-protease networks in mitochondrial protein homeostasis. *Biochim Biophys Acta*; 1833:388-99.

Wada, H., Iwasaki, M., Sato, T., Masai, I., Nishiwaki, Y., Tanaka, H., Sato, A., Nojima, Y. and Okamoto, H., 2005. Dual roles of zygotic and maternal Scribble1 in neural migration and convergent extension movements in zebrafish embryos. *Development*; 132:2273-2285.

Wada, H., Tanaka, H., Nakayama, S., Iwasaki, M., Okamoto, H., 2006. Frizzled3a and Celsr2 function in the neuroepithelium to regulate migration of facial motor neurons in the developing zebrafish hindbrain. *Development*; 133:4749-4759.

Wadhwa, R., Taira, K., Kaul, S.C., 2002. An Hsp70 family chaperone, mortalin/ mthsp70/PBP74/Grp75: what, when, and where? *Cell Stress Chaperones*; 7:309-16.

Wagner, M., Perry, R.P., 1985. Characterization of the multigene family encoding the mouse S16 ribosomal protein: strategy for distinguishing an expressed gene from its processed pseudogene counterparts by an analysis of total genomic DNA. *Mol Cell Biol*; 5:3560-76.

Wakamatsu, I., Ihara, S., Fukui, Y., 2006. Mutational analysis on the function of the SWAP-70 PH domain. *Mol Cell Biochem*; 293:137-45.

Wallingford, J.B., Rowning, B.A., Vogeli, K.M., Rothbächer, U., Fraser, S.E., Harland, R.M., 2000. Dishevelled controls cell polarity during Xenopus gastrulation. *Nature*; 405:81-5.

Wallingford, J.B., Harland, R.M., 2001. Xenopus Dishevelled signaling regulates both neural and mesodermal convergent extension: parallel forces elongating the body axis. *Development*; 128:2581-92.

Wallingford, J.B., Fraser, S., Harland, R. 2002. Convergent extension: The molecular control of polarized cell movement during embryonic development. *Dev Cell*; 2:695-706.

Wallingford, J.B., Habas, R., 2005. The developmental biology of Dishevelled: an enigmatic protein governing cell fate and cell polarity. *Development*; 132:4421-36.

Walshe, J., Maroon, H., McGonnell, I. M., Dickson, C., Mason, I., 2002. Establishment of hindbrain segmental identity requires signaling by FGF3 and FGF8. *Curr Biol*; 12:1117-1123.

Wang, Y., Macke, J.P., Abella, B.S., Andreasson, K., Worley, P., Gilbert, D.J., Copeland, N.G., Jenkins, N.A., Nathans, J., 1996. A large family of putative transmembrane receptors homologous to the product of the Drosophila tissue polarity gene frizzled. J Biol Chem; 271:4468-4476.

Wang, J.C., 2002. Cellular roles of DNA topoisomerases: a molecular perspective. *Nat Rev*; 3:430-40.

Wang, C., Ivanov, A., Chen, L., Fredericks, W.J., Seto, E., Rauscher, F.J. III, Chen, J., 2005. MDM2 interaction with nuclear corepressor KAP1 contributes to p53 inactivation. *EMBO J*; 24:3279-3290.

Wang, Y., Wang, J., Gao, L., Lafyatis, R., Stamm, S., Andreadis, A., 2005. Tau exons 2 and 10, which are misregulated in neurodegenerative diseases, are partly regulated by silencers which bind a SRp30c.SRp55 complex that either recruits or antagonizes htra2beta1. *J Biol Chem*; 280:14230-9.

Wang, Y., Guo, N., Nathans, J., 2006. The role of Frizzled3 and Frizzled6 in neural tube closure and in the planar polarity of inner-ear sensory hair cells. *J Neurosci*; 26:2147-2156.

Wang, X., Arai, S., Song, X., Reichart, D., Du, K., Pascual, G., Tempst, P., Rosenfeld, M.G., Glass, C.K., Kurokawa, R., 2008. Induced ncRNAs allosterically modify RNA-binding proteins in cis to inhibit transcription. *Nature*; 454:126-130.

Wang, H., Kadlecek, T. A., Au-Yeung, B.B., Goodfellow, H.E.S., Hsu, L.Y., Freedman, T.S., Weiss, A., 2010. ZAP-70: An Essential Kinase in T-cell Signaling. *Cold Spring Harb Pers Biol*; 2(5):a002279.

Wang, J., Yang, J., Yang, Z., Lu, X., Jin, C., Cheng, L., Wu, N., 2016. RbAp48, a novel inhibitory factor that regulates the transcription of human immunodeficiency virus type 1. *Int J Mol Med*: PMID27222146.

Wang, Y., Wang, Y., Ma, L., Nie, M., Ju, J., Liu, M., Deng, Y., Yao, B., Gui, T., Li, X., Guo, C., Ma, C., Tan, R., Zhao, Q., 2017. Heterochromatin Protein 1γ Is a Novel Epigenetic Repressor of Human Embryonic ϵ-Globin Gene Expression. *J Biol Chem*; 292:4811-4817.

Wange, R.L., Malek, S.N., Desiderio, S., and Samelson, L.E., 1993. Tandem SH2 domains of ZAP-70 bind to T cell antigen receptor ζ and CD3e from activated Jurkat T cells. *J Biol Chem*; 268:19797-19801.

Warga, R.M., Kimmel, C.B., 1990. Cell movements during epiboly and gastrulation in zebrafish. *Development*; 108:569-80.

Weaver, A.J., Sullivan, W.P., Felts, S.J., Owen, B.A., Toft, D.O., 2000. Crystal structure and activity of human p23, a heat shock protein 90 co-chaperone. *J Biol Chem*; 275:23045-52.

Weber, U., Paricio, N., Mlodzik, M., 2000. Jun mediates Frizzled-induced R3/R4 cell fate distinction and planar polarity determination in the *Drosophila* eye. *Development*; 127:3619-3629.

Weber, E., Gruetzner, R., Werner, S., Engler, C., Marillonnet, S., 2011. Assembly of Designer TAL Effectors by Golden Gate Cloning. *PLoS ONE*; 6(5):e19722.

Wei, C., Liu, J., Zhang, B., Gao, G., Jiao, R., 2013. TALEN or Cas9-Rapid, Efficient and Specific Choices for Genome Modifications. *J Genet Genom*; 40:281-289.

Weihing, R.R., 1985. The filamins: properties and functions. *Can J Biochem Cell Biol*; 63:397-413.

Weinberg, E.S., Allende, M.L., Kelly, C.S., Abdelhamid, A., Murakami, T., Andermann, P., Doerre, O.G., Grunwald, D.J., Riggleman, B., 1996. Developmental regulation of zebrafish MyoD in wild type, no tail and spadetail embryos. *Development*; 122:271-80.

Weiske, J., Huber, O., 2006. The histidine triad protein Hint1 triggers apoptosis independent of its enzymatic activity. *J Biol Chem*; 281:27356-27366.

Wen, W., Meinkoth, J.L., Tsien, R.Y., Taylor, S.S., 1995. Identification of a signal for rapid export of proteins from the nucleus. *Cell*; 82:463-73.

Wennerberg, K., Ellerbroek, S.M., Liu, R.Y., Karnoub, A.E., Burridge, K., Der, C.J., 2002. RhoG signals in parallel with Rac1 and Cdc42. *J Biol Chem*; 277:47810–7.

Westerfield, M., 2000. The zebrafish book. A guide for the labaratory use of zebrafish (*Danio rerio*). *Univ Oregon Press.*

Westfall, T.A, Brimeyer, R, Twedt, J, Gladon, J, Olberding, A, Furutani-Seiki, M, Slusarski, D.C., 2003. Wnt-5/pipetail functions in vertebrate axis formation as a negative regulator of Wnt/beta-catenin activity. *J Cell Biol*; 162:889-898.

Wharton, K.A., 2003. Runnin' with the Dvl: proteins that associate with Dsh/Dvl and their significance to Wnt signal transduction. *Dev Biol*; 253:1-17.

Whitehead, I.P., Campbell, S., Rossman, K.L., Der, C.J., 1997. Dbl family proteins. *Biochim Biophys Acta*; 1332:F1-23.

Wickramasinghe, V.O., Gonzàlez-Porta, M., Perera, D., Bartolozzi, A.R., Sibley, C.R., Hallegger, M., Ule, J., Marioni, J.C., Venkitaraman, A.R., 2015. Regulation of constitutive and alternative mRNA

splicing across the human transcriptome by PRPF8 is determined by 5' splice site strength. *Genome Biol*; 16:201.

Wiegand, G., Remington, S.J., 1986. Citrate synthase: structure, control, and mechanism. *Ann Rev Biophys Biophy Chem*; 15:97-117.

Wiellette, E.L., Sive, H., 2003. vhnf1 and Fgf signals synergize to specify rhombomere identity in the zebrafish hindbrain. *Development*; 130:3821–3829.

Wiellette, E.L., Sive, H., 2004. Early requirement for fgf8 function during hindbrain pattern formation in zebrafish. *Dev Dyn*; 229:393-399.

Willert, K., Brown, J.D., Danenberg, E., Duncan, A.W., Weissman, I.L., Reya, T., Yates, J.R. Nusse, R., 2003. Wnt proteins are lipid-modified and can act as stem cell growth factors. *Nature*; 423: 448-452.

Willert, K., Nusse, R., 2012. Wnt proteins. *Cold Spring Harb Perspect Biol*; 4(9):a007864.

Williams, D.B., 2006. Beyond lectins: the calnexin/calreticulin chaperone system of the endoplasmic reticulum. *J Cell Sci*; 119:615-623.

Wilson, C.M., High, S., 2007. Ribophorin I acts as a substrate-specific facilitator of N-glycosylation. *J Cell Sci*; 120:648-57.

Wilson, C.M., Roebuck, Q., High, S., 2008. Ribophorin I regulates substrate delivery to the oligosaccharyltransferase core. *Proc Natl Acad Sci USA*; 105:9534-9.

Wolffe, A.P., Urnov, F.D., Guschin, D., 2000. Co-repressor complexes and remodelling chromatin for repression. *Biochem Soc Trans*; 28:379-86.

Wong, H.C., Bourdelas, A., Krauss, A., Lee, H.J., Shao, Y., Wu, D., Mlodzik, M., Shi, D.L., Zheng, J., 2003. Direct binding of the PDZ domain of Dishevelled to a conserved internal sequence in the C-terminal region of Frizzled. *Mol Cell*; 12:1251-60.

Wool, I.G., Chan, Y.L., Glük, A., 1996. Mammalian ribosomes: The structure and the evolution of the proteins. In: Hershey, J.W.B., Mathews, M.B., Sonenberg, N., editors. Translational control. *NY: Cold Spring Harb Lab Press*; 685-732.

Worthmann, K., Leitges, M., Teng, B., Sestu, M., Tossidou, I., Samson, T., Haller, H., Huber, T.B., Schiffer, M., 2013. Def-6, a Novel Regulator of Small GTPases in Podocytes, Acts Downstream of Atypical Protein Kinase C (aPKC) λ/ι. *Am J Pathol*; 183:1945-1959.

Worthylake, D.K., Rossman, K.L., Sondek, J., 2000. Crystal structure of Rac1 in complex with the guanine nucleotide exchange region of Tiam1. *Nature*; 408:682-8.

Worthylake, D.K., Rossman, K.L., Sondek, J., 2004. Crystal structure of the DH/PH fragment of Dbs without bound GTPase. *Structure*; 12:1079-1086.

Wu, S., Romfo, C.M., Nilsen, T.W., Green, M.R., 1999. Functional recognition of the 3' splice site AG by the splicing factor U2AF35. *Nature*; 402:832-5.

Wu, Y.T., Lee, H.C., Liao, C.C., Wei, Y.H., 2013. Regulation of mitochondrial FoF1ATPase activity by Sirt3-catalyzed deacetylation and its deficiency in human cells harboring 4977 bp deletion of mitochondrial DNA. *Biochim et Biophys Acta*; 1832:216–227.

Wu, Y., Liang, D., Wang, Y., Bai, M., Tang, W., Bao, S., Yan, Z., Li, D., Li, J., 2013. Correction of a genetic disease in mouse via use of CRISPR-Cas9. *Cell Stem Cell*; 13:659-62.

Wu, T.H., Shi, L., Adrian, J., Shi, M., Nair, R.V., Snyder, M.P., Kao, P.N., 2017. NF90/ILF3 is a transcription factor that promotes proliferation over differentiation by hierarchical regulation in K562 erythroleukemia cells. *bioRxiv* 189647.

Wünnenberg-Stapleton, K., Blitz, I.L., Hashimoto, C., Cho, K.W.Y., 1999. Involvement of the small GTPases XRhoA and XRnd1 in cell adhesion and head formation in early *Xenopus* development. *Development*; 126:5339-5351.

Xia, X., Cheng, A., Lessor, T., Zhang, Y., Hamburger, A.W., 2001. Ebp1, an ErbB-3 binding protein, interacts with Rb and affects Rb transcriptional regulation. *J Cell Physiol*; 187:209-217.

Xiao, S.H., Manley, J.L., 1997. Phosphorylation of the ASF/SF2 RS domain affects both protein-protein and protein-RNA interactions and is necessary for splicing. *Genes Dev*; 11:334-344.

Xu, H., Littman, D.R., 1993. A kinase-independent function of Lck in potentiating antigen-specific T cell activation. *Cell*; 74:633-43.

Xu, X., 2015. Swap70b is required for convergent and extension cell movement during zebrafish gastrulation linking Wnt11 signalling and RhoA effector function. University of Nottingham, PhD thesis.

Xuan, Y., Wang, J., Ban, L., Lu, J.J., Yi, C., Li, Z., Yu, W., Li, M., Xu, T., Yang, W., Tang, Z., Tang, R., Xiao, X., Meng, S., Chen, Y., Liu, Q., Huang, W., Guo, W., Cui, X., Deng, W., 2016. hnRNPA2/B1 activates cyclooxygenase-2 and promotes tumor growth in human lung cancers. *Mol Oncol*; 10:610-24.

Xue, Y., Zhou, Y., Wu, T., Zhu, T., Ji, X., Kwon, Y.S., Zhang, C., Yeo, G., Black, D.L., Sun, H., Fu, X.D., Zhang, Y., 2009. Genome-wide analysis of PTB-RNA interactions reveals a strategy used by the general splicing repressor to modulate exon inclusion or skipping. *Mol Cell*; 36:996-1006.

Yamaguchi, A., Takanashi, K., 2016. FUS interacts with nuclear matrix-associated protein SAFB1 as well as Matrin3 to regulate splicing and ligand-mediated transcription. *Scientific Reports*; *6*:35195.

Yamanaka, Y., Mizuno, T., Sasai, Y., Kishi, M., Takeda, H., Kim, C.H., Hibi, M., Hirano, T., 1998. A novel homeobox gene, dharma, can induce the organizer in a non-cell-autonomous manner. *Genes Dev*; 12:2345-53.

Yamashita, S., Miyagi, C., Carmany-Rampey, A., Shimizu, T., Fujii, R., Schier, A.F., Hirano, T., 2002. Stat3 Controls Cell Movements during Zebrafish Gastrulation. *Dev Cell*; 2:363-75.

Yang, Y., Liu, B., Dai, J., Srivastava, P.K., Zammit, D.J., Lefrançois, L., Li, Z., 2007. Heat Shock Protein gp96 Is a Master Chaperone for Toll-like Receptors and Is Important in the Innate Function of Macrophages. *Immunity*; 26:215-226.

Yang, L., Mali, P., Kim-Kiselak, C., Church, G., 2014. CRISPR-Cas-mediated targeted genome editing in human cells. *Methods Mol Biol*; 1114:245-67.

Yao, Y.L., Yang, W.M., 2003. The metastasis-associated proteins 1 and 2 form distinct protein complexes with histone deacetylase activity. *J Biol Chem*; 278:42560-8.

Yeh, C.M., Liu, Y.C., Chang, C.J., Lai, S.L., Hsiao, C.D., Lee, S.J., 2011. Ptenb Mediates Gastrulation Cell Movements via Cdc42/AKT1 in Zebrafish. *PLoS ONE*; 6(4):e18702.

Yin, C., Solnica-Krezel, L., 2007. Convergence and extension movements mediate the specification and fate maintenance of zebrafish slow muscle precursors. *Dev Biol*; 304:141-55.

Ying, G.G., Proost, P., van Damme, J., Bruschi, M., Introna, M., Golay, J., 2000. Nucleolin, a novel partner for the Myb transcription factor family that regulates their activity. *J Biol Chem*; 275:4152-4158.

Yoshida, M., Muneyuki, E., Hisabori, T., 2001. ATP synthase-a marvellous rotary engine of the cell. *Nat Rev Mol Cell Biol*; 2:669-77.

Yoshihama, M., Uechi, T., Asakawa, S., Kawasaki, K., Kato, S., Higa, S., Maeda, N., Minoshima, S., Tanaka, T., Shimizu, N., Kenmochi, N., 2002. The Human Ribosomal Protein Genes: Sequencing and Comparative Analysis of 73 Genes. *Genome Res*; 12:379–390.

Yu, H., Leitenberg, D., Li, B., Flavell, R.A., 2001. Deficiency of small Gtpase Rac2 affects T cell activation. *J Exp Med*; 194:915-926.

Yu, W., Ginjala, V., Pant, V., Chernukhin, I., Whitehead, J., Docquier, F., Farrar, D., Tavoosidana, G., Mukhopadhyay, R., Kanduri, C. *et al*., 2004. Poly (ADP-ribosy)lation regulates CTCF-dependent chromatin insulation. *Nat Genet*; 36:1105-1110.

Yu, H., Ye, X., Guo, N., Nathans, J., 2012. Frizzled 2 and frizzled 7 function redundantly in convergent extension and closure of the ventricular septum and palate: evidence for a network of interacting genes. *Development*; 139:4383-94.

Yu, Y., Reed, R., 2015. FUS functions in coupling transcription to splicing by mediating an interaction between RNAP II and U1 snRNP. *PNAS*; 112:8608-8613.

Yu, L., Di, Y., Xin, L., Ren, Y., Liu, X., Sun, X., Zhang, W., Yao, Z., Yang, J., 2017. SND1 acts as a novel gene transcription activator recognizing the conserved Motif domains of Smad promoters, inducing TGFβ1 response and breast cancer metastasis. *Oncogene*; 36:3903-3914.

Zahler, A.M., Lane, W.S., Stolk, J.A., Roth, M.B., 1992. SR proteins: a conserved family of pre-mRNA splicing factors. *Genes Dev*; 6:837-847.

Zalcman, G., Closson, V., Camonis, J., Honore, N., Rousseau-Mercki, M.F., Tavitian, A., Olofsson, B., 1996. RhoGDI-3 Is a New GDP Dissociation Inhibitor (GDI). *J Biol Chem*; 271:30366-30374.

Zamore, P.D., Patton, J.G., Green, M.R., 1992. Cloning and domain structure of the mammalian splicing factor U2AF. *Nature*; 355:609-614.

Zamoyska, R., Derham, P., Gorman, S.D., von Hoegen, P., Bolen, J.B., Veillette, A., Parnes, J.R., 1989. Inability of CD8 α' polypeptides to associate with p56lck correlates with impaired function *in vitro* and lack of expression *in vivo*. *Nature*; 342:278-281.

Zapun, A., Darby, N.J., Tessier, D.C., Michalak, M., Bergeron, J.J.M., Thomas, D.Y., 1998. Enhanced Catalysis of Ribonuclease B Folding by the Interaction of Calnexin or Calreticulin with ERp57. *J Biol Chem*; 273:6009-6012.

Zeng, S.X., Dai, M.S., Keller, D.M., Lu, H., 2002. SSRP1 functions as a co-activator of the transcriptional activator p63. *EMBO J*; 21:5487-5497.

Zeng, X., Tamai, K., Doble, B., Li, S., Huang, H., Habas, R., Okamura, H., Woodgett, J., He, X., 2005. A dual-kinase mechanism for Wnt co-receptor phosphorylation and activation. *Nature*; 438:873-7.

Zhang, M., Zamore, P.D., Carmo-Fonseca, M., Lamond, A.I., Green, M.R., 1992. Cloning and intracellular localization of the U2 small nuclear ribonucleoprotein auxiliary factor small subunit. *Proc Natl Acad Sci USA*; 89:8769-8773.

Zhang, Y., Ng, H.H., Erdjument-Bromage, H., Tempst, P., Bird, A., Reinberg, D., 1999. Analysis of the NuRD subunits reveals a histone deacetylase core complex and a connection with DNA methylation. *Genes Dev*; 13:1924-1935.

Zhang, Y., Woodford, N., Xia, X., Hamburger, A.W., 2003. Repression of E2F1-mediated transcription by the ErbB3 binding protein Ebp1 involves histone deacetylases. Nucleic Acids Res; 31:2168-2177.

Zhang, Y., Hamburger, A.W., 2004. Heregulin regulates the ability of the ErbB3-binding protein Ebp1 to bind E2F promoter elements and repress E2F-mediated transcription. *J Biol Chem*; 279:26126-26133.

Zhang, Z., Krainer, A.R., 2004. Involvement of SR proteins in mRNA surveillance. Mol Cell; 16:597-607.

Zhang, Y., Hamburger, A.W., 2005. Specificity and heregulin regulation of Ebp1 (ErbB3 binding protein 1) mediated repression of androgen receptor signalling. *Br J Cancer*; 92:140-146.

Zhang, D., Jiang, P., Xu, Q., Zhang, X., 2011. Arginine and glutamate-rich 1 (ARGLU1) interacts with mediator subunit 1 (MED1) and is required for estrogen receptor-mediated gene transcription and breast cancer cell growth. *J Biol Chem*; 286:17746-17754.

Zhang, F., Cong, L., Lodato, S., Kosuri, S., Church, G.M., Arlotta, P., 2011. Efficient construction of sequence-specific TAL effectors for modulating mammalian transcription. *Nat Biotechnol*; 29:149-53.

Zheng, Y., 2001. Dbl family guanine nucleotide exchange factors. *Trends Biochem Sci*; 26:724-32.

Zheng, Y., Quilliam, L.A., 2003. Activation of the Ras superfamily of small GTPases. Workshop on exchange factors. *EMBO Rep*; 4:463-8.

Zhou, A., Ou, A.C., Cho, A., Benz, E.J.Jr, Huang, S.C., 2008. Novel splicing factor RBM25 modulates Bcl-x pre-mRNA 5' splice site selection. *Mol Cell Biol*; 28:5924-36.

Zhou, Z., Fu, X.D., 2013. Regulation of Splicing by SR proteins and SR Protein-Specific Kinases. *Chromosoma*; 122:191-207.

Zhou, Z., Rawnsley, D.R., Goddard, L.M., Pan, W., Cao, X.J., Jakus, Z., Zheng, H., Yang, J., Arthur, J.S., Whitehead, K.J., *et al*., 2015. The cerebral cavernous malformation pathway controls cardiac development via regulation of endocardial MEKK3 signaling and KLF expression. *Dev Cell*; 32:168-180.

Zhu, S., Liu, L., Korzh, V., Gong, Z., Low, B.C., 2006. RhoA acts downstream of Wnt5 and Wnt11 to regulate convergence and extension movements by involving effectors Rho kinase and Diaphanous: use of zebrafish as an *in vivo* model for GTPase signaling. *Cell Signal*; 18:359-72.

Zimmerman, L.B., De Jesús-Escobar, J.M., Harland, R.M., 1996. The Spemann organizer signal noggin binds and inactivates bone morphogenetic protein 4. *Cell*; 86:599-606.

Zu, Y., Tong, X., Wang, Z., Liu, D., Pan, R., Li, Z., Hu, Y., Luo, Z., Huang, P., Wu, Q., Zhu, Z., Zhang, B., Lin, S., 2013. TALEN-mediated precise genome modification by homologous recombination in zebrafish. *Nat Methods*; 10:329-31.

Zuo, P., Manley, J.L., 1993. Functional domains of the human splicing factor ASF/SF2. *EMBO J*; 12:4727-4737.

APPENDIX-I

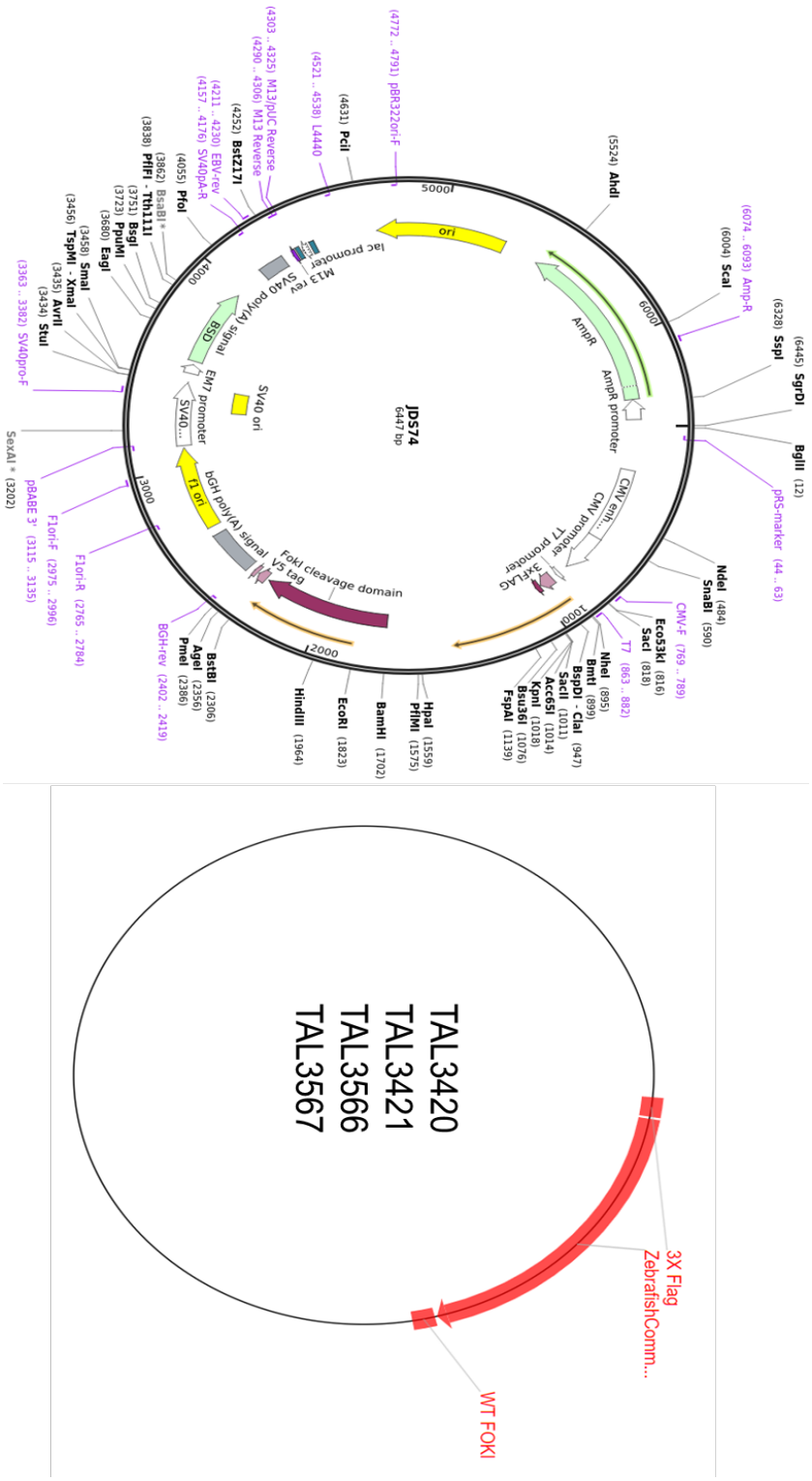


Figure 9.1 JDS74 vector backbone of TALEN constructs of *def6a* and *swap70b* genes (Adapted from www. addgene.com and Sander *et al.,* 2011).

APPENDIX-II

def6a

def6a Forward Primer

CTTCTGGTTTCAGTTCAGGTGTAAACATAAATTTCAATGAGTTTTGCTTGAGTTTTGGTCCAGCAG
GGGGTGTGATTTGTCTGCTGGAGGACGAACTCTTGTGCTCTGGGTGTGGGAGGCCCTGAACGA
CAGCGAGAGAAAGAGAAGGCAGTGAAAAAAGGGAAAACGAAGAGTAAAATTGCTGCAGTCATGG
ACTTGCG**CTCAGAACTGCTCAAGTCC**ATTTG**GTAC**GCTTTCA**CAGCTCTGGATGTGGAGA**AGAG
TGGAAAGGTCTCCAAGTCTCAACTTAAGGTGAGCTGCAAATCTGTTATTGCACTATGATGAAACT
GAGATGAGAGAGGCTGAAAATTAGGCTT

def6a Reverse Primer

- ***def6a* RESTRICTION SITE: *RsaI***
- **Left and right TALEN binding sequences are highlighted in yellow.**
- The spacer sequence is highlighted in green.
- The forward and reverse primer binding sites are highlighted in blue.

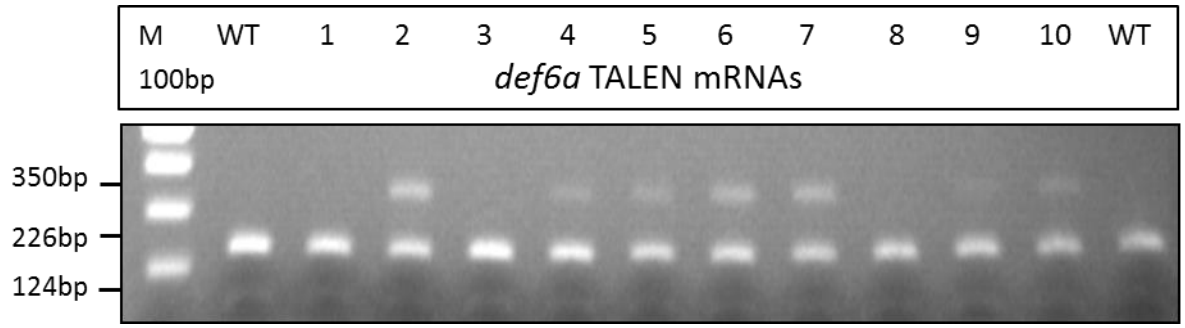


Figure 9.2 The amplified fragment size is 350bp. The digestion of sequence from restriction site generates two fragments of 226bp and 124bp.

swap70b

swap70b Forward Primer

GAAAACAGTCCACATCAAGTGCGACGCCAGTCAGCAGACGGAGAAACTACCTCTGAAAATGGGA
C**TAAGGGACGAGCTTCTC**AAGGCAATCTGG**CATG****CCTTCACAGCCCTGGA**TGTGGATAAAAGT
GGGAAAGTGTCAAAATCTCAGCTGAAGGTTTGTCGTTTTGCTCTTGAATTAATCGTGTTTTCTTTG
AGTTTGTGCACTGGAGTGTAAACGTTGTTTTTAACGCTTCACTGAAGAC

swap70b Reverse Primer

- ***swap70b* RESTRICTION SITE: *NlaIII***
- **Left and right TALEN binding sequences are highlighted in yellow.**
- The spacer sequence is highlighted in green.
- The forward and reverse primer binding sites are highlighted in blue.

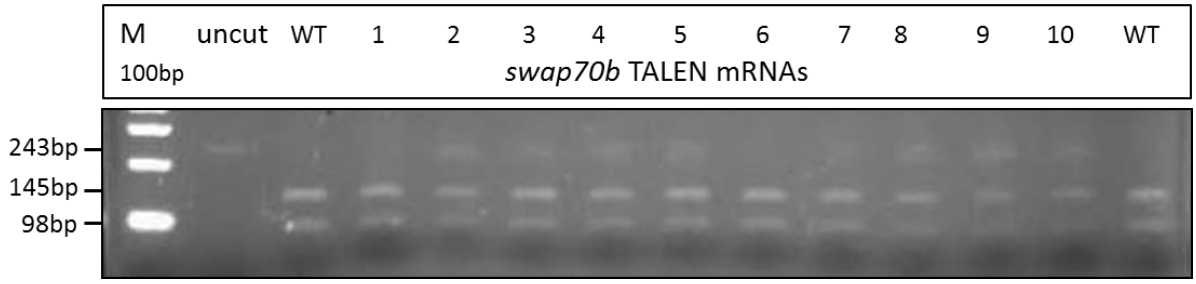


Figure 9.3 The amplified fragment size is 243bp. The digestion of sequence from restriction site generates two fragments of 145bp and 98bp.

APPENDIX-III

Zebrafish Def6a amino acid sequence-WT

MDLRSELLKSIWYAFTALDVEKSGKVSKSQLKVLSHNLYTVLKIPHEAAALEEHFRDDDD

GPVSSQGYMPYLNKYILDKVVEGTFVKENVDELCWTLTAKKNYRPEGKSILPAKDAFRLW

CLFIFLSEDRYPLVMIPDEVEYLLKKFCMAMSVELNYVELEDFISQDSVQQNGFTVWTFL

EMMNSGKLTRGIAKETVSMAIEEVYREIVGDVLKEGYLWKKGQLRRNWTERWFTLRPSTL

LYFTSEDRKDHKGNIQLDGNCCVEVLPDRDGKRCMFCLKTLTKTYELSASDTKQRQEWTT

AIQTAIRLYVEGKTSLHKDLKLKRRDQREQREKRREAKEQELQRLRALQEERERKMAELE

LLKEAQRQAQAMLEQDEQRRRQQHEQLHQALEIQLKEAEEARASMQAEMALKEAEAEKQR

TRIRELEAMQQRLEDALQQEIKARQDEEAFRYAQARLLAEEEEKMKALMGLREEQEEYIQ

RAQREKQELRQEMESKSRALEEAQRQLEETRANRYRVDQDVVAAQRKLRQASTNVKHWNV

QMNRLMHPIGPGEKRSSGGSFSSFRIPSQKDPALRQKQKSEEQDEESKENMESRGGCEAD

RRLSTNGQMEIP

Zebrafish Swap70b amino acid sequence-WT

MGLRDELLKAIWHAFTALDVDKSGKVSKSQLKVLSHNLCTVMKIPHDPVALEEHFRDDDE

GPVSNQGYMPYLNRFILDKVQDNFDRIDFNRMCWTLCARKNLNRNHLLISDDDAFKIWCI

FNFLSEDKYPLVMVSEEIEYFLRKLTEAMGGSWIEEKFEQYKLQLSSKHQCLKVWELIEL

VGMGHFSKGMDRQTLSMGITEVFHELILDVLKQGYMMKKGHKRKNWTERWFLLKPSLISY

YVSEDLTEKKGDILLDGNCCVESLPDKEGKKCLFYVKCSDKSFEISASDKKKKQEWIQAI

QTCITLLKVGRPAPHHEARQKRRELRQKQQAEQEELELRMRELQMANENKQRELEAMRKK

LEEAAANAADEERRRLQTQNELQDLYRLEMEKEKMVRQQMEEQVAQKSNELEQYLQRVRE

LENMYHSLEEALEEERQARQDEETVRKLQARLLEEEVSKRAELEEIHLYQQQTISQTQAE

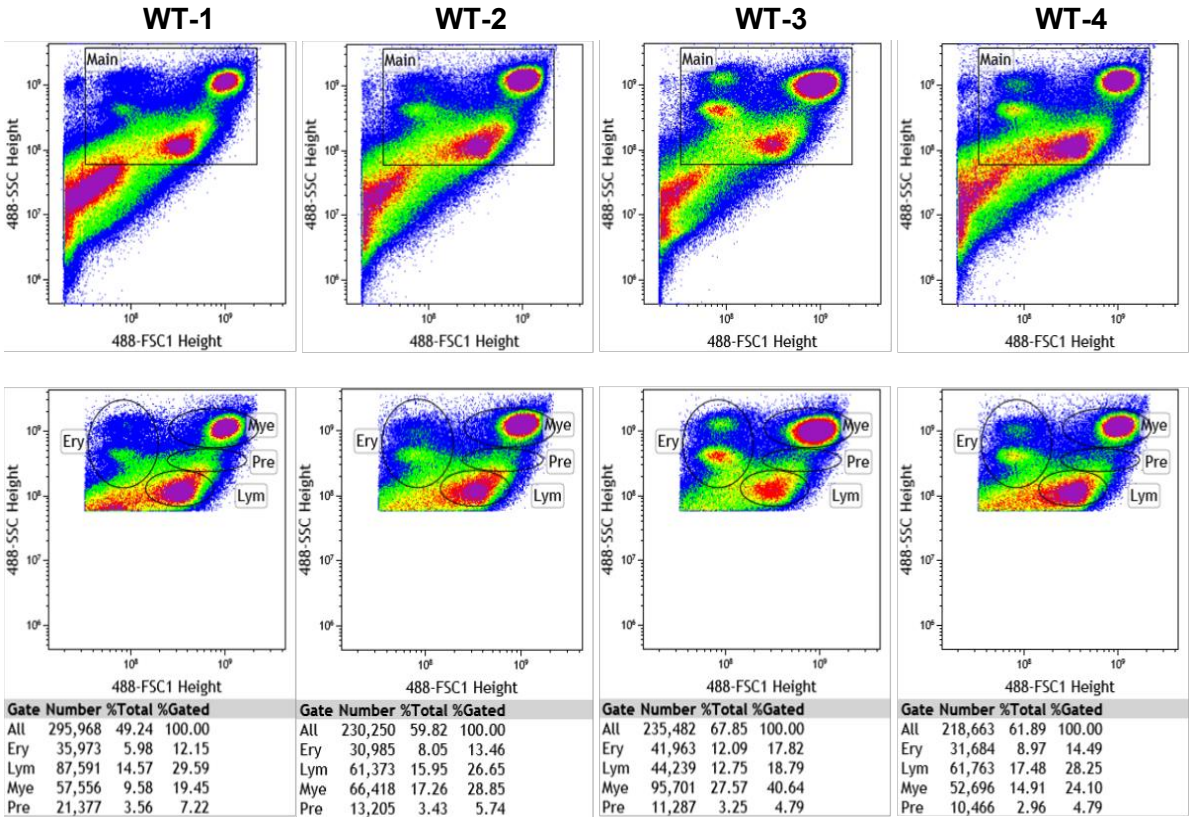
KQELERERLAKESALESAMQQLHQLEADRQGALEQYQEVMKKLSDAANNTKSWKDKVAQH

EGLIRLIQPGPKYPQKITNWGPAAFTDAELNLREKDWQEKKNRPATPQ

Figure 9.4 Zebrafish Def6a and Swap70b amino acid sequences.

APPENDIX –IV

Wild type (WT)



Gate	Number	%Total	%Gated
All	295,968	49.24	100.00
Ery	35,973	5.98	12.15
Lym	87,591	14.57	29.59
Mye	57,556	9.58	19.45
Pre	21,377	3.56	7.22

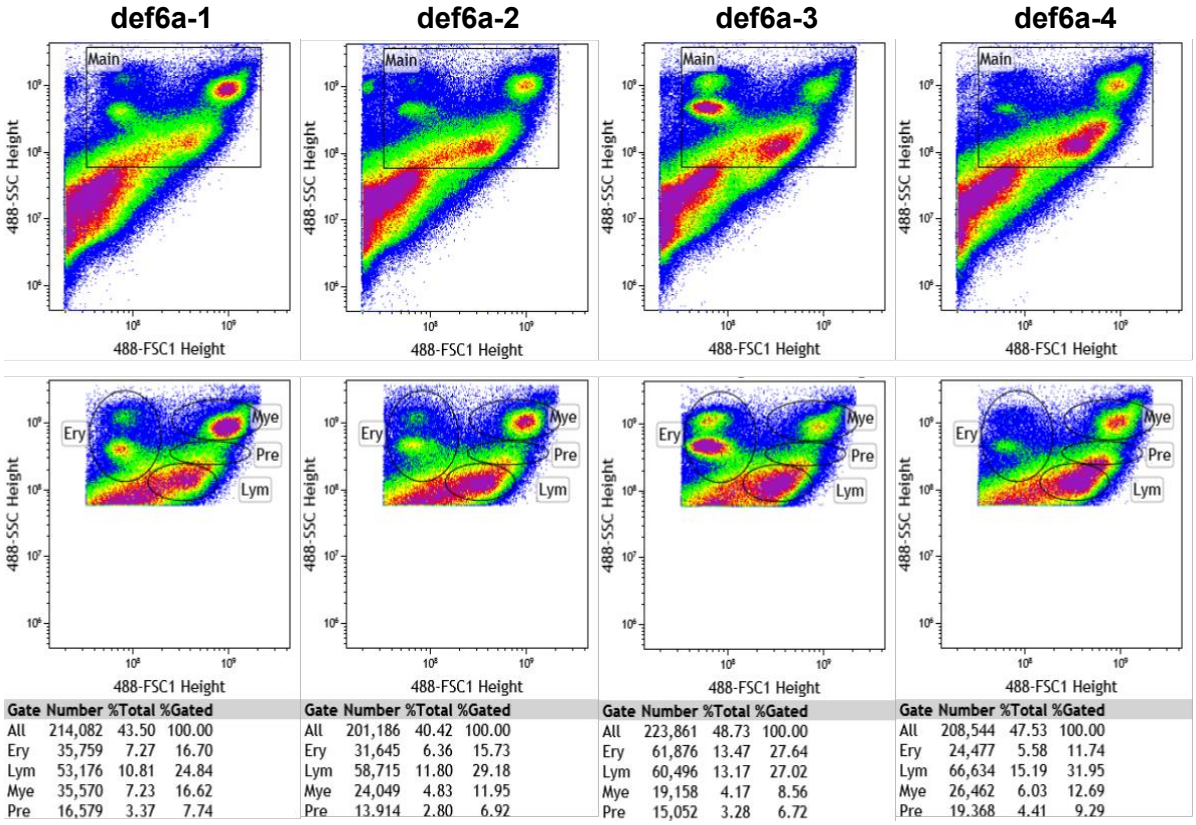
Gate	Number	%Total	%Gated
All	230,250	59.82	100.00
Ery	30,985	8.05	13.46
Lym	61,373	15.95	26.65
Mye	66,418	17.26	28.85
Pre	13,205	3.43	5.74

Gate	Number	%Total	%Gated
All	235,482	67.85	100.00
Ery	41,963	12.09	17.82
Lym	44,239	12.75	18.79
Mye	95,701	27.57	40.64
Pre	11,287	3.25	4.79

Gate	Number	%Total	%Gated
All	218,663	61.89	100.00
Ery	31,684	8.97	14.49
Lym	61,763	17.48	28.25
Mye	52,696	14.91	24.10
Pre	10,466	2.96	4.79

Figure 9.5 Flow cytometric analysis of blood cell lineages of WT zebrafish. A main gate was produced for all plots to focus only the blood cell lineages. The major blood cell linages were separated by four additional sub-gates which are erythrocytes (ery), myelomonocytes (mye), precursors (pre) and lymphocytes (lym). The number of cells were calculated by Kaluza Analysis software.

def6a$^{qmc811/qmc811}$ mutant line



Gate	Number	%Total	%Gated
All	214,082	43.50	100.00
Ery	35,759	7.27	16.70
Lym	53,176	10.81	24.84
Mye	35,570	7.23	16.62
Pre	16,579	3.37	7.74

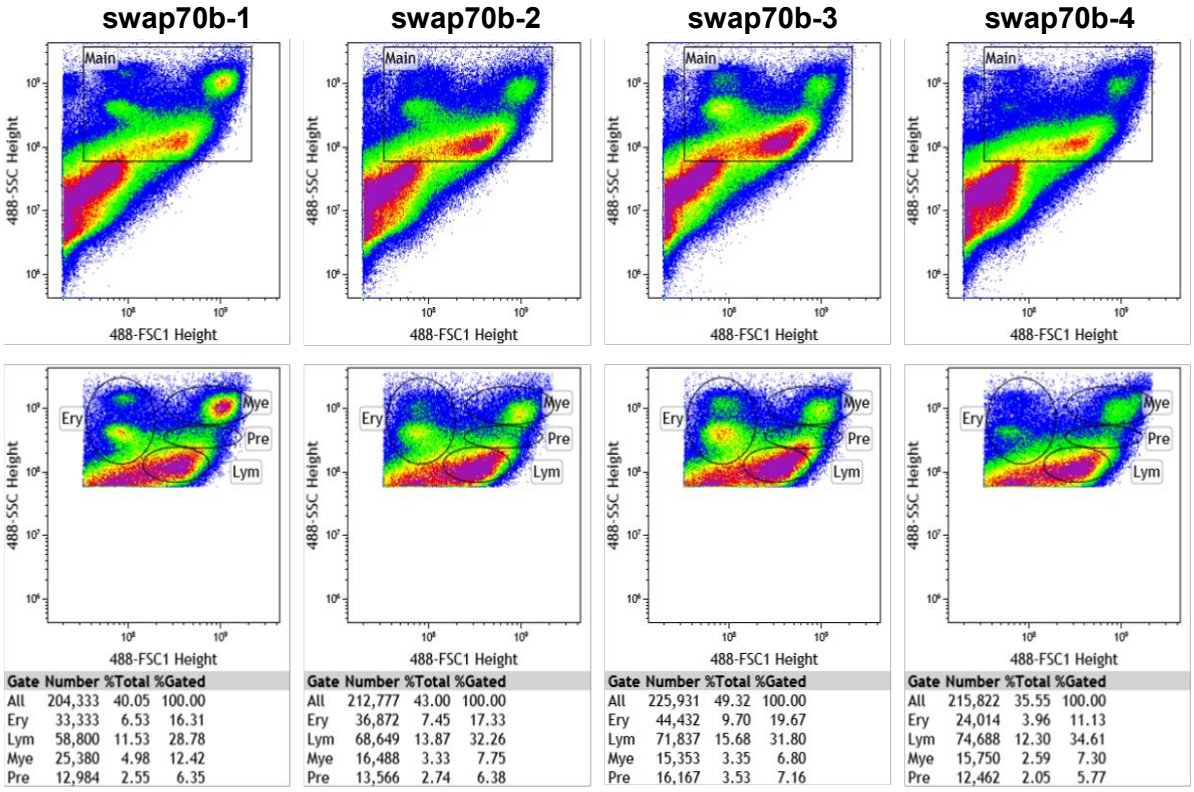
Gate	Number	%Total	%Gated
All	201,186	40.42	100.00
Ery	31,645	6.36	15.73
Lym	58,715	11.80	29.18
Mye	24,049	4.83	11.95
Pre	13,914	2.80	6.92

Gate	Number	%Total	%Gated
All	223,861	48.73	100.00
Ery	61,876	13.47	27.64
Lym	60,496	13.17	27.02
Mye	19,158	4.17	8.56
Pre	15,052	3.28	6.72

Gate	Number	%Total	%Gated
All	208,544	47.53	100.00
Ery	24,477	5.58	11.74
Lym	66,634	15.19	31.95
Mye	26,462	6.03	12.69
Pre	19,368	4.41	9.29

Figure 9.6 Flow cytometric analysis of blood cell lineages of *def6a*$^{qmc811/qmc811}$ mutant zebrafish. A main gate was produced for all plots to focus only the blood cell lineages. The major blood cell linages were separated by four additional sub-gates which are erythrocytes (ery), myelomonocytes (mye), precursors (pre) and lymphocytes (lym). The number of cells were calculated by Kaluza Analysis software.

swap70b$^{qmc809/qmc809}$ mutant line



Gate	Number	%Total	%Gated
All	204,333	40.05	100.00
Ery	33,333	6.53	16.31
Lym	58,800	11.53	28.78
Mye	25,380	4.98	12.42
Pre	12,984	2.55	6.35

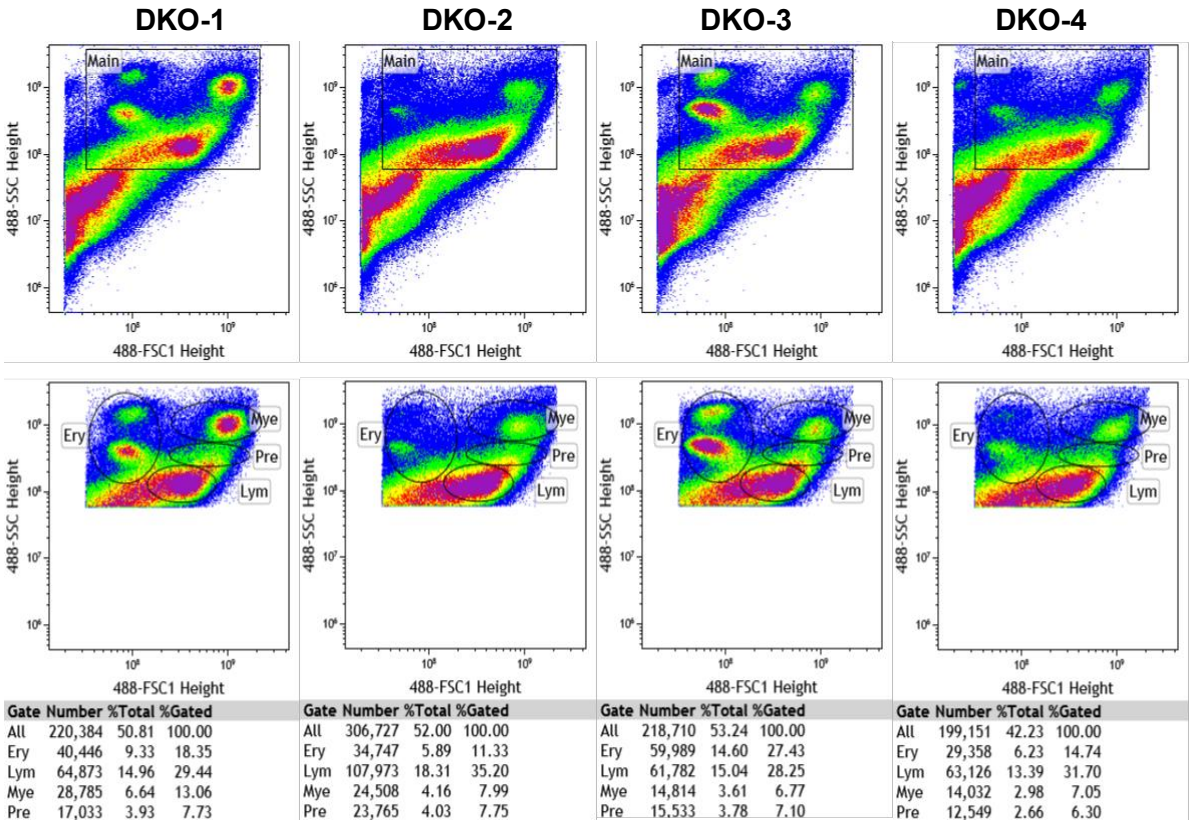
Gate	Number	%Total	%Gated
All	212,777	43.00	100.00
Ery	36,872	7.45	17.33
Lym	68,649	13.87	32.26
Mye	16,488	3.33	7.75
Pre	13,566	2.74	6.38

Gate	Number	%Total	%Gated
All	225,931	49.32	100.00
Ery	44,432	9.70	19.67
Lym	71,837	15.68	31.80
Mye	15,353	3.35	6.80
Pre	16,167	3.53	7.16

Gate	Number	%Total	%Gated
All	215,822	35.55	100.00
Ery	24,014	3.96	11.13
Lym	74,688	12.30	34.61
Mye	15,750	2.59	7.30
Pre	12,462	2.05	5.77

Figure 9.7 Flow cytometric analysis of blood cell lineages of *swap70b*$^{qmc809/qmc809}$ mutant zebrafish. A main gate was produced for all plots to focus only the blood cell lineages. The major blood cell linages were separated by four additional sub-gates which are erythrocytes (ery), myelomonocytes (mye), precursors (pre) and lymphocytes (lym). The number of cells were calculated by Kaluza Analysis software.

Double knock out (DKO: *def6a*$^{qmc811/qmc811}$*; swap70b*$^{qmc809/qmc809}$) mutant line



Gate	Number	%Total	%Gated
All	220,384	50.81	100.00
Ery	40,446	9.33	18.35
Lym	64,873	14.96	29.44
Mye	28,785	6.64	13.06
Pre	17,033	3.93	7.73

Gate	Number	%Total	%Gated
All	306,727	52.00	100.00
Ery	34,747	5.89	11.33
Lym	107,973	18.31	35.20
Mye	24,508	4.16	7.99
Pre	23,765	4.03	7.75

Gate	Number	%Total	%Gated
All	218,710	53.24	100.00
Ery	59,989	14.60	27.43
Lym	61,782	15.04	28.25
Mye	14,814	3.61	6.77
Pre	15,533	3.78	7.10

Gate	Number	%Total	%Gated
All	199,151	42.23	100.00
Ery	29,358	6.23	14.74
Lym	63,126	13.39	31.70
Mye	14,032	2.98	7.05
Pre	12,549	2.66	6.30

Figure 9.8 Flow cytometric analysis of blood cell lineages of *def6a*$^{qmc811/qmc811}$; *swap70b*$^{qmc809/qmc809}$ double mutant zebrafish. A main gate was produced for all plots to focus only the blood cell lineages. The major blood cell linages were separated by four additional sub-gates which are erythrocytes (ery), myelomonocytes (mye), precursors (pre) and lymphocytes (lym). The number of cells were calculated by Kaluza Analysis software.

APPENDIX –V

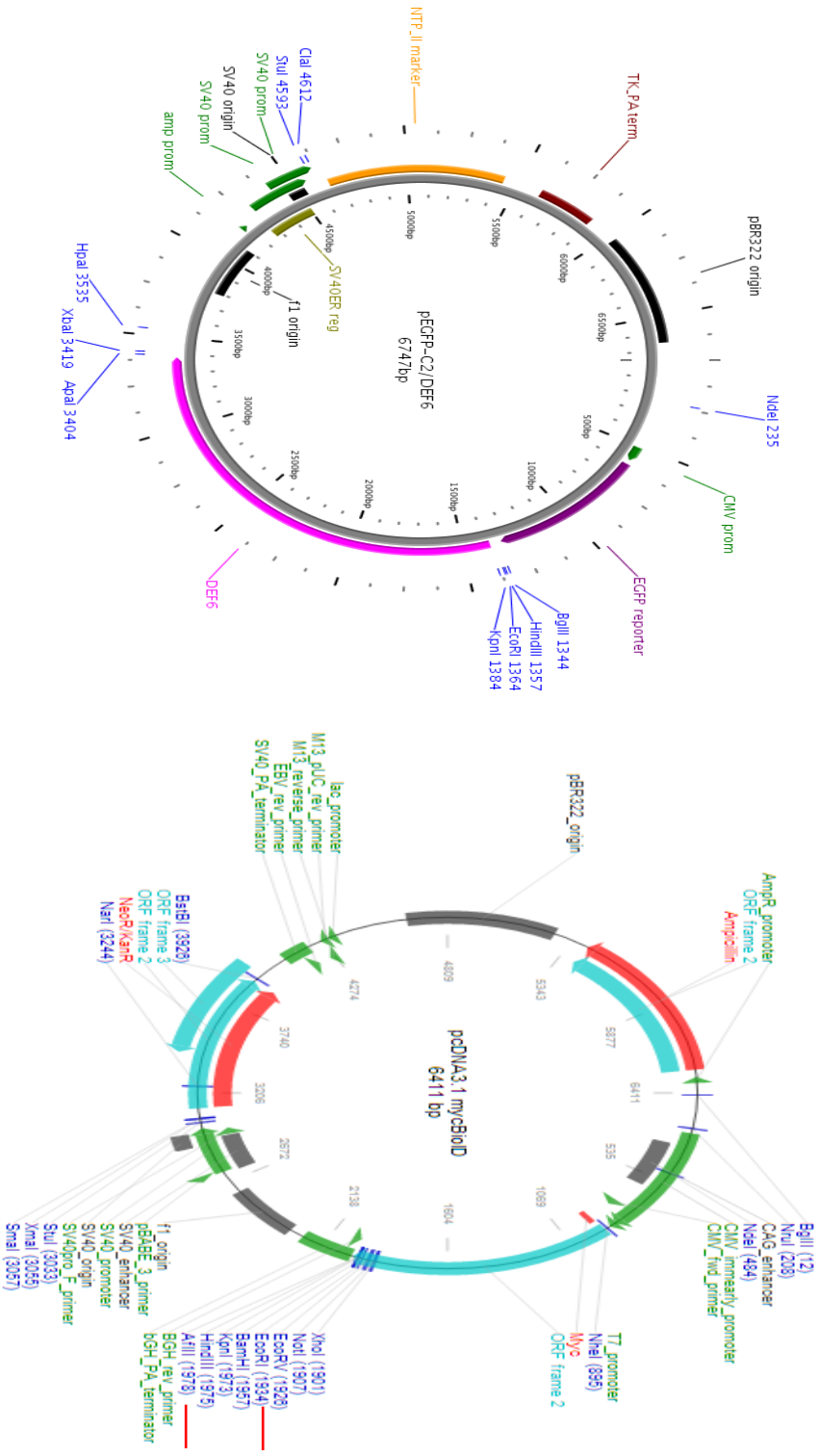
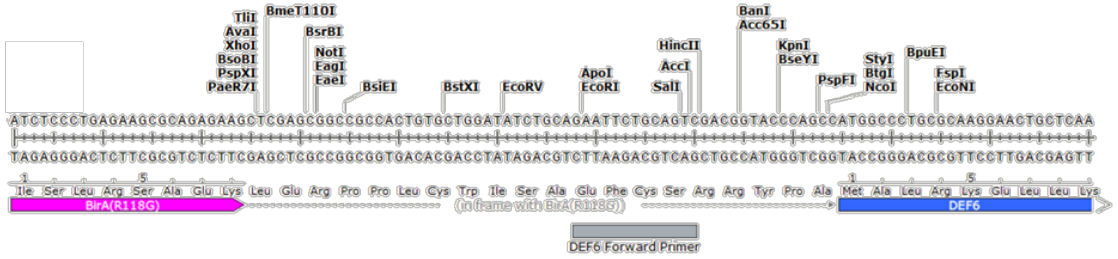


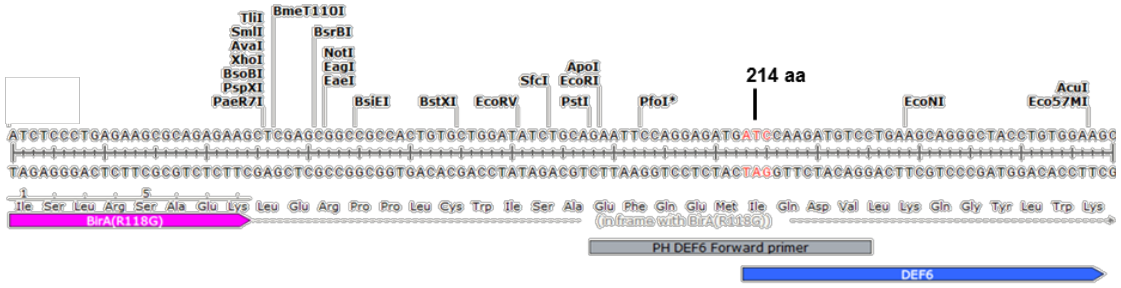
Figure 9.9. Plasmid maps of pEGFP-C2/DEF6 and pcDNA3.1 mycBioID. *EcoRI* and *AflII* restriction sites were used for generating the fusions of BirA-DEF6 and BirA-truncated DEF6. Plasmid pEGFP-C2/DEF6 was used from lab stock and pcDNA3.1 mycBioID was obtained from Addgene.

APPENDIX VI

A **FL- DEF6 and N-terminal DEF6**



B **PH DEF6**



C **C-terminal DEF6**



Figure 9.10 Sequence analysis confirming the in-frame insertions of (A) full-length (FL) DEF6, N-terminal DEF6, (B) PH-DEF6 and (C) C-terminal DEF6 into the pcDNA3.1 mycBioID vector.

APPENDIX VII

Figure 9.11 Scaffold-mediated identification of all biotinylated proteins. The proteins detected also in the negative control are indicated with blue and the proteins detected only in DEF6 or its truncation versions are indicated with red.

	Proteins	Accession No	Molecular Weight	FL Def6	N-ter Def6	PH Def6	C-ter Def6	Nega-tive control
	Cluster of Myosin-9 OS=Homo sapiens GN=MYH9 PE=1 SV=4 (P35579)	P35579 [4]	227 kDa	100% (51)	100% (52)	100% (115)	100% (88)	100% (132)
	Cluster of Heat shock protein HSP 90-beta OS=Homo sapiens GN=HSP90AB1 PE=1 SV=4 (P08238)	P08238 [4]	83 kDa	100% (52)	100% (38)	100% (64)	100% (60)	100% (67)
	Cluster of L-lactate dehydrogenase A chain OS=Homo sapiens GN=LDHA PE=1 SV=2 (P00338)	P00338 [4]	37 kDa	100% (19)	100% (20)	100% (31)	100% (28)	100% (38)
	Cluster of Tubulin beta chain OS=Homo sapiens GN=TUBB PE=1 SV=2 (P07437)	P07437 [4]	50 kDa	100% (28)	100% (18)	100% (36)	100% (28)	100% (33)
	Clathrin heavy chain OS=Homo sapiens GN=CLTC PE=1 SV=1	A0A087WVQ6 (+1)	192 kDa	100% (25)	100% (22)	100% (34)	100% (29)	100% (32)
	Cluster of DNA topoisomerase 1 OS=Homo sapiens GN=TOP1 PE=1 SV=2 (P11387)	P11387 [2]	91 kDa	100% (15)	100% (14)	100% (23)	100% (23)	100% (31)
	Cluster of Vimentin OS=Homo sapiens GN=VIM PE=1 SV=4 (P08670)	P08670 [7]	54 kDa	100% (20)	100% (10)	100% (16)	100% (9)	100% (30)
	Cluster of Tubulin alpha-8 chain (Fragment) OS=Homo sapiens GN=TUBA8 PE=1 SV=1 (V9GZ17)	V9GZ17 [5]	31 kDa	100% (25)	100% (21)	100% (26)	100% (27)	100% (29)
	Filamin-A OS=Homo sapiens GN=FLNA PE=1 SV=4	P21333 (+1)	281 kDa	100% (20)	100% (15)	100% (38)	100% (20)	100% (29)
	Pyruvate kinase PKM OS=Homo sapiens GN=PKM PE=1 SV=4	P14618	58 kDa	100% (16)	100% (14)	100% (24)	100% (22)	100% (26)
	Pyruvate carboxylase, mitochondrial OS=Homo sapiens GN=PC PE=1 SV=2	P11498	130 kDa	100% (5)	100% (3)	100% (24)		100% (26)
	Cell growth-regulating nucleolar protein OS=Homo sapiens GN=LYAR PE=1 SV=2	Q9NX58	44 kDa	100% (10)	100% (11)	100% (21)	100% (11)	100% (25)
	Elongation factor 2 OS=Homo sapiens GN=EEF2 PE=1 SV=4	P13639	95 kDa	100% (20)	100% (16)	100% (28)	100% (24)	100% (25)
	Cluster of Nucleolar protein 56 OS=Homo sapiens GN=NOP56 PE=1 SV=4 (O00567)	O00567 [2]	66 kDa	100% (19)	100% (12)	100% (25)	100% (26)	100% (24)
	RNA cytidine acetyltransferase OS=Homo sapiens GN=NAT10 PE=1 SV=2	Q9H0A0	116 kDa	100% (11)	100% (6)	100% (8)	100% (18)	100% (23)
	Cluster of Actin, cytoplasmic 1 OS=Homo sapiens GN=ACTB PE=1 SV=1 (P60709)	P60709 [7]	42 kDa	100% (20)	100% (17)	100% (28)	100% (24)	100% (22)
	ATP-dependent RNA helicase A OS=Homo sapiens GN=DHX9 PE=1 SV=4	Q08211	141 kDa	100% (16)	100% (11)	100% (23)	100% (24)	100% (22)
	T-complex protein 1 subunit alpha OS=Homo sapiens GN=TCP1 PE=1 SV=1	P17987	60 kDa	100% (15)	100% (8)	100% (22)	100% (17)	100% (22)
	Alpha-enolase OS=Homo sapiens GN=ENO1 PE=1 SV=2	P06733	47 kDa	100% (16)	100% (13)	100% (17)	100% (16)	100% (20)

	Cluster of Heterogeneous nuclear ribonucleoprotein M OS=Homo sapiens GN=HNRNPM PE=1 SV=3 (P52272)	P52272 [3]	78 kDa	100% (9)	100% (5)	100% (24)	100% (20)	100% (20)
	Heterogeneous nuclear ribonucleoprotein U OS=Homo sapiens GN=HNRNPU PE=1 SV=6	Q00839	91 kDa	100% (14)	100% (11)	100% (25)	100% (18)	100% (19)
	Glyceraldehyde-3-phosphate dehydrogenase OS=Homo sapiens GN=GAPDH PE=1 SV=3	P04406	36 kDa	100% (11)	100% (8)	100% (17)	100% (18)	100% (18)
	T-complex protein 1 subunit gamma OS=Homo sapiens GN=CCT3 PE=1 SV=4	P49368	61 kDa	100% (7)	100% (5)	100% (19)	100% (16)	100% (18)
	Cluster of Histone H2B type F-S OS=Homo sapiens GN=H2BFS PE=1 SV=2 (P57053)	P57053 [3]	14 kDa	100% (22)	100% (18)	100% (16)	100% (16)	100% (17)
	Elongation factor 1-alpha 1 OS=Homo sapiens GN=EEF1A1 PE=1 SV=1	P68104	50 kDa	100% (13)	100% (10)	100% (17)	100% (15)	100% (17)
	60S ribosomal protein L4 OS=Homo sapiens GN=RPL4 PE=1 SV=5	P36578	48 kDa	100% (15)	100% (7)	100% (18)	100% (19)	100% (17)
	ATP synthase subunit beta, mitochondrial OS=Homo sapiens GN=ATP5B PE=1 SV=3	P06576	57 kDa	100% (18)	100% (6)	100% (19)	100% (20)	100% (17)
	Eukaryotic translation initiation factor 5B OS=Homo sapiens GN=EIF5B PE=1 SV=1	A0A087WUT6 (+1)	139 kDa	100% (13)		100% (3)	100% (21)	100% (17)
	T-complex protein 1 subunit eta OS=Homo sapiens GN=CCT7 PE=1 SV=2	Q99832	59 kDa	100% (12)	100% (6)	100% (17)	100% (16)	100% (16)
	ATP-dependent RNA helicase DDX18 OS=Homo sapiens GN=DDX18 PE=1 SV=2	Q9NVP1	75 kDa	100% (10)	100% (7)	100% (9)	100% (11)	100% (16)
	Cluster of Histone H1.4 OS=Homo sapiens GN=HIST1H1E PE=1 SV=2 (P10412)	P10412 [4]	22 kDa	100% (16)	100% (27)	100% (25)	100% (11)	100% (15)
	ATP synthase subunit alpha, mitochondrial OS=Homo sapiens GN=ATP5A1 PE=1 SV=1	P25705	60 kDa	100% (18)	100% (10)	100% (14)	100% (19)	100% (15)
	60S ribosomal protein L7a OS=Homo sapiens GN=RPL7A PE=1 SV=2	P62424	30 kDa	100% (15)	100% (13)	100% (18)	100% (18)	100% (15)
	Cluster of Heat shock cognate 71 kDa protein OS=Homo sapiens GN=HSPA8 PE=1 SV=1 (P11142)	P11142 [8]	71 kDa	100% (14)	100% (8)	100% (20)	100% (21)	100% (15)
	WD repeat-containing protein 1 OS=Homo sapiens GN=WDR1 PE=1 SV=4	O75083	66 kDa	100% (7)	100% (7)	100% (15)	100% (10)	100% (15)
	Histone H4 OS=Homo sapiens GN=HIST1H4A PE=1 SV=2	P62805	11 kDa	100% (15)	100% (8)	100% (14)	100% (13)	100% (14)
	60S ribosomal protein L6 OS=Homo sapiens GN=RPL6 PE=1 SV=3	Q02878	33 kDa	100% (14)	100% (12)	100% (13)	100% (15)	100% (14)
	60 kDa heat shock protein, mitochondrial OS=Homo sapiens GN=HSPD1 PE=1 SV=2	P10809	61 kDa	100% (18)	100% (8)	100% (17)	100% (16)	100% (14)
	X-ray repair cross-complementing protein 5 OS=Homo sapiens GN=XRCC5 PE=1 SV=3	P13010	83 kDa	100% (15)	100% (7)	100% (17)	100% (15)	100% (14)
	Cluster of 40S ribosomal protein S3 OS=Homo sapiens GN=RPS3 PE=1 SV=2 (P23396)	P23396 [2]	27 kDa	100% (12)	100% (6)	100% (14)	100% (12)	100% (14)
	Eukaryotic initiation factor 4A-I OS=Homo sapiens GN=EIF4A1 PE=1 SV=1	P60842	46 kDa	100% (10)	100% (6)	100% (14)	100% (13)	100% (14)

	Cluster of Phosphoglycerate kinase 1 OS=Homo sapiens GN=PGK1 PE=1 SV=3 (P00558)	P00558 [2]	45 kDa	100% (9)	100% (4)	100% (16)	100% (13)	100% (14)
	DNA replication licensing factor MCM7 OS=Homo sapiens GN=MCM7 PE=1 SV=4	P33993	81 kDa	100% (11)		100% (19)	100% (10)	100% (14)
	Cluster of Fructose-bisphosphate aldolase A OS=Homo sapiens GN=ALDOA PE=1 SV=2 (P04075)	P04075 [2]	39 kDa	100% (5)	100% (7)	100% (12)	100% (8)	100% (14)
	Cluster of Keratin, type I cytoskeletal 10 OS=Homo sapiens GN=KRT10 PE=1 SV=6 (P13645)	P13645 [3]	59 kDa	100% (18)	100% (3)	100% (5)	100% (10)	100% (14)
	Pre-mRNA-splicing factor ATP-dependent RNA helicase DHX15 OS=Homo sapiens GN=DHX15 PE=1 SV=2	O43143	91 kDa	100% (10)	100% (4)	100% (12)	100% (12)	100% (14)
	DNA replication licensing factor MCM2 OS=Homo sapiens GN=MCM2 PE=1 SV=4	P49736	102 kDa	100% (8)	100% (3)	100% (15)	100% (8)	100% (14)
	Nucleolar protein 58 OS=Homo sapiens GN=NOP58 PE=1 SV=1	Q9Y2X3	60 kDa	100% (10)	100% (4)	100% (11)	100% (13)	100% (14)
	Histone H1.5 OS=Homo sapiens GN=HIST1H1B PE=1 SV=3	P16401	23 kDa	100% (13)	100% (13)	100% (17)	100% (9)	100% (13)
	Cluster of 40S ribosomal protein S4, X isoform OS=Homo sapiens GN=RPS4X PE=1 SV=2 (P62701)	P62701 [2]	30 kDa	100% (11)	100% (7)	100% (14)	100% (13)	100% (13)
	Receptor of activated protein C kinase 1 OS=Homo sapiens GN=RACK1 PE=1 SV=3	P63244	35 kDa	100% (11)	100% (9)	100% (14)	100% (12)	100% (13)
	40S ribosomal protein S3a OS=Homo sapiens GN=RPS3A PE=1 SV=2	P61247	30 kDa	100% (12)	100% (9)	100% (12)	100% (12)	100% (13)
	T-complex protein 1 subunit delta OS=Homo sapiens GN=CCT4 PE=1 SV=4	P50991	58 kDa	100% (5)	100% (7)	100% (12)	100% (14)	100% (13)
	DNA-dependent protein kinase catalytic subunit OS=Homo sapiens GN=PRKDC PE=1 SV=3	P78527	469 kDa	100% (9)		100% (29)	100% (6)	100% (13)
	ATP-citrate synthase OS=Homo sapiens GN=ACLY PE=1 SV=3	P53396	121 kDa	100% (6)	100% (3)	100% (15)	100% (8)	100% (13)
	pre-rRNA processing protein FTSJ3 OS=Homo sapiens GN=FTSJ3 PE=1 SV=2	Q8IY81	97 kDa	100% (5)	100% (3)	100% (4)	100% (10)	100% (13)
	Cluster of Cyclin-dependent kinase 6 OS=Homo sapiens GN=CDK6 PE=1 SV=1 (Q00534)	Q00534 [11]	37 kDa	100% (3)		100% (6)	100% (3)	100% (13)
	T-complex protein 1 subunit beta OS=Homo sapiens GN=CCT2 PE=1 SV=4	P78371	57 kDa	100% (9)	100% (6)	100% (13)	100% (13)	100% (12)
	DNA replication licensing factor MCM6 OS=Homo sapiens GN=MCM6 PE=1 SV=1	Q14566	93 kDa	100% (9)	100% (5)	100% (13)	100% (7)	100% (12)
	Fatty acid synthase OS=Homo sapiens GN=FASN PE=1 SV=1	A0A0U1RQF0 (+1)	273 kDa	100% (7)		100% (9)	100% (9)	100% (12)
	Cluster of 60S ribosomal protein L23a OS=Homo sapiens GN=RPL23A PE=1 SV=1 (P62750)	P62750 [4]	18 kDa	100% (12)	100% (8)	100% (10)	100% (13)	100% (11)
	Core histone macro-H2A.1 OS=Homo sapiens GN=H2AFY PE=1 SV=4	O75367	40 kDa	100% (14)	100% (9)	100% (9)	100% (13)	100% (11)
	60S ribosomal protein L3 OS=Homo sapiens GN=RPL3 PE=1 SV=2	P39023	46 kDa	100% (9)	100% (6)	100% (14)	100% (11)	100% (11)

	Ribosomal L1 domain-containing protein 1 OS=Homo sapiens GN=RSL1D1 PE=1 SV=3	O76021	55 kDa	100% (19)	100% (4)	100% (14)	100% (20)	100% (11)
	Heterogeneous nuclear ribonucleoprotein K OS=Homo sapiens GN=HNRNPK PE=1 SV=1	P61978	51 kDa	100% (12)	100% (6)	100% (14)	100% (14)	100% (11)
	X-ray repair cross-complementing protein 6 OS=Homo sapiens GN=XRCC6 PE=1 SV=2	P12956	70 kDa	100% (11)	100% (5)	100% (18)	100% (23)	100% (11)
	60S ribosomal protein L7 OS=Homo sapiens GN=RPL7 PE=1 SV=1	P18124	29 kDa	100% (9)	100% (3)	100% (10)	100% (7)	100% (11)
	Cluster of T-complex protein 1 subunit zeta OS=Homo sapiens GN=CCT6A PE=1 SV=3 (P40227)	P40227 [2]	58 kDa	100% (10)	100% (5)	100% (10)	100% (10)	100% (11)
	60S ribosomal protein L5 OS=Homo sapiens GN=RPL5 PE=1 SV=3	P46777	34 kDa	100% (6)	100% (4)	100% (10)	100% (12)	100% (11)
	Matrin-3 OS=Homo sapiens GN=MATR3 PE=1 SV=1	A0A0R4J2E8 (+2)	95 kDa	100% (7)	100% (5)	100% (11)	100% (7)	100% (11)
	U5 small nuclear ribonucleoprotein 200 kDa helicase OS=Homo sapiens GN=SNRNP200 PE=1 SV=2	O75643	245 kDa	100% (9)		100% (15)	100% (11)	100% (11)
	Cluster of 14-3-3 protein theta OS=Homo sapiens GN=YWHAQ PE=1 SV=1 (P27348)	P27348 [5]	28 kDa			100% (12)		100% (11)
	60S ribosomal protein L27 OS=Homo sapiens GN=RPL27 PE=1 SV=2	P61353	16 kDa	100% (10)	100% (7)	100% (5)	100% (9)	100% (10)
	Heterogeneous nuclear ribonucleoprotein A1 OS=Homo sapiens GN=HNRNPA1 PE=1 SV=2	F8W6I7 (+1)	33 kDa	100% (12)	100% (6)	100% (12)	100% (14)	100% (10)
	Probable ATP-dependent RNA helicase DDX5 OS=Homo sapiens GN=DDX5 PE=1 SV=1	J3KTA4 (+1)	69 kDa	100% (11)	100% (7)	100% (14)	100% (12)	100% (10)
	Cluster of 40S ribosomal protein S2 OS=Homo sapiens GN=RPS2 PE=1 SV=2 (P15880)	P15880 [2]	31 kDa	100% (5)	100% (4)	100% (9)	100% (11)	100% (10)
	Cluster of GTP-binding nuclear protein Ran OS=Homo sapiens GN=RAN PE=1 SV=1 (B5MDF5)	B5MDF5 [5]	26 kDa	100% (9)	100% (8)	100% (9)	100% (10)	100% (10)
	DNA replication licensing factor MCM4 OS=Homo sapiens GN=MCM4 PE=1 SV=5	P33991	97 kDa	100% (10)		100% (15)	100% (12)	100% (10)
	Cluster of Chromodomain-helicase-DNA-binding protein 4 OS=Homo sapiens GN=CHD4 PE=1 SV=1 (A0A0C4DGG9)	A0A0C4DGG9 [6]	220 kDa	100% (9)		100% (9)	100% (18)	100% (10)
	Bifunctional glutamate/proline--tRNA ligase OS=Homo sapiens GN=EPRS PE=1 SV=5	P07814	171 kDa	100% (10)	100% (4)	100% (11)	100% (11)	100% (10)
	Cluster of 60S ribosomal protein L26 OS=Homo sapiens GN=RPL26 PE=1 SV=1 (P61254)	P61254 [2]	17 kDa	100% (7)	100% (5)	100% (6)	100% (8)	100% (10)
	T-complex protein 1 subunit epsilon OS=Homo sapiens GN=CCT5 PE=1 SV=1	E7ENZ3 (+1)	54 kDa	100% (8)	100% (4)	100% (10)	100% (7)	100% (10)
	Serine hydroxymethyltransferase, mitochondrial OS=Homo sapiens GN=SHMT2 PE=1 SV=3	P34897	56 kDa	100% (9)	100% (3)	100% (10)	100% (11)	100% (10)
	C-1-tetrahydrofolate synthase, cytoplasmic OS=Homo sapiens GN=MTHFD1 PE=1 SV=1	F5H2F4 (+1)	111 kDa	100% (5)	100% (5)	100% (6)	100% (6)	100% (10)

	Splicing factor 3B subunit 1 OS=Homo sapiens GN=SF3B1 PE=1 SV=3	O75533	146 kDa	100% (5)	100% (4)	100% (6)	100% (3)	100% (10)
	Endoplasmin OS=Homo sapiens GN=HSP90B1 PE=1 SV=1	P14625	92 kDa	100% (16)	100% (5)	100% (18)	100% (23)	100% (9)
	Cluster of ADP/ATP translocase 2 OS=Homo sapiens GN=SLC25A5 PE=1 SV=7 (P05141)	P05141 [4]	33 kDa	100% (6)	100% (4)	100% (11)	100% (11)	100% (9)
	40S ribosomal protein S8 OS=Homo sapiens GN=RPS8 PE=1 SV=2	P62241	24 kDa	100% (10)	100% (6)	100% (10)	100% (9)	100% (9)
	Prohibitin-2 OS=Homo sapiens GN=PHB2 PE=1 SV=2	J3KPX7 (+1)	33 kDa	100% (10)	100% (8)	100% (7)	100% (12)	100% (9)
	Cofilin-1 OS=Homo sapiens GN=CFL1 PE=1 SV=1	E9PK25 (+2)	23 kDa	100% (6)	100% (7)	100% (7)	100% (5)	100% (9)
	Keratin, type II cytoskeletal 1 OS=Homo sapiens GN=KRT1 PE=1 SV=6	P04264	66 kDa	100% (15)	100% (6)	100% (8)	100% (7)	100% (9)
	Isocitrate dehydrogenase [NADP], mitochondrial OS=Homo sapiens GN=IDH2 PE=1 SV=2	P48735	51 kDa	100% (7)		100% (9)	100% (9)	100% (9)
	Rab GDP dissociation inhibitor beta OS=Homo sapiens GN=GDI2 PE=1 SV=2	P50395	51 kDa	100% (5)	100% (4)	100% (8)	100% (6)	100% (9)
	Poly(rC)-binding protein 1 OS=Homo sapiens GN=PCBP1 PE=1 SV=2	Q15365	37 kDa	100% (4)	100% (4)	100% (8)	100% (6)	100% (9)
	Heat shock protein 105 kDa OS=Homo sapiens GN=HSPH1 PE=1 SV=1	Q92598	97 kDa	100% (4)	100% (5)	100% (8)	100% (4)	100% (9)
	Nucleolar complex protein 3 homolog OS=Homo sapiens GN=NOC3L PE=1 SV=1	Q8WTT2	93 kDa	100% (3)			100% (6)	100% (9)
	EBNA1 binding protein 2, isoform CRA_d OS=Homo sapiens GN=EBNA1BP2 PE=1 SV=1	H7C2Q8 (+1)	41 kDa	100% (8)	100% (6)	100% (6)	100% (8)	100% (8)
	60S ribosomal protein L10 OS=Homo sapiens GN=RPL10 PE=1 SV=4	P27635 (+1)	25 kDa	100% (6)		100% (8)	100% (9)	100% (8)
	6-phosphogluconate dehydrogenase, decarboxylating OS=Homo sapiens GN=PGD PE=1 SV=3	P52209	53 kDa	100% (8)	100% (4)	100% (11)	100% (6)	100% (8)
	Probable ATP-dependent RNA helicase DDX17 OS=Homo sapiens GN=DDX17 PE=1 SV=1	H3BLZ8 (+1)	80 kDa	100% (7)		100% (10)	100% (10)	100% (8)
	Cluster of ATP-dependent RNA helicase DDX39A OS=Homo sapiens GN=DDX39A PE=1 SV=2 (O00148)	O00148 [2]	49 kDa	100% (7)	100% (5)	100% (10)	100% (9)	100% (8)
	60S acidic ribosomal protein P0 OS=Homo sapiens GN=RPLP0 PE=1 SV=1	P05388	34 kDa	100% (7)	100% (5)	100% (8)	100% (6)	100% (8)
	Adenosylhomocysteinase OS=Homo sapiens GN=AHCY PE=1 SV=4	P23526	48 kDa	100% (3)		100% (6)	100% (6)	100% (8)
	CAD protein OS=Homo sapiens GN=CAD PE=1 SV=1	F8VPD4 (+1)	236 kDa	100% (4)	100% (4)	100% (8)	100% (3)	100% (8)
	Cluster of ATP-dependent 6-phosphofructokinase, platelet type OS=Homo sapiens GN=PFKP PE=1 SV=2 (Q01813)	Q01813 [2]	86 kDa	100% (3)	100% (3)	100% (7)	100% (4)	100% (8)
	ATP-binding cassette sub-family F member 1 OS=Homo sapiens GN=ABCF1 PE=1 SV=2	Q8NE71	96 kDa	100% (5)			100% (9)	100% (8)

	Serine/arginine repetitive matrix protein 2 OS=Homo sapiens GN=SRRM2 PE=1 SV=2	Q9UQ35	300 kDa			100% (8)	100% (5)	100% (8)
	Probable ATP-dependent RNA helicase DDX27 OS=Homo sapiens GN=DDX27 PE=1 SV=1	B7Z6D5 (+1)	87 kDa	100% (3)	100% (3)		100% (4)	100% (8)
	Cullin-associated NEDD8-dissociated protein 1 OS=Homo sapiens GN=CAND1 PE=1 SV=2	Q86VP6	136 kDa			100% (6)		100% (8)
	40S ribosomal protein S9 OS=Homo sapiens GN=RPS9 PE=1 SV=1	A0A024R4M0 (+1)	23 kDa	100% (8)	100% (7)	100% (9)	100% (9)	100% (7)
	60S ribosomal protein L15 OS=Homo sapiens GN=RPL15 PE=1 SV=2	P61313	24 kDa	100% (7)	100% (4)	100% (8)	100% (8)	100% (7)
	Ubiquitin-40S ribosomal protein S27a OS=Homo sapiens GN=RPS27A PE=1 SV=2	P62979	18 kDa	100% (6)	100% (5)	100% (6)	100% (6)	100% (7)
	60S ribosomal protein L8 OS=Homo sapiens GN=RPL8 PE=1 SV=2	P62917	28 kDa	100% (7)		100% (8)	100% (8)	100% (7)
	Heterogeneous nuclear ribonucleoprotein H OS=Homo sapiens GN=HNRNPH1 PE=1 SV=1	E9PCY7 (+2)	47 kDa	100% (6)	100% (3)	100% (7)	100% (6)	100% (7)
	60S ribosomal protein L18 (Fragment) OS=Homo sapiens GN=RPL18 PE=1 SV=1	J3QQ67 (+1)	22 kDa	100% (5)	100% (5)	100% (6)	100% (7)	100% (7)
	DNA replication licensing factor MCM3 OS=Homo sapiens GN=MCM3 PE=1 SV=3	P25205	91 kDa	100% (5)	100% (3)	100% (12)	100% (9)	100% (7)
	Non-POU domain-containing octamer-binding protein OS=Homo sapiens GN=NONO PE=1 SV=4	Q15233	54 kDa	100% (4)		100% (9)	100% (6)	100% (7)
	Cluster of 60S ribosomal protein L36a-like OS=Homo sapiens GN=RPL36AL PE=1 SV=3 (Q969Q0)	Q969Q0 [3]	12 kDa	100% (4)		100% (5)	100% (4)	100% (7)
	Eukaryotic translation initiation factor 2 subunit 3 OS=Homo sapiens GN=EIF2S3 PE=1 SV=3	P41091	51 kDa	100% (3)		100% (5)	100% (4)	100% (7)
	Elongation factor Tu, mitochondrial OS=Homo sapiens GN=TUFM PE=1 SV=2	P49411	50 kDa	100% (4)		100% (5)	100% (7)	100% (7)
	Transitional endoplasmic reticulum ATPase OS=Homo sapiens GN=VCP PE=1 SV=4	P55072	89 kDa	100% (5)	100% (3)	100% (4)	100% (4)	100% (7)
	Adenosine deaminase OS=Homo sapiens GN=ADA PE=1 SV=3	P00813	41 kDa			100% (4)		100% (7)
	Cluster of Lamina-associated polypeptide 2, isoform alpha OS=Homo sapiens GN=TMPO PE=1 SV=2 (P42166)	P42166 [3]	75 kDa					100% (7)
	Cluster of Histone H3 OS=Homo sapiens GN=HIST2H3PS2 PE=1 SV=1 (Q5TEC6)	Q5TEC6 [5]	15 kDa	100% (6)	100% (6)	100% (7)	100% (9)	100% (6)
	Cluster of Neutral alpha-glucosidase AB OS=Homo sapiens GN=GANAB PE=1 SV=3 (Q14697)	Q14697 [2]	107 kDa	100% (19)		100% (11)	100% (22)	100% (6)
	60S ribosomal protein L35 OS=Homo sapiens GN=RPL35 PE=1 SV=2	P42766	15 kDa	100% (3)	100% (5)	100% (3)	100% (4)	100% (6)
	40S ribosomal protein S7 OS=Homo sapiens GN=RPS7 PE=1 SV=1	P62081	22 kDa	100% (5)	100% (4)	100% (5)	100% (4)	100% (6)

	60S ribosomal protein L17 (Fragment) OS=Homo sapiens GN=RPL17 PE=3 SV=1	A0A087WXM6 (+4)	20 kDa	100% (3)		100% (7)	100% (7)	100% (6)
	Phosphate carrier protein, mitochondrial OS=Homo sapiens GN=SLC25A3 PE=1 SV=1	F8VVM2	36 kDa	100% (3)	100% (4)	100% (7)	100% (8)	100% (6)
	60S ribosomal protein L36 OS=Homo sapiens GN=RPL36 PE=1 SV=3	Q9Y3U8	12 kDa	100% (5)	100% (3)	100% (4)	100% (4)	100% (6)
	Casein kinase II subunit alpha OS=Homo sapiens GN=CSNK2A1 PE=1 SV=1	E7EU96 (+1)	45 kDa	100% (8)	100% (4)	100% (4)	100% (10)	100% (6)
	60S ribosomal protein L13a (Fragment) OS=Homo sapiens GN=RPL13A PE=1 SV=2	M0QYS1 (+1)	24 kDa	100% (3)	100% (3)	100% (5)	100% (6)	100% (6)
	60S ribosomal protein L9 OS=Homo sapiens GN=RPL9 PE=1 SV=1	P32969	22 kDa	100% (6)	100% (4)	100% (8)	100% (7)	100% (6)
	40S ribosomal protein S18 OS=Homo sapiens GN=RPS18 PE=1 SV=3	P62269	18 kDa	100% (5)	100% (3)	100% (8)	100% (6)	100% (6)
	Cluster of 40S ribosomal protein S17 OS=Homo sapiens GN=RPS17 PE=1 SV=2 (P08708)	P08708 [2]	16 kDa	100% (4)		100% (6)	100% (5)	100% (6)
	D-3-phosphoglycerate dehydrogenase OS=Homo sapiens GN=PHGDH PE=1 SV=4	O43175	57 kDa	100% (6)		100% (8)	100% (6)	100% (6)
	Aspartate--tRNA ligase, cytoplasmic OS=Homo sapiens GN=DARS PE=1 SV=2	P14868	57 kDa	100% (6)		100% (7)	100% (5)	100% (6)
	40S ribosomal protein S13 OS=Homo sapiens GN=RPS13 PE=1 SV=2	P62277	17 kDa			100% (3)	100% (5)	100% (6)
	60S ribosomal protein L12 OS=Homo sapiens GN=RPL12 PE=1 SV=1	P30050	18 kDa	100% (4)	100% (4)	100% (5)	100% (6)	100% (6)
	60S ribosomal protein L28 OS=Homo sapiens GN=RPL28 PE=1 SV=3	P46779	16 kDa			100% (5)	100% (4)	100% (6)
	Eukaryotic translation initiation factor 3 subunit C OS=Homo sapiens GN=EIF3C PE=1 SV=1	Q99613	105 kDa	100% (3)		100% (8)	100% (4)	100% (6)
	60S ribosomal protein L24 OS=Homo sapiens GN=RPL24 PE=1 SV=1	C9JNW5 (+1)	18 kDa	100% (3)		100% (4)	100% (5)	100% (6)
	Eukaryotic translation initiation factor 3 subunit L OS=Homo sapiens GN=EIF3L PE=1 SV=1	B0QY89 (+1)	71 kDa	100% (4)		100% (5)		100% (6)
	Cluster of Treacle protein OS=Homo sapiens GN=TCOF1 PE=1 SV=1 (E7ETY2)	E7ETY2 [2]	152 kDa			100% (3)	100% (3)	100% (6)
	Exportin-1 OS=Homo sapiens GN=XPO1 PE=1 SV=1	O14980	123 kDa			100% (5)		100% (6)
	Eukaryotic initiation factor 4A-III OS=Homo sapiens GN=EIF4A3 PE=1 SV=4	P38919	47 kDa	100% (2)		100% (4)	100% (4)	100% (6)
	Eukaryotic translation initiation factor 3 subunit D OS=Homo sapiens GN=EIF3D PE=1 SV=1	O15371	64 kDa			100% (5)		100% (6)
	ATP-binding cassette sub-family E member 1 OS=Homo sapiens GN=ABCE1 PE=1 SV=1	P61221	67 kDa			100% (3)		100% (6)
	Exportin-2 OS=Homo sapiens GN=CSE1L PE=1 SV=3	P55060	110 kDa			100% (3)		100% (6)
	Peroxiredoxin-6 OS=Homo sapiens GN=PRDX6 PE=1 SV=3	P30041	25 kDa			100% (4)		100% (6)

	40S ribosomal protein S11 OS=Homo sapiens GN=RPS11 PE=1 SV=3	P62280	18 kDa	100% (5)	100% (3)	100% (7)	100% (5)	100% (5)
	60S ribosomal protein L32 (Fragment) OS=Homo sapiens GN=RPL32 PE=1 SV=1	D3YTB1 (+2)	16 kDa	100% (4)	100% (4)	100% (3)	100% (5)	100% (5)
	60S ribosomal protein L13 OS=Homo sapiens GN=RPL13 PE=1 SV=4	P26373	24 kDa	100% (4)	100% (4)	100% (5)	100% (5)	100% (5)
	Prohibitin OS=Homo sapiens GN=PHB PE=1 SV=1	P35232	30 kDa	100% (10)	100% (4)	100% (6)	100% (9)	100% (5)
	60S ribosomal protein L18a OS=Homo sapiens GN=RPL18A PE=1 SV=1	M0R117 (+1)	18 kDa	100% (5)		100% (7)	100% (5)	100% (5)
	40S ribosomal protein S14 OS=Homo sapiens GN=RPS14 PE=1 SV=3	P62263	16 kDa	100% (6)		100% (4)	100% (6)	100% (5)
	40S ribosomal protein S6 OS=Homo sapiens GN=RPS6 PE=1 SV=1	P62753	29 kDa	100% (5)	100% (4)	100% (6)	100% (3)	100% (5)
	Myb-binding protein 1A OS=Homo sapiens GN=MYBBP1A PE=1 SV=2	Q9BQG0	149 kDa	100% (8)			100% (13)	100% (5)
	Pre-mRNA-processing factor 19 OS=Homo sapiens GN=PRPF19 PE=1 SV=1	Q9UMS4	55 kDa	100% (7)		100% (5)	100% (7)	100% (5)
	40S ribosomal protein S5 (Fragment) OS=Homo sapiens GN=RPS5 PE=1 SV=1	M0R0F0 (+1)	22 kDa	100% (6)		100% (5)	100% (5)	100% (5)
	40S ribosomal protein S12 OS=Homo sapiens GN=RPS12 PE=1 SV=3	P25398	15 kDa	100% (4)		100% (5)	100% (5)	100% (5)
	Squalene synthase OS=Homo sapiens GN=FDFT1 PE=1 SV=1	P37268	48 kDa	100% (8)		100% (7)	100% (8)	100% (5)
	Keratin, type I cytoskeletal 9 OS=Homo sapiens GN=KRT9 PE=1 SV=3	P35527	62 kDa	100% (4)	100% (4)	100% (8)	100% (6)	100% (5)
	Cluster of Guanine nucleotide-binding protein G(i) subunit alpha-2 OS=Homo sapiens GN=GNAI2 PE=1 SV=3 (P04899)	P04899 [5]	40 kDa	100% (5)	100% (3)	100% (6)	100% (5)	100% (5)
	Heterogeneous nuclear ribonucleoprotein F OS=Homo sapiens GN=HNRNPF PE=1 SV=3	P52597	46 kDa	100% (3)	100% (1)	100% (4)	100% (6)	100% (5)
	Peroxiredoxin-1 OS=Homo sapiens GN=PRDX1 PE=1 SV=1	Q06830	22 kDa			100% (6)	100% (6)	100% (5)
	Cluster of Myosin light polypeptide 6 OS=Homo sapiens GN=MYL6 PE=1 SV=1 (B7Z6Z4)	B7Z6Z4 [7]	27 kDa	100% (3)		100% (6)	100% (3)	100% (5)
	40S ribosomal protein S23 OS=Homo sapiens GN=RPS23 PE=1 SV=3	P62266	16 kDa	100% (5)		100% (6)	100% (4)	100% (5)
	Poly(rC)-binding protein 2 OS=Homo sapiens GN=PCBP2 PE=1 SV=1	Q15366	39 kDa	100% (3)	100% (3)	100% (5)	100% (4)	100% (5)
	Eukaryotic translation initiation factor 3 subunit A OS=Homo sapiens GN=EIF3A PE=1 SV=1	Q14152	167 kDa	100% (3)	100% (4)	100% (4)		100% (5)
	MKI67 FHA domain-interacting nucleolar phosphoprotein OS=Homo sapiens GN=NIFK PE=1 SV=1	Q9BYG3	34 kDa	100% (7)		100% (3)	100% (5)	100% (5)
	Glucose-6-phosphate isomerase (Fragment) OS=Homo sapiens GN=GPI PE=1 SV=1	A0A0A0MTS2	65 kDa			100% (3)	100% (4)	100% (5)

	ATP-dependent RNA helicase DDX24 OS=Homo sapiens GN=DDX24 PE=1 SV=1	G3V529 (+1)	91 kDa	100% (3)			100% (7)	100% (5)
	Septin-7 OS=Homo sapiens GN=SEPT7 PE=1 SV=2	E7EPK1 (+2)	51 kDa			100% (3)	100% (3)	100% (5)
	Flap endonuclease 1 OS=Homo sapiens GN=FEN1 PE=1 SV=1	P39748	43 kDa			100% (3)		100% (5)
	Cluster of Farnesyl pyrophosphate synthase OS=Homo sapiens GN=FDPS PE=1 SV=4 (P14324)	P14324 [2]	48 kDa			100% (4)		100% (5)
	Far upstream element-binding protein 2 OS=Homo sapiens GN=KHSRP PE=1 SV=1	A0A087WTP3 (+1)	73 kDa			100% (5)		100% (5)
	Eukaryotic translation initiation factor 2 subunit 1 OS=Homo sapiens GN=EIF2S1 PE=1 SV=3	P05198	36 kDa			100% (4)		100% (5)
	Cluster of CTP synthase 1 OS=Homo sapiens GN=CTPS1 PE=1 SV=2 (P17812)	P17812 [2]	67 kDa			100% (5)		100% (5)
	Actin-related protein 3 OS=Homo sapiens GN=ACTR3 PE=1 SV=3	P61158	47 kDa			100% (3)		100% (5)
	Nuclear pore complex protein Nup93 OS=Homo sapiens GN=NUP93 PE=1 SV=1	H3BVG0 (+1)	100 kDa	100% (3)				100% (5)
	Histone H2A type 2-B OS=Homo sapiens GN=HIST2H2AB PE=1 SV=3	Q8IUE6	14 kDa	100% (5)	100% (4)	100% (4)	100% (4)	100% (4)
	Cluster of Histone H2A type 2-C OS=Homo sapiens GN=HIST2H2AC PE=1 SV=4 (Q16777)	Q16777 [5]	14 kDa	100% (6)	100% (2)	100% (5)	100% (5)	100% (4)
	Histone H1x OS=Homo sapiens GN=H1FX PE=1 SV=1	Q92522	22 kDa	100% (5)	100% (5)	100% (5)	100% (6)	100% (4)
	40S ribosomal protein S30 OS=Homo sapiens GN=FAU PE=1 SV=1	E9PR30 (+1)	11 kDa	100% (3)	100% (3)	100% (4)		100% (4)
	40S ribosomal protein S25 OS=Homo sapiens GN=RPS25 PE=1 SV=1	P62851	14 kDa	100% (4)	100% (4)	100% (4)	100% (4)	100% (4)
	60S ribosomal protein L27a OS=Homo sapiens GN=RPL27A PE=1 SV=2	P46776	17 kDa	100% (6)		100% (7)	100% (5)	100% (4)
	40S ribosomal protein S24 OS=Homo sapiens GN=RPS24 PE=1 SV=1	A0A087WUS0 (+2)	15 kDa	100% (3)		100% (4)	100% (3)	100% (4)
	Probable 28S rRNA (cytosine(4447)-C(5))-methyltransferase OS=Homo sapiens GN=NOP2 PE=1 SV=2	P46087	89 kDa	100% (8)	100% (4)		100% (11)	100% (4)
	60S ribosomal protein L14 OS=Homo sapiens GN=RPL14 PE=1 SV=1	E7EPB3 (+1)	15 kDa	100% (4)	100% (4)	100% (3)	100% (6)	100% (4)
	40S ribosomal protein S15a OS=Homo sapiens GN=RPS15A PE=1 SV=1	I3L3P7 (+1)	11 kDa			100% (4)	100% (4)	100% (4)
	60S ribosomal protein L11 OS=Homo sapiens GN=RPL11 PE=1 SV=2	P62913	20 kDa	100% (4)		100% (4)	100% (4)	100% (4)
	Cluster of ADP-ribosylation factor 3 OS=Homo sapiens GN=ARF3 PE=1 SV=2 (P61204)	P61204 [3]	21 kDa	100% (3)	100% (3)	100% (7)	100% (5)	100% (4)
	60S ribosomal protein L10a OS=Homo sapiens GN=RPL10A PE=1 SV=2	P62906	25 kDa	100% (3)		100% (4)	100% (4)	100% (4)
	Voltage-dependent anion-selective channel protein 2 (Fragment)	A0A0A0MR02 (+1)	30 kDa	100% (8)		100% (5)	100% (5)	100% (4)

	OS=Homo sapiens GN=VDAC2 PE=1 SV=1							
	Complement component 1 Q subcomponent-binding protein, mitochondrial OS=Homo sapiens GN=C1QBP PE=1 SV=1	Q07021	31 kDa	100% (4)		100% (4)	100% (4)	100% (4)
	DNA replication licensing factor MCM5 OS=Homo sapiens GN=MCM5 PE=1 SV=5	P33992	82 kDa	100% (4)		100% (7)	100% (5)	100% (4)
	40S ribosomal protein S27 OS=Homo sapiens GN=RPS27 PE=1 SV=3	P42677	9 kDa		100% (3)	100% (5)	100% (5)	100% (4)
	Ribosome biogenesis protein BRX1 homolog OS=Homo sapiens GN=BRIX1 PE=1 SV=2	Q8TDN6	41 kDa	100% (6)		100% (3)	100% (4)	100% (4)
	Cytochrome b-c1 complex subunit 2, mitochondrial OS=Homo sapiens GN=UQCRC2 PE=1 SV=3	P22695	48 kDa	100% (5)		100% (4)	100% (6)	100% (4)
	60S ribosomal protein L30 (Fragment) OS=Homo sapiens GN=RPL30 PE=1 SV=1	E5RI99 (+1)	13 kDa	100% (3)	100% (3)	100% (4)	100% (3)	100% (4)
	40S ribosomal protein S15 OS=Homo sapiens GN=RPS15 PE=1 SV=1	K7ELC2 (+1)	18 kDa			100% (4)		100% (4)
	Fumarate hydratase, mitochondrial OS=Homo sapiens GN=FH PE=1 SV=3	P07954	55 kDa	100% (5)		100% (6)	100% (6)	100% (4)
	Isoleucine--tRNA ligase, cytoplasmic OS=Homo sapiens GN=IARS PE=1 SV=2	P41252	145 kDa	100% (6)		100% (4)	100% (4)	100% (4)
	60S ribosomal protein L23 OS=Homo sapiens GN=RPL23 PE=1 SV=1	P62829	15 kDa			100% (6)	100% (3)	100% (4)
	Hydroxyacyl-coenzyme A dehydrogenase, mitochondrial OS=Homo sapiens GN=HADH PE=1 SV=1	A0A0A0MSE2 (+1)	42 kDa			100% (5)	100% (7)	100% (4)
	Heat shock protein 75 kDa, mitochondrial OS=Homo sapiens GN=TRAP1 PE=1 SV=3	Q12931	80 kDa	100% (4)		100% (3)	100% (6)	100% (4)
	Importin subunit alpha-1 OS=Homo sapiens GN=KPNA2 PE=1 SV=1	P52292	58 kDa	100% (4)		100% (3)	100% (4)	100% (4)
	ELAV-like protein 1 OS=Homo sapiens GN=ELAVL1 PE=1 SV=2	Q15717	36 kDa	100% (3)		100% (4)		100% (4)
	Leucine--tRNA ligase, cytoplasmic OS=Homo sapiens GN=LARS PE=1 SV=2	Q9P2J5	134 kDa	100% (3)		100% (6)		100% (4)
	Cluster of Nuclease-sensitive element-binding protein 1 OS=Homo sapiens GN=YBX1 PE=1 SV=3 (P67809)	P67809 [2]	36 kDa		100% (4)	100% (6)		100% (4)
	Trifunctional purine biosynthetic protein adenosine-3 OS=Homo sapiens GN=GART PE=1 SV=1	P22102	108 kDa	100% (4)		100% (5)		100% (4)
	Aminoacyl tRNA synthase complex-interacting multifunctional protein 2 OS=Homo sapiens GN=AIMP2 PE=1 SV=2	Q13155	35 kDa			100% (3)	100% (3)	100% (4)
	FACT complex subunit SPT16 OS=Homo sapiens GN=SUPT16H PE=1 SV=1	Q9Y5B9	120 kDa	100% (4)		100% (5)		100% (4)
	Guanine nucleotide-binding protein-like 3 OS=Homo sapiens GN=GNL3 PE=1 SV=2	Q9BVP2	62 kDa			100% (4)	100% (4)	100% (4)

	Threonine--tRNA ligase, cytoplasmic OS=Homo sapiens GN=TARS PE=1 SV=3	P26639	83 kDa	100% (3)		100% (5)		100% (4)
	Programmed cell death 6-interacting protein OS=Homo sapiens GN=PDCD6IP PE=1 SV=1	Q8WUM4	96 kDa			100% (5)		100% (4)
	Transgelin-2 OS=Homo sapiens GN=TAGLN2 PE=1 SV=3	P37802 (+1)	22 kDa					100% (4)
	Fermitin family homolog 3 OS=Homo sapiens GN=FERMT3 PE=1 SV=1	Q86UX7	76 kDa					100% (4)
	Coatomer subunit beta OS=Homo sapiens GN=COPB1 PE=1 SV=3	P53618	107 kDa					100% (4)
	Cytosolic acyl coenzyme A thioester hydrolase OS=Homo sapiens GN=ACOT7 PE=1 SV=3	O00154	42 kDa					100% (4)
	78 kDa glucose-regulated protein OS=Homo sapiens GN=HSPA5 PE=1 SV=2	P11021	72 kDa	100% (20)	100% (5)	100% (15)	100% (25)	100% (3)
	Nucleolar RNA helicase 2 OS=Homo sapiens GN=DDX21 PE=1 SV=5	Q9NR30	87 kDa	100% (16)	100% (3)	100% (10)	100% (20)	100% (3)
	Heterogeneous nuclear ribonucleoprotein L OS=Homo sapiens GN=HNRNPL PE=1 SV=2	P14866	64 kDa	100% (7)		100% (11)	100% (9)	100% (3)
	60S ribosomal protein L29 OS=Homo sapiens GN=RPL29 PE=1 SV=2	P47914	18 kDa		100% (3)	100% (5)		100% (3)
	Heterogeneous nuclear ribonucleoproteins C1/C2 OS=Homo sapiens GN=HNRNPC PE=1 SV=1	G3V2Q1 (+2)	34 kDa	100% (7)	100% (3)	100% (7)	100% (8)	100% (3)
	60S ribosomal protein L37a OS=Homo sapiens GN=RPL37A PE=1 SV=2	P61513	10 kDa			100% (4)	100% (3)	100% (3)
	ATP-dependent RNA helicase DDX3X OS=Homo sapiens GN=DDX3X PE=1 SV=1	A0A0D9SF53 (+2)	81 kDa	100% (6)		100% (6)	100% (4)	100% (3)
	Ribosomal protein L19 OS=Homo sapiens GN=RPL19 PE=1 SV=1	J3KTE4 (+2)	23 kDa	100% (3)		100% (4)	100% (5)	100% (3)
	Heterogeneous nuclear ribonucleoprotein A0 OS=Homo sapiens GN=HNRNPA0 PE=1 SV=1	Q13151	31 kDa	100% (3)		100% (5)	100% (5)	100% (3)
	60S ribosomal protein L21 OS=Homo sapiens GN=RPL21 PE=1 SV=2	P46778	19 kDa			100% (4)		100% (3)
	Cluster of Heterogeneous nuclear ribonucleoprotein D0 OS=Homo sapiens GN=HNRNPD PE=1 SV=1 (Q14103)	Q14103 [2]	38 kDa	100% (7)		100% (4)	100% (7)	100% (3)
	rRNA 2'-O-methyltransferase fibrillarin OS=Homo sapiens GN=FBL PE=1 SV=2	P22087	34 kDa	100% (6)		100% (7)	100% (4)	100% (3)
	40S ribosomal protein S26 OS=Homo sapiens GN=RPS26 PE=1 SV=3	P62854	13 kDa			100% (3)	100% (3)	100% (3)
	Casein kinase II subunit beta OS=Homo sapiens GN=CSNK2B PE=1 SV=1	P67870 (+1)	25 kDa	100% (5)		100% (3)	100% (4)	100% (3)
	Cluster of Tyrosine-protein kinase Lck OS=Homo sapiens GN=LCK PE=1 SV=6 (P06239)	P06239 [2]	58 kDa	100% (5)		100% (6)	100% (4)	100% (3)

	60S ribosomal protein L22 OS=Homo sapiens GN=RPL22 PE=1 SV=2	P35268	15 kDa	100% (3)	100% (3)	100% (3)	100% (3)	100% (3)
	Cluster of Guanine nucleotide-binding protein G(I)/G(S)/G(T) subunit beta-1 OS=Homo sapiens GN=GNB1 PE=1 SV=3 (P62873)	P62873 [3]	37 kDa	100% (3)		100% (4)	100% (5)	100% (3)
	Sideroflexin-1 OS=Homo sapiens GN=SFXN1 PE=1 SV=4	Q9H9B4	36 kDa	100% (5)	100% (3)	100% (5)		100% (3)
	Lamin-B receptor OS=Homo sapiens GN=LBR PE=1 SV=2	Q14739	71 kDa			100% (3)		100% (3)
	26S proteasome non-ATPase regulatory subunit 3 OS=Homo sapiens GN=PSMD3 PE=1 SV=2	O43242	61 kDa			100% (3)		100% (3)
	Serine/threonine-protein phosphatase 2A 65 kDa regulatory subunit A alpha isoform OS=Homo sapiens GN=PPP2R1A PE=1 SV=4	P30153	65 kDa			100% (4)	100% (4)	100% (3)
	60S ribosomal protein L38 OS=Homo sapiens GN=RPL38 PE=1 SV=2	P63173	8 kDa					100% (3)
	Histone deacetylase 1 OS=Homo sapiens GN=HDAC1 PE=1 SV=1	Q13547	55 kDa			100% (4)	100% (3)	100% (3)
	Eukaryotic translation initiation factor 4 gamma 1 OS=Homo sapiens GN=EIF4G1 PE=1 SV=1	E7EUU4 (+3)	172 kDa	100% (3)		100% (4)		100% (3)
	Phenylalanine--tRNA ligase alpha subunit OS=Homo sapiens GN=FARSA PE=1 SV=1	K7ER00 (+1)	62 kDa			100% (3)		100% (3)
	Activator of 90 kDa heat shock protein ATPase homolog 1 OS=Homo sapiens GN=AHSA1 PE=1 SV=1	O95433	38 kDa					100% (3)
	Casein kinase II subunit alpha' OS=Homo sapiens GN=CSNK2A2 PE=1 SV=1	P19784	41 kDa			100% (3)	100% (3)	100% (3)
	Actin-related protein 2 OS=Homo sapiens GN=ACTR2 PE=1 SV=1	P61160	45 kDa			100% (4)		100% (3)
	Protein LLP homolog OS=Homo sapiens GN=LLPH PE=1 SV=1	Q9BRT6	15 kDa			100% (3)		100% (3)
	RNA-binding protein 14 OS=Homo sapiens GN=RBM14 PE=1 SV=2	Q96PK6	69 kDa			100% (4)		100% (3)
	Cluster of RNA-binding motif protein, X chromosome (Fragment) OS=Homo sapiens GN=RBMX PE=1 SV=2 (H0Y6E7)	H0Y6E7 [4]	32 kDa			100% (4)		100% (3)
	Eukaryotic translation initiation factor 2 subunit 2 OS=Homo sapiens GN=EIF2S2 PE=1 SV=2	P20042	38 kDa			100% (3)		100% (3)
	Eukaryotic translation initiation factor 3 subunit B OS=Homo sapiens GN=EIF3B PE=1 SV=3	P55884	92 kDa	100% (3)				100% (3)
	AP-2 complex subunit mu OS=Homo sapiens GN=AP2M1 PE=1 SV=1	A0A087WY71 (+2)	50 kDa					100% (3)
	Calponin (Fragment) OS=Homo sapiens GN=CNN2 PE=1 SV=1	A0A087X271 (+3)	20 kDa					100% (3)
	Myosin regulatory light chain 12A OS=Homo sapiens GN=MYL12A PE=1 SV=1	J3QRS3 (+2)	20 kDa					100% (3)
	Ribonuclease inhibitor OS=Homo sapiens GN=RNH1 PE=1 SV=2	P13489	50 kDa			100% (3)		100% (3)
	Lysine-rich nucleolar protein 1 OS=Homo sapiens GN=KNOP1 PE=1 SV=1	Q1ED39	52 kDa					100% (3)

	Protein FRG1 OS=Homo sapiens GN=FRG1 PE=1 SV=1	Q14331	29 kDa				100% (3)	100% (3)
	Proteasome activator complex subunit 2 OS=Homo sapiens GN=PSME2 PE=1 SV=1	A0A087X1Z3 (+1)	29 kDa					100% (3)
	Chloride intracellular channel protein 1 OS=Homo sapiens GN=CLIC1 PE=1 SV=4	O00299	27 kDa					100% (3)
	14-3-3 protein epsilon OS=Homo sapiens GN=YWHAE PE=1 SV=1	P62258	29 kDa			100% (2)		100% (3)
	60S acidic ribosomal protein P2 OS=Homo sapiens GN=RPLP2 PE=1 SV=1	P05387	12 kDa					100% (3)
	Importin-5 (Fragment) OS=Homo sapiens GN=IPO5 PE=1 SV=1	H0Y8C6 (+1)	124 kDa					100% (3)
	Dipeptidyl peptidase 3 OS=Homo sapiens GN=DPP3 PE=1 SV=1	G3V180 (+2)	84 kDa					100% (3)
	Cluster of Actin-related protein 2/3 complex subunit 4 OS=Homo sapiens GN=ARPC4-TTLL3 PE=3 SV=1 (F8WCF6)	F8WCF6 [3]	21 kDa					100% (3)
	Non-histone chromosomal protein HMG-17 OS=Homo sapiens GN=HMGN2 PE=1 SV=3	P05204	9 kDa	100% (3)			100% (4)	100% (3)
	Very-long-chain enoyl-CoA reductase OS=Homo sapiens GN=TECR PE=1 SV=1	Q9NZ01	36 kDa	100% (3)			100% (4)	100% (3)
	Septin-9 (Fragment) OS=Homo sapiens GN=SEPT9 PE=1 SV=1	K7EK18 (+2)	22 kDa					100% (3)
	Importin subunit beta-1 OS=Homo sapiens GN=KPNB1 PE=1 SV=2	Q14974	97 kDa					100% (3)
	Tubulin gamma-1 chain OS=Homo sapiens GN=TUBG1 PE=1 SV=2	P23258	51 kDa					100% (3)
	60S ribosomal protein L31 OS=Homo sapiens GN=RPL31 PE=1 SV=1	B7Z4C8 (+4)	15 kDa	100% (3)	100% (3)		100% (4)	100% (3)
	Cytochrome c oxidase subunit 2 OS=Homo sapiens GN=MT-CO2 PE=1 SV=1	P00403	26 kDa				100% (3)	100% (3)
	Proliferating cell nuclear antigen OS=Homo sapiens GN=PCNA PE=1 SV=1	P12004	29 kDa	100% (4)			100% (6)	100% (3)
	Splicing factor, proline- and glutamine-rich OS=Homo sapiens GN=SFPQ PE=1 SV=2	P23246	76 kDa	100% (7)	100% (4)	100% (10)	100% (12)	100% (2)
	Histone H2A.Z OS=Homo sapiens GN=H2AFZ PE=1 SV=2	P0C0S5 (+1)	14 kDa	100% (1)		100% (2)	100% (2)	100% (2)
	Heterogeneous nuclear ribonucleoprotein A3 OS=Homo sapiens GN=HNRNPA3 PE=1 SV=2	P51991	40 kDa	100% (11)	100% (4)	100% (10)	100% (12)	
	Cluster of Stress-70 protein, mitochondrial OS=Homo sapiens GN=HSPA9 PE=1 SV=2 (P38646)	P38646 [2]	74 kDa	100% (10)	100% (4)	100% (15)	100% (13)	
	Hypoxia up-regulated protein 1 OS=Homo sapiens GN=HYOU1 PE=1 SV=1	Q9Y4L1	111 kDa	100% (15)		100% (4)	100% (20)	
	Nucleophosmin OS=Homo sapiens GN=NPM1 PE=1 SV=2	P06748	33 kDa	100% (4)		100% (6)	100% (6)	
	Signal recognition particle subunit SRP72 OS=Homo sapiens GN=SRP72 PE=1 SV=3	O76094	75 kDa	100% (9)		100% (6)	100% (19)	
	Cluster of 40S ribosomal protein S16 OS=Homo sapiens GN=RPS16 PE=1 SV=2 (P62249)	P62249 [2]	16 kDa	100% (4)		100% (4)	100% (3)	

	Cluster of T-complex protein 1 subunit theta OS=Homo sapiens GN=CCT8 PE=1 SV=4 (P50990)	P50990 [2]	60 kDa	100% (9)	100% (3)	100% (5)	100% (11)	
	Dolichyl-diphosphooligosaccharide--protein glycosyltransferase subunit 2 OS=Homo sapiens GN=RPN2 PE=1 SV=3	P04844	69 kDa	100% (8)	100% (4)	100% (8)	100% (9)	
	40S ribosomal protein SA OS=Homo sapiens GN=RPSA PE=1 SV=1	A0A0C4DG17 (+2)	33 kDa	100% (5)		100% (8)	100% (9)	
	Heterogeneous nuclear ribonucleoproteins A2/B1 OS=Homo sapiens GN=HNRNPA2B1 PE=1 SV=2	P22626	37 kDa	100% (6)		100% (8)	100% (8)	
	Heterochromatin protein 1-binding protein 3 OS=Homo sapiens GN=HP1BP3 PE=1 SV=1	Q5SSJ5	61 kDa	100% (3)		100% (4)	100% (7)	
	Elongation factor 1-gamma OS=Homo sapiens GN=EEF1G PE=1 SV=3	P26641	50 kDa	100% (5)		100% (8)	100% (7)	
	ATP synthase subunit gamma, mitochondrial OS=Homo sapiens GN=ATP5C1 PE=1 SV=1	P36542	33 kDa	100% (6)	100% (4)	100% (4)	100% (4)	
	FACT complex subunit SSRP1 OS=Homo sapiens GN=SSRP1 PE=1 SV=1	Q08945	81 kDa	100% (9)		100% (3)	100% (10)	
	Cluster of Putative RNA-binding protein Luc7-like 2 OS=Homo sapiens GN=LUC7L2 PE=4 SV=1 (A0A0A6YYJ8)	A0A0A6YYJ8 [3]	54 kDa	100% (8)		100% (5)	100% (9)	
	Dolichyl-diphosphooligosaccharide--protein glycosyltransferase subunit 1 OS=Homo sapiens GN=RPN1 PE=1 SV=1	P04843	69 kDa	100% (8)			100% (8)	
	Peptidyl-prolyl cis-trans isomerase A OS=Homo sapiens GN=PPIA PE=1 SV=2	P62937	18 kDa	100% (6)		100% (6)	100% (6)	
	Calreticulin OS=Homo sapiens GN=CALR PE=1 SV=1	P27797	48 kDa	100% (6)			100% (7)	
	Protein LYRIC OS=Homo sapiens GN=MTDH PE=1 SV=2	Q86UE4	64 kDa	100% (6)			100% (12)	
	Hemoglobin subunit alpha OS=Homo sapiens GN=HBA1 PE=1 SV=2	P69905	15 kDa	100% (6)		100% (4)	100% (5)	
	Pumilio homolog 3 OS=Homo sapiens GN=PUM3 PE=1 SV=3	Q15397	74 kDa	100% (6)	100% (3)		100% (6)	
	Cluster of ATPase family AAA domain-containing protein 3A OS=Homo sapiens GN=ATAD3A PE=1 SV=2 (Q9NVI7)	Q9NVI7 [2]	71 kDa	100% (4)		100% (6)	100% (4)	
	Transferrin receptor protein 1 OS=Homo sapiens GN=TFRC PE=1 SV=2	P02786	85 kDa	100% (7)	100% (3)	100% (3)	100% (5)	
	Gamma-interferon-inducible protein 16 OS=Homo sapiens GN=IFI16 PE=1 SV=3	Q16666	88 kDa			100% (3)	100% (8)	
	Cluster of Polyadenylate-binding protein OS=Homo sapiens GN=PABPC1 PE=1 SV=1 (A0A087WTT1)	A0A087WTT1 [5]	59 kDa	100% (5)		100% (9)	100% (3)	
	Cluster of Coronin-1A OS=Homo sapiens GN=CORO1A PE=1 SV=4 (P31146)	P31146 [2]	51 kDa	100% (3)		100% (8)	100% (4)	

	Cluster of DNA topoisomerase 2-alpha OS=Homo sapiens GN=TOP2A PE=1 SV=3 (P11388)	P11388 [3]	174 kDa	100% (3)		100% (6)	100% (9)	
	SWI/SNF-related matrix-associated actin-dependent regulator of chromatin subfamily A member 5 OS=Homo sapiens GN=SMARCA5 PE=1 SV=1	O60264	122 kDa			100% (4)	100% (8)	
	60S ribosomal protein L35a OS=Homo sapiens GN=RPL35A PE=1 SV=2	P18077	13 kDa	100% (3)		100% (3)		
	Methionine--tRNA ligase, cytoplasmic OS=Homo sapiens GN=MARS PE=1 SV=2	P56192	101 kDa	100% (3)		100% (9)		
	Staphylococcal nuclease domain-containing protein 1 OS=Homo sapiens GN=SND1 PE=1 SV=1	Q7KZF4	102 kDa	100% (9)		100% (3)	100% (5)	
	Splicing factor U2AF 35 kDa subunit-like protein OS=Homo sapiens GN=U2AF1L5 PE=1 SV=1	P0DN76 (+1)	28 kDa			100% (3)	100% (4)	
	Ubiquitin-like modifier-activating enzyme 1 OS=Homo sapiens GN=UBA1 PE=1 SV=3	P22314	118 kDa	100% (5)		100% (7)	100% (5)	
	DnaJ homolog subfamily A member 1 OS=Homo sapiens GN=DNAJA1 PE=1 SV=2	P31689	45 kDa	100% (4)			100% (4)	
	Pre-mRNA-processing-splicing factor 8 OS=Homo sapiens GN=PRPF8 PE=1 SV=2	Q6P2Q9	274 kDa			100% (7)	100% (4)	
	Cluster of High mobility group protein B1 OS=Homo sapiens GN=HMGB1 PE=1 SV=3 (P09429)	P09429 [3]	25 kDa	100% (3)		100% (3)	100% (6)	
	Filamin-B OS=Homo sapiens GN=FLNB PE=1 SV=2	O75369	278 kDa	100% (4)		100% (5)	100% (3)	
	Poly [ADP-ribose] polymerase 1 OS=Homo sapiens GN=PARP1 PE=1 SV=4	P09874	113 kDa	100% (5)		100% (5)	100% (4)	
	Bifunctional purine biosynthesis protein PURH OS=Homo sapiens GN=ATIC PE=1 SV=3	P31939	65 kDa	100% (6)		100% (6)		
	Transcriptional repressor CTCF OS=Homo sapiens GN=CTCF PE=1 SV=1	P49711	83 kDa	100% (4)			100% (8)	
	Chromobox protein homolog 3 OS=Homo sapiens GN=CBX3 PE=1 SV=4	Q13185	21 kDa	100% (4)			100% (3)	
	60S ribosomal protein L39 OS=Homo sapiens GN=RPL39 PE=1 SV=2	P62891 (+1)	6 kDa			100% (3)		
	Cluster of Glutathione S-transferase P OS=Homo sapiens GN=GSTP1 PE=1 SV=2 (P09211)	P09211 [2]	23 kDa	100% (3)		100% (3)	100% (7)	
	Heterogeneous nuclear ribonucleoprotein R OS=Homo sapiens GN=HNRNPR PE=1 SV=1	O43390	71 kDa	100% (4)		100% (5)	100% (5)	
	Calnexin OS=Homo sapiens GN=CANX PE=1 SV=2	P27824	68 kDa	100% (3)			100% (5)	
	Cluster of Transformer-2 protein homolog beta OS=Homo sapiens GN=TRA2B PE=1 SV=1 (P62995)	P62995 [2]	34 kDa	100% (4)		100% (3)	100% (5)	
	Citrate synthase OS=Homo sapiens GN=CS PE=1 SV=1	A0A0C4DGI3 (+1)	45 kDa	100% (3)		100% (3)	100% (6)	
	Multifunctional protein ADE2 (Fragment) OS=Homo sapiens GN=PAICS PE=1 SV=1	E9PBS1 (+1)	46 kDa			100% (4)	100% (4)	

	Nucleolin OS=Homo sapiens GN=NCL PE=1 SV=3	P19338	77 kDa	100% (6)		100% (6)		
	Trifunctional enzyme subunit alpha, mitochondrial OS=Homo sapiens GN=HADHA PE=1 SV=2	P40939	83 kDa			100% (6)	100% (4)	
	Ribosome biogenesis regulatory protein homolog OS=Homo sapiens GN=RRS1 PE=1 SV=2	Q15050	41 kDa	100% (4)			100% (3)	
	Stomatin-like protein 2, mitochondrial OS=Homo sapiens GN=STOML2 PE=1 SV=1	Q9UJZ1	39 kDa			100% (4)	100% (7)	
	Eukaryotic translation initiation factor 5A (Fragment) OS=Homo sapiens GN=EIF5A PE=1 SV=8	I3L397 (+2)	16 kDa	100% (3)			100% (4)	
	Heterogeneous nuclear ribonucleoprotein H3 OS=Homo sapiens GN=HNRNPH3 PE=1 SV=2	P31942	37 kDa	100% (4)		100% (4)	100% (3)	
	Glutamine--fructose-6-phosphate aminotransferase [isomerizing] 1 OS=Homo sapiens GN=GFPT1 PE=1 SV=3	Q06210	79 kDa			100% (7)		
	Protein disulfide-isomerase A6 OS=Homo sapiens GN=PDIA6 PE=1 SV=1	Q15084	48 kDa	100% (4)			100% (5)	
	Surfeit locus protein 6 OS=Homo sapiens GN=SURF6 PE=1 SV=3	O75683	41 kDa			100% (5)		
	Inosine-5'-monophosphate dehydrogenase 2 OS=Homo sapiens GN=IMPDH2 PE=1 SV=2	P12268	56 kDa	100% (3)		100% (3)	100% (5)	
	RNA-binding protein 25 OS=Homo sapiens GN=RBM25 PE=1 SV=3	P49756	100 kDa	100% (3)			100% (4)	
	KH domain-containing, RNA-binding, signal transduction-associated protein 1 OS=Homo sapiens GN=KHDRBS1 PE=1 SV=1	Q07666	48 kDa			100% (3)		
	Ribosomal RNA processing protein 1 homolog B OS=Homo sapiens GN=RRP1B PE=1 SV=3	Q14684	84 kDa	100% (3)			100% (8)	
	G patch domain-containing protein 4 OS=Homo sapiens GN=GPATCH4 PE=1 SV=2	Q5T3I0	50 kDa	100% (3)			100% (3)	
	Coiled-coil domain-containing protein 86 OS=Homo sapiens GN=CCDC86 PE=1 SV=1	Q9H6F5	40 kDa	100% (4)			100% (4)	
	Arginine and glutamate-rich protein 1 OS=Homo sapiens GN=ARGLU1 PE=1 SV=1	Q9NWB6	33 kDa	100% (3)				
	RNA-binding protein Raly OS=Homo sapiens GN=RALY PE=1 SV=1	Q9UKM9	32 kDa	100% (4)			100% (5)	
	Cluster of ATP synthase subunit O, mitochondrial OS=Homo sapiens GN=ATP5O PE=1 SV=1 (P48047)	P48047 [2]	23 kDa	100% (3)			100% (5)	
	Heterogeneous nuclear ribonucleoprotein A/B OS=Homo sapiens GN=HNRNPAB PE=1 SV=1	D6R9P3 (+2)	30 kDa	100% (3)				
	Nascent polypeptide-associated complex subunit alpha, muscle-specific form OS=Homo sapiens GN=NACA PE=1 SV=1	E9PAV3	205 kDa	100% (3)		100% (3)	100% (3)	
	Serine/threonine-protein phosphatase OS=Homo sapiens GN=PPP1CC PE=1 SV=1	F8W0W8 (+1)	38 kDa	100% (3)		100% (3)	100% (3)	

	Profilin-1 OS=Homo sapiens GN=PFN1 PE=1 SV=2	P07737	15 kDa			100% (3)		
	Stress-induced-phosphoprotein 1 OS=Homo sapiens GN=STIP1 PE=1 SV=1	P31948	63 kDa	100% (4)			100% (4)	
	Interleukin enhancer-binding factor 2 OS=Homo sapiens GN=ILF2 PE=1 SV=2	Q12905	43 kDa			100% (5)		
	Cluster of Histone-binding protein RBBP4 OS=Homo sapiens GN=RBBP4 PE=1 SV=3 (Q09028)	Q09028 [2]	48 kDa			100% (4)		
	Cluster of Polypyrimidine tract-binding protein 1 OS=Homo sapiens GN=PTBP1 PE=1 SV=1 (A0A0U1RRM4)	A0A0U1RRM4 [4]	62 kDa	100% (3)				
	Cluster of Serine/threonine-protein kinase VRK1 OS=Homo sapiens GN=VRK1 PE=1 SV=1 (Q99986)	Q99986 [2]	45 kDa			100% (5)		
	Serine/arginine-rich-splicing factor 1 OS=Homo sapiens GN=SRSF1 PE=1 SV=1	J3KTL2 (+1)	28 kDa	100% (4)			100% (4)	
	Glycine--tRNA ligase OS=Homo sapiens GN=GARS PE=1 SV=3	P41250	83 kDa			100% (4)	100% (3)	
	Interleukin enhancer-binding factor 3 OS=Homo sapiens GN=ILF3 PE=1 SV=3	Q12906	95 kDa			100% (5)		
	Leucine-rich repeat-containing protein 59 OS=Homo sapiens GN=LRRC59 PE=1 SV=1	Q96AG4	35 kDa	100% (3)			100% (5)	
	Nucleolar GTP-binding protein 1 OS=Homo sapiens GN=GTPBP4 PE=1 SV=3	Q9BZE4	74 kDa				100% (4)	
	Protein kinase C alpha type OS=Homo sapiens GN=PRKCA PE=1 SV=4	P17252	77 kDa			100% (3)		
	Serine/arginine-rich-splicing factor 3 OS=Homo sapiens GN=SRSF3 PE=1 SV=1	A0A087X2D0 (+1)	10 kDa	100% (2)				
	Cluster of Sarcoplasmic/endoplasmic reticulum calcium ATPase 2 OS=Homo sapiens GN=ATP2A2 PE=1 SV=1 (P16615)	P16615 [2]	115 kDa	100% (3)			100% (3)	
	Cluster of Sodium/potassium-transporting ATPase subunit alpha-1 OS=Homo sapiens GN=ATP1A1 PE=1 SV=1 (P05023)	P05023 [4]	113 kDa	100% (3)			100% (3)	
	Cluster of Nucleosome assembly protein 1-like 1 OS=Homo sapiens GN=NAP1L1 PE=1 SV=1 (F5H4R6)	F5H4R6 [12]	45 kDa	100% (3)			100% (3)	
	Prostaglandin E synthase 3 OS=Homo sapiens GN=PTGES3 PE=1 SV=1	A0A087WYT3 (+1)	19 kDa	100% (3)		100% (4)		
	Serine/arginine-rich-splicing factor 7 OS=Homo sapiens GN=SRSF7 PE=1 SV=1	A0A0B4J1Z1 (+2)	16 kDa	100% (4)		100% (2)	100% (2)	
	Regulator of chromosome condensation (Fragment) OS=Homo sapiens GN=RCC1 PE=1 SV=1	C9JW69 (+1)	40 kDa				100% (3)	
	ATP synthase subunit g, mitochondrial OS=Homo sapiens GN=ATP5L PE=1 SV=1	E9PN17 (+1)	8 kDa			100% (3)		

	Mitotic checkpoint protein BUB3 (Fragment) OS=Homo sapiens GN=BUB3 PE=1 SV=1	J3QT28 (+1)	32 kDa			100% (4)		
	Surfeit locus protein 4 OS=Homo sapiens GN=SURF4 PE=1 SV=3	O15260 (+1)	30 kDa				100% (3)	
	Pre-mRNA-processing factor 40 homolog A OS=Homo sapiens GN=PRPF40A PE=1 SV=2	O75400	109 kDa	100% (4)			100% (3)	
	Hypoxanthine-guanine phosphoribosyltransferase OS=Homo sapiens GN=HPRT1 PE=1 SV=2	P00492	25 kDa			100% (4)		
	26S protease regulatory subunit 7 OS=Homo sapiens GN=PSMC2 PE=1 SV=3	P35998	49 kDa				100% (3)	
	Arginine--tRNA ligase, cytoplasmic OS=Homo sapiens GN=RARS PE=1 SV=2	P54136	75 kDa			100% (3)		
	Rho-related GTP-binding protein RhoG OS=Homo sapiens GN=RHOG PE=1 SV=1	P84095	21 kDa	100% (2)		100% (3)		
	Cytoplasmic dynein 1 heavy chain 1 OS=Homo sapiens GN=DYNC1H1 PE=1 SV=5	Q14204	532 kDa			100% (3)		
	Proliferation-associated protein 2G4 OS=Homo sapiens GN=PA2G4 PE=1 SV=3	Q9UQ80	44 kDa	100% (3)			100% (3)	
	Histone H1.0 OS=Homo sapiens GN=H1F0 PE=1 SV=3	P07305	21 kDa			100% (3)		
	Ras-related C3 botulinum toxin substrate 2 OS=Homo sapiens GN=RAC2 PE=1 SV=1	P15153	21 kDa	100% (2)		100% (3)		
	Dolichyl-diphosphooligosaccharide--protein glycosyltransferase 48 kDa subunit OS=Homo sapiens GN=DDOST PE=1 SV=1	A0A0C4DGS1 (+1)	49 kDa	100% (3)				
	Propionyl-CoA carboxylase alpha chain, mitochondrial (Fragment) OS=Homo sapiens GN=PCCA PE=1 SV=1	A0A1B0GUX9 (+1)	44 kDa			100% (5)		
	Heterogeneous nuclear ribonucleoprotein Q OS=Homo sapiens GN=SYNCRIP PE=1 SV=2	O60506	70 kDa	100% (3)		100% (1)	100% (3)	
	Lysine--tRNA ligase OS=Homo sapiens GN=KARS PE=1 SV=3	Q15046	68 kDa	100% (3)				
	3-hydroxyacyl-CoA dehydrogenase type-2 OS=Homo sapiens GN=HSD17B10 PE=1 SV=3	Q99714	27 kDa	100% (4)				
	Differentially expressed in FDCP 6 homolog OS=Homo sapiens GN=DEF6 PE=1 SV=1	Q9H4E7	74 kDa				100% (5)	
	RNA-binding protein 39 (Fragment) OS=Homo sapiens GN=RBM39 PE=1 SV=1	A0A0U1RQH7 (+2)	27 kDa	100% (3)			100% (3)	
	Structural maintenance of chromosomes protein OS=Homo sapiens GN=SMC4 PE=1 SV=1	E9PD53 (+1)	144 kDa				100% (3)	
	Metastasis-associated protein MTA2 OS=Homo sapiens GN=MTA2 PE=1 SV=1	O94776	75 kDa				100% (4)	
	Retinoblastoma-associated protein OS=Homo sapiens GN=RB1 PE=1 SV=2	P06400	106 kDa			100% (3)		

	Histidine triad nucleotide-binding protein 1 OS=Homo sapiens GN=HINT1 PE=1 SV=2	P49773	14 kDa			100% (4)		
	Transcription intermediary factor 1-beta OS=Homo sapiens GN=TRIM28 PE=1 SV=5	Q13263	89 kDa				100% (3)	
	Ribosome production factor 2 homolog (Fragment) OS=Homo sapiens GN=RPF2 PE=1 SV=1	Q5VXN0 (+1)	25 kDa	100% (3)				
	MICOS complex subunit MIC60 OS=Homo sapiens GN=IMMT PE=1 SV=2	B9A067 (+2)	79 kDa				100% (3)	
	116 kDa U5 small nuclear ribonucleoprotein component OS=Homo sapiens GN=EFTUD2 PE=1 SV=1	Q15029	109 kDa	100% (3)				
	Cluster of RNA-binding protein FUS OS=Homo sapiens GN=FUS PE=1 SV=1 (P35637)	P35637 [3]	53 kDa			100% (4)		
	26S proteasome non-ATPase regulatory subunit 11 OS=Homo sapiens GN=PSMD11 PE=1 SV=3	O00231	47 kDa	100% (3)				
	Phosphoribosylformylglycinamidine synthase OS=Homo sapiens GN=PFAS PE=1 SV=4	O15067	145 kDa			100% (3)		
	Splicing factor U2AF 65 kDa subunit OS=Homo sapiens GN=U2AF2 PE=1 SV=4	P26368	54 kDa				100% (3)	
	Eukaryotic translation initiation factor 3 subunit I OS=Homo sapiens GN=EIF3I PE=1 SV=1	Q13347	37 kDa			100% (3)		
	Scaffold attachment factor B2 OS=Homo sapiens GN=SAFB2 PE=1 SV=1	Q14151 (+1)	107 kDa			100% (3)		
	Exportin-5 OS=Homo sapiens GN=XPO5 PE=1 SV=1	Q9HAV4	136 kDa			100% (3)		
	Kinectin OS=Homo sapiens GN=KTN1 PE=1 SV=1	Q86UP2	156 kDa				100% (3)	
	SRSF protein kinase 1 OS=Homo sapiens GN=SRPK1 PE=1 SV=2	Q96SB4	74 kDa				100% (3)	
	Adipocyte enhancer-binding protein 1 OS=Homo sapiens GN=AEBP1 PE=1 SV=1	Q8IUX7	131 kDa				100% (3)	
	Cisplatin resistance-associated overexpressed protein, isoform CRA_b OS=Homo sapiens GN=LUC7L3 PE=1 SV=1	J3KPP4 (+1)	58 kDa				100% (3)	
	High mobility group protein B2 OS=Homo sapiens GN=HMGB2 PE=1 SV=2	P26583	24 kDa				100% (2)	